Université du Québec
Institut National de la Recherche Scientifique
Centre Eau Terre Environnement

DÉVELOPPEMENT D'UN PROCÉDÉ D'OXYDATION PHOTOÉLÉCTROCATALYTIQUE INNOVANT UTILISANT DES ÉLECTRODES NANOSTRUCTURÉES DE Ti/TiO_2 POUR LE TRAITEMENT DES EFFLUENTS CONTAMINÉS PAR DES RÉSIDUS MÉDICAMENTEUX

Par

Rimeh DAGHRIR

Thèse présentée pour l'obtention du grade de
philosophiae doctor (Ph.D.) en sciences de l'eau

Jury d'évaluation

Examinateur externe	**Trong-On Do** **Université Laval**
Examinateur externe	**Manuel J. Rodriguez** **Université Laval**
Examinateur interne	**Satinder Kaur Brar** **INRS- ETE**
Directeur de Recherche	**Patrick Drogui** **INRS-ETE**
Co-directeurs de Recherche	**My Ali El Khakani** **INRS-EMT** **Didier Robert** **Université De Lorraine**

© Droits réservés de Rimeh Daghrir, 2013

REMERCIEMENTS

Ce travail a été effectué au Laboratoire d'Électro-technologies Environnementales et Procédés Oxydatifs (LEEPO) de l'INRS-ETE. Je tiens à exprimer, en premier lieu, à mon directeur de recherche, Monsieur le Professeur Patrick Drogui, ma profonde gratitude et mes remerciements les plus sincères pour son infaillible et stimulant encadrement, pour son inestimable aide et ses conseils précieux. Je ne peux ignorer ses qualités humaines et ne pas être reconnaissante au savoir qu'il m'a prodigué, la confiance qu'il m'a accordée et le grand soutien moral apporté de sa part grâce à quoi j'ai pu accomplir mon travail.

Je tiens aussi à témoigner mes vifs remerciements au professeur My Ali El-Khakani qui a eu l'amabilité de bien vouloir m'accueillir au sein de son équipe de recherche à l'INRS-EMT pour réaliser la majeure partie des expériences sur le simulateur solaire. Ma reconnaissance et mes remerciements pour sa disponibilité, son soutien, ses conseils judicieux, mais aussi pour la confiance qu'il m'a accordée au cours de ces années de thèse.

Je remercie énormément, Monsieur le Professeur Didier Robert, pour ses précieux conseils et sa disponibilité, mais aussi pour le grand interêt qu'il a porté à ce travail.

Je suis particulièrement reconnaissante et honorée de l'intérêt qu'ont porté à cette thèse en acceptant d'en être les rapporteurs, Messieurs les Professeurs Trong-On Do de l'Université Laval, Manuel J. Rodriguez de l'Université Laval et Madame le Professeur Satinder_Kaur Brar de l'INRS-ÉTÉ.

Je remercie vivement l'ensemble des membres du LEEPO pour leur aide précieuse lors de mes travaux de recherche. Je remercie également celles et ceux qui ont tant fait pour moi: Dr Brahima Seyhi pour son précieux coup de main et ses conseils judicieux, Dr Lea Rosine Guitaya pour ses grandes qualités, Nam Tran et Dr. François Zaviska.

Je n'oublie pas de citer mes trois stagiaires : Aicha Dimboukou-Mpira, Asmaa Errachidi et Lorene Igounet pour leur contribution, leur investissement et leur collaboration dans ce projet de recherche.

Je suis particuliérement reconnaissante envers le personnel des laboratoires de l'INRS-ETE Mesdames et Messieurs: Stéphane Prémont, Lise Rancourt, Pauline Fournier, Jean-François Dutil, Stephane Moise et Julie Perreault pour leur expertise et leurs conseils techniques, leur présence et leur aide.

Tous mes respects et sincères remerciements à tous les professeurs de l'INRS-ETE pour la qualité de la formation qu'ils m'ont fournis tout au long de mon cursus universitaire à l'INRS-ETE.

Ma gratitude s'adresse aussi à mes collégues de l'INRS-ETE pour leurs conseils, leurs encouragements et leur aide inestimable.

Enfin, si j'ai résisté durant ces années d'études, avec des hauts et des bas, c'est bien grâce à mes proches, qui ont été constamment à mes côtés. Mes pensées vont tout particulièrement à papa et maman, qui ont toujours su m'entourer de leur affection et soutenu dans la réalisation de mes projets. Je vous remercie pour votre patience, votre compréhension et votre grande confiance. Un grand merci à mes deux frères, à ma belle sœur et à ma niéce pour leur soutien dans les moments difficiles, leurs conseils, les émotions partagées et leur présence. Cette thèse, aboutissement de longues années d'études, je la dois beaucoup à mes deux fréres et à mes parents exceptionnels avec qui j'ai vécu dans un climat toujours serein, à l'abri de tous soucis affectifs. Il m'est impossible de trouver les mots pour dire à quel point je suis fière d'eux, et à quel point je les aime.

Je suis incapable de terminer cette liste de remerciement sans exprimer mon éstimation du fond du cœur à mes meilleurs ami(e)s à Québec : Dorra Hammami, Parvin Kalantari, Hoang

Kim Huong, Ahmadi Kingumbi, Shedly Baya, Sheyma Bourourou et Magdouli Sarra. Merci d'avoir souvent penser à moi et à mon bonheur, merci pour les années de soutien, merci pour vos encouragements. Je garderai le souvenir de votre sincère amitié.

AVANT-PROPOS

L'objectif principal de ce projet de thèse est de développer et optimiser un procédé d'oxydation photoélectrocatalytique utilisant une électrode nanostructurée de Ti/TiO_2 pour le traitement d'effluents contaminés par des micropolluants organiques réfractaires tels que la chlorotétracycline et la carbamazépine. Le développement d'un procédé d'oxydation photoélectrocatalytique mettant en synergie les procédés électrochimiques et les techniques photocatalytiques pourrait constituer une avenue potentielle pour le traitement à grande échelle des composés organiques persistants. Cette étude se compose de dix chapitres.

Le premier chapitre correspond à la synthèse de ce travail, laquelle comprend la revue de littérature relative à la problématique des polluants organiques réfractaires et des différents procédés de traitement existant afin d'y remédier, ainsi que les objectifs et la démarche méthodologique employée et, enfin un bilan général des résultats obtenus.

Parmi tous les contaminants émergents refractaires détectés dans l'environnement, les résidus médicamenteux de type antibiotique sont souvent cités parmi les composés les plus problématiques. De ce point de vue, le second chapitre traite de la présence des tétracyclines dans les cours d'eaux et de leur devenir dans l'environnement, lequel a fait l'objet d'un article synthèse publié dans *Environmental Chemistry Letters, DOI 10.1007/s10311-013-0404-8 :* **Rimeh Daghrir, Patrick Drogui (2013) Tetracycline antibiotics in the environment: a review.**

Vue les exigences de plus en plus strictes afin d'assurer une bonne gestion des eaux contaminées par des résidus médicamenteux, les spécialistes s'orientent vers la recherche de technologies de traitement plus avancées. C'est dans cette optique que la technique de photoélectrocatalyse a été proposée afin d'améliorer l'efficacité épuratoire lors du traitement des eaux usées résiduaires. Le troisième chapitre traite du procédé d'oxydation

photoélectrocatalytique et ses principales applications environnementales, lequel a fait également l'objet d'un article synthèse publié dans *Journal of photochemistry and photobiology A : Chemistry 238:41-52 :* **Rimeh Daghrir, Patrick Drogui, Didier Robert (2012) Photoelectrocatalytic technologies for environmental applications.**

En tenant compte de ces propriétés physico-chimiques, le TiO_2 est le photocatalyseur le plus souvent utilisé comme photoanode dans un procédé d'oxydation photoélectrocatalytique. Il a une bande interdite de 3.2 eV et est capable d'absorber les photons UV. Le développement de telles photoanodes qui absorberaient dans la partie visible du spectre solaire peut constituer un avantage majeur pour pouvoir appliquer le procédé d'oxydation photoélectrocatalytique à l'échelle réelle. Ainsi, le quatrième chapitre présente les différentes approches utilisées pour étendre la réponse spectrale de TiO_2 vers la région du visible ainsi que ses différentes applications environmentales. Cette synthèse bibliographique a fait l'objet d'un article publié dans *Industrial & Engineering Chemistry Research, 52: 3581-3599:* **Rimeh Daghrir, Patrick Drogui, Didier Robert (2013) modified TiO_2 for environmental photocatalytic applications : a review.**

Le TiO_2 utilisé comme photoanode dans un tel procédé d'oxydation photoélectrocatalytique a été synthétisé et intégré dans une cellule photoélectrocatalytique afin d'évaluer leur capacité de production d'éspéces oxydantes nécessaires à l'oxydation des micropolluants réfrcataires. La mise en évidence de ces éspéces oxygénées réactives a été réalisée en utilisant une méthode indirecte utilisant le p- nitrosodimethylaniline. Le cinquième chapitre correspond à l'étude portant sur le blanchissement du p- nitrosodimethylaniline par oxydation photoélectrocatalytique utilisant le Ti/TiO_2 nanostructuré comme photoanode. Ce chapitre a fait l'objet d'un article publié dans *Journal of Applied Electrochemistry 43 (4) : 467-479 :* **Rimeh Daghrir, Patrick Drogui, Ibrahima Ka, My Ali El Khakani and Didier Robert**

(2013) Photoelectrocatalytic bleaching of p-nitrosodimethylaniline using Ti/TiO_2 nanostructured electrodes deposited by means of a pulsed laser deposition process.

Ces résultats précédents ont permis d'exploiter ultérieurement le procédé d'oxydation photoélectrocatalytique pour le traitement d'une solution synthétique contaminée par un polluant organique persistant tel que la chlortetracycline. L'étude relative à la dégradation du chlorotétracycline par un procédé d'oxydation photoélectrocatalytique utilisant une électrode nanostructurée préparée par la méthode de déposition par ablation laser est présentée en détail dans le sixième chapitre. Les résultats issus de ces travaux ont été valorisés sous forme d'article publié dans *Journal of Hazardous Materials 199-200: 15-24:* **Rimeh Daghrir, Patrick Drogui, Ibrahima Ka, My Ali El Khakani (2012) Photoelectrocatalytic degradation of chlortetracycline using Ti/TiO_2 nanostructured electrodes deposited by means of a Pulsed Laser Deposition process.**

L'éfficacité d'oxydation photoélectrocatalytique de la chlortetracycline sous radiation UV pourrait être amélioré en utilisant une cathode appropriée pour la génération simulatnée d'un accepteur d'électron tel que le H_2O_2. De ce point de vue, le septième chapitre porte sur la dégradation photoélectrocatalytique du chlorotétracycline en utilisant le Ti/TiO_2 comme photoanode avec une production simultanée du peroxyde d'hydrogène. Cette partie des travaux a été publié dans *Electrochimica Acta*, 87: 18-31 : **Rimeh Daghrir, Patrick Drogui, My Ali El Khakani (2013) Photoelectrocatalytic oxidation of chlortetracycline using Ti/TiO_2 photo anode with simultaneous H_2O_2 production.**

L'exploitation des raditaions solaires lors de l'application du procédé d'oxydation photoélectrocatalytique constitue un avantage majeur qui pourrait contribuer à réduire les côuts du traitement. De ce point de vue, le huitième chapitre traite de l'oxydation photoélectrocatalytique du chlorotétracycline sous radiation solaire en utilisant le TiO_2 nanostructuré dopé à l'azote. Cette étude a fait l'objet d'un article accepté dans la revue *Water*

Research WR10166 (accepté le 10 Septembre 2013) : **Rimeh Daghrir, Patrick Drogui, Nazar Delegan, My Ali El Khakani (2013), Electrochemical degradation of chlortetracycline using N-doped Ti/TiO_2 photoanode under sunlight irradiations**.

En tenant compte des résultats du huitième chapitre, les meilleures conditions de traitement ont été par la suite appliquées sur un effluent réel de type municipal artificiellement contaminé par la chlortetracycline. Les résultats de cette étude sont présentés dans le neuvième chapitre qui porte sur l'application du procédé d'oxydation photoélectrocatalytique pour le traitement tertiaire d'un effluent de type municipal artificiellement contaminé par la chlorotétracycline. Cette étude a fait l'objet d'un article publié dans la revue *Science of the total Environment*, 466-467 : 300-305 : **Rimeh Daghrir, Patrick Drogui, Nazar Delegan, My Ali El Khakani (2014) Removal of chlortetracycline from spiked municipal wastewater using a photoelectrocatalytic process under sunlight irradiations.**

Dans l'optique d'étendre son spectre d'activité, le procédé photoélectrocatalytique a été testé pour la dégrdation d'une autre polluant de type pharmaceutique tel que la carbamazépine couramment rencontrée dans les eaux résiduaires. Les résultats de cette étude ont été synthétisés dans le dixième chapitre. Ce chapitre fait référence à l'étude sur la dégradation d'un antidépressif, carbamazépine par le procédé d'oxydation photoélectrocatalytique, lequel a été optimisé par la méthodologie des plans d'expériences en utilisant l'électrode Ti/TiO_2 nanostructuré comme photoanode. Ces résultats ont fait l'objet d'un article accepté dans la revue *Chemosphere CHEM 14256* (accepté le 17 Septembre 2013) : **Rimeh Daghrir, Patrick Drogui, Aicha Dimboukou-Mpira, My Ali El Khakani (2013) Photoelectrocatalytic degradation of carbamazepine using Ti/TiO_2 nanostructured electrodes deposited by means of a pulsed Laser deposition process.**

RÉSUMÉ

Depuis un certain nombre d'années, une attention scientifique particulière est portée sur l'émergence et le devenir dans l'environnement de composés organiques persistants d'origine urbaine et industrielle. Ces composés ne sont pas généralement éliminés dans les filières conventionnelles de traitement des eaux usées et s'accumulent ainsi dans le milieu récepteur. Ils provoquent des bouleversements significatifs sur la faune et la flore ainsi que sur la santé humaine. Plusieurs espèces animales et végétales sont en voie de disparition à cause des composés nocifs présents dans l'environnement. Au cours de ces dernières années, de nombreuses technologies ont été développées pour faire face à ces polluants d'intérêt émergent. De ce point de vue, les procédés d'oxydation photoélectrocatalytique sont particulièrement intéressants. L'intérêt de ces techniques réside dans leur aspect non polluant et leur facilité d'automatisation.

L'objectif de ce projet est d'évaluer l'efficacité de l'oxydation photoélectrocatalytique utilisant une électrode nanostructurée de Ti/TiO_2 dans le traitement des effluents contenant des composés organiques persistants tel que la chlorotétracycline et la carbamazépine. Le développement d'un procédé d'oxydation photoélectrocatalytique mettant en synergie les procédés électrochimiques et les techniques photocatalytiques pourrait constituer une avenue potentielle de traitement des composés organiques persistants. Le procédé photocatalytique est une technologie basée sur l'irradiation d'un catalyseur, en général un semi-conducteur (TiO_2) qui peut être photoexcité pour former des sites électro-donneurs (h^+) et des sites électro-accepteurs d'électrons (e^-) induisant ainsi des réactions d'oxydo-réduction. L'application des radiations UV ayant une énergie supérieure au gap d'énergie entre la bande de valence et la bande de conduction favorise le passage des électrons de la bande de valence à la bande de conduction créant ainsi des pairs d'électron-trou (e^-/h^+). La durée de vie de ces paires d'électron-trous (e^-/h^+) est de l'ordre de nanoseconde. Le potentiel externe appliqué

dans un procédé photoélectrocatalytique constitue un facteur clé puisqu'il est capable de retarder la recombinaison d'électron-trou e^-/h^+ photogénéré. Cet effet de synergie permet de produire *in situ* des espèces oxygénées réactives très puissantes telles que les radicaux hydroxyles ayant la capacité de dégrader efficacement les composés organiques jusqu'à sa minéralisation. Le TiO_2 est le semi-conducteur le plus utilisé comme photoanode dans les réactions photocatalytiques. Néanmoins, cette activité photo-catalytique de TiO_2 se limite souvent à l'utilisation des rayonnements ultra-violets ($\lambda < 384$ nm) qui représentent seulement 3 à 5% des radiations solaires. L'exploitation des radiations visibles en présence de TiO_2 dopé à l'azote serait une alternative pour l'application du procédé d'oxydation photoélectrocatalytique à grande échelle. Le matériel photoélectrocatalytique utilisé afin de réaliser cette étude est composé d'une cellule photoélectrocatalytique à électrode rectangulaire de Ti/TiO_2 (dopé ou non-dopé à l'azote) et alimenté par des radiations UV (ou des radiations visibles), ce qui a permis à l'échelle du laboratoire, d'évaluer et d'optimiser le procédé.

Les travaux préliminaires ont d'abord consisté à évaluer le potentiel d'oxydation d'un procédé photoélectrocatalytique. Pour ce faire, la p-nitrosodimethylaniline (RNO) a été utilisé pour évaluer la capacité de production des espèces oxygénées réactives telles que l'ozone et les radicaux hydroxyles. Un taux de blanchissement de RNO allant jusqu'à 22.6 10^{-3} mM h^{-1} a été obtenu en appliquant une intensité de courant de 0.1 A sous irradiation UV-254 nm et en utilisant la forme anatase de TiO_2 comme photoanode et le carbone vitreux à la cathode. Ces résultats permettront ultérieurement d'exploiter cette technique pour le traitement d'une solution synthétique contaminée par un polluant organique persistant tel que la chlorotétracycline, puis pour le traitement des effluents réels artificiellement contaminés par la chlorotétracycline. À titre de comparaison, la carbamazépine a été étudié. L'évaluation de la performance d'une cellule d'oxydation photoélectrocatalytique pour le traitement des eaux

usées synthétiques contaminées par la CTC a été basée sur une série d'optimisation de certains paramètres opérationnels. Les différents paramètres inhérents à ce procédé tels que l'intensité de courant, le temps de traitement, la structure cristallographique de TiO_2, le type de cathode, le pH et la concentration initiale du polluant ont été évaluées en termes d'efficacité de dégradation du polluant et de coût énergétique. Le recours à l'utilisation d'un logiciel de plan d'expérience en premier lieu a permis de décrire les différents processus de dégradation et d'évaluer les effets propres à chaque paramètres ainsi que les interactions éventuelles. Cette étude a permis également à partir des modèles mathématiques issus du plan d'expérience de déterminer les conditions opératoires optimales. L'étude de la dégradation de la chlorotétracycline par un procédé d'oxydation photoélectrocatalytique a permis de mettre en évidence l'effet de chaque paramètre et de mieux comprendre les mécanismes de dégradation mis en jeu. Des taux de dégradation de la chlorotétracycline de 99.6% et des taux d'élimination de 92.5%±0.26% et de 90.3%±1.1% de carbone organique total et d'azote totale ont respectivement été enregistrés, après 180 min du temps de traitement, sous radiation visible, en imposant une intensité de 0.6 A et en utilisant le TiO_2 dopé à 3.4 at.% d'azote et en présence d'une cathode de carbone vitreux. L'analyse des sous-produits de dégradation de la chlorotétracycline a permis de proposer un mécanisme réactionnel de dégradation. Une fois les conditions optimales de dégradation du chlorotétracycline déterminées, celles-ci ont été appliquées pour le traitement d'effluents réels issus de station d'épuration et artificiellement contaminés par ce polluant. Un rendement de degradation totale de la chlorotétracycline (99.1%±0.1%) a été enregistré après 180 min du traitement photoélectrocatalytique utilisant le TiO_2 dopé à l'azote et une intensité de courant de 0.6 A. Des taux d'élimination de 85.4% ±3.6%, 87.4%±3.1% ainsi que de 55.7% ± 2.9% ont respectivement été enregistrés pour le carbone organique total, pour l'azote total et pour l'azote ammoniacal. Une meilleure efficacité de désinfection (94.8%; abatement >1.2-log units) a été également obtenue dans les

conditions optimales du traitement d'oxydation photoélectrocatalytique. Le coût de traitement photoélectrocatalytique a été estimé à $\$4.17 \pm 0.01$ m^{-3}.

TABLE DES MATIÈRES

CHAPITRE 1 ..... **1**

1. SYNTHÈSE **3**

1.1 Introduction *3*

1.2 Synthèse bibliographique *4*

1.2.1 Propriétés physico-chimiques et impacts environnementaux des eaux usées résiduaires 4

1.2.2 Polluants organiques d'intérêt émergent retrouvés dans les eaux usées résiduaires 7

1.2.3 Stratégies de traitement des eaux résiduaires contaminées par les résidus médicamenteux de type antibiotique 17

1.2.4 Procédé d'oxydation PEC 35

1.3 Hypothèses de travail et objectifs de recherche *53*

1.3.1 Hypothèses 53

1.4 Objectifs de recherche *56*

1.4.1 Objectif Globale 56

1.4.2 Objectifs spécifiques 56

1.5 Originalité de l'étude *57*

1.6 Démarche méthodologique *58*

1.6.1 Polluants étudiés 60

1.6.2 Préparation de solutions synthétiques 62

1.6.3 Échantillonnage et caractérisation des eaux réelles 62

1.6.4 Préparation de la photoanode Ti/TiO_2 65

1.6.5 Préparation de la photoanode Ti/TiO_2 dopé à l'azote 66

1.6.6 Préparation des électrodes de carbone amorphe 67

1.6.7 Montage et caractéristiques des cellules d'oxydation PEC 68

1.6.8 Fonctionnement de l'unité expérimentale 70

1.6.9 Méthodologie de plan d'expérience 73

1.6.10 Méthodes analytiques 74

1.7 Principaux résultats et discussion générale 81

1.7.1 Production in-situ des EORs: Application de la méthode de blanchissement du RNO (Chapitre 5) 81

1.7.2 Oxydation PEC du CTC utilisant une électrode nanostructuée de Ti/TiO_2 comme photo-anode préparée par la méthode de déposition par ablation laser: Application de la méthodologie de plan d'expériences (Chapitre 6) 82

1.7.3 Oxydation PEC du CTC utilisant une électrode nanostructurée de Ti/TiO2 comme photo-anode avec une production simultanée du H2O2 (Chapitre 7) 84

1.7.4 Dégradation PEC du CTC utilisant une photoanode nanostructurée de Ti/TiO_2 dopé à l'azote (Chapitre 8) 88

1.7.5 Traitement des eaux usées municipales contaminées par la CTC en utilisant un procédé PEC sous irradiation solaire (Chapitre 9). 90

1.7.6 Méthodologie de plans d'expériences appliquée à l'oxydation PEC du CBZ utilisant une électrode nano-structurée de Ti/TiO_2 comme photo-anode (Chapitre 10) 92

1.8 Conclusions Générales 95

1.9 Recommandation 99

1.10 Références 101

CHAPITRE 2 129

2. TETRACYCLINE ANTIBIOTICS IN THE ENVIRONMENT. A REVIEW 131

2.1 Abstract 131

2.2 Keywords 132

2.3 Introduction 133

2.4 Worldwide usage of tetracycline antibiotics 138

2.5 Occurrence of tetracycline antibiotics in the environment 140

2.6 Toxicity 145

2.6.1 Effects of tetracycline antibiotics on aquatic species 146

2.6.2 Effects of tetracycline antibiotics on terrestrial organisms 147

2.6.3 Estrogenic effects of tetracycline antibiotics 148

2.7 Treatment of tetracycline antibiotics in waters 149

2.7.1 Membrane processes 150

2.7.2 Adsorption processes 150

2.7.3 Photochemical processes 151

2.7.4 Electrochemical process 154

2.7.5 Photocatalytic and photoelectrocatalytic processes 155

2.8 Area for future research 164

2.9 Conclusions 168

2.10 Acknowledgments 168

2.11 References 169

CHAPITRE 3 187

3. PHOTOELECTROCATALYTIC TECHNOLOGIES FOR ENVIRONMENTAL APPLICATIONS 189

3.1 Abstract 189

3.2 Key words 189

3.3 Introduction 190

3.4 Mechanism of the photoelectrocatalytic process 192

3.5 Parameters affecting the photoelectrocatalytic process 197

3.5.1 Effect of external potential applied on TiO_2 or effect of current intensity 197

3.5.2 Effect of light intensity 199

3.5.3 Effect of pH 200

3.5.4 Effect of dissolved oxygen 201

3.5.5 Effect of electrolytes 203

3.5.6 Effect of counter electrode (or cathode electrode) 204

3.5.7 Effect of temperature 204

3.5.8 Effect of mass transfer 205

3.6 TiO_2 electrodes: characteristics and specificities 206

3.6.1 Preparation of TiO_2 electrodes 206

3.6.2 Characteristics and specificities of TiO_2 electrodes 207

3.6.3 UV radiation of TiO_2 electrodes 212

3.7 Photoelectrocatalytic reactors 214

3.8 Application of photoelectrocatalytic processes (PECPs) 218

3.9 Current and future development of PECPs 224

3.10 Conclusion 224

3.11 Acknowledgments 225

3.12 References 226

CHAPITRE 4 241

4. MODIFIED TIO_2 FOR ENVIRONMENTAL PHOTOCATALYTIC APPLICATIONS: A REVIEW 243

4.1 Abstract 243

4.2 Key words 243

4.3 Introduction 244

4.4 Electronic and structural properties of TiO_2 249

4.5 Doping TiO_2 253

4.5.1 Cations doping of TiO_2 253

4.5.2 Drawbacks of cations doping of titanium dioxide 261

4.5.3 Anions doped TiO_2 262

4.6 Coupled semiconductor photocatalysts 270

4.6.1 Photosenitization of TiO_2 by M_xS_y nanoparticles 273

4.6.2 Coupling TiO_2 by M_xO_y nanoparticles 276

4.7 Others photosensitization of TiO_2 282

4.8 Future trends of TiO_2 for environmental applications 283

4.8.1 Preparation aspect of TiO_2 285

4.8.2 Application aspect of TiO_2 286

4.8.3 Toxicity aspect 289

4.9 Conclusion 290

4.10 Acknowledgments 291

4.11 References 292

CHAPITRE 5 321

5. PHOTOELECTROCATALYTIC BLEACHING OF P-NITROSODIMETHYLANILINE USING TI/TIO_2 NANOSTRUCTURED ELECTRODES DEPOSITED BY MEANS OF A PULSED LASER DEPOSITION PROCESS 323

5.1 Abstract 323

5.2 Keywords 323

5.3 Introduction 324

5.4 Materials and Methods 327

5.4.1 Ti/TiO_2 electrode preparation 327

5.4.2 Preparation of the synthetic solution 328

5.4.3 Experimental device 329

5.4.4 Analytical techniques 330

5.5 Results and discussions *332*

5.5.1 Characterisation of the Ti/TiO_2 electrode 332

5.5.2 Bleaching of RNO 336

5.5.3 Effect of the crystallographic structure 340

5.5.4 Effect of external potential 343

5.5.5 Effect of light intensity 344

5.5.6 Effect of pH 346

5.5.7 Effect of H_2O_2 produced at the cathode electrode 348

5.5.8 Effect of ozone production 352

5.6 Conclusion *353*

5.7 Acknowledgments *354*

5.8 References *355*

CHAPITRE 6 363

6. PHOTOELECTROCATALYTIC DEGRADATION OF CHLORTETRACYCLINE USING TI/TIO_2 NANOSTRUCTURED ELECTRODES DEPOSITED BY MEANS OF A PULSED LASER DEPOSITION PROCESS 365

6.1 Abstract *365*

6.2 Key words *365*

6.3 Introduction *366*

6.4 Materials and methods *368*

6.4.1 Ti/TiO_2 electrode preparation 368

6.4.2 Preparation of the synthetic solution 368

6.4.3 Experimental devices 371

6.4.4 Experimental design 372

6.4.5 Analytical details 373

6.4.6 Economic aspect 374

6.5 Results and discussion 374

6.5.1 Characterization of the Ti/TiO_2 electrode 374

6.5.2 Preliminary investigation of CTC degradation 376

6.5.3 Effect of the experiment parameters on the CTC degradation using the experimental factorial design methodology 380

6.5.4 Optimization conditions for CTC degradation using central composite design (CCD) methodology 386

6.6 Conclusion 395

6.7 Acknowledgements 396

6.8 References 397

CHAPITRE 7 403

7. PHOTOELECTROCATALYTIC OXIDATION OF CHLORTETRACYCLINE USING TI/TIO$_2$ PHOTO ANODE WITH SIMULTANEOUS H_2O_2 PRODUCTION 405

7.1 Abstarct 405

7.2 Key words 405

7.3 Introduction 406

7.4 Materials and methods 408

7.4.1 Preparation of the Ti/TiO_2 electrode 408

7.4.2 Preparation of the amorphous carbon electrode 409

7.4.3 Preparation of the synthetic solution 410

7.4.4 Experimental unit 412

7.4.5 Experimental procedure 413

7.4.6 Analytical techniques 414

7.4.7 Economic aspect 416

7.5 Results and discussion 417

7.5.1 Characterization of the Ti/TiO_2 electrode 417

7.5.2 Characterization of the carbon electrode 420

7.5.3 Effect of the Ti/TiO_2 crystallographic structure 422

7.5.4 Effect of the cathode material 424

7.5.5 Effect of the initial concentration of CTC 429

7.5.6 Effect of the initial pH on CTC degradation 431

7.5.7 Kinetic study of CTC degradation by PECO process 435

7.5.8 By-products identification and proposed mechanism of CTC degradation 440

7.5.9 Aquatic toxicity studies 443

7.6 Conclusion 445

7.7 Acknowledgments 445

7.8 References 446

CHAPITRE 8 453

8. ELECTROCHEMICAL DEGRADATION OF CHLORTETRACYCLINE USING N-DOPED TI/TIO_2 PHOTOANODE UNDER SUNLIGHT IRRADIATIONS 455

8.1 Abstract 455

8.2 Key words 455

8.3 Introduction 456

8.4 Material and methods 459

8.4.1 N-doped TiO_2 Photoanodes preparation 459

8.4.2 Synthetic solution preparation 459

8.4.3 Photoelectrocatalytic cell 461

8.4.4 Experimental setup 461

8.4.5 Experimental procedure 462

8.4.6 Analytical technique 463

8.4.7 Economic aspect 464

8.5 Results and Discussion 464

8.5.1 Photoanode characterization 464

8.5.2 Effect of nitrogen content on the photoelectrocatalytic properties of N-doped TiO2 photoanodes 468

8.5.3 Effect of current intensity 473

8.5.4 Effect of treatment time 474

8.5.5 By-products identification and proposed mechanism of CTC degradation 477

8.6 Conclusion 481

8.7 Acknowledgments 481

8.8 References 482

CHAPITRE 9 489

9. REMOVAL OF CHLORTETRACYCLINE FROM SPIKED MUNICIPAL WASTEWATER USING A PHOTOELECTROCATALYTIC PROCESS OPERATED UNDER SUNLIGHT IRRADIATIONS 491

9.1 Abstract 491

9.2 Key words 491

9.3 Introduction 492

9.4 Materials and methods 493

9.4.1 Preparation of the synthetic solution 493

9.4.2 Wastewater CTC-spiking 494

9.4.3 Photoelectrocatalytic cell 494

9.4.4 Experimental setup 495

9.4.5 Experimental procedure 496

9.4.6 Analytical technique 497

9.4.7 Economics 498

9.5 Results and discussions 498

9.5.1 Preliminary investigations of CTC degradation 498

9.5.2 Photoelectrocatalytic treatment of MWW contaminated by CTC 502

9.6 Conclusion 503

9.7 Acknowledgments 504

9.8 References 505

CHAPITRE 10 509

10. PHOTOELECTROCATALYTIC DEGRADATION OF CARBAMAZEPINE USING TI/TIO_2 NANOSTRUCTURED ELECTRODES DEPOSITED BY MEANS OF A PULSED LASER DEPOSITION PROCESS 511

10.1 Abstract 511

10.2 Keywords 512

10.3 Introduction 513

10.4 Materials and methods 515

10.4.1 Preparation of the Ti/TiO_2 electrode 515

10.4.2 Preparation of the amorphous carbon electrode 516

10.4.3 Preparation of the synthetic solutions 516

10.4.4 Experimental devices 517

10.4.5 Experimental design 518

10.4.6 Analytical details 519

10.4.7 Economic aspect 520

10.5 Results and discussions *520*

10.5.1 Characterization of the Ti/TiO_2 electrode 520

10.5.2 Characterization of the nanostructured carbon electrode 524

10.5.3 Efficacy of the PECO process in removing CBZ using different types of cathode electrodes 525

10.5.4 Effect of the experiment parameters on the CBZ degradation using the experimental factorial design methodology 528

10.5.5 Optimization conditions for CBZ degradation using central composite design (CCD) methodology 534

10.5.6 By-products formation and proposed mechanism of CBZ degradation 539

10.5.7 Kinetics study of CBZ degradation by PECO process 541

10.6 Conclusion *543*

10.7 Acknowledgments *544*

10.8 References *545*

LISTE DES TABLEAUX

Tableau 1-1 Composition typique des EUD (Bitton, 2005) 6

Tableau 1-2 Structure moléculaire et caractéristique de certains produits chimiques. 10

Tableau 1-3 Concentrations des antibiotiques détectés dans l'environnement 14

Tableau 1-4 Les constantes de biodégradation de cretains antibiotiques dans un systéme de traitement biologique 19

Tableau 1-5 Performances des POAs pour la dégradation des antibiotiques 32

Tableau 1-6 Performances des POAs pour la dégradation des antibiotiques (suite) 33

Tableau 1-7 Performances des POAs pour la dégradation des antibiotiques 34

Tableau 1-8 Les semi-conducteurs utilisés dans un procédé PEC 35

Tableau 1-9 Charactéristiques des deux formes cristallographiques de TiO_2 : Anatase et Rutile 48

Tableau 1-10 Propriétés physico-chimique des polluants étudiés 62

Tableau 2-1 Chemical properties of tetracycline antibiotics 137

Tableau 2-2 Variation of the residual concentration of tetracycline antibiotics with animal type. 144

Tableau 2-3 Removal of tetracycline antibiotics using different treatment processes 159

Tableau 2-4 Removal of tetracycline antibiotics using different treatment processes 160

Tableau 2-5 Removal of tetracycline antibiotics using different treatment processes 161

Tableau 2-6 Removal of tetracycline antibiotics using different treatment processes 162

Tableau 2-7 Removal of tetracycline antibiotics using different treatment processes 163

Tableau 3-1 The role and the effect of UV irradiation and current intensity in photoelectrocatalytic mechanism. 193

Tableau 3-2 Redox potential of oxidants used for water treatment 195

Tableau 3-3 Characteristics of the anatase and rutile forms of TiO_2 209

Tableau 3-4 Removal of different types of organic pollutants in aqueous solutions using PECPs 222

Tableau 3-5 Removal of dye and microbial pollutants using PECPs 223

Tableau 4-1 Common semiconductor used in photo-catalysis process 248

Tableau 4-2 Removal of organic pollutants in aqueous solution using different type of cations doped TiO_2. 268

Tableau 4-3 Removal of organic pollutants in aqueous solution using different type of anions doped TiO_2. 269

Tableau 4-4 Removal of organic pollutants in aqueous solution using photosensitization system (TiO_2/M_xO_y or TiO_2/M_xS_y) 281

Tableau 5-1 Effect of crystallographic structure on the rate of RNO removal. 342

Tableau 6-1 Chemical properties of Chlortetracycline hydrochloride. 370

Tableau 6-2 Different processes used for degradation of CTC. 377

Tableau 6-3 Chlortetracycline hydrochloride removal under various experimental conditions. 379

Tableau 6-4 Data for optimization operation: experimental range and levels of independent process variables. 380

Tableau 6-5 Experimental factorial matrix in the 2^4 design. 382

Tableau 6-6 ANOVA results for the response surface quadratic for CTC degradation. 391

Tableau 6-7 Determination of optimum operating conditions proposed by Design-Expert ® Program Software. 392

Tableau 7-1 Chemical properties of Chlortetracycline hydrochloride. 411

Tableau 7-2 Effect of TiO_2 phase structure on the removal rate of CTC. 424

Tableau 7-3 Effect of cathode materials on CTC degradation and mineralization. 428

Tableau 7-4 Influence of the initial concentrations of pollutant on the photoelectrocatalytic oxidation of CTC (Ti/TiO_2 (anatase): anode and VC: cathode) 430

Tableau 7-5 Kinetic parameters for CTC degradation 437

Tableau 7-6 Toxicity measurements before and after PECO treatment in optimal conditions. 444

Tableau 8-1 Physico-chemical properties of Chlortetracycline hydrochloride 460

Tableau 9-1 Different processes used for CTC degradation 501

Tableau 10-1 Effect of cathode materials on CBZ degradation. 527

Tableau 10-2 Experimental region and experimental results from Factorial Design matrix (2^4). 533

Tableau 10-3 Central composite matrix and experimental results 536

Tableau 10-4 ANOVA results for CBZ degradation. 537

LISTE DES FIGURES

Figure 1-1 Source et devenir des résidues d'antibiotiques dans l'environnement..... 21

Figure 1-2 Organigramme de différentes techniques pouvant être utilisées pour l'élimination des résidus d'antibiotiques présents dans les effluents médicamenteux. 22

Figure 1-3 Les réactions d'oxydoréduction qui se produisent à la surface d'un photocatalyseur. 31

Figure 1-4 Mécanisme du procédé d'oxydation PEC utilisant le TiO_2 comme photoanode..... 37

Figure 1-5 Région UV pour la photo-activitée de TiO_2 46

Figure 1-6 Représentation schématique de la maille cristalline a) Rutile et b) Anatase..... 47

Figure 1-7 Structure schématique du niveau d'énergie de TiO_2 dopé à l'azote. 50

Figure 1-8 Description schématique de la démarche méthodologique suivie. 59

Figure 1-9 Filière de traitement des eaux usées de la station d'épuration de la ville de Québec (Secteur Est), Canada..... 64

Figure 1-10 Description schématique de la déposition d'un revêtement de TiO2 par ablation laser. 66

Figure 1-11 Description schématique de la technique de pulvérisation magnetron à haute fréquence..... 67

Figure 1-12 Structure schématique de la cellule d'oxydation PEC C1..... 68

Figure 1-13 Structure schématique de la cellule d'oxydation PEC C2..... 69

Figure 1-14 Structure schématique de l'unité expérimentale U2. 72

Figure 1-15 Spectromètre UV/visible utilisé pour l'analyse de la CTC et la CBZ. 77

Figure 1-16 Chromatographie liquide couplée à deux spectrométries de masses utilisées pour l'analyse du CTC et du CBZ..... 78

Figure 2-1 Variation of the total amounts (tons) of tetracycline antibiotics used for veterinary purposes around the world. 140

Figure 2-2 Possible sources and pathways for the occurrence of TCAs in the environment. 145

Figure 3-1 Mechanism of photoelectrocatalytic process using TiO_2 photocatalyst and the reactions that occur at the surface. 197

Figure 3-2 Coupling of two different semiconductor configurations. 212

Figure 3-3 Photoreactor equipped with two electrodes: Ti/TiO_2 as anode and platinum electrode as cathode (adapted from Li et al., 2007). 214

Figure 3-4 Photoreactor equipped with three electrodes used for photoelectrocatalytic oxidation process (adapted from Xie and Li (2006)). 215

Figure 3-5 Rectangular quartz photoreacteur used for photoelectrocatalytic process (adapted from Quan et al., 2007). 216

Figure 4-1 Band gap and redox potential for different semiconductors using the normal hydrogen electrode (NHE). 250

Figure 4-2 UV region for photoactivity of TiO_2 252

Figure 4-3 Schematic energy level of iron doping TiO_2. 259

Figure 4-4 Schematic energy level of nitrogen doping TiO_2. 265

Figure 4-5 Vectorial transfer of electrons-holes (e^-/h^+) in coupled semiconductor system. 272

Figure 4-6 TiO_2/SnO_2 photocatalyst configuration. 279

Figure 4-7 Future trends of modified TiO_2 for environmental applications. 284

Figure 5-1 Schematic diagram of the photoelectrocatalytic reactor: (1) DC power supply (2) quartz window (3) UV lamp (4) photometer (5) photoanode (6) cathode (7) stirring bar (8) magnetic stirrer. 330

Figure 5-2 SEM views of PLD TiO_2 films deposited on Si at different deposition temperatures. 332

Figure 5-3 SEM views of PLD TiO_2 films deposited on silicon. 333

Figure 5-4 X-ray diffraction patterns of TiO_2 film coated at (a) 600°C and 400°C; (b) on Si substrates and; (c) Ti grids. 335

Figure 5-5 Bleaching of RNO using different processes. 337

Figure 5-6 Kinetic studies of bleaching of RNO using (a) DP (b) PC (c) EO and (d) PECO processes. 340

Figure 5-7 Bleaching of RNO using the PECO process under different current intensities (Effect of external potential) (at 254 nm and using Ti/TiO_2 anatase). 344

Figure 5-8 Bleaching of RNO using the PECO process (at 0.1 A and using Ti/TiO_2 anatase) under different light intensities. 346

Figure 5-9 Bleaching of RNO using the PECO process (at 0.1 A under 254 nm using Ti/TiO_2 anatase) at different pH. 348

Figure 5-10 H_2O_2 production during electrolysis at 0.1 A and under 254 nm. 352

Figure 6-1 Schematic diagram of the photoelectrocatalytic reactor: (1) DC power supply (2) quartz window (3) UV lamp (4) photometer (5) photoanode (6) cathode (7) stirring bar (8) magnetic stirrer. 372

Figure 6-2 SEM images of the surface morphology of the TiO_2 film deposited at 600°C. 375

Figure 6-3 X-ray diffraction patterns of TiO_2 film coated on Ti grids and on Si substrates at 600°C. 376

Figure 6-4 Graphical Pareto analysis of the effect of current intensity, treatment time, Pollutant concentration and UV lamp position on CTC degradation 383

Figure 6-5 Interaction X_{13} between current intensity and pollutant concentration. 386

Figure 6-6 The effect of current intensity (A) and pollutant concentration (mg L^{-1}) on CTC removal (application time: 90 min) three-dimensional plot; results obtained from central composite matrix; Internal UV lamp position. 389

Figure 6-7 Comparison between actual and predicted values for CTC degradation. 390

Figure 7-1 Schematic diagram of the photoelectrocatalytic reactor: (1) DC power supply (2) quartz window (3) UV lamp (4) photometer (5) photoanode (6) cathode (7) stirring bar (8) magnetic stirrer. 413

Figure 7-2 SEM views of PLD TiO_2 films deposited on Si at different deposition temperatures. 417

Figure 7-3 SEM views of PLD TiO_2 films deposited. 418

Figure 7-4 X-ray diffraction patterns of TiO_2 film coated on titanium grids and on silicon substrates at 600°C and 400°C..... 420

Figure 7-5 SEM views of PLD amorphous carbon deposited on titanium at 20°C..... 421

Figure 7-6 Hydrogen peroxide production using different cathode materials (at 0.39 A of current intensity and under 254 nm of UV irradiation)..... 426

Figure 7-7 Effect of the initial pH value on the oxidation and the mineralization of CTC (Ti/TiO_2; VC; 0.39 A of current intensity; 254 nm; $[CTC]^0 = 32\ \mu g\ L^{-1}$)..... 433

Figure 7-8 Chemical structure of CTC and the three distinct moieties (I) tricarbonylamide, (II) phenolic diketone and (III) dimethylamine..... 435

Figure 7-9 (a) Variation of the initial rate of CTC degradation versus different initial concentration and (b) the linear variation of the plot $1/r_0$ versus $1/C_0$ in the Langmuir-Hinshelwood kinetic model (Ti/TiO_2; VC; 0.39 A of current intensity; 254 nm of UV light)..... 439

Figure 7-10 (a) LC/MS/MS chromatogram presented with (b) individual MS spectra of possible by-products of CTC by PECO process..... 442

Figure 7-11 The chemical structure and the proposed photoelectrocatalytic degradation pathways of CTC..... 443

Figure 8-1 Schematic diagram of the experimental setup: (1) PVC tank, (2) peristaltic recycling pump, (3) photoelectrocatalytic reactor, (4) N-doped TiO_2 photocatalyst, (5) and (6) vitreous carbon, (7) in let, (8) out let, (9) Solar simulator..... 462

Figure 8-2 X-ray diffraction patterns of pure TiO_2 and N-doped TiO_2 coatings prepared at 650°C, by means of a magnetron sputtering process..... 465

Figure 8-3 Typical SEM micrograph of the sputter-deposited N-doped TiO_2 films..... 466

Figure 8-4 UV-Vis absorbance spectra of the N-doped TiO_2 films with various nitrogen contents (indicated by the arrows). The inset shows the variation of the optical bandgap of the N-doped TiO_2 films as a function of their N content... 468

Figure 8-5 Effect of nitrogen content doped TiO_2 photoanode on the oxidation and the mineralization of CTC (VC as cathode; 0.39 A of current intensity; visible irradiation; $[CTC]^\circ = 100\ \mu g\ L^{-1}$)..... 472

Figure 8-6 Effect of current intensity on CTC degradation and mineralization using PECO process (3.4 at.% N-doped TiO_2 photoanode; treatment time =120 min; $[CTC]^\circ = 100\ \mu g\ L^{-1}$). 474

Figure 8-7 Effect of treatment time on CTC degradation and mineralization using PECO process (N-doped TiO_2 photoanode with a N content of 3.4 at.%; Current intensity = 0.6 A; $[CTC]^\circ = 100\ \mu g\ L^{-1}$). 477

Figure 8-8 Proposed photoelectrocatalytic degradation pathways of CTC under visible irradiation using 3.4 at.% N-doped TiO_2 photoanode. 480

Figure 9-1 Schematic diagram of the experimental setup: (1) PVC tank, (2) peristaltic recycling pump, (3) photoelectrocatalytic reactor, (4) N-doped TiO_2 photocatalyst, (5) and (6) vitreous carbon, (7) in let, (8) out let, (9) Solar simulator. 496

Figure 9-2 Photoelectrocatalytic treatment of municipal wastewater contaminated by CTC under visible irradiation ($[CTC]^\circ = 100\ \mu g\ L^{-1}$; $[TOC]^\circ = 18.7 \pm 1.2$ mg L^{-1}; $[TN]^\circ = 19.8 \pm 2.1$ mg L^{-1}; $[NH_4^+]^\circ = 12.7 \pm 0.5$ mg L^{-1}; $[NO_2^- + NO_3^-]^\circ = 1.68 \pm 0.05$ mg L^{-1})..... 503

Figure 10-1 Schematic diagram of the photoelectrocatalytic reactor: (1) DC power supply (2) quartz window (3) UV lamp (4) photometer (5) photoanode (6) cathode (7) stirring bar (8) magnetic stirrer..... 518

Figure 10-2 SEM image of the surface morphology of the TiO_2 film deposited at 400°C.. 521

Figure 10-3 SEM views of PLD TiO_2 films deposited on silicon. 521

Figure 10-4 X-ray diffraction patterns of TiO_2 film coated on silicon substrates and on titanium grids at 400°C..... 524

Figure 10-5 SEM views of PLD amorphous carbon deposited on Ti at 20 °C. 525

Figure 10-6 Graphical Pareto analysis of the effect of current intensity, treatment time, pollutant concentration and cathode material. 529

Figure 10-7 Interaction X_{14} between current intensity and cathode material. 532

Figure 10-8 Interaction X_{34} between pollutant concentration and cathode material 532

Figure 10-9 The effect of current intensity (A) and pollutant concentration (mg L^{-1}) on CBZ removal (application time: 90 min); VC as cathode. 535

Figure 10-10 Comparison between actual and predicted values for CBZ degradation 539

Figure 10-11 Reaction mechanism proposed for the photoelectrocatalytic degradation of CBZ. 541

LISTES DES ÉQUATIONS

Équation 1-1 $H_2O + M \rightarrow M\,[OH°] + H^+ + e^-$ 26

Équation 1-2 $R + M\,[OH°] \rightarrow M + RO + H^+ + e^-$ 26

Équation 1-3 $2SO_4^{2-} + 2H^+ \rightarrow H_2S_2O_8 + 2e^-$ 26

Équation 1-4 $Cl^- + 2H_2O \rightarrow HClO + H_3O^+ + 2e^-$ 26

Équation 1-5 $O_{2(dissous)} + 2H^+ + 2e^- \rightarrow H_2O_2$ 26

Équation 1-6 $H_2O_2 + h\nu \rightarrow 2OH°$ 28

Équation 1-7 $O_3 + H_2O + h\nu \rightarrow 2OH° + O_2$ 29

Équation 1-8 $Fe^{2+} + H_2O_2 \rightarrow Fe^{3+} + OH^- + OH°$ 30

Équation 1-9 $Fe^{3+} + H_2O + h\nu \rightarrow Fe^{2+} + H^+ + OH°$ 30

Équation 1-10 Formation des pairs électrons-trous $TiO_2 + h\nu \rightarrow e^-_{BC} + h^+_{BV}$ 36

Équation 1-11 Oxydation de polluant adsorbé R par les phototrous $h^+_{BV} + R_{ads} \rightarrow R^+$ 36

Équation 1-12 Formation de radicaux hydroxyles $h^+_{BV} + H_2O \rightarrow OH° + H^+$ 36

Équation 1-13 Formation de radicaux superoxyde $e^-_{BC} + O_2 \rightarrow O_2^{\circ -}$ 37

Équation 1-14 Formation du peroxyde d'hydrogéne $O_2 + 2H^+ + 2e^-_{BC} \rightarrow H_2O_2$ 37

Équation 1-15 $[HO°]_S = \sqrt{\frac{(1-\alpha) I_a \Phi}{k_D}}$ 40

Équation 1-16 $O_2 + 2H^+ + 2e^- \rightarrow H_2O_2$ 42

Équation 1-17 $H_2O_2 + h\nu \rightarrow 2OH°$ 42

Équation 1-18 $2H_2O \rightarrow O_2 + 4H^+ + 4e^-$ 42

Équation 1-19 $e^- + O_{2\,(ads)} \rightarrow O_2^{\circ -}$ 42

Équation 1-20 $O_2^{\circ -} + H^+ \rightarrow HO_2°$ 42

Équation 1-21 $2HO_2° \rightarrow H_2O_2 + O_2$ 42

Équation 1-22 $O_2^{\circ -} + HO_2° \rightarrow O_2 + HO_2^-$ 42

Équation 1-23 $HO_2^- + H^+ \rightarrow H_2O_2$ 43

Équation 1-24 $O_2 + 2é_{CB} + 2H^+ \rightarrow H_2O_2$ 43

Équation 1-25 $2H_2O + 2h^+_{VB} \rightarrow H_2O_2 + 2H^+_{aq}$ 43

Équation 1-26 $Ln\left(\frac{k_1}{k_2}\right) = -\frac{E_a}{R}\left(\frac{1}{T_2} - \frac{1}{T_1}\right)$ 45

Équation 1-27 $Ce^{4+} + H_2O_2 \rightarrow Ce^{3+} + HO_2 + H^+$ 79

Équation 1-28 $Ce^{4+} + HO_2 \rightarrow Ce^{3+} + O_2 + H^+$ 79

Équation 1-29 $[Fe(O\text{-}Phen)_3]^{2+} + Ce^{4+} \rightarrow [Fe(O\text{-}Phen)_3]^{3+} + Ce^{4+}$ 79

Équation 1-30 $\mathbf{r = d[RNO]dt = -k[RNO]}$ 82

Équation 3-1 $TiO_2 + hv \rightarrow e^-_{CB} + h^+_{VB}$ 194

Équation 3-2 $h^+_{vb} + H_2O \rightarrow HO^\circ + H^+$ 194

Équation 3-3 $h^+_{vb} + OH^- \rightarrow HO^\circ_{ads}$ 194

Équation 3-4 $h^+_{vb} + R_{ads} \rightarrow R^+$ 194

Équation 3-5 $e^-_{CB} + O_2 \rightarrow O_2^{\circ-}$ 195

Équation 3-6 $e^-_{CB} + h^+_{VB} \rightarrow$ heat 195

Équation 3-7 $[HO^\circ]_S = \sqrt{\frac{(1-\alpha) I_a \Phi}{k_D}}$ 199

Équation 3-8 $2H_2O \rightarrow O_2 + 4H^+ + 4e^-$ 202

Équation 3-9 $e^- + O_{2\,(ads)} \rightarrow O_2^{\circ-}$ 202

Équation 3-10 $O_2^{\circ-} + H^+ \rightarrow HO_2^\circ$ 202

Équation 3-11 $2HO_2^\circ \rightarrow H_2O_2 + O_2$ 202

Équation 3-12 $O_2^{\circ-} + HO_2^\circ \rightarrow O_2 + HO_2^-$ 202

Équation 3-13 $HO_2^- + H^+ \rightarrow H_2O_2$ 202

Équation 3-14 $O_2 + 2\acute{e}_{CB} + 2H^+ \rightarrow H_2O_2$ 202

Équation 3-15 $2H_2O + 2h^+_{VB} \rightarrow H_2O_2 + 2H^+_{aq}$ 202

Équation 3-16 $\mathbf{f = -dCdt \times V \times Fi}$ 202

Équation 3-17 $Ln\left(\frac{k_1}{k_2}\right) = -\frac{E_a}{R}\left(\frac{1}{T_2} - \frac{1}{T_1}\right)$ 205

Équation 3-18 **IPCE = iF × P** 211

Équation 3-19 $\Phi = \frac{\frac{dn}{dt}}{I_{abs}}$ 213

Équation 4-1 $CdS\ (e^- + h^+) + TiO_2 \rightarrow CdS\ (h^+) + TiO_2$ 273

Équation 4-2 $CdS + 2H_2O \rightarrow H_2 + Cd^{2+} + S + 2OH^-$ 274

Équation 4-3 $W^{6+} + e_{(TiO2)\ CB}^- \rightarrow W^{5+}$ 277

Équation 4-4 $W^{5+} + h_{(TiO2)VB}^+ \rightarrow W^{6+}$ 277

Équation 5-1 $TiO_2 + h\nu \rightarrow e^-_{CB} + h^+_{VB}$ 324

Équation 5-2 $h_{vb}^+ + OH^- \rightarrow HO^\circ_{ads}$ 326

Équation 5-3 $e^-_{CB} + O_2 \rightarrow O_2^{\circ-}$ 326

Équation 5-4 $\boldsymbol{D = 0.9\lambda\Delta 2\theta\cos\theta}$ 334

Équation 5-5 $r = \frac{d[RNO]}{dt} = -k.[RNO]$ 337

Équation 5-6 $Ln\left(\frac{C_0}{C}\right) = k.t$ 338

Équation 5-7 $RNO_{(aq)} + H^+ \leftrightarrow RNOH^+_{(aq)}$ 347

Équation 5-8 $e^- + O_{2\ (ads)} \rightarrow O_2^{\circ-}$ 350

Équation 5-9 $O_2^{\circ-} + H^+ \rightarrow HO_2^\circ$ 350

Équation 5-10 $2HO_2^\circ \rightarrow H_2O_2 + O_2$ 350

Équation 5-11 $O_2^{\circ-} + HO_2^\circ \rightarrow O_2 + HO_2^-$ 350

Équation 5-12 $HO_2^- + H^+ \rightarrow H_2O_2$ 350

Équation 5-13 $O_2 + 2\acute{e}_{CB} + 2H^+ \rightarrow H_2O_2$ 350

Équation 5-14 $2H_2O + 2h^+_{VB} \rightarrow H_2O_2 + 2H^+_{aq}$ 350

Équation 5-15 $H_2O_2 + h\nu \rightarrow 2OH^\circ$ 350

Équation 5-16 $3\ H_2O \rightarrow O_3 + 6\ H^+ + 6e^-$ 353

Équation 5-17 $O_3 + h\nu \rightarrow O_2 + O^\circ$ 353

Équation 5-18 $O^\circ + H_2O \rightarrow 2OH^\circ$ 353

Équation 5-19 $O_3 + OH^\circ \rightarrow HO_2^\circ + O_2$ 353

Équation 6-1 $Y = b_0 + b_1X_1 + b_2X_2 + b_3X_3 + b_4X_4 + b_{12}X_1X_2 + b_{13}X_1X_3 + b_{14}X_1X_4 + b_{23}X_2X_3 + b_{24}X_2X_4 + b_{34}X_3X_4$ 380

Équation 6-2 $Y = 50.85 + 12.06X_1 + 5.65X_2 - 2.73X_3 - 2.18X_4 - 0.36X_1X_2 + 1.11X_1X_3 + 0.81X_1X_4 + 0.35X_2X_3 - 0.55X_2X_4 + 0.60X_3X_4$ 381

Équation 6-3 $P_i = \left(\frac{b_i^2}{\sum b_i^2}\right) * 100 \ (i \neq 0)$ 383

Équation 6-4 $Y = b_0 + \sum_{i=1}^{k} b_i.X_i + \sum_{i=1}^{*} b_{ii}.X^2{}_i + \sum_{j} \sum_{i=2}^{*} b_{ij}.X_iX_j + e_i$ 386

Équation 6-5 $B = (X^T X)^{-1} X^T Y$ 387

Équation 6-6 **Ui – Ui0ΔUi** 387

Équation 6-7 $Y_1 = -23.0807 + 193.235X_1 + 0{,}7462X_2 - 0.3788X_3 - 0.0966X_1X_2 - 0.712X_1X_3 + 0.000933X_2X_3 - 174.967X_1^2 - 0.003095X_2^2 - 0.00216X_3^2$ 387

Équation 6-8 $Y_1 = -34.93077 + 204.20030X_1 + 0.76658X_2 - 0.34325X_3 - 0.0966X_1X_2 - 0.712X_1X_3 + 0.000933X_2X_3 - 174.967X_1^2 - 0.003095X_2^2 - 0.00216X_3^2$ 388

Équation 7-1 $D = \frac{0.9\ \lambda}{\Delta(2\theta)\cos\theta}$ 419

Équation 7-2 $H_2O_2 + e_{CB}^- \rightarrow OH^- + OH^\circ$ 427

Équation 7-3 $OH^- + h^+ \rightarrow OH^{\circ -}$ 434

Équation 7-4 $r = -\frac{dC}{dt} = k_r\theta = \frac{k_rKC}{1+KC}$ 436

Équation 7-5 $r = -\frac{d[C]}{dt} = k_rKC = k_{app}C$ 436

Équation 7-6 $\ln\frac{C_0}{C} = k_{app}t$ 436

Équation 7-7 $r_0 = \frac{k_rKC_0}{1+KC_0}$ 438

Équation 7-8 $\frac{1}{r_0} = \frac{1}{k_r} + \frac{1}{Kk_r}\frac{1}{C_0}$ 438

Équation 8-1 $-\frac{d[C]}{dt} = k_{PECO}\,C$ 475

Équation 8-2 $\ln\frac{C_0}{C} = k_{PECO}\,t$ 475

Équation 10-1 $D = \frac{0.9\ \lambda}{\Delta(2\theta)\cos\theta}$ 522

Équation 10-2 $Y = b_0 + b_1X_1 + b_2X_2 + b_3X_3 + b_4X_4 + b_{12}X_1X_2 + b_{13}X_1X_3 + b_{14}X_1X_4 + b_{23}X_2X_3 + b_{24}X_2X_4 + b_{34}X_3X_4$ 528

Équation 10-3 $Y = 36.15 + 0.79\,X_1 + 7.65\,X_2 - 4.40\,X_3 - 1.41\,X_4 - 0.088\,X_1X_2 + 0.037\,X_1X_3 - 1.53\,X_1X_4 - 0.80\,X_2X_3 - 0.54\,X_2X_4 + 1.29\,X_3X_4$ 528

Équation 10-4 $P_i = \left(\frac{b_i^2}{\sum b_i^2}\right)*100\ (i \neq 0)$ 529

Équation 10-5 $Y = b_0 + \sum_{i=1}^{k} b_iX_i + \sum_{i=1}^{k} b_{ii}X_i^{\,2} + \sum_{j}\sum_{i=2}^{k} b_{ij}X_iX_j + e_i$ 534

Équation 10-6 $Y_1 = 2.28525 - 54.02954\,X_1 + 0.57154X_2 + 1.01299\,X_3 - 0.08125\,X_1X_2 + 0.38750X_1X_3 - 6.37510^{-3}\,X_2X_3 + 121.86609X_1^2 - 1.1208110^{-3}\,X_2^2 - 0.039642\,X_3^2$ 534

Équation 10-7 $Y_2 = 5.26173 - 32.59849X_1 + 0.58311X_2 + 0.70871\,X_3 - 0.08125\,X_1X_2 + 0.38750X_1X_3 - 6.37510^{-3}\,X_2X_3 + 121.86609X_1^2 - 1.1208110^{-3}\,X_2^2 - 0.039642\,X_3^2$ 534

Équation 10-8 $Ln\frac{C_0}{C} = k_1t$ 542

Équation 10-9 $\frac{1}{C} - \frac{1}{C_0} = k_2t$ 542

LISTE DES ABRÉVIATIONS

a-C	Carbone amorphe
AL	Ablation laser
BV	Bande de valence
BC	Bande de conduction
CBZ	Carbamazépine
CEAEQ	Centre d'expertise en analyse environnementale du Québec
CF	Coliformes fécaux
COT	Carbone organique totale
CTC	Chlortetracycline
CV	Carbone vitreux
DBO	Demande biologique en oxygène
DCO	Demande chimique en oxygène
DRX	Diffraction des rayons X
EO	Electro-oxydation
EORs	Espèces oxydantes réactives
ERU	Effluents résiduaires urbains
EUD	Eaux usées domestiques
EUI	Eaux usées industrielles
Gr	Graphite
LC-MS-MS	Liquid chromatography-Mass spectroscopy-Mass spectroscopy
MEB	Microscopie électronique à balayage
NT	Azote totale
OTC	Oxytetracycline
PC	Photocatalytique
PCC	Plan central composite
PD	Photolyse directe
PE	Perturbateur endocrinien
PEC	Photoélectrocatalytique
PF	Plan factoriel
PM	Pulvérisation magnétron
POAs	Procédés d'oxydations avancées
PPs	Produits pharmaceutiques
PPC	Procédé de photocatalyse conventionnel

PPSPs	Produits pharmaceutiques et de soins personnels
PSR	Plan de surfce de réponse
RNO	p-nitrosodimethylaniline
TCs	Tetracyclines
TC	Tetracycline

CHAPITRE 1

SYNTHÈSE

1. SYNTHÈSE

1.1 Introduction

Dès le début du XX siècle, l'utilisation de l'eau par l'être humain dans plusieurs activités s'est intensifiée. Cependant, son usage varie selon les pays car elle dépend du climat, du mode d'agriculture, du niveau d'industrialisation du pays ainsi que du niveau d'accès à l'eau potable. D'une façon générale, le secteur agricole consomme à lui seule près de 70% de l'eau disponible, le secteur industriel consomme près de 20% alors que 10% de l'eau disponible est destiné pour des utilisations domestiques (Schwarzenbach et al., 2006). L'urbanisation croissante et l'industrialisation intensive entraine une hausse de la consommation en eau et une dégradation de la qualité des ressources naturelles (eaux de surfaces et eaux souterraines). De nombreux composés chimiques sont utilisés pour des applications industrielles, domestiques et agricoles. La pollution de l'environnement par des contaminants réfractaires et persistants est un défi majeur auquel doivent faire face les scientifiques et les gestionnaires. Ces eaux usées contiennent de nombreuses substances organiques et inorganiques susceptibles de nuire gravement à l'environnement (Schwarzenbach et al., 2006). En raison de leur toxicité et de leur persistance dans l'environnement, ces contaminants ne sont pas généralement éliminés dans les filières conventionnelles de traitement des eaux usées (Watkinson et al., 2007). Certains de ces composés réfractaires sont très stables et par conséquent difficile à dégrader. D'autres parviennent à se dégrader partiellement et des composés intermédiaires plus stables et plus toxiques que le polluant de départ peuvent se former (Watkinson et al., 2007; Heberer, 2002). Ainsi, le rejet de ces contaminants dits bio-récalcitrantes dans l'environnement peuvent engendrer des bouleversements significatifs, tels que l'eutrophisation, la sous-oxygénation des lacs et des rivières et par conséquent un impact direct sur la faune et la flore. Ces composés sont également reconnus par leurs effets

cancérigènes, mutagènes ou susceptibles d'interférer avec le système hormonal des êtres vivants (Pal et al., 2010 ; Lai et al., 2009 ; Kolok et al., 2007). Pour faire face à ce problème, un fort dynamisme des recherches actuelles s'orientent de plus en plus vers le développement des technologies simples, efficaces et plus adaptés pour le traitement de ces contaminants afin de préserver les ressources en eaux et répondre à une réglementation de plus en plus contraignante.

De ce point de vue, les procédés d'oxydation photoélectrocatalytique sont particulièrement intéressants. L'intérêt de ces techniques réside dans leur aspect non polluant, leur facilité de mise en œuvre, leur faible coût et surtout en raison de leur grande efficacité sur les polluants refractaires.

1.2 Synthèse bibliographique

1.2.1 Propriétés physico-chimiques et impacts environnementaux des eaux usées résiduaires

1.2.1.1 Généralités

Compte tenu de la préoccupation mondiale face au problème de plus en plus important de la pollution de l'environnement aquatique et terrestre, la question du traitement et du devenir des eaux usées a reçu une importance croissante au cours de ces dernières années. Les eaux usées résiduaires d'origine industrielle, domestique, agricole et même urbaine contiennent des quantités non négligeables et variées de polluants organiques, inorganiques et bactériens et ne peuvent ainsi être rejetées dans l'environnement aquatique sans traitement préalables. Le rejet de ces polluants dans l'environnement sont l'une des causes principales de l'apport des composés perturbateurs endocriniens dans l'environnement et perturbent le fragile équilibre des systèmes biologiques. Ainsi, il est nécessaire de connaître les constituants majeurs qui composent les eaux usées, leurs impacts quand ils sont dispersées dans l'environnement ainsi

que les techniques de traitement préalables qui peuvent être utilisées pour enlever ces polluants afin de protéger la santé publique et l'environnement.

1.2.1.2 Eaux résiduaires domestiques

D'une façon générale, les eaux usées domestiques (EUD) comprennent les eaux de ménage qui proviennent des salles de bains, des douches, des cuisines et des buanderies. Les EUD sont une combinaison de plusieurs polluants provenant de plusieurs sources d'activités humaines. La composition de ces eaux varie significativement selon l'endroit et la saison. Elle dépend principalement du nombre d'habitant installés dans la ville, de leur niveau de vie ainsi que de la nature d'alimentation consommée (Henze et al., 2002). Les principales constituantes des EUD sont les protéines (40-60%), les carbohydrates (25-50%), les détergents, les acides humiques et fluviques, les huiles et les graisses (10%), la lignine et les tannins, ainsi que d'autres polluants organiques et inorganiques (phosphore et azote) dissous (Rebhun et Manka, 1971; Manka et al., 1974). Par exemple, les eaux de cuisine sont très riches en matière en suspensions et des matières organiques provenant des déchets végétaux et animaux. Les eaux usées provenant de la salle de bain sont très particulières. Misé à part les matières en suspension, elles renferment des détergents ainsi que des concentrations résiduelles de produits pharmaceutiques et de soins personnels. En se basant sur les données présentées par Bitton (2005), le Tableau 1-1 illustre les caractéristiques typiques des EUD.

Tableau 1-1 Composition typique des EUD (Bitton, 2005)

Paramètres	Concentrations (mg L^{-1})		
	Fort	**Moyen**	**Faible**
DBO_5	400	220	110
DCO	1 000	500	250
Azote organique	35	15	8
Azote ammoniacal	50	25	12
Azote total (N_T)	85	40	20
Phosphore total (P_T)	15	8	4
MES	350	220	100

1.2.1.3 Eaux résiduaires urbaines

Les effluents résiduaires urbains (ERU) sont un mélange complexe de plusieurs types de polluants. La composition de cet effluent varie principalement selon la taille de la communauté urbaine ainsi que les habitudes alimentaires et d'hygiène des individus. En plus des effluents domestiques et des effluents industriels, les ERU comprennent également des effluents issus des institutions, des commerces, des hôpitaux, des casernes ainsi que les eaux pluviales. Vue leur grande diversité et complexité, ces ERU peuvent être à l'origine de l'apport des contaminants émergents réfractaires dans l'environnement.

1.2.1.4 Eaux résiduaires industrielles

Les eaux usées industrielles (EUI) sont différentes des EUD et ses caractéristiques varient d'une industrie à l'autre. En plus des matières organiques et des composés azotés et phosphorées, les EUI peuvent contenir également des produits toxiques, des métaux lourds, des hydrocarbures ainsi que des micropolluants organiques. Néanmoins, une classification des effluents industriels doit être établie selon qu'il renferme ou non des substances toxiques capables d'arrêter la prolifération des microorganismes ou l'activité biologique. Cette

classification permet de distinguer les polluants organiques non biodégradables ainsi que les polluants minéraux qui inhibent les processus de dégradation biologique (Matin, 1982). Certaines industries telles que les abattoirs, les fromageries, les cartonneries, les sucreries présentent souvent des eaux usées résiduaires pouvant être traitées par voie biologique. En revanche, certaines industries telles que les industries pharmaceutiques génèrent des composés toxiques (des antibiotiques, des solvants, des substances bactéricides, etc) susceptibles d'inhiber l'activité biologique de dégradation des polluants organiques dans les stations d'épuration des eaux usées résiduaires (Adams et al., 2002 ; Snyder et al., 2003). Pour minimiser l'impact de ces polluants sur les traitements subséquents (ex. traitement biologique), un prétraitement est généralement requis avant leur rejet dans les réseaux collectifs.

1.2.2 Polluants organiques d'intérêt émergent retrouvés dans les eaux usées résiduaires

1.2.2.1 Origines et propriétés physico-chimiques

Depuis le 20^{e} siècle, une industrialisation intense et incontrôlable se développe dans plusieurs pays du monde, et ce dans différents secteurs d'activités : industries pharmaceutiques, agroalimentaires, cosmétiques, pétrolières, chimiques, etc. Au nombre de ces polluants couramment décelés dans les rejets industriels et urbains, se trouvent les produits pharmaceutiques et de soins personnels (PPSPs), les pesticides, les produits chimiques industriels et domestiques, les surfactants, les métaux, etc (Tableau 1-2). Un grand nombre de ces substances rentrent dans la catégorie des polluants émergents appelés perturbateurs endocriniens (Chang et al., 2009). Un perturbateur endocrinien (PE) se définit comme étant une substance exogène qui altère ou inhibe le fonctionnement du système endocrinien et, par conséquent, cause des effets négatifs sur un organisme intact, ou sur sa progéniture ou sa population (Lister et Van Der Kraak, 2001 ; Esplugas et al., 2007). Ces substances s'accumulent ainsi dans l'environnement engendrant des bouleversements significatifs sur la

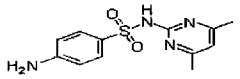
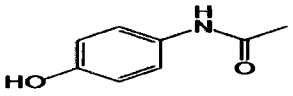
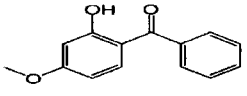
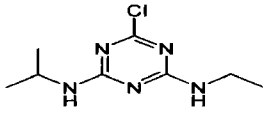
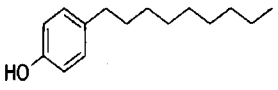
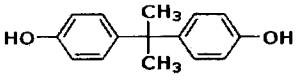
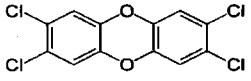
faune aquatique (féminisation et disparition de la faune aquatique) et sur la santé humaine (occurrence de certains cancers, malformation des organes génitaux, altération des thyroïdes, baisse du quotient intellectuel, etc.) (Kumar et al., 2011 ; Yoon et al., 2007). Quan et al. (2007) ont signalés que 38.000 substances chimiques ont une action sur le système endocrinien, alors que l'agence de la protection environnementale (USEPA) prévoit que 87.000 composés chimiques doivent être testés pour déterminer leurs effets sur le système endocrinien (Kumar et al., 2011).

Les rejets issus des stations d'épuration sont l'une des causes principales de l'apport de ces contaminants dans l'environnement aquatique et terrestre incluant les eaux de surface, les eaux souterraines, les sédiments et les boues (Kolpin et al., 2002). Des concentrations allant jusqu'à 100 ng L^{-1} peuvent être détecté dans les eaux usées résiduaires (Servos et al., 2005; Auriol et al., 2007), alors que des concentrations très faibles (0.1 ng L^{-1}) peuvent induire des effets oestrogéniques chez les organismes aquatiques (Auriol et al., 2007). Ces composés sont souvent présents à l'état de trace, c'est-à-dire à des concentrations allant du ng L^{-1} à quelques dizaines de µg L^{-1}, et ils ne participent globalement qu'à une très faible proportion de la matière organique dissoute (Huang et Sedlak, 2001). Cependant, leur présence dans les eaux est à prendre en considération en raison de la toxicité potentielle pour l'homme et les espèces aquatiques. Ces composés organiques réfractaires sont nombreux et échappent pour la plupart à l'épuration classique des eaux usées, comprenant un prétraitement physico-chimique suivi d'un traitement biologique par biomasse en suspension (boue activée) ou biomasse fixée (biofiltration, lit bactérien) (Auriol et al., 2006). La pollution de l'environnement par ces contaminants organiques persistants constitue aujourd'hui une des problématiques émergeantes associées au traitement des eaux usées.

Parmi tous les produits chimiques complexes, une variété de PPSPs administrés aux hommes et aux animaux ont été détectés dans les eaux usées ainsi que les eaux de surface (rivières,

lacs, etc). Même si leurs concentrations étaient dans certains cas détectables à l'état de trace (des concentrations allant du ng L^{-1} vers le µg L^{-1}), ces polluants organiques sont persistants dans l'environnement et sont par conséquent reconnus comme une menace potentielle pour la santé humaine et les écosystèmes. Les PPSPs sont des micropolluants d'intérêt émergents couramment décelés dans les effluents résiduaires de type industriel et urbain. Une description plus détaillée des produits pharmaceutiques (PPs) sera présentée dans les prochaines sections.

Tableau 1-2 Structure moléculaire et caractéristique de certains produits chimiques.

Classe	Produit chimique	Structure chimique
Pharmaceutique (antibiotique)	Sulfaméthazine (SMZ)	
Pharmaceutique (analgésique)	Acétaminophen	
Produit de soins de personnel (écran solaire)	Oxybenzone	
Pesticide	Atrazine	
Produits chimiques industriels (Surfactant)	Nonyl-phénol	
Produits chimique industriel (Plastique)	Bisphénol A	
Sous-produits de combustion	Dioxin	

1.2.2.2 Résidus médicamenteux de type antibiotique

Les composés pharmaceutiques appelés également les PPSPs sont des substances issues de la chimie fine de synthèse, regroupant une très grande variété de produits tels que les médicaments, les parfums, les produits cosmétiques, les savons, les déodorants, etc. Ces composés sont des polluants d'intérêt émergent. Plusieurs études rapportent que les PPSPs ne sont pas complètement éliminés dans les stations d'épurations des eaux usées conventionnelles (Clara *et al.*, 2005; Zuehlke *et al.*, 2006; Cirja *et al.*, 2008). Du fait de leur

caractère très persistant, ces composés pharmaceutiques ont été détectés dans les eaux de surface, les eaux souterraines, les eaux potables, et les eaux usées de plusieurs pays, notamment au Canada, aux Etats-Unis, au Brésil, en Allemagne et dans d'autres pays (Heberer, 2002; Kummerer, 2009). Dans les eaux de surface, des concentrations entre 10 et 500 ng L^{-1} ont été détectées (Ternes, 1998), alors que des concentrations résiduelles allant du ng L^{-1} au µg L^{-1} ont été mesurées dans les eaux usées municipales. Les PPSPs sont des substances très stables et très solubles dans l'eau comparés aux autres composés organiques. Etant donné la grande diversité de ce type de composés, il est difficile d'établir clairement et spécifiquement leur toxicité. Plusieurs recherches (Andreozzi et al. 2004; Fent et al. 2006) prévoient que l'exposition à long terme et à faible dose aux PPs dans l'environnement conduit à des effets néfastes sur la santé humaine et sur les espèces aquatiques.

Parmi ces produits, les médicaments constituent un groupe important et diversifié de composés organiques utilisés en grande quantité à travers le monde (Kummerer, 2001). Dans les pays développés, la consommation de médicaments progresse d'une année à une autre. Les médicaments les plus couramment détectés dans l'environnement sont les antibiotiques, les antidépresseurs, la caféine, les antalgiques, les médicaments contre le cholestérol, etc. Les antibiotiques sont souvent cités parmi les composés les plus problématiques (Homem and Santos, 2011; Gao et al., 2012; Onal, 2011; Pan et al., 2011). Les antibiotiques sont largement utilisés pour traiter et prévenir les maladies dans la médecine humaine et animale, ainsi que pour augmenter l'efficacité alimentaire et améliorer le taux de croissance chez les bétails et les volailles (Gao et al. 2012; Pan et al. 2011; Sarmah et al. 2006; Chen et al. 2011). Tel que mentionné par Martinez et al. (2011) et Halling-Sorensen et al. (1998), le volume de production annuelle de médicaments a été estimé à plusieurs centaines de tonnes, alors que son utilisation a été globalement estimée entre 100.000 et 200.000 tonnes (Kummerer, 2003). Par exemple, la capacité de production annuelle des antibiotiques en Chine est d'environ

210.000 tonnes (85% est utilisé pour l'élevage et la médecine), tandis que le rapport annuel de production d'antibiotiques au Japon est d'environ 2.200 tonnes (30% sont utilisés pour les humains et 60% sont utilisés pour le bétail) (Luo et al. 2011; Miyata et al. 2011). Aux Etats-Unis, environ 9200 tonnes d'antibiotiques ont été produites en 2003 pour des applications agricoles (AHI, 2005). Au cours de leur utilisation, les antibiotiques ne peuvent pas être absorbés ou métabolisés entièrement in vivo et une fraction importante (30 à 90%) est excrétée sous forme de métabolites dans l'environnement via l'urine (Zhou et al., 2012; Hu et al., 2010a, b; Bound and Voulvoulis, 2004). Après utilisation, ces substances chimiques persistent et peuvent contaminer les eaux de surface, les eaux souterraines et même les eaux potables (Lopez-Penalver et al. 2010; Kim and Tanaka 2009; Bautitz and Nogueira 2007). Le Tableau 1-3 présente les différentes concentrations des antibiotiques détectées dans l'environnement. Ces composés peuvent se trouver dans l'environnement aquatique à travers le rejet direct des eaux usées issues de fermes ou le rejet d'effluents des usines de traitement des eaux usées de type municipal ou industriel. L'application de fumier de ferme d'élevage sur les terres agricoles contribue également à introduire les antibiotiques dans l'environnement (Shelver et al. 2010; Chen et al. 2011). L'infiltration de ces substances dans l'environnement peut ainsi causer des problèmes environnementaux y compris les risques écologiques et des dommages de la santé humaine.

Le groupe de tétracycline (oxytétracycline (OTC), chlorotétracycline (CTC) et tétracycline (TC)) est l'un des premiers groupes d'antibiotiques utilisés en thérapie dans la médecine humaine et comme additif alimentaire dans le secteur agricole (Li et al., 2011; Ding et Mou, 2000). En raison de leur plus faible coût et de leur plus grande activité antimicrobienne, le groupe de tétracycline a été largement utilisé comme médicament dans la médecine vétérinaire pour la prévention et le traitement des animaux de ferme et pour guérir plusieurs maladies infectieuses (Onal, 2011 ; Chen et al., 2011). Ce groupe d'antibiotique a été

également utilisé comme additif alimentaire pour favoriser la croissance des animaux (Sczesny et al., 2003; Koesukwiwat et al., 2007). Du fait de leur utilisation excessive, les tétracyclines (TCs) sont souvent décelés dans l'environnement: eaux de surface (Li et al., 2011), eaux souterraines (Hernandez et al. 2007), eaux usées (Lopez Penalver et al., 2012 ; Jeong et al., 2010), les boues municipales (Liu et al., 2009), sol et sédiments (Liu et al., 2009; Andreu et al., 2009; Chen et al., 2011). D'après les études antérieures (Jjemba 2006), environ 25% à 75% et même 70% à 90% des TCs administrés aux animaux sont libérés dans l'environnement sous la forme active. Les procédés de traitement conventionnels utilisés dans les stations d'épurations des eaux usées semblent incapables d'assurer une élimination totale de ces micropolluants. Le taux d'élimination des TCs dans les stations de traitement des eaux usées varie de 12% (Spongberg et Witter, 2008) à 80% (Karthikeyan et Meyer 2006). La persistance de ces micropolluants organiques dans l'environnement peut causer une toxicité aiguë et même chronique chez les espèces aquatiques et terrestres, et entrainer des perturbations dans le système endocrinien. L'apparition de TCs dans l'environnement, leur devenir ainsi que leurs effets toxiques sur les espèces aquatiques et terrestres seront plus détaillés dans le chapitre 2.

Tableau 1-3 Concentrations des antibiotiques détectés dans l'environnement

Classe	Substance	Concentrations (ng L^{-1})	Source	Références
Sulphonamides	Sulphadiazine	4,130	Eaux de surface	Boxall et al. (2005)
	Sulphamethazine	240	Eaux souterraines	Hamscher et al. (2005)
	Sulphamethoxazole	52-1900	Eaux de surface	Christian et al. (2003)
				Kolpin et al. (2002)
		Jusqu'à 2000	Effluents des eaux usées	Hirsch et al. (1999)
		Jusqu'à 470	Eaux souterraines	Sacher et al. (2002)
		66	Eaux potables	Muckter, (2006)
Sulfamethazine	Sulfamethizol	Jusqu'à 220	Eaux de surface	Kolpin et al. (2002)
	Sulfadiazine	Jusqu'à 17	Eaux souterraines	Kolpin et al. (2002)
	Sulfadimidine	Jusqu'à 23	Eaux souterraines	Sacher et al. (2002)
Chinolones	Fluorchinolone	Jusqu'à 100	Effluents des eaux usées	Farber, (2002)
		Jusqu'à 5	Eaux de surface	Farber, (2002)
	Fluorchinolone	Jusqu'à 106	Effluent eaux usées	Giger et al. (2003)
	(ciprofloxacine,norfloxacine)	Jusqu'à 19	Eaux de surface	Giger et al. (2003)
	Ciprofloxacine	Jusqu'à 30	Eaux de surface	Kolpin et al. (2002)
		200-1400	Effluents des eaux usées	Batt et al. (2007)
Tetracyclines	Tetracycline	400	Eaux souterraines	Krapac et al. (2005)
		61-1100	Effluents des eaux usées	Batt et al. (2007)
	Chlortetracycline	Jusqu'à 690	Eaux de surface	Kolpin et al. (2002)
	Oxytetracycline	32.000	Eaux de surface	Kay et al. (2005)
Macrolides	Lincomycine	21.100	Eaux de surface	Boxall et al. (2005)
	Azithromycine	Jusqu'à 3	Eaux de surface	Christian et al. (2003)
	Erythromycine-H_2O	Jusqu'à 6000	Effluents des eaux usées	Hirsch et al. (1999)
Penicillines	Penicilline	Jusqu'à 200	Effluents des eaux usées	Farber, (2002)
	Flucloxacilline	7	Eaux de surface	Christian et al. (2003)
	Piperacilline	48	Eaux de surface	Christian et al. (2003)

1.2.2.3 Réglementation des micropolluants réfractaires dans les eaux usées résiduaires

Jusqu'à aujourd'hui, il n'existe pas de normes de rejets de micropolluants présents dans les eaux résiduaires à la sortie des stations d'épuration. Toutefois, ces rejets sont de plus en plus problématiques par leur apport de composés PEs dans l'environnement. Les PEs semblent devenir de plus en plus prioritaires pour les instances réglementaires des pays développés (Stuart et al., 2012 ; Gross et al., 2004). Certains pays, tels que ceux de l'union européennes, les Etats Unis, le Canada classent certains micropolluants organiques (hormones et ses dérivés, composés phénoliques, etc) comme des PEs prioritaires. Même si les réglementations relatives aux micropolluants organiques dans le traitement des eaux usées ne sont pas encore bien établies, les gestionnaires et les scientifiques s'orientent à imposer des réglementations de plus en plus contraignantes envers ces micropolluants réfractaires (EC, 1991; 1998; 2000; 2006; 2011).

Au cours de ces dix dernières années, des conférences et des colloques portant sur les analyses et la toxicité de certains polluants émergents tels que les PPSPs se sont multipliées à travers le monde. Par exemple, en 2002, un atelier multilatéral a été organisé par Environnement Canada et Santé Canada. Cet atelier a porté sur l'évaluation des risques et la gestion des PPs et des produits d'hygiène et de beauté dans l'environnement canadien. Un second atelier multilatéral organisé en 2004 par Environnement Canada, Santé Canada, le ministère de l'Environnement de l'Ontario, Agriculture et Agroalimentaire Canada et le Réseau canadien de l'eau, a permis d'examiner de manière approfondie trois domaines de recherche sur les PPSPs : les méthodes d'analyses, les échantillons et les effets (Ostapyk et al., 2007). Cet atelier a permis également de recommander des stratégies permettant de mettre en œuvre et de renforcer le programme de recherche. Un autre atelier a été récemment organisé en 2007 par différents organismes gouvernementaux : le ministère de l'Environnement de l'Ontario, Environnement Canada, Santé Canada, Agriculture et

Agroalimentaire Canada, le ministère de l'Agriculture, de l'Alimentation et des Affaires rurales de l'Ontario, le Réseau canadien de l'eau et le Centre de Walkerton pour l'assainissement de l'eau). A travers cet atelier, les conférenciers ont donné un aperçu de l'exposition et de la surveillance de l'environnement, des effets des PPSPs sur les écosystèmes aquatiques ainsi que des solutions alternatives pour réduire l'exposition humaine et environnementale. Ainsi, des actions sont donc entreprises par les gouvernements en appliquant le principe de précaution envers les PEs.

1.2.3 Stratégies de traitement des eaux résiduaires contaminées par les résidus médicamenteux de type antibiotique

Au Québec comme partout ailleurs dans le monde, la pollution de l'eau par des résidus pharmaceutiques de types antibiotiques demeure un problème qui peut entrainer des conséquences néfastes pour l'environnement et pour la santé publique. Les rejets de ces résidus pharmaceutiques ayant une origine industrielle et urbaine présentent des caractéristiques physico-chimiques, biologiques et écologiques très variables. L'assainissement de ces rejets, quel que soit leurs origines, devient une exigence de plus en plus stricte pour notre société. Vue la nécessité d'assurer une bonne gestion des eaux usées, les spécialistes s'orientent actuellement vers la recherche de technologies de traitement adaptés à chaque situation. Pour ce faire, des méthodes chimiques, physiques, physico-chimiques et biologiques pour le traitement des polluants de types pharmaceutiques sont étudiées et leur couplage est souvent envisagé.

1.2.3.1 Biodégradabilité des effluents médicamenteux de type antibiotique

Les effluents médicamenteux d'origines urbains et industriels sont une combinaison de plusieurs polluants provenant de plusieurs sources d'activités. La composition de ces effluents varie significativement selon l'endroit, l'activité et la saison. Les résidus d'antibiotiques sont l'un des principaux polluants présents dans ce type d'effluent. Généralement, les antibiotiques sont des substances organiques recalcitrantes (ou refractaires) qui inhibent l'activité des microorganismes dans une usine de traitement des eaux usées conventionnelles (Yahiaoui et al., 2013 ; Park and Choung, 2007). Ces composés recalcitrants non biodégradables restent sous forme inchangée vis-à vis des microorganismes. Les constantes de biodégradation de certains antibitiques dans un systéme de traitement biologique (boue activée ou bioréacteur à membrane) sont présentées dans le Tableau 1-4.

Les paramètres physico-chimiques tel que le pH, la température ainsi que la pression partielle sont des facteurs principaux qui influencent la biodégradation d'un composé. Dans le but de prévoir la biodégradabilité de ces composés organiques refractaires, de nombreux tests concernant l'étude de la biodégradabilité sont souvent réalisés. La mesure simultanée de la demande chimique en oxygène (DCO) et de la demande biologique en oxygène (DBO) est l'une des méthodes les plus simples qui a été utilisée pour vérifier la biodégradabilité des composés organiques de type antibiotique (Mansour et al., 2012; Belkheiri et al., 2011). Pour améliorer la biodégradabilité des résidues pharmaceutiques de type antibiotique, le couplage des procédés de traitement biologiques avec des méthodes de traitement physico-chimiques avancées est souvent envisagé (Basha et al., 2009 ; Yahiat et al., 2011 ; Yahiaoui et al., 2013). Une étude récente de Yahiaoui et al. (2013) utilisant un procédé d'oxydation électrochimique comme méthode de pré-traitement a montré une amélioration de la biodégradation d'une solution de tetracycline. Suite à un pré-traitement électrochimique de 5h, le rapport DBO/DCO de cette solution a été amélioré de 0.028 à 0.41. Le procédé d'ozonation-photocatalytique utilisé comme méthode de prétraitement pour les procédés biologiques a également prouvé son efficacité pour améliorer la biodégradablité d'une solution de CTC. Le rapport DBO/DCO de cette solution atteind 0.58 après un pré-traitement de 60 min et à un pH 7 (Hammad Khan et al. 2013).

Tableau 1-4 Les constantes de biodégradation de cretains antibiotiques dans un systéme de traitement biologique

Antibiotiques	Coefficient de sorption pour les boues activées K_d (L g^{-1}_{SS})	Constante de dégradation dans un systéme de traitement biologique k_{biol} (L $g^{-1}_{SS}d^{-1}$)		Références
		k_{biol} pour les boues activées	k_{biol} pour les bio-réacteurs à membrane	
Azithromycine	0.38±0,09	≤0,13	≤1,5	Gobel et al. (2005); Joss et al. (2006)
Clarithromycine	0.26±0,095	≤0,5	≤2,0	Gobel et al. (2005); Joss et al. (2006)
(Anhydro) erythromycine	0,165	≤0,12	≤1,1	Jones et al. (2002)
N^4-acetyl-sulfamethoxazole	-	5,9-7,6	3,2-5,0	Joss et al. (2006)
Roxithromycine	-	≤0,12	≤0,3	Joss et al. (2006)

1.2.3.2 Techniques de traitement des effluents médicamenteux de type antibiotique

Les résidus d'antibiotiques présents dans les effluents médicamenteux sont détéctés dans l'environnement par l'intermediaire de source diverses. Les quatres sources de ces effluents médicamenteux dans l'environnement sont présentées dans la Figure 1-1. La voie principale d'accés des résidus d'antibiotiques dans l'environnement se fait par les eaux du réseau urbain lors d'un usage domestique des médicaments ou par les hopitaux. A la suite d'un traitement, le médicament est éliminé à travers les urines et les selles comme un mélange de molécules non modifiées ou métabolisées. Ce mélange passe par les eaux usées circulant dans les égouts pour rejoindre les stations d'épuration. Il est également nécessaire de mentionner que environ 35% des médicaments non consommées sont éliminés directement dans les toilettes ou les lavabos par le consommateur (Bound et al., 2006) et rejoignant ainsi les eaux usées. Les rejets directs dans les eaux issus des industries pharmaceutiques sont considérés comme une source négligeable étant donné que l'objectif du fabricant est évidemment d'enperdre le moins possible. Les résidus d'antibiotiques issus de l'aquaculture sont rejetés directement dans les eaux de surface. Lors de l'exploitation agricole, les animaux excrétent les médicaments via les urines. Ces excrétions largement répondues sur le sol contaminent les eaux de surface et les eaux souterraines. Lors du traitement des cultures, les résidus d'antibiotiques peuvent également contaminés le sol et par conséquent la nappe aquatique (Boxall et al., 2003).

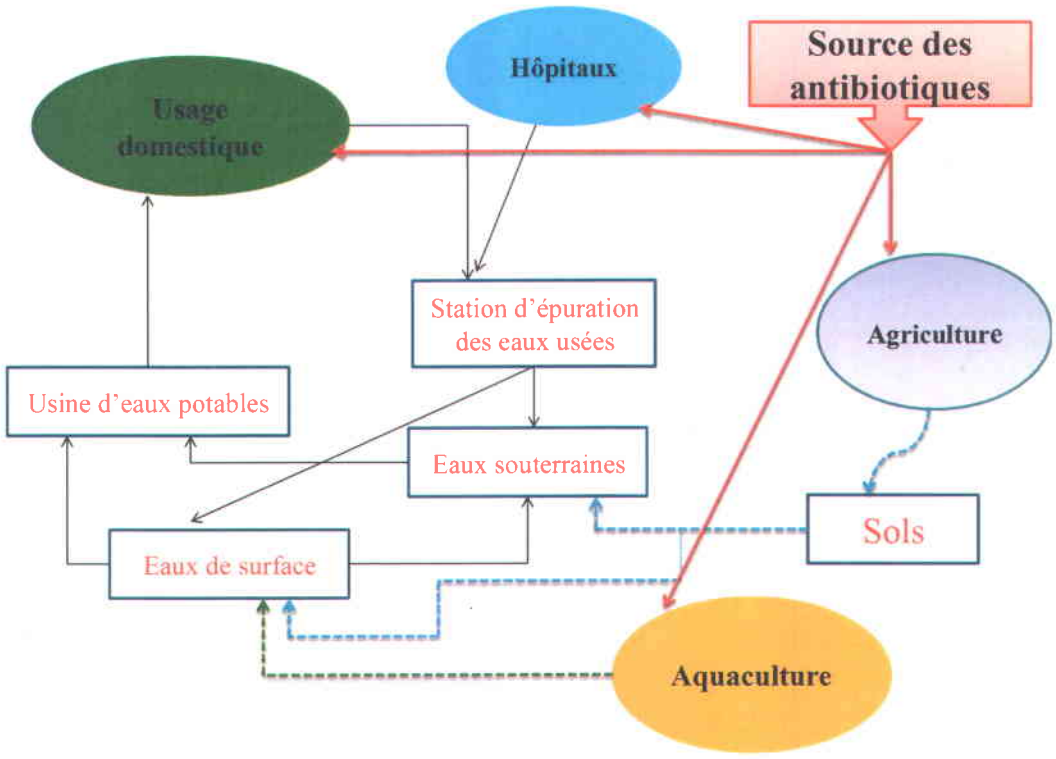


Figure 1-1 Source et devenir des résidues d'antibiotiques dans l'environnement.

Les effluents médicamenteux issus de différentes sources sont acheminés à l'usine de traitement des eaux usées. Il existe plusieurs systèmes d'épuration des eaux usées : des procédés de traitement biologiques, des procédés de traitement chimiques, des procédés de traitement physiques, etc. Le choix d'une stratégie de traitement de ces eaux usées nécessite la prise en considération de plusieurs facteurs, tels que la nature et la composition de l'effluent, la sensibilité du milieu récepteur, les normes de rejets, l'aspect économique, les objectifs de réutilisation des eaux traitées, etc. Il est également nécessaire lors du traitement des effluents médicamenteux de déterminer au préalable la concentration des réactifs, des produits et des sous-produits relargués dans l'effluent ainsi que la toxicité et la biodégradabilité des produits purs ou en mélange. L'étude antérieure effectuée par Batt et al. (2007) a montré que l'efficacité d'élimination des antibitiques (tetracycline, sulfamethoxazole, ciprofloxacine et

trimethoprime) détectés dans les stations d'épuration dépend de la combinaison des procédés de traitement chimique et biologique ainsi que des conditions opératoires imposées. La Figure 1-2 présente un organigramme des différents procédés conventionels utilisés pour l'élimination des résidus d'antibiotiques présents dans les effluents médicamenteux.

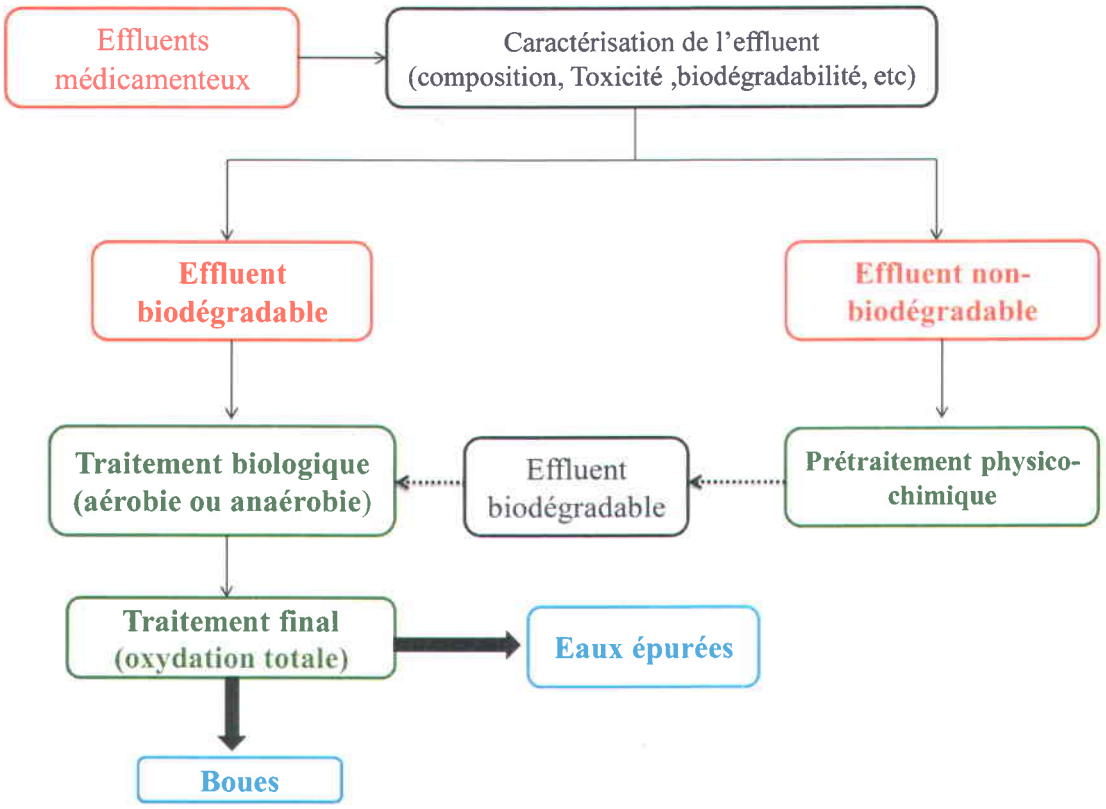


Figure 1-2 **Organigramme de différentes techniques pouvant être utilisées pour l'élimination des résidus d'antibiotiques présents dans les effluents médicamenteux.**

1.2.3.3 Traitement biologique

Les procédés de traitement biologiques sont habituellement retenus pour le traitement secondaire des eaux usées. Ces procédés où les bactéries sont les principaux acteurs de la dégradation sont généralement économiques et aisés à mettre en place. Le traitement biologique est capable de traiter un volume très important des eaux usées (Park, 2000). Les traitements biologiques sont classés en deux grandes catégories distinctes, soit la voie aérobie ou l'oxygène de l'air est associé et la voie anaérobie si la dégradation s'effectue à l'abri de l'air.

Les procédés par biofiltration et par boues activées sont classés dans la catégorie des procédés de traitement aérobie. Ces procédés (en présence d'oxygène) favorisent le développement des microorganismes qui décomposent les polluants. Le sulfamethoxazole est l'un des antibiotiques qui a été étudié par voie biologique aérobie utilisant les boues activées (Collado et al., 2013). Des taux de dégradation du sulfamethoxazole variant de 20% à 50% ont été obtenus durant deux mois avec des boues activées de station d'épuration urbaines (Collado et al., 2013). Au cours de traitement, certains microorganismes tels que Actinobacteria, Sphingobacteria, Chloroflexi and Chlorobi ont été trouvé plus vulnérables à la charge des antibiotiques et disparaissent aprés l'exposition du sulfamethoxazole. Le TC et le tylosine sont deux autres exemples d'antibiotiques qui ont été étudiés par le procédé de traitement par boues activées (Prado et al., 2009). Les résultats montrent une abscence de la biodégradabilité pour les deux antibiotiques. L'adsorption est la voie la plus favorable pour le TC dans un procédé de traitement biologique. Son adsorption inhibe l'activité des microorganismes dans un systéme biologique (Prado et al., 2009).

Les procédés anaérobies (en absence d'oxygène) permettent le développement des microorganismes qui stabilisent les substances biodégradables en les transformant en biogaz (méthane, gaz carbonique). Par comparaison au traitement aérobie, le traitement anaérobie

permet de générer moins de boue qui est stabilisée, la demande en énergie est beaucoup plus faible et les coûts d'opération sont habituellement inférieurs puisque le traitement anaérobie ne requiert pas d'apport d'oxygène (Verstraete, 2004). Les procédés de traitement anaérobies ont été largement appliqués pour la dégradation des antibiotiques (Shi et al., 2011; Tong et al., 2012 ; Arikan, 2008). Le traitement anaérobie du TC et du sulfamethoxydiazine favorise leur adsorption rapide sur la phase solide et par conséquent leur inhibition à l'activité bactérienne (Shi et al., 2011). La forte sensibilité du procédé anaérobie au pH et aux substances toxiques tels que les antibiotiques, ainsi que la faible activité bactérienne à basse température représentent les majeurs inconvénients du procédé de traitement anaérobie.

1.2.3.4 Traitement chimique par oxydation avancée

Les recherches récentes se concentrent sur le développement de nouvelles technologies pour le traitement des antibiotiques présents dans les eaux usées. La complexité de ces composés ainsi que leur caractère non-biodégradable rendent les technologies de traitement conventionnel moins attractif. Le recours à l'application des procédés d'oxydations avancées (POAs) est une solution de plus en plus prometteuse pour résoudre les problèmes environnementaux générés par ces polluants. Les technologies d'oxydation avancée sont toutes basées sur la production d'entités radicalaires, notamment les radicaux hydroxyles (OH°) ($E° = 2.80$ V) qui sont des espèces oxydantes réactives (EORs) les plus puissantes que l'on puisse utiliser dans le domaine de traitement des eaux usées (Suty et al., 2003; Zaviska et al., 2009). Les radicaux hydroxyles sont des espèces hautement actives susceptibles de réagir rapidement et de manière non sélective avec la quasi-totalité des molécules organiques. Ces espèces radicalaires ont la capacité de réagir avec un grand nombre de composés organiques avec une vitesse d'oxydation largement supérieure à celle de l'ozone (10^9 fois plus élevée) (Parsons, 2004). Ces POAs ont été largement appliqués pour le traitement des effluents médicamenteux de type antibitique (Oturan et al., 2013; Zaviska et al., 2013 ; Yao et al.,

2013; Naddeo et al., 2012; Nasuhoglu et al., 2012; Zhang et al., 2010) . Les Tableaux 1-5, 1-6 et 1-7 résument quelques applications récentes de ces procédés pour l'élimination des antibiotiques.

Les techniques d'oxydation avancées, incluant O_3/H_2O_2, UV/O_3, UV/H_2O_2, $H_2O_2/Fe^{2+}/UV$, UV/TiO_2, l'oxydation électrochimique, l'oxydation photoélectrocatalytique et l'oxydation sonochimique, peuvent être employées comme technique de prétraitement oxydatif conduisant à des composés facilement biodégradables, soit comme traitement tertiaire pour l'élimination et la minéralisation complète des polluants réfractaires tels que les antibiotiques (Drogui et al., 2007 ; Szpyrkowicz et al., 2005 ; Panniza et al., 2006). La plupart de ces techniques ont été appliqués à l'échelle du laboratoire, d'autre part mettant en combinaison l'ozone et le peroxyde d'hydrogène (O_3/H_2O_2) ont fait leur preuve à l'échelle industrielle (Galey et Palawski, 1993).

1.2.3.4.1 Traitement d'oxydation électrochimique

L'oxydation électrochimique basée sur le transfert d'électrons a reçu un intérêt considérable dans le domaine du traitement des eaux usées (Anglada et al., 2009 ; Del Rio et al., 2009 ; Zaviska et al., 2009). Par comparaison aux procédés de traitements conventionnels, l'oxydation électrochimique présente l'avantage de pouvoir réagir sur les polluants réfractaires de deux manières différentes, soit de manière directe ou indirecte. L'effet direct sur une espèce en solution s'effectue exclusivement par échange d'électron sur l'électrode. Des électrodes insolubles dites à forte surtension d'oxygène (Pt, Ti/IrO_2, Ti/SnO_2, PbO_2, BDD, Ti/RuO_2, etc) sont le plus couramment utilisées (Oturan et al., 2013 ; Yahiaoui et al., 2013 ; Zaviska et al., 2013). Cette oxydation anodique directe des polluants mène à la formation de composés plus simple, non-toxiques ou moins toxique et biodégradables (Comninellis et al., 1992). Cependant, la nature du matériau utilisé à l'anode influence de manière significative la sélectivité et l'efficacité du processus d'oxydation directe. Le

mécanisme de la réaction directe consiste à l'oxydation de molécule d'eau (décharge anodique de l'eau) conduisant à la formation de radicaux hydroxyles adsorbés à la surface de l'anode (Équation 1-1 et Équation 1-2).

Équation 1-1 $H_2O + M \rightarrow M\,[OH^\circ] + H^+ + e^-$

Équation 1-2 $R + M\,[OH^\circ] \rightarrow M + RO + H^+ + e^-$

Dans certains cas, l'électrolyse peut être inefficace ou lente. Il est alors nécessaire de générer par voie électrochimique un oxydant qui va réagir par la suite avec les polluants réfractaires présents en solution. Des espèces oxydantes puissantes telles que l'acide hypochloreux (HClO) et l'acide persulfurique ($H_2S_2O_8$) peuvent être générées par oxydation anodique des ions chlorures et des ions sulfates, respectivement (Équation 1-3 et Équation 1-4). Ces oxydants puissants sont capables d'oxyder ou de modifier la structure des molécules organiques réfractaires (Canizares et al., 2005) et conduire ainsi à la formation des composés plus oxydés. IL est également possible lors de l'électrolyse de générer *in situ* d'autres espèces oxydantes tel que le peroxyde d'hydrogène (H_2O_2) par réduction cathodique de l'oxygène dissous (Équation 1-5) (Oturan et al., 2013).

Équation 1-3 $2SO_4^{2-} + 2H^+ \rightarrow H_2S_2O_8 + 2e^-$

Équation 1-4 $Cl^- + 2H_2O \rightarrow HClO + H_3O^+ + 2e^-$

Équation 1-5 $O_{2(dissous)} + 2H^+ + 2e^- \rightarrow H_2O_2$

L'oxydation électrochimique est considérée comme une stratégie très effective pour le traitement des effluents médicamenteux de type antibiotique (Oturan et al., 2013; Cheng et

al., 2013; Zaviska et al., 2013; Haidar et al., 2013). L'oxydation électrochimique utilisant le Ti/IrO_2 comme anode à une intensité de 1.5 A a assuré l'élimination de 99% de l'OTC présent dans les eaux usées de l'élevage après 6 h de traitement (Miyata et al., 2011), alors que un taux de minéralisation allant jusqu'à 98% a été obtenu lors d'un traitement électrochimique de 6 h d'une soultion contaminée par le TC (100 mg L^{-1}) utilisant une électrode de BDD à l'anode et à une intensité de courant de 0.5 A (Oturan et al., 2013). Les techniques de traitement électrochimiques se caractérisent par leur aspect non polluant et une facilité d'automatisation et constituent l'une des méthodes visant à réduire l'emploi de réactif chimiques. Néanmoins, le coût opérationnel très élevé due à la consommation énergétique reste le majeur inconvénient qui limite l'application des procédés d'oxydation électrochimiques (Anglada et al., 2009).

1.2.3.4.2 Les procédés photochimiques

Au cours des années récentes, les technologies photochimiques sont devenues très attractives et sont susceptibles de remplacer les techniques de traitement conventionnelles telles que la biodégradation et l'adsorption sur charbon actif. Les procédés photochimiques basés sur les radiations UV sont simples d'utilisation, propres et peu couteuses. De plus, ces technologies ont la particularité d'assurer à la fois la désinfection et le traitement des contaminants. Lors de la photolyse directe, les radiations UV absorbées par les molécules de H_2O permettent la génération des espèces oxydantes puissantes telles que les radicaux hydroxyles (OH°) et le peroxyde d'hydrogène (H_2O_2) (Heit et al., 1998 ; Kim and Tanaka, 2009). Cependant, l'application des radiations UV lors du traitement des eaux usées est généralement affectée par plusieurs facteurs tels que la qualité des eaux, le coût de la maintenance ainsi que le coût énergétique. Les études récentes sont plus focalisées vers le couplage des radiations UV avec des oxydants puissants tels que l'ozone et le peroxyde d'hydrogène (UV/H_2O_2, UV/O_3).

1.2.3.4.2.1 Couplage peroxyde/ultraviolet (H_2O_2/UV)

Ce procédé est basé sur la formation des radicaux hydroxyles suite à la photolyse du peroxyde d'hydrogène présent en solution (Pera-Titus et al., 2004). L'irradiation à des longueurs d'ondes comprises entre 200 nm et 300 nm provoque une coupure homolytique de la liaison O-O de la molécule de H_2O_2 et conduit à la formation de radiaux hydroxyles (Équation 1-6).

Équation 1-6 $H_2O_2 + h\nu \rightarrow 2OH°$

La vitesse de production des radicaux libres dépend de plusieurs facteurs dont le pH, la dose du H_2O_2 ainsi que les caractéristiques des lampes UV. L'addition des quantités de H_2O_2 lors du traitement photochimiques améliore l'oxydation des antibiotiques (Kim et al., 2009). Par exemple, l'addition d'une dose de 10 mmoL L^{-1} de H_2O_2 à l'irradiation UV (254 nm) diminue la concentration du carbone organique totale (COT) (une élimination de 27.4%) et la toxicité des sous-produits générés durant l'oxydation du CTC (Lopez-Penalver et al. 2010). Cette association mettant en évidence le couplage H_2O_2/UV (3.36 x 10^{-6} Einstein L^{-1} s^{-1} d'irradiation UV et 30 mg L^{-1} de H_2O_2) a permis également d'assurer une meilleure dégradation de l'ionophore (une constante de dégradation allant jusqu'à 1.14 min^{-1}) (Yao et al., 2013). Du à la quantité limitée des radicaux hydroxyles produites durant le procédé et le coût de l'énergie élevé, les recherches s'orientent aujourd'hui vers l'utilisation d'autres catalyseurs dans le but d'améliorer la décomposition de H_2O_2.

1.2.3.4.2.2 Couplage ozone/ultraviolet (O_3/UV)

Au cours des dernières années, il y a un grand intérêt dans l'utilisation de l'ozone pour traiter des effluents médicamenteux de type antibiotioque (Homem et Santos, 2011). Par comparaison à d'autres espèces oxydantes (H_2O_2, HClO, etc), l'ozone est un oxydant très

puissant (E° = 2.07 V) qui a été largement utilisé pour la désinfection des eaux potables mais son application dans les filières de traitement des eaux usées reste très limité du au coût énergétique très élevé (Pera-Titus et al., 2004 ; Guivarch, 2004). En solution, l'ozone est capable d'oxyder les polluants par voie directe et indirecte. Le couplage de l'ozone avec les radiations UV (O_3/UV) conduit à la production de radicaux libres qui sont des espèces oxydantes très réactives et efficaces pour éliminer les polluants organiques refractaires (Équation 1-7). Le procédé d'ozonation utilisant une concentration de 11 mg O_3 L^{-1} a assuré une dégradation totale de l'OTC (100-200 mg L^{-1}) (Li et al., 2008). L'application d'un procédé d'ozonation (10 mg O_3 L^{-1}) en couplage avec les radiations UV (238-366 nm) a assuré également une dégradation totale de sulfamethoxazole (10^{-4} mol L^{-1}) après 10 min de traitement (Beltran et al., 2009). La dose de l'ozone ajoutée ainsi que les radiations UV appliquées ont une grande influence sur l'efficacité du procédé.

Équation 1-7 $O_3 + H_2O + h\nu \rightarrow 2OH° + O_2$

1.2.3.4.2.3 Couplage réactif de Fenton/ultraviolet (Fe^{2+}/H_2O_2/UV)

Le procédé photo-Fenton est un POA hybride qui utilise une source de radiation (généralement l'UV) pour augmenter le taux de production de radicaux hydroxyles en stimulant la réduction du Fe^{3+} en Fe^{2+}. La combinaison entre le procédé Fenton (H_2O_2/Fe^{2+}) et les radiations UV permet de décomposer par photolyse le peroxyde d'hydrogène pour former des radicaux hydroxyles mais aussi d'augmenter l'activité catalytique du fer (Équation 1-8 et Équation 1-9). Le procédé photo-Fenton a été efficacement utilisé par Bautitz et Nogueira (2007) pour le traitement de la TC (24 mg L^{-1}) présent dans les boues. Un taux d'élimination de 80% de TC a été obtenu en utilisant des radiations UV (365 nm), 0.20 mM de $Fe(NO)_3)_3$ et 3.0 mM de H_2O_2. Une dégradation compléte du Sulfamethoxazole (200 mg L^{-1}) a été

enregistrée en appliquant une dose de 300 mg L^{-1} de H_2O_2, 100 mg L^{-1} de Fe^{2+} et sous une radiation UV ayant une longueur d'onde de 365 nm. Néanmoins, la dose du fer et du peroxyde d'hydrogène utilisée dans la réaction photo-Fenton est un paramètre important qui détermine l'efficacité du procédé. Il faut également tenir compte des caractéristiques spectrales et de la puissance des lampes utilisées, de leur encrassement, de la turbidité des effluents limitant le parcours des rayonnements ainsi que des coûts d'installation et de fonctionnement supplémentaires.

Équation 1-8 $Fe^{2+} + H_2O_2 \rightarrow Fe^{3+} + OH^- + OH°$

Équation 1-9 $Fe^{3+} + H_2O + h\nu \rightarrow Fe^{2+} + H^+ + OH°$

1.2.3.4.2.4 Le procédé photocatalytique

Au cours des dernières années, l'application de la photocatalyse hétérogène pour le traitement des effluents médicamenteux de type antibiotique a reçu un intérêt considérable (Elmolla et Chaudhuri, 2010; Li et al., 2012 ; Nasuhoglu et al., 2011; Hapeshi et al., 2010). Cette technologie est basée sur l'irradiation d'un catalyseur, en général un semi-conducteur (ex. TiO_2, ZnO) qui peut être photo-excité pour former des sites électro-donneurs et des sites électro-accepteurs et ainsi induire des réactions d'oxydoréduction. Sous radiation UV, si les photons absorbés possèdent une énergie supérieure au gap d'énergie (> 3.2 eV pour le TiO_2) entre la bande de valence (BV) et la bande de conduction (BC) de TiO_2, des pairs électrons-trous se créent dans le semi-conducteur (Figure 1-3). Les électrons photo-générés dans la BC favorisent la réduction de l'oxygène à des radicaux superoxydes, alors que les trous photo-générés dans la BV peuvent oxyder directement le contaminant adsorbé ou alors oxyder les groupes hydroxyles à la surface de TiO_2 pour former des radicaux hydroxyles. La dégradation

de polluants contenus dans les eaux usées peut ainsi s'effectuer directement à la surface du semi-conducteur ou indirectement en interagissant avec des radicaux hydroxyles.

La durée de vie du pairs (e^-/h^+) est de quelques nanosecondes (Zalazar et al., 2005). Ces paires électron-trou peuvent se recombiner pour libérer de la chaleur. La recombinaison du pair électron-trou photo-générés représente le majeur inconvénient qui limite l'application du procédé photocatalytique. Aujourd'hui, les recherches récentes s'orientent vers la combinaison des procédés photocatalytiques (PC) avec les procédés électrochimiques (procédé photoélectrocatalytique (PEC)). Cette synergie améliore le taux de dégradation des polluants récalcitrants (Rajeshwar et al., 1994). La technique d'oxydation PEC sera plus étudiée en détail dans les prochaines sections.

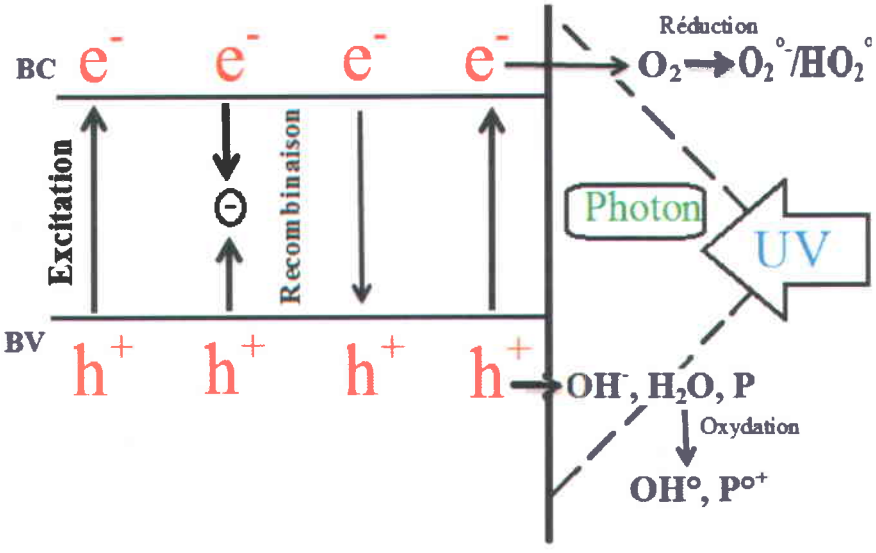


Figure 1-3 Les réactions d'oxydoréduction qui se produisent à la surface d'un photocatalyseur.

Tableau 1-5 Performances des POAs pour la dégradation des antibiotiques

POAs	Type de Matrice	Type de polluant	Conditions opératoires	Résultats et commentaires	Réferences
Electrooxydation (EO)	Eaux usées d'élevage	Oxytetracycline (OTC)	$[OTC]_0$ = 100 mg L^{-1}; Ti/IrO_2:anode; Ti : cathode; I = 1.5 A; Na_2SO_4;V = 500 mL; [DCO] = 1,5 mg L^{-1}; temps de traitement = 6 h;	$[OTC]_F$ = 0,7 mg L^{-1}	Miyata et al. 2011
	Solution aqueuse	Tétracycline (TC)	[TC] = 200 mg L^{-1}; Ti/RuO_2-IrO_2: anode; Inox: cathode; i = 47,6 mA cm^{-2}; $[Na_2SO_4]$ = 0,1 mol L^{-1}; pH = 3,9; V =200 mL; temps de traitement = 60 min	% TC éliminé = 82,2%	Zhang et al. 2009
	Solution aqueuse	Sulfamethoxazole (SMX)	Diamant dopé au bore (BDD): anode; carbon felt: cathode; I= 300mA; pH = 3; V = 250 mL; $[Na_2SO_4]$ = 0,05 M; room temperature; treatment time = 360 min.	% SMX éliminé = 95%	Dirany et al. 2010
	Solution aqueuse	Chlortetracycline	C° = 10 mg L^{-1}; Ti/IrO_2 and Ti/PbO_2: anode; Ti: cathode; V = 2 L; intensité de courant = 1,0-3,0 A; temps de traitement = 20-60 min; température = 5-22°C ; $[Na_2SO_4]$ = 100 mg L^{-1} ; [NaCl] = 100 mg L^{-1}.	%chlortetracycline éliminé = 96 % à une intensité de courant = 2 A, après 49 min de traiment, à une température = 14°C et en utilisant Ti/PbO2 comme anode.	Zaviska et al. 2013
	Solution aqueuse	Sulfachloropyridazine	BDD : anode; feutre de carbone = cathode; 25 mg L^{-1} de carbone organique totale de Sulfachloropyridazine ; $[Na_2SO_4]$ = 0,05 mol L^{-1} ; C° = 0,2 mmol L^{-1} ; pH = 4,5	Taux de minéralization = 95% après un temps de traitement de 8h et à une intensité de courant de 350 mA.	Haidar et al., 2013
	Solution aqueuse	Tetracycline	Anode = Ti/RuO_2-IrO_2, Pt et BDD; cathode = feutre de carbone et inox ; pH = 3-4,3;C° = 100 mg L^{-1}; $[Na_2SO_4]$=0,05mol L^{-1} ; V = 220 mL ; température = 23±2°C ; intensité de courant = 500 mA.	Taux de minéralization = 98% est atteind après un temps de traitemenyt de 6h utilisant le BDD à l'anode	Oturan et al., 2013

Tableau 1-6 Performances des POAs pour la dégradation des antibiotiques (suite)

POAs	Type de Matrice	Type de polluant	Conditions opératoires	Résultats et commentaires	Références
H_2O_2/UV	Solution aqueuse	Tétracycline (TC); Chlortétracycline (CTC); Oxytetracycline (OTC)	Lampe à faible pression (254 nm); $[H_2O_2]$ = 10 mmol L^{-1} ; pH = 2-4,5; $[TC]_0$= 20 mg L^{-1}; $[CTC]_0$ = 20 mg L^{-1}; $[OTC]_0$ = 20 mg L^{-1}; T° = 298 K; temps de traitement = 60 min	% COT (TC) = 18.2%; % COT (CTC) = 27.4%; %COT (OTC) = 27.8%; Toxicité (TC) = 35%; Toxicité (CTC) = 18%; Toxicité (OTC) = 25%.	Lòpez-Penalver et al. 2010
	Solution aqueuse	Sulphamethoxazole (SMX)	Lampe à moyenne pression (200-300 nm); $[H_2O_2]$ = 0- 4,41 mmol L^{-1}; pH = 6.0; $[SMX]_0$ = 3,2 µM	Taux de dégradation du SMX = 0.021s^{-1} at 2.94 mM	Lester et al. 2010
	Eaux de surface Eaux usées	Ionophore	C°= 0,8-3,0µM ; pH=7 ; lampe UV(254 nm ; 2,0 mW cm^{-2}; $[H_2O_2]$ = 30 mg L^{-1}	Constantes de dégradation: 0.81-1.14 min^{-1} (eau déionisée); 0.51-0.60 min^{-1} (eaux de surface); 0.28-0.31min^{-1}(eaux usées).	Yao et al., 2013
H_2O_2/Fe^{2+}/UV	Station de traitement des boues	Tétracycline (TC)	Lampe UV (365 nm); $[Fe(NO_3)_3]$ = 0,20 mmol L^{-1}; $[H_2O_2]$ = 3,0 mmol L^{-1}; [TC] = 24 mg L^{-1}; COT = 19 mg°L^{-1}; temps de traitement = 50 min	%TC éliminé = 80%; %COT éliminé = 34%	Bautitz and Nogueira, 2007
	Effluents de pénicilline	Procaine Penicilline G	Lampe UV (365 nm); DCO = 600 mg L^{-1}; DBO_5 = 53 mg L^{-1}; COT_0 = 450 mg L^{-1}; temps de traitement = 30 min	% DCO éliminé = 56 %; %COT éliminé = 42%; le ratio DBO_5/DCO augmente de 0.10 à 0,45 dans les conditions optimales ($[Fe^{3+}]$ = 1,5 mM; $[H_2O_2]$ = 25 mM; pH = 3)	Arslan-Alaton and Gurses, 2004

Tableau 1-7 Performances des POAs pour la dégradation des antibiotiques

POAs	Type de Matrice	Type de polluant	Conditions opératoires	Résultats et commentaires	Réferences
Photocatalyse (PC)	Solution aqueuse	Tylosine	Illumination UV (365 nm); Plaque de verre avec TiO_2 immobilisé (P25, PC105, PC500); $[Tylosine]_0$ = 200 mg L^{-1}; T° = 25°C; débit= 0.4 L min^{-1}	Meilleure dégradation du Tylosine (70%) a été obtenue avec le P25 après 7 h.	Alatrache et al. 2010
	Solution aqueuse	Ciprofloxacine	Irradiation UV (365 nm); semi-conducteur ZnO (20 mg L^{-1}); pH = 4-10	Après 60 min, une efficacité de dégradation élevée (50%) du Ciprofloxacin a été observée à pH = 10	El-Kemary et al. 2010
	Solution aqueuse	Acide Oxolinique (AO)	Radiations UV (365 nm); TiO_2 en suspension Degussa P25 (0,2-1,5 g L^{-1}); pH (7,5-11); $[OA]_0$= 20 mg L^{-1}	Sous un pH 7,5 et 1,0 g L^{-1} du TiO_2, 80% and 100% du OA a été éliminé après 10 min et 30 min d'irradiation, respectivement. Après 30 min, le photocatalyseur TiO_2 est capable de réduire la toxicité de la solution par 60% et 53%	Giraldo et al. 2010
	Solution aqueuse	Flumequine	TiO_2 (forme pure, urea-TiO_2, thiourea-TiO_2); irradiation solaire stimulé (500 W m^{-2}); [Flumequine] = 20 mg L^{-1};	Après 15 min irradiation, 90% de la dégradation du flumequine a été enregistrée en utilisant urea-TiO_2 et thiourea-TiO_2 comparé à 55% de la dégradation du flumequine a été enregistré en utilisant le TiO_2 pure. La dégradation élevé de la FQ a été obtenu à pH en dessous de 7 et en utilisant une quantité de catalyseur de 1,6 g L^{-1}.	Nieto et al. 2008
	Solution aqueuse	Ofloxacine, norfloxacine, ciprofloxacine, eurofloxacine	$[TiO_2]$=0,1-1,5 g L^{-1}; lampeUV(800 W xenon); [ofloxacine]= 0,028 mmol L^{-1}; [norfloxacine]= 0,031mmol L^{-1}; [ciprofloxacine] =0,027mmol L^{-1};[eurofloxacine]=0,028 mmol L^{-1}; pH=2-9;temperature = 23±2°C;volume=500mL ; $[H_2O_2]$= 0-330 mg L^{-1}	%de dégradation de ofloxacine =98% ;%de dégradation de norfloxacine =99%;%de dégradation de ciprofloxacine=96% ;%de dégradation de enrofloxacine=100% pour un pH=9, à une concentration de TiO_2=0,5 g L^{-1}, $[H_2O_2]$ 82,5 mg L^{-1} et après 90 min d'irradiation	Li et al., 2012
	Solution aqueuse	Amoxicilline, ampicilline, cloxacilline	[ZnO]= 0,2-2g L^{-1}; [amoxicilline] =104 mg L^{-1}; [ampicilline]=105 mg L^{-1}; [cloxacilline]=103 mg L-1;pH=5-11; temps de traitement=0-300min; V=500mL; lampe UV=365nm	100% dégradation de amoxicilline, ampicilline, cloxacilline à une dose de 0,5 g L^{-1} de ZnO, après 180 min du temps de traitement et à un pH11 ;% d'élimination de DCO=23,9% ;% d'élimination du COD=9.7%.	Elmolla et Chaudhuri, 2010

1.2.4 Procédé d'oxydation PEC

1.2.4.1 Intérêts et spécificité de la photoéléctrocatalyse

Le procédé d'oxydation PEC est basé sur les approches mettant en synergie les procédés électrochimiques et les techniques PC activées par un rayonnement UV. Le processus PC est basé sur l'irradiation d'un catalyseur, en général un semiconducteur, qui peut être photo-excité pour former des sites électro-donneurs et des sites électro-accepteurs d'électrons. Plusieurs matériaux semi-conducteurs (ZnO, WO_3, SnO_2 et TiO_2, CdS, etc.) peuvent être utilisés comme photocatalyseurs dans ces procédés ultra-oxydatifs (Tableau 1-8) (Robert, 2007; Rehman et al., 2009). En revanche, l'instabilité chimique de ZnO (photo-stabilité insuffisante), la photocorrosion de CdS et sa possiblité de subir une oxydation en solution (relargage de Cd^{2+}) (Colmenares et al., 2009; Robert, 2007; Bessekhouad et al., 2006) et la methode de préparation trop complexe et coûteuse de $SrTiO_3$ tendent à privilégier le TiO_2 comme photocatalyseur fiable. En effet, le TiO_2 est chimiquement et biologiquement inerte, possède une photosensibilité élevée et une bonne efficacité d'oxydation, et se caractérise par une stabilité à long terme contre la corrosion (Ouyang et al., 2012 ; Zhang et al., 2010 ; Valentin et al., 2007). Par ailleurs, le TiO_2 est un matériau qui a été largement étudié dans la littérature.

Tableau 1-8 Les semi-conducteurs utilisés dans un procédé PEC

Semi-conducteur	Band gap (eV)	Longueur d'onde (nm)	Absorption de la lumière	BV (V vs NHE)	BC (V vs NHE)
TiO_2	3.2	387	UV	+3,1	-0,1
SnO_2	3.8	318		+4,1	+0,3
ZnO	3.2	387		+3,0	-0,2
ZnS	3.7	335		+1,4	-2,3
WO_3	2.8	443	Visible	+3,0	+0.4
CdS	2.5	496		+2,1	-0,4
CdSe	2.5	729		+1,6	-0,1

L'exposition du photocatalyseur au rayonnement UV ayant une énergie supérieure à la bande interdite du semiconducteur (> 3.2 eV pour le TiO_2) favorise le passage des électrons de la BV vers la BC. Ce processus mène à la création des paires d'électron-trou (e^-_{BC}/h^+_{BV}) (Équation 1-10), qui sont à l'origine des réactions d'oxydoréduction à la surface du matériau semi-conducteur (Yang et al., 2009). Les charges ainsi photogénérées sont exploitées pour l'oxydation des polluants. La durée de vie des paires électron-trou (e^-_{BC}/h^+_{BV}) est dans le régime de la nanoseconde (Daghrir et al., 2012; Zalazar et al., 2005). Cependant, le potentiel externe appliqué dans un tel procédé PEC permet de retarder la recombinaison des paires (électrons-trous) et d'allonger ainsi leur durée de vie pour oxyder plus efficacement les polluants (Figure 1-4). Les photo-trous (h^+_{BV}) formés peuvent soit, oxyder directement les contaminants adsorbés (R_{ads}) (Équation1-11) ou oxyder la molécule de H_2O à la surface de TiO_2 pour former des radicaux hydroxyles OH° (Équation 1-12) (Esquivel et al. 2009). Il est à rappeler que les radicaux OH° sont les oxydants les plus forts que l'on puisse utiliser pour le traitement des eaux (Drogui et al., 2007).

Équation 1-10 Formation des pairs électrons-trous $TiO_2 + h\nu \rightarrow e^-_{BC} + h^+_{BV}$

Équation 1-11 Oxydation de polluant adsorbé R par les phototrous $h^+_{BV} + R_{ads} \rightarrow R^+$

Équation 1-12 Formation de radicaux hydroxyles $h^+_{BV} + H_2O \rightarrow OH° + H^+$

Les photoélectrons (e^-) éjectés vers la BC de TiO_2 réagiront à leur tour avec des accepteurs d'électrons tel que l'oxygène adsorbé (O_2) pour former des espèces oxygénées réactives (EORs) (ex. $O_2°^-$, $HO_2°$, H_2O_2, etc.) (Macphee et al., 2011; Daghrir et al., 2012) (Équation 1-13 et Équation 1-14). Aussi, ces photo-électrons peuvent être directement acheminés dans le circuit électrique externe au lieu d'être transférés à l'oxygène moléculaire (Daghrir et al.,

2012). Les espèces donneuses d'électrons (ex. $E°_{O2/H2O}$ = 1.23 V) ayant un potentiel d'oxydoréduction inférieur à celui de la BV de TiO_2 (+2.5 V/ENH à pH 7) seront oxydées par les photon-trous, alors que les espèces accepteuses d'électrons (ex. $E°_{O2/O2°}$ = - 0.33V) ayant un potentiel supérieur à celui de la BC de TiO_2 (-0.52 V/ENH à pH 7) seront réduites à la surface du catalyseur.

Équation 1-13 Formation de radicaux superoxyde $e^-_{BC} + O_2 \rightarrow O_2^{\circ-}$

Équation 1-14 Formation du peroxyde d'hydrogéne $O_2 + 2H^+ + 2e^-_{BC} \rightarrow H_2O_2$

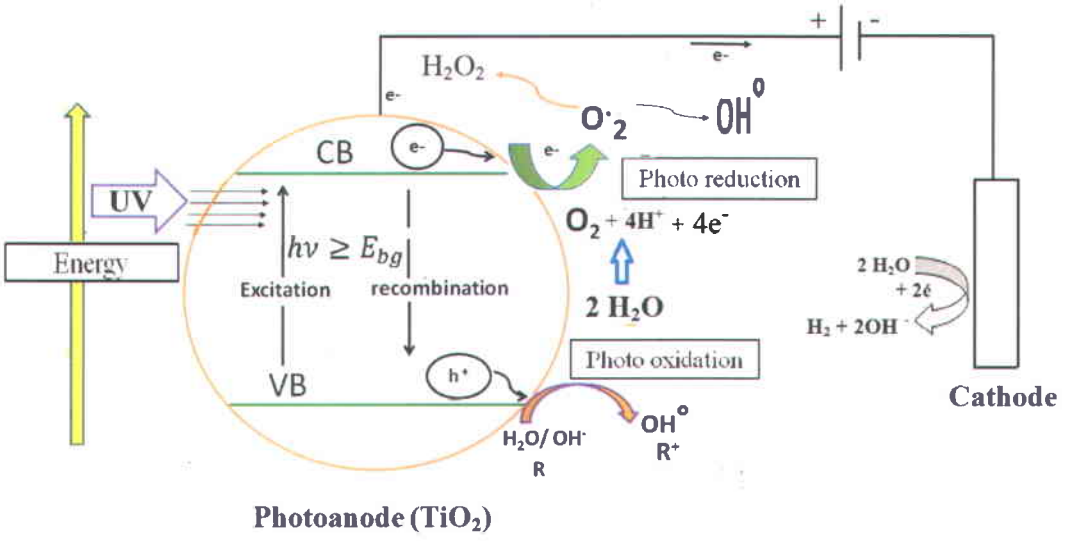


Figure 1-4 Mécanisme du procédé d'oxydation PEC utilisant le TiO_2 comme photoanode.

Ces réactions à la surface de la photo-anode et celles induites par les EORs permettront d'assurer une oxydation efficace des polluants organiques jusqu'à leur minéralisation. Le

procédé PEC se distingue de la photocatalyse conventionnelle souvent limitée à une oxydation partielle des contaminants à cause de la recombinaison prématurée des paires d'électron-trou. Un autre avantage intéressant du procédé PEC (par rapport au procédé PC) est la possibilité d'utiliser une électrode cathodique appropriée (contre électrode), tel que le carbone vitreux (CV), sur laquelle le peroxyde d'hydrogène (H_2O_2) peut être généré par voie électrochimique et ce, par réduction cathodique de l'oxygène dissous (Leng et al., 2006; Xie et Li, 2006). Cela pourrait se faire par régulation du courant électrique en jouant sur le bilan électronique et en contrôlant également les conditions hydrodynamiques à l'intérieur de la cellule PEC (Drogui et al., 2007). De plus, le peroxyde d'hydrogène (H_2O_2) induit des produits de réduction inoffensifs contrairement aux oxydants chimiques les plus utilisés comme le chlore (Drogui et al., 2001).

Sous irradiation UV, le H_2O_2 piège les photoélectrons de la BC et génère ainsi des radicaux hydroxyles (Daghrir et al., 2012; Leng et al., 2006; Xie et Li., 2006), qui viennent s'ajouter à ceux générés directement sur la surface de la photoanode TiO_2. Ceci a pour effet d'amplifier d'avantage l'efficacité de dégradation des polluants dans les eaux. Par ailleurs, la génération *in-situ* d'un accepteurs d'électrons (tel que H_2O_2) empêcherait la recombinaison des électron-trous et augmenterait potentiellement l'efficacité photocatalytique du procédé PEC (Xie et Li, 2006). En somme, la force de l'approche PEC-UV réside en sa capacité de mettre à profit à la fois les réactions anodiques, photocatalytiques et cathodiques pour ainsi produire simultanément plusieurs EORs sans apport d'électrolyte. Cette technique qui a rarement été appliquée sur des effluents réels, a surtout été utilisée sur des solutions synthétiques pour la dégradation de molécules organiques spécifiques (ex. bisphénol A, pentachlorophénol, dichlorophénol, acide humique, colorants, antibiotiques, etc.) (Xie et Li, 2006; Quan et al., 2007; Li et al., 2007; Selcuk et al., 2003; Esquivel et al., 2009; Li et al., 2000; Liu et al.,

2009). Les paramètres expérimentaux affectant l'efficacité d'un procédé d'oxydation PEC seront plus présentés en détails dans les sections suivantes.

1.2.4.2 Paramètres expérimentaux affectant l'oxydation PEC

L'efficacité d'un processus PEC est basée principalement sur les conditions opératoires imposées telles que le potentiel externe, l'intensité lumineuse, le pH, la température, la concentration de l'électrolyte ainsi que la nature de l'électrode (matériau de cathode).

1.2.4.2.1 Effet du potentiel externe appliqué

Le potentiel externe appliqué est l'un des paramètres opératoires les plus importants dans un processus d'oxydation PEC. Plusieurs études ont montré que le potentiel externe appliqué sur le TiO_2 (photo-anode) contribue à séparer les électrons et les trous photo-générés et évite le plus possible la recombinaison entre eux (Waldner et al., 2003; Li et al., 2002). Dans un procédé PEC, l'application d'une différence de potentiel évite la recombinaison des charges (e^-/h^+) et augmente leur durée de vie. Par conséquent, les électrons et les trous peuvent davantage oxyder directement le polluants à la surface de TiO_2 ou réagir indirectement avec les espèces actives (telles que les radicaux hydroxyles). L'influence de l'intensité de courant imposée sur la production des radicaux hydroxyles a été étudiée par Jiang et al. (2006). Il a été montré que la concentration totale de radicaux hydroxyles (plus que 20 $\mu mol\ L^{-1}$) générée sous irradiation UV (20 W) a été améliorée suite à l'application d'un potentiel externe de 0.6 V. L'application de ce potentiel favorise une meilleure dégradation des polluants. L'influence de l'intensité de courant a été également mise en évidence par Selcuk et al. (2003) et Wang et al. (2009) lors du traitement de l'acide humique et du 4-chlorophenol, respectivement. L'étude a montré que l'efficacité de la dégradation PEC du 4-chlorophenol et de l'acide humique est majorée d'un facteur 2 suite à l'application d'un potentiel externe optimal de 0.6 V et de 1.5 V, respectivement. Ainsi, il semblerait qu'il y aurait un seuil au-delà duquel le

potentiel externe appliqué aurait une influence significative sur la dégradation du polluant. L'augmentation du potentiel externe au dessus de la valeur optimale peut soit diminuer l'efficacité de la dégradation du polluant ou ne pas avoir d'effet. Par l'application d'un potentiel externe, le gradient du potentiel électrochimique pourrait augmenter jusqu'à une séparation complète des charges e^-/h^+ (conditions d'épuisement complet). Dans ces conditions, la cinétique de la réaction est seulement limitée par le flux de photons (Neuman-Spallart, 2007). Dans les conditions d'épuisement de charges, la séquence de réactions incluant la réduction des molécules d'oxygène serait absente, réduisant ainsi la dégradation PEC du polluant.

1.2.4.2.2 *Effet de l'intensité lumineuse*

La recombinaison des électrons-trous est une étape limitante dans les réactions photocatalytiques (Sohrabi et Ghavami, 2010). Dans un procédé PC, le taux de dégradation des polluants dépend fortement de l'intensité lumineuse appliquée sur la surface du catalyseur. Des études antérieures ont montré que l'augmentation de l'intensité lumineuse UV favorise une meilleure excitation du catalyseur et par conséquent une meilleure dégradation des polluants organiques (Wang et al. 2010; Wang et al. 2009; Chen et al. 2010). L'amélioration de l'efficacité de dégradation PC des polluants est principalement attribuée à une augmentation de la concentration des EORs générées sur la surface du TiO_2. La concentration des radicaux hydroxyles générée sur la surface de TiO_2 est décrite par Chen et al (2010) et par Cho et al (2004) comme suit :

Équation 1-15 $$[HO^\circ]_S = \sqrt{\frac{(1-\alpha) I_a \Phi}{k_D}}$$

Dans cette expression, I_a est le nombre de photons absorbés par seconde; Φ est le rendement quantique; k_D est la constante de diffusion et α est un paramètre qui dépend du pH.

Une étude effectuée par Li et al. (2002) sur la dégradation de l'acide humique a montré que le taux de dégradation est proportionnel à l'intensité lumineuse ($k° = k_2 I^b$, dont $k°$ est le taux de dégradation, I c'est l'intensité lumineuse, k_2 et b sont des constantes cinétiques). Dans le domaine de traitement des eaux usées, certaines études ont montré qu'une intensité lumineuse relativement élevé est nécessaire pour atteindre des meilleures réactions PC(Chong et al., 2010). L'efficacité de la dégradation des polluants est fortement liée à la distribution de l'intensité lumineuse à l'intérieur du réacteur (Pareek et al., 2008). Il est donc nécessaire de déterminer l'intensité lumineuse appropriée pour assurer une bonne dégradation des polluants tout en minimisant la consommation énergétique. Pour des applications pratiques à grande échelle, il sera intéressant d'utiliser les radiations UV émises par le spectre solaire en présence de TiO_2 dans le but de minimiser le coût du traitement. Cependant, si les radiations UV émise par le spectre solaire sont insuffisantes, ces derniers peuvent être combinés avec des irradiations de la lampe UV artificiel.

1.2.4.2.3 *Effet de la cathode*

Par comparaison au procédé photocatalytique conventionnel, l'utilisation des électrodes comme le CV à la cathode représente un avantage intéressant dans l'application des techniques d'oxydation PEC. Des études précédentes ont montré que l'utilisation des électrodes comme le VC ou le graphite (Gr) à la cathode favorise la production électrochimique du peroxyde d'hydrogène suite à une réduction cathodique des molécules d'oxygène (Équation 1-16) (Xie et Li, 2006). Sous irradiations UV, le peroxyde d'hydrogène peut se décomposer pour former des radicaux hydroxyles (en plus des radicaux hydroxyles produits à la surface de TiO_2) (Équation 1-17). L'addition d'un électron accepteur tel que le

H_2O_2 permet d'éviter la recombinaison des électrons-trous, augmentant ainsi l'efficacité PEC (Ding et al., 2010; Sohrabie et Ghavami, 2010; Xie et Li, 2006).

Équation 1-16 $O_2 + 2H^+ + 2e^- \rightarrow H_2O_2$

Équation 1-17 $H_2O_2 + h\nu \rightarrow 2OH^\circ$

1.2.4.2.4 *Influence de l'oxygène dissous*

Lors de la dégradation PEC des polluants organiques, l'oxygène dissous évite la recombinaison des paires électron-trou photo-générés en agissant comme accepteurs d'électrons. Il contribue à la formation des EORs telles que les radicaux superoxydes (Yang et al., 2009 ; Leng et al., 2006 ; Zhang et al., 2003). Une quantité d'oxygène suffisante est nécessaire pour favoriser les réactions d'oxydation et de réduction des polluants. Dans un procédé PEC, un système d'aération ou une oxydation des molécules de H_2O à l'anode représente une source principale d'approvisionnement en O_2 (Équation 1-18). Ces molécules de O_2 jouent le rôle d'accepteurs d'électron qui réagissent avec les électrons dans la BC pour former des radicaux superoxydes ($O_2^{\circ-}$) ainsi que d'autres espèces oxydantes telles que H_2O_2, HO_2° et HO_2^- (Équations 1-19-1-25).

Équation 1-18 $2H_2O \rightarrow O_2 + 4H^+ + 4e^-$

Équation 1-19 $e^- + O_{2\,(ads)} \rightarrow O_2^{\circ-}$

Équation 1-20 $O_2^{\circ-} + H^+ \rightarrow HO_2^\circ$

Équation 1-21 $2HO_2^\circ \rightarrow H_2O_2 + O_2$

Équation 1-22 $O_2^{\circ-} + HO_2^\circ \rightarrow O_2 + HO_2^-$

Équation 1-23 $HO_2^- + H^+ \rightarrow H_2O_2$

Équation 1-24 $O_2 + 2é_{CB} + 2H^+ \rightarrow H_2O_2$

Équation 1-25 $2H_2O + 2h^+_{VB} \rightarrow H_2O_2 + 2H^+_{aq}$

La présence des EORs en grande quantité dans le milieu réactionnel peut limiter la recombinaison des paires électron-trou et améliorer ainsi l'efficacité d'oxydation.

1.2.4.2.5 *Influence du pH*

L'oxydation PEC des composés organiques peut fortement dépendre du pH de la solution à traiter (Wang et al., 2009; Quan et al., 2007). Le pH affecte la capacité d'adsorption et de dissociation des composés cibles, la distribution des charges sur la surface du catalyseur ainsi que le potentiel d'oxydation de la BV (Chong et al., 2010; Wang et al., 2009; Quan et al., 2007). Dans le cas de TiO_2, le point de charge nulle possède une valeur de pH autour de 6 (Selcuk et al., 2003). Sous ces conditions, la surface de TiO_2 est neutre et l'interaction électrostatique entre le polluant et le TiO_2 est absente. La surface du catalyseur est chargée négativement (TiO^-) lorsque des valeurs de pH imposées sont supérieures au point de charge nulle de TiO_2. Une répulsion électrostatique vis-à-vis des composés anioniques prédomine. Cependant, pour des valeurs de pH en dessous du point isoélectrique (ou point de charge nulle), la surface du TiO_2 devient positive ($TiOH_2^+$). Des études effectuées avec quelques composés organiques tels que l'acide humique (Li et al., 2002), le benzotriazole (Ding et al., 2010), le pentachlorophenol (Quan et al., 2007) ont démontré que le maximum de dégradation est plus rapide dans des conditions acides que dans des conditions alcalines.

1.2.4.2.6 *Influence de l'électrolyte*

Dans un procédé électrolytique, l'addition de l'électrolyte joue un rôle essentiel dans le passage de courant à travers la cellule électrochimique. Le passage du courant électrique à travers le milieu aqueux se fait par conductivité ionique, c'est-à-dire que sous l'action du

champ électrique généré entre les deux électrodes. Les espèces ioniques présentes en solution vont donc migrer vers les électrodes et induire des réactions d'oxydo-réduction. Généralement, la conductivité de la solution affecte l'efficacité de l'intensité de courant, la tension et la consommation de l'énergie électrique. La conductivité doit être élevée dans le but d'assurer un bon transfert ionique dans l'effluent. NaCl et Na_2SO_4 sont les deux électrolytes les plus utilisés. D'après l'étude de Wang et al. (2009), le type et la concentration de l'électrolyte affecte le procédé de dégradation PEC. Dans le cas du 4-chlorophenol, la dégradation PEC de ce polluant a été améliorée en augmentant la concentration du Na_2SO_4 de 0.05 M à 0.2 M. De même, un meilleur taux d'élimination du pentachlorophenol a été enregistré en augmentant la concentration du Na_2SO_4 de 0.005 M à 0.01 M (Quan et al., 2007). Durant le procédé PEC, l'addition d'un électrolyte améliore la conductivité de la solution, facilite le passage du courant électrique dans la solution et par conséquent évite toute recombinaison entre les électrons et les trous photogénérés.

1.2.4.2.7 *Influence de la température*

La température est un paramètre qui influence les réactions photo-catalytiques. Une augmentation de la température (T > 80°C) favorise la recombinaison des charges (e^-/h^+) et réduit l'adsorption des composés organiques sur la surface de TiO_2 (Chong et al., 2010). Malato et al. (2009) prévoit qu'une température entre 20°C et 80°C est considéré comme optimale pour assurer une meilleure photo-minéralisation des polluants. En se basant sur l'étude de Chen et Ray (1998), la dégradation du 4-chlorophenol (20 mg L^{-1}) est meilleure lorsque la température passe de 288 K à 323 K. L'augmentation de la température favorise la fréquence de collision des molécules dans la solution et augmente ainsi le taux de dégradation des polluants. Ceci a été prouvé par l'équation de Van't Hoff-Arrhenius (Équation 1-26) dont la constante k de la réaction est proportionnel à exp (-1/T).

Équation 1-26 $$Ln\left(\frac{k_1}{k_2}\right)=-\frac{E_a}{R}\left(\frac{1}{T_2}-\frac{1}{T_1}\right)$$

Ou k_1 et k_2 sont les constants de la température T_1 et T_2, respectivement; E_a est l'énergie de l'activation et R est la constant de gaz.

1.2.4.2.8 *Influence du transfert de masse*

Il est connu que les conditions hydrodynamique (ou le coefficient de transfert de masse) à l'intérieur du réacteur sont fortement liées à la configuration et à la conception de la cellule (Kim et al., 2003; Chen, 2004; Rajeshwar et Ibanez, 1997). Durant l'oxydation PEC, les polluants doivent être transportés vers la photo-anode et puis oxydés à la surface du catalyseur (TiO_2). Cependant, des essais complémentaires sont nécessaires pour déterminer la valeur du coefficient de transfert de masse et pour étudier les conditions hydrodynamiques du réacteur.

1.2.4.2.9 *Effet de la structure cristallographique de TiO_2 (anatase versus rutile) dans l'UV*

Le TiO_2 existe sous plusieurs phases cristallographiques, dont les plus connues sont le rutile, l'anatase et la brookite. Seuls l'anatase et le rutile sont les plus utilisés dans les réactions photocatalytiques car ils présentent une bande interdite, respectivement de 3,23 eV (387 nm) et 3,02 eV (405 nm), qui correspondent au domaine ultraviolet et une petite partie du visible (Figure 1-5) (Rivera et al., 1993; Ye et al., 1997; Thiruvenkatachari et al., 2008 ; Egerton et al., 2004). Toutefois, l'anatase est reconnue pour être la phase la plus active en photocatalyse grâce à un niveau de Fermi un peu plus élevé et a sa forte capacite d'adsorption de l'oxygéne (Linsebigler et al., 1995). Ainsi, le piégeage des électrons est plus efficace et la recombinaison des charges (électron-trou) est limitée (Sclafani et Herrmann 1996).

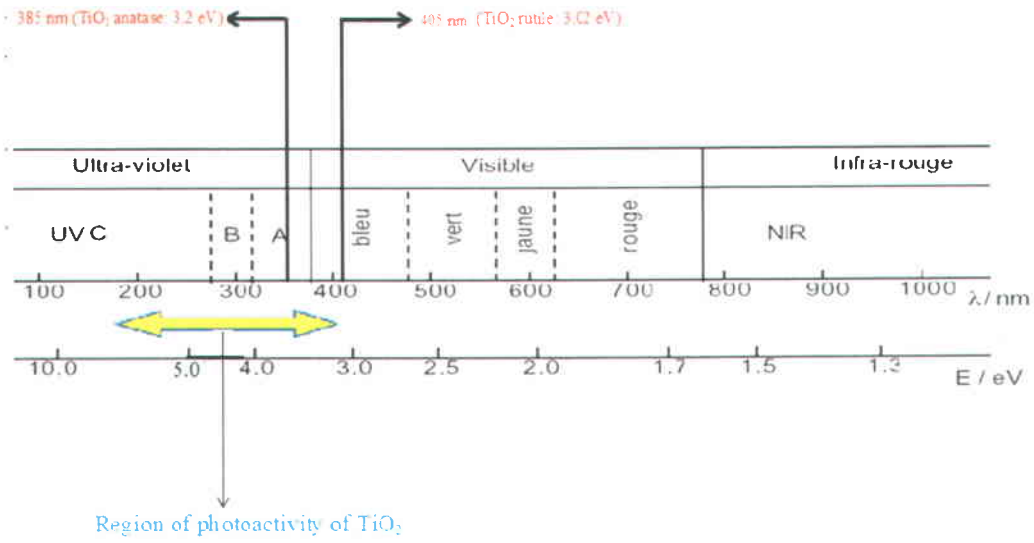


Figure 1-5 Région UV pour la photo-activitée de TiO_2

Le TiO_2 anatase est une phase métastable, alors que le TiO_2 rutile est une phase stable. Les deux formes de TiO_2 cristallisent dans un systéme quadratique. Une maille cristalline de rutile contient deux unités de TiO_2, dans lesquelles un atome de Ti est entouré de 6 atomes d'oxygénes voisins, via deux liaisons longues (en position axiale) et 4 liaisons courtes (en position équatoriale) (Figure 1-6a). Les longueurs des liaisons sont de 1,976 Å et 1,946 Å respectivement. Chaque atome d'oxygéne est relié à trois atomes Ti par l'intermédiaire d'une liaison longue et de deux liaisons courtes.

Par comparison, une maille tétragonale de la forme anatase contient quatre unités TiO_2 (Figure 1-6b). La coordination des atomes de Ti et O est la même que dans le rutile, mais l'octaèdre est plus déformé avec une longueur de liaison Ti-O de 1,979 Å (en position axiale) et 1,932 Å en position équatoriale (Angenault 2001). Pour des tailles de particules inférieures à 14 nm, Zhang et Banfield ont montrés que l'anatase devient plus stable que le rutile (Zhang

et Banfield 1998). Plus de détails sur les chracatéristiques des deux formes cristallographiques anatase et rutile de TiO_2 sont présentés dans le Tableau 1-9.

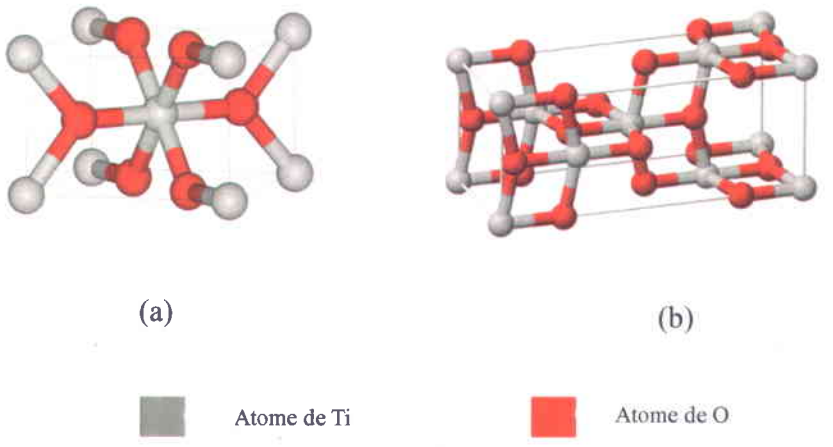


Figure 1-6 Représentation schématique de la maille cristalline a) Rutile et b) Anatase

Tableau 1-9 Charactéristiques des deux formes cristallographiques de TiO_2 : Anatase et Rutile

Paramétres	Anatase	Rutile
Structure cristalline	Quadratique	Quadratique
Stabilité	Thermodynamiquement métastable	Thermodinamiquement stable
Elaboration	Faible température	Haute température
Surface spécifique	Elevée	Faible
Bande gap (ev)	3,2	3,02
Bande d'absorption (nm)	385	405
Paramétres de maille	a = 3,7852; c = 9,5139	a = 4,5930; c = 2,9590
Photoconductivité	Elevé	Faible
Activité	Plus active en photocatalyse	Moins active en photocatalyse
Mobilité de charges	Charges plus mobiles	Charges moins mobiles
Densité	3,89	4,27

1.2.4.3 Photo-réactivité de TiO_2 dans le visible

La complexité d'un procédé de traitement d'effluents peut constituer un obstacle majeur à son application à grande échelle. La forme anatase de TiO_2 souvent employée dans les procédés photo-catalytiques peut absorber les photons UV ayant une longueur d'onde ≤ 385 nm (Ren et al., 2007). Pour rendre le TiO_2 photosensible dans la partie visible du spectre solaire (qui offre 4 fois plus de photons que dans l'UV), il est possible de réduire sa bande interdite par l'ingénierie du dopage par l'azote (Figure 1-7) et/ou par les défauts structurels liés aux vacances d'oxygène (i.e.; contrôle du bombardement ionique pendant la croissance des films par plasma de pulvérisation magnétron). De telles photoanodes actives dans le visible permettraient de développer une technologie d'oxydation PC plus efficace et permettant

d'utiliser directement le rayonnement solaire, contribuant ainsi à réduire les coûts du traitement. Le développement de telles photoanodes qui absorberaient dans le visible devrait prendre en compte les critères suivants : (*i*) une bande interdite la plus étroite possible en deçà de 3.0 eV ; (*ii*) des potentiels appropriés pour la BV et la BC de TiO_2 pour assurer les réactions d'oxydo-réduction et; (*iii*) la mobilité des charges entre la BV et la BC de TiO_2. Plusieurs approches peuvent être utilisées pour étendre la réponse spectrale du TiO_2 dans la région du visible. La technique de dopage de TiO_2 par des cations (Fer, zinc, nickel, cérium, etc) ou par des anions (azote, sulfure, carbone, etc.) ont fait l'objet de plusieurs travaux de recherche (Zhang et al., 2012; Valentin et al., 2007; Wang et Lewis, 2005; Chen et al., 2007; Parck et al., 2006). D'autres travaux ont été plutôt orientés vers le couplage de TiO_2 avec d'autres semi-conducteurs photoactifs dans le visible (ex. WO_3, CdS, SnO_2, FeO_3, etc) (Ouyang et al., 2012; Robert, 2007; De Tacconi et al., 2003 ; Zhang et al., 2009). Bien que le dopage de TiO_2 avec des cations (Ga^{3+}, Cr^{3+}, Al^{3+}) assure l'extension de la réponse spectrale de TiO_2 vers le visible, ces derniers peuvent cependant constituer un centre de recombinaison pour les paires (e^-_{CB}/h^+_{VB}) photo-créées, réduisant même l'activité photocatalytique (Burda et al., 2003; Di Paola et al., 2001).

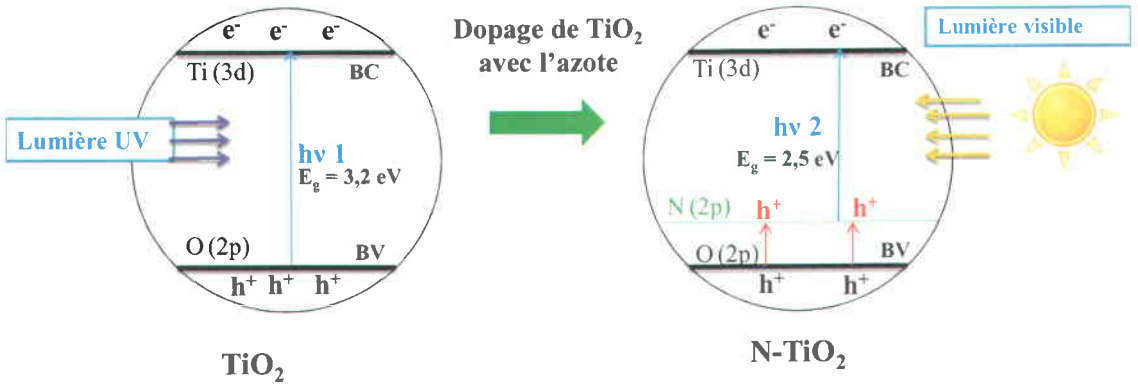


Figure 1-7 Structure schématique du niveau d'énergie de TiO_2 dopé à l'azote.

En particulier, le dopage à l'azote peut être avantageusement utilisé pour réduire la bande interdite du TiO_2:N à au moins 2.25 eV (qui correspond au maximum de l'insolation). Des travaux antérieurs ont rapporté la possibilité de réduire la bande interdite du TiO_2 (à 2.55 eV) par dopage d'azote (Wang et Lewis, 2006). Il est important de souligner que l'azote a la capacité de remplacer simultanément les atomes d'oxygène et de titane dans la structure cristalline de TiO_2 pour former des composés du type $Ti_{1-y}O_{2-x}N_{x+y}$ (Rehman et al., 2009; Peng et al., 2008). La substitution de l'oxygène par l'azote peut être cependant complexe car le rayon ionique de l'azote (1.71 A°) est supérieur à celui de l'oxygène (1.4 A°) (Guo et al., 2007). Le dopage du TiO_2 à l'azote consistera à remplacer trois molécules d'oxygène avec deux molécules d'azote dans l'optique de maintenir l'électroneutralité et former des lacunes

d'oxygène. Ces lacunes d'oxygène favorisent l'activation de TiO_2 dopé dans la région du visible. Cependant, la concentration de l'azote utilisée pour le dopage de TiO_2 reste un facteur critique qui influence l'activité PC de TiO_2 dopé à l'azote (Wang et Lewis, 2006).

Les avantages et les inconvénients de ces différentes approches utilisées pour étendre la réponse spectrale de TiO_2 vers la région du visible ainsi que les différentes applications PC du TiO_2 modifié seront plus détaillés dans le chapitre 4 relatif à l'article synthèse :

Rimeh Daghrir, Patrick Drogui, Didier Robert (2013) Modified TiO_2 for environmental photocatalytic applications: a review. Industrial & Engineering Chemistry Research, 52: 3581-3599.

1.2.4.4 Applications de la photoélectrocatalyse pour le traitement de divers types d'effluents

L'application des procédés PEC utilisant le TiO_2 comme photocatalyseur pour la dégradation des polluants organiques réfractaires présent dans les eaux et les eaux usées a reçu un intérêt considérable dans le domaine de la protection environnementale. La photoélectrocatalyse a été utilisée pour le traitement d'effluent toxique contenant divers types de polluants organiques (ex. des colorants, des composés phénoliques et des substances humiques) et microbiens (ex. E. coli). Le procédé d'oxydation PEC a été largement appliqué pour la dégradation et la minéralisation de différents types de colorants (Azo orange II, Rose bengal, Bleu Brilliant, etc) présents dans les eaux usées de textiles ainsi que des eaux de surfaces (Xu et al., 2008; Li et al., 2000 ; Fraga et al., 2009 ; Esquivel et al., 2009). En particulier, Esquivel et al (2009) en appliquant la technique de la photoélectrocatalyse à des eaux usées de textiles contenant le colorant orange azo obtiennent des taux d'élimination du COT de 57%, alors que des taux allant jusqu'à 63% du COT ont été éliminé lors du traitement des eaux usées de textiles contenant le colorant orange disperse (Paschoal et al., 2009). En outre, plusieurs

études ont démontré le potentiel de la photoélectrocatalyse pour la dégradation de divers types de polluants réfractaires tels que par exemple le bisphénol A (Xie et Li, 2006), le pentachlorophenol (Quan et al., 2007), le rhodamine B (Li et al., 2006) et le benzotriazole (Ding et al., 2010) parmi d'autres polluants. Les différentes applications récentes du procédé d'oxydation PEC ainsi que son efficacité pour le traitement de différents types de polluants seront indiquées dans le chapitre 3 présenté sous formes d'article synthèse:

Rimeh Daghrir, Patrick Drogui, Didier Robert (2012) Photoelectrocatalytic technologies for environmental applications. *Journal of photochemistry and photobiology A : Chemistry 238:41-52.*

1.3 Hypothèses de travail et objectifs de recherche

1.3.1 Hypothèses

Les eaux résiduaires traitées par les filières conventionnelles d'assainissement des eaux contiennent encore des quantités non négligeables de polluants organiques réfractaires, notamment des résidus médicamenteux. Au nombre de ces résidus médicamenteux décelés dans les rejets municipaux et industriels, se trouvent des antibiotiques, des hormones et des dérivés hormonaux, etc., lesquels composés sont à l'origine de nombreuses perturbations de la faune aquatique et constituent un risque pour la santé humaine. Dans l'optique de limiter l'arrivée de ces divers types de contaminants (notamment les résidus médicamenteux) dans l'environnement, ces eaux usées résiduaires doivent être soumises à des traitements plus poussés. Des stratégies de traitement efficaces devront être adoptées par les industries, les scientifiques et gestionnaires pour limiter ces rejets. C'est dans cette optique que la technique de photoélectrocatalyse a été proposée afin d'améliorer l'efficacité épuratoire lors du traitement des eaux usées résiduaires. Cette technique d'oxydation PEC devrait permettre de réagir sur les doubles liaisons -C=C- et attaquer les noyaux aromatiques, composants majeurs des résidus médicamenteux de type antibiotique des eaux usées résiduaires.

1.3.1.1 Hypothèse I : Allongement de la durée de vie des paires électron-trou (e^-_{BC}/h^+_{BV}) par ajout de la dimension électrolytique à la photocatalyse.

La durée de vie des paires électron-trou (e^-_{CB}/h^+_{VB}) dans un procédé de photo-catalyse conventionnel est dans le régime de la nanoseconde. La recombinaison prématurée des paires électron-trou limite la photocatalyse conventionnelle et est souvent à l'origine d'une oxydation partielle des contaminants. Le potentiel externe appliqué par électrolyse (ajout de la dimension électrolytique à la photocatalyse) est capable de retarder la recombinaison des paires (électrons-trous) et d'allonger ainsi leur durée de vie pour oxyder plus efficacement les

polluants jusqu'à leur minéralisation. Les photo-trous (h^+_{BV}) formés peuvent soit, oxyder directement les contaminants adsorbés ou oxyder la molécule H_2O à la surface de TiO_2 (photoanode) pour former des radicaux OH°. Les photoélectrons (e^-) éjectés vers la BC de TiO_2 sont capables de réagir à leur tour avec des accepteurs d'électrons tel que l'oxygène adsorbé (O_2) pour former des EORs (ex. $O_2^{\circ-}$, HO_2°, etc.). Aussi, il est possible que ces photo-électrons soient directement acheminés dans le circuit électrique externe au lieu d'être transférés à l'oxygène moléculaire.

1.3.1.2 Hypothèse II : Forme et structure nanométrique de la photoanode de TiO_2

Les procédés de traitement électrolytique ou photocatalytique des eaux sans ajout de produits chimiques mettent souvent en jeu des réactions de surface (catalyse hétérogène). La structure cristalline, la composition chimique et la morphologie des matériaux (surface spécifique, porosité, etc.) sont parmi les caractéristiques fondamentales qui commandent leur réactivité de surface, et donc leur capacité d'oxydation catalytique (Ohtani et al., 1997; Sun et Xu, 2010; Yu et al., 2007). Comme il s'agit de procédés contrôlés par les réactions de surfaces, les nanomatériaux constituent un substrat catalytique de choix qui offre des rapports surface/volume inégalés (la surface spécifique du TiO_2 serait de plusieurs dizaines de m^2/g et augmente lorsque la taille moyenne des nanocristaux de TiO_2 diminue). Ainsi, le développement de nanomatériaux de TiO_2, dont la capacité photocatalytique serait amplifiée (par la grande surface spécifique accessible) constitue un élément clé pour oxyder plus efficacement les contaminants des eaux jusqu'à leur minéralisation.

1.3.1.3 Hypothèse III : Utilisation d'une cathode appropriée pour la génération simultanée d'un accepteur d'électron

Il est important de souligner que les réactions cathodiques peuvent être mises à profit pour générer simultanément du peroxyde d'hydrogène (H_2O_2) par réduction cathodique de

l'oxygène dissous sur une électrode appropriée. Il est possible de produire le peroxyde d'hydrogène par réduction cathodique de l'oxygène dissous sur une électrode de CV ou de Gr. L'addition *in situ* d'un accepteur d'électron tel que H_2O_2 dans la solution permet d'éviter la recombinaison des électrons-trous photo-générés et augmente ainsi l'efficacité PC. Sous radiation UV, le peroxyde d'hydrogéne se décompose à des radicaux hydroxyles (en plus des radicaux hydroxyles produits sur la surface de la photoanode). Cela suppose que la génération *in situ* de ces EORs (OH°, H_2O_2) dans la solution contribue à améliorer l'efficacité de l'oxydation PEC des polluants organiques réfractaires.

1.3.1.4 Hypothèse IV : Photo-réactivité de TiO_2 par dopage à l'azote

Le dopage anionique du dioxyde de titane permet d'introduire des états d'énergie intermédiaires dans la bande interdite du TiO_2 et permet ainsi d'élargir sa gamme spectrale en l'étendant vers le visible. Par conséquent, cette modification dans la masse de TiO_2 est capable de favoriser l'exploitation des radiations visibles présentes dans le spectre solaire et d'améliorer simultanément les performances des procédés d'oxydation PEC à base de TiO_2 pour des applications environnementales à grande échelle. Cela suppose qu'une telle photoanode de dioxyde de titane dopé à l'azote contribue à réduire les coûts du traitement PEC en exploitant la lumiére visible présente dans le spectre solaire.

1.4 Objectifs de recherche

1.4.1 Objectif Globale

L'objectif général de cette étude consiste à concevoir, tester et optimiser un procédé de traitement d'oxydation PEC utilisant une électrode nano-structurée de TiO_2 comme photo-anode à l'échelle du banc d'essai en laboratoire pour le traitement des eaux résiduaires contenant des résidus médicamenteux de type antibiotique tels que que la CTC.

1.4.2 Objectifs spécifiques

Le *premier objectif* est de concevoir et tester, à l'échelle de banc d'essai en laboratoire, le procédé PEC capable de produire *in situ* des oxydants dérivés de l'oxygène (EORs: OH°, O_3 et H_2O_2, etc.) et ce, pour le traitement des eaux usées résiduaires contaminées par les résidus médicamenteux de type antibiotique. La mise au point de cellules photoélectrocatalytiques (parallélépipédique) permettra d'évaluer la capacité de production des EORs. Le *second objectif* est de développer une méthodologie statistique par une analyse rationnelle de la combinaison des différents facteurs opérationnels dans le but d'atteindre les meilleurs conditions de traitement de la CTC (ou de la carbamazépine (CBZ)) en utilisant le procédé d'oxydation PEC sous rayonnement UV. Le *troisième objectif* vise le développement des méthodes couplées de traitement, mettant en synergie les techniques électrochimiques et les procédés photocatalytiques utilisant les photoanodes nanostructurées (dopées à l'azote) pour la dégradation de la CTC sous rayonnement solaire (simulateur solaire). Le *quatrième objectif* est d'identifier les sous-produits de la CTC et de proposer un mécanisme réactionnel de dégradation du CTC par voie PEC sous radiation solaire. Le *cinquième objectif* est de valider les performances épuratoires du procédé PEC sur un effluent réel de type municipal artificiellement contaminé par la CTC.

1.5 Originalité de l'étude

L'originalité de ce projet de recherche se situe à plusieurs niveaux. Si les procédés électrolytiques et photo-catalytiques ont été séparément étudiés par plusieurs auteurs, la combinaison des deux procédés dans un même réacteur (procédés PEC) n'a pas encore été amplement explorée et constitue la pierre angulaire de ce projet de recherche. L'intérêt de développer des techniques hybrides profitant de la synergie des mécanismes photoéléctrocatalytiques réside dans leur aspect non polluant, leur facilité d'automatisation ainsi que leur capacité d'action à deux niveaux sur les polluants (action directe et indirecte). Bien que des études récentes ont exploité les procédés d'oxydation PEC pour la dégradation des pollunants organiques réfractaires tel que le Bisphenol A, le benzotriazole, le pentachlorophenol, etc., cette technique a été rarement appliquée pour le traitement des effluents médicamenteux de type antibiotique. Ce travail contribuera donc à élargir les applications des procédés PEC, une technologie propre et économiquement viable, dans l'industrie des électrotechnologies environnementales.

1.6 Démarche méthodologique

Les premiers travaux ont consisté en la conception et au montage de la cellule du procédé PEC. La partie subséquente portait sur l'évaluation et la caractérisation de la cellule PEC en termes de sa capacité de production des EORs (ex. H_2O_2, O_3, HO°, etc.). Par la suite, la performance du procédé PEC a été évaluée sur une solution synthétique artificiellement contaminée par la CTC. Les performances épuratoires du procédé PEC ont été comparées avec les procédés de photocatalyse conventionnelle (PCC), de photolyse directe (PD) et d'électro-oxydation (EO). Par la suite, l'optimisation du système PEC pour la dégradation du CTC (sous rayonnement ultraviolets) a été effectuée grâce à une stratégie expérimentale basée sur une étude quantitative des facteurs (matrice factorielle), suivie du plan de surface de réponse. Subséquemment, le procédé PEC a été testé sous simulateur solaire (dans le visible) à l'aide d'une photanode nanostructurée de dioxyde de titane dopé à l'azote (n-TiO_2 : N) pour la dégradation du CTC en solution synthétique et dans un effluent réel de type municipal. Finalement, dans l'optique d'étendre son spectre d'activité, le procédé PEC a été testé pour la dégradation d'un autre polluant de type pharmaceutique, la CBZ couramment rencontrée dans les eaux usées résiduaires. Une description schématique de la démarche méthodologique suivie est présentée à la Figure 1-8.

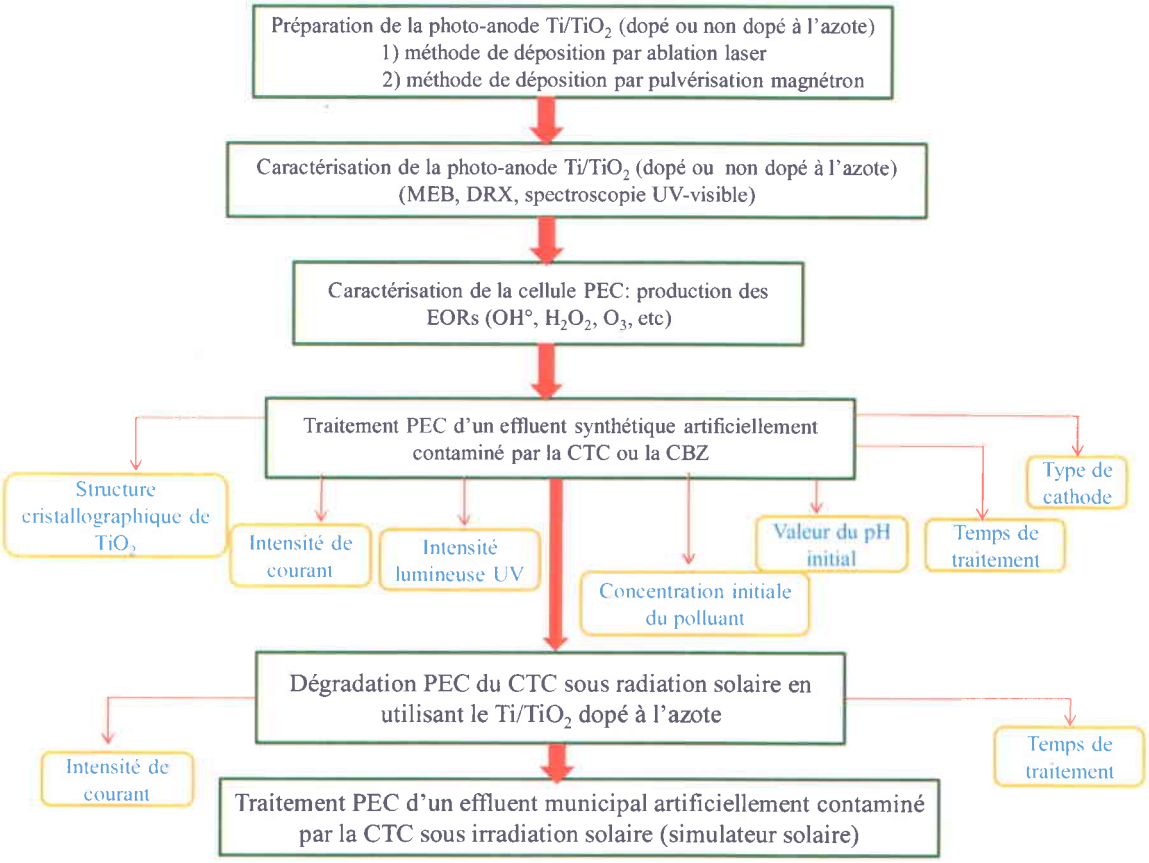


Figure 1-8 Description schématique de la démarche méthodologique suivie.

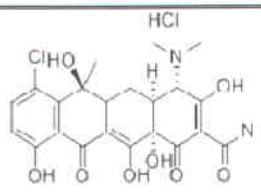
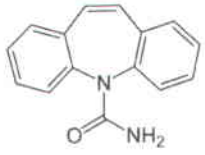
1.6.1 Polluants étudiés

La CTC est le polluant qui a été principalement étudié. La CTC est un exemple d'antibiotique très répandu dans le monde et principalement employé dans les industries d'élevage ainsi que dans le secteur agricole (Jeong et al. 2010; Yang and Carlson 2004; Lopez Penalver et al. 2012). La solubilité élevé de la CTC dans l'eau (0.008 moL L^{-1}) ainsi que son faible coefficient de partition eau-octanol (Log K_{ow} = -0.62) définie son caractère hydrophile (Lopez-Penalver et al., 2010; Kim et al., 2009). Le rejet des antibiotiques dans l'environnement aquatique représente un sujet de précaution en raison de leur impact potentiel sur les êtres vivants. Après utilisation, seulement une faible proportion des antibiotiques ingérés est métabolisée, la majorité est ainsi excrétée à travers les urines et les excréments des animaux sous la forme active. Le résidu de ces antibiotiques rejeté par les stations d'épuration des eaux usées est généralement détecté dans les eaux de surface, les eaux souterraines, les eaux usées et même dans les eaux potables à des concencentrations allant de 61 ng L^{-1} à 32 µg L^{-1} (Li et al. 2011; Hernandez et al. 2007; Lopez Pen˜alver et al. 2012; Jeong et al. 2010 ; Batt et al., 2007; Kolpin et al., 2002; Kay et al., 2005). Grâce aux groupements fonctionnels chargés (phénol, amine, alcool, etc) présent dans la molécule de CTC, divers interactions peuvent exister entre les multiples fonctionnalités et peuvent fortement influencer leur enlèvement dans les eaux usées.

La CBZ a également été étudiée afin d'élargir le domaine d'activité du procédé PEC. La CBZ est un antidépressif utilisé principalement pour soigner l'épilepsie, pour contrôler les douleurs chroniques ainsi que pour traiter les différents troubles et maladies mentales (Chong et al., 2012; Scheytt et al., 2005; Martinez et al., 2011). Une fois que la CBZ est administrée, son absorption dans le corps est lente avec environ 2 à 3% de la dose appliquée est excrétée à travers l'urine. Approximativement, 72% de la dose de CBZ administrée par voie orale est absorbée, alors que 28% reste inchangée et est excrétée à travers les selles (RxList, 2006). La

CBZ ne peut être traité efficacement par les filières de traitement classique des eaux et se retrouve ainsi dans les eaux de surface, les eaux souterraines et même dans l'eau potable à des concencentrations allant de 60 ng L^{-1} jusqu'à 800 ng L^{-1} (Calisto et al., 2011 ; Ternes et al., 1998). Les propriétés physico-chimiques des différents polluants étudiés sont présentées dans le Tableau 1-10.

Tableau 1-10 Propriétés physico-chimique des polluants étudiés.

Polluant	Formule moléculaire	Structure chimique	Poids moléculaire ($g.mol^{-1}$)	Solubilité ($mg.L^{-1}$)	Log K_{ow}
Chlorotétracycline (CTC)	$C_{22}H_{24}Cl_2N_2O_8$		515.3	0.008	-0.62
Carbamazépine (CBZ)	$C_{15}H_{12}N_2O$		236.26	112	2,45

1.6.2 Préparation de solutions synthétiques

Les solutions synthétiques de CTC et de CBZ ont été préparées individuellement à partir d'eau distillée et de composés organiques de grade analytique provenant de la compagnie Sigma Aldrich (Ontario, Canada). La solution synthétique de CTC a été préparée en ajoutant 100 mg de CTC à un volume de 2.0 L d'eau distilée. La solution est maintenue sous agitation magnétique jusqu'à dissolution compléte de la CTC. La solution synthétique de CBZ a été préparée en ajoutant 28.6 mg de CBZ à un volume de 1L d'eau distilée. La solution est maintenue sous agitation magnétique jusqu'à dissolution compléte de la CBZ. Par la suite ce mélange a été dilué pour atteindre des concentrations finales de CBZ de 20 mg L^{-1} et de 10 mg L^{-1}. Une conductivité minimale de la solution synthétique est nécessaire pour assurer la conductivité de la solution synthétique. Le sulfate de sodium est ajouté à cette solution synthétique dans une gamme de concentration allant de 0.05 mol L^{-1} à 0.07 moL L^{-1}.

1.6.3 Échantillonnage et caractérisation des eaux réelles

Dans l'optique d'évaluer l'efficacité du procédé d'oxydation PEC sur des effluents réels contenant des micropolluants organiques, des échantillons des eaux usées ont été prélevés et

artificiellement contaminés par la CTC (100 µg L^{-1}). Ces effluents proviennent de la station municipale d'eaux usées de la ville de Québec. La filière de traitement de cette station se compose d'un prétraitement comprenant un dégrillage et un dessablage, d'un traitement primaire caractérisé par une décontamination gravitaire, suivi d'un traitement secondaire par biofiltration et enfin d'un traitement de désinfection aux ultraviolets fonctionnant exclusivement en période estivale. Une description détaillée de la filière de traitement des eaux usées de la station municipale de la ville de Québec est présentée dans la Figure 1-9. Les effluents utilisés dans le cadre de cette étude ont été prélevé après traitement secondaire, à la sortie d'une unité de biofiltration. L'échantillonnage de ces effluents a été effectué deux fois durant le mois d'Avril. Les effluents ont été prélevés dans des contenants en polypropylène et conservés dés leur réception dans une chambre froide à 4°C jusqu'à leur utilisation. L'effluent prélevé se caractérise par une DCO = 56.7 ± 9 mg L^{-1}, un COT = 16.5±1.2 mg L^{-1}, un azote totale (NT) = 17.9±2.2 mg L^{-1}, des coliformes fécaux (CF) = 1900 ± 565 UFC/100 mL, $[NH_4^+]$ = 10.5 ± 0.3 mg L-1, un pH = 6.9 ± 0.18 et une conductivité de 1018 ± 12 µs cm^{-1}. Les échantillons ont été collectés et stockés dans des bouteilles en propylène et conservé à 4°C.

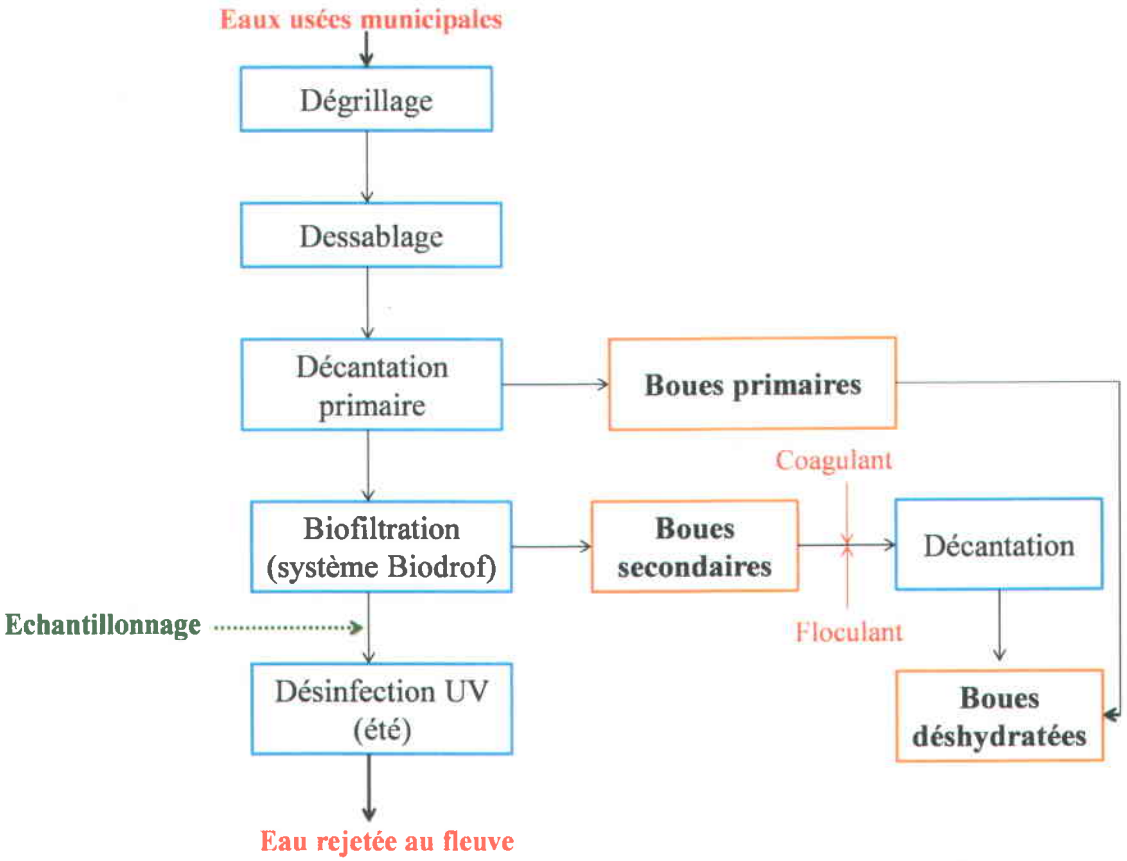


Figure 1-9 **Filière de traitement des eaux usées de la station d'épuration de la ville de Québec (Secteur Est), Canada.**

1.6.4 Préparation de la photoanode Ti/TiO_2

Les revêtements du TiO_2 sont préparés en utilisant la méthode de déposition par ablation laser (Figure 1-10). Des radiations laser (λ = 248 nm, durée de l'impulsion est de 15 ns) ayant un taux de répétitions de 30 Hz ont été opérées à un angle d'incidence de 45° sur une cible tournante de TiO_2 (une pureté de 99.95%). La densité énergétique des radiations laser a été fixée à 4.5 J cm^{-2}. Les films de TiO_2 sont déposés sur des grilles de titanes (pour des études photoélectrocatalytique) et sur un substrat de silicium (pour des buts de caractérisation du matériau). Les films de TiO_2 sont déposés à une température de 600°C et 400°C, respectivement, sous une pression d'oxygène de 1 mTorr. L'épaisseur nominal du revêtement de TiO_2 a été estimé à 400 nm pour la forme rutile et 1 µm pour la forme anatase. L'épaisseur du film a été déterminée directement à partir de la section transversale en utilisant la microscopie électronique à balayage (MEB). La structure cristallographique des films de TiO_2 a été examinée par la technique de la diffraction des rayons X (DRX) utilisant un diffractomètre de type Philips X'pert-MPD X (des radiations Cu K_α) ayant un angle d'incidence de 1°.

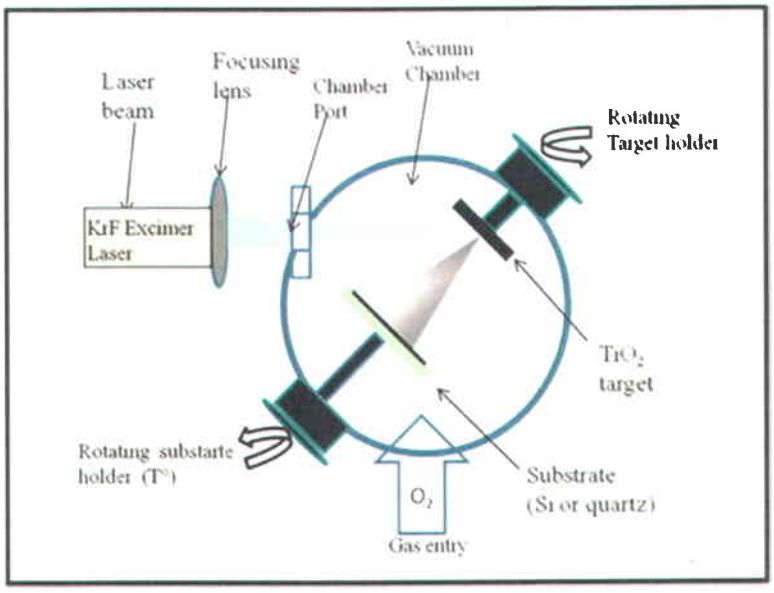


Figure 1-10 Description schématique de la déposition d'un revêtement de TiO2 par ablation laser.

1.6.5 Préparation de la photoanode Ti/TiO_2 dopé à l'azote

Les photoanodes ont été préparées en déposant les revêtements de TiO_2 dopés à l'azote sur des grilles de titane en utilisant la technique de pulvérisation magnetron à haute fréquence (Figure 1-11), qui permet leur dopage *in situ* par l'incorporation de l'azote gazeux (N) avec l'argon (Ar). La teneur en azote des revêtements de TiO_2 dopés est contrôlée en ajustant le rapport du débit de gaz $[N_2]$ / ($[Ar] + [N_2]$) au cours du processus de pulvérisation-déposition, tout en maintenant la pression totale à 1,4 mTorr dans la chambre de dépôt. Avant le dépôt et entre chaque dépôt, la pression de la chambre de fond a été maintenu à une valeur d'ultravide aussi bas que ~ 2 x 10^{-8} Torr. La température de déposition des revêtements a été maintenue à 650 ° C, tandis que la puissance de radiofréquence pour la pulvérisation magnétron a été fixée à 350 W. Plus de détails expérimentaux sur notre système de pulvérisation magnetron peuvent être trouvées ailleurs (Brassard et al, 2006; Hajjaji et al., 2011). Ainsi, des photoanodes de TiO_2 dopés ayant des teneurs d'azote allant de 0 à environ ~6 at.% ont été réalisés.

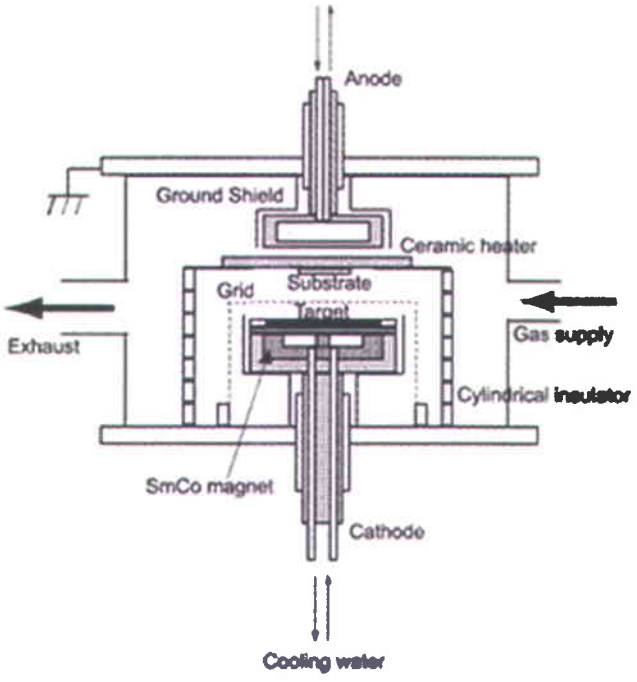


Figure 1-11 Description schématique de la technique de pulvérisation magnetron à haute fréquence.

1.6.6 Préparation des électrodes de carbone amorphe

Les films de carbone amorphe (a-C) sont déposés en utilisant la méthode de déposition par ablation laser. Des radiations laser (λ = 248 nm, durée de l'impulsion est de 15 ns) ayant un taux de répétitions de 30 Hz ont été opérées à un angle d'incidence de 45° sur une cible tournante de graphite (une pureté de 99.95%). La densité énergétique des radiations laser a été fixée à 4.5 J cm^{-2}. Les revêtements de carbone amorphe sont déposés sur un disque de titane ayant un diamètre de 1 cm (pour des buts d'analyses) et sur des grilles de titane spécialement désignées pour des études photoélectrocatalytique. Les films de carbone amorphe sont déposés à deux températures différentes : 20°C et 600°C. L'épaisseur du film du revêtement du carbone amorphe (500 nm) a été déterminée directement à partir de la section transversale en utilisant la MEB.

1.6.7 Montage et caractéristiques des cellules d'oxydation PEC

1.6.7.1 Cellule d'oxydation PEC C1

L'application du traitement d'oxydation PEC a été effectuée en premier lieu dans un réacteur fait en matériaux acrylique et ayant une capacité de 1 L avec des dimensions de 12.7 cm de largeur, 16.51 cm de longueur et 11.43 cm de profondeur. Une fenêtre en quartz (8.89 cm x 8.89 cm) a été disposée sur l'une des faces du réacteur. Cette cellule PEC est constituée d'une électrode anodique et une électrode cathodique rectangulaire placées verticalement et connectées individuellement au générateur de courant. Ces électrodes qui disposent d'une surface de 110 cm^2 sont placées en parallèle avec une distance inter-électrode de 1 cm (Figure1-12). Le matériau constituant l'anode est du titane recouvert de l'oxyde de titane (Ti/TO_2) alors qu'au niveau de la cathode des électrodes de Gr, CV, inox et a-C nano-structuré ont été utilisées. Ces électrodes sont disposées sur un support perforé en plexiglas situé à 2 cm du fond.

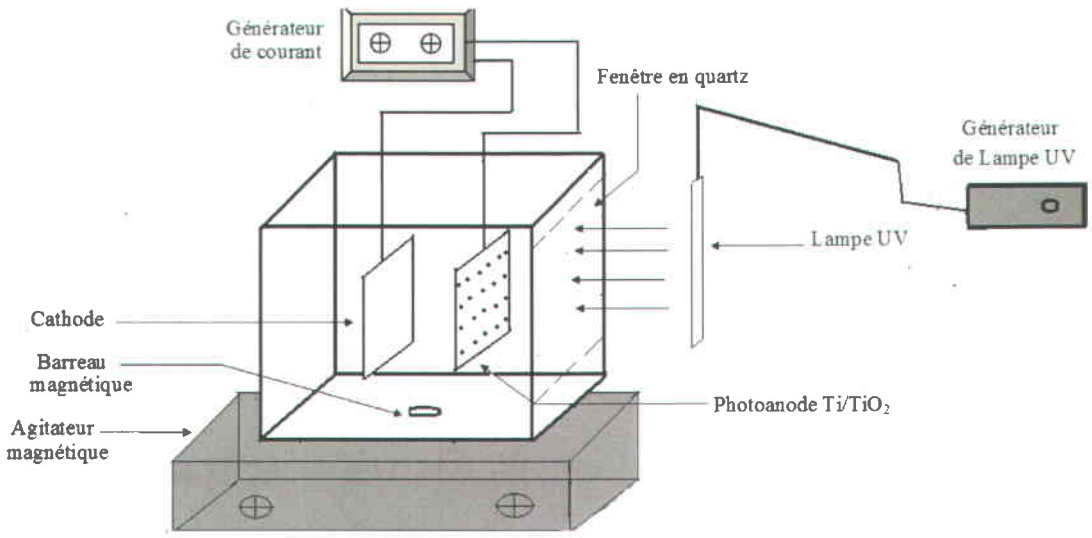


Figure 1-12 Structure schématique de la cellule d'oxydation PEC C1.

1.6.7.2 Cellule d'oxydation PEC C2

L'application du traitement d'oxydation PEC a été effectuée en deuxième lieu dans un réacteur fait en matériaux PVC et ayant une capacité de 1 L avec des dimensions de 10 cm de largeur, 10 cm de longueur et 13 cm de profondeur. Cette cellule d'oxydation PEC est constituée de deux électrodes cathodiques placées verticalement et connectées individuellement au générateur de courant. Des électrodes de CV ayant une surface pleine de 24 cm^2 (6 cm de hauteur et 4 cm de largeur) sont situées à 6 cm appart et sont utilisées à la cathode. Le matériau constituant l'anode (6 cm de hauteur et 4 cm de largeur) est du titane recouvert par l'oxyde de titane (soit le Ti/TiO_2 dopé ou non dopé à l'azote) placé horizontalement entre les deux électrodes cathodiques. Ces électrodes sont disposées sur un support perforé également en plexiglas situé à 2 cm du fond (Figure 1-13).

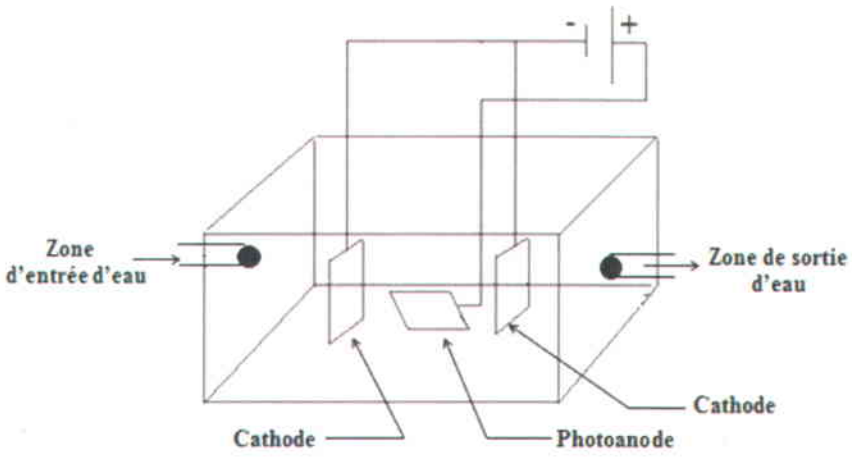


Figure 1-13 Structure schématique de la cellule d'oxydation PEC C2.

1.6.8 Fonctionnement de l'unité expérimentale

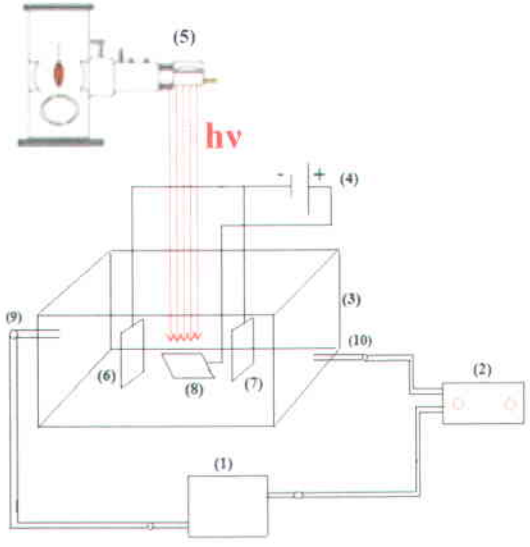
Deux unités expérimentales (U1 et U2) ont été utilisées pour le traitement d'oxydation PEC. La première utilisait la cellule C1 et fonctionnait en mode batch (en mode statique) ou le mélange dans la cellule était assuré par une agitation mécanique ; la deuxième utilisait la cellule C2 et où la circulation ou la recirculation de l'effluent était assuré par une pompe.

1.6.8.1 Unité expérimentale U1

L'unité expérimentale décrite schématiquement en Figure 1-12 fonctionnait en mode batch avec un volume utile de 1.0 L. L'agitation dans la cellule C1 était assurée par un agitateur magnétique placé au fond de la cuve. Des intensités de courant variant entre 0.02 A et 0.59 A ont été imposées pendant une période de temps variant entre 20 et 140 min. Les électrodes sont connectées à un générateur de courant de modèle 3030D, Circuit-Test Electronics (Burnaby, BC, Canada) permettant de délivrer une intensité maximale de 3.0 A et une tension maximale de 30 V. Deux lampes de mercures ayant une longueur d'onde de 254 nm (intensité lumineuse = 6.9 mW cm^{-2}) et 365 nm (intensité lumineuse = 0.3 mW cm^{-2}) ont été utilisées durant le traitement PEC pour irradier la surface catalytique de la photo-anode Ti/TiO_2. La lampe est positionnée verticalement sur un support à l'intérieur (ou à l'extérieur) du réacteur. L'intensité lumineuse est mesurée à l'aide d'un photomètre de Modèle PS-3, 99-0057-01(compagnie UVP, USA). Pour éviter toute interférence avec la lumière du jour, la cellule photoélectrocatalytique est placée dans une chambre obscure. Tous les essais d'oxydation PEC ont été effectués à une température ambiante (25°C). Au cours de chaque essai, le pH a été mesuré avant et après traitement. Un apport en électrolyte de Na_2SO_4 (Laboratoire MAT, Québec, Qc, Canada) dans des concentrations de 0.05 mol L^{-1} a été utilisé pour améliorer la conductivité.

1.6.8.2 Unité expérimentale U2

L'unité expérimentale décrite schématiquement en Figure 1-14 fonctionne en circuit fermé. Ce système PEC est constitué d'un réservoir en PVC d'une capacité de 0.6 L (1), d'une pompe de recirculation (2), d'une cellule PEC C2 (3), d'un générateur de courant (4) et d'un simulateur solaire (5). La pompe (Master flex, Model 77200-50, USA) fixée à un débit de 0.25 L min^{-1} assure la recirculation de l'eau à travers le système. Les électrodes sont connectées à un générateur de courant de modèle 3030D, Circuit-Test Electronics (Burnaby, BC, Canada) permettant de délivrer une intensité maximale de 3.0 A et une tension maximale de 30 V. La photoanode (Ti/TiO_2 dopé et non dopé à l'azote) a été illuminée sous des radiations visibles en utilisant un simulateur solaire modèle SS50AAA (Photo émission Tech., INC, Camarillo, USA) équipé avec une lampe xénon de 150 W. Toutes les expériences ont été effectuées sous des conditions d'illumination solaire de 1.5 AM. Pour tous les tests, un volume total de 0.6 L a été utilisé. Une concentration de 0.07 mol L^{-1} en électrolyte de Na_2SO_4 (Laboratoire MAT, Québec, Qc, Canada) a été ajoutée dans l'effluent synthétique pour améliorer sa conductivité électrique.



(1) Réservoir PVC (0.6 L)

(2) Pompe de recirculation

(3) Cellule d'oxydation photoélectrocatalytique

(4) Générateur de courant

(5) Simulateur solaire

(6) cathode : carbone vitreux

(7) cathode : carbone vitreux

(8) Photoanode : Ti/TiO_2 dopé ou non dopé à l'azote

(9) Zone d'entré de l'eau

(10) Zone de sortie de l'eau

Figure 1-14 Structure schématique de l'unité expérimentale U2.

1.6.9 Méthodologie de plan d'expérience

Le recours à l'utilisation de plan d'expérience dans le domaine du développement de procédés est un outil indispensable afin d'appréhender correctement les différents mécanismes de fonctionnement d'un processus expérimental (Myers and Montgomery, 2002; Olmez, 2009). La méthodologie de plan d'expérience est l'une des méthodes d'analyses statistiques et mathématiques permettant dans une optique d'optimisation, de prédire avec justesse une réponse comprise dans le domaine expérimental et de caractériser un processus d'une façon très précise. La méthodologie de plan d'expérience permettant avec un minimum d'essais expérimentaux de déterminer les éventuelles interactions entre les différents paramètres régissant ce processus, d'en déduire les éventuelles erreurs d'ajustement du modèle, ainsi que ses éventuelles erreurs expérimentales. Cependant, vu que cette méthode statistique nécessite une multitude de calculs afin de valider le modèle mathématique, un logiciel de plan d'expérience Design-Expert version 7 offrant une multitude de possibilité a été utilisé afin de planifier les expérimentations.

1.6.9.1 Plan factoriel

Le plan factoriel (PF) est l'un des plans expérimentaux les plus courants (Box et al., 2005). C'est un outil de décision qui permet de mettre en évidence très rapidement l'existence d'interaction entre les facteurs. L'hypothèse de base est d'assigner pour chaque facteur sa valeur la plus basse (-1) et sa valeur la plus haute (+1). Ainsi, pour k facteurs, il est possible de construire une matrice d'expérience de 2^k valeurs possibles permettant de planifier les différents essais expérimentaux à réaliser. Le PF est basé sur le critère d'orthogonalité c'est-à-dire que les niveaux de chaque paramètre (-1 et +1) sont combinés les uns avec les autres. Le PF est un outil de décision qui permet d'obtenir le maximum d'informations sur les effets et interactions des différents facteurs influençant la réponse. Néanmoins, il ne peut être utilisé exclusivement pour optimiser un processus.

1.6.9.2 Plan central composite

Le plan central composite (PCC) est un plan de surface de réponse (PSR) qui permet de décrire le processus dans l'ensemble du domaine expérimental, de déterminer les conditions opératoires optimales et d'assurer même une région pour les facteurs pour se rencontrer. Le PCC présente un certain nombre d'avantages tels que : *i)* la capacité d'explorer l'ensemble de la région expérimentale ; *ii)* la possibilité de déterminer le coefficient d'ajustement en utilisant une équetion polynomiale du second ordre et *iii)* la facilité d'interpoler la réponse (Myers and Montgomery, 2002 ; Zaviska et al., 2011). Le PCC s'avère très intéressant d'un point de vue expérimental car celui-ci est basé sur un PF (2^k) complété par un plan en « étoile » ou chaque facteur varie un à un à une distance ± α du centre (les autres facteurs sont au centre du domaine). Le PCC utilise 5 niveaux pour les facteurs expérimentaux. Il permet ainsi à partir d'un PF d'évoluer progressivement vers un PSR.

1.6.10 Méthodes analytiques

1.6.10.1 Mesure des paramètres opératoires

Lors de différentes expérimentations, des mesures de pH et de la conductivité ont été effectué afin de suivre le bon fonctionnement du processus d'oxydation PEC, de comprendre les différents mécanismes mis en jeu et d'établir certaine conclusion en terme d'efficacité. Les mesures du pH ont été effectuées en utilisant un pH-mètre (Fisher Acumet, modèle 915) équipé d'une électrode Cole-Palmer à double jonction (référence Ag/AgCl). Un conductimètre (Oakton, modèle 510) a été également utilisé afin de déterminer la conductivité électrique de l'effluent traité et non-traité.

1.6.10.2 Mesure des contaminants organiques et inorganiques

La DCO se caractérise par la consommation en oxygène induite lors de l'oxydation de substances organiques et minérales dans l'eau. Cette mesure permet d'évaluer la quantité de

matière organique en solution et par conséquent d'évaluer l'efficacité de dégradation PEC. L'analyse de la DCO a été effectuée selon la méthode prescrite par le ministère du Développement durable de l'Environnement et des Parcs du Québec (Méthode d'analyse-MA.315-DCO 1.1) (CEAEQ, 2012) en utilisant un spectrophotomètre de type Varian UV 0811 M136 (Australie). Pour évaluer le degré de minéralisation du polluant, des mesures du COT et de NT ont été effectuées. Les mesures du COT et de NT ont été effectuées grâce à un appareil TOC-5000A Shimadzu (Corporation Shimadzu, Japon). Les mesures de la concentration des ions ammoniums (NH_4^+), des ions nitrates et des ions nitrites présents dans les eaux usées ont été effectuées en utilisant un auto-analyseur de marque Lachat (modèle FIA+, Zellweger Analytics, Lachat Instruments Division, WI., Etats-Unis).

1.6.10.3 Mesure des contaminants microbiens

L'analyse des CF présents dans les eaux usées municipales (SM-9222D) a été effectuée en duplicata par le laboratoire Bodycote (Québec, Qc, Canada). La technique consiste à recueillir, identifier et dénombrer les bactéries recherchées à la surface des boites de pétrie. Un volume de 1 mL d'échantillon brut est déposé à l'aide d'outils stériles dans un tube stérile contenant 9 mL de solution saline stérile. Les 10 mL de solution sont agité au vortex pendant 5 min. Dans ce tube stérile, l'échantillon d'eau brute est dilué (1 :10) afin d'obtenir une solution d'extraction dont la concentration attendue est entre 30 et 300 colonies sur chaque milieu de culture. Trois dilutions au moins sont étalées sur le milieu de culture solide mFC agar, préalablement coulé dans la boite de pétrie et refroidi dans des conditions aseptiques. Le volume d'étalon est de 100 mL. Chaque concentration est étalée en triplicata. Les boites de pétris sont incubées à l'étuve pendant une période de 24h à 44.5±1°C. L'utilisation du milieu sélectif mFC agar et la température d'incubation à 44.5°C est idéale et primordiale pour éliminer ou ralentir la croissance non souhaitée des bactéries, des champignons et levures et de former un amas de cellules (colonies). Le nombre N de micro-organismes dénombrés par

millilitre de produit est obtenu de facon générale, en chaoississant le nombre de colonies acceptables, de préférence à l'intérieur des limites de quantification, et le résultats est exprimé en unité formation des colonies (UFC) par 100 mL d'échantillon selon l'équation générale suivante :

$$UFC/100\ mL = \frac{nombre\ de\ colonies\ de\ coliformes}{Volume\ d'échantillon\ analysé\ en\ mL}$$

1.6.10.4 Mesure du CTC et du CBZ au spectrophotomètre UV

La spectrométrie UV-visible est une technique analytique basée sur la loi de Beer-Lambert qui consiste à mesurer l'absorbance ou la densité optique d'une solution contenant des espèces capables d'absorber certains rayonnements UV ou visibles. La concentration d'une espèce est déterminée par analogie entre la mesure de la densité optique et la droite d'étalonnage effectuée préalablement au maximum d'absorbance de ce composé (λ_{max}). La CTC et la CBZ sont les deux composés qui ont été analysés par spectrophotométrie UV-visible. Le spectromètre utilisé est un modèle Varian UV 0811 M136 (Australie) (Figure 1-15). La concentration résiduelle de CTC a été évaluée à une longueur d'onde de 368 nm, alors que la concentration résiduelle de CBZ a été évaluée à 286 nm. Une courbe de calibration a ainsi été réalisée à cette longueur d'onde pour évaluer la concentration résiduelle des deux polluants (CTC et CBZ).



Figure 1-15 Spectromètre UV/visible utilisé pour l'analyse de la CTC et la CBZ.

1.6.10.5 Mesure du CTC au LC-MS/MS

Le suivi de la dégradation PEC du CTC et de ces sous-produits a été réalisé par analyse au LC-MS/MS (Thermo TSQ Quantum Access) (Figure 1-16). Les analyses au LC ont été réalisées en utilisant une colonne chromatographique Beta Basic C18 ayant une taille de particule de 3µm et un diamètre intérieur de 2.1 mm x 100 mm. Un flux isocratic de 200 µL min^{-1} d'éluan constitué de A : 50% d'eau et 0.1% d'acide formique et B: 50% d'acétonitrile et 0.1% d'acide formique a été appliqué. La détection a été conduite par un système MS/MS utilisant une interface electrospray (ESI) en mode ionisation positive. L'analyse quantitative du CTC et de ces sous-produits a été déterminée en utilisant le sulfamethazine C13 comme standard interne.

1.6.10.6 Mesure du CBZ au LC-MS/MS

Le suivi de la dégradation PEC du CBZ et de ces sous-produits (acridine et l'acide anthranilique) a été réalisé par analyse au LC-MS/MS (Thermo TSQ Quantum Access) (Figure 1-16). Les analyses au LC ont été réalisées en utilisant une colonne

chromatographique Hypersil Gold C18 (100 * 2.1 mm * 3 µm). Un flux isocratic de 200 µL min^{-1} d'éluan constitué de A : 50% d'eau et 0.1% d'acide formique et B: 50% d'acétonitrile et 0.1% d'acide formique a été appliqué. La détection a été conduite par un système MS/MS utilisant une interface electrospray (ESI) en mode ionisation positive. L'analyse quantitative du CBZ ainsi que de ces sous-produits (acridine et l'acide anthranilique) a été déterminée en utilisant le sulfamethazine C13 comme standard interne.



Figure 1-16 Chromatographie liquide couplée à deux spectrométries de masses utilisées pour l'analyse du CTC et du CBZ.

1.6.10.7 Mesure de la concentration des EORs

La mesure des EORs incluant les radicaux hydroxyles et l'ozone a été déterminée en utilisant la méthode de blanchissement du RNO (Simonsen et al., 2010). Le taux de blanchissement du RNO a été suivi par mesure de l'absorbance du RNO à 440 nm en utilisant le spectrophotomètre UV-Visible (UV 0811 M136, Varian, Australia). Les EORs (O_3 et OH°) produites *in situ* sont capables d'assurer le blanchissement du RNO par oxydation chimique

(Muff et al., 2011). Les trous (h^+) qui sont photo-générés au niveau de la BV sont capables également d'assurer le blanchissement du RNO.

1.6.10.8 Mesure de la concentration du peroxyde d'hydrogène

La détermination de la concentration du peroxyde d'hydrogène a été effectuée en suivant une méthode de dosage volumétrique basé sur une oxydation de H_2O_2 par une solution de cérium ($Ce(SO_4)_2$, $2(NH_4)_2SO_4$, $2H_2O$) en milieu acide et en présence d'un indicateur coloré (orthophénanthroline ferreuse). Les principaux réactifs qui ont été utilisés lors du dosage sont les suivants: une solution d'acide sulfurique (H_2SO_4 4.5 M); une solution de sulfate de cérium (5.88×10^{-3} M) et une solution d'othophénanthroline. Le changement progressif de la couleur de la solution du rouge vers le bleu pâle signifie un dosage de la quantité de H_2O_2 présent dans l'échantillon. Les réactions chimiques qui expliquent bien le dosage du peroxyde d'hydrogène à l'aide d'une solution de cérium (IV) sont comme suit (Sigler et Master, 1957):

Équation 1-27 $Ce^{4+} + H_2O_2 \rightarrow Ce^{3+} + HO_2 + H^+$

Équation 1-28 $Ce^{4+} + HO_2 \rightarrow Ce^{3+} + O_2 + H^+$

Équation 1-29 $[Fe(O\text{-}Phen)_3]^{2+} + Ce^{4+} \rightarrow [Fe(O\text{-}Phen)_3]^{3+} + Ce^{4+}$

1.6.10.9 Mesure de la concentration d'ozone

La concentration de l'ozone a été déterminée en utilisant la méthode de l'indigo (Bader and Hoigne, 1981). Une solution stock du réactif d'indigo a été préparée en faisant dissoudre 770 mg L^{-1} du trisulphonate du potassium d'indigo dans un 1 mL d'acide phosphorique. Pour des faibles concentrations d'ozone, 20 mL de la solution stock d'indigo ($2.49\ 10^{-5}$M) est dissoute dans 10g du phosphate de sodium monobasique (Na_2HPO_4) et dans 7 mL d'acide phosphorique. Les solutions standards de l'ozone ayant des concentrations allant de 0.0 moL

L^{-1} à 1.87 10^{-6} moL L^{-1} sont préparées en utilisant un générateur d'ozone (OzoStar, model WL7, Ozocan Corporation, Ontario, Canada).

1.7 Principaux résultats et discussion générale

Les résultats de la présente étude ont permis d'évaluer l'efficacité d'un procédé d'oxydation PEC utilisant une électrode nanostructurée de TiO_2 comme photoanode pour le traitement d'effluents contaminés en micropolluants organiques tels que la CTC et la CBZ. Cette section consiste en une discussion générale des différents résultats obtenus.

1.7.1 Production in-situ des EORs: Application de la méthode de blanchissement du RNO (Chapitre 5)

Les photoanodes de Ti/n-TiO_2 (préparées par la méthode de déposition par ablation laser à 400 et 600°C) ont été respectivement intégrées dans une cellule PEC développée sur mesure (Cellule C1, Figure 1-11) afin d'évaluer leur capacité de production d'espèces oxydantes (notamment les radicaux hydroxyles (OH°) et l'ozone (O_3)) nécessaires à l'oxydation des micropolluants réfractaires. La mise en évidence de ces espèces oxygénées a été réalisée en utilisant une méthode indirecte dite "Spin trapping", qui consiste à piéger le radical par le p-nitrosodimethylaniline (RNO) en un adduit stable, lequel est par la suite analysé par spectrophotométrie d'absorption UV-visible (pic d'absorption à 440 nm) (Muff et al., 2011). Un taux de dégradation relativement élevé de RNO a été enregistré comparativement aux valeurs mesurées lors de l'application des procédés conventionnels d'oxydation électrochimique (EO), de photolyse directe (PD) et de photocatalyse (PC). L'influence de différents paramètres tels que la structure cristalline de Ti/TiO_2 (anatase versus rutile), le type de cathode, le potentiel appliqué, le temps d'électrolyse, l'irradiation UV et le pH initial ont été étudiés. La cellule PEC utilisant Ti/n-TiO_2 (de structure anatase) comme photo-anode et le CV à la cathode et fonctionnant à une intensité de courant de 0.1A pendant 120 min en présence d'un rayonnement UV à 254 nm ont été identifiées comme étant les meilleurs

conditions d'oxydation du RNO (22.610^{-3} mM h^{-1}). La vitesse de production des espèces oxydantes (ex. OH°, O_3, h^+) est égale à la vitesse de disparition du RNO :

Équation 1-30 $$r = \frac{d[RNO]}{dt} = -k[RNO]$$

Dans cette équation "[RNO]" représente la concentration de RNO, "k" est une constante de cinétique de premier ordre et "r" la vitesse de production des espèces oxydantes (tels que OH°, O_3, h^+). La constante cinétique de premier ordre enregistrée lors de l'application du procédé d'oxydation PEC était de 0.02 min^{-1}. Par comparaison, les constantes cinétiques enregistrées pour les procédés conventionnels (PD, PC et EO) étaient de 0.0038 mn^{-1}, 0.0058 min^{-1} et 0.012 min^{-1}, respectivement. Ceci démontre que la vitesse de production des espèces oxydantes par notre procédé PEC est 5.3, 3.5 et 1.7 fois plus rapide que pour les procédés conventionnels PD, PC et EO, respectivement. Les résultats de cette partie des travaux (incluant les aspects matériaux) ont fait l'objet d'un article publié dans la revue de calibre international Journal of Applied Electrochemistry.

1.7.2 Oxydation PEC du CTC utilisant une électrode nanostructuée de Ti/TiO_2 comme photo-anode préparée par la méthode de déposition par ablation laser: Application de la méthodologie de plan d'expériences (Chapitre 6).

La dégradation PEC de la CTC en milieu aqueux synthétique a été étudiée en utilisant une électrode nanostructurée de Ti/TiO_2 comme photoanode sous une irradiation UV. La première étape de cette étude a consisté à caractériser l'électrode nanostructurée de TiO_2 déposé sur une grille de Ti par ablation laser. L'analyse utilisant la MEB montre que les revêtements de TiO_2 déposé à une température de 600°C sont très uniformes en épaisseur et forme une interface lisse et continue avec le substrat. L'analyse utilisant la technique de DRX montre que le TiO_2 déposé à 600°C correspond à la forme rutile avec une taille moyenne des cristallites de 10 nm.

Cette électrode nanostructurée de Ti/TiO_2 a été utilisée dans les prochains essais en tant que photoanode pour la dégradation PEC de la CTC.

Le procédé PEC a par la suite été testé pour la dégradation de résidus médicamenteux de type antibiotique couramment rencontrés dans les eaux de surface, souterraines et résiduaires. Les essais ont été effectués sur des effluents synthétiques reconstitués et artificiellement contaminés par la CTC. Lors de l'application du procédé PEC avec des photoanodes de n-TiO_2, plusieurs paramètres tels que, l'intensité de courant, le temps de traitement, la position de la lampe UV et la concentration initiale du CTC ont été étudiés.

En utilisant un PF 2^4, les meilleures performances épuratoires (74.3 % d'élimination) ont été obtenues pour une intensité de courant de 0.5 A pendant une période de 120 min de traitement et lorsque la lampe UV est directement immergée dans l'effluent à traiter en présence d'une concentration initiale de 25 mg L^{-1} de CTC. L'intensité de courant et le temps d'électrolyse étaient des paramètres principaux les plus influents lors de la dégradation de la CTC. Les contributions de l'intensité de courant et du temps de traitement étaient de 76.2 % et 16.7 %, respectivement, alors que les contributions de la concentration en polluant et de la position de la lampe UV étaient de 4 % et 2.5%, respectivement.

Il est également nécessaire de signaler que les interactions les plus significatives font systématiquement intervenir l'intensité de courant avec une prédominance pour l'interaction X_1X_3 (intensité de courant et concentration en polluant). Dans un procédé d'oxydation PEC, la différence de potentiel appliqué est un facteur clé qui influence l'efficacité de dégradation des polluants. L'intensité de courant appliquée évite la recombinaison du paires électron-trou photo-générés, lesquels contribuent à la dégradation du CTC directement sur la surface de l'électrode nanostructurée Ti/TiO_2. Néanmoins, les meilleures dégradations PEC de la CTC sont enregistrées à des faibles concentrations initiales de CTC. La dégradation du CTC reste toujours limitée par la quantité des EORs produite *in situ*. A des fortes concentrations en

CTC, les espèces oxydantes produites *in situ* sont insuffisantes pour améliorer l'efficacité de la dégradation. On comprend ainsi aisément pourquoi l'intensité de courant imposée et la concentration du polluant peuvent être liées. Le modèle construit sur la base du PF n'étant pas suffisant pour permettre la prédiction des conditions optimales, l'étape suivante s'est donc orientée vers un PCC.

Un plan de surface de réponse (Plan Central Composite, PCC) a été employé pour déterminer les conditions optimales de dégradation de la CTC. Les critères choisis pour l'optimisation sont les suivants : l'intensité de courant et la concentration du polluant ont été minimisés, le temps de traitement a été maximisé, alors que la position de la lampe UV qui est restée libre dans son domaine de variation sans application de condition particulière. Ainsi, la meilleure solution proposée par le logiciel satisfaisant au mieux les différents critères imposés consiste à imposer une intensité de courant de 0.39 A, pendant 120 min du temps de traitement à une concentration initial de CTC de 25 mg L^{-1} et en gardant la lampe UV en position interne immergé dans l'effluent. Un taux d'abattement allant jusqu'à 97% ± 1.12% de la CTC pour un coût de \$4.55 ± 0.01 m^{-3} a été enregistré dans ces conditions optimales. Un article, portant sur nos résultats originaux sur la dégradation du CTC par notre procédé PEC avec n-TiO_2, a été publié dans la revue internationale: Journal of Hazardous Materials.

1.7.3 Oxydation PEC du CTC utilisant une électrode nanostructurée de Ti/TiO2 comme photo-anode avec une production simultanée du H2O2 (Chapitre 7)

D'autres travaux ont consisté à évaluer l'efficacité épuratoire du procédé PEC sur des concentrations relativement faibles de CTC (32 à 230 µg L^{-1}) en utilisant une cellule constituée d'une photo-anode de Ti/TiO_2 (structure anatase, rutile ou amorphe). Les paramètres qui ont été étudiés sont la structure cristallographique de la photoanode Ti/TiO_2, le type de matériau utilisé à la cathode, le pH et la concentration du polluant. Lors de cette étude, une intensité de courant de 0.39 A a été imposée durant 120 min du temps de

traitement et en utilisant la lampe UV (254 nm) en position interne immergée dans l'effluent à traiter.

La première partie de cette étude a consisté à caractériser une électrode de TiO_2 déposée sur des grilles de titane par ablation laser. Il est important de signaler que les revêtements du film de TiO_2 ont été déposés à deux températures différentes: 600°C et 400°C. L'étude morphologique effectuée par MEB montre que les revêtements du TiO_2 sont très denses et uniformes formant une interface lisse et continue avec le substrat. De même, en augmentant la température de 400°C à 600°C, une augmentation de la taille des cristallites du revêtement de TiO_2 a été observée. Les analyses utilisant la technique de DRX montrent que le revêtement de TiO_2 déposé à 400°C et à 600°C correspondent à la forme anatase et rutile, respectivement. La taille moyenne des cristallites de TiO_2 sous la forme rutile ont été estimé à 10 nm, alors que la taille moyenne des cristallites de TiO_2 sous la forme anatase ont été estimé à 15 nm. Vu que chaque forme cristalline de TiO_2 (anatase ou rutile) réagit différemment vis-à vis d'un même polluant organique, ces électrodes nano-strustructurées ont été par la suite utilisées pour des traitements PEC du CTC.

Des électrodes cathodiques nanostructurées de a-C déposés sur des grilles de titane par ablation laser à deux températures différentes (20°C et 600°C) ont également été caractérisées. L'étude morphologique par MEB montre que le revêtement du carbone amorphe déposé sur des grilles de titane est considéré comme très dense formant des grains fins (de l'ordre de nanomètre) plus ou moins sphériques. Ces électrodes nanostructurées de a-C ont été ensuite utilisées à la cathode pour le traitement PEC de la CTC.

Les expériences suivantes ont permis de mettre en évidence l'effet de la structure cristallographique de Ti/TiO_2 (anatase, rutile et amorphe) utilisé comme photoanode sur la dégradation PEC de la CTC. Les résultats montrent qu'en utilisant la forme anatase du Ti/TiO_2 comme photoanode, les rendements d'abattement de la CTC sont nettement plus

élevés que ceux enregistrés avec la forme rutile et amorphe. Un taux de dégradation de la CTC allant jusqu'à 97.5 ±0.6% a été obtenu en utilisant la forme anatase. En utilisant cette même structure cristallographique de Ti/TiO_2 (forme anatase), des taux d'élimination de 55.6% et de 63.1% de COT et de NT ont été respectivement enregistrés. Cette meilleure dégradation et minéralisation de la CTC enregistrée en utilisant la forme anatase par rapport à la forme rutile est principalement due à la différence au niveau de la structure cristalline qui influence l'activité de la réaction photocatalytique (Ma et Tu, 2011). Il est également nécessaire de signaler que la quantité de défaut présent dans la structure amorphe de Ti/TiO_2 peut entrainer une augmentation du nombre de sites de recombinaison des paires électron-trou photogénérés par le procédé PEC. Ceci contribue à limiter l'oxydation et la minéralisation du CTC (Xiang et al., 2011).

L'effet du matériel cathodique a été évalué en comparant cinq types de matériaux : Inox, CV, Gr, a-C déposé à 20°C et a-C déposé à 600°C. Il est possible en utilisant des électrodes à base de carbone de produire du peroxyde d'hydrogène qui est un oxydant pouvant contribuer à l'oxydation de la matière organique. Les essais réalisés avec le CV étaient plus satisfaisants en termes de production du peroxyde d'hydrogène et de dégradation du polluant CTC. Après 120 min d'oxydation PEC, une concentration de 0.2 ±0.01 mM du peroxyde d'hydrogène a été enregistrée à une intensité de courant imposée de 0.39 A, en utilisant la forme anatase du Ti/TiO_2 comme photoanode et le CV à la cathode et sous une radiation UV de 254 nm. De meilleurs taux de dégradation (98.0 ± 0.2%) et de minéralisation du CTC (élimination de 67.3±2.15% du COT et 69.3 ±3.10% de l'NT) ont été également obtenus dans ces conditions opératoires. Il a été démontré précédemment que la génération électrochimique des espèces oxydantes (autre que le radical hydroxyle) telles que H_2O_2 améliore l'efficacité des réactions PEC (Xie et Li, 2006).

L'effet de la concentration initiale en CTC a été évalué pour des concentrations variant entre 32 $\mu g\ L^{-1}$ et 230 $\mu g\ L^{-1}$. Des taux de dégradation variant de 97.10 ±0.47% à 92.34 ± 0.23% ont été enregistrés. La diminution du taux de dégradation lors de l'augmentation de la concentration initiale du CTC peut être attribuée à une insuffisance des espèces oxygénées oxydantes produites lors du procédé PEC. Les sous-produits du CTC générés lors de l'oxydation PEC peuvent entrer en compétition avec la molécule mère (CTC) en réagissant avec les espèces oxydantes, réduisant ainsi le taux de dégradation et de minéralisation.

Enfin, l'efficacité du procédé d'oxydation PEC du CTC a été étudiée pour différents valeurs de pH (3.12; 5.51; 7.06 et 9.02). Il est important de souligner que dans un tel traitement, le pH est un paramètre qui affecte la capacité d'adsorption et de dissociation des polluants, la distribution de la charge sur la surface du photocatalyseur et le potentiel d'oxydation de la bande de valence (Ahmed et al., 2011). Des meilleurs taux de dégradation de CTC (97.3% ± 0.41%) et d'élimination du COT (67.9 ± 1.11%) ont été obtenus sans ajustement de pH. Sous ces conditions, la surface du catalyseur est chargée positivement ($TiOH_2^+$) et une attraction électrostatique entre la forme zwitterionic du CTC ($CTCH_2^{\pm}$) et la surface de TiO_2 prédomine.

L'ensemble de ces essais a permis de définir les conditions optimales pour la dégradation du CTC : utilisation de la forme anatase du Ti/TiO_2 comme photoanode, le CV à la cathode, à une intensité de courant de 0.39 A et sous une radiation UV de 254 nm dont la lampe est immergée dans l'effluent, pour une concentration initial du CTC de 32 $\mu g\ L^{-1}$ et un pH initial neutre. Dans ces conditions, la totalité du CTC est dégradée après un temps de traitement de 120 min. L'étude cinétique effectuée dans ces conditions optimales montre que le taux de dégradation PEC initial du CTC peut être bien décrit par le modèle Langmuir-Hinshelwood avec une constante cinétique de 17.3 $\mu g\ L^{-1}\ min^{-1}$. L'analyse par LC-MS/MS a permis d'identifier les différents sous-produits de dégradation du CTC formés lors du traitement PEC. Enfin, la dernière partie de cette étude a consisté à évaluer la toxicité de l'effluent traité

sur des espèces aquatiques. Les tests de microtox (*vibrio fisheri*), de micro-algue (*Pseudokirchneriella Subcapitata*) et de Daphnie (*Daphnia magna*) montrent une diminution de la toxicité dans l'effluent traité par comparaison à l'effluent non-traité (une réduction de la toxicité de 62% et de 78% sur la *Pseudokirchneriella Subcapitata et la vibrio fisheri,* respectivement). Les résultats de cette partie des travaux ont fait également l'objet d'un article publié dans la revue de calibre international Electrochimica Acta.

1.7.4 Dégradation PEC du CTC utilisant une photoanode nanostructurée de Ti/TiO_2 dopé à l'azote (Chapitre 8)

Les photoanodes n-TiO_2 ont été réalisées en déposant des couches minces nanostructurées sur des substrats appropriés de Ti en utilisant la technique de pulvérisation magnétron (Brassard et al., 2006; Hajjaji et al., 2011). Les films de n-TiO_2 ont été dopés à l'azote pour réduire leur bande interdite de l'UV (~3.2 eV pour l'anatase) au visible ($\leq$ 2.25 eV), les rendant ainsi photoactifs à l'insolation. La teneur en azote incorporée dans les photoanodes de n-TiO_2:N a été contrôlée en ajustant le ratio de flux gazeux $[N_2]/([N_2]+[Ar])$ lors de la préparation des électrodes. Le ratio de flux gazeux variait entre 0 à 20%, alors que les teneurs en azote incorporées dans le film de n-TiO_2:N. variaient entre 0 à 5.8at%.

L'analyse utilisant la technique de DRX montre que le revêtement de n-TiO_2 : N correspond à la forme anatase avec une taille des cristallites allant de 51 nm pour le TiO_2 non dopé à 29 nm pour le TiO_2 dopé à 3.4 at% d'azote. Il est également nécessaire de mentionner que le revêtement de TiO_2 dopé avec une teneur de 0.2 at% d'azote présente des pics moins intensifs qui correspondent à la forme rutile. Le film de TiO_2 dopé à 0.2at.% d'azote semble consister en un mélange d'anatase (comme composante majeure) et de rutile. La forme rutile est plus dense que la forme anatase. Néanmoins, la forme anatase possède une activité photocatalytique plus importante que la forme rutile (Tsai and Cheng, 1997; Ohno et al., 2001; Sakatani et al., 2006).

L'étude morphologique examinée par MEB montre que le revêtement de n-TiO_2 : N est très dense et présente une certaine porosité. L'étude des propriétés optoélectroniques utilisant la spectroscopie d'absorption UV-visible montre que l'absorption des films de TiO_2 dopé à différents teneurs d'azote (de 0 at% à 5.8at%) est décalée de la région UV vers la région du visible (de 380 nm pour le film de TiO_2 non dopé à 550 nm pour le TiO_2 dopé avec une teneur de 3.4 at% d'azote). L'incorporation de l'azote dans le film de TiO_2 favorise la réduction de la largeur de la bande interdite de 3.2 eV (pour le TiO_2 non dopé) à 2.3 eV (pour le TiO_2 dopé à 3.4 at% de la teneur d'azote). Une bande interdite ayant une valeur de 2.3 eV absorbe à une longueur d'onde de 539 nm, qui est très proche de l'énergie solaire. Une telle amélioration de l'absorption dans le visible entrainera une meilleure performance photocatalytique (Peng et al., 2012; Cheng et al., 2013; Ananapattarachai et al., 2009; Senthilnathan and Philip, 2010). Les photoanodes à base de n-TiO_2:N ont été par la suite intégrées dans une cellule PEC en conjonction avec des cathodes à base de carbone.

Le traitement d'oxydation PEC a été réalisé en utilisant un simulateur de radiation solaire pour une période de 120 min et à une intensité de courant de 0.39A. Une concentration initiale de 100 $\mu g\ L^{-1}$ de CTC a été imposée dans l'effluent synthétique. Les photoanodes de TiO_2 dopé à l'azote étaient plus efficaces que le TiO_2 non-dopé. Un rendement de dégradation de la CTC allant jusqu'à $98.2 \pm 0.1\%$ a été enregistré en utilisant n-TiO_2:N ayant une teneure de 3.4 at% d'azote. En utilisant la même photoanode, des meilleurs taux d'élimination du COT (80%) et de l'NT (77%) ont été également enregistré.

Les expériences suivantes ont permis de mettre en évidence l'effet de l'intensité du courant (de 0.1 A à 0.8 A) et du temps de traitement (de 20 min à 240 min) sur la dégradation PEC de la CTC sous irradiation solaire. L'ensemble de ces essais a permis de définir les conditions optimales qui assurent une meilleure dégradation et minéralisation d'un effluent synthétique contaminé par la CTC (100 $\mu g\ L^{-1}$): une intensité de courant de 0.6 A imposée pendant 180

min et en utilisant une photoanode de n-TiO_2:N ayant une teneur de 3.4% d'azote. Dans ces conditions, 99.6% de la CTC est dégradé, 92.5% ±0.26 % et 90.3%±1.1% du COT et de l'NT sont respectivement éliminés. L'analyse des sous-produits de dégradation a permis de proposer un mécanisme réactionnel de dégradation PEC de la CTC. La voie de dégradation principale de la CTC favorise la formation du N-dedismethyl-CTC suite à une perte de deux groupements méthyl à la position C4 du CTC. La déchlorination du N-dedismethyl-CTC favorise la formation N-dedismethyl tétracycline. L'attaque du N-dedismethyl tétracycline par des radicaux hydroxyles favorise la rupture des groupements amines et la formation de l'acide carboxylique et du groupement cétone en position C2 et C4, respectivement. L'oxydation continue du N-dedismethyl tétracycline conduit à la formation des intermédiaires aromatiques bicycliques et tricycliques puis à l'ouverture du cycle aromatique pour former divers composés aliphatiques de faible poids moléculaire. Les résultats de cette partie des travaux ont fait l'objet d'un article qui a été publié dans la revue Water Research.

1.7.5 Traitement des eaux usées municipales contaminées par la CTC en utilisant un procédé PEC sous irradiation solaire (Chapitre 9).

Cette partie des travaux a consisté à évaluer l'efficacité de ce procédé (procédé PEC) d'oxydation du CTC sur une matrice réelle issue de station d'épuration. Pour cela, des eaux usées de type municipal ont été artificiellement contaminées par du CTC puis soumises au traitement d'oxydation PEC dans les conditions optimales déterminées au chapitre 8 lors de l'application du procédé PEC à la lumière du soleil (UV et visible). Ces effluents réels sont issus d'un traitement secondaire (unité de biofiltration) et ont été artificiellement contaminés par 100 $\mu g\ L^{-1}$ de CTC.

L'application du procédé PEC sur une telle matrice permet d'enregistrer une dégradation quasi-totale de CTC (99.1%±0.1%) en imposant une intensité de courant de 0.6A pendant 180 min de traitement et en présence d'une photoanode de n-TiO_2:N ayant une teneur de 3.4%

d'azote. Une différence est cependant observée entre les résultats obtenus en solution synthétique et ceux obtenus en solutions réelles. La présence de contaminants organiques autre que la CTC dans les effluents réels influence l'efficacité de minéralisation de la solution. Des taux d'élimination de 85.4% ±3.6% ainsi que de 87.4%±3.1% ont respectivement été enregistrés pour le COT et pour l'NT. Ces taux de dégradation relativement élevés indiquent que la majeure partie des composés organiques a été transformée en eau et en dioxyde de carbone. Aussi, des taux d'élimination de 55.7% ± 2.9% d'azote ammoniacal et de 71.1% ± 3.1% nitrites/nitrates ont été enregistrés. Par ailleurs, un taux d'abattement de 95% de CF (1.2 unités d'abattement logarithmique a été enregistré suite à l'application du procédé PEC. Cette étude a permis de mettre en évidence l'intérêt de l'application du procédé PEC en tant que traitement tertiaire des eaux usées pour l'élimination des polluants organiques réfractaires (tels que la CTC) tout en assurant une désinfection des eaux. Dans ces conditions, un coût de traitement du procédé PEC de \$4.17 ± 0.01 m^{-3} a été enregistré. Ce coût de traitement incluant seulement la consommation énergitique peut être comparé avec ceux (de 0.63 \$ m^{-3} à 278 \$ m^{-3}) répertoriés dans la littérature lors de l'application des POAs (Annexe 1). Par exemple, un coût de traitement de 9.42 \$ m^{-3} a été enregistré par Olya et al. (2013) (incluant le coût de fonctionnement et de consommation en électrolyte) lors de l'oxydation PEC d'un colorant industriel (Acide Red 88) sous radiation solaire. Plus de 95% de colorant a été éliminé. Pour sa part, Martinetti (2007) a enregistré des coûts de traitement de 12.88 et de 24.41 \$ m^{-3} pour l'élimination de la DCO réfractaire (plus de 90% d'abattement de la DCO) des eaux résiduaires issues d'industrie de textile en appliquant respectivement les procédés photo-Fenton et d'oxydation photo-catalytique. Ces coûts de traitement dépendent de plusieurs paramètres tels que la structure chimique et la concentration du polluant cible, le type de matrice (eaux municipales ou industrielles) et le type du POAs appliqués.

1.7.6 Méthodologie de plans d'expériences appliquée à l'oxydation PEC du CBZ utilisant une électrode nano-structurée de Ti/TiO_2 comme photo-anode (Chapitre 10)

Dans l'optique d'élargir le spectre d'activité d'oxydation du procédé PEC à d'autres types de polluants pharmaceutiques, des travaux additionnels ont été entrepris afin de vérifier les performances du procédé pour la dégradation de la CBZ.

Une étude préliminaire a permis de comparer le comportement PEC de la dégradation du CBZ en utilisant différents cathodes (Gr, CV, inox et a-C nano-structuré) dans l'optique de sélectionner l'électrode la plus appropriée pour la réalisation d'un plan de surface de réponse. Une dégradation de CBZ allant jusqu'à $51\% \pm 2.6$ % a été enregistrée en utilisant une électrode nanostructurée de Ti/TiO_2 comme photoanode, le CV à la cathode, à une intensité de courant de 0.1 A imposée durant 120 min. Le CV s'avère nettement plus efficace. Le CV est une électrode capable de générer *in situ* du peroxyde d'hydrogène (0.14 ± 0.01 mmol L^{-1}) suite à une réduction cathodique de l'oxygéne.

Afin de décrire et optimiser le processus de dégradation PEC du CBZ, plusieurs paramétres tels que, l'intensité de courant, le temps de traitement, le type de cathode et la concentration initiale du CBZ ont été par la suite étudiés. En utilisant, un PF 2^4, les meilleures performances épuratoires (53.5% d'élimination) ont été obtenues pour une intensité de courant de 0.3 A pendant une période de 120 min de traitement et en utilisant le CV à la cathode et en présence d'une concentration de 10 mg L^{-1} de CBZ. Le temps d'électrolyse et la concentration initiale de CBZ étaient des paramètres principaux les plus influents lors de la dégradation de la CBZ. Les contributions du temps de traitement et de la concentration en polluant étaient de 70.6% et 23.3%, respectivement, alors que les contributions de la nature de la cathode et de l'intensité de courant étaient de 2.4% et 0.75%, respectivement. Il est également nécessaire de signaler que les interactions les plus significatives font systématiquement intervenir le type de cathode avec une prédominance pour l'interraction X_1X_4 (intensité de courant et type de

cathode). L'utilisation des électrodes comme le CV à la cathode représente un avantage intéressant dans l'application des techniques PEC. L'addition électrochimique d'un électron accepteur tel que le H_2O_2 permet d'éviter la recombinaison des électrons-trous, augmentant ainsi la dégradation PEC du CBZ. Le modèle construit sur la base du PF n'étant pas suffisant pour permettre la prédiction des conditions optimales, l'étape suivante s'est donc orientée vers un PSR.

Un plan de surface de réponse (Plan Central Composite, PCC) a été employé pour déterminer les conditions optimales de dégradation de la CBZ. Les critères choisis pour l'optimisation sont les suivants : la concentration du polluant a été minimisés, le temps de traitement a été maximisé, alors que l'intensité de courant et le type de cathode sont restées libre dans son domaine de variation sans application de condition particulière. Ainsi, la meilleure solution proposée par le logiciel satisfaisant au mieux les différents critères imposés consiste à imposer une intensité de courant de 0.3 A, pendant 120 min du temps de traitement, à une concentration initiale de CBZ de 10 mg L^{-1} et en utilisant le CV à la cathode. Un taux d'abattement allant jusqu'à 73.5% ± 2.8% de la CBZ pour un coût de 2.98 ± 0.1 \$ m^{-3} a été enregistré dans ces conditions optimales. Sous ces conditions, un taux d'élimination de 21.2% ± 7.7% du COT a été enregistré. Seulement une faible fraction de la CBZ a été complétement oxydé en eau et en dioxyde de carbone. La majorité du polluant a été transformé à des sous-produits. Le test Microtox appliqué sur la vibrio fisheri montre une réduction de la toxicité dans l'effluent traité par comparaison à l'effluent non-traité. Le pourcentage d'inhibition enregistré initialement est de 32.25%, alors que le pourcentage d'inhibition obtenu à la fin du traitement PEC est de 20.45%.

L'analyse des sous-produits de dégradation a permis de proposer un mécanisme réactionnel de dégradation PEC de la CBZ. La voie de dégradation principale favorise la formation du 10, 11-epoxycarbamazepine par attaque radicalaire. La perte d'un groupement -$CONH_2$ dans le

10, 11-epoxycarbamazepine mène à la formation d'un intermédiaire très instable aboutissant à la formation de l'acridine. Une voie de dégradation alternative mène à la réaction de la CBZ avec le radical hydroxyle pour former des dérivés hydroxylés (10, 11-dihydroxycarbamazépine). L'oxydation continue du 10, 11-dihydroxycarbamazépine conduit à la formation de l'acide anthranilique et de l'acide salicylique. L'étude cinétique appliquée dans les conditions optimales montre que la dégradation PEC de la CBZ suit une cinétique du second ordre avec une constante cinétique de 6 10^{-4} L mg^{-1} mn^{-1} (R^2 = 0.994). Un article, portant sur nos résultats originaux sur la dégradation du CBZ par notre procédé PEC avec n-TiO_2, a été soumis dans la revue internationale: Chemosphere.

1.8 Conclusions Générales

Cette étude a permis de développer et d'évaluer les performances épuratoires d'un procédé d'oxydation PEC combinant la photocatalyse et l'électrolyse. Ce procédé a été conçu pour le traitement tertiaire des eaux résiduaires (de type municipal ou industriel) contenant des résidus médicamenteux.

Des cellules PEC constituées de photoanodes nanostructurées de TiO_2 (anatase, rutile ou amorphe) et d'électrodes cathodiques (CV, Gr, acier inoxydable ou a-C nanostructuré) ont été conçues et caractérisées en terme de leur capacité de production d'EOR (H_2O_2, O_3, OH°, etc.) nécessaires à l'oxydation de composés organiques réfractaires. Plus spécifiquement, la possibilité de générer simultanément des éspéces oxydantes telles que OH°, O_3, h^+ a été mis en évidence en présence de la molécule de RNO. Les cellules PEC fonctionnaient sous irradiations ultraviolettes et/ou solaire. Après avoir établi les caractéristiques de la cellule PEC, le procédé a été testé pour la dégradation de micropolluants réfractaires de type pharmaceutique (la CTC et la CBZ) et pour le traitement tertiaire des eaux usées de type municipal.

Plus spécifiquement, l'étude menée sur la CTC (résidus médicamenteux de type antibiotique) a fait ressortir les points suivants:

- La méthodologie des plans d'expérience a permis de décrire le processus de dégradation de la CTC. Les résultats de cette étude ont permis de confirmer l'hypothèse I.
- L'intensité de courant appliqué et le temps de traitement représentent les paramètres les plus influents dans le processus de dégradation PEC de la CTC. La contribution de l'effet de l'intensité de courant et du temps de traitement sur la réponse est estimée à environ de 76.2 % et 16.7 %, respectivement, alors que les effets de la concentration

intiale du CTC, de la position de la lampe UV et les autres interactions représentent moins de 5%.

- Subséquemment, un PCC a été employé pour définir les conditions optimales de dégradation de CTC. L'intensité de courant imposée et le temps de traitement ont des effets positifs sur la réponse. Imposer une intensité de courant de 0.39A, pendant 120 min du temps de traitement à une concentration initial de CTC de 25 mg L^{-1} et en gardant la lampe UV en position interne immergé dans l'effluent a été retenue comme conditions optimales en termes de coût et d'efficacité. Dans ces conditions, 97% ± 1.12% d'abattement de CTC a été obtenu, pour un coût total de \$4.55 ± 0.01 m^{-3} (incluant seulement les coûts d'énergie et d'électrolyte).

- Des essais complémentaires de dégradation de la CTC ayant des concentrations relativement faibles (de 32 à 230 µg L^{-1}) ont montré que l'oxydation PEC utilisant la forme anatase du Ti/TiO_2 comme photoanode, le CV à la cathode et à un pH neutre est très efficace. Dans ces conditions, la totalité du CTC (32 µg L^{-1}) est dégradée sous irradiation UV (254 nm) et après un temps de traitement de 120 min. Des taux de minéralisation relativement élevées (une élimination de 67.3 ± 2.15% et 69.3 ± 3.10% de carbone organique total et d'azote total, respectivement) ont été également énregistrés. Ces résultats obtenus ont permis de confirmer l'hypothèse II et III.

- L'étude de la toxicité sur des éspéces aquatiques telles que la *vibrio fisheri,* la *Pseudokirchneriella Subcapitata* et la *Daphnia magna* montre une diminution de la toxicité dans l'effluent traité par comparison à l'effluent non-traité (une réduction de la toxicité de 62% et de 78% sur la *Pseudokirchneriella Subcapitata* et la *vibrio fisheri,* respectivement).

- Aussi, l'efficacité épuratoire du procédé PEC a été testé sous simulateur solaire (dans le visible) à l'aide d'une photanode nanostructurée de dioxyde de titane dopé à l'azote (n-TiO_2 : N) pour la dégradation du CTC en solution synthétique (100 µg L^{-1}). Un rendement de dégradation de la CTC allant jusqu'à 99.6% a été enregistré en utilisant n-TiO_2:N ayant une teneur de 3.4 at% d'azote. En utilisant la même photoanode, des meilleurs taux d'élimination du COT (92.5% ±0.26 %) et de l'NT (90.3%±1.1%) ont été également enregistré. A travers ces résultats enregistrés, l'hypothése VI a été confirmé.
- La voie de dégradation principale de la CTC sous radiation solaire favorise la formation du N-dedismethyl-CTC et N-dedismethyl-TC. L'oxydation PEC du CTC durant 180 min du temps de traitement conduit à la formation des intermédiaires aromatiques bicycliques et tricycliques puis à l'ouverture du cycle aromatique pour former divers composés aliphatiques de faible poids moléculaire.

L'étude menée sur la CBZ (résidus médicamenteux de type antiépileptique) a fait ressortir les points suivants:

- La méthodologie des plans d'expérience a permis de décrire le processus de dégradation de la CBZ.
- Le temps de traitement et la concentration initiale du CBZ représentent les paramètres les plus influents dans le processus de dégradation de la CBZ. La contribution du temps de traitement et de la concentration en CBZ sur la réponse est estimée à environ 70.6% et 23.3% respectivement, alors que les effets de l'intensité, de la nature de la cathode et les autres interactions représentent moins de 3%.
- Pour définir les conditions optimales de dégradation du CBZ, un PCC a été ultérieurement employé. L'utilisation du CV à la cathode fonctionnant à une intensité de courant de 0.3 A pendant 120 min et à une concentration initiale en CBZ de 10 mg L^{-1} a

été retenue comme conditions optimales en termes de coût et d'efficacité. Dans ces conditions, un taux d'abattement allant jusqu'à 73.5% ± 2.8% de la CBZ a été enregistré pour un coût total de 2.98 ± 0.1 $ m^{-3} (incluant seulement les coûts d'énergie et d'électrolyte).

- Une minéralisation partielle du CBZ (21.2 ± 7.7% d'élimination du COT) a été enregistrée dans les conditions optimales. La majorité du CBZ a été transformé à des sous-produits durant le traitement PEC. L'acridine, l'acide antharnilique et l'acide salicylique sont les principaux sous-produits de dégradation du CBZ par voie PEC.

L'étude menée sur le traitement tertiaire des eaux usées municipales contaminées par la CTC a fait ressortir les points suivants:

- L'application du procédé PEC sur une telle matrice permet d'enregistrer une dégradation quasi-totale de CTC (99.1%±0.1%) en imposant une intensité de courant de 0.6A pendant 180 min de traitement et en présence d'une photoanode de n-TiO_2:N ayant une teneur de 3.4% d'azote.
- La présence de contaminants organiques autre que la CTC dans les effluents réels influence l'efficacité de minéralisation de la solution. Des taux d'élimination de 85.4% ±3.6% ainsi que de 87.4%±3.1% ont respectivement été enregistrés pour le carbone organique total et pour l'azote total. Aussi, des taux d'élimination de 55.7% ± 2.9% d'azote ammoniacal et de 71.1% ± 3.1% nitrites/nitrates ont été enregistrés.
- Par ailleurs, un taux d'abattement de 95% de coliformes fécaux (1.2 unités d'abattement logarithmique) a été enregistré suite à l'application du procédé PEC.

1.9 Recommandation

Ce travail a permis de montrer l'efficacité du procédé PEC pour le traitement tertiaire de micropolluants réfractaires. Cependant, il serait très important d'effectuer des travaux supplémentaires dans le but d'optimiser l'efficacité de ce procédé.

- Tester le procédé PEC sur d'autres substances prioritaires (polluants émergeants) couramment rencontrées dans les eaux usées et identifiées par les agences environmentales (Di (2-ethylhexyl) phthalate (DEHP), 17 α Ethyléne estradiol (EE2), Naphtaléne, etc).
- Evaluer la performance du procédé PEC en utilisant une photo-anode de TiO_2 couplé avec d'autres semi-conducteurs tels que TiO_2/WO_3, $TiO_2/CdSe$, TiO_2/CdS, etc. Le couplage de TiO_2 avec d'autres types de semiconducteurs (WO_3, CdS, CdSe, etc) est une alternative pour élargir sa gamme spectrale en déplaçant vers la région du visible. Cette modification permettrait de favoriser l'exploitation des radiations visibles présentes dans le spectre solaire et permmetrait d'améliorer simultanément les performances des procédés d'oxydation PEC pour des applications environmentales à grande échelle.
- Tester le procédé en mode d'opération continu tout en ajustant la configuration hydrodynamique de l'unité expérimentale. Le choix judicieux des conditions hydrodynamiques serait favorable à la production des EORs. Suivant l'agitation (écoulement laminaire ou turbulent) au voisinage de l'électrode anodique ou cathodique, il est possible de produire *in situ* différents oxydants à partir de l'oxygéne dissous. Par exemple, le peroxyde d'hydrogéne peut être avantageusement formé en régime laminaire sur une électrode cathodique appropriée. Par la suite, ces éspéces réactives (ex. H_2O_2) peuvent dans la couche de diffusion capter des électrons dans la

bande de condution de TiO_2 et conduire à la formation de radicaux hydroxyles (OH°) suivant la réaction :

$$H_2O_2 + e_{BC}^- \rightarrow OH^- + OH°$$

- Tester à grande échelle le procédé d'oxydation PEC afin de développer son domaine d'application. Ces essais complémentaires permettraient de définir et de confirmer le coût de traitement associé à l'application du procédé d'oxydation PEC (étude technico-économique) et de récueillir les paramétres nécessaires pour la conception d'une unité permanente de grande capacité.

1.10 Références

Adams C, Wang Y, Loftin K & Meyer M (2002) Removal of antibiotics from surface and distilled water in conventional water treatment processes. *J. Environ. Eng.* 128(3): 253-260.

AHI (Animal Health Institute) (2005) www.ahi.org/documents/ antibioticuse2003.pdf.

Ahmed S, Rasul MG, Brown R & Hashib MA (2011) Inluence of parameters on the heterogeneous photocatalytic degradation of pesticides and phenolic contaminants in wastewater: A short review. *J. Environ. Manag.* 92:311-330.

Alatrache A, Laoufi NA, Pons MN, Deik JV & Zahraa O(2010) Tylosin abatement in water by photocatalytic process. *Water Sci. Technol.* 62(2): 435-441.

Ananapattarachai J, Kajitvichyanukul P, Seraphin S (2009) Visible light absorption ability and photocatalytic oxidation activity of various interstitial N-doped TiO_2 prepared from different nitrogen dopants. *J.Hazard. Mater.* 168: 253-261.

Andreozzi R, Campanella L, Fraysse B, Garric J, Gonnella A, Lo Giudice R, Marotta R, Pinto G & Pollio A (2004) Effects of Advanced oxidation processes (AOPs) on the toxicity of a mixture pharmaceuticals. *Water Sci. Technol.* 50:23–28.

Andreu V, Vazguez-Roig P, Blasco C & Pico Y (2009) Determination of tetracycline residues in soil by pressurized liquid extraction and liquid chromatography tandem mass spectrometry. *Anal. Bioanal. Chem.* 394:1329–1339.

Angenault J (2001) Symétrie et structure : cristallochimie du solide : cours et exercices corrigés (Premier et deuxième cycles universitaires). Edition Vuibert, Paris, 646p.

Anglada A, Urtiaga A & I Ortiz (2009) Contributions of electrochemical oxidation to waste-water treatment: fundamentals and review of applications. *J. Chem. Technol. Biotechnol.* 84: 1747-1755.

Arikan OA (2008) Degradation and metabolization of chlortetracycline during the anaerobic digestion of manure from medicated calves. *J. Hazard. Mater.* 158(2-3) 485-490.

Arslan-Alaton I & Gurses F (2004) Photo-Fenton-like and photo-Fenton-like oxidation of Procaine Penicillin G formulation effluent. *J. Photochem. Photobiol.A.* 165 : 165-175.

Auriol M, Filali-Meknassi Y & Tyagi RD (2007) Présence et devenir des hormones stéroïdiennes dans les stations de traitement des eaux usées. *Rev. Sci. Eau* 20(1) : 89-108.

Auriol M, Filali-Meknassi Y, Tyagi RD, Adams CD & Surampalli RY (2006) Endocrine disrupting compounds removal from wastewater, a new challenge. *Procc.Biochem.* 41(3): 525-539.

Bader H & Hoigné J (1981) Determination of ozone in water by the indigo method. *Water Res.* 15 (4): 449-456.

Basha CA, Chithra NK & Sripriyalakshmi NK (2009) Electro-degradation and biological oxidation of non-biodegradable organic contaminants. *Chem.Eng.J.* 149: 25-34.

Batt AL, Kim S & Aga DS (2007) Comparison of the occurrence of antibiotics in four full-scale wastewater treatment plants with varying designs and operations. *Chemosphere* 68:428-435.

Bautitz IR & Nogueira RFP (2007) Degradation of tetracycline by photo-Fenton process-Solar irradiation and matrix effects. *J. Photochem. Photobiol. A.* 187:33–39.

Belkheiri D, Fourcade F, Geneste F, Floner D, Ait-Amar H & Amrane A (2011) Feasibility of an electrochemical pre-treatment prior to a biological treatment for tetracycline removal. *Sep. Purif. Technol.* 83(1): 151-156.

Beltràn FJ, Aguinaco A & Garcia-Araya JF (2009) Mechanism and kinetics of sulfamethoxazole photocatalytic ozonation in water. *Water Res.* 43(5): 1359-1369.

Bessekhouad Y, Chaoui N, Trzpit M, Ghazzal N, Robert D & Weber JV (2006) UV-vis versus visible degradation of acid orange II in a coupled CdS/TiO_2 semiconductors suspension. *J. photochem. Photobiol. A.* 183: 218-224.

Bitton G (2005) *Wastewater Microbiology. Third Edition.* Department of Environmental Engineering Sciences, University of Florida, Willey, Gainesville, FL, 768 p.

Bound JP, Kitsou K & Voulvoulis N (2006) Household disposal of pharmaceuticals and perception of risk to the environment. *Environ Toxicol. Pharmacol.* 21(3) 301-307.

Bound JP & Voulvoulis N (2004) Pharmaceuticals in the aquatic environment—a comparison of risk assessment strategies. *Chemosphere* 56:1143–1155.

Boxall ABA, Fogg LA, Baird DJ, Lewis C, Telfer TC, Kolpin D & Gravell A (2005) Targeted monitoring study for veterinary medecines in the UK environment. Final report to the UK Environment Agency.

Boxall A, Kolpin D, Sorensen B & Toll J (2003) Are veterinary medicines causing environmental risks? *Environ.Sci.Technol.* 37: 286A-294A.

Box GEP, Stuart Hunter J & Hunter WG (2005) Statistics for Experimenters: Design, Innovation, and Discovery, 2nd Edition, 664p.

Burda C, Lou Y, Chen X, Samia ACS, Stout J & Gole JL (2003) Enhanced Nitrogen doping in TiO_2 nanoparticles. *Nano Lett.* 3: 1049-1051.

Brassard D, Sarkar DK, El Khakani MA & Ouellet L (2006) Compositional effect on the dielectric properties of high-k titanium silicate thin films deposited by means of a co-sputtering process. *J. Vacu. Sci. Technol. A* 24: 600-605.

Calisto V, Domingues MRM, Erny GL, Esteves VI (2011) Photodegradation of psychiatric pharmaceuticals in aquatic environments - Kinetics and photodegradation products. *Water Res.* 45 (18):1095-1104.

Canizares P, Lobato J, Paz R, Rodrigo MA, Saez CJ & Rodrigo MA (2005) Electrochemical oxidation of phenolic wastes with boron-doped diamond anodes. *Water Res.* 39: 2687-2703.

Canizares P, Paz R, Sàez C & Rodrigo MA (2009) Costs of the electrochemical oxidation of wastewaters: A comparison with ozonation and Fenton oxidation processes. *J. Environ. Manage.* 90 :410-420.

CEAEQ (2012) Centre d'expertise en analyse environnementale du Québec. Méthode d'analyse. MA. 315-DCO 1.1. Détermination de la demande chimique en oxygéne: méthode de reflux en système fermé suivi d'un dosage par calorimétrie avec le bicharbonate de potassium. Québec, Qu, Canada, 10p.

Chang H-S, Choo KH, Lee B & Choi SJ (2009) The methods of identification, analysis, and removal of endocrine disrupting compounds (EDCs) in water. *J.Hazard.Mater.*172 (1): 1-12.

Chen F, Yang X, Mak HKC & Chan DWT (2010) Photocatalytic oxidation for antimicrobial control in built environment: A brief literature overview. *Build. Environ.* 45 (8): 1747-1754.

Chen G, Zhao L & Dong Yh (2011) Oxidative degradation kinetics and products of chlortetracycline by manganese dioxide. *J. Hazard. Mater.* 193:128–138.

Chen D, Jiang Z, Geng J, Wang Q &Yang D (2007) Carbon and nitrogen Co-doped TiO_2 with enhanced visible light photocatalytic activity. *Ind. Eng. Chem. Res.* 46: 2741-2746.

Chen G (2004) Electrochemical technologies in wastewater treatment. *Sep. Purif. Technol.* 38 (1): 11-41.

Chen D & Ray AK (1998) Photodegradation kinetics of 4-nitrophenol in TiO_2 suspension. *Water Res.* 32 (11): 3223-3234.

Cheng W, Yang M, Xie Y, Fang Z, Nan J & Tsang PE (2013) Electrochemical degradation of the antibiotic metronidazole in aqueous solution by the Ti/SnO2-Sb-Ce anode. Environ.Technol. DOI: 10.1080/09593330.2013.796010.

Cho M, Chung H, Choi W & Yoon J (2004) Linear correlation between inactivation of E.Coli and OH radical concentration in TiO_2 photocatalytic disinfection. Water Res. 38: 1069-1077.

Chong MN & Jin B (2012). Photocatalytic treatment of high concentration carbamazepine in synthetic hospital wastewater. *J. Hazard. Mater. 199-200: 135-142*

Chong MN, Jin B, Chow CWK & Saint C (2010) Recent developments in photocatalytic water treatment technology: A review. *Water Res.* 44: 2997-3027.

Christian T, Schneider R, Farber HA, Skutlarek D, Meyer MT & Glodbach HE (2003) Determination of antibiotic residues in manure, soil, and surface waters. *Acta Hydrochim. Hydrobiol.* 31:36-44.

Cirja M, Ivashechkin P, Scheffer A & Corvini PFX (2008) Factors affecting the removal of organic micropollutants from wastewater in conventional treatment plants (CTP) and membrane bioreactors (MBR). *Rev.Environ.Sci.Biotechnol.* 7(1): 61-78.

Clara M, Strenn B, Gans O, Martinez E, Kreuzinger N & Kroiss H (2005) Removal of selected pharmaceuticals, fragrances and endocrine disrupting compounds in a membrane bioreactor and conventional wastewater treatment plants. *Water Res.* 39: 4797-4807.

Collado N, Buttiglieri G, Marti E, Ferrando-Climent, Rodriguez-Mozaz S, Barcelo D, Comas J & Rodriguez-Roda I (2013) Effects on activated sludge bacterial community exposed to sulfamethoxazole. Chemosphere *DOI: 10.1016/j.chemosphere.2013.04.094.*

Colmenares JC, Luque R, Campelo JM, Colmenares F, Karpinski Z & Romero AA (2009) Nanostructured photoatalysts and their applications in the photocatalytic transformation of Lignocellulosic biomass: An overview. *Materials 2*: 2228-2258.

Comninellis C (1992) Electrochemical treatment of wastewater containing phenol. *Trans. Inst. Chem. Engineers.* 70(4): 219-224.

Daghrir R, Drogui P & Didier R (2012) Photoelectrocatalytic technologies for environmental applications. *J.Photochem.Photobiol.A.*238 : 41-52.

Del Rio AI, Molina J, Bonastre J & Cases F (2009) Study of the electrochemical oxidation and reduction of C.I. Reactive Orange 4 in sodium sulphate alkaline solutions. *J. Hazard.Mater.* 172: 187-195.

De Tacconi NR, Chenthamarakshan CR, Rajeshwar K, Pauporté T & Lincot D (2003) Pulsed electrodeposition of WO_3-TiO_2 composite films. *Electrochem. Commun.* 5: 220-224.

Ding Y, Yang C, Zhu L & Zhang J (2010) Photoelectrochemical activity of liquid phase deposited tio_2 film for degradation of benzotriazole. *J. Hazard. Mater.*175: 96-103.

Ding X & Mou S (2000) Ion chromatographic analysis of tetracyclines using polymeric column and acidic eluent. *J. Chromatogr. A.* 897:205–214.

Di Paola A, Ikeda S, Marci G, Ohtani B & Palmisano L (2001) Transition metal doped TiO_2: physical properties and photocatalytic behavior. *Int. J. photoenergy* 3: 171-176.

Dirany A, Sirés I, Oturan N & Oturan MA (2010) Electrochemical abatement of the antibiotic sulfamethoxazole from water. Chemosphere 81(5): 594-602.

Drogui P, Blais JF & Mercier G (2007) Review of electrochemical technologies for environmental applications. *Recent Patent Eng.* 1: 257-272.

Drogui P, Elmaleh S, Rumeau M, Bernard C & Rambaud A (2001) Oxidising and disinfecting by hydrogen peroxide produced in a two-electrode cell. *Water Res.* 35(13): 3235-3241.

Duran A, Monteagudo JM & Martin S (2012) Photocatalytic treatment of an industrial effluent using artificial and solar UV radiation: An operational cost study on a pilot plant scale. *J.Environ. Manage.* 98: 1-4.

EC (1991) Plant Protection Products Directive 91/414/EC. European Commission.

EC (1998) Biological Products Directive 98/8/EC. European Commission.

EC (2000) Water Framework Directive 2000/60/EC. European Commission.

EC (2006) Groundwater Daughter Directive 2006/118/EC. European Commission.

EC (2011) Review of priority substances under the WFD.

Egerton TA & Christensen PA (2004) *Advanced oxidation processes for water and wastewater treatment.* Ed. Simon Parsons, IWA Publishing, London, p356.

El-Kemary M, El-Shamy H & El-Mehasseb I (2010) Photocatalytic degradation of ciprofloxacin drug in water using ZnO nanoparticles. *J. Luminesc.* 130: 2327-2331.

Elmolla ES & Chaudhuri M (2010) Degradation of amoxicillin, ampicillin and cloxacillin antibiotics in aqueous solution by the UV/ZnO photocatalytic process. *J. Hazard. Mater.* 173: 445-449.

Esquivel K, Arriaga LG, Rodriguez FJ, Martinez L & Godinez LA (2009) Degradation of chlorophenols by means of advanced oxidation processes: A general review. *Water Res.* 43: 3593-3603.

Esplugas S, Bila DM, Krause LGT & Dezotti M (2007) Ozonation and advanced oxidation technologies to remove endocrine disrupting chemicals (EDCs) and pharmaceuticals and personal care products (PPCPs) in water effluents. *J.Hazrd.Mater.* 149(3): 631-642.

Farber H (2002) Antibiotika im Krankenhausabwasser (Antibiotics in the hospital sewage). Hyg.Med.27, 35

Fent K, Weston AA & Caminada D (2006) Ecotoxicology of human pharmaceuticals. *Aquat Toxicol.* 76:122–159.

Fraga LE, Anderson MA, Beatriz MLPMA, Paschoal FMM, Romao LP & Zanoni MVB (2009) Evaluation of the photoelectrocatalytic method for oxidizing chloride simultaneous removal of microcystin toxins in surface waters. *Electrochem. Acta.* 54: 2069-2076.

Galey C & PaSlawski D (1993) Élimination des micropolluants par l'ozone couplé avec le peroxyde d'hydrogène dans le traitement de potabilisation des eaux. *L'Eau, L'Industrie, Les Nuisances*, 161: 46-49.

Gao P, Ding Y, Li H & Xagoraraki I (2012) Occurrence of pharmaceuticals in a municipal wastewater treatment plant: mass balance and removal processes. *Chemosphere* 88:17–24.

Giger W, Alder AC, Golet EM, Kohler HPE, McArdell CS, Molnar E, Siegrist H & Suter MJF (2003) Occurrence and fate of antibiotics as trace contaminants in wastewaters, sewage sludges, and surface waters. *Chimia* 57: 485-491.

Giraldo AL, Penuela GA, Torres-Palma RA, Pino NJ, Palominos RA & Mansilla HD (2010) Degradation of the antibiotic oxolinic acid by photocatalysis with TiO_2 in suspension. *Water Res.* 5158-5167.

Gobel A, Thomsen A, McArdell CS, Joss A & Giger W (2005) Occurrence and sorption behavior of sulfonamides, macro-lides and trimethoprim in conventional activated sludge treatment. *Env. Sci. Tech.* 39: 3981-3989.

Guo Y, Zhang XW, Weng WH & Han GR (2007) Structure and properties of nitrogen-doped titanium dioxide thin films grown by atmospheric pressure chemical vapor deposition. *Thin Solid Films* 515: 7117-7121.

Guivarch ZE (2004) Traitement des polluants organiques en milieux aqueux par procédé éléctrochimique d'oxydation avancée « Éléctro-Fenton ». Application à la minéralisation des colorants synthétiques. Thése de Doctorat, Université de Marne –la-Vallée, Institut Francilien des Géosciences, Marne-la –Valée, France, 235p.

Gross B, Montgomery-Brown J, Naumann A, Reinhard M (2004) Occurrence and Fate of pharmaceuticals and Alkylphenol Ethoxylate Metabolites in An effluent-Dominated River and Wetland. Environ.Toxicol. Chem. 23: 2074-2083.

Haidar M, Dirany A, Sirés I, Oturan N & Oturan MA (2013) Electrochemical degradation of the antibiotic sulfachloropyridazine by hydroxyl radicals generated at a BDD anode. *Chemosphere* 91(9): 1304-1309.

Halling-Sorensen B, Nielsen SN, Lanzky PF, Ingerslev F, Lutzhoft HCH & Jorgensen SE (1998) Occurrence, fate and effects of pharmaceutical subsatnces in the environment-a review. *Chemosphere* 36:357–394.

Hammad Khan M, Jung HS, Lee W & Jung JY (2013) Chlortetracycline degradation by photocatalytic ozonation in the aqueous phase: Mineralization and the effect on biodegradability. *Environ. Technol* (United Kingdom) 34(4): 495-502.

Hamscher G, Pawelzick HT, Hoper H, Nau H (2005) Different behavior of tetracyclines and sulfonamides in sandy soils after repeated fertilization with liquid manure. *Environ.Toxicol.Chem.* 24: 861-868.

Hapeshi E, Achilleos A, Vasquez MI, Michael C, Xekoukoulotakis NP, Mantzavinos D & Kassinos D (2010) Drugs degrading photocatalytically: Kinetics and mechanisms of ofloxacin and atenolol removal on Titania suspensions. *Water Res.* 44(6): 1737-1746.

Hajjaji A, Gaidi M, Bessais B, El Khakani MA (2011) Effect of Cr incorporation on the structural and optoelectronic propert ies of TiO_2: Cr deposited by means of a magnetron co-sputtering process. *Appl. Surf. Sci.* 25: 10351-10357.

Heberer T (2002) Occurrence, fate, and removal of pharmaceutrical residues in the aquatic environment: a review of recent research data. *Toxicol. Lett.*131 (1-2): 5-17.

Heit G, Neuner A, Saugy PY & Braun AM (1998) Vacuum-UV (172 NM) Actinometry-the quantum yield of the photolysis of water. *J. Phys. Chem. A.* 102: 5551-5561.

Henze M, Harremoes P, Jansen J, Cour LA & Arvin E (2002) *Wastewater Treatment: Biological and Chemical Process. Third Edition.* Springer, Berlin, Allemagne, 430 p.

Hernandez F, Sancho JV, Ibanez M & Guerrero C (2007) Antibiotic residue determination in environment waters by LC-MS. *TrACTrend Anal. Chem.* 26:466–485.

Hirsch R, Ternes T, Haberer K & Kratz KL (1999) Occurrence of antibiotics in the aquatic environment. *Sci.Total Environ.* 225: 109-118.

Homem V & Santos L (2011) Degradation and removal methods of antibiotics from aqueous matrices-a review. *J. Environ. Manag.* 92:2304–2347.

Hu L, Martin HM & Strathmann TJ (2010a) Oxidation kinetics of antibiotics during water treatment with potassium permanganate. *Environ. Sci. Technol.* 44:6416–6422

Hu X, Zhou Q & Luo Y (2010b) Occurrence and source analysis of typical veterinary antibiotics in manure, soil, vegetables and groundwater from organic vegetable bases, northern China. *Environ. Pollut.* 158: 2992–2998.

Huang CH & Sedlak DL (2001) Analysis of estrogenic hormones in municipal wastewater effluent and surface water using enzyme-linked immunosorbent assay and gaz chromatography/tandem mass spectrometry. *Environ Toxicol Chem* 20(1):133-139.

Jeong J, Song W, Cooper WJ, Jung J & Greaves J (2010) Degradation of tetracycline antibiotics: mechanisms and kinetic studies for advanced oxidation/reduction processes. *Chemosphere* 78(5): 533–540.

Jiang YL, Liu HL, Wang QH & Jiang ZH (2006) Determination of hydroxyl radicals in TiO_2/Ti photoelectrocatalytic oxidation system using $Fe(phen)_3^{2+}$ spectrophotometry. *J. Environ.Sci.* 18:158-161.

Jjemba PK (2006) Excretion and ecotoxicity of pharmaceutical and personal care products in the environment. *Ecotox. Environ. Safe.* 63:113–130.

Jones OAH, Voulvoulis N & Lester JN (2002) Aquatic environmental assessment of the top 25 English prescription pharmaceuticals. *Water Res.* 36: 5013-5022.

Joss A, Zabczynski S, Gobel A, Hoffmann B, Loffler D, McArdell CS, Ternes TA, Thomsen A & Siegrist H (2006) *Water Res.* 40: 1686-1696.

Karthikeyan KG & Meyer MT (2006) Occurrence of antibiotics in wastewater treatment facilities in Wisconsin, USA. Sci. Total Environ. 361:196–207.

Kay P, Blackwell PA, Boxall ABA (2005) Transport of veterinary antibiotics in overland flow following the application of slurry to arable land. *Chemosphere* 59: 951-959.

Khataee AR, Safarpour M, Zarei M & Aber S (2012) Combined heterogeneous and homogeneous photodegradation of a dye using immobilized TiO_2 nanophotocatalyst and modified graphite electrode with carbon nanotubes. *J.Mol.Catal.A.Chem.* 363-364: 58-68.

Kim I & Tanaka H (2009) Photodegradation characteristics of PPCPS in water with UV treatment. *Environ. Inter.* 35:793–802.

Kim I, Yamashita N & Tanaka H (2009) Photodegradation of pharmaceuticals and personal care products during UV and UV/H_2O_2 treatments. *Chemosphere* 77: 518-525.

Kim S, Kim T, Park C & Shin EB (2003) Electrochemical oxidation of polyvinylalcohol using a RuO_2/Ti anode. *Desalination*. 155 (1): 49-57.

Koesukwiwat U, Jayanta S & Leepipatpiboon N (2007) Validation of a liquid chromatography–mass spectrometry multi-residue method for the simultaneous determination of sulfonamides, tetracyclines, and pyrimethamine in milk. *J. Chromatogr. A.* 1140: 147–156.

Kolok AS, Snow DD, Kohno S, Sellin MK, Guillette LJ (2007) Occurrence and biological effect of exogenous steroids in the Elkhorn River, Nebraska, USA. *Sci. Total. Environ.* 388: 104-115.

Kolpin DW, Furlong ET, Meyer MT, Thurman EM, Zaugg SD, Barber LB & Buxton HT (2002) Pharmaceuticals, hormones, and other organic wastewater contaminants in U.S. streams, 1999-2000: a national reconnaissance. *Environ.Sci.Technol.* 36: 1202-1211.

Kumar AK, Chiranjeevi P, Mohanakrishna G & Mohan SV (2011) Natural attenuation of endocrine-disrupting estrogens in an ecologically engineered treatment system (eets) designed with floating, submerged and emergent macrophytes. *Ecol.Eng.* 37(10): 1555-1562.

Kummerer K (2009) Antibiotics in the aquatic environment—a review-part I. *Chemosphere* 75:417–434.

Kuemmerer K (2003) significance of antibiotics in the environment. *J. Antimicrob. Chemother.* 52(1): 5-7.

Kummerer K (2001) Drugs in the environment: Emission of drugs, diagnostic aids and disinfectants into wastewater by hospitals in relation to other sources-A review. *Chemosphere* 45 (6-7): 957-969.

Krapac IG, Koike S, Meyer MT, Snow DD, Chou SFJ, Mackie RI, Roy WR & Chee-Sandford JC (2005) Long-term monitoring of the occurrence of antibiotic residues and antibiotic resistance in groundwater near swine confinement facilities. Report of the CSREES project 2001-35102-10774.

Lai HT, Hou JH, Su CI, Chen CI (2009) Effects of Chloramphenicol, florfenicol, and thiamphenicol on growth of algae Chlorella pyrenoidosa, Isochrysis galbana, and Tetraselmis chui. *Ecotoxicol. Environ. Safe.* 72: 329-334.

Leng WH, Zhu WC, Ni J, Zhang Z, Zhang JQ & Cao CN (2006) Photoelectrocatalytic destruction of organics using Ti_{O2} as photoanode with simultaneous production of H_2O_2 at the cathode. *Appl. Catal.A.* 300: 24-35.

Lester Y, Avisar D & Mamane H (2010) Photodegradation of the antibiotic sulphamethoxazole in water with UV/H_2O_2 advanced oxidation process. *Environ. Technol.* 31 (2): 175-183.

Li R, Zhang Y, Lee CC, Liu L & Huang Y (2011) Hydrauphilic interaction chromatography separation mechanisms of tetracyclines on amino-bonded silica column. *J. Sep. Sci.* 34:1508–1516.

Li W, Guo C, Su B & Xu J (2012) Photodegradation of four fluoroquinolone compounds by titanium dioxide under simulated solar light irradiation. *J.Chem.Technol.Biotechnol.* 87: 643-650.

Li K, Yediler A, Yang M, Schulte-Hostede S & Wong MH (2008) Ozonation of oxytetracycline and toxicological assessment of its oxidation by-products. Chemosphere 73(3) 473-478.

Li XZ, Zhao BX & Wang P (2007) Degradation of 2, 4-dichlorophenol in aqueous solution by a hybrid oxidation process. *J. Hazard. Mater.* 147 (1-2): 281-287.

Li XZ, Li FB, Fan CM & Sun YP (2002) Photoelectrocatalytic degradation of humic acid in aqueous solution using a Ti/TiO_2 mesh photo electrode. *Water Res.* 36: 2215-2224.

Li XZ, Liu HL, Yue PT & Sun YP (2000) Photoelectrocatalytic oxidation of rose Bengal in aqueous solution using a Ti/TiO_2 mesh electrode. *Environ.Sci.Technol.* 34 (20): 4401-4406.

Linsebigler AL, Lu G & Yates JT (1995) Photocatalysis on TiO_2 surfaces: Principles, mechanisms, and selected results. *Chem. Rev.* 95(3): 735-758.

Lister AL & Van Der Kraak GJ (2001) Endocrine disruption: Why is it so complicated? *Water Qual. Res. J. Can.* 36(2): 175-190.

Liu F, Ying GG, Tao R, Zhao JL, Yang JF & Zhao LF (2009) Effects of six selected antibiotics on plant growth and soil microbial and enzymatic activities. *Environ. Pollut.* 157:1636–1642.

Liu Y, Gan X, Zhou B, Xiong B, Li J, Dong C, Bai J & Cai W (2009) Photoelectrocatalytic degradation of tetracycline by highly effective TiO_2 nanopore arrays electrode. *J. Hazard.Mater.* 171: 678-683.

Lopez Pen˜alver JJ, Gomez Pacheco CV, Sanchez Polo M & Utrilla JR (2012) Degradation of tetracyclines in different water matrices by advanced oxidation/reduction processes based on gamma radiation. *J. Chem. Technol. Biot.* doi:10.1002/jctb.3946.

Lopez-Penalver JJ, Sa`nchez-Polo M, Go`mez-Pacheco CV & Rivera-Utrilla J (2010) Photodegradation of tetracyclines in aqueous solution by using UV and UV/H_2O_2 oxidation processes. *J. Chem. Technol. Biot.* 85:1325–1333.

Lucas MS, Peres JA & Puma GL (2010) Treatment of winery wastewater by ozone-based advanced oxidation processes (O_3, O_3/UV and O_3/UV/H_2O_2) in a pilot-scale bubble column reactor and process economics. *Sep. Purf. Technol.* 72: 235-241.

Luo Y, Xu L, Rysz M, Wang Y, Zhang H & Alvarez PJJ (2011) Occurrence and transport of tetracycline, sulfonamide, quinolone, and macrolide antibiotics in the Haihe River Basin, China. *Environ. Sci. Technol.* 45:1827–1833.

Ma L & Tu SX (2011) Removal of Arsenic from aqueous solution by two types of nano TiO_2 crystals. *Environ. Chem.Lett.* 9: 465-472.

Macphee DE, Rosenberg D, Skellern MG, Wells RP, Duffy JA & Killham KS (2011) A tungsten oxide-based photoelectrocatalyst for degradation of environmental contaminants. *J. Solid State Electrochem.*15: 99-103.

Malato S, Fernandez-Ibanez P, Maldonado MI, Blanco J & Gernjak W (2009) Decontamination and disinfection of water by solar photocatalysis : Recent overview and trends. *Catal. Today* 147 (1): 1-59.

Malato S, Blanco J, Vidal A & Richter C (2002) Photocatalysis with solar energy at a pilot-plant scale: An overview. *Appl.Catal.B.* 37(1): 1-15.

Manka J, Rebhun M, Mandelbaum A & Bortinger A (1974) Characterization of organics in secondary effluents. *Environ. Sci. Technol.* 8: 1017-1020.

Mansour D, Fourcade F, Bellakhal N, Dachraoui M, Hauchard D & Amrane A (2012) Biodegradabilily improvement of sulfamethazine solutions by means of an electro-fenton process. *Water, Air soil Pollut.* 223(5): 2023-2034.

Martinetti R (2007) Industrial liquid effluents in the textile industry. In M. Cox, P. Négré & L. Yurramendi (Eds). A guide book on the treatment of effluents from the Mining/Metallurgy, Paper, Plating and Textile Industries San Sebastiàn, Spain: Inasment tecnalia, 137-173.

Martinez C, Canle ML, Ferna`ndez MI, Santaballa JA & Faria J (2011) Kinetics and mechanism of aqueous degrdation of carbamazepine by heterogenous photocatalysis using nanocristalline TiO_2, ZnO_2 and multi-walled carbon nanotube-anatase composites. *Appl. Catal. B Environ.* 102:563–571.

Marugàn J, Aguado J, Gernjak W & Malato S (2007) Solar photocatalytic degradation of Dichloroacetic acid with silica-supported titania at pilot-plant scale. *Catal.Today* 129: 59-68.

Matin G (1982) Point sur l'épuration et le traitement des effluents. Technique et Documentation Lavoisier, Paris, France, 298p.

Myers & Montgomery DC (2002) Response surface methodology: Process and product optimization using designed experiments, 2nd ed, John Wiley and Sons, New York, NY, USA, 798 pp.

Miyata M, Ihara I, Yoshid G, Toyod K & Umetsu K (2011) Electrochemical oxidation of tetracycline antibiotics using a Ti/IrO_2 anode for wastewater treatment of animal husbandry. *Water Sci. Technol.* 63 (3): 456-461.

Muckter H (2006) Antibiotika-Ruckstande im Trinkwasser. 47. Arbeitstagung des Arbeitsgebiets Lebensmittelhygiene, Garmisch-Patenkirchen.

Muff J, Bennedsen LR & Søgaard EG (2011) Study of electrochemical bleaching of p-nitrosodimethylaniline and its role hydroxyl radical probe compound. *J. Appl. Electrochem.* 41(5): 599-607.

Naddeo V, Ricco D, Scannapieco D, Belgiorno V (2012) Degradation of Antibiotics in Wastewater during Sonolysis, Ozonation, and Their Simultaneous Application: Operating Conditions Effects and Processes Evaluation. *Inter. J. Photoener.* ID 624270. doi:10.1155/2012/624270.

Nasuhoglu D, Yargeau V & Berk D (2011) Photo-removal of sulfamethoxazole (SMX) by photolytic and photocatalytic processes in a batch reactor under UV-C radiation (λ_{max} = 254 nm). *J.Hazrd.Mater.*186: 67-75.

Neuman-Spallart M (2007) Aspects of Photocatalysis on Semiconductors: Photoelectrocatalysis. *Chimica Inter. J. Chem.* 61: 806–809.

Nieto J, Freer J, Contreras D, Candal RJ, Sileo & Mansilla HD (2008) Photocatalysed degradation of flumequine by doped TiO_2 and simulated solar light. *J. Hazard. Mater.* 155: 45-50.

Ohno T, Sarukawa K & Matsumura M (2001) Photocatalytic Activities of Pure Rutile Particles Isolated from TiO_2Powder by Dissolving the Anatase Component in HF Solution. *J. Phys.Chem. B.* 105: 2417–2420.

Ohtani B, Ogawa Y & Nishimoto S-I (1997) Photocatalytic activity of amorphousanatase mixture of titanium (IV) oxide particles suspended in aqueous solutions. *J.phys.Chem. B.* 101(19): 3746-3752.

Olmez T (2009) The optimization of Cr(VI) reduction and removal by electrocoagulation using response surface methodology. *J.Hazard.Mater.* 162: 1371-1378.

Olya ME, Pirkarami A, Soleimani M & Bahmaei M (2013) Photoelectrocatalytic degradation of acid dye using Ni-TiO2 with the energy supplied by solar cell: Mechanism and economical studies. *J.Environ.Manage.* 121: 210-219.

Onal A (2011) Overview on liquid chromatographic analysis of tetracycline residues in food matrices. *Food Chem* 127:197–203.

Ostapyk K, Innes E, Servos M, Boudrias R & Van Sickle K (2007) Vers la création d'un réseau de surveillance: un atelier technique sur les produits pharmaceutiques et de soins personnels présents dans l'environnement. Forum scientifique de Santé Canada 2007: Intégrer la science, la réglementation et l'élaboration de politiques pour améliorer la santé des Canadiens. Bureau de l'expert scientifique en chef de Santé Canada Ottawa (Ontario) 8 et 9 novembre 2007.

Oturan N, Wu J, Zhang H, Sharma VK & Oturan MA (2013) Electrocatalytic destruction of the antibiotic tetracycline in aqueous medium by electrochemical advanced oxidation processes: Effect of electrode materials. *Appl. Catal. B.* 140-141: 92-97.

Ouyang J, Chang M & Li X (2012) CdS-sensitized ZnO nanorod arrays coated with TiO_2 layer for visible light photoelectrocatalysis. *J. Mater. Sci.* 47: 4187-4193.

Pal A, Gin KYH, Yy-Chen Lin A, Reinhard M (2010) Impacts of emerging organic contaminants on freshwater resources: Review of recent occurences, sources, fate and effects. *Sci. Total. Environ.* 408: 6062-6069.

Pan X, Qiang Z, Ben W & Chen M (2011) Residual veterinary antibiotics in swine manure from concentrated animal feeding operations in Shandong Province, China. *Chemosphere* 84:695–700.

Panizza M, Zolezzi M & Nicolella C (2006) Biological and electrochemical oxidation of naphthalenesulfonates. *J. Chem. Technol. Biotechnol.* 81: 225-232.

Parck H & Choung YK (2007) Degradation of antibiotics (tetracycline, sulfathiazole, ampicillin) using enzyme of glutathione S-transferase. *Hum. Ecol. Risk Assess.* 13(5):1147-1155.

Park JH, Kim S & Bard AJ (2006) Novel Carbon-doped TiO_2 nanotube arrays with high aspect Ratios for efficient solar water splitting. *Nano Lett.* 6: 24-28.

Pareek V, Chong S, Tadé M & Adesina AA (2008) Light intensity distribution in heterogeous photocatalytic reactors. *Asia-Pacific J. Chem. Eng.* 3 (2): 171-201.

Park JW. (2000) *Surimi and Surimi Seafood.* Marcel Dekker, Taylor and Francis, New York, NY, 500 p.

Parsons S (2004) Advanced oxidation processes for water and wastewater treatment. *IWA Publishing,* Alliance House, Londres, Angleterre, 356 p.

Paschoal FMM, Anderson MA & Zanoni MVB (2009) The Photoelectrocatalytic oxidative treatments of textile wastewater containing disperse dyes. *Desalination* 249 (3): 1350-1355.

Peng YP, Yassitepe E, Yeh YT, Ruzybayev I, Shah SI & Huang CP (2012) Photoelectrochemical degradation of azo dye over pulsed laser deposited nitrogen-doped TiO_2 thin film. *App.Catal. B.* 125: 465-472.

Peng F, Cai L, Huang L, Yu H & Wang H (2008) Preparation of nitrogen-doped titanium dioxide with visible-light photocatalytic activity using a facile hydrothermal method. *J. Phys. Chem. Solids* 69: 1657-1664.

Pera-Titus M, Garcia-Molina V, Banos MA, Giménez J, Esplugas S (2004) Degradation of chlorophenols by means of advanced oxidation processes: A general review. *Appl. Catal. B. Environ.* 47: 219-256.

Prado N, Ochoa J & Amrane A (2009) Biodegradation and biosorption of tetracycline and tylosin antibiotics in activated sludge system. *Proc.Biochem.* 44: 1302-1306.

Quan X, Ruan X, Zhao H, Chen S & Zhao Y (2007) Photoelectrocatalytic degradation of pentachlorophenol in aqueous solution using TiO_2 nanotube film electrode. *Environ. Pollut.* 147 (2): 409-414.

Rajeshwar K and J. Ibanez (1997) Environmental Electrochemistry: Fundamentals and Applications in Pollution Abatement, *Academic Press*, San Diego, CA.

Rajeshwar K, Ibanez JG & Swain GM (1994) Electrochemistry and the environment. *J. Appl. Electrochem.* 24 (11): 1077-1091.

Rajkumar D & Palanivelu K (2004) Electrochemical treatment of industrial wastewater. *J.Hazard.Mater.* B113: 123-129.

Rebhun M. & Manka J (1971) Classification of organics in secondary effluents. *Environ. Sci. Technol.* 5: 606-609.

Ren W, Ai Z, Jia F, Zhang L, Fan X & Zou Z (2007) Low temperature preparation and visible light photocatalytic activity of mesoporous carbon-doped crystalline TiO_2. *Appl.Catal. B.* 69: 138-144.

Rehman S, Ullah R, Butt AM & Gohar ND (2009) Strategies of making TiO_2 and ZnO visible light active. *J. Hazard. Mater.* 170: 560-569.

Rivera AP, Tanaka K & Hisanaga T (1993) Photocatalytic degradation of pollutant over TiO_2 in different crystal structures. *Appl.Catal.B.* 3 (1): 37-44.

Robert D (2007) Photosensitization of TiO_2 by M_xO_y and M_xS_y nanoparticles for heterogeneous photocatalysis applications. *Catal. Today* 122: 20-26.

RxList (2006) The Internet Drug Index. http://www.rxlist.com.

Sakatani Y, Grosso D, Nicole L, Boissière C, Soler-Illia G, Sanchez C (2006) Optimized photocatalytic activity of grid-like mesoporous TiO_2 films: effect of crystallinity, pore size distribution, and pore accessibility. *J. Mater. Chem.*16: 77-82.

Sarmah AK, Meyer MT, Boxall ABA (2006) A global perspective on the use, sales, exposure pathways, occurrence, fate and effects of veterinary antibiotics (VAs) in the environment. *Chemosphere* 65:725–759.

Sacher F, Gabriel S, Metzinger M, Stretz A, Wenz M, Lange FT, Brauch HJ & Blankenhorn I (2002) Active pharmaceutical ingredients in ground water-the results of a monitoring program in BadenWurttemberg (Germany) Vom Wasser 99: 183-196.

Scheytt TP, Mersmann R, Heberer LT (2005) 1-Octanol/water partition coefficients of 5 pharmaceuticals from human medical care: Carbamazepine, clofibric acid, diclofenac, ibuprofen, and propyphenazone. *Water Air Soil Pollut.* 165 (1-4): 3-11.

Schwarzenbach RP, Escher BI, Fenner K, Hofstetter TB, Johnson CA, Gunten Uv, Wehrli B (2013) The challenge of micropollutants in aquatic systems. *Science* 313: 1072-1077.

Sclafani A & Herrmann JM (1996) Comparison of the photoelectronic and photocatalytic activities of various anatase and rutile forms of titania in pure liquid organic phase and in aqueous solutions. *J. Phys. Chem.* 100: 13655-13661.

Sczesny S, Nau H & Hamscher G (2003) Residue analysis of tetracyclines and their metabolites in eggs and in the environment by HPLC coupled with a microbiological assay and tandem mass spectrometry. *J. Agric. Food Chem.* 51:697–703.

Selcuk H, Sene JJ & Anderson MA (2003) Photoelectrocatalytic humic acid degradation kinetics and effect of pH, applied potential and inorganic ions. *J. Chem.Technol. Biotechnol.*78 (9): 979-984.

Senthilnathan J & Philip L (2010) Photocatalytic degradation of lindane under UV and visible light using N-doped TiO_2. *Chem. Eng. J.* 161: 83-92.

Servos MR, Bennie DT, Burnison BK, Jurkovic A, Mclnnis R, Neheli T, Schnell A & Ternes TA (2005) Distribution of estrogens, 17β-estradiol and estrone, in Canadian municipal wastewater treatment plants. *Sci. Total Environ.* 336 (1-3): 155-170.

Shelver WL, Hakk H, Larsen GL, DeSutter TM & Casey FXM (2010) Development of an ultra-high-pressure liquid chromatography– tandem mass spectrometry multi-residue sulfonamide method and its application to water, manure slurry, and soils from swine rearing facilities. *J.Chromatogr. A.* 1217:1273–1282.

Shi JC, Liao XD, Wu YB & Liang JB (2011) Effect of antibiotics on methane arising from anaerobic digestion of pig manure. Anim.Feed Sci. Technol 166-167.

Simonsen ME, Muff J, Bennedsen LR, Kowalski KP & SØgaard EG (2010) Photocatalytic bleaching of p-nitrosodimethylaniline and a comparison to the performance of other AOP technologies. *J. Photochem. Photobiol .A.* 216: 244-249.

Sigler PB.& Masters BJ (1957) The hydrogen peroxide-induced Ce(III)-Ce(IV) exchange system. *J. Amer. Chem. Soc.* 79: 6353-6357.

Snyder SA, Wersterhoff P, Yoon Y & Sedlak DL (2003) Pharmaceuticals, personal care products, and endocrine disruptors in water: Implication for water industry. *Environ. Eng. Sci.* 20(5): 449-469.

Sohrabi MR & Ghavami M (2010) Comparison of direct yellow 12 dyes degradation efficiency using uv/semiconductor and UV/H_2O_2/semiconductor systems. *Desalination* 252: 157-162.

Spongberg AL & Witter JD (2008) Pharmaceutical compounds in the wastewater process stream in Northwest Ohio. *Sci. Total Environ.* 397:148–157.: 457-463.

Sun Q & Xu Y (2010) Evaluating intrinsic photocatalytic activities of anatase and rutile TiO_2 for organic degradation in water. *J phys. Chem.C* 114 (44): 18911-18918.

Suty H, De Traversay C & Coste M (2003) Application of advanced oxidation processes: present: Present and future. Dans: *Proceedings of the 3rd conference on oxidation technologies for water and wastewater treatment.* 18 au 22 mai, Goslar, Germany, p. 8.

Szpyrkowicz L, Kaul SN & Neti RN (2005) Tannery wastewater treatment by electro-oxidation coupled with a biological process. *J. Appl. Electrochem.* 35(4): 381-390.

Ternes TA (1998) Occurences of drugs in German sewage treatment plants and rivers. *Water Res.* 32: 3245-3260.

Tong ZL, Liu YL, Hu ZH & Yuan SJ (2012) Anaerobic digestion of animal manure contaminated by tetracyclines. *Environ. Sci.* 33(3):1028-1032.

Thiruvenkatachari R, Vigneswaran S & Moon IS (2008) A review on UV/TiO_2 photocatalytic oxidation process. *Korean J.Chem.Eng.*25 (1): 64-72.

Tsai SJ & Cheng S (1997) Effect of TiO_2 crystalline structure in photocatalytic degradation of phenolic contaminants. *Catal. Today* 33: 227-237.

Valentin CD, Finazzi E, Pacchioni G, Selloni A, Livraghi S, Paganini MC & Giamello E (2007) N-doped TiO_2: Theory and experiment. *Chem. Phys.* 339: 44-56.

Verstraete W (2004) *European Symposium on Environmental Biotechnology*, ESEB, CRC Press, Boca Raton, FL, 928 p.

Waldner G, Pourmodjib M, Bauer R & Neumann-Spallart M (2003) Photoelectrocatalytic degradation of 4-chlorophenol and oxalic acid on titanium dioxide electrodes. *Chemosphere* 50: 989-998.

Wang WY, Yang ML, Ku Y (2010) Photoelectrocatalytic decomposition of dye in aqueous solution using nafion as an electrolyte. *Chem. Eng. J.* 165: 273–280.

Wang N, Li X, Wang Y, Quan X & Chen G (2009) Evaluation of bias potential enhanced photocatalytic degradation of 4-chlorophenol with tio_2 nanotube fabricated by anodic oxidation method, *Chem.Eng. J.* 146: 30-35.

Wang H & Lewis JP (2006) Second-generation photocatalytic materials: anion-doped TiO_2. *J. Phys.Condens. Matter.* 18: 421-434.

Wang H & Lewis JP (2005) Effects of dopant states on photoactivity in carbon-doped TiO_2, *J. Phys.:* Condens. Matter. 17: L209-L213.

Watkinson AJ, Murby EJ, Costanzo SD (2007) Removal of antibiotics in conventional and advanced wastewater treatment: Implications for environmental discharge and wastewater recycling. *Water Res.* 41: 4164-4176.

Xiang Q, Yu J & Wong PK (2011) Quantitative characterization of hydroxyl radicals produced by various photocatalysts. *J.Colloid. Interf. Sci.* 357 (1):163-167.

Xie YB & Li XZ (2006) degradation of Bisphenol A in aqueous solution by H_2O_2-assisted photoelectrocatalytic oxidation. *J. Hazard.Mater.* B138, 526-533.

Xu Y, Zhong D & Jia J (2008) Degradation of Dye wastewater using a rotating TiO_2/Ti disc photoanode. *2nd International Conference on Bioinformatics and Biomedical Engineering*. Article n°. 4535306: 3696-3699.

Yang L, Yu LE & Ray MB (2009) Photocatalytic oxidation of paracetamol: Dominant Reactants, Intermediates and Reactions mechanisms. *Environ. Sci. Technol.* 43: 460-465.

Yang J, Dai J, Chen C & Zhao J (2009) Effect of hydroxyl radicals and oxygen species on the 4-chlorophenol degradation by Photoelectrocatalytic reactions with TiO_2-film electrodes. *J. Photochem. Photobiol A.* 208: 66-77.

Yang S & Carlson K (2004) Routine monitoring of antibiotics in water and wastewater with a radioimmunoassay technique. *Water Res.* 38(14-15): 3155-3166.

Yahiaoui I, Aissani-Benissad F, Fourcade F & Amrane A (2013) Removal of tetracycline hydrochloride from water based on direct anodic oxidation (Pb/PbO_2 electrode) coupled to activated sludge culture. *Chem. Eng. J.* 221: 418-425.

Yahiat S, Fourcade F, Brosillon S & Amrane A (2011) Removal of antibiotics by an integrated process coupling photocatalysis and biological treatment-case of tetracycline and tylosin. *Int. Biodeter. Biodegr.* 65: 997-1003.

Yao H, Sun P, Minakata D, Crittenden JC & Huang CH (2013) Kinetics and modeling of degradation of Ionophore antibiotics by UV and UV/H_2O_2. *Environ.Sci.Technol.* 47: 4581-4589.

Ye X, Sha J, Jiao Z & Zhang L (1997) Thermoanalytical characteristics of nanocrystalline brookite-based titanium dioxide. *Nanostruct.Mater.* 8(7): 919-927.

Yoon Y, Westerhoff P, Snyder SA, Wert EC & Yoon J (2007) Removal of endocrine disrupting compounds and pharmaceuticals by nanofiltration and ultrafiltration membranes. *Desalination* 202 (1-3): 16-23.

Yu J, Wang G, Cheng B & Zhou M (2007) Effects of hydrothermal temperature and time on the photocatalytic activity and microstructures of bimodal mesoporous TiO_2 powders. *Appl.Catal. B. Environ.* 69: 171-180.

Zalazar CS, Martin CA & Cassano AE (2005) Photocatalytic intrinsinc reaction kinetics. II: Effect of oxygen concentration on the kinetics of the photocatalytic degradation of dichloroacetic acid. *Chem. Eng. Sci.* 60 (15): 4311-4322.

Zaviska F, Drogui P, Blais JF, Mercier G & DE la Rochebrochard d'Auzay S (2013) Electrochemical oxidation of chlortetracycline using Ti/IrO_2 and Ti/PbO_2 anode electrodes: Application of electrochemical design methodology. *J. Environ. Eng.* 139 : 810-821..

Zaviska F, Drogui P, Blais JF, Mercier G & Lafrance P (2011) Experimental design methodology applied to electrochemical oxidation of the herbicide atrazine using Ti/IrO_2 and Ti/SnO_2 circular anode electrodes. Journal of Hazardous Materials 185: 1499-1507.

Zaviska F, Drogui P, Mercier G & Blais JF (2009) Procédés d'oxydation avancée dans le traitement des eaux et des effluents industriels : Application à la dégradation des polluants réfractaires. *Revue des Sciences de l'eau 22(4): 535-564.*

Zhang Y, Xiong X, Han Y, Zhang X, Shen F, Deng S, Xiao H, Yang X, Yang G & Peng H (2012) Photoelectrocatalytic degradation of recalcitrant organic pollutants using TiO_2

film electrodes: an overview. *Chemosphere* 88: 145-154.Zhang J, Fu D, Xu Y & Liu C (2010) Optimization of parameters on photocatalytic degradation of chloramphenicol using TiO_2 as photocatalyist by response surface methodology. *J. Environ. Sci.* 22(8): 1281-1289.

Zhang H, Liu F, Wu X, Zhang J & Zhang D (2009) Degradation of tetracycline in aqueous medium by electrochemical method. *Pac. J. Chem. Eng.* 4: 568-573.

Zhang L, Lv L, Zhang W, Li R, Zhong H, Zhao Y, Zhang Y & Wang X (2009) Photo degradation of methyl orange by attapulgite-SnO_2-TiO_2 nanocomposites. *J. Hazard. Mater.* 171: 294-300.

Zhang YG, Ma LL, Li JL & Yu Y (2007) In situ Fenton reagents generated from TiO_2/Cu_2O Composite film: a new way to utilize TiO_2 under visible light irradiation. *Environ. Sci. Technol.* 41: 6264-6269.

Zhang W, An T, Xiao X, Fu J, Sheng G, Cui M & Li G (2003) Photoelectrocatalytic degradation of reactive brilliant orange K-R in a new continuous flow Photoelectrocatalytic reactor. *Appl.Catal.A.* 255: 221-229.

Zhang H & Banfield JF (1998). Thermodynamic analysis of phase stability of nanocrystalline titania. *J. Mater. Chem* 8: 2073-2076.

Zhou Q, Zhang MC, Shuang CD, Li ZQ & Li AM (2012) Preparation of a novel magnetic powder resin for the rapid removal of tetracycline in the aquatic environment. *Chin. Chem. Lett.* 23:745–748.

Zuehlke S, Duennbier U, Lesjean B, Gnirss R & Buisson H (2006) Long-term comparison of trace organics of removal performances between conventional and membrane activated sludge processes. *Water Environ. Res.* 78(13): 2480-2486.

CHAPITRE 2

TETRACYCLINE ANTIBIOTICS IN THE ENVIRONMENT. A REVIEW

Le Chapitre 2 est constitué de l'article suivant :

Rimeh Daghrir, Patrick Drogui, (2013) Tetracycline antibiotics in the environment. A review.

Environmental Chemistry Letters. DOI: 10.1007/s10311-013-0404-8

2. TETRACYCLINE ANTIBIOTICS IN THE ENVIRONMENT. A REVIEW

2.1 Abstract

Tetracycline antibiotics are one of the primarily antibiotics groups used for veterinary purposes, for human therapy and in agriculture sector. Amongst the different antibiotics used, more attention is paid to tetracycline's as it exhibits serious environmental problems including ecological risk and human health damage. Due to their extensive usage, most of the evidence until date suggests that tetracycline antibiotics are omnipresent compounds found in different ecological compartments. After medication, more than 70% of tetracycline antibiotics were excreted and released in active form into the environment via urine and feces from humans and animals. Their higher hydrophilic character and low volatility have resulted in significant persistent in aquatic matrix. Very few studies describe the fate and toxicity of tetracycline antibiotics in the environment. Here, we review several important issues with regard to (1) the toxicity of these compounds on aquatic and terrestrial organisms, (2) their estrogenic effects, (3) their behavior in different ecological systems and (3) the by-products generated during water treatment. These tetracycline antibiotics residues promote the development of antibiotic resistant microorganisms, which can induce adverse effect to human health by increasing the risk of certain infections. Based on recent research results, the occurrence of these residual compounds in the environment inhibits the growth of terrestrial and aquatic species such as crops, *Microcystis aeruginosa, Rhodomonas salina and Selenastrum capricornutum* among others. Additionally, the residual concentrations of such drugs could affect steroidogenic pathway and consequently may cause endocrine disruption. Up to now, wastewater treatment plants are not capable of removing effectively the tetracycline antibiotics. There is therefore a need of knowledge the different treatment processes that could be used and developed to remove residual concentrations of tetracycline antibiotics from environment. This review

highlights also the conventional chemical, physical and physicochemical methods used to eliminate tetracycline antibiotics during the treatment of drinking water and wastewaters. Accordingly, the research gaps and the future trends related to tetracycline antibiotics removal are also discussed. Novel approaches that use and integrate the chemical data including advanced oxidation processes have been proposed as alternative methods to ensure higher degradation and mineralization of tetracycline antibiotics among others bio-recalcitrant compounds present in water and wastewater.

2.2 Keywords

Antibiotics; Tetracyclines; Occurrence; Fate; Toxicity; Treatment; Waters.

2.3 Introduction

Over the past few years, the use of pharmaceuticals in the medical field for preserving human and animal health has resulted in their undesirable accumulation in the environment. Most of these pharmaceuticals are stable and difficult to oxidize by conventional treatment processes (Gao et al., 2012). A significant number of these compounds have been frequently detected in different type of waters (wastewater, surface water, drinking water, ground water) and solids (sludge, soil, and sediments) (Christian et al., 2003; Gobel et al., 2005; Kim and Carlson 2007; Kummerer, 2009). Due to their excessive occurrences and their persistent characters in the environment, there is a considerable interest for pharmaceutical residues. The long-term and the low-dosed exposures to PPs in the environment lead to the adverse impacts to the target organisms including endocrine disruption, chronic toxicity and antibiotic resistance (Andreozzi et al., 2004; Fent et al., 2006).

Among the pharmaceutical compounds present in the environment, special interest has been given to antibiotics (Homem and Santos, 2011; Gao et al., 2012; Hu et al., 2010; Pan et al., 2011; Onal, 2011). Antibiotics belong to a class of pharmaceuticals used extensively to treat and to prevent the disease in human and animal medicine, as well as to increase feed efficiency and improve the growth rate in livestock and poultry industries (Gao et al., 2012; Pan et al., 2011; Sarmah et al., 2006; Chen et al., 2011). The use of antibiotics in feed for growth promotion is banned in European Union (EU; Commission of the European Communities, 1998a, b). In some countries such as Canada, USA and Korea, their uses are still common (Sarmah et al., 2006). According to Martinez et al. (2011) and Halling-Sorensen et al. (1998), the annual production volume of drugs has been estimated in several hundreds of tons, whereas its annual use has been globally estimated between 100,000 and 200,000 tons (Kuemmerer, 2003). For instance, it was estimated in 2003 that about 9200 tons of antibiotics were produced for farming in the United States (A.H.I., 2005). By comparison, the annual

production capacity of antibiotics in China is around 210 000 tons (85 % is used for animal husbandry and medicine), while the annual production of antibiotics in Japan is around 2 200 tons (30% are used for humans and 60% are used for livestock) (Luo et al., 2011; Miyata et al., 2011). During their use, antibiotics cannot be absorbed or metabolized entirely in vivo and a significant fraction (from 30 to 90%) is excreted in metabolite forms into the environment via urine and feces (Zhou et al., 2012; Hu et al., 2010; Bound and Voulvoulis, 2004).

Antibiotics and their metabolites have been detected in surface water, ground water, sewage water and drinking water at a concentration ranging from ng°L^{-1} to µg L^{-1} (Lòpez-Penalver et al., 2010; Kim and Tanaka, 2009; Bautitz and Nogueira, 2007). According to previous research (Karthikeyan and Meyer, 2006; Xu et al., 2007), antibiotic can enter in the aquatic environment through the direct discharge of animal wastewater and the discharge of effluents from wastewater treatment plants. Besides, the application of manure from livestock farm onto agriculture land contributes to introduce antibiotics in the environment (Shelver et al., 2010; Chen et al., 2011). The introduction of these residual compounds into environment through different sources will lead to serious environmental problems including ecological risk and human health damage.

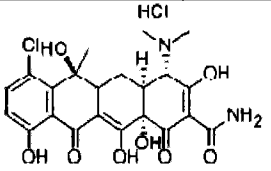
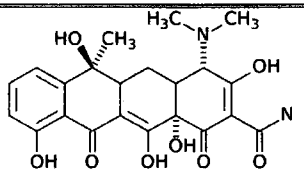
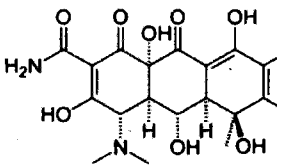
Tetracycline antibiotics are broad spectrum antibiotics, and exhibit antibiotic activity against infections caused by both Gram (+) and Gram (-) microorganisms as well as mycoplasma, chlamydia, rickettsiae and protozoan parasites (Samanidou et al., 2007; Onal, 2011; Ding and Mou, 2000). Tetracycline antibiotics are one of the primarily antibiotics groups used for veterinary purposes, for human therapy and in agriculture sector as feed additive (Li et al., 2011; Ding and Mou, 2000). Owing to their lower cost and their higher antimicrobial activity, Tetracycline antibiotics are widely used as veterinary drugs for the prevention and treatment of animal farm to cure several infectious diseases (Onal, 2011; Chen et al., 2011). Tetracycline antibiotics are also used as feed additives to promote the growth of animal

(Sczesny et al., 2003; Koesukwiwat et al., 2007). As reported by Halling-SØrensen et al., (2002), more than 2.500 tons of TCAs are used annually in Europe in veterinary therapy. Clinical studies of TCAs (Han et al., 1999; Li et al., 2000) have showed that this group of antibiotics have an auxiliary treatment of tumor, inhibit the activity of collagen enzyme and promote bone absorption.

Chlortetracycline, oxytetracycline and tetracycline, which are a kind of tetracycline antibiotics, were the most often used throughout the world (Lòpez-Penalver et al., 2010; Jeong et al., 2010; Halling-SØrensen et al., 2002). Their structural formulas and their physico-chemical properties are listed in Table 2.1. Their relatively low Henry's constant (from 3.45 10^{-24} to 3.91 10^{-26} atm m^3 mol^{-1}) indicates that these molecules are weakly lost by volatilization. Their high water solubility (0.008 - 0.062 mol L^{-1}) and lower octanol–water partition coefficient (log K_{ow} from -1.25 to -1.12) defines their hydrophilic character. Tetracycline antibiotics are characterized by three pKa values (Table 2-1). Tetracycline antibiotics are relatively stable in acids, but not in alkaline media (Halling-SØrensen et al., 2002). Tetracycline is one of the most frequently used antibiotics in aquaculture and veterinary medicine (Lopez Penalver et al., 2012), whereas chlortetracycline and oxytetracycline are two of the ten antimicrobials licensed as growth promoters in the United States (Jeong et al. 2010; Yang and Calson 2003). Chlortetracycline is the most commonly used in swine production in USA, although oxytetracycline and tetracycline are also frequently used (Wei et al., 2011). Due to their extensive usage and their higher adsorption capability, Tetracycline antibiotics have been detected in terrestrial and aquatic environment: surface water (Li et al., 2011), ground water (Hernández et al., 2007), wastewater (Lopez Penalver et al. 2012; Jeong et al. 2010), municipal sewage (Liu et al., 2009), soil and sediments (Liu et al., 2009; Andreu et al., 2009; Chen et al., 2011). Hence, conventional wastewater treatment plants appear unable to completely eradicate these micropollutants. In

wastewater treatment plants, the removal efficiency of tetracycline varied from 12 % (Spongberg and Witter, 2008) to 80% (Karthikeyan and Meyer 2006). By considering the risks of tetracycline antibiotics in the ecosystem, the search for new alternatives to prevent environment contamination is become necessary. This review highlights various issues concerning the tetracycline antibiotics occurrence, toxicity, distribution, fate and the different technologies applied so far for their removal from waters.

Tableau 2-1 Chemical properties of tetracycline antibiotics

Molecule	Molecular formula	Chemical structure	Molecular weight (g mol^{-1})	Solubility (mol L^{-1})	Log K_{OW}	Henry's law constant (atm m^3 mol^{-1})	Isoelectric point	pK_{a1}	pK_{a2}	pK_{a3}
Chlortetracycline	$C_{22}H_{24}Cl_2N_2O_8$		515.3	0.008	-0.62	3.45 E-24	2.27	3.3±0.3	7.55±0.02	9.3±0.3
Tetracycline	$C_{22}H_{25}Cl\,N_2O_8$		480.9	0.041	-1.25	-	-	3.2±0.3	7.78±0.05	9.6±0.3
Oxytetracycline	$C_{22}H_{25}Cl\,N_2O_9$		496.9	0.062	-1.12	3.91 E-26	-	3.2±0.3	7.46±0.03	8.9±0.3

2.4 Worldwide usage of tetracycline antibiotics

The tetracycline antibiotics were discovered in the 1940s and their therapeutic use for preserving human health began in the 1950s (Chopra and Roberts, 2001; Roberts, 2003). Besides, the use of tetracycline antibiotics has become integral to the livestock production industry as growth promoters and in agriculture sector as feed additive in North America since the 1950s (Roberts, 2012; Arikan et al., 2009). Each year, the worldwide production of tetracycline antibiotics is estimated to be in thousands of tons (Michalova et al., 2004).

Recent research (Xie et al., 2010; Chen, 2005) show that tetracycline antibiotics are ranked second in the production and usage of antibiotics worldwide and are ranked first in China. Tetracyclines are considered one of the cheapest classes of antibiotics available today. It makes them attractive for use in developing countries with limited health care budgets (Roberts, 2012; Michalova et al., 2004). For instance, the amount of tetracycline antibiotics used in European Union in 1997 for therapeutic purpose was around 2294 tons, whereas during the period 2000 to 2001 the consumption of tetracycline antibiotics in USA was increase from 3000 to 3200 tons, respectively (Michalova et al., 2004).

According to several works (Ding and Mou, 2000; Samanidou et al., 2007; Kim et al., 2011; Chen et al., 2012), tetracycline antibiotics still widely used in many countries for the prevention and treatment of diseases and promotion of growth in animal such as cattle, pigs, sheeps, and poultries, among others. Tetracycline antibiotics are widely applied in veterinary medicine for the treatment of gastrointestinal, respiratory and skin bacterial infections, infectious diseases of locomotive organs and of genito-urinary tract as well as systematic infections and sepsis (Prescott et al., 2000; Michalova et al., 2004). The world wide variation of the total amounts of tetracycline antibiotics used in veterinary medecine is shown in Figure 2-1. The USA was the biggest consumer of tetracycline antibiotics (3200 tons $years^{-1}$) followed by Korea (723 tons $Years^{-1}$). The uses of tetracycline antibiotics in veterinary

medicine were significantly higher than some European countries (such as Sweeden, Danemark, France, among others) due to the high numbers of livestocks in both Korea and USA and the common agriculture practice of tetracycline antibiotics as feed supplements to promote the growth (Kim et al., 2011).

In human medicine, tetracycline antibiotics have been used for the treatment of different types of infections, especially respiratory infections (pneumonia) due to *Mycoplasma pneumonia, Chlamydia pneumonia, and Chlamydia psittaci*. In the past decade, they have been also the drug of choice for the treatment of malaria due *Plasmodium falciparum* (Roberts 2003). In addition, it has been suggested by Smith and Rajan (2000) that tetracycline antibiotics could be benefit for the treatment of human infected with flarial nematodes, whereas Chopra and Roberts (2001) show that tetracycline antibiotics are effective to treat infections with Entamoeba histolytica, Giardia lamblia, Leishmania major, Trichomonas vaginalis, and Toxoplasma gondii. This successful use of tetracycline antibiotics around the world is due to the nonantibacterial effects including anti-inflammation, immunosuppression, inhibition of lipase and collagenase activity, wound healing, and enhancement of gingival fibroblast cell attachment, antibacterial effects or the combination between the two properties (Chopra and Roberts, 2001; Chaidemenos, 2001; Ramamurthy et al., 2002; Roberts, 2003).

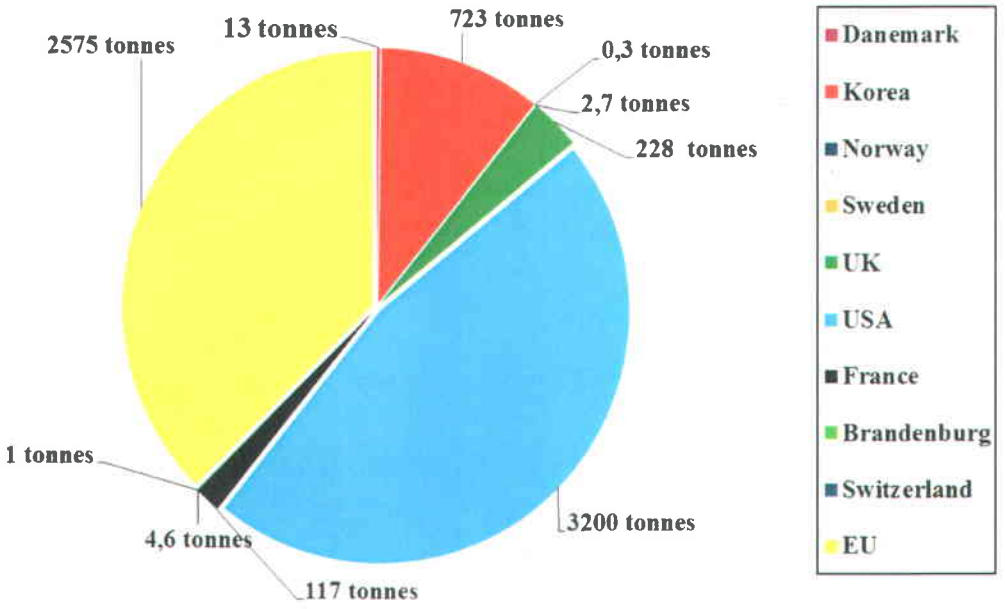


Figure 2-1 Variation of the total amounts (tons) of tetracycline antibiotics used for veterinary purposes around the world.

2.5 Occurrence of tetracycline antibiotics in the environment

In the last decades, the abusive use of tetracycline antibiotics in veterinary and human medicine was widespread, and consequently, the possibility of environmental contamination with such compounds increased (Chen et al., 2011; Arikan et al., 2009). The occurrence of tetracycline antibiotics in the aquatic environment has received a great attention due to their potential contribution toward increasing bacterial resistance to anti-infective (Sarmah et al., 2006; Baquero et al., 2008). After using such compounds, a fraction of tetracycline antibiotics is metabolized into inactive compounds. Another fraction is excreted as parent compounds or actives metabolites products or both forms by a diversity of input source as shown in Figure 2.2 (Kim et al., 2005; Xie et al., 2010). The most of tetracycline antibiotics are released via urine, feces, and manure from humans and animals after medication. As shown by some monitoring data, around 25% to 75% or even 70% to 90% of tetracycline antibiotics

administrated to animals were excreted and released in active form into the environment via urine and feces (Jjemba, 2002; Halling-Sorensen, 2000). When tetracycline antibiotics are released from animal, manure can contaminated soil and consequently surface and ground waters through leaching or run-off. Similarly, human tetracycline antibiotics are introduced into the environment through excretion, entering in the sewer network and reaching the wastewater treatment plants.

Up to now, wastewater treatment plants are not capable of removing effectively the tetracycline antibiotics. For instance, residual concentrations from 0.15 $\mu g\ L^{-1}$ to 0.97 $\mu g\ L^{-1}$ of tetracycline have been detected by Miao et al. (2004) in the final effluent from wastewater treatment plants in Canada. Residual concentrations up to 2.37 $\mu g\ L^{-1}$ have been also detected by Deblonde et al. (2011) in the effluents from wastewater treatment plants. Therefore, they can be transported to surface water and reach ground water after leaching. A residual concentration of 400 $ng\ L^{-1}$ of tetracycline was recorded in ground waters, whereas 32 $ng\ L^{-1}$ of oxytetracycline and less than 690 $ng\ L^{-1}$ of chlortetracycline were measured in overland flow water and surface water, respectively (Krapac et al., 2005). Another important contamination source is the direct release from pharmaceutical production plants.

In their monitoring investigations of various sewages, surface and groundwater in Germany, Hirsch et al. (1999) did not detect tetracycline antibiotics. This result is not surprising because tetracycline antibiotics are easily precipitated with cations such as calcium and accumulate in sewage sludge or sediments (Daughton and Ternes, 1999). However, tetracycline antibiotics including tetracycline, chlortetracycline and oxytetracycline have been detected by Kolpin et al. (2002) and Lindsey et al. (2001) in US surface water samples. The average concentrations of tetracycline, oxytetracycline and chlortetracycline detected in US surface water were 0.11$\mu g\ L^{-1}$, 1.34 $\mu g\ L^{-1}$ and 0.15 $\mu g\ L^{-1}$, respectively (Lindsey et al., 2001). By comparison, tetracycline was the most commonly detected (0.11 $\mu g\ L^{-1}$) by Kolpin et al., (2002).

Usually, tetracycline antibiotics are accumulated with organic manure in soil. For instance, in Germany the residual concentration of tetracycline and chlortetracycline recorded by Hamscher et al. (2002) in soil were up to 86-199 μg Kg^{-1} and 4.6-7.3 μg Kg^{-1}, respectively, whereas the maximum concentrations of oxytetracycline measured by Boxall et al. (2006) in soil were 305 μg Kg^{-1}. Oxytetracycline remained biologically active in soil under field conditions at a concentration greater than 25 μg L^{-1} for at least 40 days (Kulshrestha et al., 2004; Polubesova et al., 2006).

Furthermore, the release of tetracycline antibiotics can be taken up by various plants, crops and soil animals on farmland. For instance, chlortetracycline has been shown quite persistent in soil. Research group of Hamscher et al. (2000) have reported an average concentration of 9.5 μg Kg^{-1} chlortetracycline in the upper 10 cm of the soil. Previous investigations showed that the excretion rate and the total amount used influence the residual concentration of tetracycline antibiotics detected in the environment (Table 2-2). Due to its persistent character in soil, chlortetracycline is the most antibiotic frequently detected in the environment at higher concentrations up to 880 μg Kg^{-1} in pig manure (Hamscher et al., 2000). After 10 days of chlortetracycline medication, the concentrations of chlortetracycline and its metabolites (Epi-chlortetracycline and Iso- chlortetracycline) in pig faeces recorded by the research group of Grote were 281.000 μg Kg^{-1}, 157.000 μg Kg^{-1} and 67.000 μg Kg^{-1}, respectively (Grote et al., 2004). Hamscher et al. (2000) detected higher concentrations of chlortetracycline in pig manure slurry (1435 μg Kg^{-1}) compared to 11 μg Kg^{-1} of chlortetracycline recorded in the cattle manure slurry. Chlortetracycline has been also detected in water samples at the maximum concentrations of 0.03 μg L^{-1} (Arikan et al., 2008), 0.16 μg L^{-1} (Yang and Carlson, 2003) and 0.69 μg L^{-1} (Kolpin et al., 2002) and even in sediment at concentrations from 2 to 10 μg Kg^{-1} dry weight (Arikan et al., 2008). In the investigation of veterinary antibiotics used for livestock, Hu et al. (2010) have detected residual concentrations of tetracycline,

chlortetracycline and oxytetracycline in both manure and soil. The amount of oxytetracycline, tetracycline and chlortetracycline recorded in soil (in winter) were up to 2683 μg Kg^{-1}, 105 μg Kg^{-1} and 1079 μg Kg^{-1}, respectively, whereas residual concentrations of 183.5 mg Kg^{-1}, 43.5 mg Kg^{-1} and 26.8 mg Kg^{-1} for oxytetracycline, tetracycline and chlortetracycline, respectively have detected in manure. Thereby, the occurrence and the accumulation of these tetracycline antibiotics in the environment could lead to toxic effects in animals as well as humans.

Tableau 2-2 Variation of the residual concentration of tetracycline antibiotics with animal type.

Animal type	Manure generated tetracycline antibiotics (tons years^{-1})	Tetracycline antibiotics used (tons years^{-1})	Tetracycline antibiotics concentrations (µg Kg^{-1})			References
			Chlortetracycline	Oxytetracycline	Tetracycline	
Cattle	16 676 949	42.4	11-208	-	-	Hamscher et al., 2000; Arikan, 2008; Kim et al., 2011
Pig	14 363 192	366	46-880	29-78	23-81	Aust et al., 2008; Martinez-Carballo et al., 2007; Hamscher et al., 2000; Xian-Gang et al., 2008; Kim et al., 2011
Poultry	4 349 489	104.5	57. 94.7	62	69	Xian-Gang et al., 2008; Bao et al., 2009; Kim et al., 2011

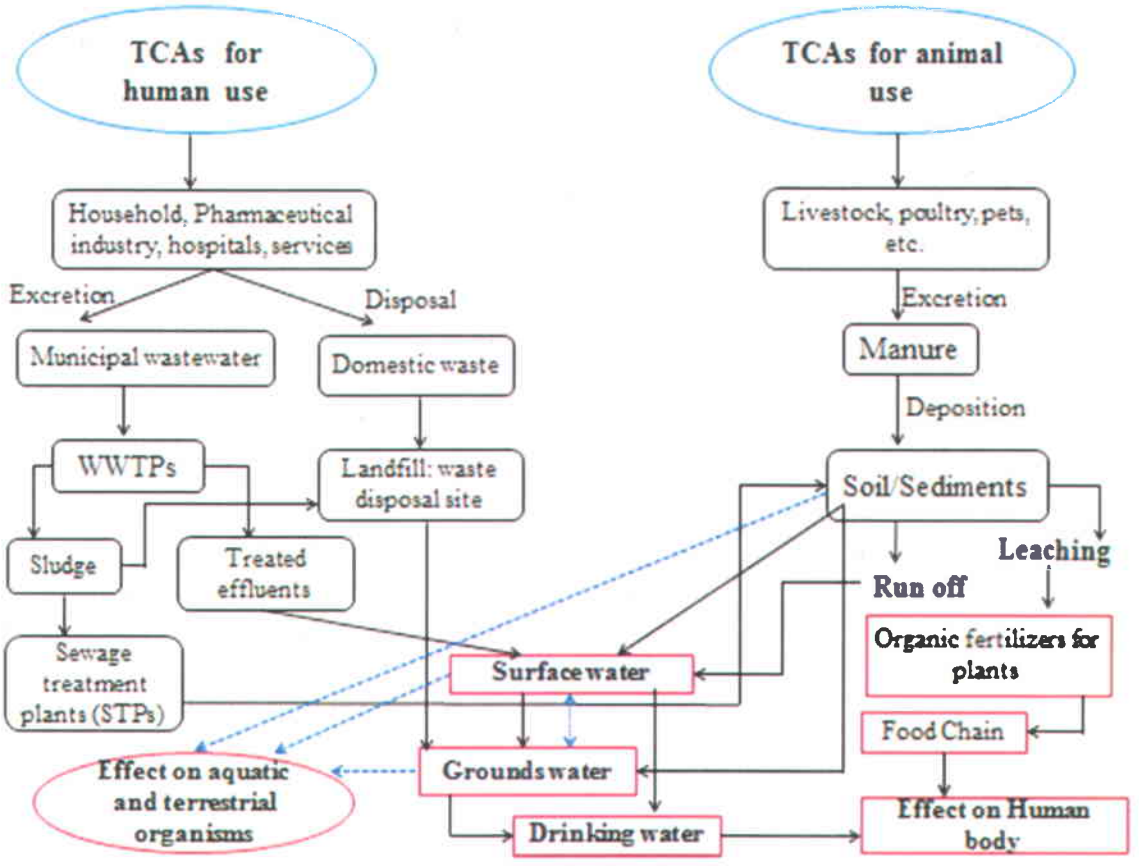


Figure 2-2 Possible sources and pathways for the occurrence of TCAs in the environment.

2.6 Toxicity

Up to now, more attention has been paid to ecological risk and potential toxic effects of tetracycline antibiotics residues in the environment (Xie et al., 2010; Haling-Sorensen, 2000; Hui-zhu et al., 2008). These tetracycline antibiotics residues promotes the evolution or the development of antibiotic resistant microorganisms, which can induce adverse effect to human health when present in drinking water or irrigation water used for fruit and vegetable (Stackelberg et al., 2007; Lopez Penalver et al., 2012; Arikan, 2008). These antimicrobial

agents may disturb the microflora of the human intestinal and increase the risk of certain infections (Heuer et al., 2009). Given this fact, it is not surprising to find many researches trying to determine and estimate the toxicity of tetracycline antibiotics on aquatic and terrestrial species, and even their estrogenic effects.

2.6.1 Effects of tetracycline antibiotics on aquatic species

The chronic and acute toxic effects of tetracycline antibiotics on various aquatic species have been widely conducted. As reported by Halling-Sorensen (2000), tetracycline antibiotics are mainly bacteriostatic, with a broad spectrum of antimicrobial activity. Owing to an active transport process, tetracycline antibiotics are taken up into sensitive bacterial cell. Once within the cell, they bind reversibly to the 30S subunit of the ribosome, they prevent the binding of aminoacyl transfer to DNA and they inhibit protein synthesis and hence cell growth.

Photoautotrophic microalgae, as primary producers, play an important role in the structure and functioning of the whole aquatic ecosystem (Yang et al., 2008). As reported in the literature data, microalgae are more sensitive than crustaceans and fish to antibacterial agents such as tetracycline antibiotics. Study of Yang et al. (2008) has shown that chlortetracycline could potentially affect the growth of green alga in freshwater systems. On the basis of the growth inhibiting test, Yang and his co-worker calculated the median inhibitory concentration value of chlortetracycline to be 3.49 μM. On the other hand, it has been found by Brain et al. (2004) that chlortetracycline had photo-toxicity to the aquatic plant *Lemna gibba* with effective concentration EC25 values of 114 μg L^{-1}. The toxic effect of oxytetracycline (growth inhibition) on various aquatic species (*Microcystis aeruginosa, Rhodomonas salina and Selenastrum capricornutum*) has been investigated by Holten Lutzhoft et al. (1999). Oxytetracycline was found in water and sediment from the outflow of a breeding pond and below fish farms (Migliore et al., 1996). The few tests done by Holten Lutzhoft show that

Microcystis aeruginosa (the half live effective concentration (EC_{50}) = 0.207 mg L^{-1}) was more sensitive to oxytetracycline compared to both *Rhodomonas salina* (EC_{50} = 1.6 mg L^{-1}) *and Selenastrum capricornutum* (EC_{50} = 4.5 mg L^{-1}).

The same aquatic species (*Microcystis aeruginosa* and *Selenastrum capricornutum*) have been also used by Halling Sorensen (2000) to evaluate the effects of tetracycline and chlortetracycline. In this investigation, *Microcystis aeruginosa* and *Selenastrum capricornutum* were found to be more sensitive to chlortetracycline and tetracycline than oxytetracycline. It was observed that the growth inhibition rates (EC_{50}) of *Microcystis aeruginosa* and *Selenastrum capricornutum* by tetracycline were 0.09 mg L^{-1} and 2.2 mg L^{-1}, respectively, while the growth inhibition rates of *Microcystis aeruginosa* and *Selenastrum capricornutum* using chlortetracycline were 0.05 mg L^{-1} and 3.1 mg L^{-1}, respectively.

The acute toxicity of tetracycline and chlortetracycline on aquatic organisms such as Daphnia magna, Danio rerio and Carassius auratus has been evaluated by Hui-zhu et al. (2008). According to this research group, it has been found that chlortetracycline toxicity to the three organisms was significantly higher than that of tetracycline. The acute toxicity of Daphnia magna, Danio rerio and Carassius auratus to TC were 617.2 mg L^{-1} (48h-EC50), 406.0 mg L^{-1} (96h-LC50) and 322.8 mg L^{-1} (96h-LC50), respectively. By comparison, the acute toxicity of Daphnia magna, Danio rerio and Carassius auratus to chlortetracycline were 137.59 mg L^{-1} (48h-EC50), 61.15 mg L^{-1} (96h-LC50) and 34.68 mg L^{-1} (96h-LC50), respectively.

2.6.2 Effects of tetracycline antibiotics on terrestrial organisms

Research on toxic effects of tetracycline antibiotics in terrestrial organisms including crops is still scarce. As mentioned by Xie et al. (2010), knowledge of the dual effect (promotion and inhibition) on the growth and genotoxicity of chlortetracycline in plants as crops is lacking. The first report on the phototoxic effects of tetracycline antibiotics in crops shows that the

presence of chlortetracycline influences negatively the growth of pinto beans in soil (Michael et al., 2007). It has been also reported by Xie et al. (2010) that chlortetracycline at higher concentrations significantly inhibited the percentage germination of wheat (25-300 mg L^{-1}), the root length (25-300 mg L^{-1}), the bud length (50-300 mg L^{-1}) and the mitotic index (25-300 mg L^{-1}). In addition, the lowest concentration of chlortetracycline slightly increased the frequency of micronucleus (MN), the chromosomal aberration (CA) and the sister chromatid exchange (SCE) in the root tips, thus resulting in acute cell toxicity. Xie et al. (2010) pointed out that sister chromatid exchange was the most sensitive to chlortetracycline followed by chromosomal aberration, and micronucleus was the least sensitive to chlortetracycline genotoxicity in wheat.

2.6.3 Estrogenic effects of tetracycline antibiotics

Among others antibiotics (tylosin, amoxicillin), oxytetracycline can modulate the expression of gene and the production of hormone related to steroidogenesis (Gracia et al., 2007). The effects of tetracycline antibiotics related to the reproduction have been reported for Japanese medaka fish. For example, oxytetracycline and chlortetracycline induce the production of vitellogenin in male Japanese medaka fish as *Oryzias Latipes* (Kang et al., 2005; Kim, 2007). The results recorded by Kim (2007) show that CTC induces vitellogenin in male medaka, and consequently may cause endocrine disruption in fishes. From 10 mg L^{-1}, chlortetracycline is an inducer of vitellogenin in male fishes, whereas it was a reducer of vitellogenin in female fishes from 0.1 mg L^{-1} of chlortetracycline concentration (Kim, 2007).

In addition, chlortetracycline and oxytetracycline affected several reproduction related endpoint such as the first day of the reproduction, the number of young per female and the growth rate of populations (Park and Choi, 2008). Chlortetracycline and oxytetracycline have been also tested by Ji et al. (2010) to evaluate their effects on steroidogenesis in vivo with male medaka fish. The concentration of 17β-estradiol (E2) in the plasma of male medaka fish

increased significantly after 14 days exposure to chlortetracycline (40 mg L^{-1}) and oxytetracycline (50 mg L^{-1}).

Furthermore, the effects of chlortetracycline and oxytetracycline on steroidogenesisin in vitro with human adrenocarcinoma (H295R) cells have been tested by Ji and his co-workers. Both chlortetracycline (from 0 mg L^{-1} to 20 mg L^{-1}) and oxytetracycline (from 0 mg L^{-1} to 20 mg L^{-1}) affected the production mechanism of 17β-estradiol (E2) by increasing the catalytic activity of aromatase and enhancing the expression of CYP17, CYP19, and 3βHSD mRNAs of H295R cells. However, further investigations are needed because the residual concentrations of tetracycline antibiotics are relatively low in the environment (from μg L^{-1} to ng L^{-1}).

2.7 Treatment of tetracycline antibiotics in waters

As mentioned above, most conventional wastewater treatment plants are not designed to remove tetracycline antibiotics from waters and wastewaters. To this end, practical and economical processes must be developed and applied in order to reduce the tetracycline antibiotics discharges into the environment. Physicochemical methods such as membrane filtration and adsorption using activated carbon have been applied to remove tetracycline antibiotics. However, the main disadvantage of such methods is that they do not destroy the pollutants but transfer the pollutant from one phase to another. Nowadays, advanced oxidation processes have been proposed as alternative methods for the elimination of tetracycline antibiotics among others biorecalcitrant compounds in wastewater (Daghrir et al., 2012; Palominos et al., 2009; Jeong et al., 2010; Bautitz and Nogueira, 2007). The principle of advanced oxidation processes (including O_3/H_2O_2, UV/O_3, UV/H_2O_2, H_2O_2/Fe^{2+}, and UV-TiO_2) is to produce hydroxyl radical in water, a very powerful oxidant ($E° = 2.8$ V) capable of oxidizing a wide range of organic compounds with one or many double bonds (Homem and Santos, 2011; Esquivel et al., 2009; Yu and Chuang, 2008). As reported by Homem and Santos (2011), hydroxyl radicals are produced from oxidizing agents such as ozone, hydrogen

peroxide, often combined with UV radiation or semiconductor/metallic catalysts. An overview of the recent research studies using different processes for tetracycline antibiotics removal is summarized in Table 2-3-Table 2-7.

2.7.1 Membrane processes

The reverse osmosis, nanofiltration and ultrafiltration are membrane processes (Li et al., 2004; Radjenovic et al., 2008; Koyuncu et al., 2008). The reverse osmosis constitutes one of the membranes processes that has been widely used in combination with nanofiltration (or ultrafiltration) to remove tetracycline antibiotics (Li et al., 2004; Kosutic et al., 2007). Oxytetracycline was removed using either reverse osmosis/nanofiltration or reverse osmosis/ultrafiltration processes (Li et al., 2004; Kosutic et al., 2007). These studies revealed for example, that reverse osmosis/ultrafiltration technique is considered as an effective method to remove oxytetracycline (≈87.5%) from pharmaceutical wastewater (Li et al., 2004). By comparison, 50 to 80 % of tetracycline antibiotics were removed while treating distilled water spiked with calcium chloride, humic acid and NaCl using nanofiltration technique (Koyuncu et al., 2008). Nevertheless, reverse osmosis, nanofiltration and ultrafiltration techniques are very sensible to the amounts of organic material occurring naturally in the water matrices and the concentration of the dissolved salts (Homem and Santos, 2011). The presence of higher levels of these compounds in water could cause the fouling of the membrane.

2.7.2 Adsorption processes

In the adsorption process, the pollutant is transferred from liquid phase to solid surface. Granular activated carbon is the most popular adsorbent used but its cost and the difficulties of regeneration represent the major drawbacks (Crisafully et al., 2008). Despite the fact that the adsorption is a well-known process, this technology has not been widely used to remove

tetracycline antibiotics. Adsorption using granular activated carbon in combination with coagulation process was applied by Choi et al. (2008) to remove tetracycline antibiotics (10-100 μg L^{-1}) from synthetic water and river water. Higher removal rate of tetracycline antibiotics drugs up to 94% has been recorded from synthetic water, whereas the removal rate of tetracycline antibiotics does not exceed 67% from river water. Furthermore, Chen and Huang (2010) analyzed the adsorption of three tetracycline antibiotics (chlortetracycline, oxytetracycline and tetracycline) on aluminum oxide. These compounds were adsorbed and they concluded that structural transformations were produced along the adsorption process. Different sorbents described earlier have been applied to remove tetracycline antibiotics. The physical-chemical properties (pH, salinity, temperature, etc.) and the chemical composition of water or wastewater (including tetracycline antibiotics and other antibiotics) are main criteria in the selection of sorbents. Choosing the best sorbent for tetracycline antibiotics removal should take into account not only the efficiency but also the cost. From this point of view, biosorbent generated from activated sludge could be an interesting alternative for tetracycline antibiotics removal. However, the main disadvantage of such method is that they do not destroy the pollutant. The adsorption is a process to concentrate the contaminants.

2.7.3 Photochemical processes

In the recent years, the use of UV light irradiations for the degradation of tetracycline antibiotics is one of the approaches that have been widely investigated. Tetracycline antibiotics are very sensitive to the light irradiation. Photolysis processes using UV radiation are simple, clean and less expensive. In direct photolysis, UV radiations absorbed by H_2O molecule allow the generation of powerful oxidizing species such as the hydroxyl radicals (OH°) and the hydrogen peroxide (H_2O_2) (Heit et al., 1998; Kim and Tanaka, 2009). The oxidation efficiency of UV radiation (365 nm) promotes the degradation rates of 50%, 90% and 75% of chlortetracycline, oxytetracycline and tetracycline, respectively (Chen et al.,

2012, Jiao et al., 2008, Shaojun et al., 2008). Despite this higher degradation of tetracycline antibiotics, a lower mineralization rate (14-15% of total organic carbon removal) has been reached depending on the types of tetracycline antibiotics tested and the experimental conditions. The low removal of total organic carbon indicates the presence of intermediate compounds, which can be more toxic than the original one (Jiao et al., 2008, Shaojun et al., 2008).

The performance of the photolysis process in wastewater treatment is affected by several factors such as the absorption spectrum of the target compounds, the type of matrix and the intensity of the radiation (Kummerer, 2009; Homem and Santos, 2011). The maintenance and the electrical energy costs are also some limiting factors for the application of UV system in wastewater treatment. To this end, researches focus on the combinations of UV radiations with oxidant species such as H_2O_2 and O_3 (UV/H_2O_2 and UV/O_3).

Ozonation technique was applied to remove oxytetracycline and chlortetracycline from water and livestock wastewater, respectively (Lee et al., 2011; Li et al., 2008). The ozone is a strong oxidant ($E° = 2.07$ V) capable to act direct or indirectly with pollutants (Homem and Santos, 2011). Otherwise, the presence of hydroxide ions could initiate the decomposition of ozone in water to form hydroxyl radicals (Andreozzi et al., 1999). A 100% removal of oxytetracycline has been reached using 11 mg O_3 L^{-1} after 20 min of treatment time, whereas 30% of chlortetracycline has been removed from livestock wastewater after 40 min and at 7.0 g O_3 m^{-3}.

In order to improve the performance of this kind of treatment, it is possible to combine ozone with UV irradiation (O_3/UV) or hydrogen peroxide (O_3/H_2O_2). Lee et al. (2011) verified that H_2O_2 (0-200 mg L^{-1}) combined with O_3 (namely perozonation process) increased the removal efficiency of chlortetracycline (up to 65 % removal in 40 min), but the ecotoxicity was not totally removed. Another pathway to enhance the ozonation performance is to combine O_3

with UV irradiation. According to Hernandez et al. (2002), the photolysis of ozone produces hydrogen peroxide, which initiates the further decomposition of residual ozone into hydroxyl radical. This technique (O_3/UV) has been investigated by Lee et al. (2011). The inactivation of chlortetracycline-resistant HPCs has been recorded after 10 min, while less than 2 log-reduction of chlortetracycline was achieved in 1 h using O_3 alone. According to the results reported above, the efficiency of the ozonation process on the removal of tetracycline antibiotics showed a difference. The operating conditions imposed during the treatment (pH, Type of tetracycline antibiotics, dose of ozone, mixing inside the reactor, etc) and the mass transfer limitations are a relevant factor to be considered in the oxidation process with ozone.

As reported by Homem and Santos (2011), this system requires the transfer of ozone molecules from gas phase to liquid phase, where the attack on the organic molecules occurs. It is worth noting that the presence of organic matter, suspended solids, carbonate/bicarbonate and chlorine ions could also affect the performance of ozone process (Gunten, 2003; Andreozzi et al., 1999). As far as, the high cost of the equipment and maintenance, as well as the energy required to supply the process constitutes one of the disadvantages of the ozonation technique.

Photo-Fenton process (UV/Fe^{2+}/H_2O_2) is another attractive oxidation system because it uses low cost reagents, iron is abundant and a non-toxic element and hydrogen peroxide is easy to handle and environmentally safety. The use of UV radiation increases the efficiency of the oxidation process due to the highly generation of hydroxyl radicals by the photolysis of ferric complexes and the regeneration of ferrous ions (Gonzalez et al., 2007, Bautitz and Nogueira, 2010). As shown in Table 2.3, 100% degradation rate of tetracycline was obtained at 0.14 J cm^{-2} (1.5 min irradiation) using 3.0 mmol L^{-1} of H_2O_2 and 0.20 mmol L^{-1} of FeOx (Bautitz and Nogueira, 2010). Tetracycline was removed from different water sources (Spiked wastewater treatment plants effluent, surface and deionized water) under solar irradiation.

Under these conditions, the average mineralization rate recorded in wastewater treatment plants, surface water and deionized water were 77 %, 83 % and 91 %, respectively. These results suggest that the radiation may have been attenuated by the organic matter in the wastewater treatment plants matrices. The photolysis of aqueous $Fe(OH)^{2+}$ has been hindered and consequently, the generation of OH° was limited. Photo-Fenton process is generally inapplicable to wastewater with high organic matter such as hospital and antibiotic manufacturing wastewater because the turbity prevents the penetration of UV radiations (Homem and Santos, 2011). The high chemical consumption which sometimes produces a secondary pollution and a huge volume of sludge, and the relatively higher treatment cost constitutes another major drawback for large scale application of these processes (Martinez-Huitle and Ferro, 2006; Panizza and Cerisola, 2004).

2.7.4 Electrochemical process

Nowadays, electrochemical technologies applied for the treatment of tetracycline antibiotics have received considerable attention in the environmental field (Miyata et al., 2011, Rossi et al., 2009). Electrochemical method combining chemistry and electronic science (electron transfer) has widely proved to be a clean, flexible and powerful technique for water and wastewater treatment (Grimm et al., 1998). Electrochemical treatment is characterized by simple equipment, easy operation, safety, selectivity, environmental compatibily and brief retention time (Rajeshwar and Ibanez, 1997). Compared to chemical oxidation, no addition of chemicals is necessary in the process of electrochemical degradation. In electrochemical oxidation processes, pollutant can be removed electrochemically by a direct anodic oxidation, where pollutant are firstly adsorbed on the anode surface and then destroyed through the anodic electron exchange. On the other hand, pollutants could be also degraded indirectly in the liquid bulk through reactive oxidant species (OH°, O_3, H_2O_2, chlorinated species, etc), which act as intermediates for electrons transference between the electrode and the refractory

organic compounds (Panizza and Cerisola, 2009; Homem and Santos, 2011). This technology has been widely applied to remove tetracycline antibiotics under different experimental conditions. More than 90% of tetracycline degradation has been recorded by Zhang et al. (2009) using Ti/RuO_2-IrO_2 as anode electrode at 47.6 mA cm^{-2} of current density, after 60 min of electrolysis time, at pH value of 3.9 and using of 0.1 moL L^{-1} of Na_2SO_4. By comparison, electrochemical oxidation (chlortetracycline, oxytetracycline, tetracycline and doxycycline) promote the reduction of tetracycline antibiotics from 100 mg/L to 0.6 mg/L in aqueous solution (removal of 99% of tetracycline antibiotics) at 1.5 A of current intensity, after 6h of electrolysis time and using Ti/IrO_2 as anode (Miyata et al., 2011). The same electrochemical process applied by Miyata et al. (2011) favored the reduction of oxytetracycline in livestock wastewater from 100 mg L^{-1} to 0.7 mg L^{-1} after 6 h of treatment. Microbiological studies with Staphylococcus aureus ATCC 29213 have shown that oxytetracycline lost antibacterial activity after 120 min of electrolysis time and at 50 mA cm^{-2} (Rossi et al., 2009). According to Homem and Santos, (2011), electrochemical processes seem to be suitable to treat manufacturing wastewaters containing high concentrations of antibiotics and COD. Despite this higher degradation of tetracycline antibiotics recorded using electrochemical technology, the applicability of this process for large scale remains limited. The high operating cost due to the high energy consumption is still the main drawback which limits the application of the electrochemical process (Anglada et al., 2009).

2.7.5 Photocatalytic and photoelectrocatalytic processes

Over the past twenty years, there has been a growing interest in system employing heterogeneous photocatalytic process (Zouaghi et al., 2007; McCullagh et al., 2011; Tsai and Cheng, 1997; Chen et al., 2010; Leary and Westwood, 2011; Braham and Harris, 2009). Photocatalytic technology has a great potential due to the low treatment cost, environmental friendly and a sustainable treatment process in the field of wastewater treatment (Chong et al.,

2011). In photocatalysis process, the reactions of oxidative degradation require the presence of two basic components: a catalytic photo-sensitive surface (such as TiO_2, ZnO) and a source of photon energy. As reported in several review, the principle of this methodology is mainly based on the generation of oxidant reactive species upon absorption of artificial UV light (or sunlight) by the photo-catalyst (Daghrir et al., 2012). The application of energy greater or equal to the energy of the band gap of the photo-catalyst leads to the transfer of the electron from the valence band to the conduction band and the formation of a positive hole in the valence band. In water and wastewater treatment, the pollutant species such as antibiotic could be degraded directly on the surface of the semi-conductor or indirectly by reacting with hydroxyl radical and through other radical species derived from oxygen (Homem and Santos, 2011; Daghrir et al., 2012). Several authors studied the applications of this method to degrade tetracycline antibiotics and they concluded that semiconductor photocatalysis process was very efficient. Addamo et al. (2005) studied the application of this technique to treat aqueous solution contaminated with tetracycline. They concluded that the rate of tetracycline degradation above 98% occur within 2h, associated with total mineralization (100 % removal of total organic carbon) using TiO_2 (anatase/rutile) as photo-catalyst irradiated with UV light. By comparison, Reyes et al. (2006) who studied TC degradation using photocatalytic process show 100% of tetracycline degradation after 120 min and higher mineralization level (≈90%) using 0.5 g L^{-1} of TiO_2 and under 254 nm of UV irradiation. These results were consistent with those obtained by Palominos et al. (2009), who studied the degradation of TC using photocatalytic process. The degradation rates of tetracycline were high using either TiO_2 or ZnO (≈100%), as well as mineralization (≈50% using TiO_2 and ≈100% using ZnO). A recent study of Bu and Zhuang (2013) using photo-catalysis process (0.4g of Cu/TiO_2 as photo-catalyst and under 360 nm of UV irradiation) could be effective to remove more than 80% of chlortetracycline.

Under these conditions, 75%, 28.1% and 50% of chemical oxygen demand, total organic carbon and biological oxygen demand were recorded, respectively. It has been shown by Homem and Santos (2011) that photocatalytic processes seem to be very promising for the treatment of waters (drinking water, surface and groundwater) containing low concentrations of organic matter. In addition, the practical application of photocatalytic processes at large scale remain limit due to the fast recombination of photo-generated electrons/holes pairs (e^-/h^+).

Nowadays, recent research focus on improving the photocatalytic process by combining catalytic reaction with electrochemical technology named photo-electrocatalytic process (Daghrir et al., 2012; Liu et al., 2012). However, the application of this technology to remove tetracycline antibiotics remains limited compared to the conventional photocatalytic process. Photoelectrocatalytic process has been applied by Liu et al. (2012) to remove 30 mg L^{-1} of tetracycline antibiotics (chlortetracycline, oxytetracycline and tetracycline). In this study, about 95% of the three antibiotics were achieved after 180 min of treatment time at 3.0 V of external potential applied, under UV irradiation and at neutral pH. Moreover, the photoelectrocatalytic treatment of tetracycline (10 mg L^{-1}) in aqueous solution during 3h, at 0.5V and using 254 nm of UV irradiation promotes the removal of 80%. On the other hand, Daghrir et al. (2013) also studied the use of Photoelectrocatalytic oxidation process for the removal of chlortetracycline (30-230 μg L^{-1}). They obtained higher degradation efficiency of chlortetracycline (98.0 ± 0.2% of chlortetracycline removal) followed by higher mineralization (67.3 ± 2.15% of total organic carbon removal and 69.3 ± 3.10% of total nitrogen removal) after 120 min of treatment time, using Ti/TiO_2 as photo-anode, vitreous carbon as cathode at 0.39 A of current intensity and under 254 nm of UV light.

Due to the successful results at the laboratory scale for the degradation of tetracycline antibiotics, the photoelectrocatalytic processes merit further research, particularly for the

design of pilot units to remove tetracycline antibiotics and others recalcitrant compounds from drinking water and from different effluents (municipal, industrial and domestic wastewaters).

Tableau 2-3 Removal of tetracycline antibiotics using different treatment processes

Tetracycline antibiotics	Matrix	Treatment	Operating conditions	Results and comments	References
CTC	Manure slurry	Anaerobic digestion	Treatment Time = 33 days, T = 35°C, pH = 7.5, [chlortetracycline]° = 100 mg L^{-1}, COD = 52, 240-49	75% degradation rate of chlortetracycline	Arikan 2008
	Distilled water	Photoelectrocatalytic oxidation	[chlortetracycline]° = 32-230 µg L^{-1}, treatment time = 120 min, Ti/TiO_2 (anatase, rutile, amorphous) = photoanode, cathode (vitreous carbon, graphite, stainless steel, amorphous carbon), current intensity = 0.39 A, UV light (254 nm), pH = 3.12- 9.02.	• 98.0 ± 0.2% of chlortetracycline • 67.3 ± 2.15% of total organic carbon removal • 69.3 ± 3.10% of total nitrogen removal	Daghrir et al. 2013
	Aqueous solution	Photocatalysis	50 mg L^{-1} of chlortetracycline, 0.4 g (Cu/TiO_2), high-pressure mercury lamp (500 W, 360 nm), T = 20°C±2°C, treatment time = 0-90 min	• More than 80% degradation rate of chlortetracycline • ≈75% removal of chemical oxygen demand • ≈28.1% of total organic carbon removal • ≈50% of biological oxygen demand removal	Bu and Zhuang 2013
	Beef manure	Composting	Treatment Time = 30 days, temperature = 25-55°C, chlortetracycline = 22 mg Kg^{-1} day^{-1},	• Concentrations of chlortetracycline/epichlortetracycline decreased 99% and 98% (from 113 µg g^{-1} dry weight to 0.7 µg g^{-1} dry weight and 2.0 µg g^{-1} dry weight) at T= 55°C. • Concentration of chlortetracycline/epichlortetracycline decreased 49% and 40% (from 113 µg g^{-1} dry weight to 58 µg/g^{-1} dry weight and 68 µg/g dry weight) at T= 25°C.	Arikan et al. 2009
	Distilled water	Manganese dioxide	pH = 3.0-6.0, $[MnO_2]$ = 50-200 mg/L, Temperature = 15-35°C, [chlortetracycline]° = 65 µmol L^{-1},	• k_{obs} = 4.1 ±0.1 10^{-3} µM $^{-1}$ h^{-1} at pH =5.02, [CTC]° = 65 µM, and [δ-MnO_2]° = 50 mg L^{-1}	Chen et al. 2011

Tableau 2-4 Removal of tetracycline antibiotics using different treatment processes

Tetracycline antibiotics	Matrix	Treatment	Operating conditions	Results and comments	References
CTC	Livestock wastewater	Ozonation	UV light (4.9 W, 253.7 nm), working volume = 1L, O_3 (7.0 g m^{-3}, 4.9 mg/min), [H_2O_2] = 0-200 mg L^{-1}, T = 20°C, treatment time = 0-60 min, [chlortetracycline]° = 20 µg mL^{-1}	• 30% of chlortetracycline was degraded by O_3 in 40 min • 65% of chlortetracycline was degraded by O_3/H_2O_2 in 40 min. • Less than 2 log-reduction was achieved in 1 h using O_3. • 4 log-reduction in 20 min and 5-log reduction in 40 min using UV • Inactivation of chlortetracycline -resistant HPCs after 10 min using O_3/UV	Lee et al., 2011
	Distilled water	Direct photolysis	150-W Xenon short Arc lamp, [chlortetracycline]°= 200 µmol L^{-1}, pH = 6.0-9.0, irradiation time = 0-90 min.	• 50% of Chlortetracycline degradation • [H_2O_2] production = 0.027-0.086µmol L^{-1} min^{-1}	Chen et al., 2012.
TC	Distilled water	Semiconductor photocatalysis	MP UV (125 W); pH = 6.0; [TC]°= 10-50 mg L^{-1}; TiO_2 (100% anatase or anatase/rutile = 4/1; 1 and 0.4 g L^{-1} of catalyst	More than 98% of tetracycline was oxidized within about 2 h; 100% of total organic carbon removal using TiO_2 (anatase/rutile).	Addamo et al., (2005)
	Deionised water	Semiconductor photocatalysis	UV (254 nm, 365 nm); solarium device (300-400 nm); TiO_2 catalyst; 05-1.0 g L^{-1} catalyst; [tetracycline]° = 40 mg L^{-1}; treatment time = 120 min.	• 100% degradation and 90% total organic carbon removal (UV 254 nm; 0.5 g/L TiO_2; after 120 min). • 100% degradation and 70% total organic carbon removal (Solarium device; 0.5g/L TiO_2; after 120 min). • 50% degradation and 10% total organic carbon removal (UV 365 nm; 0.5 g/L TiO_2; after 120 min).	Reyes et al., (2006)
	Ultra-pure water	Direct photolysis	UV at 365 nm; pH = 6; [tetracycline]° = 10-40 mg L^{-1}	73% tetracycline degradation; 15% total organic carbon removal	Jiao et al., 2008

Tableau 2-5 Removal of tetracycline antibiotics using different treatment processes

Tetracycline antibiotics	Matrix	Treatment	Operating conditions	Results and comments	References
TC	Distilled water	Electrochemical oxidation	pH = 3.9-10.0, current density = 15.9-63.5 mA cm^{-2}, treatment time = 60 min, [Na_2SO_4] = 0.05-0.20 mol L^{-1}, Ti/RuO_2-IrO_2: anode, stainless steel: cathode, [OH°] = 0-4.20 mmol L^{-1}, [tetracycline]° = 50-200 mg L^{-1}, volume = 200 mL	More than 90% of tetracycline degradation at pH = 3.9, current density = 47.6 mA/cm^2, [Na_2SO_4] = 0.1 mol/L and [tetracycline] = 100 mg L^{-1}	Zhang et al., 2009
	Distilled water	Photoelectrocatalytic process	TiO_2 photoanode, UV light (254 nm, 2.5 mW cm^{-2}), 0.5 V, pH = 5.5, [NaSO4]° = 0.02 moL L^{-1}, [tetracycline]° = 10 mg L^{-1}, treatment time = 3h	More than 80% of tetracycline degradation	Liu et al., 2009
	Spicked STP effluent, surface and deionised water	Photo-Fenton	Black light (15 W); solar irradiation; 1-10 mM H_2O_2; 0.20 mM ferrioxalate or $Fe(NO_3)_3$; [tetracycline]° = 24 mg L^{-1}	100 % tetracycline degradation under solar irradiation;	Bautitz and Nogueira, 2007
	Distilled Water	Semiconductor photocatalysis	Xe lamp (300-800 nm); TiO_2 and ZnO as catalyst ; 0.5-1.5 g L^{-1} TiO_2; 0.2-1.5g L^{-1} ZnO ; pH = 3-10 (TiO_2) ; pH= 6-11 (ZnO); [tetracycline]° = 20 mg L^{-1}	• 100% tetracycline degradation and 50% total organic carbon removal (after 15 min, 1.5 g L^{-1} TiO_2, pH = 8.7) • 100% tetracycline degradation and mineralization (after 10-60 min, 1.0 g L^{-1} ZnO, pH = 11).	Palominos et al., (2009)
OTC	Pharmaceutical wastewater	Reverse osmosis Ultrafiltration	• **Reverse osmosis**: NTR-7450 membrane ; NTR-7459 membrane ; Area = 155 cm^2 ; T = 21-23°C; pressure = 1.8 MPa; volume reduction = 3.5. • **Ultrafiltration**: Stirred cell; 3,10,30,50 K Da cut-off membranes; operational pressure = 0.30 MPa; volume reduction = 10. • [oxytetracycline]° = 1000 mg L^{-1}; [COD] = 10000 mg L^{-1}	• **Reverse osmosis**: The organic content in the permeate was decreased from 10000 mg COD L^{-1} to 200 mg COD L^{-1} (98% removal); oxytetracycline was reduced from 1000 mg L^{-1} to 80 mg L^{-1} (87.5% removal). • Ultrafiltration: the oxytetracycline recovery ratio was higher than 60%, the purity higher than 80%.	Li et al., 2004

Tableau 2-6 Removal of tetracycline antibiotics using different treatment processes

Tetracycline antibiotics	Matrix	Treatment	Operating conditions	Results and comments	References
OTC	Ultrapure water	Ozonation	11 mg L^{-1} O_3; [oxytetracycline]° = 100-200 mg L^{-1} ; pH = 3-11	• 100% oxytetracycline degradation after 20 min; BOD_5/COD was higher than 0.3 biodegradable effluent; By-products were more toxic than parent compounds.	Li et al., 2008
	Ultrapure water	Direct photolysis	UV at 365 nm, pH =4-9; [oxytetracycline]° = 10-40 mg L^{-1}.	90% oxytetracycline degradation, 14% total organic carbon removal, 47% of inhibition rate after 240 min of irradiation	Shaojun et al. (2008)
	Distilled water	Electrochemical oxidation	Current density = 50 mA cm^{-2}, pH = 2.10-4.45, T° = 21±1.0°C, electrolysis time = 0-120 min, anode= RuO_2, [oxytetracycline] = 4.8310^{-5}-8.8510^{-5} mol dm^{-3}	• Rate constants: 9.9 x 10^{-5} s^{-1} (pH 2.10), 1.9 10^{-4} s^{-1} (pH 5.45). • Complete loss of the antimicrobial activity of oxytetracycline after 120 min of electrolysis time and at 50 mA cm^{-2}.	Rossi et al., 2009
	Pharmaceutical wastewater	Reverse osmosis Nanofiltration	[oxytetracycline]° = 10 mg L^{-1}, XLE and HR95PP membranes (Reverse osmosis), NF90 and HL Desal membrane (nanofiltration).	Higher degradation using reverse osmosis followed by nanofiltration	Kosutic et al. (2007)
CTC OTC TC	Distilled water	Adsorption with aluminium oxide	C° = 20-110 µg L^{-1}, 0.8-3.5 g L^{-1} Al_2O_3	Rapid adsorption of tetracycline (43%), chlortetracycline (57%) and oxytetracycline (44%).	Chen and Huang, 2010

Tableau 2-7 Removal of tetracycline antibiotics using different treatment processes

Tetracycline antibiotics	Matrix	Treatment	Operating conditions	Results and comments	References
CTC OTC TC	Aqueous solution	Photoelectrocatalytic process	[tetracycline]° = 10 mg L^{-1}; [chlortetracycline]° = 10 mg L^{-1}; [oxytetracycline]° = 10 mg L^{-1}; medium pressure mercury lamp (15 W, $\lambda \geq 365$ nm, 21.2 µW cm^{-2}, [Na_2SO_4] = 0.1 moL L^{-1}, potential applied = 0.6-3.0 V, treatment time = 0-180 min, pH =3-12	About 95% of tetracycline antibiotics degradation	Liu et al., 2012
CTC Doxycycline OTC TC	Aqueous solution Wastewater animal husbandry	Electrochemical oxidation	Current intensity = 1.5 A, Ti/IrO_2 (or Ti/PbO_2) : anode, Ti: cathode, electrode gap = 10 mm, [NaCl] (or [Na_2SO_4]) = 1000 mg L^{-1}, treatment time = 6h, [Tetracycline antibiotics]° = 100 mg L^{-1}, [oxytetracycline]° = 100 mg L^{-1}	[Tetracycline antibiotics] final = 0.6 mg L^{-1}, [oxytetracycline]° = 0.7 mg L^{-1} after 6h of treatment time	Miyata et al., 2011
CTC Doxycycline OTC TC	Distilled water spicked with calcium chloride, humic acid and NaCl	Nanofiltration	NF 200 membranes (14.6 cm^2 area), pH = 7, T = 20°C.	Degradation of tetracycline antibiotics between 50-80% after 90 min.	Koyuncu et al., 2008
CTC Doxycycline OTC TC	Distilled water	Oxidation/reduction	pH = 7.0±0.1, 5 mM phosphate buffer, T° = 22.0 ±1.0°C, Xe arc lamp (172 nm), [TOC]° = 13 µg L^{-1}, electron pulse radiolysis (472 nm, G =5.2 x 10^{-4} m^2 J^{-1}	• The efficiencies for OH° reaction = 32-60% • The efficiencies for e^- reaction= 15-29%, for chlortetracycline = 97%.	Jeong et al., 2010
CTC OTC TC	Ultrapure water Surface water Ground water Wastewater	Gamma radiation	Temperature = 25°C±1.0°C, pH= 2-10, radiation dose = 1.66-3.83 Gy min^{-1}, [HCO_3^-] = 0.0-7.2 meq L^{-1}, [SO_4^{2-}] = 0.0-41.0 mg L^{-1}, [NO_3^-] =0.0-4.4 mg L^{-1}, [Tetracycline antibiotics] = 20-100 mg L^{-1}	• Toxicity inhibition: surface water (43.2% of tetracycline, 36.3% of chlortetracycline, 47.2% of oxytetracycline); Ground water (32.7% of tetracycline, 55.6% of chlortetracycline, 44.4% of oxytetracycline)	Lopez-Penalver et al. 2012
CTC Doxycyline OTC TC Demeclocycline Minocycline	Spiked synthetic and river water	Coagulation adsorption with activated carbon	Contact time 5 min, 10 µg L^{-1} for adsorption process, 100 µg L^{-1} for coagulation, coagulation PACI (5-60 mg L^{-1}), granular activated carbon filtration: calgon F400 and coconut-based carbon.	• **Synthetic water**: 43-94% removal of the drugs (40 mg L^{-1} of coagulant). • **River water**: 44-67% removal of the drugs.	Choi et al., 2008

2.8 Area for future research

This paper underlines the worldwide usage of tetracycline antibiotics, their fate and toxicity in the aquatic and terrestrial environment. On one hand, the cheapest cost and the therapeutic effects of tetracycline antibiotics make it more suitable for preserving human and animal health and even as feed additive in agriculture sector; and on the other hand, it also make it potentially significant as environmental contaminants due to its higher stability and persistence. Halling-Sorensen et al. (2005) found that the average degradation half live of CTC varied from 25 to 34 days in two Danish soils, whereas Samuelsen et al. (1994) reported that no degradation was observed for OTC after 6 months of incubation in marine sediment. Up to now, the environmental consequences of the presence of tetracycline antibiotics and the resistant bacteria in the environment remain indistinct. Generally, the impact of tetracycline antibiotics drugs administrated for example to animals in terrestrial and aquatic environments depends not only on the amount used and the type of the administration, but also on animal husbandry practices, metabolism within the animal, manure handling and storage and degradation rate in it. Thus, the prudent use of tetracycline antibiotics and the claim for "co-ordination" between human, veterinary and the different environmental sectors become mandatory.

Although extensive studies have been conducted on the tetracycline antibiotics (tetracycline, chlortetracycline and oxytetracycline), the fate and effect of its metabolites is still unknown and pose challenges. Major studies focus to develop new remediation techniques for the removal of TCAs from environmental media, for the general protection of human health and ecosystems. The lower mineralization yields recorded at the end of the most treatment processes indicated that only a small fraction of tetracycline antibiotics was completely oxidized into water and carbon dioxide. The majority of the contaminant was transformed into by-products. Thus, more attention has to be paid to these intermediates. Halling-Sorensen et

al. (2002) have investigated the fate of important tetracycline antibiotics and their degradation products under environmentally relevant conditions (pH, chelation and photo-degradation). They analyzed whether these degradation products were potent to environmentally relevant sludge and soil bacteria. According to Halling-Sorensen et al. (2002), the tetracycline antibiotics degradation products were formed dependently on the pH, the presence of cations and the light exposure. At pH levels exceeding 6.5, iso-chlortetracycline, iso-tetracycline, keto-chlortetracycline and iso-oxytetracycline are the major by-products formed, whereas epi-tetracycline, epianhydro-tetracycline, epi-chlortetracycline, epi-anhydrochlortetracycline, keto-chlortetracycline, α-Apo-oxytetracycline and β-Apo-chlortetracycline were considered as the major degradation products to be found in the environmental aquatic matrices at pH below 6.5. Majors of these degradation products were found potent to both sludge and soil bacteria, especially anhydro-tetracycline, epi-anhydrotetracycline, epi-chlortetracycline and anhydro-chlortetracycline which are very toxic to all the resistant isolates. According to Backwood and English (1970), the corresponding potency of anhydro-tetracycline, iso-tetracycline, epi-tetracycline, epi-oxytetracycline was 270%, 0.09%, 54% and 29%, respectively. Belong to the "atypical tetracycline antibiotics", anhydro-tetracycline, anhydro-chlortetracycline and epi-anhydrochlortetracycline have a different mode of action than tetracycline antibiotics by being bactericidal instead of bacteriostatic (Halling-Sorensen et al., 2002). They interfere with membrane permeability and they exhibit activity against organisms that are resistant to chlortetracycline, oxytetracycline and tetracycline (Chopra et al., 1994; Chopra et al., 1992).

Furthermore, it is clear that there is a gap of reliable studies on the relationship between the occurrence of residual concentrations of tetracycline antibiotics and the antibiotic resistance microorganisms. This resistance is mainly due to the repeated exposition of bacteria to sub-lethal dosages of antibiotics (Kemper et al., 2008). Generally, tetracycline antibiotics is regularly fertilized in soils with manure (Hamscher et al., 2002). Thus, the long term

dispersion of liquid manure on fields may result in serious contamination due to the accumulation character of tetracycline antibiotics in the environment (Kemper et al., 2008). Consequently, a transfer of antimicrobial is possible. According to Richter et al. (1996), the transmission of these antibiotic resistance microorganisms is possible via the direct contact or via the food chain.

Besides, reported concentrations of tetracycline antibiotics in different environmental compartments are still detected in lower trace levels and ultimately depend on spatial and climatic variations. Given this fact, techniques developed for the detection cannot be extrapolated. In this context, analytical method for the detection should have higher sensitivity, selectivity and specificity. According to Shelver et al. (2012), sensitive analytical methods should be used to demonstrate the presence of chlortetracycline for example in manure, agriculture wastewater and in ground water at lower concentrations (from ng L^{-1} to $\mu g\ L^{-1}$). Thus, it is critical to find multi-residual method to detect tetracycline antibiotics and its by-products. Liquid chromatography coupled to mass spectrometry which provides new opportunities for analysis of tetracycline antibiotics in water, is highly recommended. Liquid chromatography coupled to mass spectrometry has been developed and effectively implemented by several research groups (Daghrir et al., 2013; Arikan et al., 2009; Arikan, 2008) for the determination of tetracycline antibiotics mainly due to the known advantage of mass spectrometry detection over conventional detection method such as UV and fluorescence. According to Onal et al. (2011), mass spectrometry - mass spectrometry proves to be a useful analysis technique able to identify and clarify the structure of the compound in complex matrices.

It should be also mentioned that several questions remain unanswered for the conventional treatment processes (biological or physico-chemical treatments) generally applied to remove tetracycline antibiotics through wastewater treatment plants. The occurrence of tetracycline

antibiotics in the aquatic and terrestrial environmental is mainly due to the unsuccessful of conventional treatment processes (coagulation, sedimentation, UV irradiation, and biological) applied in wastewater treatment plants in the removal of these compounds. These tetracycline antibiotics promote the proliferation of antibiotic resistant microorganisms, which can pose a major public health concern. Previous studies (Auerbach et al., 2007) have investigated wastewater treatment plants as possible sources for the development and proliferation of tetracycline antibiotics resistance genes in the activated sludge. According to the results reported with Auerbach et al. (2007), the concentrations of tet(Q) resistance genes were found to be highest in wastewater influent while the concentrations of tet(G) genes were highest in activated sludge. As a matter of fact, investigations of the effects of UV disinfection as a tertiary treatment process in wastewater treatment plants showed no reduction in the number of detectable resistant gene types (tet^R).

To overcome this drawback, novel approaches that use and integrate the chemical data including advanced oxidation processes have been developed and applied to remove tetracycline antibiotics from water, wastewater, soil and sludge. Until date, applications of advanced oxidation processes for tetracycline antibiotics removal were carried out at the laboratory scale. Future research should be focused on the development of advanced oxidation processes for large scale applications. Advanced oxidation processes are one of the most powerful processes for the removal of antibiotics from the environment (Homem and Santos, 2011). In addition, these processes can be effectively used to remove by-products toxicity and enhance the mineralization rate of tetracycline antibiotics. The microorganisms used in biological process are sensible to the toxic pollutants. Thus, advanced oxidation processes could be applied as pre-treatment step in which the pollutant are oxidized to by-products that are easily biodegradable and less toxic. This combined process avoids the death of microorganisms that are present in biological treatment (Tekin et al., 2006). Likewise,

coupling a biodegradation process with physicochemical process would improve tetracycline antibiotics removal and reduce the operating cost.

2.9 Conclusions

This review emphasizes the widespread usage of tetracycline antibiotics, their occurrence and their toxicity in different aquatic and terrestrial compartments. Due to their extensive applications in the medical field and in the agriculture sector, residual concentrations of such drugs have been detected in the environment. The introduction of these residual compounds into environment through different sources will lead to serious environmental problems including ecological risk and human health damage. Despite the extensive knowledge about tetracycline antibiotics, advanced studies need to be carried out to evaluate the toxicity of tetracycline antibiotics. Today, most conventional wastewater treatments are not able to remove tetracycline antibiotics from water and waste water. To this end, practical and economical processes have been developed and applied in order to reduce the discharges of tetracycline antibiotics into the environment. Advanced oxidation processes have been proposed as alternative methods to ensure the higher degradation and mineralization of tetracycline compounds.

2.10 Acknowledgments

Sincere thanks are extended to the National Sciences and Engineering Research Council of Canada and Premier Tech Ltee for their financial support for this study.

2.11 References

Addamo M, Augugliaro V, Di Paola A, García-López E, Loddo V, Marcì G & Palmisano L (2005) Removal of Drugs in aqueous systems by photoassisted degradation. *J. App. Electrochem.* 35: 765-774.

Andreozzi R, Campanella L, Fraysse B, Garric J, Gonnella A, Lo Giudice R, Marotta R, Pinto G & Pollio A (2004) Effects of Advanced oxidation processes (AOPs) on the toxicity of a mixture pharmaceuticals. *Water Sci. Technol.* 50: 23-28.

Andreozzi R, Caprio V, Insola A & Marotta R (1999) Advanced oxidation processes (AOP) for water purification and recovery. *Catal. Today* 53: 51-59.

Andreu V, Vazguez-Roig P, Blasco C, Pico Y (2009) Determination of tetracycline residues in soil by pressurized liquid extraction and liquid chromatography tandem mass spectrometry. *Anal. Bioanal. Chem.* 394: 1329-1339.

Anglada A, Urtiaga A, Ortiz I (2009) Contributions of electrochemical oxidation to waste-water treatment: fundamentals and review of applications. *J. Chem. Technol. Biotechnol.* 84: 1747-1755.

AHI (2005) *Animal Health Institute*, www.ahi.org/documents/antibioticuse2003.pdf.

Arikan OA, Mulbry W & Rice C (2009) Management of antibiotic residues from agricultural sources: use of composting to reduce chlortetracycline residues in beef manure from treated animals. *J. Hazard. Mater.* 164: 483-489.

Arikan OA, Rice C & Codling E (2008) Occurrence of antibiotics and hormones in a major agricultural watershed. *Desalination* 226: 121-133.

Auerbach EA, Seyfried EE, McMahon KD (2007) Tetracycline resistance genes in activated sludge wastewater treatment plants. *Water Res.* 41: 1143-1151.

Aust MO, Godlinski F, Travis GR, Hao X, McAllister TA, Leinweber P & Thiele-Bruhn S (2008) Distribution of sulfamethazine, chlortetracycline and Tylosin in manure and soil of Canadian feedlots after subtherapeutic use in cattle. *Environ. Pollut.* 156: 1243-1251.

Bao Y, Zhou Q, Guan L & Wang Y (2009) Depletion of chlortetracycline during composting of aged and spiked manures. *Waste Manage.* 29: 1416-1423.

Baquero F, Martinez JL & Canton R (2008) Antibiotics and antibiotic resistance in water environments. *Curr. Opin. Biotech.* 19: 260-265.

Bautitz I R & Nogueira RFP (2007) Degradation of tetracycline by photo-Fenton process-Solar irradiation and matrix effects. *J. photochem. photobiol. A.* 187: 33-39.

Blackwood RK & English AR (1970) Structure-activity relationship in the tetracycline series. *Adv. appl. Microbiol.* 13: 237-266.

Braham RJ & Harris AT (2009) Review of major design and scale-up considerations for solar photocatalytic reactors. *Ind. Eng. Chem. Res.* 48 (19): 8890-8905.

Brain RA, Johnson DJ, Richards SM, Sanderson H, Sibley PK & Solomon KR (2004) Effects of 25 pharmaceutical compounds to Lemna gibba using a seven-day static-renewal test. *Environ. Toxicol. Chem.* 23: 371-382.

Bound JP & Voulvoulis N (2004) Pharmaceuticals in the aquatic environment - A comparison of risk assessment strategies. *Chemosphere* 56: 1143-1155.

Boxall A B, Johnson P & Smith E (2006) Uptake of Veterinary Medicines from Soils into Plants. *J. Agric. Food Chem.* 54: 2288-2297.

Bu D & Zhuang H (2013) Biotemplated synthesis of high specific surface area copper-doped hollow spherical titania and its photocatalytic research for degradating chlorotetracycline. *Appl. Surf. Sci.* 265: 677-685.

Commission of the European Communities (1998a) Council regulation 2788/98. Official Journal of the European Communities Legislation, L347, 32.

Commission of the European Communities (1998b) Council Regulation 2821/98. Official Journal of the European Communities Legislation, L351, 4.

Chaidemenos GC (2001) Tetracycline and niacinamide in the treatment of blistering skin diseases. *Clin. Dermatol.* 19: 781-785.

Chen Y, Li H, Wang Z, Tao T, Wei D & Hu C (2012) Photolysis of chlortetracycline in aqueous solution: Kinetics, toxicity and products. *J. Environ. Sci.* 24: 254-260.

Chen G, Zhao L & Dong Yh (2011) Oxidative degradation kinetics and products of chlortetracycline by manganese dioxide. *J. Hazard. Mater.* 193: 128-138.

Chen F, Yang X, Mak HKC & Chan DWT (2010) Photocatalytic oxidation for antimicrobial control in built environment: A brief literature overview. *Build. Environ.* 45: 1747-1754.

Chen WR & Huang CH (2010) Adsorption and transformation of tetracycline antibiotics with aluminum oxide. *Chemosphere* 79: 779–785.

Cheng G (2005) Interaction of tetracycline with aluminum and iron hydrous oxides. *Environ. Sci. Technol.* 39: 2660–2667.

Chong MN, Jin B, Laera G & Saint CP (2011) Evaluating the photodegradation of carbamazepine in a sequential batch photoreactor system: impacts of effluent organic matter and inorganic ions. *Chem. Eng. J.* 174(2-3): 595-602.

Chopra I (1994) Tetracycline analogs whose primary target is not the bacterial ribosome. *Antimicrob Agents Che* 38: 637-664.

Chopra I, Hawkey PM & Hinton M (1992) Tetracyclines, molecular and clinical aspects. *J Antimicrob Ch* 29: 245-277.

Chopra I & Roberts M (2001) Tetracycline Antibiotics: Mode of Action, Applications, Molecular Biology, and Epidemiology of Bacterial Resistance. *Microbiol. Mol. Biol. R.* 65: 232–260.

Choi KJ, Kim SG & Kim SH (2008) Removal of antibiotics by coagulation and granular activated carbon filtration. *J. Hazard. Mater.* 151: 38-43.

Christian T, Schneider RJ, Farber HA, Skutlarek D, Meyer MT & Goldbach HE (2003) Determination of antibiotic residues in manure, soil, and surface waters. *Acta Hydroch. Hydrob.* 31: 36-44.

Crisafully R, Milhome MAL, Rivelino M, Cavalcante RM, Silveira ER, Keukeleire DD & Nascimento RF (2008) Removal of some polycyclic aromatic hydrocarbons from petrochemical wastewater using low-cost adsorbents of natural origin. Bioresource Technol. 99: 4515–4519.

Daghrir R, Drogui P & El Khakani MA (2013) Photoelectrocatalytic oxidation of chlortetracycline using Ti/TiO_2 photo-anode with simultaneous H_2O_2 production. *Electrochim. Acta* 87: 18-31.

Daghrir R, Drogui P, Ka I & El Khakani MA (2012) Photoelectrocatalytic degradation of chlortetracycline using Ti/TiO_2 nanostructured electrodes deposited by means of a Pulsed Laser Deposition process. *J. Hazard. Mater.* 199– 200: 15– 24

Daghrir R, Drogui P & Robert D (2012) Photoelectrocatalytic technologies for environmental applications. *J. Photochem. Photobiol. A.* 238: 41-52.

Daughton CG & Ternes TA (1999) Pharmaceuticals and Personal Care Products in the Environment: Agents of Subtle Change. *Environ. Health Perspect.* 107: 907-938.

Deblonde T, Cossu-Leguille C & Hartemann P (2011) Emerging pollutants in wastewater: A review of the literature. *Int. J. Hyg. Envir. Heal.* 214: 442-448.

Ding X & Mou S (2000) Ion chromatographic analysis of tetracyclines using polymeric column and acidic eluent. *J. Chromatogr. A* 897: 205-214.

Esquivel K, Arriaga L G, Rodriguez F J, Martinez L & Godinez L A (2009) Development of a TiO_2 modified optical fiber electrode and its incorporation into a photoelectrochemical reactor for wastewater treatment. *Water Res.* 43: 3593-3603.

Fent K, Weston AA & Caminada D (2006) Ecotoxicology of human pharmaceuticals. *Aquat. Toxicol.* 76: 122–159.

Gao P, Ding Y, Li H & Xagoraraki I (2012) Occurrence of pharmaceuticals in a municipal wastewater treatment plant: Mass balance and removal processes. *Chemosphere* 88: 17-24.

Gobel A, Thomsen A, McArdell C S, Joss A & Giger W (2005) Occurrence and sorption behavior of sulfonamides, macrolides, and trimethoprim in activated sludge treatment. *Environ. Sci. Technol.* 39: 3981-3989.

Gonzàlez O, Sans C & Esplugas S (2007) Sulfamethoxazole abatement by photo-Fenton. Toxicity, inhibition and biodegradability assessment of intermediates. *J. Hazard. Mater.* 146: 459-464.

Gracia T, Hilscherova K, Jones PD, Newsted JL, Higley EB, Zhang X, Hecker M, Murphy MB, Yu RMK, Lam PKS, Wu RSS & Giesy JP (2007) Modulation of steroidogenic gene expression and hormone production of H295R cells by pharmaceuticals and other environmentally active compounds. *Toxicol. Appl. Pharmacol.* 255: 142-153.

Grote M, Vockel A, Schwarze D, Mehlich A & Freitag M (2004) Fate of antibiotics in food chain and environment originating from pig fattening (Part 1). *Fresenius Environ. Bull.* 13:1216-1224.

Grimm J, Bessarabov D & Sanderson R (1998) Review of electro-assisted methods for water purification. *Desalination* 155: 285-294.

Gunten U (2003) Ozonation of drinking water: Part I, Oxidation kinetics and product formation. *Water Res.* 37: 1443-1467.

Halling-Sorensen B, Sengelov G & Tjornelund J (2002) Toxicity of tetracyclines and tetracycline degradation products to environmentally relevant bacteria, including selected tetracycline-resistant Bacteria. *Arch. Environ. Con. Tox.* 42: 263-271.

Halling-Sorensen B (2000) Algal toxicity of antibacterial agents used in intensive farming. *Chemosphere* 40: 731-739.

Halling-Sorensen B, Nielsen SN, Lanzky PF, Ingerslev F, Lutzhoft HCH & Jorgensen SE (1998) Occurrence, fate and effects of pharmaceutical subsatnces in the environment-a review. *Chemosphere* 36: 357-394.

Halling-Sorensen B, Jacobsen AM, Jensen J, Sengelov G, Vaclavik E & Ingerslev F (2005) Dissipation and effects of chlortetracycline and tylosin in two agricultural soils: A field-scale study in southern Denmark. Environ. Toxicol. Chem. 24: 802-810.

Hamscher G, Sczesny S, Höper H & Nau H (2002) Determination of Persistent Tetracycline Residues in Soil Fertilized with Liquid Manure by High-Performance Liquid

Chromatography with Electrospray Ionization Tandem Mass Spectrometry. Anal. Chem. 74:1509–1518.

Hamscher G (2000) Substances with pharmacological effects including hormonally active substances in the environment: Identification of tetracyclines in soil fertilized with animal slurry. Deu. Tierarztl. Woch. 107: 332-334.

Han Y & Lucy Zhou ZH (1999) Ransohoff R M TNF-α suppresses IFN-γ-induced MHC class II expression in HT1080 cells by destabilizing class II trans-activator mRNA. J. Immun. 163: 1435-1440.

Hernandez F, Sancho JV, Ibanez M & Guerrero C (2007) Antibiotic residue determination in environment waters by LC-MS. *TrAC-Trend Anal. Chem.* 26: 466-485.

Hernandez-Alonso MD, Coronado JM, Javier Maira A, Soria J, Loddo V & Augugliaro V (2002) Ozone enhanced activity of aqueous titanium dioxide suspensions for photocatalytic oxidation of free cyanide ions. *Appl. Catal. B.* 39: 257-267.

Heit G, Neuner A, Saugy PY & Braun AM (1998) Vacuum-UV (172 nm) actinometry- the quantum yield of the photolysis of water. *J. Phys. Chem. A.* 102: 5551-5561.

Heuer O E, Kruse H, Grave K, Collignon P, Karunasagar I & Angulo FJ (2009) Human Health Consequences of use of antimicrobial agents in aquaculture. *Clin. Infect. Dis.* 49: 1248-1253.

Hu L, Martin HM & Strathmann TJ (2010) Oxidation Kinetics of Antibiotics during Water Treatment with Potassium Permanganate. *Environ. Sci. Technol.* 44: 6416–6422.

Hu X, Zhou Q, Luo Y (2010) Occurrence and source analysis of typical veterinary antibiotics in manure, soil, vegetables and groundwater from organic vegetable bases. *Northern China. Environ Pollut* 158: 2992-2998.

Hui-zhu W, Yi L, Wen-qing X, Qi-xing Z, Bao-hua T & Yuan-yuan W (2008) Ecotoxic Effects of Tetracycline and Chlortetracycline on Aquatic Organisms. *J. Agro.Environ Sci.* http://en.cnki.com.cn/Article_en/CJFDTOTAL-NHBH200804048.htm

Homem V & Santos L (2011) Degradation and removal methods of antibiotics from aqueous matrices- A review. *J. Environ. Manage.* 92: 2304-2347.

Holten Lützhøft HC, Halling-Sørensen B & Jørgensen SE (1999) Algal toxicity of antibacterial agents applied in Danish fish farming. *Arch. Environ. Con. Tox.* 36: 1-6.

Hirsch R, Ternes T, Haberer K & Kratz KL (1999) Occurrence of antibiotics in the aquatic environment. *Sci. Total Environ.* 225: 109-118.

Jeong J, Song W, Cooper WJ, Jung J & Greaves J (2010) Degradation of tetracycline antibiotics: Mechanisms and kinetic studies for advanced oxidation/reduction processes. *Chemosphere* 78(5): 533-540.

Jiao S, Zheng S, Yin D, Wang L & Chen L (2008) Aqueous photolysis of tetracycline and toxicity of photolytic products to luminescent bacteria. *Chemosphere* 73: 377-382.

Ji K, Choi K, Lee S, Park S, Khim JS, Jo EH, Choi K, Zhang X & Giesy JP (2010) Effects of sulfathiazole, oxytetracycline and chlortetracycline on steroidogenesis in the human adrenocarcinoma (H295R) cell line and freshwater fish Oryzias Latipes. *J. Hazard. Mater.* 182: 494-502.

Jjemba PK (2006) Excretion and ecotoxicity of pharmaceutical and personal care products in the environment. *Ecotox. Environ. Safe.* 63:113-130.

Kang HJ, Kim HS, Choi KH, Kim KT & Kim PG (2005) Several human pharmaceutical residues in aquatic environment may result in endocrine disruption in Japanese medaka (Oryzias latipes). *Korean J. Environ. Health* 31: 227-233.

Karthikeyan KG, Meyer MT (2006) Occurrence of antibiotics in wastewater treatment facilities in Wisconsin, USA. *Sci. Total Environ.* 361: 196-207.

Kemper N, Farber H, Skutlarek D & Krieter J (2008) Analysis, of antibiotic residues in liquid manure and leachates of dairy farms in Northern Germany. *Agr. Water Manage.* 95:1288-1292.

Kim I & Tanaka H (2009) Photodegradation characteristics of PPCPS in water with UV treatment. *Environ. Inter.* 35: 793-802.

Kim SC & Carlson K (2007) Temporal and spatial trends in the occurrence of human and veterinary antibiotics in aqueous and river sediment matrices. Environ. Sci. Technol. 41: 50-57

Kim KR, Owens G, Kwon SI, So KH, Lee DB & Ok YS (2011) Occurrence and environmental fate of veterinary antibiotics in the terrestrial Environment. *Water Air Soil Poll.* 214:163-174.

Kim PG (2007) Chlortetracycline caused vitellogenin induction at male Japanese medaka (Oryzias Latipes). *Korean J. Environ. Health* 33: 513-516.

Kim S, Eichhorn P, Jensen J & Weber AS (2005) Removal of Antibiotics in Wastewater: Effect of Hydraulic and Solid Retention Times on the Fate of Tetracycline in the Activated Sludge Process. *Environ. Sci. Technol.* 39: 5816-5823.

Koesukwiwat U, Jayanta S & Leepipatpiboon N (2007) Validation of a liquid chromatography–mass spectrometry multi-residue method for the simultaneous determination of sulfonamides, tetracyclines, and pyrimethamine in milk. *J. Chromatogr. A.* 1140:147–156.

Kosutic K, Dolar D, Asperger D & Kunst B (2007) Removal of antibiotics from a model wastewater by RO/NF membranes. *Sep.Purif.Technol.* 53:244-249.

Koyuncu I, Arikan OA, Wiesner MR & Rice C (2008) Removal of hormones and antibiotics by nanofiltration membranes. *J. Membr. Sci.* 309: 94-101.

Kummerer K (2003) Significance of antibiotics in the environment. *J. Antimicrob. Chemother.* 52: 5–7.

Kummerer K (2009) Antibiotics in the aquatic environment- A review-Part I. *Chemosphere* 75: 417-434.

Kummerer K (2009) The presence of pharmaceuticals in the environment due to human use-present knowledge and future challenges. *J. Environ. Manage.* 90: 2354-2366.

Kulshrestha P, Giese RF, Aga DS (2004) Investigating the Molecular Interactions of Oxytetracycline in Clay and Organic Matter: Insights on Factors Affecting Its Mobility in Soil. *Environ. Sci. Technol.* 38: 4097-4105.

Kolpin DW, Furlong E, Meyer M, Thurman EM, Zaugg S, Barber L, Buxton H (2002) Pharmaceuticals, Hormones, and Other Organic Wastewater Contaminants in U.S. Streams, 1999-2000: A National Reconnaissance. *Environ. Sci. Technol.* 36: 1202-1211.

Krapac IG, Koike S, Meyer MT, Snow DD, Chou SFJ, Mackie RI, Roy WR & Chee-Sandford JC (2005) Long-term monitoring of the occurrence of antibiotic residues and antibiotic resistance in groundwater near swine confinement facilities. Report of the CSREES project 2001-35102-10774.

Leary R & Westwood A(2011) Carbonaceous nanomaterials for the enhancement of TiO_2 photocatalysis. *Carbon.* 49: 741-772.

Lee H, Lee E, Lee CH & Lee K (2011) Degradation of chlortetracycline and bacterial disinfection in livestock wastewater by ozone-based advanced oxidation. *J. Ind. Eng. Chem.* 17: 468-473.

Li JJ, Cao Y, Young MR, Colburn & NH (2000) Induced expression of dominant-negative c-jun downregulates NFκB and AP-1 target genes and suppresses tumor phenotype in human keratinocytes. *Mol. Carcinogen* 29: 159-169.

Lindsey ME, Meyer M & Thurman EM (2001) Analysis of trace levels of sulfonamides and tetracycline antimicrobials in groundwater and surface water using solid phase ectraction and liquid chromatography/mass spectrometry. *Anal. Chem.* 73: 4640-4646.

Liu H, Liu G, Fan J, Zhou Q, Zhou H, Zhang N, Hou Z, Zhang M & He Z (2011) Photoelectrocatalytic degradation of 4, 4`-dibromobiphenyl in aqueous solution on TiO_2 and doped TiO_2 nanotube arrays. *Chemosphere* 82: 43-47.

Liu F, Ying GG, Tao R, Zhao JL, Yang JF & Zhao LF (2009) Effects of six selected antibiotics on plant growth and soil microbial and enzymatic activities. *Environ. Pollut.* 157: 1636-1642.

Liu C, Fua D & Lia H (2012) Behaviour of multi-component mixtures of tetracyclines when degraded by photoelectrocatalytic and electrocatalytic technologies. *Environ. Technol.* (United Kingdom) 33: 791-799.

Li K, Yediler A, Yang M, Schulte-Hostede S & Wong MH (2008) ozonation of oxytetracycline and toxicological assessment of its oxidation by-products. *Chemosphere* 72: 473-478.

Li SZ, Li XY & Wang DZ (2004) Membrane (RO-UF) filtration for antibiotic wastewater treatment and recovery of antibiotics. *Sep. Purif. Technol.* 34: 109-114.

Li R, Zhang Y, Lee CC, Liu L & Huang Y (2011) Hydrauphilic interaction chromatography separation mechanisms of tetracyclines on amino-bonded silica column. *J. Sep. Sci.* 34: 1508-1516.

Lòpez-Penalver JJ, Sànchez-Polo M, Gòmez-Pacheco CV & Rivera-Utrilla J (2010) Photodegradation of tetracyclines in aqueous solution by using UV and UV/H_2O_2 oxidation processes. *J. Chem. Technol. Biot.* 85: 1325–1333.

López Peñalver J J, Gómez Pacheco CV, Sánchez Polo M & Utrilla JR (2012) Degradation of tetracyclines in different water matrices by advanced oxidation/reduction processes based on gamma radiation. *J. Chem. Technol. Biot.* DOI: 10.1002/jctb.3946.

Luo Y, Xu L, Rysz M, Wang Y, Zhang H & Alvarez PJJ (2011) Occurrence and Transport of Tetracycline, Sulfonamide, Quinolone, and Macrolide Antibiotics in the Haihe River Basin, China. *Environ. Sci. Technol.* 45: 1827-1833.

Martinez C, Canle ML, Fernàndez MI, Santaballa JA & Faria J (2011) Kinetics and mechanism of aqueous degrdation of carbamazepine by heterogenous photocatalysis using nanocristalline TiO_2, ZnO_2 and multi-walled carbon nanotube-anatase composites. *Appl. Catal. B.* 102: 563-571.

Martinez-Carballo E, Gonzalez-Barreiro C, Scharf S & Gans O (2007) Environmental monitoring study of selected veterinary antibiotics in animal manure and soils in Austria. *Environ. Pollut.* 148: 570-579.

Martínez-Huitle CA & Ferro S (2006) Electrochemical oxidation of organic pollutants for the wastewater treatment: direct and indirect processes. *Chem. Soc. Rev.* 35: 1324-1340.

McCullagh C, Skillen N, Adams M, Robertson PKJ (2011) Photocatalytic reactors for environmental remediation: a review. *J. Chem. Technol. biotechnol.* 86: 1002-1017.

Michalova E, Novotna P & Schlegelova J (2004) Tetracyclines in veterinary medicine and bacterial resistance to them. *Vet. Med.* 49: 79-10.

Michael HF, James OB & Diana SA (2007) Chlortetracycline detoxification in maize via induction of glutathione-S-transferases after antibiotic exposure. *Environ. Sci. Technol.* 41: 1450-1456.

Migliore L, Brambilla G, Casoria P, Civitareale C, Cozzolino S & Gaudio L (1996) Effects of Antimicrobials for Agriculture as Environmental Pollutants. *Fresenius Environ. Bull.* 5:735-739.

Miyata M, Ihara I, Yoshid G, Toyod K & Umetsu K (2011) Electrochemical oxidation of tetracycline antibiotics using a Ti/TiO_2 anode for wastewater treatment of animal husbandry. *Water Sci. Technol.* 63: 456-461.

Miao XS, Bishav F, Chen M & Metcalfe CD (2004) Occurrence of antimicrobials in the final effluents of wastewater treatment plants in Canada. *Environ. Sci. Technol.* 38: 3533-3541.

Onal A (2011) Overview on liquid chromatographic analysis of tetracycline residues in food matrices. *Food Chem.* 127: 197-203.

Palominos RA, Mondaca MA, Giraldo A, Penuela G, Pérez-Moya M & Mansilla HD (2009) Photocatalytic oxidation of the antibiotic tetracycline on TiO_2 and ZnO suspenssions. *Catal. Today* 144: 100-105.

Pan X, Qiang Z, Ben W & Chen M (2011) Residual veterinary antibiotics in swine manure from concentrated animal feeding operations in Shandong Province, China. *Chemosphere* 84: 695-700.

Panizza M & Cerisola G (2004) Electrochemical Oxidation as a Final Treatment of Synthetic Tannery Wastewater. *Environ. Sci. Technol.* 38: 5470-5475.

Panizza M & Cerisola G (2009) Direct and mediated anodic oxidation of organic pollutants. *Chem. Rev.* 109: 6541-6569.

Park S & Choi K (2008) Hazard assessment of commonly used agricultural antibiotics on aquatic ecosystems. *Ecotoxicology* 17: 526-538.

Polubesova T, Zadaka D, Groisman L & Nir S (2006) Water remediation by micelle–clay system: Case study for tetracycline and sulfonamide antibiotics. *Water Res.* 40: 2369-2374.

Prescott JF, Baggot JD & Walker RD (2000) *Antimicrobial Therapy in Veterinary Medicine*, Iowa State University Press, Ames. p277.

Radjenovic J, Petrovic M, Ventura F & Barcelo D (2008) Rejection of pharmaceuticals in nanofiltration and reverse osmosis membrane drinking water treatment. *Water Res.* 42: 3601-3610.

Rajeshwar K & Ibanez J (1997) Environmental Electrochemistry: Fundamentals and applications in pollution abatement. Academic Press, San Diego, CA, p776.

Ramamurthy NS, Rifkin BR, Greenwald RA, Xu JW, Liu Y, Turner G, Golub LM & Vernillo AT (2002) Inhibition of matrix metalloproteinase-mediated periodontal bone loss in rats: a comparison of 6 chemically modified's tetracyclines. *J.Periodontal.*73:726-734.

Reyes C, Fernandez J, Freer J, Mondaca MA, Zaror C, Malato S & Mansilla H (2006) Degradation and inactivation of tetracycline by TIO_2 photocatalysis. *J. Photochem. Photobiol. A.* 184: 141-146.

Roberts MC (2003) *Tetracycline Therapy: Update. Clin. Infect. Dis.* 36: 3462-467.

Roberts JA, Norris R, Paterson DL, Martin JH (2012) Therapeutic drug monitoring of antimicrobials. *Brit. J. Clinical Pharmaco.* 7: 27-36.

Rossi A, Alves VA, Da Silva LA, Oliveira MA, Assis DOS, Santos FA, De Miranda RRS (2009) Electrooxidation and inhibition of the antibacterial activity of oxytetracycline hydrochloride using a RuO_2 electrode. *J. Appl. Electrochem.* 39: 329-337.

Richter A, Loscher W & Witte W (1996) Leistungsforderer mit antibakterieller Wirkung: Probleme aus pharmakologisch-toxikologischer und mikrobiologischer Sicht. *Prakt. Tierarzt.* 7: 603-624.

Samanidou VF, Nikolaidou KI, Papadoyannis IN (2007) Development and validation of an HPLC confirmatory method for the determination of seven tetracycline antibiotics residues in milk according to the European Union Decision 2002/657/EC. *J. Sep. Sci.* 30: 2430-2439.

Samuelsen OB, Lunestad BT, Ervik A & Fielde S (1994) Stability of antibacterial agents in an artificial marine aquaculture sediment studied under laboratory conditions. *Aquaculture* 126: 283-290.

Sarmah AK, Meyer MT, Boxall ABA (2006) A global perspective on the use, sales, exposure pathways, occurrence, fate and effects of veterinary antibiotics (VAs) in the environment. *Chemosphere* 65: 725-759.

Sczesny S, Nau H, Hamscher G (2003) Residue analysis of tetracyclines and their metabolites in eggs and in the environment by HPLC coupled with a microbiological assay and tandem mass spectrometry. *J Agr Food Chem* 51: 697-703.

Shelver WL, Hakk H, Larsen GL, DeSutter TM & Casey FXM (2010) Development of an ultra-high-pressure liquid chromatography–tandem mass spectrometry multi-residue sulfonamide method and its application to water, manure slurry, and soils from swine rearing facilities. *J. Chromatogr. A.* 1217:1273–1282.

Shelver WL & Varel VH (2012) Development of a UHPLC-MS/MS method for the measurement of chlortetracycline degradation in swine manure. *Anal. Bioanal. Chem.* 402: 1931-1939.

Shajoun J, Shourong Z, Daqiang Y, Lianhong W & Liangyan C (2008) Aqueous oxytetracycline degradation and the toxicity change of degradation compounds in photoirradiation process. *J. Environ. Sci.* 20: 806-813.

Smith H L & Rajan T V (2000) Tetracycline Inhibits Development of the Infective-Stage Larvae of Filarial Nematodes *in Vitro*. *Exp. Parasitol.* 95: 265-270.

Stackelberg PE, Gibs J, Furlong ET, Meyer MT, Zaugg SD & Lippincott RL (2007) Efficiency of conventional drinking water-treatment processes in removal of pharmaceuticals and other organic compounds. *Sci. Total Environ.* 377: 255-272.

Stuart M, Lapworth D, Crane E, Hart A (2012) Review of risk from potential emerging contaminants in UK groundwater. *Sci.Total.Environ.* 416: 1-21.

Spongberg AL & Witter JD (2008) Pharmaceutical compounds in the wastewater process stream in Northwest Ohio. *Sci. Total Environ.* 397:148-157.

Tsai SJ & Cheng S(1997) Effect of TiO_2 crystalline structure in photocatalytic degradation of phenolic contaminants. *Catal. Today*. 33 (1-3): 227-237.

Tekin H, Bilkav O, Ataberk SS, Balta TH, Ceribasi IH, Sanin FD, Dilek FB & Yetis U (2006) Use of Fenton oxidation to improve the biodegradability of a pharmaceutical wastewater. *J. Hazard. Mater.* 136: 258-265.

Wei R, Ge F, Huang S, Chen M & Wang R (2011) Occurrence of veterinary antibiotics in animal wastewater and surface water around farms in Jiangsu Province, China. *Chemosphere* 82: 1408-1414.

Xie X, Zhou Q, He Z & Bao Y (2010) Physiological and potential genetic toxicity of chlortetracycline as an emerging pollutant in wheat (Triticum aestivum L.). *Environ. Toxicol. Chem.* 29: 922-928.

Xiang-Gang H, Yi L, Qi-xing Z & Lin X (2008) Determination of thirteen antibiotics residues in manure by solid phase extraction and high performance liquid chromatography. *Chinese J. Analyt. Chem.* 36: 1162-1166.

Xu W, Zhang G, Li X, Zou S, Li P, Hu Z & Li J (2007) Occurrence and elimination of antibiotics at four sewage treatment plants in the Pearl River Delta (PRD), South China. *Water Res.* 41: 4526-4534.

Yang S & Carlson K (2003) Evolution of antibiotic occurrence in a river through pristine, urban and agricultural landscapes. *Water Res.* 37: 4645-4656.

Yang LH, Ying GG, Su HC, Stauber JL, Adams MS & Binet MT (2008) Growth-inhibiting effects of 12 antibacterial agents and their mixtures on the freshwater microalga Pseudokirchneriella subcapitata. *Environ. Toxicol. Chem.* 27: 1201-1208.

Yu Z & Chuang SSC (2008) The effect of Pt on the photocatalytic degradation pathway of methylene blue over TiO_2 under ambient conditions. *Appl. Catal. B.* 83: 277-285

Zhang H, Liu F, Wu X, Zhang J & Zhang D (2009) Degradation of tetracycline in aqueous medium by electrochemical method. *Asia-Pac J. Chem. Eng.* 4: 568-573.

Zhou Q, Zhang M C, Shuang C D, Li Z Q & Li AM (2012) Preparation of a novel magnetic powder resin for the rapid removal of tetracycline in the aquatic environment. *Chin. Chem. Lett.* 23: 745-748.

Zouaghi R, Zertal A, David B & Guittonneau S (2007) Photocatalytic degradation of Monolinuron and Linuron in an aqueous suspension of Titanium Dioxide under Simulated solar irradiation. *J. Water Sci.* 20: 163-172.

CHAPITRE 3

PHOTOELECTROCATALYTIC TECHNOLOGIES FOR ENVIRONMENTAL APPLICATIONS

Le chapitre 3 est constitué de l'article suivant :

Rimeh Daghrir, Patrick Drogui, Didier Robert (2012) Photoelectrocatalytic technologies for environmental applications. *Journal of Photochemistry and Photobiology A: Chemistry. 238: 41-52.*

3. PHOTOELECTROCATALYTIC TECHNOLOGIES FOR ENVIRONMENTAL APPLICATIONS

3.1 Abstract

This paper summarizes recent research works dealing with the development of photoelectrocatalytic oxidation technologies combining both electrolytic and photocatalytic processes. Photoelectrocatalytic technologies have received particular attention due to their potential and effectiveness in the photodegradation of refractory organic and microbial pollutants present in water and wastewater. Here, titanium dioxide (TiO_2) plays the most important role compared to other semiconductor photocatalysts (CdS, ZnO, SnO_2, etc.) due to its excellent chemical and physical properties. The recombination of the photogenerated electrons and holes is the main factor that generally limits the application of photocatalytic processes (PCPs) in the environmental field. Considerable efforts have been made to increase the photocatalytic efficiency and decrease the charge recombination by means of photoelectrocatalytic processes (PECPs), also referred to as electrochemically assisted photocatalytic processes, which consists of applying an external potential on photocatalysts. This paper deals with the mechanism of photoelectrocatalytic processes, the characteristics and methods for preparing a TiO_2 electrode, the irradiation sources, and the types of reactors used. Moreover, the key factors affecting the photoelectrocatalytic oxidation efficiency are discussed, including the applied electrical potential, light intensity, pH, dissolved oxygen concentration, electrolyte concentration, and temperature. Finally, the paper emphasizes the recent applications of photoelectrocatalytic processes and suggests new research directions for the development of this promising technology.

3.2 Key words

TiO_2 photocatalyst, Photoelectrocatalytic degradation, Catalytic electrode, Water purification

3.3 Introduction

Treatment of a range of recalcitrant contaminants derived from agricultural processes (herbicides, pesticides, etc.), sewage (oestrogens, pathogens, etc.), industrial effluents phenolics compounds, etc.) and natural runoff (soil and plant derived colorants) is a significant challenge throughout the world. Oxidation processes (physical, chemical or biological) are one of the main steps in water treatment (Li and Qu, 2009). Chemical oxidation using several oxidants such as chlorine, hydrogen peroxide and ozone rarely leads to a total mineralization of water contaminants. Biological oxidation is considered to be very economical and widely applicable. However, the presence of toxic and refractory pollutants in water and wastewaters makes this latter method inappropriate in many cases. Conventional methods such as ultrafiltration and adsorption using activated carbon have been applied to remove refractory organic compounds. The main disadvantage of such methods is that they do not destroy the pollutants but rather transfer the pollutant from one phase to another (Ozcan et al., 2004; Tahir and Rauf, 2006). Advanced oxidation processes (AOPs) have been proposed as alternative methods for the elimination of many toxic organic compounds in wastewaters, air and soil. As such, they are used for the elimination of biorecalcitrant compounds in wastewater (Gogate and Pandit, 2004; Ikehata et al., 2006; Ikehata and El-Din, 2006; Pera-Titus et al., 2004). The principle of AOPs (including O_3/H_2O_2, UV/O_3, UV/H_2O_2, H_2O_2/Fe^{2+}, and $UV\text{-}TiO_2$) is to produce hydroxyl radical in water, a very powerful oxidant capable of oxidizing a wide range of organic compounds with one or many double bonds (Esquivel et al., 2009; Yu and Chuang, 2008; Tomovska et al., 2007; Lou and Huang, 2008). Although photocatalytic process ($UV\text{-}TiO_2$) using semiconductor as photocatalyst under UV illumination has been extensively studied, its practical exploitation for the oxidation of refractory organic pollutant has been restricted due to the low photonic efficiency (Egerton, 2011). The fast recombination of the photo-generated electron/hole (e^-/h^+) represents the

major drawback of photocatalytic process applications (Waldner et al., 2003). Therefore, it is important to retard the recombination of the charge carriers. According to the literature (Wang et al., 2009; Bandara et al., 2007; Skoumal et al., 2009; Martinez-Huitle et Brillas, 2009), a great interest in electrochemical advanced oxidation processes (EAOPs) has been emerging. Combining electrochemical and photo-catalysis technologies (called photoelectrocatalytic technology) offers the opportunity to separate electron–hole photo-generated (e^-/h^+) and to prevent their recombination. Photoelectrocatalytic process allows not only to increase efficiency and decrease costs, but also to increase the rate of degradation of recalcitrant pollutants (Rajeshwar et al., 1994). Photoelectrocatalytic oxidation (PEO) in which a small positive potential is applied across the photo-catalyst has proven to be more efficient than photocatalytic process and a better use of the photogenerated holes (Liu et al., 2009). Heterogeneous PEO using semiconductors as photocatalysts has been largely applied over the last ten years for removing organic pollutants (Fujishima et al., 2000; Mills and Le Hunte, 1997; Dominguez et al., 1998). This photoelectrocatalytic technique has received increasing attention in the environmental field because of its ability to destroy undesirable organic compounds in aqueous phase and to remove traces of organic species that are stable and difficult to oxidize by means of conventional water treatment methods (Fujishima et al., 2000; Hoffmann et al., 1995; Li and Shen, 2006).

The present review aims to provide a comprehensive analysis of the mechanism of PEO processes, the characteristics of photo-catalyst materials, the source of irradiation, and the different types of photoelectrocatalytic reactors. The final section of the manuscript presents some applications of photoelectrocatalytic processes in the field of water and wastewater treatment.

3.4 Mechanism of the photoelectrocatalytic process

The photoelectrocatalytic technique combines both electrolytic and photocatalytic processes. Recently, the photoelectrocatalytic treatment process has received considerable attention in the environmental field owing to its ability to retard the recombination of electron–hole pairs (e^-_{CB}/h^+_{VB}) and the possibility to increase the lifetime of the latter. The applied external potential is a key factor in the photoelectrocatalytic technique because it accelerates photocatalytic reaction. The role of UV irradiation and the applied potential on the photoelectrocatalytic mechanism are indicated in Table 3-1.

Tableau 3-1 The role and the effect of UV irradiation and current intensity in photoelectrocatalytic mechanism.

Parameters	Reactions	Comments
UV irradiation	$TiO_2 + h\nu \rightarrow e^-_{CB} + h^+_{VB}$	• The TiO_2 is exposed to the UV light with energy greater than the band gap energy (> 3.2 eV). Electrons are excited from the TiO_2 valence band into the TiO_2 conduction band.
	$h^+_{vb} + H_2O \rightarrow OH° + H^+$ $h^+_{vb} + OH^- \rightarrow OH_{ad}°$ $e^-_{cb} + O_2 \rightarrow O_2°-$	• In the valence band of TiO_2 photocatalyst, the holes can react with adsorbed water (or hydroxyl ions) to produce free radical such as OH°. • The ejected electrons react with electron acceptors such as oxygen adsorbed to form superoxide radicals.
Current intensity	$e^-_{CB} + h^+_{VB} \rightarrow$ heat	• The current intensity applied prevents as much as possible the recombination between the photogenerated electrons and holes. The recombination between electrons and holes releases the heat. • Photogenerated electrons in the excited TiO_2 anode can be taken away via the external circuit, instead of the electron transfer to molecular oxygen, and consequently, the photogenerated hole or OH° is left at the surface of the TiO_2 electrode.

The basic process of photocatalysis consists of ejecting an electron from the valence band (VB) to the conduction band (CB) of the TiO_2 semi-conductor, thereby creating an "h+" hole in the valence band. This is due to the UV irradiation of TiO_2 with an energy equal or superior to the band gap (>3.2 eV). These charge carriers (e^-/h^+) can migrate to the surface of the catalyst, where they are then available to undergo redox reactions with substrates (Yang et al., 2009).

Équation 3-1 $$TiO_2 + h\nu \rightarrow e^-_{CB} + h^+_{VB}$$

This is followed by the formation of extremely reactive radicals (such as HO•) at the semi-conductor surface and/or a direct oxidation of the polluting species (R). Table 3-2 presents the redox potential of different oxidants. Therefore, pollutants in wastewater can be degraded directly on the surface of the semiconductor (Esquivel et al., 2009) or indirectly by reacting with hydroxyl radicals. The photogenerated hole in the valence bond can react with an adsorbed water molecule (or surface hydroxyl) to form oxidative species such as OH• which subsequently attack the pollutant. It was reported by Chong et al. (2010) that in the absence of water molecules, the powerful oxidant hydroxyl radicals could not be formed and impedes the photodegradation of liquid phase organics.

Équation 3-2 $$h^+_{vb} + H_2O \rightarrow HO^\circ + H^+$$

Équation 3-3 $$h^+_{vb} + OH^- \rightarrow HO^\circ_{ads}$$

Équation 3-4 $$h^+_{vb} + R_{ads} \rightarrow R^+$$

The electrons ejected to the conduction band can either react with electron acceptors such as adsorbed oxygen (O_2) to form superoxide radicals (Equation 3-5) or react with adsorbed water molecule (H_2O) to form oxidative species such as hydroxyl radicals (Macphee et al., 2010).

Équation 3-5 $e^-_{CB} + O_2 \rightarrow O_2^{\circ -}$

Tableau 3-2 Redox potential of oxidants used for water treatment.

Redox couples	E°, (V) at 25°C	References
OH°/H_2O	2.81	Schaller, 1996
O_3/O_2	2.07	Guivarch, 2004
$S_2O_8^{2-}/SO_4^{2-}$	2.05	Doré, 1989
H_2O_2/H_2O	1.77	Doré, 1989
MnO_4^-/Mn_2^+	1.51	Doré, 1989
$HClO/Cl^-$	1.49	Doré, 1989
Cl_2/Cl^-	1.36	Doré, 1989

The photogenerated electrons (e^-) reduce the recombination rate of the photogenerated electron–hole pairs and enhance the photocatalytic activity (Fujishima et al., 2000). The lifetime of the pairs (e^-_{CB}/h^+_{VB}) is a few nanoseconds. Without electron donors or acceptors these electron–hole pairs can recombine to release heat or migrate to the surface of the semiconductor and react with species that have been adsorbed there.

Équation 3-6 $e^-_{CB} + h^+_{VB} \rightarrow$ heat

The recombination of the photogenerated electron–hole pairs reduces the quantum efficiency and limits the application of photocatalysis in the field of wastewater treatment (Ding et al., 2010). Every recombination means a loss of a hole that might otherwise have promoted the degradation reaction. In order to achieve good photoelectrocatalytic efficiency, recombination between electrons and holes must be avoided. This is possible by trapping of free charges at

intermediate energy levels (Hoffmann et al., 1995). Further reactions can lead to other oxidant species such as HO_2•, HO_2^-, and H_2O_2 that can promote oxidizing conditions that are not described here. Figure 3-1 shows the general mechanism of the photoelectrocatalytic process and the main reaction that occurs at the surface of TiO_2. According to the literature (Selcuk et al., 2003; Wang et al., 2009), potential applied is a key factor that improves photoelectrocatalytic efficiency. In fact, when a positive bias is applied to the Ti/TiO_2 photoanode, the thereby generated electrons can be transferred into the external circuit instead of to the oxygen molecule. As a result, the photogenerated hole or OH• will be left at the surface of the TiO_2 electrode. Therefore, the rate of photogenerated electron–hole recombination is limited while a possibility exists to improve the efficiency oxidation at the semiconductor–electrolyte interface (Gogate and Pandit, 2004; Ikehata et al., 2006). In the photoelectrocatalytic process, the rate of conversion does not depend directly on the applied potential but depends on several factors: *(i)* the specific feature of the semiconductors, *(ii)* diffusion light, *(iii)* adsorption and desorption of the reactant and products, and (iv) the intensity of the electric field in the space charge region (Selcuk et al., 2003).

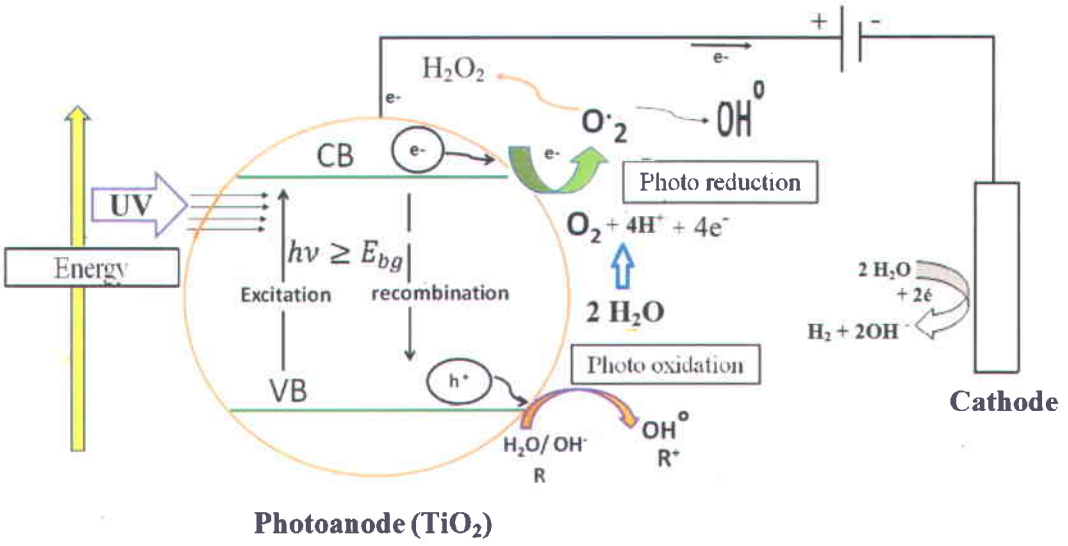


Figure 3-1 Mechanism of photoelectrocatalytic process using TiO_2 photocatalyst and the reactions that occur at the surface.

3.5 Parameters affecting the photoelectrocatalytic process

3.5.1 Effect of external potential applied on TiO_2 or effect of current intensity

Applying an external potential on TiO_2 (photo-anode) contributes to the separation of the photo-generated electrons and holes and prevents as much as possible the recombination between them (Waldner et al., 2003; Li et al., 2002). In the photoelectrocatalytic process, applying an external potential prevents charge recombination and increases the lifetimes of the active holes The electrons and holes have more opportunities to either oxidize the pollutants directly on the surface of Ti/TiO_2 photo-anode (adsorption) or react indirectly with active species (such as hydroxyl radicals) (Adams et al., 2002). The effect of electrical potential on hydroxyl radical production has been studied by Jiang et al. (2006). That study showed that the total concentration of hydroxyl radicals (higher than 20 mol L^{-1}) generated under UV irradiation (20 W) was effectively enhanced with a small applied potential (0.6 V).

Consequently, higher efficiency in the degradation of pollutants is recorded. The influence of current intensity was also put into evidence by Daghrir et al. (2012) while studying photoelectrocatalytic degradation of chlortetracycline hydrochloride (CTC) using TiO_2 nano-structured photo-anode and a mercury lamp (λ= 254 nm). The degradation experiments were carried out at different initial concentrations of CTC (from 25 to 50 mg L^{-1}) in 0.5 M of Na_2SO_4 using a current intensity varying from 0.25 to 0.50 A. When pollutant concentration is fixed at the highest level (50 mg L^{-1}), current intensity has a significant influence on the removal of CTC. The degradation rate passed from 34.9% to 61.3% when the current intensity passed from 0.25 to 0.50 A. The efficiency of photoelectrocatalytic degradation of some contaminants such as humic acid (Selcuk et al., 2003; Li et al., 2002) and 4-chlorophenol (Wang et al., 2009) is maximized by applying an optimal value of external potential (0.6 and 1.5 V is an optimal potential for the photoelectrocatalytic degradation of 4-chlorophenol and humic acid, respectively). The increase of the applied potential above the optimal value may decrease the degradation efficiency but it may also have no effect on the degradation. By applying an external potential, the gradient of the electrochemical potential could be increased to an extent that ensures complete separation of all charge carriers (depletion conditions) (Neuman-Spallart, 2007). In electrically biased system (full depletion conditions), the majority of the electron are drawn inside the semiconductor and are extracted at the back contact. Under these conditions, the current under UV radiation cease to increase and the kinetics of the reaction is only limited by the photon flux. This phenomenon was discussed in detail by Neuman-Spallart (2007). Under biased conditions, the whole reaction sequence involving reduced oxygen species will be absent and the degradation efficiency of pollutant will be reduced. According to Maeda et al. (1999), the oxidation and reduction reactions could be occurred simultaneously on the illuminated TiO_2 photo-catalyst in an

electrically unbiased system, where the consumption of photoexcited electrons is slow in the conduction band (reduction site).

3.5.2 Effect of light intensity

Electron–hole recombination is a limiting step in photocatalytic reactions (Sohrabi and Ghavami, 2010). The photocatalytic degradation rates depend strongly on the light intensity applied on the surface of the catalyst. According to Wang et al. (2010), the light intensity influences on the extent of the electron–hole pairs photo-generated and consequently on the progress of the photocatalytic reaction. By increasing the intensity of the incident light, the probability of excitation of the catalyst and the re-excitation of recombined electrons can be increased (Wang et al., 2009). Moreover, with the increase of UV light intensity, the decomposition of organic compounds or the inactivation rate of bacteria (especially under UVC irradiation) increases due to the increasing concentration of reactive oxygen species and hydroxyl radicals formed on the TiO_2 surface (Wang et al., 2009; Chen et al., 2010). The steady concentration of HO• on the TiO_2 surface is described by Chen et al. (2010) and Cho et al. (2004) as follows:

Équation 3-7

$$[HO^{\circ}]_S = \sqrt{\frac{(1-\alpha) I_a \Phi}{k_D}}$$

Where, I_a is the number of light quanta absorbed per second; Φ the quantum yield; k_D the diffusion-limited rate constant and α the parameter depending on the pH. Some authors studied the relationship between light intensity and photoelectrocatalytic oxidation used for degradation of humic acid (Li et al., 2002). It has been proven that the degradation reaction rate is proportional to the light intensity ($k^{\circ} = k_2 I^b$, where k° is the degradation reaction rate; I the light intensity and k_2 and b the kinetic constants). In the field of water treatment, Chong et al. (2010) indicated that a relatively high light intensity is required to achieve a high photocatalytic reaction rate. Some authors (Yang and Liu, 2007; Hermann, 2005; Ollis et al.,

1991) argued that under low light intensities (lower than 250 W m^{-2}), the reaction rate is proportional to the light intensity, while under moderate light intensities (above 250 W m^{-2}) the reaction rate is proportional to the square root of the light intensity. Nevertheless, under high light intensities, the reaction rate is independent of the light intensity. Limit values range between 22 and 44 kW m^{-2} (Malato et al., 2002). Pareek et al. (2008) show that the degradation efficiency of pollutants is strongly linked to the light intensity distribution within the reactor. According to the same authors, it is very difficult to maintain a uniform light intensity distribution within the reactor. For this reason, it is very important to determine the appropriate light intensities to minimize energy consumption and to increase the rate of pollutant degradation. For practical application (i.e. large-scale application), it could be interesting to use the natural UV irradiations emitted by the solar spectrum in the presence of a TiO_2 photocatalyst material in order to minimize treatment costs. However, if the natural UV irradiations emitted by the solar spectrum are insufficient, these can be combined with artificial UV lamp irradiation.

3.5.3 Effect of pH

According to the literature (Wang et al., 2009; Quan et al., 2007), in the field of wastewater treatment, pH is one of the most important parameters that influence the removal of pollutants. It affects the capacity of adsorption and dissociation of the target compounds, the charge distribution to photocatalyst surface, and the oxidation potential of the valence band (Chong et al., 2010; Wang et al., 2009; Quan et al., 2007). Many authors (Chong et al., 2010; Ding et al., 2010; Selcuk et al., 2003; Wang et al., 2009; Elsellami et al., 2010) used the point of zero charge (PZC) to study the performance of photocatalytic oxidation using TiO_2 as photocatalyst. The PZC has a pH value of approximately 6 (pHPZC) for TiO_2 (Selcuk et al., 2003). Under these conditions, the surface charge of TiO_2 is neutral and the electrostatic interaction between the pollutant and TiO_2 is absent. For pH values higher than the PZC of

TiO_2, the surface becomes negatively charged and an electrostatic repulsion toward anionic compounds dominates. However, the surface of the catalyst becomes positive when the pH is lower than the PZC of TiO_2. For a pH value between 3 and 10, the distribution of TiOH is greater than or equal to 80%, whereas for a pH value above 10 or below 3 the distribution of TiO^- and $TiOH_2^+$, respectively, is greater than or equal to 20% (Chong et al., 2010). In the photoelectrocatalytic process, the maximum degradation rate of certain pollutants such as pentachlorophenol (Quan et al., 2007), humic acid (Li et al., 2002), benzotriazole (Ding et al., 2010) and dye (Carneiro et al., 2010) is much faster in an acidic solution than in an alkaline solution. Nonetheless, Wang et al. (2009) have proven that the degradation rate of 4 chlorophenol was enhanced in both alkaline and acid solutions. However, the effect of pH in photocatalytic reactions cannot be generalized. Laboratory experiments are required in order to determine optimum pH conditions, unless data are available from previous studies conducted under similar operating conditions (Gogate and Pandit, 2004). Three possible reaction mechanisms can contribute to the degradation of pollutants in photoelectrocatalytic processes: (i) direct attack of hydroxyl radicals, (ii) direct photo-oxidation by the positive hole in the valence band, and; (iii) direct photo-reduction by the electron in the conduction band. Each of these depends on the pH value and the nature of the substrate.

3.5.4 Effect of dissolved oxygen

In the photoelectrocatalytic degradation of organic pollutants, the dissolved oxygen avoids the recombination of photo-generated electron–hole pairs by acting as electron acceptors and participates in the formation of reactive oxygen species as the superoxide radical $O_2^{\bullet}$ (Yang et al., 2009; Leng et al., 2006; Zhang et al., 2003). A sufficient amount of O_2 promotes oxidizing conditions. The oxygen is well-known for its effective role in the oxidation/reduction reactions of pollutants. The dissolved oxygen source is the aeration system and/or the H_2O molecule electrooxidation at the anode (Equation 3-8). In the photo-electrocatalytic process,

the electron ejected in the conduction band reacts with electron acceptors such as O_2 to form superoxide radicals $O_2^{\bullet -}$ and subsequently other oxidant species such as H_2O_2, $HO_2^{\bullet}$ and HO_2^- (Equations 3-9–3-15) (Wang and Hong, 1999). Moreover, hydrogen peroxide H_2O_2 (oxidant) can be electrogenerated by the cathodic reduction of dissolved oxygen on the electrode.

Équation 3-8 $2H_2O \rightarrow O_2 + 4H^+ + 4e^-$

Équation 3-9 $e^- + O_{2\,(ads)} \rightarrow O_2^{\circ -}$

Équation 3-10 $O_2^{\circ -} + H^+ \rightarrow HO_2^{\circ}$

Équation 3-11 $2HO_2^{\circ} \rightarrow H_2O_2 + O_2$

Équation 3-12 $O_2^{\circ -} + HO_2^{\circ} \rightarrow O_2 + HO_2^-$

Équation 3-13 $HO_2^- + H^+ \rightarrow H_2O_2$

Équation 3-14 $O_2 + 2\acute{e}_{CB} + 2H^+ \rightarrow H_2O_2$

Équation 3-15 $2H_2O + 2h^+_{VB} \rightarrow H_2O_2 + 2H^+_{aq}$

The presence of reactive oxygen species in high quantity can limit the recombination of photo-generated electron–hole and improve the efficiency oxidation at the semiconductor interface. The performance of the photoelectrocatalytic cell in term of pollutant degradation could be evaluated using Faradayic efficiency (Equation 3-16). A simple relationship between photocurrent density and the amount of pollutant removal could be derived from Faraday's law (Waldner et al., 2003).

Équation 3-16 $$f = \frac{\left(-\frac{dC}{dt}\right) \times V \times F}{i}$$

Where, (−dc/dt) represents the disappearance rate of pollutant, V is the working volume (m^3) of the reactor, F is the Faraday constant (coulombs) and i is the photocurrent density (A cm^{-2} nm^{-1}). Some authors (Chong et al., 2010; Wang and Hong, 2000) suggest that the presence of dissolved oxygen provides the cleavage mechanism for aromatic pollutants present in water. The pressure of oxygen applied during the reaction is also important. A higher organic photomineralization rate was obtained by applying a higher pressure of oxygen (Wang and Hong, 2000). For instance, by increasing the airflow in the photoelectrocatalytic process, Liang et al. (2008) demonstrated that the oxidation of 2,3-dichlorophenol can be increased. When the oxygen molecule is in excess in the medium, the transfer rate of photogenerated electrons from the surface of the titania to the molecular oxygen will be maximized. However, according to Almquist and Biswas (2001), in the photocatalytic process, the electron transfer rate depends on the type and characteristics of the titania as well as the rate of the charge transfer.

3.5.5 Effect of electrolytes

In an electrolytic process, the conductivity of the solution affects the efficiency of current intensity, voltage, and the consumption of electrical energy. The conductivity must be high in order to ensure good ion transfer in the effluent. If the conductivity is too low, the resistance is too high and consequently, an increase of the applied voltage is observed. NaCl and Na_2SO_4 are the two electrolytes most often used. The type of electrolyte and its concentration affect the photoelectrocatalytic degradation process (Wang et al., 2009). The results of a 4-chlorophenol degradation study showed that photoelectrocatalytic efficiency improved in the presence of sodium sulfate and that the degradation process increased with the concentration of electrolyte (from 0.05 to 0.2 M). In the photoelectrocatalytic process, the electrolyte Na_2SO_4 is the electrolyte that has been widely used by several authors (Esquivel et al., 2009; Ding et al., 2010; Selcuk et al., 2003; Xu et al., 2008; Li et al., 2006; Philippidis et al., 2010;

Li et al., 2007). For instance, pentachlorophenol degradation was improved when Na_2SO_4 was added to the solution. The removal rate of pentachlorophenol was accelerated by increasing the electrolyte concentration (from 6.0 mg pentachlorophenol/L at 0.005 M Na_2SO_4 to 3.0 mg pentachlorophenol/L at 0.01 M Na_2SO_4) (Quan et al., 2007). During the photoelectrocatalytic process, the addition of an electrolyte improves treatment efficiency since it modifies the conductivity of the solution and facilitates the passage of the electrical current in solution, which in turn prevents the fast recombination between photo-generated electrons and holes

3.5.6 Effect of counter electrode (or cathode electrode)

Another interesting advantage of the photo electrocatalytic process (compared to conventional photocatalytic process) could be the use of a cathode material, such as vitreous carbon (VC) on which hydrogen peroxide (H_2O_2) can be electrochemically generated by cathodic reduction of dissolved oxygen (Xie and Li, 2006). This peroxide induces non offensive by-products contrarily to chlorine. Under UV irradiation, hydrogen peroxide can be decomposed into hydroxyl radical (in addition to hydroxyl radical produced on the surface of photocatalyst). This should contribute to enhance pollutant degradation. Likewise, the addition of an electron acceptor (e.g. H_2O_2) should prevent the electron–hole recombination and increase the photocatalyst efficiency (Ozer and Ferry, 2001). According to previous studies (Ding et al., 2010; Sohrabi and Ghavami, 2010; Xie and Li, 2006), such an oxidant agent (H_2O_2) is beneficial for photocatalytic reaction by trapping the conduction band electron in order to generate more hydroxyl radical.

3.5.7 Effect of temperature

According to our knowledge, the effect of temperature on PECPs has not been studied in the literature. However, its effect has been widely studied on photocatalytic processes (Chong et al., 2010; Gaya and Abdullah, 2008; Evgenidou et al., 2005). The increase in photocatalytic

temperature (T > 80 °C) promotes and enhances the charge recombination. Under these conditions, adsorption of organic compounds on TiO_2 surface decreases (Chong et al., 2010). According to Malato et al. (2009), a temperature range between 20 and 80°C is considered as optimum for photomineralization. In a photodisinfection reaction, an increase in temperature enhances the inactivation rate of microorganisms (Rincon et al., 2004). Based on studies carried out by Chen and Ray (1998), the degradation rate constants of 4-nitrophenol increased with increasing temperature from to 288 to 323 K (at an initial concentration of 4-nitrophenol = 20 ppm; pH 4.3; TiO_2 = 2 g L^{-1}, flow rate = 250 mL min^{-1}, and O_2 saturated). By increasing temperature, the collision frequency of molecules in solution increases and the reaction rate constant improves. This was proven by the Van't Hoff–Arrhenius equation (Equation 3-17), where the rate constant k is linearly proportional to the exp(−1/T).

Équation 3-17

$$Ln\left(\frac{k_1}{k_2}\right) = -\frac{E_a}{R}\left(\frac{1}{T_2} - \frac{1}{T_1}\right)$$

Where, k_1 and k_2 are the constants of temperature T_1 and T_2, respectively; E_a is the energy activation; and where R is the universal gas constant.

3.5.8 Effect of mass transfer

It is well-known that, hydrodynamic conditions (or mass transfer coefficient) inside reactors are greatly linked to the cell configuration or cell design (Kim et al., 2003; Rajeshwar and Ibanez, 1997; Chen, 2004). Indeed, in the PECP, the oxidation of pollutants can occur heterogeneously. Pollutants must be transported to the photo-anode surface first, and then be oxidized there as a result of hydroxyl radical formation ($OH^{\bullet}$) (Drogui et al., 2001; Grimm et al., 1998; Martinez-Huitle and Ferro, 2006) or owing to the photogenerated hole (Yang et al.,

2009; Li et al., 2007; Konstantinou and Albanis, 2004). Experiments are required to determine the value of the mass transfer coefficient and to study the hydrodynamic conditions of the reactor prior to the development of practical applications.

3.6 TiO_2 electrodes: characteristics and specificities

3.6.1 Preparation of TiO_2 electrodes

Several methods can be used to prepare TiO_2 electrodes for PECPs. The anodizing method has been widely used by several authors to prepare Ti/TiO_2 electrodes (Quan et al., 2007; Xie, and Li, 2006; Li et al., 2000; Li and Liu, 2005). Anodizing titanium metal can be carried out in acid (Hitchman et al., 1996) or alkaline (Zane et al., 1993) solution. Commercial titanium foils with appropriate dimensions (25 mm × 50 mm) were used to prepare TiO_2 films by anodization. The initial surface was polished with abrasive papers and rinsed in an ultrasonic bath containing cold distilled water. Prior to anodization, the titanium plate was first immersed in an $HF/HNO_3/H_2O$ solution and then cleaned with alcohol and distilled water. The treated Ti served as an anode and a platinum (Pt) foil served as a cathode. Both were placed in acid or alkaline solution and an electrical current was applied at a constant voltage and for an appropriate time. The anodization process was accompanied by a significant generation of heat (Li et al., 2000). The freshly generated TiO_2 electrode was then rinsed in distilled water, and then dried first in the atmosphere and then at 105 °C for 2 h (Li and Liu, 2005). The sol–gel method has also been used by many authors (Waldner et al., 2003; Xu et al., 2008; Christensen et al., 2005) to prepare the TiO_2/Ti electrode. Sol–gel electrodes were fabricated by coating a layer of TiO_2 sol onto the titanium substrates via repetitive heat treatments. The plate titanium substrate formed was dip-coated into a TiO_2 sol solution prepared by the method according to Xu et al. (Xu et al., 2008), and dried for 10 min at 500 °C. The coating and drying process was repeated several times and the resulting materials were heated between 500 and 550 °C for 1 h (Leng et al., 2006) or 2 h (Xu et al., 2008). The

TiO_2 electrode can be prepared with chemical deposition methods. Sun et al. (Sun et al., 2010) used nickel plates coated with a 500 nm thick titanium film as a substrate. The titanium film was deposited on nickel plates by means of arc ion plating. The deposition of film was conducted at a temperature of 200 °C and a rate between 50 and 60 nm s^{-1}. After deposition, the substrate formed was cooled to temperature at 3°C min^{-1}, dipped in the solution, and pulled out with a constant speed. During each dip-coating procedure, the gel film was dried at 300°C during 15 min. An electrophoretic deposition method was also used for TiO_2 preparation (Esquivel et al., 2009). A TiO_2 film was deposited on the pre-treated fibers coated with SnO_2:Sb (optical fiber with a 600 μm silica core and a polymer optical cladding). The fiber was immersed at room temperature during 1 h in a colloidal suspension of TiO_2 powder under a potential difference applied between the optical fiber and a stainless steel sheet. Afterward, the electrode was placed in an oven at 450°C to sinter the TiO_2 film. Compared to the common synthesis methods described above for the preparation of TiO_2 electrodes, new method using for instance a pulsed laser deposition (PLD) process has been investigated by Daghrir et al. (2012). A KrF excimer laser (wavelength = 248 nm, pulse duration = 15 ns) operating at a repetition rate of 30 Hz was focused, at an incidence angle of 45°, onto the TiO_2 rotating target (99.95% purity). The on-target laser energy density was set to 4.5 J cm^{-2}. For photoelectrocatalytic studies, the TiO_2 films were deposited on titanium grids. The TiO_2 deposits were performed at a deposition temperature 600°C under an oxygen background pressure of 1 mTorr. More details on the PLD system and it schematics have been investigated by Desbiens and El Khakani (2003).

3.6.2 Characteristics and specificities of TiO_2 electrodes

Many researches (Ollis et al., 1991; Li et al., 2000; Hidaka et al., 1992) have shown that the semiconductor TiO_2 is an excellent photocatalyst that can, under UV light irradiation, break down many refractory organic pollutants such as pesticides, herbicides, halophenols, dyes and

detergents. Titanium dioxide (TiO_2) was widely used for the degradation of dyes that could not be easily oxidized by chemical or biological processes (Yun et al., 2008; Paschoal et al., 2009). Several authors (Ding et al., 2010; Wang et al., 2009; Yu et al., 2009; Yun et al., 2008) show that TiO_2 is the most suitable photocatalyst for environmental applications due to its excellent chemical and physical properties such as high photosensitivity, non-toxicity, long-term stability against photocorrosion and chemical corrosion, and strong oxidizing power. Titanium dioxide exits in three different crystal forms: anatase, rutile and brookite. Anatase and rutile forms have been the most studied phases of nanostructure TiO_2 (Table 3-3), whereas, brookite forms are still scarce (Rivera et al., 1993; Ye et al., 1997; Thiruvenkatachari et al., 2008). The rutile form of TiO_2 begins to adsorb strongly at 405 nm, whereas the anatase form adsorbs until 385 nm (Egerton and Christensen, 2004). In the anatase form, the energy gap between the valence and conduction bands is slightly larger (3.25 eV) (Sun et al., 2010). The anatase form shows a higher photocatalytic activity than the rutile form (Linsebigler et al., 1995).

Tableau 3-3 Characteristics of the anatase and rutile forms of TiO_2

Parameters	Anatase	Rutile
Crystalline structure	Quadratic	Quadratic
Stability	Thermodynamically metastable	Thermodynamically stable
Elaboration	Low temperature	High temperature
structure	Nanostructured	Grain size greater than anatase
Specific surface	High	lower
Band gap (ev)	3.2	3.0
Absorption edge (nm)	385	405
Ti-Ti distances (A°)	3.04-3.79	2.96-3.57
Ti-O distances (A°)	1.934-1.980	1.949 - 1.980
Photoconductivity	High	Lower
Activity	More active in photocatalysis	Less active in photocatalysis
Mobility of charge	More mobile charge carrier	Less mobile charge carrier
Density	3.89	4.27

In photocatalytic degradation using TiO_2/UV, a TiO_2 catalyst can be utilized in two different forms: (1) TiO_2 suspended in aqueous medium and (2) TiO_2 immobilized on support inert materials (TiO_2 on robust substrates). By comparison, only the immobilized TiO_2 on support materials can be used in photoelectrocatalytic processes. The active surface area available for photocatalytic reactions is much larger in suspension systems than in film systems (Li et al., 2006; Zaviska et al., 2009). The use of TiO_2 particles in photocatalytic oxidation (PO) has two drawbacks: (i) the separation of the suspension of TiO_2 from the aqueous phase is very difficult and (ii) it involves heat loss due to the recombination of the electron–hole pairs (Waldner et al., 2003; Christensen et al., 2005). Recent research works tried to immobilize the TiO_2 film on support materials such as sand, glass media, SiC foams (Kouame et al., 2011),

ceramic membrane or resins by means of coating, soaking, precipitating or spinning methods in order to solve the problem of TiO_2 particle separation from wastewater (Li et al., 2000). According to Thiruvenkatachari et al. (2008), an immobilized TiO_2 film is preferable compared to dispersed TiO_2 because the addition of a post-treatment (filtration step) is not necessary after the oxidation process. By using the TiO_2 film, the quantum efficiency will decrease in comparison to TiO_2 particulate suspension. The limit diffusion of the target compounds to the surface of the catalysts and the reduction in the surface area of the catalysts are the two factors that are responsible for the decrease of quantum efficiency (Quan et al., 2007). Photoelectrocatalytic oxidation process in which a differential potential is applied to photo-catalyst enhances the quantum efficiency and consequently increases the degradation rate of the pollutant. The potential applied across the immobilized photo-catalyst is a key factor that prevents the fast recombination of the photo-generated electron–hole and enhances the quantum efficiency of the process (Wang et al., 2009). The analysis of the current–voltage curves gives direct information about what is to be expected if a selected voltage is applied. In the field of electrochemistry, cyclic voltammetry is a very important analytical characterization. Any process that includes electron transfer can be investigated using this analytical method. In order to select the appropriate potential in photoelectrocatalytic process, a voltamperometric study was performed by several authors (Paschoal et al., 2009; Li et al., 2006; Li and Liu, 2005) under and without illumination. Furthermore, reactors using fixed catalysts need to obtain a stable and active catalyst layer. Irradiation in the reactor must be uniform over the entire surface of the catalyst (Zaviska et al., 2009). The quantity and type of catalyst depends mainly on the radiation source, and the type and concentration of the pollutant and reactor (Zaviska et al., 2009). According to Paschoal et al. (2009), the h^+/e^- are generated on the layer of TiO_2 under UV illumination. Besides, oxidation reactions can be initiated owing to the potential gradient between the surface and the bulk of the

semiconductor. As the photocurrent depend on light intensity, it could be possible to determine the efficiency of transforming light flux into electron flow namely IPCE (incident-photon to current conversion efficiency) (Equation 3.18) (Waldner et al., 2003).

Équation 3-18 $$\text{IPCE} = \frac{i}{F \times P}$$

Where, i represents the photocurrent density (A cm^{-2} nm^{-1}), F is the Faraday constant (coulombs) and P is the incident light (Einstein s^{-1} cm^{-2}).

In order to improve electron–hole separation, De Tacconi et al. (2003) proposed the coupling of the TiO_2 semiconductor with another semiconductor such as CdS (coupled nanoparticles CdS/TiO_2) (Bessekhouad et al., 2004). Other studies (Wu, 2004; Wu and Chang, 2006) suggested combined semiconductor powders such as TiO_2 + ZnO and TiO_2 + SnO_2. According to Zhang et al. (2009), using different semiconductors simultaneously allows to reduce electron–holes recombination in individual photoelectrodes. Figure 3-2 presents a semiconductor configuration in which a vectorial transfer of photogenerated charge carriers between corresponding band levels ensures a spatial separation between electrons and holes (Robert, 2007). For instance, combining SnO_2/TiO_2 photoelectrodes was used by several authors (Vinodgopal and Kamat, 1995 ; Vinodgopal et al., 1996; Hattori et al., 2000; Hattori et al., 2001) to oxidize different types of molecules (Acid Orange 7, to degrade naphthol blue black, formic acid and 1,3,5,7-tetramethylcyclotetrasiloxane). SnO_2/TiO_2 coupled with film was found to be more effective than TiO_2 film used alone.

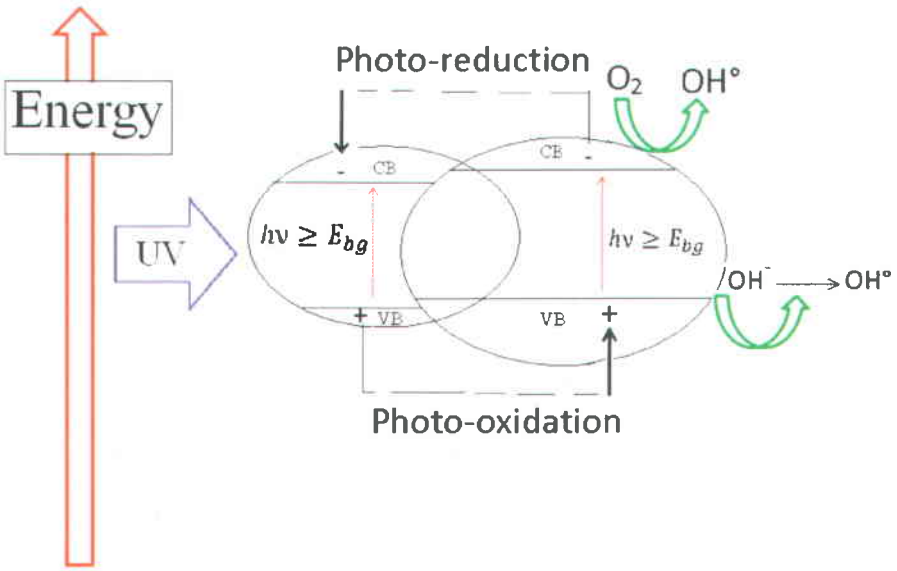


Figure 3-2 Coupling of two different semiconductor configurations.

3.6.3 UV radiation of TiO_2 electrodes

In the case of the photocatalysis process, the photoactivation of TiO_2 requires irradiations emitted at a wavelength less than or equal to 384 nm (Thiruvenkatachari et al., 2008). UV irradiations are a critical parameter in photocatalysis and photoelectrocatalysis reactions. Different types of lamps emitting ultraviolet radiation were used. Quasi-monochromatic low pressure lamps transmit at wavelengths ranging at 254 nm, while polychromatic medium pressure lamps emit at a wavelengths ranging between 185 and 400 nm (Locas et al., 2008). The degradation efficiency of certain organic compounds was increased by applying UV-C radiation (between 200 and 280 nm) followed by UV-A radiation (between 320 and 380 nm) (Matthews and McEvoy, 1992; Puma and Yue, 1999). In the photoelectrocatalysis process, a combination between the catalysis effect as TiO_2, UV illumination and electrochemical process allows enhancing the degradation of emerging contaminants such as benzotriazole (Ding et al., 2010) and 2,4-dichlorophenol (Li et al., 2007) and inactivation of bacteria

(Philippidis et al., 2010). In this case, both UV light radiations and the applied potential between anode and cathode are responsible for the photogenerated electron–hole on TiO_2 catalysts, and consequently for oxidizing the organic substrate. Previous studies (Thiruvenkatachari et al., 2008; Tsai and Cheng, 1997) have demonstrated the positive effect of UV radiation on the TiO_2 catalyst activation. Rapid electron–hole recombination is the major factor limiting the process when UV light was used alone. To enhance the UV radiation effect on TiO_2 and to improve the quantum yield (Φ), the application of current intensity on the TiO2 anode electrode is increasingly an object of study (Liu et al., 2011; Monllor-Satoca and Gomez, 2010; Esquivel et al., 2009; Li and Liu, 2005). According to Zhang et al. (2009) and Rosenfeldt and Linden (2004), quantum yield is defined as the ratio of the reactant molecules consumed or formed to the quantity of absorbed photons at a given wavelength. By calculating the number of photons absorbed during the reaction, we can determine the quantum yield of a reaction (Equation 3.19). Quantum yield depends on pH, wavelength, pollutant concentration, solvent, temperature, and the concentration of dissolved oxygen. Quantum yields are determined at specific wavelengths.

Équation 3-19

$$\Phi = \frac{\frac{dn}{dt}}{I_{abs}}$$

where: Φ is the quantum yield, n is the number of molecules that react in this process during time t, and I_{abs} is the number of photons absorbed during the same time and in the same volume.

3.7 Photoelectrocatalytic reactors

The main advantage of using the photoelectrocatalytic process is the simplicity of the reactor in terms of construction and management (Li and Qu, 2010). Several configurations of photoreactors have been described in the literature. Li et al. (2007) have used a cylindrical quartz cell with a dimension of 25 mm (diameter) × 50 mm (height) (Figure 3-3).

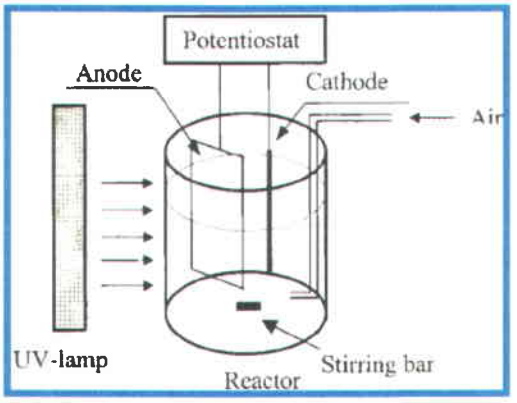


Figure 3-3 Photoreactor equipped with two electrodes: Ti/TiO_2 as anode and platinum electrode as cathode (adapted from Li et al., 2007).

A UV lamp (20 W) with a maximum UV irradiation at 365 nm has also been used outside the photoreactor. The working volume of this reactor was 10 mL and two Ti/TiO_2 and platinum (Pt) electrodes were connected with a potentiostat were used as anode and cathode, respectively. A cylindrical quartz cell has also been used by Xie and Li (2006) but with three electrodes (working electrode, counter electrode and reference electrode). In this configuration (Figure 3-4), Ti/TiO_2 or $Au\text{-}TiO_2/Ti$ (anode) was placed at the bottom of the reactor to receive UV light irradiation (power: 8 W; light intensity: 0.68 mW cm^{-2}, main emission: 365 nm) by using a medium-pressure mercury lamp. Reticulated vitreous carbon (RVC) or Pt used as a cathode was placed at one side of the cell nearby an air diffuser. A

saturated calomel electrode (SCE) was used as the reference electrode. The current applied on the electrode was regulated by a potentiostat–galvanostat.

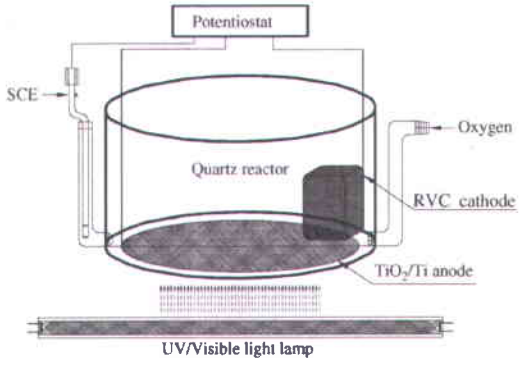


Figure 3-4 Photoreactor equipped with three electrodes used for photoelectrocatalytic oxidation process (adapted from Xie and Li (2006)).

A further type of configuration, used by Quan et al. (2007), is comprised of a rectangular quartz photoreactor (40 mm × 50 mm × 60 mm with a 2.0 mm wall) with TiO_2 at the anode and Pt at the cathode. In this type of photoreactor, a mercury lamp (365 nm) was positioned vertically outside the reactor. An SCE served as the reference electrode. A schematic diagram of the reactor is shown in Figure 3-5.

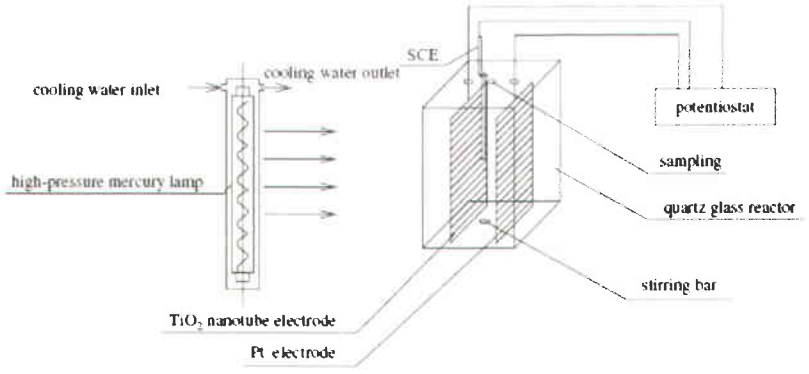


Figure 3-5 Rectangular quartz photoreacteur used for photoelectrocatalytic process (adapted from Quan et al., 2007).

A semi-arc quartz cell of 8.5 cm diameter has been used by Xu et al. (2008) to oxidize dye from textile effluent. A Ti/TiO_2 disc (diameter of 7.5 cm and thickness of 1.5 mm) and Cu sheet electrodes were respectively used as anode and cathode in this photo-reactor-cell. The inter-distance between anode and cathode was 1.0 cm. A mercury lamp (11 W) with a wavelength 254 nm was placed horizontally in front of the photoanode Ti/TiO_2. For the disinfection of water inoculated with Escherichia coli, a vertical cylindrical reactor has been used by Christensen et al. (2003) for photoelectrocatalytic applications. The photo-reactor was fitted with two concentric Pyrex tubes (external diameter 42 mm and inner diameter 80 mm) and the solution occupied the annular volume. The UV source was located in internal configuration along the axis of the reactor. To ensure high mass transfer of reactant to the electrode inside the photo-reactor, mesh electrodes (100 mm long × 44 mm diameter) and gas sparging with small bubbles have been used. With the exception of the photoreactor described by Christensen et al. (2003), in the experimental units described above, the UV lamp was installed outside of the photo-reactor and the illumination passed through the window quartz. However, UV lamp position could influence the efficiency of the photoelectrocatalytic

process. For instance, it has been shown by Daghrir et al. (2012) that UV lamp installed inside the reactor was more effective to remove CTC compared to UV lamp installed outside the photoreactor. Indeed, UV radiations absorbed by H_2O molecules allow the generation of powerful oxidizing species such as H_2O_2 and $OH^{\bullet}$ (Kim and Tanaka, 2009; Heit et al., 1998). The direct contact of UV light with polluted water induced high oxidation of pollutant (Daghrir et al., 2012). Using internal UV configuration for laboratory scale applications enhances the distribution of irradiation across the photo-catalyst and consequently increases the generation rate of reactive oxygen species. The distance between the UV source and the working electrode is also an important parameter that must be taken into account in the designing of photo-reactors. It has been reported by Egerton (2011) that a large distance between the light source and the working electrode in a practical photoreactor reduces the radiation flux and consequently reduces the efficiency of the process. Besides, mixing in the three photoreactors (Figure 3-3; Figure 3-4; Figure 3-5) was achieved by a Teflon-covered stirring bar installed at the bottom of the cell. Nevertheless, high recycling flow rate of a fraction of treated-water provided by recycling pump promotes the turbulence near the photocatalyst and increase the coefficient of mass transfer at the interface electrode–electrolyte. The structure of the electrode could also enhance the mass transfer coefficient. For instance, the electrode in the form of sheet used by Quan et al. (2007) limits the turbulence around the photocatalyst and reduces the mass transfer coefficient. The turbulent effect required to promote mass transfer and to minimize fouling can be achieved in the reactor using mesh electrodes and gas sparging with small bubbles (Christensen et al., 2005; Christensen et al., 2003). It has been shown by Egerton (2011) that the development of spinning disc and gas sparging inside the reactor influenced the mass transfer.

3.8 Application of photoelectrocatalytic processes (PECPs)

Applications of heterogeneous PECPs using semiconductors as a catalyst for the degradation of refractory organic pollutants present in water and wastewater have received increasing attention in the field of environmental protection. The photoelectrocatalytic oxidation process has been applied for the treatment of different effluents containing varied and high amounts of organic compounds (dye, phenolic compounds, and humic substances) and bacteria (E. coli) that are difficult to oxidize biologically or chemically (Table 3-4 and Table 3-5). A 100% removal of TOC can be reached depending on the type of organic compounds tested and the experimental condition imposed. The performance of PECPs for the degradation of refractory organic pollutants is best examined on the basis of dyes, which are by far the organic compounds that have been the most studied (Table 3-5). For instance, when applying the photo-electro-catalytic process (using TiO_2 anode and carbon cathode electrodes) for the treatment of textile wastewater effluent (containing azo dye Orange), Esquivel et al. (2009) obtained 57% of TOC removal. The reactor was equipped with a low pressure mercury lamp of 21 W cm^{-2} light intensity and operated at 254 nm. By comparison, 63% of TOC was removed when Paschoal et al. (2009) studied the photoelectrocatalytic method using a medium pressure mercury lamp operated at the same wavelength for the treatment of textile wastewater (containing a Disperse Orange dye). The reactor was comprised of TiO_2 and Pt electrodes, used as anode and cathode, respectively. Likewise, PEO could be a good alternative for discoloration and mineralization of dispersed dyes. UV irradiations (254 nm) have been applied to treat textile wastewater before and after conventional treatment (biological method). During the treatment, a potential difference of 1.0 V was applied on the nanoporous photoanode Ti/TiO_2. A degradation rate varying from 53% to 69% of COD could be reached, whereas 80% to 89% of discoloration was recorded. Quan et al., (2007) also used an electrochemically assisted photocatalytic method for the degradation of pentachlorophenol

(PCP) in aqueous solution using a TiO_2 nanotube film electrode as well as UV irradiation. A degradation rate of 82% was obtained after 2 h of treatment. PECPs have also been used to remove endocrine disrupting compounds such as bisphenol-A. Xie and Li (2006) studied PEO of bisphenol-A by using Ti/TiO_2 as an anode and RVC as a cathode. An RVC electrode was used to generate H_2O_2 in the aqueous solution during the treatment. The production of H_2O_2 assisted with the TiO_2 photocatalysis reaction led to a good performance of bisphenol-degradation (up to 99% of degradation). The residual H_2O_2 concentrations recorded (0.2 mM) in the absence of bisphenol-A was lower than that measured (0.98 mM) in the presence of bisphenol-A while the same experimental conditions were applied (current intensity imposed of 1.5 mA for 240 min). The study conducted by Christensen et al. (2005) moreover showed that PEO is able to mineralize 75% of 4-nitrophenol (after 10 h), whereas only 30% of 4-nitrophenol was destroyed in the absence of applied potential (photocatalytic process). Photoelectrocatalytic technology using TiO_2 as a photoanode has been applied by Philippidis et al. (2010) and Christensen et al. (2003) to ensure the disinfection of a suspension of E. coli. The particular advantage associated with this technology is to avoid the use of chlorine, which has serious negative impacts, among them the production of toxic compounds, and carcinogenic and mutagenic chlorinated organic products and the partial inactivation of pathogenic microorganisms. The study of Philippidis et al. (2010) showed that PEO assured a 100% photoinactivation efficiency when applying an anodic potential of 1.0 V. However, electrolysis contributed to the inactivation of less than 5% of E. coli colonies after 3 h of reaction time, while the photocatalytic process eliminates 80% of E. coli. Based on the study of Christensen et al. (2003), the rates of photoelectrochemical disinfection with an illuminated geometric area of the electrode of 100 cm^2 significantly exceed the rate of photocatalytic disinfection for a surface area of 50 $m^2\ g^{-1}$. According to the results presented in Tables 3-4 and Table 3-5, the efficiency of the photo-electrocatalytic process on the removal of pollutant

showed a difference. The nature of the pollutant, the operating conditions imposed during the treatment (pH, pollutant concentration, irradiation source, current density, mixing inside the photoelectrocatalytic cell, etc.) and the photo-reactor configuration could influence on photoelectrocatalytic efficiency.

To the best of our knowledge, photoelectrocatalytic applications have been most often carried out at the laboratory scale. By comparison, conventional photocatalytic processes have been tested in large reactors for practical applications by using a wide variety of photoreactor designs (e.g. parabolic trough, inclined plate, fixed/fluidized bed, packed bed, corrugated plate, and falling film photoreactors). This was discussed in detail by Braham and Harris (2009) and by McCullagh et al. (2010). Indeed, the industrial implementation of the conventional photocatalytic process must be taken into consideration for practical installations and the application of the photoelectrocatalytic process for treating real wastewater (scale up of photoelectrocatalytic reactors). In fact, in photoelectrocatalytic reactor development, parameters such as current density, mass transfer, reaction kinetics, catalyst installation and, catalyst illumination (photoanode) are relevant. The current density is obtained by dividing the current intensity imposed by the surface area of the photoanode (catalyst). Thus, in large-scale application, the imposed current intensity will depend on the size of reactor and the photoanode surface area. On the other hand, the illumination of the photoanode during electrolysis determines the amount of water that may be treated per effective unit area of deployed photoanode. As indicated by several authors (McCullagh et al., 2010; Ray and Beenackers, 1998), the main difficulty of this type of reactor is the provision of sufficient high specific area of catalyst and the uniform distribution of illumination across this area. Here, it could be interesting to use the natural UV radiation emitted by the solar spectrum in the presence of a TiO_2 photocatalyst material a measure that would also allow to reduce the treatment costs (solar photoelectrocatalytic reactors). However, if the solar UV irradiations

are insufficient, it could be combined with UV lamp irradiation. Likewise, the hydrodynamic conditions of the reactor have to be carefully studied and optimized. The mass transfer coefficient (kd) between photoanode and electrolyte need to be improved to increase the reaction rate at the surface of the electrode. For this, the photoanode could be presented in the form of expanded titanium (Ti) covered with titania (TiO_2). Such an electrode structure provides good mechanical strength and, a high surface area (compared to solid plate electrodes), and could moreover be used as a turbulence promoter near the photoanode for increasing the mass transfer coefficient at the electrode–electrolyte interface. In addition, a high recycling flow rate of a fraction of treated-water could be of benefit to decrease the thickness of the diffusion layer near the photoanode electrode, and possibly result in a higher performance of the system. It is worth noting that, during electrolysis the photoanode surface may be covered with organic substances that reduce its electrode active surface. This may affect the treatment performance in long-term experiments. To circumvent these drawbacks, the use of photoanodes in the form of expanded metal (Ti/TiO_2) and the application of a high recycling flow rate during the treatment could be one of the easier and more feasible regeneration methods of the photoanode surface. Likewise, the polarity reversal could be used to maintain electrode longevity.

Tableau 3-4 Removal of different types of organic pollutants in aqueous solutions using PECPs

Matrix	Type of pollutant	Operating conditions	Results and comments	References
Aqueous solution	Bisphenol A	8 W medium pressure mercury lamp (365 nm); $AuTiO_2/Ti$ or TiO_2/Ti(anode); RVC or Pt(cathode); 110 W high pressure sodium vapor lamp (450-650 nm); C^0 (bisphenol A) = 1.12 mg L^{-1}; Na_2SO_4 = 0.01 M; flow rate of air = 120 mL min^{-1}; initial pH = 6.17; current intensity applied = 0-1.5 mA; treatment time = 180 min.	% Bisphenol A removal = 13%- 99%	Malato et al., (2009)
Aqueous solution	Benzotriazole (BTA)	15 W UV lamp (253.7 nm); TiO_2 (working electrode); Pt(counter electrode); SCE(reference electrode); Volume = 100mL; Na_2SO_4= 0.5M; pH(initial) = 6.2; C^0(BTA) = 210-4M; potential applied = 0-0.8V; Treatment time = 180 min; pH= 2-10; calcinations temperature = 100-500°C; Na_2SO_4 = 0.05-0.5 M; C(BTA) = 0.05-0.5 mM	EO(0% removal); DP(65% removal); PO (70% removal); PEO(89.8-90% removal)	Yang et al., (2009)
Aqueous solution	Pentachlorophenol (PCP)	300 W high pressure mercury lamp (365 nm); C0 (PCP)=20 ppm; pH = 7.03; C0(Na_2SO_4) = 0.01M; TiO_2 (anode); Pt (cathode); potential applied=0.0-0.6V; treatment time = 2h; pH=3.25-8.00; C(Na_2SO_4)=0-0.01 M	EO(0% removal); DP(44% removal);PO(62% removal); PEO(82-86% removal)	Wang et al., (2010)
Aqueous solution	2,4 dichlorophenol	8 W medium pressure mercury lamp (365 nm); TiO_2/Ti(first anode); graphite (cathode); Fe(second anode); Na_2SO_4=0.02 M; Oxygen gas flow= 40 mL min^{-1}; treatment time = 60 min.	2,4-dichlorophenol degradation (93%); mineralization of 78%	Leng et al., (2006)
Aqueous solution	4-chlorophenol, Oxalic acid	45 W Hg medium pressure lamp (365 nm); TiO_2 film (anode); Ag/AgCl (reference electrode; Na_2SO_4 = 0.1 M; T<35°C; natural pH; treatment time = 5h	Oxalic acid: 100% of the total organic carbon degradation 4-chlorophenol: less CO_2 was detected	Ding et al., (2010)
Aqueous solution	Rhodamine B	30 W mercury UVA lamp, Ti/TiO_2(working electrode); Pt(counter electrode); SCE(reference electrode); Na_2SO_4= 0.1 mol L^{-1}; potential applied = 0.05-0.5 V; treatment time= 30 min; pH=2-10	Efficient and complete oxidation of Rhodamine B	Elsellami et al., (2010)
Aqueous solution	Humic acid	450 W Xe-Hg UV light lamp (254 nm and 400 nm); TiO_2 (anode); Pt(counter electrode); SCE (reference electrode); oxygen is bubbled during all experiments; C^0 (humic acid) = 25 mg dm^{-3}; potential applied = 0-2 V; treatment time = 2h; Na_2SO_4 = 0.01 mol dm^{-3}; pH (initial) = 7	Color removal (96%); Humic acid removal (98%); TOC removal (85%)	Chong et al., (2010)

Tableau 3-5 Removal of dye and microbial pollutants using PECPs

Matrix	Type of pollutant	Operating conditions	Results and comments	References
Dye wastewater	Textile effluent, Brilliant Blue X-BR (RBB)	11 W mercury lamp (254 nm); radiation power = 15 mW cm^{-2}; flow rate = 7.7 L h^{-1}; TiO_2/Ti sheet: (anode); Cu sheet (cathode); applied potential = 0.6-1.0 V; pH = 10; Na_2SO_4 = 0.5 g L^{-1}; C^0 (dye) = 20-150 mg L^{-1}.	44-83% of RBB (flowing aqueous film photoelectrocatalytic reactor); 12%-75% of RBB removed (conventional photoelectrocatalytic reactor);	Quan et al., (2007)
Textile wastewater	Azo dye Orange II	UV lamp (254 nm), TiO_2(anode); carbon cloth(cathode), C^0 (azo dye Orange II=15 mg L^{-1}; Na_2SO_4 = 0.05 M; pH=3; [Fe^{2+}]=0.2 mM; [H2O2]= 80 mg L^{-1}; treatment time = 60 min; reactor volume = 640 mL; flow rate = 80 L h^{-1}	Azo dye Orange II removal (100%); TOC removal (57%)	Esquivel et al., (2009)
Textile wastewater	Dispersal orange dye (DOD), dispersal ruby dye (DRD), dispersal red dye (DRR), borax, emulsogen (naphthalene)	125 W medium pressure mercury lamp (254nm); TiO_2(working electrode; Pt gauze (counter electrode); Ag/AgCl (reference electrode); C^0(DOD) = 77 mg L^{-1}; C0(DRD) = 72 mg L^{-1}, C^0(DRR) = 92 mg L^{-1}; C^0(borax) = 1500 mg L^{-1}; C^0(emulsogen) = 800 mg L^{-1}; C^0(Na_2SO_4) = 0.1 mol L^{-1}; potential applied = 1.0V	DOD (90% discoloration, reduction 63% of TOC); DRD (94% discoloration, reduction 45% of TOC); DRR (100% discoloration, reduction 61% of TOC)	Li et al., (2007)
Dye solution	Rose Bengal	20 W UV lamp (365 nm); Ti/TiO_2 (anode); Pt (cathode); light intensity = 1.4-2.2 mW cm^{-2}; treatment time = 6h; C^0 (Rose Bengal) = 20 mg L^{-1}	Rose Bengal removed = 65% after 0.5h and 85% after 6h.	Rincon et al., (2004)
Surface water	Microcystin aeruginosa	125 W Philips medium pressure mercury lamp UV light (365-400 nm); Ti/TiO_2(working electrode); Pt (counter electrode); bubbling of compressed air, C0 (chloride)>0.010 mol L^{-1}; pH=4; current density = 30 mA cm^{-2}; treatment time = 150 min; C^0(NaCl) = 0.05 mol L^{-1}; C^0 (microcystin aeruginosa) = 50 µg L^{-1}	TOC reduction (90%); Turbidity removal (100%); color decrease (93%); COD removal (96%); bacteria removal (100%)	Monllor-Satoca and Gomez, (2010)
E.coli colonies Solution	Escherichia-Coli XL-1 Blue	9W/78 UVA lamp (365 nm); TiO_2/Ti, Pt-TiO_2/Ti, R-TiO_2/Ti (anode); Pt(cathode); Ag/AgCl (reference electrode); potential applied = 1.0 V; C0(E. Coli) = 10^3-10^7CFU; C^0 (Na_2SO_4) = 0.1 mol L^{-1}; pH= 5.6; T°=25°C	EO (removal 5% of E.coli after 3h); PO (removal 80% of E.coli after 1h); PEO (removal 100% of E.coli after 1 h)	Wu, 2004

3.9 Current and future development of PECPs

The photoelectrocatalytic process is considered as a good alternative to conventional photocatalysis for improving the degradation rate of refractory organic pollutants. The introduction of electrochemical technology into photocatalytic reactions increases the efficiency of processes and also expands the degradation capacity of the recalcitrant organic pollutants. Due to the successful results at the laboratory scale, the photoelectrocatalytic process merits further research, in particular concerning the design of pilot units for the treatment of different effluents (industrial, municipal and domestic effluents). In order to promote the feasibility of phototoelectrocatalytic technology for large-scale applications, several key technical constraints should be addressed. These include: (i) a better exploitation of solar irradiation to be used as a free energy light source; (ii) development of TiO_2 photocatalyst material able to operate as much as possible using the solar spectrum (5% of solar energy is emitted as UV irradiation); (iii) research should be focused on the use of mathematical models for the optimization of parameters affecting the efficiency of PECPS. It should also be noted that the total cost of the photoelectrocatalytic process, including energy, electrodes, and UV lamps, is relatively high. Decreasing those costs thus poses a further research challenge.

3.10 Conclusion

Heterogeneous photoelectrocatalytic degradation using TiO2 as a photocatalyst has proven to be a good alternative for the degradation of several persistent organic contaminants (hormones, phenolic compounds, antibiotics, pesticides, halogenated compounds, etc.) that are present in wastewater. These pollutants, coming from pharmaceuticals, food waste, cosmetics, and the chemical and oil industries, among other sources, can be directly degraded on the surface of the semiconductor or indirectly by reacting with hydroxyl radicals or by

reacting with superoxide radicals produced in situ. Up to now, the applications of photoelectrocatalytic technologies for water and wastewater treatment were carried out at the laboratory scale. Future research should be focused on the development of photoelectrocatalytic technology for large-scale applications. PECPs can be effectively combined with biological processes when treating effluents containing refractory organic compounds. For example, coupling a biodegradation process with a physicochemical process would lead to a reduction of operating costs as well as a shorter retention time. In effluent that has been treated with PECPs, the non-biodegradable organic pollutants can be transformed into biodegradable compounds, which contribute to increasing the depurative efficiency of the subsequent biological process. When installed downstream of biological processes, PECP combustion yields water and carbon dioxide, forgoing the need for any further treatment. In this way, the residence time and reaction volume for the biological treatment could be significantly reduced.

3.11 Acknowledgments

Sincere thanks are extended to the National Sciences and Engineering Research Council of Canada and Premier Tech Ltee for their financial support for this study.

3.12 References

Adams C, Wang MY, Loftin K & Meyer M (2002) Removal of antibiotics from surface and distilled water in conventional water treatment processes. *J. Environ. Eng.* 128: 253-260.

Almquist CB & Biswas P (2001) A mechanistic approach to modeling the effect of dissolved oxygen in photo-oxidation reactions on titanium dioxide in aqueous system. *Chem.Eng. Sci.*56: 3421-3430.

Bandara J, Wansapura PT & Jayathilaka SPB (2007) Indium tin oxide coated conducting glass electrode for electrochemical destruction of textile colorants. *Electrochim.Acta.* 52 (12): 4161–4166.

Bessekhouad Y, Robert D & Weber JV (2004) Bi_2S_3/TiO_2 and CdS/TiO_2 heterojunctions as an available configuration for photocatalytic degradation of organic pollutant. *J. Photochem. Photobiol.A.* 163(3): 569-580.

Braham RJ & Harris AT (2009) Review of major design and scale-up considerations for solar photocatalytic reactors. *Ind. Eng. Chem.Res.* 48 (19): 8890-8905.

Carneiro PA, Oliveira DP, Umbuzeiro GA & Boldrin Zanoni MV (2010) Mutagenic activity removal of selected disperse dye by Photoelectrocatalytic treatment. *J.Appl.Electrochem.* 40 (3): 485-492.

Chen F, Yang X, Mak HKC & Chan DWT (2010) Photocatalytic oxidation for antimicrobial control in built environment: A brief literature overview. *Build. Environ.* 45 (8): 1747-1754.

Chen G (2004) Electrochemical technologies in wastewater treatment. *Sep. Purif. Technol.* 38 (1): 11-41.

Chen D & Ray AK (1998) Photodegradation kinetics of 4-nitrophenol in TiO_2 suspension. *Water Res.* 32 (11): 3223-3234.

Cho M, Chung H, Choi W & Yoon J (2004) Linear correlation between inactivation of E.Coli and OH radical concentration in TiO_2 photocatalytic disinfection. *Water Res.* 38: 1069-1077

Chong MN, Jin B, Chow CWK & Saint C (2010) Recent developments in photocatalytic water treatment technology: A review. *Water Res.* 44: 2997-3027.

Christensen PA, Egerton TA, Kosa SAM, Tinlin JR & Scott K (2005) The photoelectrocatalytic oxidation of aqueous nitrophenol using a novel reactor. *J. Appl. Electrochem.* 35 (7-8): 683-692.

Christensen PA, Curtis TP, Egerton TA, Kosa SAM & Tinlin JR (2003) Photoelectrocatalytic and photocatalytic disinfection of E.Coli suspensions by titanium dioxide. *Appl.Catal.B.* 41: 371-386.

Daghrir R, Drogui P, Ka I & El-Khakani MA (2012) Photoelectrocatalytic degradation of chlortetracycline using Ti/TiO_2 nanostructured electrodes deposited by means of a Pulsed Laser Deposition process. *J. Hazard. Mater.* 199–200: 15-24.

De Tacconi NR, Chenthamarakshan CR, Rajeshwar K, Pauporté T & Lincot D (2003) Pulsed electrodeposition of WO_3-TiO_2 composite films. *Electrochem.Commun.* 5 (3): 220-224.

Desbiens E & El Khakani MA (2003) Growth of high-k silicon oxynitride thin films by means of a pulsed laser deposition-atomic nitrogen plasma source hybrid system for gate dielectric applications. *J.Appl. Phys.* 94(9): 5969-5975.

Ding Y, Yang C, Zhu L & Zhang J (2010) Photoelectrochemical activity of liquid phase deposited tio_2 film for degradation of benzotriazole. *J. Hazard. Mater.*175: 96-103.

Dominguez C, García J, Pedraz MA, Torres A & Galán MA (1998) Photocatalytic oxidation of organic pollutants in water. *Catal. Today*. 40 (1): 85-101.

Doré M (1989) *Chimie des oxydants et traitement des eaux.* Tec & Doc. Lavoisier, Paris, France, p505.

Drogui P, Elmaleh S, Rumeau M, Bernard C & Rambaud A (2001) Hydrogen peroxide production by water electrolysis: Application to disinfection. *J. Appl. Electrochem.*31: 877-882.

Egerton TA (2011) Does photoelectrocatalysis by TiO_2 work? *J. Chem. Technol. Biotechnol.* 86: 1024-1031.

Egerton TA & Christensen PA (2004) *Advanced oxidation processes for water and wastewater treatment.* Ed. Simon Parsons, IWA Publishing, London, p356.

Elsellami L, Vocanson F, Dappozze F, Puzenat E, Paisse O, Houas A & Guillard C (2010) Kinetic of adsorption and of photocatalytic degradation of phenylalanine effect of pH and light intensity. *Appl.Catal.A.* 380 (1-2): 142-148.

Esquivel K, Arriaga LG, Rodriguez FJ, Martinez L & Godinez LA (2009) Degradation of chlorophenols by means of advanced oxidation processes: A general review. *Water Res.* 43: 3593-3603.

Evgenidou E, Fytianos K & Poulios I (2005) Semiconductor-sensitized photodegradation of dichlorvos in water using TiO_2 and ZnO as catalysts. *Appl.Catal. B.* 59: 81–89.

Fraga LE, Anderson MA, Beatriz MLPMA, Paschoal FMM, Romao LP & Zanoni MVB (2009) Evaluation of the photoelectrocatalytic method for oxidizing chloride simultaneous removal of microcystin toxins in surface waters. *Electrochem. Acta.* 54: 2069-2076.

Fujishima A, Rao TN & Tryk DA (2000) Titanium dioxide photocatalysis. *J. Photochem. Photobiol. C.* 1(1): 1-21.

Gaya UI & Abdullah AH (2008) Heterogenous photocatalytic degradation of organic contaminants over titanium dioxide: A review of fundamentals, progress and problems. *J.Photochem.Photobiol.C.* 9: 1-12.

Gogate PR & Pandit AB (2004) A review of imperative technologies for wastewater treatment I: Oxidation technologies at ambient conditions. *Adv. Environ. Res.* 8 (3-4): 501-551.

Grimm J, Bessarabov D & Sanderson R (1998) Review of electro-assisted methods for water purification. *Desalination* 115 (3): 285-294.

Guivarch ZE (2004) *Traitement des polluants organiques en milieux aqueux par procédé éléctrochimique d'oxydation avancée « Éléctro-Fenton ». Application à la minéralisation des colorants synthétiques*. Thése de Doctorat, Université de Marne – la-Vallée, Institut Francilien des Géosciences, Marne-la –Valée, France, p235.

Hattori A, Tokihisa Y, Tada H, Tohge N, Ito S, Hongo K, Shiratsuchia R & Nogami G (2001) Patterning effect of a sol-gel TiO_2 over layer on the photocatalytic activity of a TiO_2/SnO_2 bilayer-type photocatalyst. *J. Sol-Gel Sci. Technol.* 22 (1-2): 53-61.

Hattori A, Tokihisa Y, Tada H & Ito S (2000) Acceleration of oxidations and retardation of reductions in photocatalysis of a TiO_2/SnO_2 bilayer-type catalyst. *J Electrochem.Soc.* 147 (6): 2279-2283.

Heit G, Neuner A, Saugy PY & Braun AM (1998) vacuum-UV (172 nm) actinometry-the quantum yield of the photolysis of water. *J. phys. Chem.A.* 102: 5551-5561.

Hermann JM (2005) Heterogeneous photocatalysis: state of the art and present applications. *Top.Catal.* 34: 49-65.

Hidaka H, Nohara K, Zhao J, Serpone N & Pelizzetti E (1992) Photo-oxidative degradation of the pesticide permethrin catalyzed by irradiated TiO_2 semiconductor slurries in aqueous media. *J Photochem. Photobiol.A.* 64 (2): 247-254.

Hitchman ML, Spackman RA & Agra C (1996) Photoelectrochemical study of titanium dioxide films prepared by anodisation of titanium metal in sulfuric acid. *J. Chem.Soc. Faraday Trans*. 92 (20): 4049-4052.

Hoffmann MR, Martin ST, Choi W & Bahnemann DW (1995) Environmental applications of semiconductor photocatalysis. *Chem. Rev.* 95: 69-96.

Ikehata K, Naghashkar NJ & El-Din MG (2006) Degradation of aqueous pharmaceuticals by ozonation and advanced oxidation processes: A review. *Ozone: Sci. Eng.*28 (6): 353-414.

Jiang YL, Liu HL, Wang QH & Jiang ZH (2006) Determination of hydroxyl radicals in TiO_2/Ti photoelectrocatalytic oxidation system using $Fe(phen)_3^{2+}$ spectrophotometry. *J. Environ.Sci.* 18:158-161.

Kim S, Kim T, Park C & Shin EB (2003) Electrochemical oxidation of polyvinylalcohol using a RuO_2/Ti anode. *Desalination.* 155 (1): 49-57.

Kim I & Tanaka H (2009) Photodegradation characteristics of PPCPs in water with UV treatment. *Environ.Inter.* 35:793-802.

Konstantinou IK & Albanis TA (2004) TiO_2-assisted photocatalytic degradation of azo dyes in aqueous solution: Kinetic and mechanistic investigation: A review. *Appl.Catal.B.* 49(1): 1-14.

Kouamé NA, Robert D, Keller V, Keller N, Pham C & Nguyen P (2011) Preparation and optimization of TiO_2/β-SiC foam for Industrial photocatalytic water treatment. *Catal.Today* 161 (1): 3-7.

Leng WH, Zhu WC, Ni J, Zhang Z, Zhang JQ & Cao CN (2006) Photoelectrocatalytic destruction of organics using Ti_{O2} as photoanode with simultaneous production of H_2O_2 at the cathode. *Appl. Catal.A.* 300: 24-35.

Locas A, Demers J & Payment P (2008) Evaluation of photoreactivation of Escherichia coli and enterococci after UV disinfection of municipal wastewater. *Canad. J. Microbiol.*54 (11): 971-975.

Lou JC & Huang SW (2008) Treating isopropyl alcohol by a regenerative catalytic oxidizer. *Sep. Purif. Technol.* 62: 71-78.

Li D & Qu J (2009) The progress of catalytic technologies in water purification: A review. *J. Environ.Sci.* 21: 713-719.

Li J, Zheng L, Li L, Xian Y & Jin L (2007) Fabrication of TiO_2/Ti electrode by laser-assisted anodic oxidation and its application on Photoelectrocatalytic degradation of methylene blue. *J. Hazard. Mater.* B139 (1): 72-78.

Li MC & Shen JN (2006) Photoelectrochemical oxidation behavior of organic substances on TiO_2 thin-film electrodes. *J. Solid State Electrochem.*10 (12): 980-986.

Li XZ, Li FB, Fan CM & Sun YP (2002) Photoelectrocatalytic degradation of humic acid in aqueous solution using a ti/tio_2 mesh photo electrode. *Water Res.* 36: 2215-2224.

Li J, Li L, Zheng L, Xian Y & Jin L (2006) Photoelectrocatalytic degradation of rodhamine B using Ti/TiO_2 electrode prepared by laser calcination method. *Electrochim Acta.* 51: 4942-4949.

Li XZ, Zhao BX & Wang P (2007) Degradation of 2, 4-dichlorophenol in aqueous solution by a hybrid oxidation process. *J. Hazard. Mater.* 147 (1-2): 281-287.

Li XZ & Liu HS (2005) Development of an E-H_2O_2/TiO_2 photoelectrocatalytic oxidation system for water and wastewater treatment. *Environ. Sci. Technol.* 39 (12): 4614-4620.

Li XZ, Liu HL, Yue PT & Sun YP (2000) Photoelectrocatalytic oxidation of rose Bengal in aqueous solution using a Ti/TiO_2 mesh electrode. *Environ.Sci.Technol.* 34 (20): 4401-4406.

Liang HC, Li XZ, Yang YH & Sze KH (2008) Effects of dissolved oxygen, pH, and anions on the 2, 3-dichlorophenol degradation by photocatalytic reaction with anodic TiO_2 nanotube films. *Chemosphere*. 73: 805-812.

Linsebigler AL, Lu G & Yates JT (1995) Photocatalysis on TiO_2 surfaces: Principles, mechanisms, and selected results. *Chem. Rev*. 95(3): 735-758.

Liu Y, Gan X, Zhou B, Xiong B, Li J, Dong C, Bai J & Cai W (2009) Photoelectrocatalytic degradation of tetracycline by highly effective TiO_2 nanopore arrays electrode. *J. Hazard.Mater.* 171: 678-683.

Liu H, Liu G, Fan J, Zhou Q, Zhou H, Zhang N, Hou Z, Zhang M & He Z (2011) Photoelectrocatalytic degradation of 4, 4`-dibromobiphenyl in aqueous solution on TiO_2 and doped TiO_2 nanotube arrays. *Chemosphere* 82 (1): 43-47.

Macphee DE, Rosenberg D, Skellern MG, Wells RP, Duffy JA & Killham KS (2011) A tungsten oxide-based photoelectrocatalyst for degradation of environmental contaminants. *J. Solid State Electrochem.*15: 99-103.

Maeda H, Ikeda K, Hashimoto K, Ajito K, Morita M & Fujishima A (1999) Microscopic Observation of TiO_2 Photocatalysis Using Scanning Electrochemical Microscopy. *J. Phys.Chem.* 103: 3213–3217.

Malato S, Fernandez-Ibanez P, Maldonado MI, Blanco J & Gernjak W (2009) Decontamination and disinfection of water by solar photocatalysis : Recent overview and trends. *Catal. Today* 147 (1): 1-59.

Malato S, Blanco J, Vidal A & Richter C (2002) Photocatalysis with solar energy at a pilot-plant scale: An overview. *Appl.Catal.B.* 37(1): 1-15.

Martínez-Huitle CA & Brillas E (2009) Decontamination of wastewaters containing synthetic organic dyes by electrochemical methods: A general review. *Appl.Catal. B.* 87 (3-4): 105-145.

Martínez-Huitle CA & Ferros S (2006) Electrochemical oxidation of organic pollutants for the wastewater treatment: direct and indirect processes. *Chem.Soc.Rev.*35 (12): 1324-1340.

Matthews RW & McEvoy SR (1992) Photocatalytic degradation of phenol in the presence of near-UV illuminated titanium dioxide. *J. Photochem. Photobiol. A.* 64 (2): 231-246.

McCullagh C, Skillen N, Adams M & Robertson PKJ (2011) Photocatalytic reactors for environmental remediation: a review. *J.Chem.Technol. Biotechnol.* 86 (8): 1002-1017.

Mills A & Le Hunte S (1997) An overview of semiconductor photocatalysis. *J. Photochem. Photobiol. A.* 108 (1): 1-35.

Monllor-Satoca D & Gomez R (2010) A photoelectrochemical and spectroscopic study of phenol and catechol oxidation on titanium dioxide nanoporous electrodes. *Electrochim. Acta.* 55 (15): 4661-4668.

Neuman-Spallart M (2007) Aspects of Photocatalysis on Semiconductors: Photoelectrocatalysis. *Chimica Inter. J. Chem.* 61: 806–809.

Ollis DF, Pelizzetti E & Serpone N (1991) Destruction of water contaminants. *Environ. Sci. Technol.*25: 1522-1529.

Ozcan AS, Erdem B & Ozcan A (2004) Adsorption of acid blue 193 from aqueous solutions onto Na-bentonite and DTMA-bentonite. *J Colloid Interface Sci.* 280: 44-54.

Ozer RR & Ferry JL (2001) Investigation of the photocatalytic activity of TiO2 polyoxometalate systems. *Environ. Sci. Technol.* 35:3242-3246.

Pareek V, Chong S, Tadé M & Adesina AA (2008) Light intensity distribution in heterogeous photocatalytic reactors.*Asia-Pacific J. Chem. Eng.* 3 (2): 171-201.

Paschoal FMM, Anderson MA & Zanoni MVB (2009) The Photoelectrocatalytic oxidative treatments of textile wastewater containing disperse dyes. *Desalination* 249 (3): 1350-1355.

Pera-Titus M, Garcia-Molina V, Banos MA, Giménez J & Esplugas S (2004) Degradation of chlorophenols by means of advanced oxidation processes: A general review. *Appl. Catal.B.* 47: 219-256.

Philippidis N, Nikolakaki E, Sotiropoulos S & Poulios I (2010) Photoelectrocatalytic inactivation of E.Coli XL-1 blue colonies in water. *J. chem. Technol. Biotechnol.* 85: 1054-1060.

Puma GL & Yue PL (1999) Photocatalytic oxidation of chlorophenols in single-component and multicomponent systems. *Ind. Eng. Chem.Res.* 38 (9): 3238-3245.

Quan X, Ruan X, Zhao H, Chen S & Zhao Y (2007) Photoelectrocatalytic degradation of pentachlorophenol in aqueous solution using TiO_2 nanotube film electrode. *Environ.Pollut.* 147 (2): 409-414.

Rajeshwar K & Ibanez J (1997) *Environmental Electrochemistry: Fundamentals and Applications in Pollution Abatement.* Academic Press, San Diego, CA, p804.

Rajeshwar K, Ibanez JG & Swain GM (1994) Electrochemistry and the environment. *J. Appl. Electrochem.* 24 (11): 1077-1091.

Ray AK & Beenackers ACM (1998) Novel photocatalytic reactor for water purification. *AIChE J.* 44(2): 477-483.

Rincon AG & Pulgarin C (2004) Photocatalytic inactivation of E.Coli: effect of (continuous-intermittent) light intensity and of (suspended-fixed) TiO_2 concentration. *Appl.Catal.B.*44: 263-284.

Rivera AP, Tanaka K & Hisanaga T (1993) Photocatalytic degradation of pollutant over TiO_2 in different crystal structures. *Appl.Catal.B.* 3 (1): 37-44.

Robert D (2007) Photosensitization of TiO_2 by M_xO_y and M_xS_y nanoparticles for heterogeneous photocatalysis applications. *Catal. Today* 122: 20–23.

Rosenfeldt EJ & Linden KJ (2004) Degradation of endocrine disrupting chemicals bisphenol A, ethinyl estradiol, and estradiol during UV photolysis and advanced oxidation processes. *Environ. Sci. Technol.* 38 (20): 5476-5483.

Schaller V (1996) *Oxydation électrochimique du phénol sur des électrodes du type métal support/dépôt conducteur.* Thèse de Doctorat, École Polytechnique Fédérale de Lausanne, Lausanne, Switzerland, p250.

Selcuk H, Sene JJ & Anderson MA (2003) Photoelectrocatalytic humic acid degradation kinetics and effect of pH, applied potential and inorganic ions. *J. Chem.Technol. Biotechnol.*78 (9): 979-984.

Sohrabi MR & Ghavami M (2010) Comparison of direct yellow 12 dyes degradation efficiency using uv/semiconductor and UV/H_2O_2/semiconductor systems. *Desalination* 252: 157-162.

Skoumal M, Rodríguez RM, Cabot PL, Centellas F, Garrido JA, Arias C & Brillas E (2009) Electro-Fenton, UVA photoelectron-Fenton and solar photoelectron-Fenton degradation of the drug ibuprofen in acid aqueous medium using platinium and boron-doped diamond anodes. *Electrochim. Acta.* 54 (7): 2077–2085.

Sun P, Liu H, Yang H, Fu W, Liu S, Li M, Sui Y, Zhang Y & Li Y (2010) Synthesis and characterization of TiO_2 thin films coated on metal substrate. *Appl.Surf.Sci.* 256 (10): 3170-3173.

Tahir SS & Rauf N (2006) Removal of a cationic dye from aqueous solutions by adsorption onto bentonite clay. *Chemosphere* 63: 1842-1848.

Thiruvenkatachari R, Vigneswaran S & Moon IS (2008) A review on UV/TiO_2 photocatalytic oxidation process. *Korean J.Chem.Eng.*25 (1): 64-72.

Tomovska R, Marinkovski M & Frajgar R (2007) Current state of nanostructured TiO_2-based catalysts: Preparation methods. *NATO Sec. Sci. C: Environ. Sec.* 207-229.

Tsai SJ & Cheng S (1997) Effect of TiO_2 crystalline structure in photocatalytic degradation of phenolic contaminants. *Catal. Today.* 33 (1-3): 227-237.

Vinodgopal K, Bedja I & Kamat PV (1996) Nanostructured semiconductor films for photocatalysis. Photoelectrochemical behavior of SnO_2/TiO_2 composite systems and its role in photocatalytic degradation of a textile azo dye. *Chem. Mater.* 8(8): 2180-2187.

Vinodgopal K & Kamat PV (1995) Enhanced rates of photocatalytic degradation of an azo dye using SnO_2/TiO_2 coupled semiconductor thin films. *Environ.Sci. Technol.* 29 (3): 841-845.

Waldner G, Pourmodjib M, Bauer R & Neumann-Spallart M (2003) Photoelectrocatalytic degradation of 4-chlorophenol and oxalic acid on titanium dioxide electrodes. *Chemosphere* 50: 989-998.

Wang WY, Yang ML, Ku Y (2010) Photoelectrocatalytic decomposition of dye in aqueous solution using nafion as an electrolyte. *Chem. Eng. J.* 165: 273–280.

Wang N, Li X, Wang Y, Quan X & Chen G (2009) Evaluation of bias potential enhanced photocatalytic degradation of 4-chlorophenol with tio_2 nanotube fabricated by anodic oxidation method, *Chem.Eng. J.* 146: 30-35.

Wang K, Guo J, Yang M, Junji H & Deng R (2009) Decomposition of two haloacetic acids in water using UV radiation, ozone and advanced oxidation processes. *J. Hazard.Mater.* 162 (2-3): 1243–1248.

Wang Y, Hong CS (2000) TiO_2-mediated photomineralization of 2-chlorobiphenyl: The role of O_2. *Water Res.* 34 (10): 2791-2797.

Wang Y & Hong CS (1999) Effects of hydrogen peroxide, periodate and persulfate on photocatalysis of 2-chlorobiphenyl in aqueous TiO2 suspensions. *Water Res.* 33:2031-2036.

Wu, CH & Chang CL (2006) Decolorization of reactive red 2 by advanced oxidation processes: Comparative studies of homogeneous and heterogeneous system. *J.Hazard. Mater.* B128 (2-3): 265–272.

Wu CH (2004) Comparison of azo dye degradation efficiency using UV/Single semiconductor and UV/coupled semiconductor systems. *Chemosphere* 57: 601–608.

Xie YB & Li XZ (2006) Degradation of Bisphenol A in aqueous solution by H_2O_2-assisted photoelectrocatalytic oxidation. *J.Hazard.Mater.* B138:526-533.

Xu Y, Zhong D & Jia J (2008) Degradation of Dye wastewater using a rotating TiO_2/Ti disc photoanode. *2nd International Conference on Bioinformatics and Biomedical Engineering*. Article n°. 4535306: 3696-3699.

Yang J, Dai J, Chen C & Zhao J (2009) Effect of hydroxyl radicals and oxygen species on the 4-chlorophenol degradation by Photoelectrocatalytic reactions with TiO_2-film electrodes. *J. Photochem. Photobiol A.* 208: 66-77.

Yang L & Liu Z (2007) Study on light intensity in the process of photocatalytic degradation of indoor gaseous formaldehyde for saving energy. *Energ. Convers. Manage.* 48: 882-889.

Ye X, Sha J, Jiao Z & Zhang L (1997) Thermoanalytical characteristics of nanocrystalline brookite-based titanium dioxide. *Nanostruct.Mater.* 8(7): 919-927.

Yu J, Wang W, Cheng B & Su BL (2009) Enhancement of photocatalytic activity of mesoporous TiO_2 powders by hydrothermal surface fluorination treatment. *J.phys.Chem.C.* 113 (16): 6743-6750.

Yu Z & Chuang SSC (2008) The effect of Pt on the photocatalytic degradation pathway of methylene blue over TiO_2 under ambient conditions, *Appl. Catal. B.* 83 (3-4): 277–285.

Yun SM, Palanivelu K, Kim YH, Kang PH & Lee YS (2008) Preparation and characterization of carbon covered TiO_2 using sucrose for solar photodegrdation. *J. Indus. Eng.Chem.* 14: 667–671.

Zane D, Decker F & Razzini G (1993) Characterization of electrodeposited TiO_2 films. *Electrochim. Acta.* 38 (1): 37-42.

Zaviska F, Drogui P, Mercier G & Blais JF (2009) Procédé d'oxydation avancée dans le traitement des eaux et des effluents industriels : Application à la dégradation des polluants réfractaires. *Rev. Sci. Eau.* 22 (4): 535-564.

Zhang H, Chen G & Bahnemann DW (2009) Photoelectrocatalytic for environmental application. *J. Mater Chem.* 19 (29): 5089-5121.

Zhang W, An T, Xiao X, Fu J, Sheng G, Cui M & Li G (2003) Photoelectrocatalytic degradation of reactive brilliant orange K-R in a new continuous flow Photoelectrocatalytic reactor. *Appl.Catal.A.* 255: 221-229.

CHAPITRE 4

MODIFIED TIO_2 FOR ENVIRONMENTAL PHOTOCATALYTIC APPLICATIONS: A REVIEW.

Le chapitre 4 est constitué de l'article suivant :

Rimeh Daghrir, Patrick Drogui, Didier Robert (2013) Modified TiO_2 For Environmental Photocatalytic Applications: a review. *Industrial & Enginnering Chemistry Research. 52 (10) 3588-3599.*

4. MODIFIED TIO_2 FOR ENVIRONMENTAL PHOTOCATALYTIC APPLICATIONS: A REVIEW.

4.1 Abstract

This paper summarizes recent research dealing with development of titanium dioxide (TiO_2) used for environmental applications. TiO_2 plays the most important role owing to its excellent chemical and physical properties. However, the TiO_2 band edge lies in the UV region which makes them inactive under visible irradiation. In this regard, considerable efforts have been made to increase the visible light activity of TiO_2 via the modification of its electronic and optical properties. Doping TiO_2 using either anions or cations is one of the typical approach that has been largely applied. Coupling TiO_2 with a narrow bad gap semiconductor (M_xO_y/TiO_2 or M_xS_y/TiO_2) represents another approach. This work aims to encompass the new progress of TiO_2 for an efficient application in water and wastewater treatment under visible light, emphasizes the future trends of TiO_2 in the environment and suggests new research direction including preparation aspect for the development of this promising material.

4.2 Key words

Titanium dioxide, dopant, sensitization, photocatalysis, environmental applications.

4.3 Introduction

Over the past few years, the abusive use of pharmaceutical and personal care products (PPCPs), pesticides, surfactants, industrial chemicals and combustion by-products have resulted in their undesirable accumulation in the environment. Several pollutants are soluble in water and have been detected in surface water, ground water, sewage water and drinking water. The excessive occurrence of these residues in the environmental has received a great attention as emerging contaminants due to its persistent characters. The complex mixture of these compounds and the non-biodegradability character make conventional wastewater treatment methods (physical, chemical and biological methods) unable to completely remove them (Zhang et al., 2010).

Advanced oxidation processes (AOPs) have been proposed as alternative methods for the elimination of many toxic organic compounds in wastewaters, air and soil. The principle of AOPs (including O_3/H_2O_2, UV/O_3, UV/H_2O_2, H_2O_2/Fe^{2+}, and $UV\text{-}TiO_2$) is to produce hydroxyl radical in water, a very powerful oxidant capable of oxidizing a wide range of organic compounds with one or many double bonds (Yu and Chuang, 2008). In spite of the good oxidation of refractory organic pollutants, the complexity of these methods (AOPs), the high chemical consumption, and the relatively high treatment costs constitute the major barriers for large scale applications (Martinez-Huitle and Ferro, 2006).

Nowadays, photocatalytic process using semiconductor as photocatalyst (ex. TiO_2) under UV irradiation has been extensively applied for the oxidation of various refractory organic compounds such as bisphenol A, tetracycline, sulfamethazine, etc (Reyes et al., 2006; Fukahori et al., 2003; Kaniou et al., 2005). Nonetheless, the fast recombination of the photogenerated electron/hole (e^-/h^+) reduces the photonic efficiency and represents the major drawback of photocatalytic applications (Waldner et al., 2003; Daghrir et al., 2012a). A renewed interest in photocatalysis has been spurred by the search for reliable, cost-effective

water treatment processes. From this point of view, photoelectrocatalytic oxidation (PECO) technique combining photocatalytic and electrolytic processes represents an alternative method (Daghrir et al., 2012a; Liu and Du, 2011). Recently, this photoelectrocatalytic process has received an increasing attention in the environmental field because of its ability to destroy undesirable organic compounds in aqueous phase and to remove traces of organic species that are stable and difficult to oxidize by means of conventional water treatments methods (Daghrir et al., 2012a; Li and Shen, 2006; Chang et al., 2012; He et al., 2003).

The combination of electrochemical and photocatalysis technologies offer the opportunity to promote the separation between the electron-hole photogenerated (e^-/h^+) and to prevent their recombination. According to the previous research (Daghrir et al., 2012b), the applied external potential is a key factor in the photoelectrocatalytic technique because it accelerates the photocatalytic reactions. The basic of such process consists of ejecting an electron from the valence band (VB) to the conduction band (CB) of the semi-conductor, thereby creating an "h^+" hole in the valence band. This is due to the UV irradiation of TiO_2 with an energy equal or superior to the band gap (>3.2 eV for TiO_2 photocatalyst). These charge carriers (e^-/h^+) can migrate to the surface of the catalyst, where they are then available to undergo redox reactions with substrates (Yang et al., 2009). This is followed by the formation of extremely reactive oxygen species (OH°, $O_2^{\circ-}$, H_2O_2, O_3, etc) at the surface of the semi-conductor and/or a direct oxidation of the polluting species (R).

Most of the materials used for photoelectrocatalytic degradation of pollutants are titanium dioxide (TiO_2) and zinc oxide (ZnO) (Sapkal et al., 2012; Zhang et al., 2012; Ojani et al., 2012; Zhang et al., 2008). TiO_2 and ZnO are considered as semi-conductors with a wide band gap (E_g = 3.2 eV and 3.4 eV for TiO_2 anatase and ZnO, respectively). Titanium dioxide remains one of the most promising materials due to its high oxidation efficiency, non-toxicity, high photostability, chemical inertness and environmentally friendly nature (Zhang et al.,

2010; Ouyang et al., 2012; Valentin et al., 2007). Another advantage of TiO_2 is its low cost owing to the abundance of Ti (0.44% of the earth crust) (Robert, 2007; Westerhoff et al., 2011). With worldwide resereve in excess of 600 million tons, the annual production of Ti metal is approximately 90 000 tons and the annual production of TiO_2 is around 4.3 million tons (Westerhoff et al., 2011). Previous research (Daghrir et al., 2012a; Mills and Le Hunte, 1997; Agrios and Pichat, 2005; Li et al., 2000) have shown that the TiO_2 semiconductor is an excellent photocatalyst that can under UV irradiation mineralize a large range of refractory organic pollutants such as herbicides, dyes, pesticides, phenolic compounds among others. TiO_2 could be activated under UV irradiation having a wavelength lower than 387 nm due its large band gap (3.0-3.2 eV). Such an oxide absorbs only a small fraction of solar light (less than 5% of solar energy is emitted as UV irradiation) (Ren et al., 2007). This major drawback limits the TiO_2 application for large scale. Owing to the successful results at the laboratory scale, TiO_2 material merits further research, in particular concerning the better environmental applications at large scale.

Recently, the development of new TiO_2 photocatlyst by extend the absorption of the wavelength range into the visible light region has received a great interest (Ouyang et al., 2012; Valentin et al., 2007; Robert, 2007; Wang and Lewis, 2006; Sakthivel et al., 2004). The scientists are exploring methods to modify titanium dioxide by shifting its optical response to the visible range. Impurities doping of TiO_2 (either cations or anions) is one of the typical approaches that has been applied by several research works to extend the spectral response to visible light region (Zhang et al., 2012; Valentin et al., 2007; Wang and Lewis, 2005; Chen et al., 2007; Park et al., 2006). For example, the doping of carbon (Khan et al., 2002; Irie et al., 2003; Choi et al., 2004), nitrogen (Asahi et al., 2001; Burda et al., 2003; Diwald et al., 2004) and sulfur (Ohno et al., 2003; Umebayashi et al., 2002) in TiO_2 can lower its band gap and shift its optical response to the visible light range. Another approach is to couple TiO_2 with a

narrow band gap semiconductor (M_xO_y/TiO_2 or M_xS_y/TiO_2) possessing a higher conduction band than that of TiO_2 (Ouyang et al., 2012; Robert, 2007; De Tacconi et al., 2003; Zhang et al., 2009). The common semiconductors used in photocatalyst process are shown in Table 4-1. These new photocatalyst materials (TiO_2/ZnO; TiO_2/CdS; TiO_2/WO_3, TiO_2/CdSe etc) ensure to extend light absorption toward the visible light and prevent the fast recombination of exited electron/holes during photocatalytic and photoelectrocatalytic processes (Ouyang et al., 2012).

Despite the extensive knowledge assembled by the scientists around the world showing the importance of the topic, there are a number of key questions which need to be answered: (i) the electronic structure of doped TiO_2 or coupled TiO_2 with others materials; (ii) the advantages and the drawbacks of each one, their efficiency; (iii) and their expansive environmental applications at large scale. To this end, the present review aims to provide a comprehensive analysis of the electronic and structural properties of the TiO_2 photocatalyst, review the recent progress of the photocatalytic efficiency of doped TiO_2 or coupled TiO_2 semiconductors and to evaluate their potential applications in environmental field.

Tableau 4-1 Common semiconductor used in photo-catalysis process

Semi-conductor	Band gap (eV)	Wavelength (nm)	Light absorption	Valence band (V vs NHE)	Conduction band (V vs NHE)
TiO_2	3.2	387		+3.1	-0.1
SnO_2	3.8	318		+4.1	+0.3
ZnO	3.2	387	UV	+3.0	-0.2
ZnS	3.7	335		+1.4	-2.3
WO_3	2.8	443		+3.0	+0.4
CdS	2.5	496	Visible	+2.1	-0.4
CdSe	2.5	729		+1.6	-0.1

4.4 Electronic and structural properties of TiO_2

Due to its excellent chemical and physical properties, titanium dioxide has gained a great success for environmental applications (Yun et al., 2008; Yu et al., 2009; Wang et al., 2009). In 1972, Fujishima and Honda were the first to propose the photocatalytic splitting of water on TiO_2 electrode. Since this discovery, TiO_2 has become the most suitable semiconductor, and research works increasingly focused over the years to enhance its efficiency in the environmental applications (Fang et al., 2011; Fujishima and Honda, 1972). Belong to the family of semiconductors, TiO_2 is classified as photocatalyst where two reactions were occurred simultaneously: (a) oxidation reactions from the photo-generated holes on the valence band and (b) reduction reactions from photo-generated electrons on the conduction band (Leary and Westwood, 2011). Among other semiconductors, one of the key advantages of the TiO_2 is that it allows simultaneously the reduction of the protons (E_{NHE} (H^+/H_2) = 0.0 eV) and the oxidation of water (E_{NHE} (O_2/H_2O) = 1.23 eV) (Figure 4-1) (Hernàndez-Alonso et al., 2009). More specifically, the redox potential of the donor species (E° (O_2/H_2O) = 1.23 V) adsorbed on the TiO_2 photocatalyst is more negative than the potential of the TiO_2 valance band (+2.5 V/ENH at pH 7), whereas the redox potential of the acceptor molecules (E° ($O_2/O_2°$) = -0.33V) is more positive than the potential of the TiO_2 conduction band (-0.52 V/ENH at pH 7) (Hernàndez-Alonso et al., 2009; Carp et al., 2004).

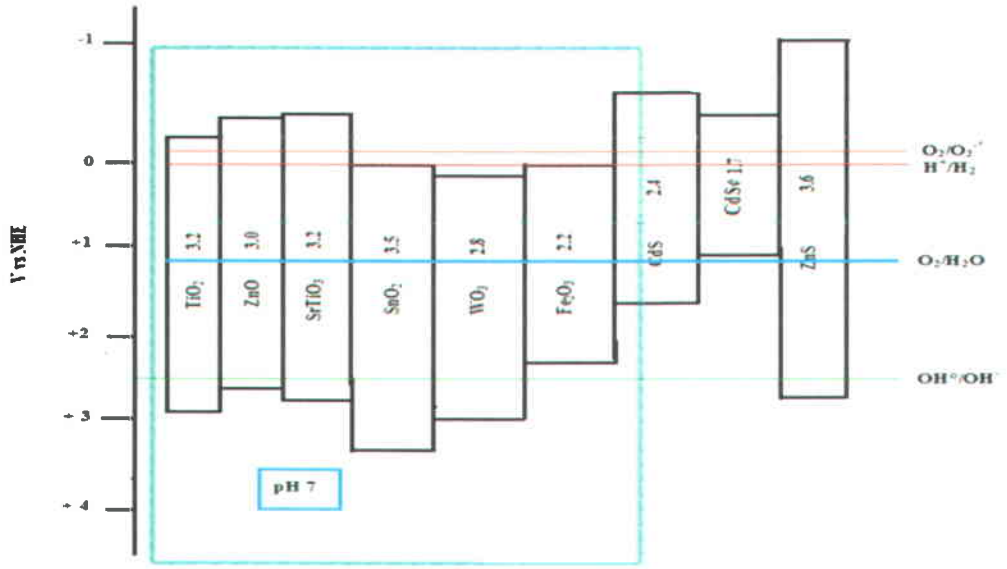


Figure 4-1 **Band gap and redox potential for different semiconductors using the normal hydrogen electrode (NHE).**

The presence of small amount of oxygen vacancies which are compensated by the presence of Ti^{3+} centers classes TiO_2 as n-type semi-conductor (Hernàndez-Alonso et al., 2009). In the TiO_2 material, the lower part of the conduction band is formed by the 3d orbitals of Ti^{4+}, while the valence band is mainly formed by the overlapping of the oxygen 2p orbitals. Titanium dioxide exists in three different crystal forms: anatase, rutile and brookite (Diebold, 2003; Tanemura et al., 2005). Anatase and rutile are the most studied forms of nanostructured TiO_2, whereas brookite forms are still scarce (Rivera et al., 1993; Ye et al., 1997; Thiruvenkatachari et al., 2008; Kitazawa et al., 2006). In fundamental studies, the rutile TiO_2 is the most explored, whereas the anatase TiO_2 is the most investigated form in the applied

studies (Fang et al., 2011). According to previous research (Chen and Mao, 2007; Fujishima et al., 2008), TiO_2 anatase form plays a central role in the industrial applications such as photonic crystals, photocatalytic process, photovoltaic cells, and photo/electrochromics among others. It has been found by Ohtani et al., (1997) that the anatase structure has higher photocatalytic activity than the rutile one. Most researchers in the field argue that the physical properties of TiO_2 such as crystal structure (anatase or rutile), crystal size distribution, surface hydroxyl group density, surface roughness and so on, influence the photocatalytic activity (Ohtani et al., 1997; Lee and Kim, 1993). In the morphology of TiO_2 rutile, the dominant faces are (110), (100) and (101), whereas (011) and (001) are the dominant faces in the morphology of TiO_2 anatase (Wang and Lewis, 2006). Rutile is the thermodynamically most stable phase (Dunnill et al., 2012). The (110) face of TiO_2 rutile has the lowest energy and it is the most intensely studied surface (Tanemura et al., 2005). By comparison, theoretical studies (Fang et al., 2011) show that the surface (001) of anatase TiO_2 is much more reactive, since it largely affects the stability, the adsorptive properties and the catalytic reactivities of TiO_2 anatase form. Upon heating, the TiO_2 anatase is transformed into rutile (Kitazawa et al., 2006). Anatase form can be easily synthetized at lower temperature (below 400°C), whereas rutile form is frequently synthetized at moderate temperature (from 400°C to 600°C) (Hernàndez-Alonso et al., 2009; Chen and Mao, 2007). Besides, the crystalline structure of rutile and anatase TiO_2 are both tetragonal. The tetragonal anatase structure contains 12 atoms per conventional unit cell compared to the tetragonal rutile structure which contains only 6 atoms per conventional unit cell (Wang and Lewis, 2006). According to Fujishima et al. (2000), the octahedral of TiO_2 rutile are slightly orthorhombic and each octahedron is connected to 8 surrounding octahedrons, while those of TiO_2 anatase are distorted orthorhombic and each octahedron is connected to 10 surrounding octahedrons. These differences in lattice structures are responsible for the different mass densities and electronic

band structures between the two forms of TiO_2 (anatase and rutile) and consequently could contribute to higher photocatalytic efficiency for anatase form under UV irradiations (Fang et al., 2011; Ma and Tu, 2011). The most reason for the low conversion efficiency of TiO_2 under visible light is due to the width of the band gap which is 3.2 eV and 3.0 eV for the anatase and rutile phase, respectively (Leary and Westwood, 2011). This relatively wide band gap means that both TiO_2 forms could be stimulated only under UV irradiation. According to Egerton and Christensen (2004), the rutile form of TiO_2 absorbs until 405 nm, while the anatase form absorbs until 385 nm (Figure 4-2). Thus, the development of TiO_2 photocatalyst able to adsorb visible light region of the spectrum requires (i) engineering the band-gap to less than 3.0 eV; (ii) suitable potentials of the conduction and/or valence band edges and (iii) higher mobility of the charge carriers within in the valence and the conduction bands (Zhang et al., 2009).

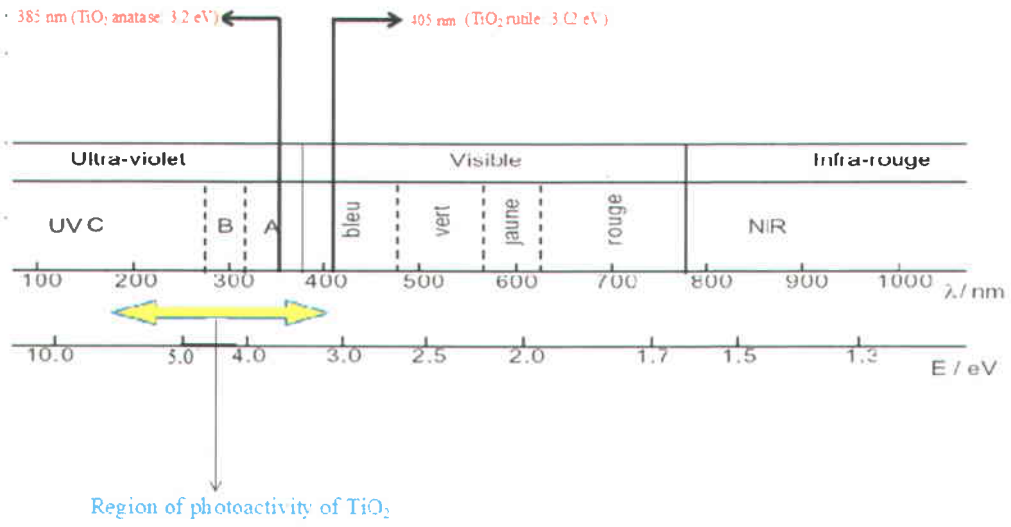


Figure 4-2 UV region for photoactivity of TiO_2

4.5 Doping TiO_2

To extend the spectral response of TiO_2 into the visible region and to enhance its photocatalytic activity, several strategies have been developed (Zhao et al., 2004; Liu et al., 2006). Doping pure TiO_2 with either anions or cations is one ways for sensitizing TiO_2 to visible light (Zhang et al., 2012; Wang and Lewis, 2006; Teh and Mohamed, 2011). This route promotes the use of the main part of the solar spectrum and also to ensure the charge traps to keep electron-hole photogenerated separate (Fujishima et al., 2008). The recent photocatalytic applications using TiO_2 doped with cations and anions are summarized in Table 4-2 and Table 4-3, respectively.

4.5.1 Cations doping of TiO_2

Titanium dioxide doped with cations such as rare earth metals, noble metals, poor metals and transition metals have been widely investigated (Teh and Mohamed, 2011; Yalcin et al., 2010). According to previous research (Yalcin et al., 2010; Zhang et al., 2009; Robert, 2007), the metallic ions doped TiO_2 widen the light absorption range, increase the redox potential of the photogenerated radicals and enhance the quantum efficiency by inhibing the recombination of the electrons and holes photo-generated on the conduction and valence bands, respectively. However, the nature and the concentration of dopant, the length of the induced space charge layer as well as photocorrision process change the properties at the surface of the materials and consequently influence the photocatalytic activity (Carp et al., 2004). This phenomenon has been demonstrated for example by Karakitsou and Verykios (1993). The concentration and the valence of the doping cations (In^{3+}, Zn^{2+}, W^{6+}, Nb^{5+}, Li^{+}, etc) influenced the enhancement or the reduction of the photocatalytic activity.

Although there are a large of number of research (Zhu et al., 2006; Ghicov et al., 2007) that demonstrate how metal ion doping TiO_2 improve the visible light absorption properties of the

material. It should be also mentioned that the increase of the visible light absorption is not a sufficient condition to promote the photoactivity of doped TiO_2 (Zhang et al., 2009; Dunnill et al., 2012; Gracia et al., 2004). Indeed, during the implantation of cations, a certain amounts of defects could be created and acted as recombination centers which decrease the photocatalytic activity. This adverse effect could be avoided by reannealing the doped TiO_2 (Zhang et al., 2009). Besides, another feature of TiO_2 doped with metals cations has been mentioned by Dunnils et al. (2012). Doping TiO_2 with cations having either higher or lower oxidation state promotes the increase in the electrical conductivity. For instance, in the case of doping TiO_2 with metallic cations having lower oxidation state (Fe^{3+} in low concentration), the electro-neutrality was achieved by removing electrons from the valence band (Bally et al., 1998). The hopping of the electrons creates holes in the valence band of the system and increases the electrical conductivity (conduction p-type). By comparison, in the case of doping TiO_2 with metallic action having higher oxidation rate such as Nb^{5+}, electro-neutrality in the system was achieved by injection of the electrons into the conduction band already empty (Furubayashi et al., 2005). These electrons which passed into the conduction band increase the electrical conductivity (conduction n-type).

4.5.1.1 Doped TiO_2 with rare earth metals

Rare earth metals including Scandium (Sc), yttrium (Y) and the 15 Lanthanoids are a group of 17 chemical elements in the periodic table. According to Teh and Mohamed (2011), these metals having incompletely occupied 4f and empty 5d orbitals could be used as catalyst or to promote catalysis. Various studied have been extensively incorporated rare earth elements into the TiO_2 matrix for improving the photoactivity (Stengl et al., 2009; Xu et al., 2009; El-Bahy et al., 2009). Research carried out by Fan et al. (2006) showed that the cerium (Ce) doped TiO_2 (mixture of anatase and rutile) is able to retard the development of the grain size of TiO_2, to decrease its crystallite size (increase the specific surface area), hence improving

the photocatalytic activity. Besides, the redox pair of Ce (Ce^{3+}/Ce^{4+}) could act as an electron scavenger which trap the bulk electrons into TiO_2 and lead to an increase in the performance of the photocatalytic activity (Teh and Mohamed, 2011). It was also concluded that the amount of Ce significantly influence the photocatalytic activity. When the content of doping is excessively high, the space charge region becomes narrow and the penetration depth of light exceeds the space charge layer. Thus, the recombination of the photo-generated electron–hole pairs becomes easier, which lead to reduce the photocatalytic activity (Stengl et al., 2009). Higher photocatalytic activity of gadolinium (Gd) doped TiO_2 has been also recorded by El-Bahy et al. (2009) compared with pure TiO_2. Results recorded by El-Bahy et al. (2009) show also that Gd^{3+}/TiO_2 prepared by sol gel method has lowest band-gap and particle size and highest surface area and pore volume. It was found by Teh and Mohamed (2011) that a higher surface area promotes the adsorption of more reactant molecule on the surface of the photocatalyst and consequently avoids the recombination of the electron-hole photogenerated. The lowest crystallite size increases the specific surface area of the photocatalyst, promotes the shifting of photogenerated carriers to the surface of the photocatalyst and enhances the interaction with reactant molecules (Shi et al., 2009).

Others rare earth elements such as neodymium (Nd) (Stengl et al., 2009; Xu et al., 2009) and holmium (Ho) (Shi et al., 2009) have been also used for doping TiO_2. According to Stengl et al. (2009), the higher photocatalytic activity in rare earth metals was mainly due to the transition of 4f electrons, which led to decrease the energy band gap by allowing the transfer of charge between the TiO_2 valence/conduction band and the 4f level in rare earth ions (Xu et al., 2009).

4.5.1.2 Doped TiO_2 with noble metal

Nobel metals including osmium (Os), palladium (Pd), ruthenium (Ru), rhodium (Rh), silver (Ag), iridium (Ir), platinum (Pt) and gold (Au), have high resistance to corrosion and oxidation in moist air, unlike most base metals (Teh and Mohamed, 2011). Their precious nature derives from their rarity in the earth's crust. It has been reported by Grabowska et al. (2010) that noble metals such as platinum, palladium, silver, and gold ions allow to extend the light absorption of TiO_2 band gap semiconductor to the visible light. The Effect of noble metal (Pt and Au) doped TiO_2 photocatalyst has been recently investigated by Dozzi et al. (2012) for the degradation of formic acid. Kich and co-worker also investigated the photocatalytic degradation of 4-chlorophenol under visible irradiation of TiO_2 modified with chloride complexes of Pt. The presence of noble metals nanoparticles contributes in increasing the separation of photo-generated charge carriers, and consequently improves the photocatalytic performances on the surface and bulk modified photocatalyst systems. According to Yoon et al. (2005), the surface of noble metal serves as visible light absorbing sensitizers and centers of charge separation.

In addition, the effect of silver (Ag) doped TiO_2 has been largely studied by several research (Seery et al., 2007; Tomas et al., 2009; Binitha et al., 2009). The addition of amounts of silver enhances the photocatalytic activity of TiO_2 and thus, increase the rate of degradation of rhodamine 6G dye (Seery et al., 2007), methylene blue (Tomas et al., 2009) and methyl orange (Binitha et al., 2009; You et al., 2005). The photocatalytic activity improvement of silver (Ag)-doped TiO_2 was mainly attributed to the increase of specific surface area which promotes more reactive sites available to take part in photoreactions (Teh and Mohamed, 2011). On the other hand, doping TiO_2 with Ag retards the recombination rate of electron-hole pair by enhancing the charge carrier separation and hence improves the photocatalytic activity (Seery et al., 2007; Tomas et al., 2009). It has been reported by Sobana et al. (2006)

and Xin et al., (2005), that Ag nanoparticles deposited on TiO_2 act as electron traps, enhances the electron-hole separation and ensure afterwards the transfer of the trapped electron to the adsorbed O_2 acting as an electron acceptor.

4.5.1.3 Doped TiO_2 with transitions metals

According to the IUPAC definition, transition metal is an element whose atom has an incomplete d sub-shell or which can give rise to cations with an incomplete d sub-shell. A number of research groups have doped TiO_2 with transition metals such as iron (Ambrus et al., 2008), cobalt (Subramanian et al., 2008), nickel (Martinez et al., 2006), manganese (Mohamed et al., 2007), chromium (Wu et al., 2004), vanadium (Tsuyumoto and Nawa, 2008), copper (Li et al., 2008), zinc (Wang et al., 1997), zirconium (Venkatachalam et al., 2007; Lippens et al., 2008) among others, in the attempt to create shift of the band gap energy and to extend the spectral response of the TiO_2 to the visible light region. According to previous studies (Zhang et al., 2012; Zhang and Zeng, 2011; Hsieh et al., 2009), doping TiO_2 with transition metals tunes the electronic structure, shifts the light absorption region from UV to visible light, thus enhancing the photocatalytic activity of TiO_2. The shift of the absorption edge to the visible light region is caused by the charge-transfer transition between the d electrons of the transition metals and the conduction or the valence band of TiO_2 (Teh and Mohamed, 2011). Such metal creates a new electron state inside the electronic structure of TiO_2, which can capture the excited electrons from the TiO_2 valance band and prevents as possible the recombination of charge carriers (Kment et al., 2010; Di Paola et al., 2002).

However, the type of the transition metal, its concentrations and the microstructural characteristics of the catalyst are the mains factors that influence the photocatalytic degradation of various substrates under visible region (Kment et al., 2010). It has been found by He et al., (2002), that there is a critical doping concentration which influences the

photocatalytic activity. The further increase in dopant concentration could increase the recombination of the charge carriers (e^-/h^+), thus lowering the photoactivity of TiO_2. For instance, it has been reported by He et al., (2002) that a suitable amount of dopant Ag (2-4 mol %) could effectively increase the photocatalytic activity of the TiO_2 film. It has been also showed by Karakitsou and Verykios (1993) that doping TiO_2 with transition metals having a valency higher than + 4 could increase the photoreactivity, while others studies (Mu et al., 1989) showed that doping TiO_2 with trivalent or pentavalent metal ions decrease the photoreactivity of TiO_2 even under UV irradiation. The transition metals which exhibit two or more oxidation states usually ensure an enhancement in the TiO_2 photocatalytic activity (Sun et al., 2009). For instance, iron (Fe) with different ion forms (Fe^{4+}, Fe^{3+} and Fe^{2+}) acts as traps for the electron-hole pairs and consequently inhibits their recombination (Figure 4-3) (The and Mohamed, 2011). On the other hand, the radius of Fe^{3+} (0.79 A°) is similar to that of Ti^{4+} (0.75 A°). This trait promotes the easy incorporation of Fe^{3+} ions into the crystal lattice of TiO_2 (Zhang et al., 1998; Wang et al., 2009). Research group of Asilturk's et al. (2009) studied also the effect of Fe^{3+}doped TiO_2 photocatalyst. It was found that Fe^{3+} doping TiO_2 prevents the agglomeration of the particles, forming well nanocrystalline particles with high surface area and, thus ensuring high photocatalytic efficiency. Among a great variety of transition metal ion dopant investigated previously (Wu et al., 2009; Melghit et al., 2009; Fuerte et al., 2001), Fe^{3+} having band-gap of 2.6 eV has been found to be the best candidate to enhance the photocatalytic activity, while some research groups (Adan et al., 2007; Li et al., 2008) have found that the presence of this cation in TiO_2 is detrimental for the photocatalytic degradation reactions of organic pollutants in aqueous systems. Due to the widely varying experimental conditions, it remains so difficult until this time to make direct comparison between metal transitions doping TiO_2 and to unify conclusions.

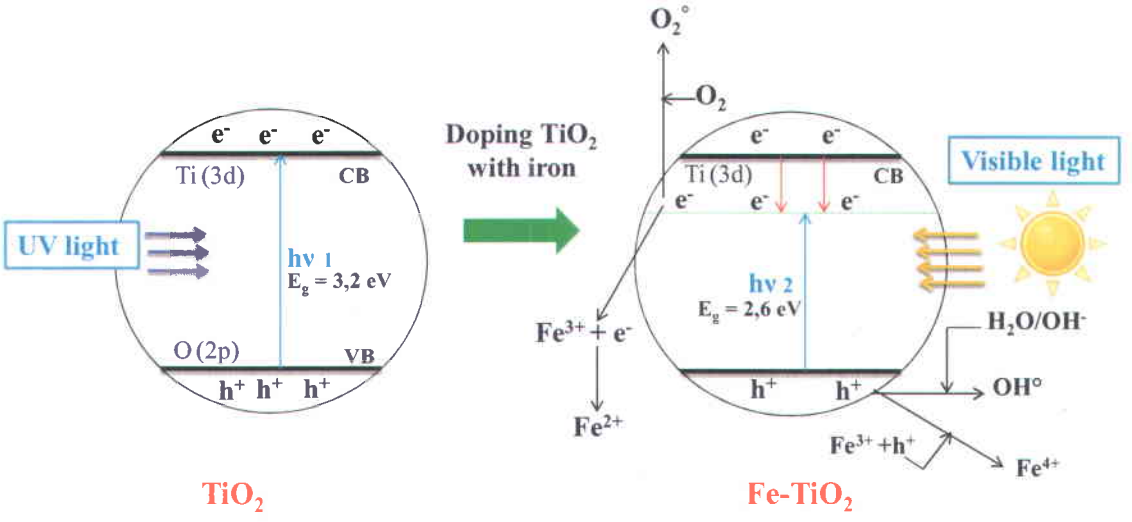


Figure 4-3 Schematic energy level of iron doping TiO_2.

4.5.1.4 Doped TiO_2 poor metals

Otherwise, Poor metals known post transition metals are the metallic elements in the p-block of the periodic table, situated between the metalloids and the transition metals (including groups 13, 14 and 15). A characteristic of the poor metals is that they have lower melting and boiling points than the transition metals; they are also softer and have a higher electronegativity. Compared to the metalloids in the same raw (Bore (B), Silicium (Si), Germanium (Ge), Arsenic (As), etc), post transition metals have significantly higher boiling points. Post transition metals including aluminum (Al), gallium (Ga), indium (In), tin (Sn), thalium (TI), lead (Pb) and bismuth (Bi), are a group of 7 chemical elements in the periodic table (Teh and Mohamed, 2011). Aluminum is a silvery-white chemical element and is one of

the most abundant metal found in the earth's crust. In nature, it doesn't occur in metallic form but is found with soils, clays and rocks. It can be found also in vegetation and in all of the earth's water. According to research study conducted by Choi and Depero (Choi et al., 2007; Depero et al., 2000), doping TiO_2 with aluminum shows retardation of TiO_2 phase transformation from anatase to rutile by stabilizing the surface state of TiO_2 particles and also inhibits grain growth. Liu and his co-workers (2010) also studied the effect of Al-doped TiO_2 photocatalysts. They found them to be promising photocatalyst where they show (Al-doped TiO_2) excellent photodegradation behavior for Congo Red.

Recently, Bismuth (Bi) is another example of post transition metal which has received a great attention for doping TiO_2 (Ji et al., 2009; Xu et al., 2002; Zuo et al., 2007). Compared to the undoped TiO_2, Bi doping TiO_2 can enlarge the wavelength response range and also intrinsically narrows the band gap transition of the catalyst, hence enhancing the photocatalytic activity under visible light for degradation of methylene blue (Ji et al., 2009). Bi doped TiO_2 has proved an effective way to increase the photocatalytic activity for the degradation of different organic pollutants. Under visible light, higher mineralization of Sulforhodamine-B (61.6% of TOC removal) and higher degradation rate of rhodhamine B (more than 90% at 0.25% of Bi-TiO_2) have been recorded by Jiang et al. (2010) and Li et al. (2009), respectively. The incorporation of Bi induces the Bi^{4+}/Bi^{3+} species, which trap the electrons and thus ensure the separation of the electron-hole pairs (Li et al., 2009). Besides, research conducted in the last years (Jiang and Dou, 2011; Sui and Young, 2010; Tu et al., 2009) show that a suitable amount of tin (Sn) doping TiO_2 could be an effective way to increase the photocatalytic activity. For example, as reported by Zheng et al. (2002), the photocatalytic activity of TiO_2 thin film in the degradation of rhodamine B dye was efficiently improved by Sn implantation, whereas the photocatalytic activity of Sn doped TiO_2 was doubled for the degradation of toluene in the gas phase (Fresno et al., 2006). The

incorporation of Sn into the TiO_2 lattice has been shown to be very effective because of the similar ionic radius of the two metals ($Sn_{(IV)}$ = 0.71 A°; $Ti_{(IV)}$ = 0.68 A°) (Sui et al., 2010). Doped Sn^{4+} inhibits the phase transformation of TiO_2 from anatase to rutile, decrease the diameter of TiO_2 photocatalyst and enhance significantly the photoctalytic activity. According to Sui et al. (2010), the Sn^{4+} doped into TiO_2 exerts a synergistic effect on their photocatalytic activity.

4.5.2 Drawbacks of cations doping of titanium dioxide

As discussed in the previous section, doping TiO_2 with metallic cations has shown positive effects on photocatalysis. However, several authors (Nah et al., 2010; Qiu and Burda, 2007; Wang and Lewis, 2006; Choi et al., 1994), have reported that metal doping TiO_2 have also considerable drawbacks. The photocatalytic activities of a cation-doped TiO_2 decrease even under UV irradiation. The metals doped materials have been shown to suffer from thermal instability and the metals centers act as an electron traps which encourage the recombination of the photogenerated electrons/holes pairs (Burda et al., 2003; Di Paola et al., 2001). It has be reported by Lu et al. (2007), that the cationic dopant could be localized in the d-level deep of TiO_2 band gap which serve as carriers recombination centers leading to decrease the photocatalytic activity. For instance, Gallium (Ga^{3+}), chromium (Cr^{3+}) and aluminum (Al^{3+}) known as acceptor centers (p-type doping agents) act as a trap for photogenerated electrons and promote the easy recombination with the positive holes. On the opposite, n-type doping agent such as niobium (Nb^{5+}), antimony (Sb^{5+}) and tantalum (Ta^{5+}) known as donor centers, act as trap for photogenerated holes, ensure the attraction of the electrons and thus promoting the recombination of e^-/h^+ (Teh and Mohamed, 2011; Matos et al., 2007). In noble metals, the difference between the Fermi level of noble metals and that of titania is ascribed to the electron-hole pairs separation. Yet, once the metal centers become negatively charged, hole will be attracted especially for highly loaded samples (more than 5%) and the recombination

is favored. Current research support the conclusion that the desired TiO_2 band gap narrowing of TiO_2 can be better achieved using anionic dopant rather than cationic dopant (Asahi et al., 2001; Burda et al., 2003; Yu et al., 2002).

4.5.3 Anions doped TiO_2

Recently, various approaches have been made in the bid to hinder the recombination of the photogenerated electron-hole pairs. Doping TiO_2 with anionic nonmetals such as carbon (C) (Wang and Lewis, 2005; Khan et al., 2002; Irie et al., 2003; Choi et al., 2004), nitrogen (N) (Valentin et al., 2007; Asahi et al., 2001; Sakthivel and Kisch, 2003; Lindgren et al., 2003 ; Yang and Gao, 2008), sulfur (S) (Ohno et al., 2003; Umebayashi et al., 2002; Umebayashi et al., 2002) and iodine (I) (Hong et al., 2005) have received much attention. Compared to cations doping, their role as recombination centers might be minimized (Wang and Lewis, 2006; Chen et al., 2007). Tan et al. (2011) show that nonmetal dopant have the ability to improve the morphology and the photocatalytic performance of TiO_2, whereas Ren et al. (2007) showed that the anionic metals doping TiO_2 can lower its band gap and shift its optical response to the visible light region. Over the last several years, it has been demonstrated by many researchers that TiO_2 doped with non-metal elements (carbon, sulfur, fluorine, nitrogen, etc) show positive effect in the visible region and higher photocatalytic activity. The impurity states are near to the valence band edge but don't act as charge carriers (Ren et al., 2007; Wang and Lewis, 2005; Yu et al., 2002; Liu et al., 2009). Among all the anions, the doping TiO_2 with carbon or nitrogen has been found to ensure higher photocatalytic activity under visible light irradiation (Chen et al., 2007).

Significant attention has been directed towards the carbon doping TiO_2 (Leary and Westwood, 2011; Rehman et al., 2009; Shen et al., 2006). The substitution of carbon atom in the TiO_2 photocatlyst introduces new states (C 2p) close to the valence band edge of TiO_2 (O 2p).

Accordingly, the conduction band edge shifts to narrow the band gap. The incorporation of carbon into TiO_2 may form carbonaceous species at the surface of the photocatalyst which are reported to facilitate the absorption in the visible light (Rehman et al., 2009; Wong et al., 2008). Furthermore, the high surface area of the doped sample is another factor that increases the photocatalytic activity of the C-doped TiO_2 (Teh and Mohamed, 2011). The higher surface area provides more reactive sites and promotes the adsorption of more target pollutants. Shen and his co-workers (Shen et al., 2006) reported that C-doped TiO_2 appears to be much efficient to degrade trichloroacetic acid under visible light irradiation than pure TiO_2. The electron excited from these surface states (C-doped TiO_2) had the ability to form sufficient of $O_2^{\circ-}$ and OH° radicals under visible irradiation and consequently to ensure higher degradation and mineralization of pollutants.

On the other hand, doping TiO_2 with nonmetals like nitrogen has received nowadays a specific attention (Rehman et al., 2009; Asahi and Morikawa, 2007; Peng et al., 2008; Guo et al., 2012; Peng et al., 2008; Viswanathan and Viswanathan, 2012; Long and Cai, 2011). The photocatalytic proprieties of N-doped TiO_2 under visible light show a promising extension for environmental application where the conventional TiO_2 is not used (Viswanathan and Viswanathan, 2012). Doping Nitrogen into titania changes the refraction index, hardness, electrical conductivity, elastic modulus and the photocatalytic activity towards visible light absorption (The and Mohamed, 2011; Peng et al., 2008; Wong et al., 2006; Ao et al., 2009). The nitrogen species resulting from the TiO_2 doping could be either substitutional or interstitial N atom in the TiO_2 matrix. The substitutional species are most localized above the valence band, whereas the interstitial form is present at 0.73 eV above the valence band (Asahi and Morikawa, 2007). By comparison to ZnO, nitrogen has the ability to simultaneously substitute both O and Ti sites in TiO_2 to form $Ti_{1-y}O_{2-x}N_{x+y}$ instead of $TiO_{2-x}N_x$ (Rehman et al., 2009; Peng et al., 2008). According to Guo et al. (2007), it is so difficult

to make the substitution of O by N because the ionic radius of N (1.71 A°) is so greater compared to that of O (1.4 A°). Thus, to maintain the electroneutrality and to form an oxygen vacancy, three oxygen atoms should be replaced by two nitrogen atoms. In the presence of nitrogen impurities in titania, the energy of oxygen vacancies is reduced from 4.2 to 0.6 eV, indicating hence that nitrogen favors the formation of oxygen vacancies (Valentin et al., 2007; Di Valentin et al., 2005). As shown in Figure 4-4, these oxygen vacancies promote the absorption in the visible region (from 400 nm to 600 nm) and ensure the activation of N-doped TiO_2 (E_g = 2.5 eV) under visible light. For instance, research of Peng et al. (2008) and Ao et al. (2009) showed that N-doped TiO_2 has a narrower energy band gap and can be activated under visible irradiations. Under visible light, more electrons and holes are generated and promote the photocatalytic redox reactions.

Asahi research group suggested that the N_{2p} level could mix with O_{2p} which results in the narrowing of the band gap and enhancing the photocatalytic activity (Asahi et al., 2001). However, recent experimental and theoretical researches show that the formation of the localized midgap state above the top of the valence band is responsible to increase the photoactivity of TiO_2 in visible region (Zhang et al., 2010). Yet, the localized midgap would decrease the oxidation power of the photogenerated hole compared to that of pure TiO_2. Likewise, the formation of oxygen vacancies in the bulk usually resulting from the doping of N into the lattice of TiO_2, could act as recombination centers for carriers which decrease the photocatalytic efficiency (Zhang et al., 2010). Another problem with N-doped TiO_2 is the low concentration of nitrogen used for doping TiO_2. Compared to carbon-doped TiO_2, there is no significant energy shift (< 0.05 eV) in the valence band edge for higher concentration of nitrogen (5.2%). The significant shift of band gap (2.55 eV) is only observed in the lower nitrogen doping concentration (0.52%) (Wang and Lewis, 2006). At the same time, the decrease in N concentration at the surface layer after photoelectrolysis of water under visible

light irradiation could worse the stability of N-doped TiO_2 and consequently decreases the photocatalytic activity (Kitano et al., 2006). A deactivation of N-doped TiO_2 has been observed by Nosaka et al. (2005) during the oxidation of 2 propanediol under visible irradiation. This is mainly due to the loss of N concentrations.

Furthermore, it has been also observed that the techniques or the preparation methods employed for doping N into TiO_2 influence the state of N in titania and its effectiveness in the visible light absorption (Rehman et al., 2009; Viswanathan and Krishanmurthy, 2012). Thus, it is very important to choice the appropriate preparation methods for N doping TiO_2 which promote extending of the light absorption and to ensure higher photocatalytic efficiency.

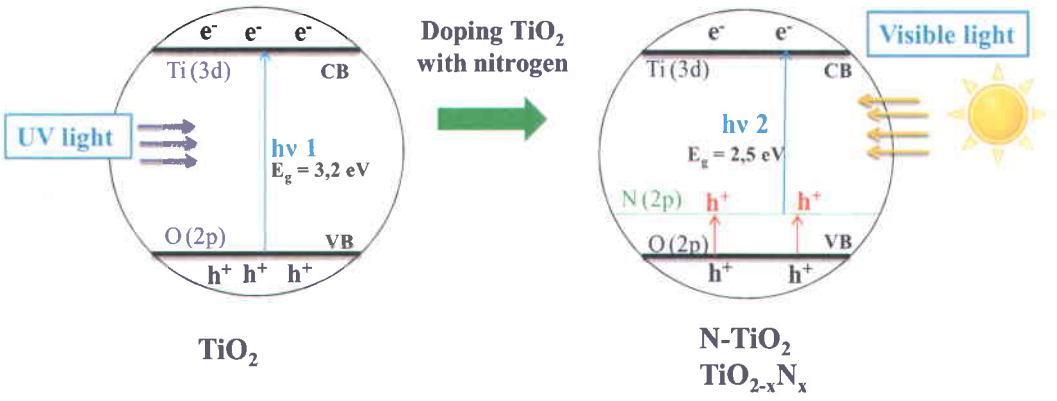


Figure 4-4 Schematic energy level of nitrogen doping TiO_2.

In addition to nitrogen and carbon doping, sulfur and fluorine have been successfully used for TiO_2 doping (Yu et al., 2002; Umebayashi et al., 2003; Liu et al., 2009). Fluorine atoms (1.33 A° for F^-) could easily substitute for O atoms (1.4 A° for O^{2-}) owing to their similar ionic radius (Rehman et al., 2009). Fluoride ions have been detected not only at subtitutional sites in the lattice but also physically adsorbed on the surface of nanoparticles doped TiO_2 (Yu et al., 2002; Todorova et al., 2008).

By comparison, sulfur can be used as anion for doping TiO_2 by substituting O sites (Ohno et al., 2003) and also as cation by replacing Ti^{4+} in the bulk (Wang et al., 2008) or at the surface (Zhou et al., 2008; Wei et al., 2008). The substitutional doping of S into the TiO_2 distorts the crystal lattice because the ionic radius of S (1.8 A°) is so greater compared to that of O (1.4 A°) (Zhang et al., 2009; Rehman et al., 2009). The incorporation of an S_{3p} band above the valence band edge shifts the ban gap and ensures higher photocatalytic efficiency (Rehman et al., 2009). Furthermore, it was found that S-doped TiO_2 is able to extend the photocatalytic activity to the visible region and to ensure excellent photocatalytic degradation of organic pollutant under visible irradiation (Umebayashi et al., 2003; Liu et al., 2009). For instance, higher degradation of Trichloroethylene (80%) and methyl-tertiary butyl ether (75%) have been recorded by Jo and Yang (2010) when S-doped TiO_2 (weight of S = 2.6 mg cm^{-2}) has been used under daylight irradiation (1.8 mW cm^{-2}). By incorporating sulfur into TiO_2, it is also possible to modifie the ratio of anatase and rutile and to improve the photocatalyst efficiency of doped TiO_2 under visible irradiation (Hamadanian et al., 2009; Ho and Yu, 2006). According to Tian et al., (2009), the anatase/rutile phase composition ratio was strongly influenced by the amount of sulfure. By increasing the amount of S (doping TiO_2 with 1.5% of sulfure), the phase composition ratio is enhanced.

Despite the several advantages achieved by doping TiO_2 with non metal anionic, researchers have found that the content of dopant would decrease during the annealing process, thus

reducing the photoactivity under visible radiation (Teh and Mohamed, 2011). This major drawback limits the incorporation of non metallic anion for doping TiO_2. Others researches focus towards the coupling of two semi-conductors as one way to compensate the drawbacks of doped TiO_2. This approach will be more discussed in the following section.

Tableau 4-2 Removal of organic pollutants in aqueous solution using different type of cations doped TiO_2.

Matrix	Type of polluant	Operating conditions	Results and comments	References
Aqueous solution	4-nitrophenol	1.0 x 10^{-2} mol L^{-1} of 4-nitrophenol; 2g L^{-1} **Fe-TiO_2**; %Fe =0.0-1.00; 5 x 8 W black light fluorescence lamps; Temperature = 22±3°C; pH =5.9±0.2; treatment time = 120 min.	80.05% of nitrophenol removal at 0.25% of Fe doped TiO_2 and after 120 min of treatment time	Yalcin et al., (2010)
Aqueous solution	Rhodamine B	10^{-4} mol L^{-1} Rhodamine B; volume 10 mL; treatment time =140 min; 400W high-pressure mercury lamp (290 nm; 20 mW cm^{-2}); **M/TiO_2 (M= Ag, Zr, Fe)**; distance lamp-reactor =10 cm;	K_{app} (TiO_2) = 5.71 10^3 min^{-1}; K_{app} (TiO_2/Ag) = 10.1 $10^3 min^{-1}$; K_{app} (TiO_2/Zr) = 7.3 10^3 min^{-1}; K_{app} (TiO_2/Fe) = 6.2 10^3 min^{-1}.	Kment et al., (2010)
Aqueous solution	DB53 dye	100 mg L^{-1} of DB53 dye ; pH =2-9; treatment time =5-60 min; xenon lamp at 150 W; λ>320 nm; **Lanthanide ions-doped TiO2 (La^{3+}; Nd^{3+}, Sm^{3+}, Eu^{3+}, Gd^{3+}, Yb^{3+}) = 0.1-0.5 g L^{-1}**; temperature = 25°C.	100% removal of DB53 dye after 40 min at pH 4 and 0.3g/L of photocatalyst loading (Gd^{3+}/TiO_2)	El-Bahy et al., (2009)
Aqueous solution	4-chlorophenol	100 mg L^{-1} of 4-chlorophenol, pH= 5.8; 200 mL min^{-1} oxygen/argon (20 vol% oxygen); **Ce-doped TiO_2 = 0.2-1 g L^{-1}**; medium-pressure mercury UV-visible light (366, 405 and 436 nm); treatment time = 20-180 min.	100% removal of 4-chlorophenol after 120 min of treatment time at 0.6 g/L of Ce/TiO_2 and pH 10	Silva et al., (2009)
Aqueous solution	2,4dichlorophenol	100 mg L^{-1} of 2,4 dichlorophenol; 1000 W tungsten halogen lamp (λ>420 nm); volume= 50 mL; **0.25-5.00 mol %V/TiO_2**; treatment time =8 h	more than 90% removal of 2,4 dichlorophenol after 8h of treatment and 1 mol% of V/TiO_2.	Tian et al., (2009)
Aqueous solution	Methylene blue	12.8 mg L^{-1} of methylene blue, 500 W Xenon lamp (simulate solar light), **1.5-10wt% W^{6+}/TiO_2**, treatment time =60 min.	Around of 35% removal of methylene blue after 60 min of treatment and using 3.0wt%of W^{6+}/TiO_2.	Yang et al., (2009)
Aqueous solution	Malachite Green dye	2.5-5.0 mg L^{-1} of malachite green dye; distance UV lamp-reactor = 20 cm; UV and visible light irradiation; volume = 25 mL; **0.3-0.7 $FeTiO_2$**	80% removal of malachite green dye after 115 min of irradiation time and using 0.3$FeTiO_2$.	Asilturk et al., 2009
Aqueous solution	Rhodamine 6G dye	5 10^{-6} mol L^{-1} of Rhodamine 6G dye; Q-Sun solar test chamber (0.68 W/m^2; 340 nm); volume =50 mL; **1-5 mol% Ag/TiO_2**	The rate of degradation of Rhodamine 6G dye increase from 0.06 min^{-1} for TiO_2 to 0.34 min^{-1} for 5mol%Ag/TiO_2.	Seery et al., (2007)
Aqueous solution	Methylene blue	10^{-5} mol L^{-1} of methylene blue; visible light irradiation (λ>420 nm); **0-0051 mol%Bi/TiO_2.**	More than 60% removal of methylene blue after 180 of irradiation and using 0.051 mol%Bi/TiO_2	Ji et al., (2009)

Tableau 4-3 Removal of organic pollutants in aqueous solution using different type of anions doped TiO_2.

Matrix	Type of polluant	Operating conditions	Results and comments	References
Aqueous solution	Rhodamine B	5 mg L^{-1} Rhodamine B; volume = 100 mL; distance light source-bottom of the solution = 15 cm; temperature = 25°C; treatment time = 5h; visible irradiation ($\lambda > 420$ nm); **C-doped TiO_2**.	59% degradation of rodhamine B (C-doped TiO_2); 29% degradation of rodhamine B (TiO_2 alone)	Ren et al., 2007
Aqueous solution	Methyl Orange	20 mg L^{-1} of methyl orange; volume =100 mL; distance lamp-solution = 30 cm; 12 W light Emitting diode lamp (460 nm); **0-4wt%S doped TiO_2**; treatment time = 5h.	More than 95% removal of methyl orange after 5h and using 0.8wt%S-TiO_2.	Liu et al., 2009
Aqueous solution	Reactive Brillant Red dye X-3B (C.I.Reactive Red 2)	25 mg L^{-1} of X-3B; volume = 200 mL; 250 W halogen lamp (λ>400 nm); **1-2mol%N-doped TiO_2**; treatment time = 2h.	85% removal of X-3B after 2h and using 2 mol%N-TiO_2	Ao et al., 2009
Aqueous solution	Lindane	500 W high pressure tungsten visible lamp ($\lambda > 400$ nm); oxygen flow rate = 300 mL/min; 8.6210^{-5}-5.1710^{-4} mmol; **N-doped TiO_2 (Ti:N ratio = 1:0.4, 1:0.8, 1:1.2, 1:1.6 and 1:2.0)**; treatment time 330-450 min; Volume = 400 mL; temperature = 25-30°C	100% removal of Lindane after 450 min of treatment time and using N-doped TiO_2 (ratio: 1:1.6)	Senthilnathan and Philip, 2010
Aqueous solution	Trichloroethylene and methyl-tertiary butyl ether	0.1-1.0 mg L^{-1} of Trichloroethylene; 0.1-1.0 mg L^{-1} of methyl-tertiary butyl ether; fixed flow rate = 0.5 L min^{-1}; **S-doped TiO_2** (weight of S = 2.6 mg cm^{-2}); **N-doped TiO_2** (weight of N = 2.5 mg cm^{-2}); 8W fluorescent daylight lamp (1.8 mW cm^{-2})	75% removal of methyl-tertiary butyl ether and 80% removal of Trichloroethylene.	Jo and Yang, 2010

4.6 Coupled semiconductor photocatalysts

Coupling between different semiconductors with different energy levels, is another interesting approach which have received a great of interest in the last decade (Robert, 2007; Zhang et al., 2009; Hernàndez-Alonso et al., 2009; Ilieva et al., 2012). In photocatalytic systems, coupling TiO_2 with others semi-conductors was designed to extend the absorption wavelength range into the visible light region and to alleviate the charge carrier recombination in individual photo-electrodes (Ouyang et al., 2012; Robert, 2007). It has been reported by Zhang et al., (2009) that the good matching of the conduction band and valence band of the two semiconductors could ensure an efficient transfer of the charge carriers from one to another. When the large band gap of TiO_2 is coupled with a small band gap semiconductor having more negative conduction band level, the electron can be injected from the small band gap of the semiconductor used as sensitizer to the TiO_2. The energy gap between corresponding band levels ensure the transfer of charge carriers from one particle to its neighbor and promote the separation between the electron-holes photo-generated (Zhang et al., 2009). Figure 4-5 presents semiconductors configuration in which a vectorial transfer of electron-hole photogenerated between corresponding band levels ensure a spatial separation between them. The efficient transfer of electrons and holes photogenerated between TiO_2 and the sensitizer depends on the difference between the conduction band and the valence band potentials of the two semiconductors (Bessekhouad et al., 2004). According to Robert (2007), the efficient transfer of electron between TiO_2 and the sensitizer was occurred when the conduction band of TiO_2 is more anodic than the corresponding band of the sensitizer. Under visible irradiation, only the sensitizer is excited and the electrons photogenerated will flow into the conduction band of the adjacent TiO_2 (Figure 4-5a). On the other hand, if the valence band of the sensitizer is more cathodic than that of TiO_2 one, the holes photogenerated behind in the valence band of the sensitizer (Figure 4-5b). As mentioned in certain number of studies,

the photocatalytic activity of TiO_2 coupled with metal oxides such as CdS (Kannaiyan et al., 2010), SnO_2 (Shang et al., 2004), WO_3 (Ren et al., 2011) and FeO_3 (Kuang et al., 2009). Bi_2S_3 (Bessekhouad et al., 2004) among other has been largely used for improving the process under visible irradiation. For photocatalytic application intended for water and wastewater treatment, the systems M_xO_y/TiO_2 and M_xS_y/TiO_2 are the most widely used (Robert, 2007). The different photocatalytic and photoelectrocatalytic applications using photosensitization system (TiO_2/M_xO_y or TiO_2/M_xS_y) are shown in Table 4-4. TiO_2/CdS is an example of TiO_2/M_xS_y system which has been applied by Zyoud et al. (2010) to ensure the degradation of 75% of phenazopyridine after 60 min of treatment time and using solar simulator lamp (400-800 nm; 0.0212 W cm^{-2}). By comparison, SnO_2/TiO_2 and ZnO/TiO_2 are examples of TiO_2/M_xO_y system which have been applied by Zhang et al. (2009) and Ge et al. (2009), respectively. Higher degradation rate of methyl orange (95% and 98.13%) have been recorded using SnO_2/TiO_2 and ZnO/TiO_2, respectively.

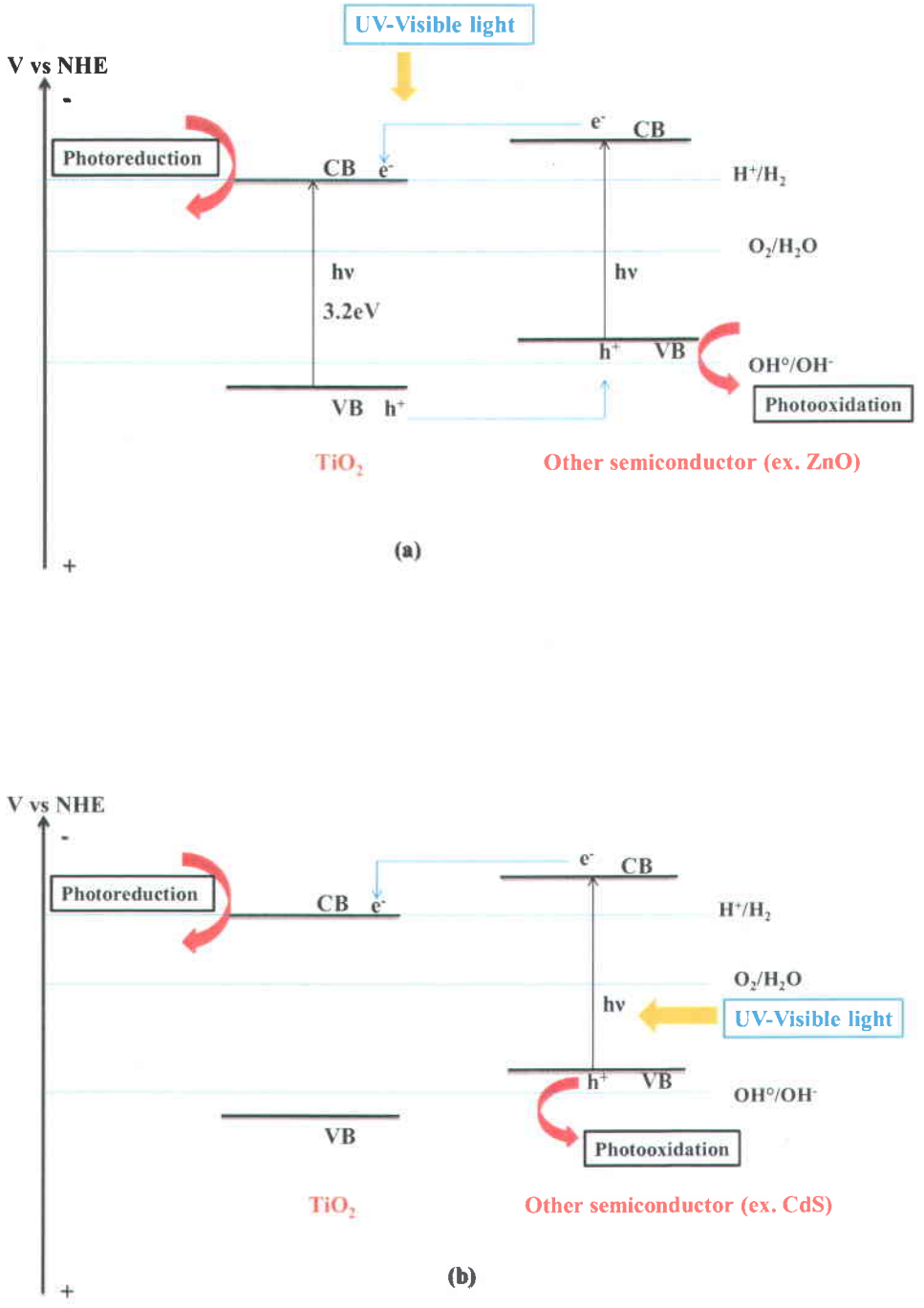


Figure 4-5 Vectorial transfer of electrons-holes (e^-/h^+) in coupled semiconductor system.

4.6.1 Photosenitization of TiO_2 by M_xS_y nanoparticles

Coupling TiO_2 with cadmium sulphide (CdS) is highly promising approach in the field of research (Robert, 2007; Wang et al., 2012). Cadmium sulfide with a narrow band gap of 2.4 eV, is one of the very well-known semiconductors (Huo et al., 2011). Both the conduction band and the valence band of CdS are higher than their counterparts in the TiO_2 (Zhang et al., 2009). The conduction band potentials of TiO_2 and CdS versus Normal Hydrogen Electrode (NHE) at pH7 are -0.5 V and 0.95 V, respectively (Rehman et al., 2009). Such appropriate alternation in the energy levels of the valence and conduction bands allows CdS act as photosensitizer to absorb visible irradiation and to generate electrons and holes. Subsequently, the electrons are injected into the conduction band of the inactivated TiO_2, leaving the holes behind in the valence band of CdS (equation 4-1). The TiO_2 accepts photoelectrons generated from the CdS, which could effectively inhibits the recombination of photoelectrons and holes in CdS (Yu et al., 2003; Kang et al., 1999). Owing to this charge separation under visible light illumination, the couple TiO_2/CdS has been widely applied to enhance the degradation of organic pollutants (Acid Orange II; organic dye Drimaren red, Phenazopyridine, Methyl Orange, etc) by photocatalytic and photoelectrocatalytic reactions (Zyoud et al., 2010; Bessekhouad et al., 2006; Jiang et al., 2011; Tristao et al., 2006).

Équation 4-1 $CdS\ (e^- + h^+) + TiO_2 \rightarrow CdS\ (h^+) + TiO_2$

A small amount of CdS dispersed in TiO_2 matrix can absorb visible light making the photocatalyst TiO_2/CdS sensitive to visible light. Bessekhouad et al. (2006) prepared TiO_2/CdS by a sol-gel method with a CdS loading varied from 5 to 50%. Higher photocatalytic activity of TiO_2/CdS containing low proportion of CdS (from 5 to 10%) has

been recorded toward the degradation of acid orange II (removal more than 50% of Acid Orange II) under visible (less than 20% of Acid Orange II degradation) light irradiation ($\lambda > 400$ nm) compared to the pure TiO_2 or CdS. This higher activity is mainly due to the electron transfer from CdS to TiO_2 which prevent the recombination of charge carriers (Zhang et al., 2009). The same trend has been also reported by Tristao et al., (2006) while studying the photodegrdation of organic dye Drimaren red using the same catalyst. The photocatalytic efficiency of the couple TiO_2/CdS is highly dependent on the proportion of CdS. For instance, higher degradation of 4 organic dye Drimaren red (more than 95%) has been recorded when the TiO_2/CdS system containing lower amounts of CdS (only 5%) (Tristao et al., 2006). In water, organic compounds are adsorbed on the CdS surface than the TiO_2 and the suitable level suggest that the transfer of the electrons from the dye to CdS contributes to the degradation mechanism (Robert, 2007; Bessekhouad et al., 2006).

Another interest of thus structured couple is that the surrounding TiO_2 matrix can protect the CdS against photocorrosion, which represents the major problem of CdS photocatalyst in environmental application (Bessekhouad et al., 2006). The photoanodic corrosion occurs when the photogenerated holes don't react quickly with the water molecular or with organic pollutants (Robert, 2007). According to Colmenares et al. (2009), the S^{2-} in CdS photocatalyst is easily oxidized by photogenerated holes, which accompanied by the release of Cd^{2+} into the solution and the formation of the elemental sulfur layer on the surface of the CdS (equation 4-2). This phenomenon could negatively affect the photocatalytic reactions (Robert, 2007).

Équation 4-2 $CdS + 2H_2O \rightarrow H_2 + Cd^{2+} + S + 2OH^-$

Compared to other sulphide semiconductor such as Bi_2S_3, the visible light activity of Cd/TiO_2 is reported to be much lower (Bessekhouad et al., 2006). Bi_2S_3 is able to absorb light up to

800 nm, whereas CdS adsorb visible light only at 600 nm (Bessekhouad et al., 2006). Owing to its narrow band gap (1.3 eV), Bi_2S_3 photocatalyst appears to be a good for photocatalytic application (Gupta and Tripathi, 2011). The conduction band and the valence band potentials of TiO_2 is more negative and less positive respectively than that the corresponding band of the Bi_2S_3 used as sensitizer (Nayak et al., 1983). However, the conduction band position of Bi_2S_3 (-0.76 V) is lower than the conduction band position of CdS (-0.95V). It has been reported by Rehman et al. (2009) that the extent of the visible light absorption of the sensitizer, in addition to the location of the band edges of the two coupled semiconductors are the mains factors that determine the photocatalytic activity under visible irradiation. The Bi_2S_3/TiO_2 junction has been studied by Bessekhouad et al. (2004) at different concentrations of Bi_2S_3 onto TiO_2 for photocatalytic degradation of organic pollutants (4 hydroxybenzoique acid, Orange II). It has been reported in this work that the Bi_2S_3 absorbs a large part of visible light and when the junction contains 10 wt% of Bi_2S_3, the absorbance started at 800 nm. By performing photocatalytic test, Bi_2S_3 (10 wt%)/TiO_2 demonstrate high ability to remove more than 60% of 4 hydroxybenzoique acid and 100% of Orange II in both visible light and UV-Vis light.

Furthermore, a new approach has been developed by Ho et al. (2004) for the fabrication of visible light photocatalysts using molibenum and tungsten dichalcogenides (MoS_2 and WS_2). The major interest using these semiconductors is their photostability against the corrosion and their narrow band gaps (1.1-1.7 eV) that closely match the solar spectrum (Coehoorn et al., 1987). Unfortunately, the conduction band energy level of bulk MoS_2 and WS_2 are also less negative than that of TiO_2. This structure avoids the transfer of electrons from the potential of sensitizer to titanium dioxide. Accordingly to same research group (Ho et al., 2004), MoS_2 and WS_2 exhibited quantum confinement effects. Owing to this confinement, the band gaps of MoS_2 and WS_2 can be increased significantly, leading to a change in their redox potentials. Such appropriate energy levels of the valence and conduction bands edge promote MoS_2 and

WS_2 to act as photosensitizer under visible irradiation in the heterogeneous semiconductor systems. Under visible light irradiation ($\lambda > 400$ nm), both MoS_2/TiO_2 and WS_2/TiO_2 are efficient in the degradation of methylene blue and 4-chlorophenol.

Cadmium selenide (CdSe) is another material that has been widely used as photosensitizer in the $CdSe/TiO_2$ system. CdSe has a lower band gap ($E_g = 1.74$ eV) and has been considered as potential material to form a composite semi-conductor with TiO_2 (Ho and Yu, 2006). More than 30% of 4-chlorophenol degradation and more than 20% of total organic carbon were achieved under visible light irradiation using $CdSe/TiO_2$ as photocatalyst (Ho and Yu, 2006). By comparison, similar study of Lo et al. (2004) has used $CdSe/TiO_2$ for photocatalytic degradation of 4-chlorophenol under 420 nm irradiation. Only 10% of 4-chlorophenol photodegradation was obtained using $CdSe/TiO_2$ under visible irradiation. This lower result is mainly due to the insufficient amount of CdSe on the TiO_2 (only 27.6% of CdSe). Until this date, the photocatalytic properties of $CdSe/TiO_2$ have not been extensively investigated compared to the CdS/TiO_2. According to Lo et al. (2004), use of CdS to couple with TiO_2 seems to be most favorable than CdSe.

4.6.2 Coupling TiO_2 by M_xO_y nanoparticles

The TiO_2/WO_3 hybrid system has received attracting much attention in the field of photoelectrochemistry (Ilieva et al., 2012; Tada et al., 2004; Lin et al., 2008). TiO_2/WO_3 is a system of semiconductor-semiconductor coupled material, which has been widely used as a photocatalyst for decades (Gupta and Tripathi, 2011). The band gap of WO_3 is lower (2.8 eV) and both the upper edge of the valence band and the lower edge of the conduction band of WO_3 are lower than those of TiO_2 (Gupta and Tripathi, 2011). Thus, WO_3 can be excited by visible light and the photogenerated holes can be transferred from WO_3 to TiO_2 (Miyauchi et al., 2002). The electron in the conduction band of TiO_2 could be easily accepted by WO_3 because the standard reduction potential between W(VI) and W(V) is only - 0.03 V (Gupta

and Tripathi, 2011). The electrons in the WO_3 would then be transferred to the oxygen molecules adsorbed on the surface of TiO_2. The increase of photocatalytic activity of TiO_2 was confirmed by several research groups as a result of coupling with WO_3 for the decomposition of benzene (Tae Kwon et al., 2000), methylene blue (Tae Kwon et al., 2000), butyl acetate (Keller et al., 2003) and dichlorobenzene (Do et al., 1994). Higher rates of pollutant degradation were recorded owing to the increase of electron transfer from TiO_2 to WO_3 via the formation of an intermediate W(V) species, together with the increased surface acidity in the TiO_2/WO_3 couple. It has been reported by Papp et al. (1994), the surface acidity and the protonated surface hydroxyl groups promote the transfer of electron from the conduction band of TiO_2 to the adsorbed oxygen molecules, and hence increase the photocatalytic activity. However, the TiO_2/WO_3 coupling doesn't always enhance the photocatalytic activity of TiO_2. The two much loading of WO_3 could act as centers of charge recombination (equations 4-3 and 4-4) (Zhang et al., 2009). Furthermore, the preparation technique of coupled semiconductor TiO_2/WO_3 remains a critical parameter which influences the band structure properties and consequently the photocatalytic activity (Zhang et al., 2009).

Équation 4-3 $W^{6+} + e_{(TiO2)\ CB}^{-} \rightarrow W^{5+}$

Équation 4-4 $W^{5+} + h_{(TiO2)VB}^{+} \rightarrow W^{6+}$

As mentioned in the previous works (Zhang et al., 2009; Gupta and Tripathi, 2011; Vinodgopal and Kamat, 1995; Cao et al., 2000), tin dioxide (SnO_2) semi conductor attracts much interest because it posses interesting electrochemical and photoelectrochemical properties. Traditionally, SnO_2 has been viewed as a poor candidate for photocatalytic application even under UV illumination due to its very large band gap (3.8 eV) and its instability to reduce oxygen (Zhang et al., 2009; Vinodgopal and Kamat, 1995). To overcome such limitations and

achieve efficient charge separation, systematic research was conducted to use SnO_2 as a coupled semiconductor. The couple system SnO_2/TiO_2, where TiO_2 play the role of photosensitizer for SnO_2 has received a great attention (Tada et al., 2004; Hattori et al., 2001; Tada et al., 2000; Vinodgopal and Kamat, 1995). The conduction band of SnO_2 is more positive (0.5V) than that of TiO_2 and could act as a sink for the photogenerated electrons (Zhang et al., 2009; Robert, 2007; Vinodgopal and Kamat, 1995). Using SnO_2 coupled to TiO_2, the photogenerated electrons can accumulate on the SnO_2 and the photogenerated holes can accumulate on the TiO_2 owing to the formation of a heterojunction at the SnO_2/TiO_2 (Figure 4-6). According to Yu et al. (2006), Zhang et al. (2009) and El-Maghraby et al. (2008) SnO_2/TiO_2 system avoids the recombination rate of photogenerated charge carriers, ensures higher quantum efficiency and better photocatalytic efficiency in organic pollutant degradation. For instance, more than 15% of 4-chlorophenol removal has been recorded by Lin et al. (2008) using TiO_2/SnO_2 under 369 nm of UV irradiation compared to single TiO_2 and SnO_2 system (around 5% of degradation rate of 4-chlorophenol). Besides, higher decolorization of Acid orange 7 (more than 97%) has been recorded after 60 min of photoelectrocatalytic treatment at 0.83 V and using the similar system (TiO_2/ SnO_2) as photocatalyst (Vinodgopal and Kamat, 1995).

Despite the higher photocatalytic and the photoelectrocatalytic performance of TiO_2/ SnO_2 configuration under UV irradiation, the incorporation of this system for environmental applications at large scale remains limited due to the large band gap of both TiO_2 and SnO_2. Recently, a new approach towards the improvement of photocatalytic activity of TiO_2 under visible illumination moves to the substitution of Sn for Ti in the TiO_2 lattice. This substitution enhances the absorption of visible light by the doped Sn-TiO_2 and leads to better separation of charge carriers (Cao et al., 2000; Pilkenton and Raftery, 2003).

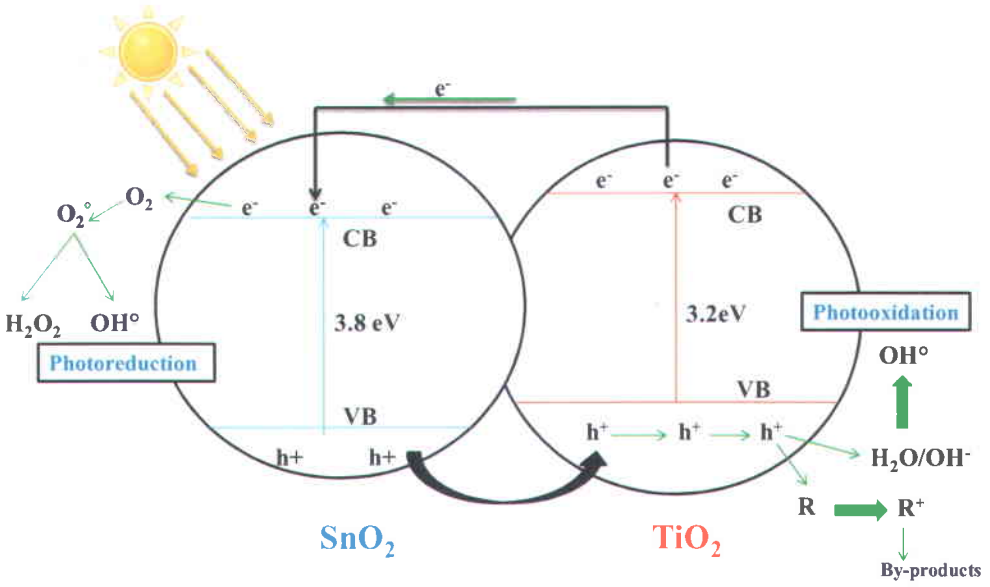


Figure 4-6 TiO_2/SnO_2 photocatalyst configuration.

Cuprous oxide (Cu_2O) is another interaction metal oxide p-type semiconductor. Owing to its lower band gap (2.0 eV) (Zhang et al. (2007), Cu_2O is a promising material for the conversion of solar energy into chemical energy (Jin et al., 2012). Nevertheless, the application of Cu_2O as photocatalyst is very limited due to the fast recombination of charge carriers. Combining Cu_2O with TiO_2 represent a promising way because the absorption of sunlight was achieved and the separation of the e^-/h^+ was ensured (Robert, 2007). Compared to TiO_2, Cu_2O possess higher conduction band (-1.4 eV) and valence band edge (Zhang et al., 2005). Under visible light, the photogenerated electrons in the conduction band of Cu_2O were transferred to the conduction band of TiO_2 and the photogenerated holes in the valence band of TiO_2 were transferred to the valence band of Cu_2O (Jin et al., 2012). As the result, high concentration of electrons and holes were obtained in the conduction band of TiO_2 and valence band of Cu_2O,

respectively. Thus, Ti^{3+} electron centers could be formed, which may lead to enhance the photocatalytic efficiency of Cu_2O/ TiO_2. More than 90% of photocatalytic degradation efficiency of methylene blue (Jin et al., 2012) and dye brilliant red x-3B (Li et al., 2004) have been recorded using Cu_2O/ TiO_2 as photocatalyst.

However, it well known that the photocatalytic activity is closely related with the surface area. It has been reported by Bassekhouad et al. (2005), while studying the photocatalytic activity of Cu_2O/ TiO_2, that the physical chemical properties and the structure of the photocatalyst influence the performance of the process. Some other oxide such as ZnO (Ge et al., 2009), Bi_2O_3 (Bassekhouad et al., 2005), ZrO_2 (Smirnova et al., 2006) among other have been used in previous research for enhancing the photoactivity of titanium dioxide. Yet, the application of these different photocatalysts in coupling with TiO_2 remains limited in the photocatalytic treatment of water (Robert, 2007).

Tableau 4-4 Removal of organic pollutants in aqueous solution using photosensitization system (TiO_2/M_xO_y or TiO_2/M_xS_y)

Systems	Matrix	Type of polluant	Operating conditions	Results and comments	References
TiO_2/M_xS_y	Aqueous solution	Methylene blue	300 W xenon lamp (390-770 nm); room temperature; 5 x 10^{-6} mol L^{-1}; external potential = 0-0.2 V; 0.10 mol L^{-1} $NaNO_3$; treatment time = 90 min; volume = 75 mL; **ZnO/CdS/TiO_2**	91.3% removal of methylene blue at 0.2 V after 90 min, using ZnO/CdS/TiO_2	Ouyang et al., (2012)
	Aqueous solution	Acid Orange II	Visible irradiation (λ>400nm); 0-50% **CdS/TiO_2**; treatment time = 35 min	Removal more than 50% removal of acid orange II using 10% CdS/TiO_2	Bessekhouad et al. (2006)
	Aqueous solution	Phenazopyridine	50W Xe solar simulator lamp (400-800 nm; 0.0212 W cm^{-2}); 2x 10^{-5}- 6x10^{-5} mol L^{-1} of phenazopyridine; Treatment time = 60-120 min; pH =4-10; temperature = 30-60°C; **TiO_2/CdS** (0.05 g, 0.1 g and 0.15 g).	Removal more than 75% of phenazopyridine at pH 9.5, temperature 30°C, after 60 min of treatment time	Zyoud et al. (2010)
	Aqueous solution	Orange II, 4-hydroxybenzoïque acid benzamide	Treatment time = 30 min; 10-50% wt **Bi_2S_3/TiO_2**; visible irradiation (λ = up to 800 nm); 10 mg L^{-1} of Orange II; 30 mg L^{-1} of 4-hydroxybenzoïque acid; 20 mg L^{-1} of benzamide.	100% removal of orange II, removal more than 60% of 4-hydroxybenzoïque acid and removal more than 20% of benzamide using Bi_2S_3 (10wt %)/TiO_2.	Bessekhouad et al., (2004)
TiO_2/M_xO_y	Aqueous solution	Methyl orange	3000 W high pressure mercury lamp; 20 mg L^{-1} of methyl orange; pH=5; volume = 400 mL; air flow rate =20 mL min^{-1}; 1g L^{-1} of **SnO_2/TiO_2**	Removal of 95% of methyl orange	Zhang et al., (2009)
	Aqueous solution	Malachite green	0.1 mol L^{-1} of Na_2SO_4; 10 mg L^{-1} of malachite green; 0.01-0.2 mol L^{-1} of methanol; 0.001-0.055 mol L^{-1} $Na_2C_2O_4$; volume = 35 mL; pH = 6.5; Radium Ralutec 9W/78 UVA lamp (λ= 350-400 nm; λ_{max} = 370nm; 12.45 mW cm^{-2});Radium Ralutec 9W/71 VIS light lamp (λ>400 nm; λ_{max}=437 nm; 11.6 Mw cm^{-2}); distance lamp-sample = 2 cm; external potential = 0.7 V; anode = **TiO_2/WO_3**; counter electrode = platinum plate; reference electrode = acid mercury/mercury sulfate; treatment time = 120 min.	Removal more than 70% of malachite green	Ilieva et al., 2012
	Aqueous solution	Methylene blue	500 W Xe lamp irradiation; 15 mg L^{-1} of methylene blue; treatment time = 210 min; **TiO_2/Cu_2O** double wall nanotubes.	Degradation of more than 90% methylene blue within 210 min.	Jin et al., 2012
	Aqueous solution	Methyl orange	300 W medium pressure mercury lamp (365 nm); 60 mg of **ZnO/TiO_2**, 5 10^{-5} mol L^{-1} of methyl orange; volume = 200 mL; pH= 2-11; treatment time =30-60 min	98.13% removal of methyl orange at pH =2 and after 60 min; 85.14% removal of methyl orange at pH = 11 and before 30 min	Ge et al., (2009)

4.7 Others photosensitization of TiO_2

The photocatalytic activity of TiO_2 under visible light could be also enhanced by coupling of organic and inorganic dyes to TiO_2 surface (Park et al., 2012; Rehman et al., 2009). Dye sensitized TiO_2 has been widely and successfully applied to the degradation of pollutants. Various electron transfer steps are involved in this process. Physical adsorption of dyes occurs through the week Van der Waals interaction between dye molecule and the TiO_2 surface. The photochemical process is initiated by photo-excitation of dye molecules upon illumination by visible light, followed by the transfer of the electrons from the excited dye to the conduction band of TiO_2. Subsequently, in the presence of suitable electron donors (e.g., EDTA, organic acids, water, alcohols, etc), the oxidized dye is regenerated. The injection of electron into the conduction band of TiO_2 is favorable due to the more negative potential of the lowest unoccupied molecular orbital (LUMO) of the dye molecules as compared to the potential of the TiO_2 conduction band (Rehman et al., 2009). The electrons injected by dye molecules to the surface of titania are scavenged by molecules of oxygen to promote the generation of superoxide radical $O_2^{\circ-}$ and hydrogen peroxide radical °OOH. These radicals attack the aromatic rings of organic pollutants forming intermediates and mineralizing them to carbon dioxide and water. Despite the popular utilization of dyes as sensitizer of TiO_2, the quantity of the dye adsorbed on the TiO_2 surface is a crucial parameter because only this amount contributes to photocatalytic process. The frequent desorption of dye molecules reduces significantly the potential use of this technique for practical applications. The extent of dye adsorption depends on the initial concentration of dye, the nature of dye, the surface of the photocatalyst and the pH of the solution (Moon et al., 2003; Kaur and Singh, 2007). Besides, the photochemical properties of dyes and the interfacial transfers of electrons between dyes and TiO_2 are very important parameters to ensure high photocatalytic efficiency (Park et al., 2012).

Another mechanism of sensitizing TiO_2 by visible light is the direct charge transfer between surface adsorbate and TiO_2. In the charge transfer sensitization, the electron is photo-excited directly from the ground state adsorbate to the conduction band of TiO_2. The formation of the charge transfer complex on the surface of TiO_2 usually accompanies the appearance of a visible light absorption band, which is not seen in either the adsorbate or TiO_2 alone (Park et al., 2012). Aromatic compounds having hydroxyl or carboxyl anchoring group are the common examples of formation of charge transfer complex on TiO_2 surface. TiO_2-catechol complex is a classical example of charge transfer complex (Park et al., 2012). According to Wang et al. (2003) the formation of complex between catechol and TiO_2 creates a broad new band centered at 390 nm, which is extended into the visible region at 600 nm. The excitation of visible light induces the direct transfer of electron from the organic substrates into the conduction band of TiO_2. The application of such mechanism could be a promising alternative for the development of visible light active photo-catalysts.

4.8 Future trends of TiO_2 for environmental applications

This review has emphasized some key areas concerning the electronic properties and structure of TiO_2, doping TiO_2 with cationic and anionic metals, coupling TiO_2 with others semiconductors. Its efficiency in the degradation of pollutants using photocatalytic or photoelectrocatalytic process has been also discussed. Metals doping TiO_2 has been extensively explored as a way to improve the photoactivity under visible light (Carp et al., 2004). However, foreign cations could act as a recombination center and therefore the significant separation between e^-/h^+ are only possible at low concentrations of dopants (Hernàndez-Alonso et al., 2009). Moreover, doping TiO_2 with anionic metals or coupling TiO_2 with other semiconductors represent another approaches to increase the photonic efficiency and the photocatalytic activity of TiO_2. On one hand, doping TiO_2 with anionic nonmetals (such as nitrogen, carbon, etc) or the increase of its photosensitization in the

presence of others semiconductors (such as CdS, WO_3, etc) make it more suitable for environmental applications. On the other hand, it also makes it potentially significant as promising photocatalyst due to its higher chemical and physical properties (high oxidation efficiency, non-toxicity, high photostability and chemical inertness among others).

Despite these achievements and remarkable improvements in TiO_2 structure (doping TiO_2 or coupling TiO_2), several challenges (toxicity and preparation aspects) have to be considered for practical environmental applications as illustrated in Figure 4-7.

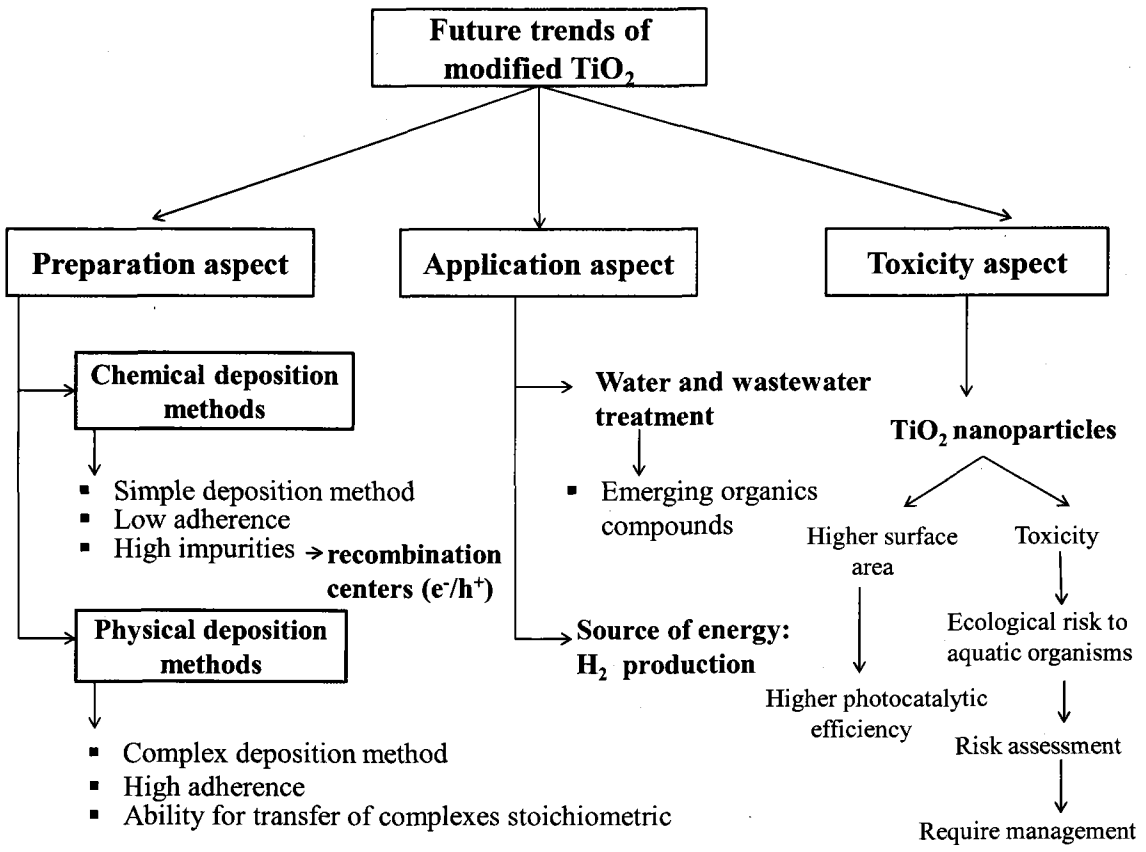


Figure 4-7 Future trends of modified TiO_2 for environmental applications.

4.8.1 Preparation aspect of TiO_2

It is well known that the photocatalytic activity remains an inconclusive area for all the TiO_2 investigations. The photocatalytic activity is mainly related with surface morphology (Colmenares et al., 2009).The provision of sufficient high specific area of catalyst remains one of the major difficulties. Evidently, there is a clear relation between the surface properties, the rational development of improved synthesis ways and the potential usefulness of the material prepared for specific applications (Diebold, 2003; Mohammadi et al., 2006). Thus, various methods including physical and chemical deposition techniques (hydrothermal synthesis, chemical vapor deposition, pulsed laser deposition, magnetron sputtering, nitrogen plasma, sol-gel) have been recently adopted to achieve photocatalysts exhibiting desirable physical properties and high activity and stability for photocatalytic applications under visible irradiation using a main part of solar spectrum. For instance, doping transition metals into titania lattice has been mostly carried out using chemical sol-gel technique (Anpo and Takeuchi, 2003; Yamashita et al., 2003) whereas doping TiO_2 with nitrogen as an example of anionic metals was mostly conducted under gaseous flow of molecular nitrogen (N_2) (Rehman et al., 2009; Asahi and Morikawa, 2007), nitrous oxide (Guo et al., 2007) and ammonia (Irie et al., 2003). Besides, pulsed Laser deposition (PLD) method is one of the techniques that was used by Peng et al. (2012) to prepare nitrogen-doped TiO_2 thin film. Results showed a significant visible light response at 595 nm and a decrease of the band gap as evidence of 3% N doping. The same method has been successfully conducted by Dabney et al. (2008) and Zhao et al. (2008) to prepare Nb-doped TiO_2 and N-doped TiO_2, respectively. Different molecules, different operating conditions and different methods of analysis make the comparison between deposition techniques so difficult. Compared to the common and available synthesis methods, PLD has become a widely used technique for the deposition of thins films due to its several advantages (Zhao et al., 2008). Among the advantages of the

PLD method, one can mention the high density of the deposited film with their enhanced adhesion to the substrate because of the rather energetic species involved in the ablation (Gyorgy et al., 2005). It also offers the possibility to achieve nanostructured coating which is known for high specific area (Peng et al., 2012; Yoshida et al., 2005). Compared to other plasma deposition technique, PLD method offers a quite independent control of the growth parameters while making deposit wide range of pressure and temperature. The PLD technique is well known not only for its versatility but more importantly for its unique ability for transfer of complexes stoichiometric (Peng et al., 2012; Zhou et al., 2009; Chrisey and Hubler, 1994). Magnetron sputtering is also among the very powerful technique that has been used for the synthesis of TiO_2 materials for photocatalytic applications (Yamagishi et al., 2003; Takeuchi et al., 2009; Herman et al., 2006). As reported by Abdollahi Nejand et al. (2010), magnetron sputtering is a suitable method for doping the metal and non-metal elements. This technique allows the deposition of well adherent, uniform, mechanical durable and transparent film with a controllable density (Abdollahi Nejand et al., 2010; Eufinger et al., 2007). Until the current time, it is very difficult to assess which of the many deposition techniques is the most effective for photocatalytic application at large scale. The choice of one method among other should take into consideration the cost, the effectiveness and the operation for large scale. Thus, extensive research should be more conducted to achieve this objective.

4.8.2 Application aspect of TiO_2

Nowadays, the presence of emerging organic pollutants such as hormones, phenolic compounds, pharmaceutical compounds, personal care products, and pesticides among others in the aquatic environment has received much attention. The application of photocatalytic or photoelectrocatalytic processes using new TiO_2 photocatalyst structure could be a good alternative to avoid the major drawbacks of conventional treatment methods. Up to now, the

application of these new technologies using doped TiO_2 or coupled TiO_2 as photo-catalyst for water and wastewater treatment were carried out at the laboratory scale. Thus, the industrial implementation of photocatalytic process using modified TiO_2 under solar irradiation must take into consideration some parameters such as the illumination of the photo-catalyst. To the best of our knowledge, conventional photocatalytic processes have been tested in large reactors for practical applications by using a wide variety of photo-reactor designs (e.g. parabolic trough, inclined plate, fixed/fluidized bed, packed bed, corrugated plate, and falling film photoreactors). This was discussed in detail by Braham and Harris (2009) and by McCullagh et al. (2010) The commercial development of photocatalytic technologies using modified TiO_2 photo-catalyst should take into account these designs of the photo-reactor in order to promote as possible as contact between solar irradiation and the surface of the photo-catalyst and consequently to ensure higher efficiency of photocatalytic process.

It is worth noting that during the photocatalytic reaction, the surface of the doped photocatalyst may be covered with organic substances that reduce its active surface. This may affect the treatment performance in long term experiments. To circumvent these major drawbacks, the use of doped photocatalyst in the form of expanded metal (titanium covered with doped titania) and the application of a high recycling flow rate during the treatment could be one of the easier and more feasible regeneration methods of the photo-catalyst surface. Such structure of photo-catalyst provides a good mechanical strength and promotes higher turbulence near the catalyst for increasing the mass transfer coefficient at the electrode-electrolyte interface. Moreover, the high recycling flow rate could be benefit to decrease the thickness of the diffusion layer near the photo-catalyst and consequently to increase the performance of the photocatalytic process. Likewise, the polarity reversal could be also used to maintain the longevity of doped TiO_2 photo-catalyst.

Future research should be also focused to combine this novel technology with biological processes when treating effluents containing refractory organic compounds. Coupling a biodegradation process with a physicochemical process transforms the non-biodegradable organic pollutants into biodegradable compounds, which contributes to increase the depurative efficiency of the subsequent biological process. Besides, when biological process was installed downstream, the residence time and reaction volume for the biological treatment could be significantly reduced. In this way, the operating cost of treatment will be decreased.

Although extensive studies have emphasized on TiO_2 semiconductor for photocatalytic and photoelectrocatalytic oxidation of persistent organic pollutants present in water and wastewater (Daghrir et al., 2012; Ma and Tu, 2011; Zhang et al., 2009; Peng et al., 2012), other potential environmental uses of TiO_2 photocatalyst as source of energy have gathered a great deal of interest (Hernàndez-Alonso et al., 2009; Ni et al., 2007; Yu et al., 2012). Hydrogen energy is a storable, clean and environmentally friendly fuel for the future.[222, 224] Fujishima and Honda[45] have discovered the hydrogen production from photoelectrochemical water splitting using TiO_2 photocatalyst. Subsequently, scientific interests have been focused in enhancing the photocatalytic H_2 production for energy generation. For hydrogen production, the conduction band level should be more negative than hydrogen production level ($E_{H2/H2O}$), while the valence band should be more positive than water oxidation level ($E_{O2/H2O}$) for efficient oxygen production from water by photocatalysis. Unfortunately, the photocatalytic production efficiency of H_2 on a bare TiO_2 is very low due to the following reasons: *(i)* the rapid recombination of e^-/h^+ photo-generated, *(ii)* the large H_2 production overpotential *(iii)* and the fast backward between hydrogen and oxygen (Yu et al., 2011; Jin et al., 2007; Xu and Sun, 2009). Likewise, the inability use of visible light is another drawback that limits the efficiency of solar photocatalytic for hydrogen production at large scale (Ni et al., 2007). However, to overcome the above listed problems and make solar photocatalytic

hydrogen production feasible, more efforts have been made to the deposition method such as metal cations doping (Yu and Hu, 2009), carbon and nitrogen doping (Khan et al., 2002; Asahi et al., 2001), etc. Thus, the development of novel TiO_2 photocatalyst merits further research for environmental applications. The future challenge should more focus on the development of novel TiO_2 photocatalyst which would be able to ensure simultaneously the generation of H_2 and the oxidation of refractory organic pollutants.

4.8.3 Toxicity aspect

The development of TiO_2 nanocrystalline photocatalyst is another emerging area where a considerable interest has been shown (Beydoun et al., 1999; Kamat, 2012; Paronyan et al. , 2008). Such a nanometric grain size (range from a few tens up to a few hundreds of nm) is expected to have an important effect on the photocatalytic activity of the TiO_2 coating (Kim et al., 2007). Indeed, with the decrease in particle size, the catalytic activity is enhanced due to the huge increase in the surface area of the material (Daghrir et al., 2012). Nevertheless, nanomaterials can be an important emerging class of contaminants (Farré et al., 2009; Klaine et al., 2008; Nel et al., 2006), which have a wide ecological impacts within marine and estuarine ecosystems (Miller et al., 2012). TiO_2 uses include different area such as medical applications (Hugo Ricardo and Angelo Fernando, 2001), catalyst for water and air purification (Li et al., 2005; Ryu and Choi, 2008), energy storage (Deng et al., 2009; Tatsuma et al., 2002) and antimicrobial applications (Keleher et al., 2002), among others. In 2005, the global production of TiO_2 nanoscale was estimated to be 2000 ton, whereas in 2010 the production had increased to 5000 ton (Weir et al., 2012). According to Westerhoff et al. (2011), nanomaterials engineering could pose an ecology risk to aquatic organisms. Among the most commonly used nanoparticles, higher concentrations of TiO_2 have been reached in surface water and pose a significant problem to aquatic ecosystem (Miller et al., 2012). During the photocatalytic process, the nanoparticles TiO_2 could diffuse in the aquatic

environment. These nanomaterials are then released to surface waters, where they can interact with living organisms. This major drawback limits the use of TiO_2 nano-structured for photocatalytic applications at large scale.

The development of modified TiO_2 photo-catalyst by introducing anions or cations could pose an ecological risk to aquatic ecosystem. Indeed, the release of these anionic or cationic compounds in aquatic system could lead to the adverse impacts on the target organisms. For example, the presence of nitrogen as an example of anionic compounds contribute mainly to eutrophication of water bodies, in addition to the risks associated with toxicity and bad odors (Adhoum et al., 2004). The presence of sulfide compounds in water is also very toxic for many microorganisms because the reaction of sulfide with iron from cytochromes inhibiting the respiration (Visser et al., 1997). Besides, the release of cations compounds (such as Pb, Ni, Cr, Zn and Cu among others) in the aquatic environment are still very toxic and can cause several problems such as extermination of aquatic organisms, as well as risks to human health (Martins et al., 2012; Adhoum et al., 2004). Metals are persistent compounds, toxic and absolutely non-biodegradable (Martins et al., 2012). Thus, they can accumulate in the environment and increase their toxicity. To avoid these major drawbacks, research should be focused on the development of preparation techniques in order to increase the photo stability of the material.

4.9 Conclusion

This research highlights the importance of TiO_2 photocatalyst for environmental applications. As it has been stated in this review, a number of research studies have focus on the development of a new TiO_2 photocatalyst able to absorb visible light as a main part of solar spectrum. The limitations of pure TiO_2, which require the use of UV light and its high photogenerated electrons and holes recombination rate, can be overcome by introducing foreign species into the titanium dioxide matrix. The Doping TiO_2 with either cationic or

anionic metals and coupling TiO_2 with other semiconductor are the major approaches that have been reviewed. Up to now, the successful applications of TiO_2 photocatalyst under visible light for water and wastewater treatment were carried out at the laboratory scale. Future research should be focused on the use of novel TiO_2 photocatalyst (doped TiO_2 or photosensitization TiO_2) for large scale applications.

4.10 Acknowledgments

Sincere thanks are extended to the National Sciences and Engineering Research Council of Canada and Premier Tech Ltee for their financial support for this study.

4.11 References

Abdollahi Nejand B, Sanjabi S & Ahmadi V (2010) Optical and photocatalytic characteristics of nitrogen doped TiO_2 thin film deposited by magnetron sputtering. *Sci. Iran.* 17: 102-107.

Adhoum N, Monser L, Bellakhal N & Belgaied JE (2004) Treatment of electroplating wastewater containing Cu^{2+}, Zn^{2+} and Cr(VI) by electrocoagulation. *J. Hazard. Mater.* 112: 207-213.

Adan C, Bahamonde A, Fernandez-Garcia M & Martinez-Arias A (2007) Structure and activity of nanosized iron-doped anatase TiO_2 catalyst for phenolic photocatalytic degradation. *Appl. Catal. B-Environ.* 72: 11-17.

Agrios AG & Pichat P (2005) State of the art and perspectives on materials and applications of photocatalysis over TiO_2. *J. Appl. Electrochem. 35*: 655-663.

Ambrus Z, Balàzs N, Alapi T, Wittmann G, Sipos P, Dombi A & Mogyorosi K (2008) Synthesis, structure and photocatalytic properties of Fe(III)-doped TiO_2 prepared from $TiCl_3$. *Appl. Catal. B-Environ.* 81: 27-37.

Anpo M & Takeuchi M (2003) The design and development of highly reactive titanium oxide photocatalysts operating under visible light irradiation. *J. Catal.* 216 (1-2): 505-516.

Ao Y, Xu J, Fu D & Yuan C (2009) A simple method to prepare N-doped titania hollow spheres with high photocatalytic activity under visible light. *J. Hazard. Mater.* 167: 413-417.

Asahi R & Morikawa T (2007) Nitrogen complex species and its chemical nature in TiO_2 for visible light sensitized photocatalysis. *Chem. Phys.* 339: 57-63.

Asahi R, Morikawa T, Ohwaki T, Aoki K & Taga Y (2001) Visible light photocatalysis in nitrogen-doped titanium oxides. *Science* 293 (5528): 269-271.

Asilturk M, Sayilkan F & Arpac E (2009) Effect of Fe^{3+} ion doping to TiO_2 on the photocatalytic degradation of Malachite Green dye under UV and vis-irradiation. *J. Photochem. Photobiol. A.* 203: 64-71.

Bally AR, Korobeinikova EN, Schmid PE, Lévy F, Bussy F (1998) Structural and electrical properties of Fe-doped TiO_2 thin films. *J. Phys. D: Appl. Phys.* 31: 1149-1154.

Bessekhouad Y, Chaoui N, Trzpit M, Ghazzal N, Robert D & Weber JV (2006) UV-vis versus visible degradation of acid orange II in a coupled CdS/TiO_2 semiconductors suspension. *J. photochem. Photobiol. A.* 183: 218-224.

Bessekhouad Y, Robert D & Weber JV (2005) Photocatalytic activity of Cu_2O/TiO_2, Bi_2O_3/TiO_2 and $ZnMn_2O_4/TiO_2$ heterojunctions. *Catal. Today* 101: 315-321.

Bessekhouad Y, Robert D & Weber JV (2004) Bi_2S_3/TiO_2 and CdS/TiO_2 heterojunctions as an available configuration for photocatalytic degradation of organic pollutant. *J. Photochem. Photobiol. A.* 163: 569-580.

Beydoun D, Amal R, Low G & McEvoy S (1999) Role of nanoparticles in photocatalysis. *J. Nanopart. Res.* 1: 439-458.

Binitha NN, Yaakob Z, Reshmi MR, Sugunan S, Ambili VK & Zetty AA (2009) Preparation and characterization of nano silver-doped mesoporous titania photocatalysts for dye degradation. *Catal. Today* 147: S76-S80.

Braham RJ & Harris AT (2009) Review of major design and scale-up considerations for solar photocatalytic reactors. *Ind. Eng. Chem. Res.* 48: 8890-8905.

Burda C, Lou Y, Chen X, Samia ACS, Stout J & Gole JL (2003) Enhanced Nitrogen doping in TiO_2 nanoparticles. *Nano Lett.* 3: 1049-1051.

Cao Y, Zhang X, Yang W, Du H, Bai Y, Li T & Yao J (2000) A bicomponent TiO_2/SnO_2 particulate film for photocatalysis. *Chem. Mater.* 12: 3445-3448.

Carp O, Huisman CL & Reller A (2004) Photoinduced reactivity of titanium dioxide. *Prog. Solid. State. Ch.* 32: 33-177.

Chang CY, Hsieh YH & Chen YY (2012) Photoelectrocatalytic degradation of sodium oxalate by TiO_2/Ti thin film electrode. *Int. J. Photoenergy.* art n° 576089.

Chen D, Jiang Z, Geng J, Wang Q &Yang D (2007) Carbon and nitrogen Co-doped TiO_2 with enhanced visible light photocatalytic activity. *Ind. Eng. Chem. Res.* 46: 2741-2746.

Chen X, Mao SS (2007) Titanium dioxide nanomaterials: Synthesis, properties, modifications and applications. *Chem. Rev.* 107: 2891-2959.

Coehoorn R, Haas C & De Groot RA (1987) Electronic structure of $MoSe_2$, MoS_2, and WSe_2.II. The nature of the optical band gaps. *Phys. Rev.* B35: 6203-6206.

Choi YJ, Seeley Z, Bandyopadhyay A, Bose S & Akbar SA (2007) Aluminium-doped TiO_2 nano-powders for gas sensors. *Sens. Actuators, B.* 124: 111-117.

Choi Y, Umebayashi T & Yoshikawa M (2004) Fabrication and characterization of C-doped anatase TiO_2 photocatalyst. *J. Mater. Sci.* 39: 1837-1839.

Choi W, Termin A & Hoffmann MR (1994) The role of metal ion dopants in quantum-sized TiO_2: Correlation between photoreactivity and charge carrier recombination dynamics. *J. Phys. Chem.* 98: 13669-13679.

Chrisey DB & Hubler GK (1994) Pulsed Lase deposition of Thin films. John Wiley& Sons. Inc., New York, p613.

Colmenares JC, Luque R, Campelo JM, Colmenares F, Karpinski Z & Romero AA (2009) Nanostructured photoatalysts and their applications in the photocatalytic transformation of Lignocellulosic biomass: An overview. *Materials* **2009**, *2*, 2228-2258.

Dabney MS, van Hest MFAM, Telpin CW, Arenkiel SP, Perkins JD & Ginley DS (2008) Pulsed Laser deposition Nb doped TiO_2 as a transparent conducting oxide. *Thin Solid Films* 516: 4133-4138.

Daghrir R, Drogui P, Ka I & El Khakani MA (2012) Photoelectrocatalytic degradation of chlortetracycline using Ti/TiO_2 nanostructured electrodes deposited by means of a pulsed Laser deposition process. *J.Hazard. Mater.* 199-200: 15-24.

Daghrir R, Drogui P & Robert D (2012) Photoelectrocatalytic technologies for environmental applications, *J. Photochem. Photobiol. A.* 238: 41-52.

Depero LE, Marino A, Allieri B, Bontempi E, Sangaletti L, Casale C &Notaro M (2000) Morphology and microstructural properties of TiO_2 nanopowders doped with trivalent Al and Ga cations. *J. Mater. Res.* 15: 2080-2086.

De Tacconi NR, Chenthamarakshan CR, Rajeshwar K, Pauporté T & Lincot D (2003) Pulsed electrodeposition of WO_3-TiO_2 composite films. *Electrochem. Commun.* 5: 220-224.

Deng D, Kim MG, Lee JY & Cho J (2009) Green energy storage materials: Nanostructured TiO_2 and Sn-based anodes for lithium-ion batteries. *Energ. Environ. Sci.* 2: 818-837.

Diebold U (2003) Structure and properties of TiO_2 surfaces: a brief review. *Appl. Phys. A. Mater.* 76: 681-687.

Diwald O, Thompson TL, Goralski EG, Walck SD & Yates Jr JT (2004) Photochemical activity of nitrogen-doped rutile TiO_2 (110) in visible light. *J. phys. Chem B.* 108: 52-57.

Di Paola A, Garcia-Lopez E, Ikeda S, Marc G, Ohtani B & Palmisano L (2002) Photocatalytic degradation of organic compounds in aqueous systems by transition metal doped polycristalline TiO_2. *Catal. Today.* 75: 87-93.

Di Paola A, Ikeda S, Marci G, Ohtani B & Palmisano L (2001) Transition metal doped TiO_2: physical properties and photocatalytic behavior. *Int. J. photoenergy* 3: 171-176.

Di Valentin C, Pacchioni G, Selloni A, Livraghi S & Giamello E (2005) Characterization of paramagnetic species in N-doped TiO_2 powders by EPR spectroscopy and DFT calculations. *J. Phys. Chem. B.* 109: 11414-11419.

Dozzi MV, Saccomanni A & Selli E (2012) Cr(VI) photocatalytic reduction : Effects of simultaneous organics oxidation and of gold nanoparticles photodeposition on TiO_2. *J. Hazard. Mater.* 211-212: 188-195.

Do YR, Lee W, Dwight K & Wold A (1994) The effect of WO_3 on the photocatalytic activity of TiO_2. *J. Solid State Chem.* 108: 198-201.

Dunnill By Charles W, Kafizas A & Parkin IP (2012) CVD production of doped titanium dioxide thin films. *Chem. Vapor. Depos.* 18: 89-101.

Egerton TA & Christensen PA (2004) *Advanced oxidation processes for water and wastewater treatment*; in: S. Parsons, IWA Publishing: London, p356.

El-Bahy ZM, Ismail AA & Mohamed RM (2009) Enhancement of titania by doping rare earth for photodegradation of organic dye (Direct blue). *J. Hazard. Mater.* 166: 138-143.

El-Maghraby EM, Nakamura Y & Rengakuji S (2008) Composite TiO_2-SnO_2 nanostructured films prepared by spin-coating with high photocatalytic performance. *Catal. Commun.* 9: 2357-2360.

Eufinger K, Poelman D, Poelman H, De Gryse R & Marin GB (2007) Photocatalytic activity of dc magnetron sputter deposited amorphous TiO_2 thin films. *Appl. Surf. Sci.* 254: 148-152.

Fan C, Xue P & Sun Y (2006) Preparation of Nano-TiO_2 doped with cerium and its photocatalytic activity. *J. Rare Earth.* 24: 309-313.

Fang D, Luo Z, Huang K & Lagoudas DC (2011) Effect of heat treatment on morphology, crystalline structure and photocatalysis properties of TiO_2 nanotubes on Ti substrate and freestanding membrane. *Appl. Surf. Sci.* 257: 6451-6461.

Fang WQ, Gong XQ & Yang HG (2011) On the Unusual properties of anatase TiO_2 exposed by highly reactive facets. *J. Phys. Chem. Lett.* 2: 725-734.

Farré M, Gajda-Schrantz K, Kantiani L & Barcelo D (2009) Ecotoxicity and analysis of nanomaterials in the aquatic environment. *Anal. Bioanal. Chem.* 393: 81-95.

Fuerte A, Hernàndez-Alonso MD, Maira AJ, Martinez-Arias A, Fernàndez-Garcia M, Conesa JC & Soria J (2001) Visible light-activated nanosized doped TiO_2 photocatalysts. *Chem. Commun.* 24: 2718-2719.

Fujishima A, Zhang X, Tryk DA (2008) TiO_2 photocatalysis and related surface phenomena. *Surf. Sci. Rep.* 63: 515-582.

Fujishima A, Rao AN & Tryk DA (2000) Titanium dioxide photocatalysis. *J. Photochem. Photobiol. C.* 1: 1-21.

Fujishima A & Honda K (1972) Electrochemical photolysis of water at a semiconductor electrode. *Nature* 238: 37-38.

Fukahori S, Ichiura H, Kitaoka T & Tanaka H (2003) Photocatalytic Decomposition of Bisphenol A in Water Using Composite TiO_2-Zeolite Sheets Prepared by a Papermaking Technique. *Environ. Sci. Technol.* 37: 1048–1051.

Furubayashi Y, Hitosugi T, Yamamoto Y, Inaba K, Kinoda G, Hirose Y, Shimada T, Hasegawa T (2005) A transparent metal: Nb-doped anatase TiO_2. *Appl. Phys. Lett.* 86: art no 252101, 1-3.

Fresno F, Tudela D, Javier Maira A, Rivera F, Coronado JM & Soria J (2006) Triphenyltin hydroxide as a precursor for the synthesis of nanosized tin-doped TiO_2 photocatalysts. *Appl. Organomet. Chem.* 20: 220-225.

Ge M, Guo C, Zhu X, Ma L, Han Z, Hu W & Wang Y (2009) Photocatalytic degradation of methyl orange using ZnO/TiO_2 composites. *Front. Environ. Sci. Engin.* 3: 271-280.

Ghicov A, Schmidt B, Kunze J & Schmuki P (2007) Photoresponse in the visible range from Cr doped TiO_2 nanotubes. *Chem. Phys. Lett.* 433: 323-326.

Grabowska E, Remita H & Zaleska A (2010) Photocatalytic activity of TiO_2 loaded with metal clusters. *Physicochem. Probl. MI.* 45: 29-38.

Gracia F, Holgado JP & Gonzalez-Elipe AR (2004) Photoefficiency and optical, microstructural, and structural properties of TiO_2 thin films used as photoanodes. *Langmuir* 20: 1688-1697.

Guo S, Han S, Mao H, Wu C, Jia L, Chi B, Pu J & Jian L (2012) Synthesis and characterization of nitrogen and phosphate codoped titanium dioxide with excellent visible light photocatalytic activity. *J. Alloys Compd.* 544: 50-54.

Guo Y, Zhang XW, Weng WH & Han GR (2007) Structure and properties of nitrogen-doped titanium dioxide thin films grown by atmospheric pressure chemical vapor deposition. *Thin Solid Films* 515: 7117-7121.

Gupta SM & Tripathi MA (2011) review of TiO_2 nanoparticles. *Chin. Sci. Bull.* 56: 1639-1657.

Gyorgy E, Socol G, Axente E, Mihailescu IN, Ducu C & Ciuca S (2005) Anatase phase TiO_2 thin films obtained by pulsed Laser deposition for gas sensing applications. *Appl. Surf. Sci.* 247: 429-433.

Hamadanian M, Reisi-Vanani A & Majedi A (2009) Preparation and characterization of S-doped TiO_2 nanoparticles, effect of calcination temperature and evaluation of photocatalytic activity. *Mater. Chem. phys.* 116: 376-382.

Hattori A, Tokihisa Y, Tada H, Tohge N, Ito S, Hongo K, Shiratsuchi R & Nogami G (2001) Patterning effect of a sol-gel TiO_2 overlayer on the photocatalytic activity of a TiO_2/SnO_2 bilayer-type photocatalyst. *J. Sol-Gel Sci. Technol.* 22: 53-61.

He C, Xiong Y, Chen J, Zha C & Zhu X (2003) Photoelectrochemical performance of Ag-TiO_2/ITO film and photoelectrocatalytic activity towards the oxidation of organic pollutants. *J. Photochem. Photobiol. A.* 157: 71-79.

He C, Yu Y, Hu X & Larbot A (2002) Influence of silver doping on the photocatalytic activity of titania films. *Appl. Surf. Sci.* 200: 239-247.

Herman D, Sicha J & Musil J (2006) Magnetron sputtering of TiOxNy films. *Vacuum* 81: 285-290.

Hernàndez-Alonso MD, Fresno F, Suàrez S & Coronado JM (2009) Development of alternative photocatalyst to TiO_2: Challenges and opportunities. *Energy Environ. Sci.* *2*: 1231-1257.

Ho W & Yu JC (2006) Sonochemical synthesis and visible light photocatalytic behavior of CdSe and CdSe/TiO_2 nanoparticles. *J. Mol. Catal A.* 247: 268-274

Ho W, Yu JC, Lin J, Yu J & Li P (2004) Preparation and photocatalytic behavior of MoS_2 and WS_2 nanocluster sensitized TiO_2. Langmuir 20: 5865-5869.

Hong X, Wang Z, Cai W, Lu F, Zhang J, Yang Y, Ma N & Liu Y (2005) Visible light activated nanoparticle photocatalyst of iodine-doped titanium dioxide. *Chem. Mater.* 17: 1548-1552.

Hugo Ricardo ZS & Angelo Fernando P (2001) Processing, microstructure and properties of Nb-TiO_2 ODS materials for surgical implants. *Zeitschrift fur Metallkunde* 92: 904-909.

Huo Y, Yang X, Zhu J & Li H (2011) Highly active and stable CdS-TiO_2 visible photocatalyst prepared by in situ sulfurization under supercritical conditions. *Appl. Catal. B.* 106: 69-75.

Hsieh CT, Fan WS, Chen WY & Lin JY (2009) Adsorption and visible light derived photocatalytic kinetics of organic dye on Co doped titania nanotubes prepared by hydrothermal synthesis. *Sep. Purif. Technol.* 67: 312-318.

Ilieva M, Nakova A & Tsakova V (2012) TiO_2/WO_3 hybrid structures produced through a sacrificial polymer layer technique for pollutant photo-and photoelectrooxidation under ultraviolet and visible light illumination. *J. Appl. Electrochem.* 42: 121-129.

Irie H, Watanabe Y & Hashimoto K (2003) Carbon doped Anatase TiO_2 powders as a visible light sensitive photocatalyst. *Chem. Lett.* 32: 772-773.

Irie H, Watanabe Y & Hashimoto K (2003) Nitrogen-Concentration Dependence on photocatalytic activity of $TiO_{2-x}N_x$ powders. *J. phys. Chem.* B. 107: 5483-5486.

Ji T, Yang F, Lv Y, Zhou J & Sun J (2009) Synthesis and visible light photocatalytic activity of Bi-doped TiO_2 nanobelts. *Mater. Lett.* 63: 2044-2046.

Jiang CZ & Dou YL (2011) Preparation of Sn^{4+} doped TiO_2 and investigation of its photocatalytic activity. *Adv. Mater. Res. 239-242*: 2671-2674.

Jiang D, Zhou T, Sun Q, Yu Y, Shi G & Jin L (2011) Enhanced Visible-Light-Induced Photoelectrocatalytic Degradation of Methyl Orange by CdS Sensitized TiO_2 Nanotube Arrays Electrode. *Chin. J. Chem.* 29: 2505-2510.

Jiang X, Fang Y, Deng A, Xiao F, Huang Y, Pan J & Yang T (2010) Preparation of Bi-doped nano-TiO_2 and degradation of organic pollutants under visible light. *Acta Energiae Solaris Sinica* 31: 291-296.

Jin Z, Tao Fei G, Hu XY, Wang M & De Zhang L (2012) Synthesis and photocatalytic activity of Cu_2O/TiO_2 Double wall nanotube arrays. J. Nanoeng. *Nanomanuf.* 2: 49-53.

Jin Z, Zhang X, Li Y, Li S & Lu G (2007) 5.1% Apparent quantum efficiency for stable hydrogen generation over eosin-sensitized CuO/TiO_2 photocatalyst under visible light irradiation. *Catal. Commun.* 8: 1267-1273.

Jo WK & Yang CH (2010) Visible-light-induced photocatalysis of low-level methyl-tertiary butyl ether (MTBE) and trichloroethylene (TCE) using element-doped titanium dioxide. *Build. Environ.* 45: 819-824.

Kamat PV (2012) TiO_2 Nanostructures: Recent Physical Chemistry Advances. *J. Phys. Chem.* 116: 11849-11851.

Kannaiyan D, Kim E, Won N, Kim KW, Jang YH, Cha MA, Ryu DY, Kim S & Kim DH (2010) On the synergistic coupling properties of composite CdS/TiO_2 nanoparticle arrays confined in nanopatterned hybrid thin films. *J. Mater.Chem.* 20: 677-682.

Kaniou S, Pitarakis K, Barlagianni I & Poulios I (2005) Photocatalyticoxidation of sulfamethazine, *Chemosphere* 60: 372-380.

Kang MG, Han HE & Kim KJ (1999) Enhanced photodecomposition of 4-chlorophenol in aqueous solution by deposition of CdS on TiO_2. *J. photochem. Photobiol. A.* 125: 119-125.

Karakitsou KE & Verykios XE (1993) Effects of altervalent cation doping of TiO_2 on its performance as a photocatalyst for water cleavage. *J. Phys. Chem.* 97: 1184-1189.

Kaur S & Singh V (2007) Visible light induced sonophotocatalytic degradation of reactive red dye 198 using dye sensitized TiO_2. *Ultrason. Sonochem.* 14: 531-537.

Keller V, Bernhardt P & Garin F (2003) Photocatalytic oxidation of butyl acetate in vapor phase on TiO_2, Pt/TiO_2 and WO_3/TiO_2 catalysts. *J. Catal.* 215: 129-138.

Keleher J, Bashant J, Heldt N, Johnson L & Li Y (2002) Photocatalytic preparation of silver-coated TiO_2 particles for antibacterial applications. *World J. Microb. Biot.* 18: 133-139.

Khan Shahed UM, Al-Shahry M & Ingler Jr WB (2002) Efficient photochemical water splitting by a chemically modified n-TiO_2. *Science* 297: 2243-2245.

Kim SY, Lim TH, Chang TS & Shin CH (2007) Photocatalysis of methylene blue on titanium dioxide nanoparticles synthesized by modified sol-hydrothermal process of $TiCl_4$. *Catal. Lett.* 117: 112-118.

Kitano M, Funatsu K, Matsuoka M, Ueshima M & Anpo M (2006) Preparation of nitrogen-substituted TiO_2 thin film photocatalysts by the radio frequency magnetron sputtering deposition method and their photocatalytic reactivity under visible light irradiation. *J. phys. Chem. B.* 110: 25266-25272.

Kitazawa S-I, Choi Y, Yamamoto S & Yamaki T (2006) Rutile and anatase mixed crystal TiO_2 thin films prepared by pulsed laser deposition. *Thin solid films* 515: 1901-1904.

Klaine SJ, Alvarez PJJ, Batley GE, Fernandes TF, Handy RD, Lyon DY, Mahendra S, McLaughlin MJ & Lead JR (2008) Nanomaterials in the environment: Behavior, fate, bioavailability, and effects. *Environ. Toxicol. Chem.* 27: 1825-1851.

Kment S, Kmentova H, Kluson P, Krysa J, Hubicka Z, Cirkva V, Gregora I, Solcova, O & Jastrabik L (2010) Notes on the photo-induced characteristics of transition metal-doped and undoped titanium dioxide thin films. *J. Colloid Interface Sci.* 348: 198-205.

Kuang S, Yang L, Luo S & Cai Q (2009) Fabrication, characterization and photoelectrochemical properties of Fe_2O_3 modified TiO_2 nanotube arrays. *Appl. Surf. Sci.* 255: 7385-7388.

Leary R & Westwood A (2011) Carbonaceous nanomaterials for the enhancement of TiO_2 photocatalysis. *Carbon* 49: 741-772.

Lee HY & Kim HG (1993) The role of gas phase nucleation in the preparation of TiO_2 films by chemical vapor deposition. *Thin solid Films* 229: 187-191.

Lin CF, Wu CH & Onn ZN (2008) Degradation of 4-Chlorophenol in TiO_2, WO_3, SnO_2, TiO_2/WO_3 and TiO_2/SnO_2 systems. *J. Hazard. Mater.* 154: 1033-1039.

Lo SF, Lin CF, Wu CH & Hsieh PH (2004) Capability of coupled CdSe/TiO_2 for photocatalytic degradation of 4-Chlorophenol. *J. Hazard. Mater.* B114: 183–190.

Li H, Wang D, Wang P, Fan H & Xie T (2009) Synthesis and studies of the visible light photocatalytic properties of near monodisperse Bi-doped TiO_2 nanospheres. *Chem. Eur. J.* 15: 12521-12527.

Li G, Dimitrijevic NM, Chen L, Rajh T & Gray KA (2008) Role of surface/interfacial Cu^{2+} sites in the photocatalytic activity of coupled CuO-TiO_2 nanocomposites. *J. Phys. Chem. C.* 112: 19040-19044.

Li J, Yun H & Lin CJ (2008) Investigations on the Fe-doped TiO_2 nanotube arrays as a photoanode for cathodic protection of stainless steel. *ESC Transactions* 3: 1-9.

Li MC & Shen JN (2006) Phoelectrochemical oxidation behavior of organic substance on TiO_2 thin-film electrodes. *J. Solid State Electrochem.* 10: 980-986.

Li D, Haneda H, Hishita S & Ohashi N (2005) Visible light-Driven N-F-Codoped TiO_2 photocatalyst.2. Optical Characterization, photocatalysis and potential application to air purification. *Chem. Mater.* 17: 2596-2602.

Li J, Liu L, Yu Y, Tang Y, Li H & Du F (2004) Preparation of highly photocatalytic active nano-size TiO_2–Cu_2O particle composites with a novel electrochemical method. *Electrochem. Commun.* 6: 940-943.

Li XZ, Liu HL & Yue PT (2000) Photoelectrocatalytic Oxidation of Rose Bengal in Aqueous Solution Using a Ti/TiO_2 Mesh Electrode. *Environ. Sci. Technol.* 34: 4401-4406.

Lindgren T, Mwabora JM, Avandano E, Jonsson J, Hoel A, Granqvist CG & Lindquist SE (2003) Photoelectrochemical and optical properties of nitrogen doped titanium dioxide films prepared by reactive DC magnetron sputtering. *J. Phys. Chem. B.* 107: 5709-5716.

Lippens PE, Chadwick AV, Weibel A, Bouchet R & Knauth P (2008) Structure and chemical bonding in Zr-doped anatase TiO_2 nanocrystals. *J. Phys. Chem. C.* 112: 43-47.

Liu Y & Du H (2011) Study on photoelectrocatalytic technology of three-dimentional electrode. Advances in Intelligent and soft computing. 104: 447-451.

Liu S, Liu G & Feng Q (2010) Al-doped TiO_2 mesoporous materials: Synthesis and photodegradation properties. *J. Porous Mater.* 17: 197-206.

Liu Y, Liu J, Lin Y, Zhang Y & Wei Y (2009) Simple fabrication and photocatalytic activity of S-doped TiO_2 under low power LED visible light irradiation. *Ceram. Int.* 35: 3061-3065.

Liu C, Chen W, Tao H & Lin T (2009) Performance of solar/S-doped TiO_2 on the decomposition of bisphenol A. *Environ. Sci.* 30: 1653-1657.

Liu Y, Li J, Qui X & Burda C (2006) Novel TiO_2 nanocatalysts for wastewater purification: Tapping energy from the sun. *Water Sci. Technol.* 54: 47-54.

Long M & Cai W (2011) Visible light responsive TiO_2 modification with nonmetal elements. *Front. Chem. China.* 6: 190-199.

Lu YM, Liu CK & Huang CM (2007) The visible photocatalyst properties of Nitrogen-doped TiO_2 thin film. *ECS Transactions* 2: 101-107.

Ma L & Tu SX (2011) Removal of arsenic from aqueous solution by two types of nano TiO_2 crystals. *Environ. Chem. Lett.* 9: 465-472.

Martins R, Britto-Costa PH & Ruotolo LAM (2012) Removal of toxic metals from aqueous effluents by electrodeposition in a spouted bed electrochemical reactor. *Environ Technol.* 33: 1123-1131.

Martinez-Huitle CA & Ferro S (2006) Electrochemical oxidation of organic pollutants for the wastewater treatment: Direct and indirect processes. *Chem. Soc. Rev.* 35: 1324-1340.

Martinez TLM, Montes de Correa C, Odriozola JA & Centeno MA (2006) Synthesis and characterization of xerogel titania modified with Pd and Ni. *J. Mol. Catal. A: Chem. 253*, 252-260.

Matos J, Laine J, Herrmann JM, Uzcategui D & Brito JL (2007) Influence of activated carbon upon titania on aqueous photocatalytic consecutive runs of phenol photodegradation. *Appl. Catal. B.* 70: 461-469.

McCullagh C, Robertson PKJ, Adams M, Pollard PM & Mohammed A (2010) Development of a slurry continuous flow reactor for photocatalytic treatment of industrial wastewater, *J. Photochem. Photobiol. A.* 211: 42-46.

Melghit K, Al-Shukeili OS & Al Amri I (2009) Effect of M-doping (M=Fe, V) on the photocatalytic activity of nanorod rutile TiO_2 for Congo red degradation under the sunlight. *Ceram. Int.* 35: 433-439.

Miller RJ, Bennett S, Keller AA, Pease S & Lenihan HS (2012) TiO_2 nanoparticles are phototoxic to marine phytoplankton. *Plos one* 7: 1-7.

Mills A & Le Hunte S (1997) An overview of semiconductor photocatalysis, *J. Photochem. Photobiol. A. 108*: 1-35.

Miyauchi M, Nakajima A, Watanabe T & Hashimoto K (2002) Photoinduced hydrophilic conversion of TiO_2/WO_3 layered thin films. *Chem. Mater.* 14: 4714-4720.

Mohamed MM, Othman I, Mohamed RM (2007) Synthesis and characterization of $MnOx/TiO_2$ nanoparticles for photocatalytic oxidation of indigo carmine dye. *J. Photochem. Photobiol. A.* 191: 153-161.

Mohammadi MR, Cordero-Cabrera MC, Ghorbani M & Fray DJ (2006) Synthesis of high surface area nanocrystalline anatase-TiO_2 powders derived from particulate sol-gel route by tailoring processing parameters. *J. Sol-Gel Sci. Technol.* 40: 15-23.

Moon J, Yun CY, Chung KW, Kang MS & Yi J (2003) Photocatalytic activation of TiO_2 under visible light using Acid Red 44. *Catal. Today* 87: 77-86.

Mu W, Herrmann JM & Pichat P (1989) Room temperature photocatalytic oxidation of liquid cyclohexane into cyclohexanone over neat and modified TiO_2. *Catal. Lett.* 3: 73-84.

Nah YC, Paramasivam I & Schmuki P (2010) Doped TiO_2 and TiO_2 nanotubes: Synthesis and applications. *Chem. Phys. Chem.* 11: 2698-2713.

Nayak BB, Acharya HN, Mitra GB & Mathur BK (1983) Structural characterization of Bi2-xSbxS_3 films prepared by the dip-dry method. Thin solid Films 105: 17-24.

Nel A, Xia T, Madler L & Li N (2006) Toxic potential of materials at the nanolevel. *Science* 311: 622-627.

Ni M, Leung MKH, Leung DYC, Sumathy K (2007) A review and recent developments in photocatalytic water-splitting using TiO2 for hydrogen production. *Renew. Sust. Energ. Rev.* 11: 401-425.

Nosaka Y, Matsushita M, Nishino J & Nosaka AY (2005) Nitrogen-doped titanium dioxide photocatalysts for visible response prepared by using organic compounds. *Sci. Technol. Adv. Mater.* 6: 143-148.

Ohno T, Mitsui T & Matsumura M (2003) Photocatalytic activity of S-doped TiO_2 photocatalyst under visible light. *Chem. Lett.* 32: 364-365.

Ohtani B, Ogawa Y, Nishimoto S-I (1997) Photocatalytic activity of Amorphous-Anatase Mixture of Titanium(IV) oxide Particles Suspended in Aqueous Solutions. *J. Phys. Chem. B.* 101: 3746-3752.

Ojani R, Raoof JB, Khanmohammadi A & Zarei E (2012) Photoelectrocatalytic degradation of 3 nitrophenol at surface of Ti/TiO_2 electrode. *J. Solid State Electrochem.* 1-16. DOI 10.1007/s10008-012-1853-x.

Ouyang J, Chang M & Li X (2012) CdS-sensitized ZnO nanorod arrays coated with TiO_2 layer for visible light photoelectrocatalysis. J. Mater. Sci. 47: 4187-4193.

Papp J, Soled S, Dwight K & Wold A (1994) Surface acidity and photocatalytic activity of TiO_2, WO_3/TiO_2 and MoO_3/TiO_2 photocatalysts. *Chem. Mater.* 6: 496-500.

Park H, Park Y, Kim W & Choi W (2012) Surface modification of TiO_2 photocatalyst for environmental applications, *J. Photochem. Photobiol. C.* 15: 1-20

Park JH, Kim S & Bard AJ (2006) Novel Carbon-doped TiO_2 nanotube arrays with high aspect Ratios for efficient solar water splitting. *Nano Lett.* 6: 24-28.

Paronyan TM, Kechiantz AM & Lin MC (2008) Highly active nanocrystalline TiO_2 photoelectrodes. *Nanotechnology* 19: art n°115201.

Peng YP, Yassitepe E, Yeh YT, Ruzybayev I, Shah SI & Huang CP (2012) Photoelectrochemical degradation of azo dye over pulsed laser deposited nitrogen-doped TiO_2 thin film. *Appl. Catal. B.* 125: 465-472.

Peng F, Cai L, Huang L, Yu H & Wang H (2008) Preparation of nitrogen-doped titanium dioxide with visible-light photocatalytic activity using a facile hydrothermal method. *J. Phys. Chem. Solids* 69: 1657-1664.

Pilkenton S & Raftery D (2003) Solid-state NMR studies of the adsorption and photooxidation of ethanol on mixed TiO_2-SnO_2 photocatalysts. Solid State Nucl. Mag. 24: 236-253.

Qiu X & Burda C (2007) Chemically synthesized nitrogen-doped metal oxide nanoparticles. *Chem. Phys.*, 339: 1-10.

Rehman S, Ullah R, Butt AM & Gohar ND (2009) Strategies of making TiO_2 and ZnO visible light active. *J. Hazard. Mater.* 170: 560-569.

Ren G, Gao Y, Yin J, Xing A & Liu H (2011) Synthesis of high-activity TiO_2/WO_3 photocatalyst via environmentally friendly and microwave assisted hydrothermal process. J. Chem. Soc. Pakistan 33: 666-670.

Ren W, Ai Z, Jia F, Zhang L, Fan X & Zou Z (2007) Low temperature preparation and visible light photocatalytic activity of mesoporous carbon-doped crystalline TiO_2. *Appl. Catal. B.* 69: 138-144.

Reyes C, Fernandez J, Freer J, Mondaca MA, Zaror C, Malato S & Mansilla H (2006) Degradation and inactivation of tetracycline by TiO_2 photocatalysis. *J. Photochem. Photobiol. A.* 184: 141–146.

Reyes-Avila J, Razo-Flores E, Gomez J (2004) Simultaneous biological removal of nitrogen, carbon and sulfur by dentrification. *Water Res.* 38: 3313-321.

Rivera AP, Tanaka K & Hisanaga T (1993) Photocatalytic degradation of pollutant over TiO_2 in different crystal structures. *Appl. Catal. B-Environ.* 3: 37-44.

Robert D (2007) Photosensitization of TiO_2 by M_xO_y and M_xS_y nanoparticles for heterogeneous photocatalysis applications. *Catal. Today* 122: 20-26.

Ryu J & Choi W (2008) Substrate-specific Photocatalytic activities of TiO_2 and multiactivity test for water treatment application. *Environ. Sci. Technol.* 42: 294-300.

Sakthivel S, Janczarek M & Kisch H (2004) Visible light activity and photoelectrochemical properties of nitrogen-doped TiO_2. *J. Phys. Chem. B.* 108: 19384-19387.

Sakthivel S & Kisch H (2003) Photocatalytic and photoelectrochemical properties of nitrogen-doped titanium dioxide. *Chem. Phys. Chem.* 4: 487-490.

Sapkal RT, Shinde SS, Mahadik MA, Mohite VS, Waghmode TR, Govindwar SP, Rajpure KY & Bhosale CH (2012) Photoelectrocatalytic decolorization and degradation of textile effluent using ZnO thin films. J. *Photochem. Photobiol.* B. 114: 102-107.

Seery MK, George R, Floris P & Pillai SC (2007) Silver doped titanium dioxide nanomaterials for enhanced visible light photocatalysis. *J. Photochem. Photobiol. A.* 189: 258-263.

Senthilnathan J & Philip L (2010) Photocatalytic degradation of lindane under UV and visible light using N-doped TiO_2. *Chem. Eng. J.* 161: 83-92.

Shen M, Wu Z, Huang H, Du Y, Zou Z & Yang P (2006) Carbon-doped anatase TiO_2 obtained from TiC for photocatalysis under visible light irradiation. *Mater. Lett.* 60: 693-697.

Silva AMT, Silva CG, Drazic G & Faria JL (2009) Ce-doped TiO_2 for photocatalytic degradation of chlorophenol. *Catal. Today* 144: 13-18.

Sobana N, Muruganadham M & Swaminathan M (2006) Nano-Ag particles doped TiO_2 for efficient photodegradation of Direct azo dyes. *J. Mol. Catal. A: Chem.* 258: 124-132.

Stengl V, Bakardjieva S & Murafa N (2009) Preparation and photocatalytic activity of rare earth doped TiO_2 nanoparticles. *Mater. Chem. Phys.* 114: 217-226.

Subramanian M, Vijayalakshmi S, Venkataraj S & Jayavel R (2008) Effect of cobalt doping on the structural and optical properties of TiO_2 films prepared by sol-gel process. *Thin Solid Films* 516: 3776-3782.

Sui R, Young JL & Berlinguette CP (2010) Sol-gel synthesis of linear Sn-doped TiO_2 nanostructures. *J. Mater. Chem.* 20: 498-503.

Sun L, Li J, Wang CL, Li SF, Chen HB & Lin CJ (2009) An electrochemical strategy of doping Fe^{3+} into TiO_2 nanotube array films for enhancement in photocatalytic activity. *Sol. Energy Mater. Sol. Cells*. 93: 1875-1880.

Shang J, Yao W, Zhu Y & Wu N (2004) Structure and photocatalytic performance of glass/SnO_2/TiO_2 interface composite film. *Appl. Catal. A.* 257: 25-32.

Shi JW, Zheng JT & Wu P (2009) Preparation, characterization and photocatalytic activities of holmium-doped Titanium dioxide nanoparticles. *J. Hazard. Mater.* 161: 416-422.

Smirnova N, Gnatyuk Y, Eremenko A, Kolbasov G, Vorobetz V, Kolbasova I & Linyucheva O (2006) Photoelectrochemical characterization and photocatalytic properties of mesoporous TiO_2/ZrO_2 films. *Int.J. photoenergy* art 85469.

Tada H, Kokubu A, Iwasaki M & Ito S (2004) Deactivation of the TiO_2 photocatalyst by coupling with WO_3 and the electrochemically assisted high photocatalytic activity of WO_3. *Langmuir* 20: 4665-4670.

Tada H, Hattori A,Tokihisa Y, Imai K, Tohge N & Ito S (2000) A Patterned TiO_2/SnO_2 Bilayer Type photocatalyst. *J. Phys. Chem. B.* 104: 4585-4587.

Takeuchi M, Sakai S, Matsuoka M & Anpo M (2009) Preparation of the visible light responsive TiO_2 thin film photocatalysts by the RF magnetron sputtering deposition method. *Res. Chem. Intermed.* 35: 973-983.

Tan, YN, Wong CL, Mohamed AR (2011) An overview on the photocatalytic activity of nano-doped-TiO_2 in the degradation of organic pollutants. *Inter.Scho. Res.Net.* 2011: ID261219, 1-18.

Tanemura S, Miao L, Wunderlich W, Tanemura M, Mori Y, Toh S & Kaneko K (2005) Fabrication and characterization of anatase/rutile-TiO_2 thin films by magnetron sputtering: A review. *Sci. Technol. Advan. Mater.* 6: 11-17.

Tae Kwon Y, Yong Song K, In Lee W, Jin Choi G & Rag Do Y (2000) Photocatalytic behavior of WO_3-loaded TiO_2 in an oxidation reaction. *J. Catal.* 191 (1): 192-199.

Tatsuma T, Saitoh S, Ngaotrakanwiwat P, Ohko Y & Fujishima A (2002) Energy storage of TiO_2-WO_3 photocatalysis systems in the gas phase. *Langmuir.* 18: 7777-7779.

The CM & Mohamed AR (2011) Role of titanium dioxide and ion-doped titanium dioxide on phtotocatalytic degradation of organic pollutants (phenol compounds and dyes) in aqueous solutions: A review. *J. Alloys Compd.* 509: 1648-1660.

Thiruvenkatachari R, Vigneswaran S & Moon IS (2008) A review on UV/TiO_2 photocatalytic oxidation process. *Korean J. Chem. Eng.* 25: 64-72.

Tian H, Ma J, Li K & Li J (2009) Hydrothermal synthesis of S-doped TiO_2 nanoparticles and their photocatalytic ability for degradation of methyl orange. *Ceram. Int.* 35: 1289-1292.

Tomas SA, Luna-Resendis A, Cortés-Cuautli LC & Jacinto D (2009) Optical and morphological characterization of photocatalytic TiO_2 thin films doped with silver. *Thin Solid Films* 518: 1337-1340.

Todorova N, Giannakopoulou T, Vaimakis T & Trapalis C (2008) Structure tailoring of fluorine-doped TiO_2 nanostructured powders. *Mat. Sci. Eng. B-Solid.* 152: 50-54.

Tsuyumoto I & Nawa K (2008) Thermochromism of Vanadium-titanium oxide prepared from peroxovanadate and peroxotitanate. *J. Mater. Sci.* 43: 985-988.

Tu YF, Huang SY, Sang JP & Zou XW (2009) Synthesis and photocatalytic properties of Sn-doped TiO_2 nanotube arrays. *J. Alloys Compd.* 482: 382-387.

Tristao JC, Magalhaes F, Corio P & Sansiviero MTC (2006) Electronic characterization and photocatalytic properties of CdS/TiO_2 semiconductor composite. *J. photochem. Photobiol. A.* 181: 152–157.

Umebayashi T, Yamaki T, Tanaka S & Asai K (2003) Visible light induced degradation of methylene blue on S-doped TiO_2. *Chem. Lett.* 32: 330-331.

Umebayashi T, Yamaki T, Itoh H & Asai K (2002) Analysis of electronic structures of 3d transition metal-doped TiO_2 based on band calculations. *J. Phys. Chem. Solids.* 63: 1909-1920.

Valentin CD, Finazzi E, Pacchioni G, Selloni A, Livraghi S, Paganini MC & Giamello E (2007) N-doped TiO_2: Theory and experiment. *Chem. Phys.* 339: 44-56.

Venkatachalam N, Palanichamy M, Arabindoo B & Murugesan V (2007) Enhanced photocatalytic degradation of 4-chlorophenol by Zr^{4+} doped nano TiO_2. *J. Mol. Catal. A: Chem.* 266: 158-165.

Vinodgopal K & Kamat PV (1995) Enhanced rates of photoccatalytic degradation of an azo dye using SnO_2/TiO_2 coupled semiconductor thin films. *Environ. Sci. Technol.* 29: 841-845.

Visser JM, Robertson LA, Van Verseveld HW, Kuenen JG (1997) Sulfur production by obligately chemolithoautotrophic Thiobacillus species. *Appl. Environ. Microbiol.* 60: 2300-2305.

Viswanathan B & Krishanmurthy KR (2012) Nitrogen incorporation in TiO_2: Does it make a visible light photoactive material. *Inter. J. Photoenergy*. ID 269654: 1-10.

Waldner G, Pourmodjib M, Bauer R & Neumann-Spallart M (2003) Photoelectrocatalytic degradation of 4-chlorophenol and oxalic acid on titanium dioxide electrodes. *Chemosphere* 50: 989–998.

Wang MC, Lin HJ, Wang CH & Wu HC (2012) Effects of annealing temperature on the photocatalytic activity of N-doped TiO_2 thin films. *Ceram. Int.* 38: 195-200.

Wang X, Hu Z, Chen Y, Zhao G, Liu Y & Wen Z (2009) A novel approach towards high performance composite photocatalyst of TiO_2 deposited on activated carbon. *Appl. Surf. Sci.* 255: 3953-3958.

Wang MC, Lin HJ & Yang TS (2009) Characteristics and optical properties of iron ion (Fe^{3+})-doped titanium oxide thin films prepared by sol-gel spin coating. *J. Alloys Compd.* 473: 394-400.

Wang Y, Li J, Peng P, Lu T & Wang L (2008) Preparation of S-TiO_2 photocatalyst and photodegradation of L-acid under visible light. *Appl. Surf. Sci.* 254: 5276-5280.

Wang H & Lewis JP (2006) Second-generation photocatalytic materials: anion-doped TiO_2. *J. Phys.Condens. Matter.* 18: 421-434.

Wang H & Lewis JP (2005) Effects of dopant states on photoactivity in carbon-doped TiO_2, *J. Phys.: Condens.* Matter. 17: L209-L213.

Wang YH, Hang K, Anderson NA & Lian TQ (2003) Comparison of Electron Transfer Dynamics in Molecule-to-Nanoparticle and Intramolecular Charge Transfer Complexes, *J. Phys. Chem. B.* 107: 9434-9440.

Wang CL, Lee HY, Azough F & Freer R (1997) The microstructure and microwave dielectric properties of zirconium titanate ceramics in the solid solution system $ZrTiO_4$-$Zr_5Ti_7O_{24}$. *J. Mater. Chem.* 32: 1693-1701.

Wong MS, Chu WC, Sun DS, Huang HS, Chen JH, Tsai PJ, Lin NT, Yu MS, Hsu SF, Wang SL & Chang HH (2006) Visible light induced bactericidal activity of a nitrogen-doped titanium photocatalyst against human pathogens. *Appl. Environ. Microbiol.* 72: 6111-6116.

Wei F, Ni L & Cui P (2008) Preparation and characterization of N-S codoped TiO_2 photocatalyst and its photocatalytic activity. *J. Hazard. Mater.* 156: 135-140.

Weir A, Westerhoff P, Fabricius L, Hristovski K & von Goetz N (2012) itanium Dioxide nanoparticles in food and personnel care products. *Environ. Sci. Technol.* 46: 2242-2250.

Westerhoff P, Song G, Hristovski K & Kiser MA (2011) Occurrence and removal of titanium at full scale wastewater treatment plants: implication for TiO_2 nanomaterials. *J. Environ. Monit.* 13: 1195-1203.

Wong MS, Hsu SW, Rao KK & Kumar CP (2008) Influence of cristallinity and carbon content on visible light photocatalysis of carbon doped titania thin films. *J. Mol. Catal. A: Chem.* 279: 20-26.

Wu Y, Long M, Cai W, Dai S, Chen C, Wu D & Bai J (2009) Preparation of photocatalytic anatase nanowire films by in situ oxidation of titanium plate. *Nanotechnology* 20: 185703-185711.

Wu SX, Ma Z, Qin YN, Qi XZ, Liang ZC (2004) Photocatalytic redox activity of doped nanocrystalline TiO_2. *Acta Phys-Chim Sin.* 20: 138-143.

Xin B, Ren Z, Hu H, Zhang X, Dong C, Shi K, Jing L & Fu H (2005) Photocatalytic activity and interfacial carrier transfer of Ag-TiO_2 nanoparticle films. *Appl. Surf. Sci.* 252: 2050-2055.

Xu D, Feng L & Lei A (2009) Characterizations of lanthanum trivalent ions/TiO_2 nanopowders catalysis prepared by plasma spary. *J. Colloid Interface Sci.* 329: 395-403.

Xu S & DD Sun (2009) Significant improvement of photocatalytic hydrogen generation rate over TiO_2 with deposited CuO. *Int. J. Hydrogen Energy.* 34: 6096-6104.

Xu XH, Wang M, Hou Y, Yao WF, Wang D & Wang H (2002) Preparation and characterization of Bi-doped TiO_2 photocatalyst. *J. Mater. Sci. Lett.* 21: 1655-1656.

Yalcin Y, Kiliç M & Cinar Z (2010) Fe^{3+}-doped TiO_2: A combined experimental and computational approach to the evaluation of visible light activity. *Appl. Catal. B.* 99: 469-477.

Yamagishi M, Kuriki S, Song PK & Shigesato Y (2003) Thin film TiO_2 photocatalyst deposited by reactive magnetron sputtering. *Thin solid Films* 442: 227-231.

Yamashita H, Harada M, Misaka J, Takeuchi M, Neppolian B, Anpo M (2003) Photocatalytic degradation of organic compounds diluted in water using visible light-responsive metal ion-implanted TiO_2 Catalysts, Fe ion implanted TiO_2. *Catal Today* 84: 191-196.

Yang L, Yu LE & Ray MB (2009) Photocatalytic oxidation of paracetamol: Dominant Reactants, Intermediates and Reactions mechanisms. *Environ. Sci. Technol.* 43: 460-465.

Yang Y, Wang H, Li X & Wang C (2009) Electrospun mesoporous W^{6+} doped TiO_2 thin films for efficient visible-light photocatalysis. *Mater. Lett.* 63: 331-333.

Yang S & Gao L (2008) New method to prepare nitrogen-doped titanium dioxide and its photocatalytic activities irradiated by visible light. *J. Am. Ceram. Soc.* 87: 1803-1805.

Ye X, Sha J, Jiao Z, Peng Z & Zhang L (1997) Structural phase transition in nanostructured TiO_2. *J. Mater. Sci. Technol.* 13: 359-360.

Yoon JW, Sasaki T & Koshizaki N (2005) Dispersion of nanosized noble metals in TiO_2 matrix and their photoelectrode properties. *Thin Solid Films* 483: 276-282.

Yoshida T, Fukami Y, Okoshi M & Inoue N (2005) Improvement of photocatalytic efficiency of TiO_2 thin films prepared by pulsed Laser deposition. *Jpn. J. Appl. Phys. Part 1.* 44: 3059-3062.

You X, Chen F & Zhang J (2005) Effects of calcination on the physical and photocatalytic properties of TiO_2 powders prepared by sol-gel template method. *J. Sol-Gel Sci. Technol.* 34: 181-187.

Yu Y, Zhao N, Shi C, He C, Liu E, Li J (2012) Electrochemical hydrogen storage of expanded graphite decorated with TiO_2 nanoparticles. *Int. Journal of Hydrogen Energ.* 37: 5762-5768.

Yu J, Hai Y & Cheng B (2011) Enhanced photocatalytic H_2-production activity of TiO_2 by $Ni(OH)_2$ cluster modification. *Journal Phys. Chem. C.* 115: 4953-4958.

Yu J, Xiang Q & Zhou M (2009) Preparation, characterization and visible light driven photocatalytic activity of Fe-doped titania nanorods and first principles study for electronic structures. *Appl. Catal. B.* 90: 595-602.

Yu HF & Hu FC (2009) Preparation and Characterization of transparent TiO_2 thin films coated on fused-silica substrates. *J. Sol-Gel.Sci. Technol.* 52: 158-165.

Yu Z & Chuang SSC (2008) The effect of Pt on the photocatalytic degradation pathway of methylene blue over TiO_2 under ambient conditions. *Appl. Catal. B. Environ.* 83: 277-285.

Yu ER, Chibirova YKh, Kulova TL & Skundin AM (2006) Products of lithium interaction with nanostructured oxides SnO_2-TiO_2 and mechanism of charge-discharge of electrodes in a lithium-ion battery. *Russ. J. Electrochem.* 42: 355-362.

Yu JC, Wu L, Jin J, Li P & Li Q (2003) Microemulsion-mediated solvothermal synthesis of nanosized CdS-sensitized TiO_2 crystalline photocatalyst. *Chem. Commun.* 9: 1552-1553.

Yu JC, Yu J, Ho W, Jiang Z & Zhang L (2002) Effects of F-doping on the photocatalytic activity and microstructures of nanocristalline TiO_2 powders. *Chem. Mater.* 14: 3808-3816.

Yun H, Lin C, Li J, Wang J & Chen H (2008) Low temperature hydrothermal formation of a net like structured TiO_2 film and its performance of photogenerated cathode protection. *Appl. Surf. 255*: 2213-2217.

Zhang Y, Xiong X, Han Y, Zhang X, Shen F, Deng S, Xiao H, Yang X, Yang G & Peng H (2012) Photoelectrocatalytic degradation of recalcitrant organic pollutants using TiO_2 film electrodes: an overview. *Chemosphere* 88: 145-154.

Zhang D & Zeng F (2011) Photocatalytic oxidation of organic dyes with visible light driven codoped TiO_2 photocatalysts. *Russ. J. Phys. Chem. A.* 85: 1077-1083.

Zhang J, Wu Y, Xing M, Khan Leghari SA & Sajjad S (2010) Development of modified N doped TiO_2 photocatalyst with metals, nonmetals and metal oxides. *Energy Environ. Sci.* 3: 715-726.

Zhang L, Lv L, Zhang W, Li R, Zhong H, Zhao Y, Zhang Y & Wang X (2009) Photo degradation of methyl orange by attapulgite-SnO_2-TiO_2 nanocomposites. *J. Hazard. Mater.* 171: 294-300.

Zhang H, Chen G & Behnemann DW (2009) Photoelectrocatalytic materials for environmental applications. *J. Mater. Chem.* 19: 5089-5121.

Zhang Z, Yuan Y, Liang L, Cheng Y, Shi G, Jin L (2008) Preparation and photoelectrocatalytic activity of ZnO nanorods embedded in highly ordered TiO_2 nanotube arrays electrode for azo dye degradation. *J. Hazard. Mater.* 158: 517-522.

Zhang YG, Ma LL, Li JL & Yu Y (2007) In situ Fenton reagents generated from TiO_2/Cu_2O Composite film: a new way to utilize TiO_2 under visible light irradiation. *Environ. Sci. Technol.* 41: 6264-6269.

Zhang H, Shen C, Chen S, Xu Z, Liu F, Li J & Gao H (2005) Morphologies and microstructures of nano-sized Cu_2O particles using a cetyltrimethylammonium template. *Nanotechnology* 16: 267-272.

Zhang X, Cao Y, Kan S, Chen Y, Tang J, Jin H, Bai Y, Xiao L, Li T & Li B (1998) Study on the photo-induced interfacial charge transfer in TiO_2/Fe_2O_3 heterostructured composite film. *Thin solid Films*. 327-329: 568-570.

Zhao L, Han M & Lian J (2008) Photocatalytic activity of TiO_2 films with mixed anatase and rutile structures prepared by pulsed Laser deposition. Thin Solid Films. 516: 3394-3398.

Zhao M, Fang L, Zhang G & Zhuang D (2004) Absorption property in visible region of $TiO_{2-x}N_x$ films prepared by reactive sputtering. *Chin. J. Mater. Res.* 18: 108-112.

Zheng SK, Wang TM, Hao WC & Shen R (2002) Improvement of photocatalytic activity of TiO_2 thin film by Sn ion implantation. *Vacuum* 65: 155-159.

Zhou B, Schulz M, Lin HY, Shah SI, Qu J & Huang C.P (2009) Photoelectrochemical generation of hydrogen over carbon-doped TiO_2 photoanode. *Appl. Catal.* B. 92: 41-49.

Zhou LM, Wang YP, Huang QW & Liu ZR (2008) Preparation and visible light activity of silver, sulfur and carbon co-doped nano-TiO_2. *Semiconduct. Optoelect.* 29: 365-369+373.

Zhu J, Deng Z, Chen F, Zhang J, Chen H, Anpo M, Huang J & Zhang L (2006) Hydrothermal doping method for preparation of Cr^{3+}-TiO_2 photocatalysts with concentration gradient distribution of Cr^{3+}. *Appl. Catal. B.* 62: 329-335.

Zuo H, Sun J, Deng K, Su R, Wei F & Wang D (2007) Preparation and characterization of Bi^{3+}-TiO_2 and its photocatalytic activity. *Chem. Eng. Technol.* 30: 577-582.

Zyoud AH, Zaatar N, Saadeddin I, Ali C, Park D, Campet G & Hilal HS (2010) CdS-sensitized TiO_2 in phenazopyridine photo-degradation: Catalyst efficiency, stability and feasibility assessment. *J. Hazard. Mater.* 173: 318-325.

CHAPITRE 5

PHOTOELECTROCATALYTIC BLEACHING OF P-NITROSODIMETHYLANILINE USING TI/TIO_2 NANOSTRUCTURED ELECTRODES DEPOSITED BY MEANS OF A PULSED LASER DEPOSITION PROCESS

Le chapitre 5 est constitué de l'article suivant :

Rimeh Daghrir, Patrick Drogui, Ibrahima Ka, My Ali El Khakani and Didier Robert (2013) Photoelectrocatalytic bleaching of p-nitrosodimethylaniline using Ti/TiO_2 nanostructured electrodes deposited by means of a pulsed laser deposition process. *Journal of Applied Electrochemistry, 43 (4): 467- 479.*

5. PHOTOELECTROCATALYTIC BLEACHING OF P-NITROSODIMETHYLANILINE USING TI/TIO_2 NANOSTRUCTURED ELECTRODES DEPOSITED BY MEANS OF A PULSED LASER DEPOSITION PROCESS

5.1 Abstract

This study investigated the potential use of oxidation in a photoelectrocatalytic cell for bleaching p-nitrosodimethylaniline. The Ti/TiO_2 used as photo-anode was prepared by a pulsed laser deposition method. The TiO_2 coatings were found to have rutile and anatase structures consisting of approximately 10 nm and 15 nm in diameter, respectively. A relatively high degradation rate of p-nitrosodimethylaniline was recorded using the photoelectrocatalytic cell, compared to those measured during conventional electrochemical oxidation, direct photolysis and photocatalysis processes. The influence of different parameters such as crystallographic structure of the Ti/TiO_2, type of cathode, potential applied, electrolysis time, UV irradiation and initial pH were investigated. The photoelectrocatalytic cell using Ti/TiO_2 (anatase structure) as photo-anode and vitreous carbon as cathode operated at a current intensity of 0.1 A for 120 min with 254 nm of UV irradiation were found to be the best conditions to remove high amounts of p-nitrosodimethylaniline (22.6 10^{-3} mM h^{-1}).

5.2 Keywords

Photoelectrocatalytic oxidation; p-nitrosodimethylaniline; reactive oxygen species; Titanium dioxide semiconductor photocatalyst

5.3 Introduction

Photo-oxidation, using semiconductors as photocatalysts, has been widely applied over the last ten years for removing organic pollutants (Hoffmann et al., 1995; Jiang et al., 2006; Xiang et al., 2011). These techniques are capable of destroying undesirable organic compounds (such as herbicides, pesticides, dyes, detergents and phenol compounds) in aqueous media and removing traces of organic species that are stable and difficult to oxidise by means of conventional water treatment methods (Li et al., 2000; Ollis et al., 1991; Hidaka et al., 1992; Li et al., 2006). Nowadays, photocatalytic process using semiconductor as photocatalyst (ex. TiO_2) under UV irradiation has been extensively applied for the oxidation of various refractory organic compounds such as bisphenol A, tetracycline, sulfamethazine, etc (Reyes et al., 2006; Fukahori et al., 2003; Kaniou et al., 2005). The basic mechanism of photocatalysis (PC) involves ejecting an electron from the valence band (VB) to the conduction band (CB) of the titanium dioxide (TiO_2) semiconductor, thereby creating an "h^+" hole in the VB (Equation 5-1). The delocalization of electrons occurs during UV irradiation of TiO_2 with energy equal to or greater than the band gap (> 3.2 eV). These charge carriers (e^- /h^+) can migrate to the surface of the catalyst, where they are then available to undergo redox reactions with substrates (Ollis et al., 1991). Nonetheless, the fast recombination of the photogenerated electron/hole (e^-/h^+) reduces the photonic efficiency and represents the major drawback of PC applications (Waldner et al., 2003; Daghrir et al., 2012). According to Meng et al. (2012), the PC efficiency of a semiconductor depends on three physical processes, including the light absorption, the transport of charge carriers and the recombination of photogenerated electron–hole pairs.

Équation 5-1 $TiO_2 + h\nu \rightarrow e^-_{CB} + h^+_{VB}$

Recently, scientists are exploring methods to modify the photo-catalyst. An impurity doping the photo-catalyst (either cations or anions) is one of the typical approaches that has been applied by several research works to enhance the photocatalytic activity toward the organic compounds such as the methyl orange (Meng et al., 2012; Cushing et al., 2012). Another approach using for example ZnO photo-catalyst coupled to another semi-conductor (CeO_2) has been conducted by Ma et al. (2010) to ensure higher photocatalytic performance for the degradation of rhodamine B. These new photo-catalyst materials ensure to extend the response toward the visible light and prevent the fast recombination of excited electron/holes during photocatalytic process (Meng et al., 2012; Ma et al., 2010). Despite the several advantages achieved by doping photo-catalyst with cations or anions, some researchers have found that the content of dopant would decrease during the annealing process, thus reducing the photocatalytic activity (Teh and Mohamed, 2011). As reported in previous research (Burda et al., 2003), the metal doped material have been shown to suffer from thermal instability and metals centers act as an electron traps which encourage the recombination of the e^-/h^+ pairs.

By comparison, photoelectrocatalytic treatment has received considerable attention in the environmental field owing to its ability to retard the recombination of electron-hole pairs (e^-_{CB}/h^+_{VB}) and the possibility to increase the lifetime of the electron-hole pairs. The photoelectrocatalytic technique combines both electrolytic and photocatalytic processes (Wang et al., 2009). The applied external potential is a key factor in the process because it accelerates the PC reaction (Waldner et al., 2003; Wang et al., 2009; Selcuk et al., 2003; Li et al., 2002). The applied external potential prevents the recombination between the photogenerated electrons and holes. Photogenerated electrons in the excited TiO_2 anode can be removed via an external bias, instead of electron transfer to molecular oxygen. As reported by Fujishima et al. (2000), the photogenerated electrons (e^-) increase the TiO_2 conductivity

and enhance the photocatalytic activity. However, the recombination between e^-/h^+ pairs reduces the quantum efficiency (Ding et al., 2010). Every recombination means a loss of a hole, a reduction in the TiO_2 conductivity and thus a decrease in the photoelectrocatalytic reaction. The external potential applied in photoelectrocatalytic process avoids their recombination by ejecting the electrons in the CB. Consequently, a photogenerated hole, or OH°, is left at the surface of the TiO_2 electrode. In the VB of the TiO_2 photocatalyst, the holes can react with adsorbed water to form hydroxyl radicals (OH°) (Equation 5-2), whereas in the CB of TiO_2, the excited electrons are trapped by O_2 to form the superoxide radical ion (O_2^-) (Equation 5-3) (Simonsen et al., 2010).

Équation 5-2 $h_{vb}^{+} + OH^- \rightarrow HO_{ads}^{\circ}$

Équation 5-3 $e^-_{CB} + O_2 \rightarrow O_2^{\circ -}$

Other reactive oxygen species (e.g., O_3, H_2O_2, etc.) can be formed during photo-electro-catalysis (Ozer and Ferry, 2001; Xie et Li, 2006; Sohrabi and Ghavami, 2010). The addition of an electron acceptor to the system, such as hydrogen peroxide and ozone, prevents the electron-hole recombination and increases the photocatalyst efficiency (Ozer and Ferry, 2001). Among these reactive oxygen species (ROS), hydroxyl radical is by far one of the most powerful oxidants that can be used in water treatment. It is highly reactive and characterised by a half-life of approximately 10^{-9} s (Xiang et al., 2011; Ishibashi et al., 2000). However, the short lifetime and the high reactivity of the hydroxyl radical make its detection very difficult. Methods for detecting hydroxyl radicals include electron paramagnetic resonance (EPR) spectroscopy (Halpern et al., 1995), fluorometric assay (Ishibashi et al., 2000) and high performance liquid chromatography (Jen et al., 1998). Nevertheless, the application of these methods is very difficult due to the need for expensive reagents and

complex operation procedures (Jiang et al., 2006). UV-visible absorption spectroscopy method is applied to investigate the hydroxyl radical (Jiang et al., 2006; Xiang et al., 2011; Simonsen et al., 2010; Kraljie and Trumbore, 1965; Zang et al., 1997). p-Nitrosodimethylaniline (RNO) is an organic dye molecule having a strong yellow colour in aqueous solution and is easy to detect using UV-visible absorption spectroscopy (440 nm) (Muff et al., 2011). RNO is bleached selectively by oxidation with hydroxyl radicals and does not react with singlet oxygen ($^1O_2$), superoxide anions (O_2^-) or other peroxy compounds (Simonsen et al., 2010; Muff et al., 2011). However, ozone, hypochlorous acid and hypochlorite are other strong chemical oxidants have also been shown to bleach RNO by chemical oxidation (Simonsen et al., 2010).

The aim of this study is to evaluate the oxidation potential of a photoelectrocatalytic cell with a nanocrystalline TiO_2 photo-anode under UV irradiation (Photoelectrocatalytic Oxidation Process (PECO)). RNO was used as a probe molecule to assess the production of reactive oxygen species. Different parameters such as current intensity, crystallographic structure of the deposited TiO_2 films, UV irradiation, initial pH and the effect of ozone and hydrogen peroxide produced *in situ* were investigated.

5.4 Materials and Methods

5.4.1 Ti/TiO_2 electrode preparation

TiO_2 coatings were prepared using a pulsed laser deposition (PLD) method. A KrF excimer laser (wavelength = 248 nm, pulse durations 15 nanoseconds) operating at a repetition rate of 30 Hz was focused, at an incidence angle of 45°, onto the TiO_2 rotating target (99.95% purity). The on-target laser energy density was set to 4.5 J cm^{-2}. The TiO_2 films were deposited on both titanium grids (for photoelectrochemical studies) and on silicon substrates (for material characterisations). The TiO_2 films were deposited at a temperature of 600°C and

400°C, respectively, under an oxygen background pressure of 1 mTorr. The PLD deposition chamber was first turbo-pumped to approximately 10^{-6} Torr before filling it with oxygen. More details on the pulsed laser deposition system and it schematics can be found elsewhere (Desbiens and El Khakani, 2003). Prior to coating the substrates, the TiO_2 target was systematically cleaned by laser-ablating its surface for 5 min. The nominal thickness of the coating was estimated to 400 nm for rutile TiO_2 and 1 μm for anatase TiO_2. The film thickness was determined directly from cross-sectional scanning electron microscopy (SEM) observations. The crystallographic structure of the PLD-deposited TiO_2 films was examined by means of X-ray diffraction (XRD) using a Philips X'pert-MPD X-ray diffractometer (Cu K_α radiation) at a glancing incident angle of 1°. The composition and chemical bonding states of the TiO_2 films were investigated by means of X-ray photoelectron spectroscopy (XPS) using Al K_a monochromatic radiation (1487 eV) in an ESCALAB 200I-XL spectrophotometer after a systematic *in situ* surface cleaning by 5 keV Ar+ ion sputtering.

5.4.2 Preparation of the synthetic solution

RNO (N, N-Dimethyl-4-nitroso-aniline) was an analytical grade reagent supplied by Sigma Aldrich (purity 97%). An RNO stock solution (4 10^{-3} mol L^{-1}) was prepared in a glass tank containing 1 L of buffer in which 600. 72 mg of RNO was added. Solubilisation of RNO was carried out by stirring at a speed of 900 rpm for 120 min. Mixing was achieved using a Teflon-covered stirring bar deposited in the bottom of the beaker. The RNO stock solution is stable for periods up to several weeks when protected from light. At the end of this conditioning stage, a fraction of the mixture (12 mL) was transferred into a 2 L tank containing 1 L of buffer solution. The resulting mixture constituted the synthetic RNO solution (final concentration of 4.80 10^{-5} mol L^{-1}) in which 0.05 mol L^{-1} of sodium sulphate was added to increase the electrical conductivity. Buffer solutions were prepared using

anhydrous dibasic sodium phosphate (99% purity) and crystalline monobasic potassium phosphate (99% purity). The pH value of the buffer solution was 7.0.

5.4.3 Experimental device

The reactor unit was made of an acrylic material with dimensions of 12.7 cm (width), 16.51 cm (length) and 11.43 cm (depth). A quartz window (8.89 cm x 8.89 cm) was disposed on one face of the reactor for the photoelectrocatalysis experiments (Figure 5-1). All of the assays were conducted in batch mode. The photoelectrocatalytic cell was comprised of one anode (Ti/TiO_2) and one cathode, each having a surface area of 110 cm^2 (10 cm width x 11 cm high), placed in parallel and submerged in the solution. Different cathode materials were investigated: stainless steel (SS), vitreous carbon (VC) and graphite (Gr). The electrodes were installed vertically on a perforated Plexiglas plate placed 2 cm from the bottom of the cell. The inter-electrode gap was 1.0 cm. Both the anode and cathode were connected to the positive and negative outlets, respectively, of a regulated DC power supply (PS 3030 D, Circuit-Test Electronics, Burnaby, BC, Canada) with a maximum current rating of 3.0 A at an open circuit potential of 30 V. The photoelectrocatalytic cell was operated at currents ranging from 0.02 A to 0.1 A for treatment periods of 120 min. Two mercury lamps with 254 nm (light intensity = 6.9 mW cm^{-2}) and 365 nm (light intensity = 0.3 mW cm^{-2}) illumination were used to irradiate the catalytic surface of Ti/TiO_2 photo-anode. The lamp was positioned vertically on a support inside the reactor. The light intensity was measured with a photometer (Model PS-3, 99-0057-01; UVP Company, USA). The light intensity is the luminous power imposed per unit area of photoelectrocatalytic reactor. The photoelectrocatalytic reactor was placed in a dark chamber to avoid interference from the daylight. Mixing in the cell was achieved using a Teflon-covered stirring bar installed between the perforated plate and the bottom of the cell. All experiments were carried out at room temperature (25°C). For all tests a total volume of 1.0 L was used. Na_2SO_4 (0.05 M) was used as the supporting electrolyte.

For the reactions at different pH, hydrochloric acid or sodium hydroxide solutions were added to adjust the initial pH of the RNO solution. Sodium sulphate was an analytical grade reagent supplied by Mat laboratory (Quebec, QC, Canada). Anhydrous dibasic sodium phosphate and crystalline monobasic potassium phosphate were analytical grade reagents and supplied by EMD Chemicals (Darmstadt, Germany).

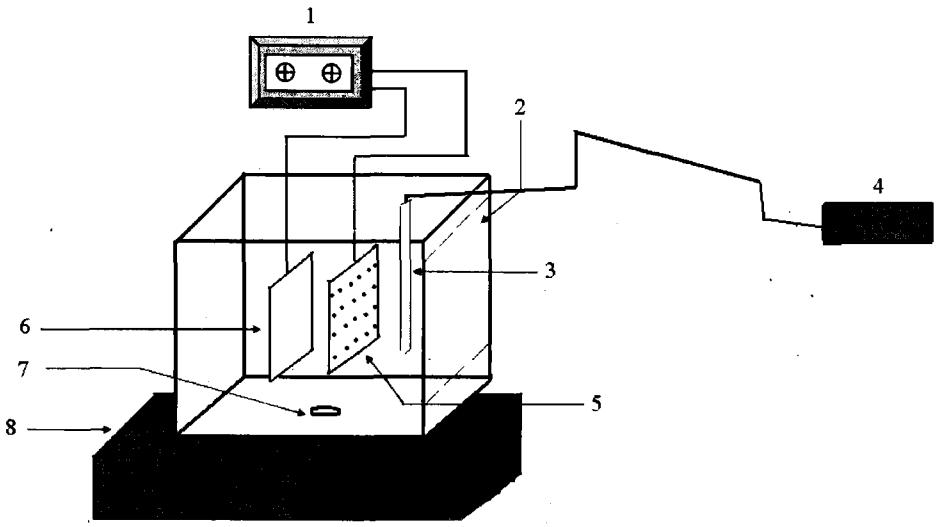


Figure 5-1 Schematic diagram of the photoelectrocatalytic reactor: (1) DC power supply (2) quartz window (3) UV lamp (4) photometer (5) photoanode (6) cathode (7) stirring bar (8) magnetic stirrer.

5.4.4 Analytical techniques

The pH was determined using a pH meter (Fisher Acumet model 915) equipped with a double-junction Cole-Palmer electrode with an Ag/AgCl reference cell. The bleaching rate was monitored by absorbance measurements of RNO at 440 nm using an UV-visible

absorption spectrophotometer (UV 0811 M136, Varian, Australia). The RNO calibration curve was obtained by plotting the RNO absorbance at 440 nm as a function of RNO concentration (from 0.0 mol L^{-1} to 5.32 10^{-5} mol L^{-1}). ROS (O_3 and OH°) produced *in situ* have been shown to bleach RNO by chemical oxidation (Simonsen et al., 2010). The oxidizing species include the "h^+" holes created in the VB.

The hydrogen peroxide concentration was measured using volumetric dosage. The cerium ion solution (Ce $(SO_4)_2$, $2(NH_4)_2$ SO_4, 2 H_2O) (5.88 10^{-3} M) was used under acidic conditions (H_2SO_4, 9N) in the presence of three drops of $Fe(o\text{-}phen)_3^{2+}$ as an indicator. To quantitatively determine the concentration of hydrogen peroxide, the H_2O_2 calibration curve was obtained by plotting the cerium volume (mL) as a function of H_2O_2 concentration (from 0 mol L^{-1} to 2.94 10^{-3} mol L^{-1}). The gradual change of the solution colour from red to the blue indicates a total oxidation of hydrogen peroxide using the cerium solution.

The ozone concentration was determined using the indigo method (Bader et Hoigne, 1981). A stock solution of the indigo reagent was prepared by dissolving 770 mg L^{-1} of potassium indigo trisulphonate in 1 mL phosphoric acid. When the absorbance at 600 nm had decreased to below 80% of the initial value, the stock solution of indigo was replaced (typically after 3-4 months storage). For low concentrations of ozone, 20 mL of indigo stock solution (2.49 10^{-5} M) was dissolved in 10 g monobasic sodium phosphate (Na_2HPO_4) and 7 mL phosphoric acid. The ozone calibration curve was obtained by plotting the absorbance as a function of O_3 concentration (standard solution with different concentrations from 0.0 moL L^{-1} to 1.87 10^{-6} moL L^{-1}). The standard solutions of ozone were prepared using an ozone generator (OzoStar, model WL7, Ozocan Corporation, Ontario, Canada).

5.5 Results and discussions

5.5.1 Characterisation of the Ti/TiO_2 electrode

The surface morphology of the TiO_2 photocatalytic coating was examined by scanning electron microscopy. Figure 5-2 shows a top view of a TiO_2 film deposited at 600°C and 400°C onto silicon substrates. The coating is densely featured with fine spherical grains of a few tens of diameters. By increasing the temperature from 400°C to 600°C, the deposited TiO_2 showed an increase in crystallite size.

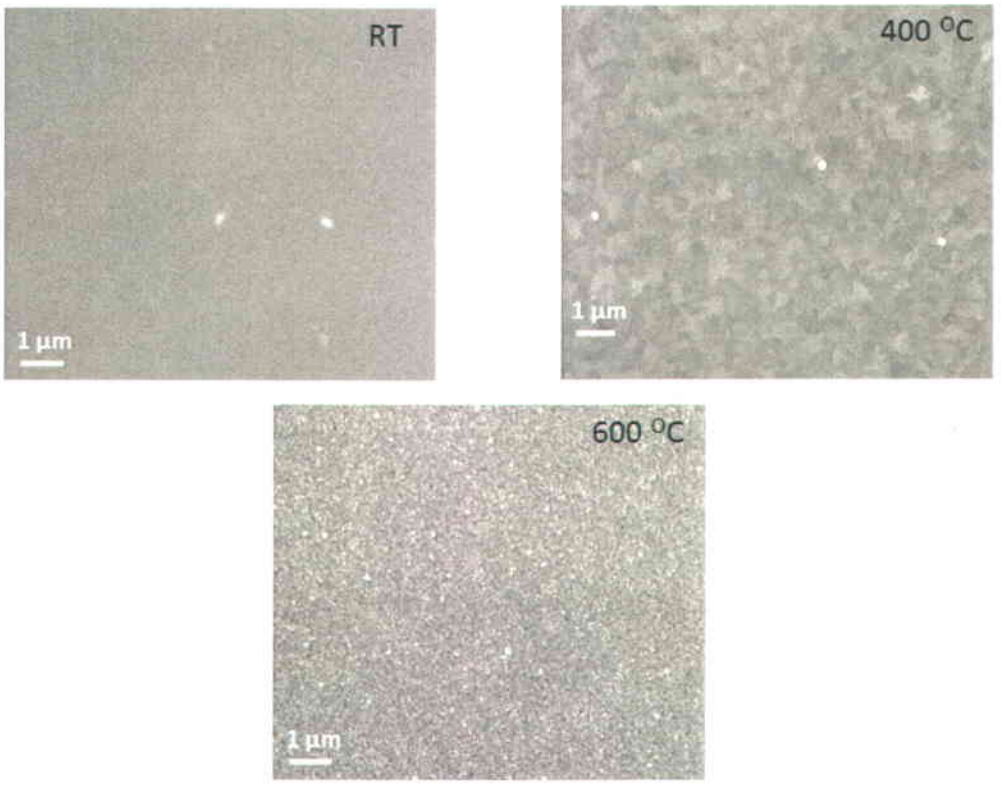


Figure 5-2 SEM views of PLD TiO_2 films deposited on Si at different deposition temperatures.

Figure 5-3 (a, b) shows that the TiO_2 columns are densely packed with a uniform thickness across the film, forming a smooth and continuous interface with the underlying substrate.

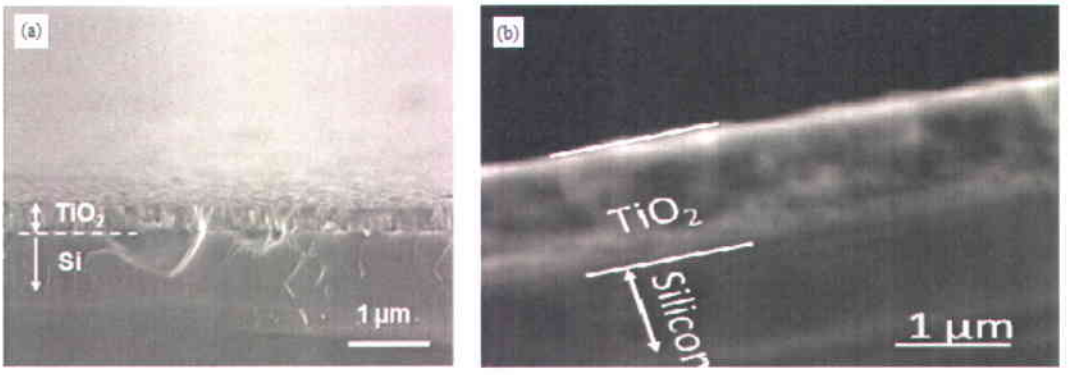


Figure 5-3 SEM views of PLD TiO_2 films deposited on silicon.

The crystallographic structure of the TiO_2 coating prepared by PLD was characterised by XRD (Figure 5-4). The XRD analysis indicates that our TiO_2 coatings deposited at 600°C and 400°C are polycrystalline and crystallise in the TiO_2 rutile phase and in the TiO_2 anatase phase, respectively (Figure 5-4 (a)). The TiO_2 rutile phase is generally obtained for deposition at temperatures above 550°C (Kitazawa et al., 2006; Jaroenworaluck et al., 2010; Regonini et al., 2010), while at temperature below 500°C only the TiO_2 anatase phase is found (Fang et al., 2011). The XRD spectrum of the TiO_2 coating on the Ti-grid confirms the presence of the same TiO_2 rutile phase and the same TiO_2 anatase phase obtained on Si (the peak intensities are less prominent than the peaks of the underlying metallic Ti grid because of the thinness of the TiO_2 coating compared to the Ti grid substrate) (Figure 5-4(b), Figure 5-4(c)). Interestingly, one can note that the main (110) and (101) XRD peak of the TiO_2 phase is broader in the case of the films deposited onto the Ti grid than on Si substrates. The average size of TiO_2 crystallites is smaller on the Ti grid than on Si. To quantify this substrate-

dependent grain size effect, the average size (D) of the TiO_2 crystallites was estimated using the Debye–Scherer equation (Guinier, 1962):

Équation 5-4 $$D = \frac{0.9\lambda}{\Delta(2\theta)\cos\theta}$$

Where D is the grain size in a particular orientation (i.e.; (110) and (101) here), λ is the X-ray wavelength, 2θ is the diffraction angle corresponding to the particular orientation and Δ (2θ) is the width at half maximum of the peak.

Thus, the average size of the TiO_2 rutile crystallites was estimated to approximately 29 nm on silicon and only approximately 10 nm on the Ti-grid substrates. By comparison, the average size of the TiO_2 anatase crystallites was estimated to approximately 26 nm on silicon and only approximately 15 nm on the Ti-grid substrates. The smoothness of the silicon substrate promotes the growth of TiO_2 crystallites with increasing temperature.The average size of the TiO_2 particles (anatase) deposited on the Ti-grid is greater than the average size of TiO_2 rutile structure deposited on the Ti-gird. This result agrees with the data obtained from the SEM images and is likely due to the rougher surface of the Ti grids compared to silicon grids. This nanometre scale grain size is expected to have an important effect on the photocatalytic activity of the TiO_2 coating (Kim et al., 2007). Indeed, with a decrease in particle size, the catalytic activity is enhanced due to the huge increase in the surface area (or surface to volume ratio) of the material.

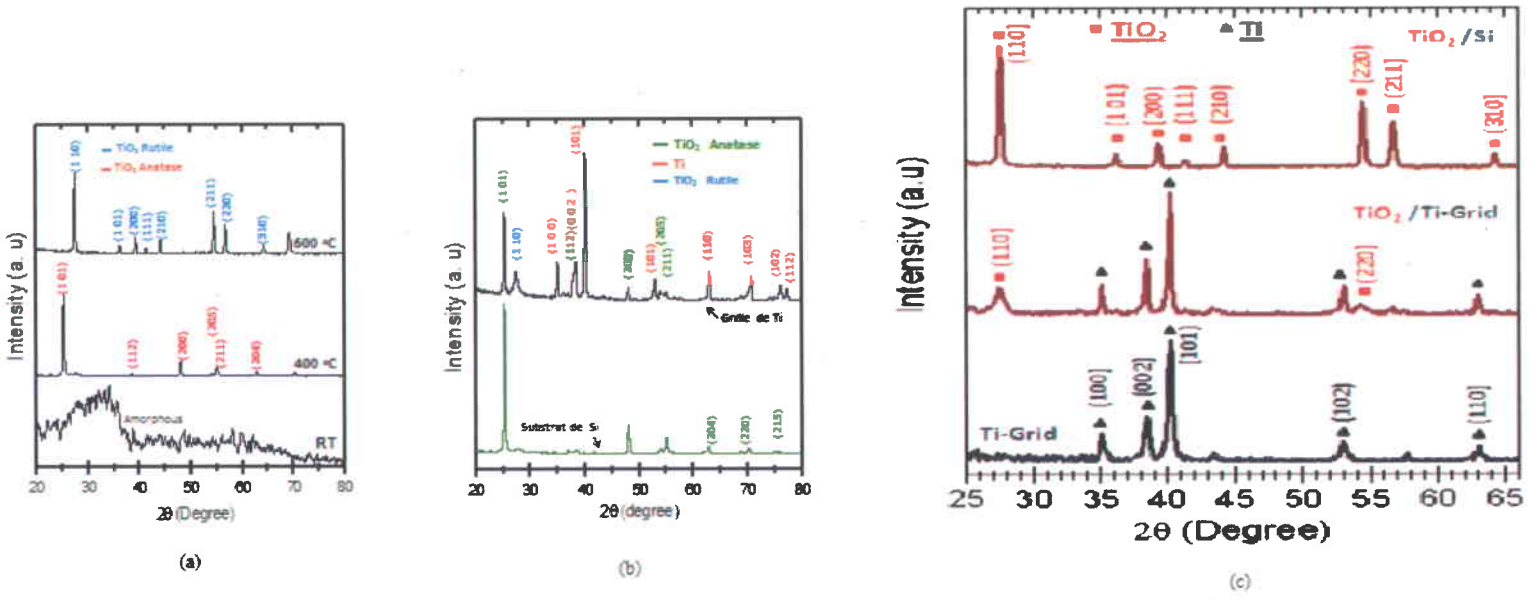


Figure 5-4 X-ray diffraction patterns of TiO_2 film coated at (a) 600°C and 400°C; (b) on Si substrates and; (c) Ti grids.

5.5.2 Bleaching of RNO

Experiments using direct photolysis (DP), electro-oxidation (EO), PC and PECO processes were carried out to compare the degradation efficiencies of RNO. The DP process involved exposing the RNO solution to UV irradiation at 254 nm, whereas in the PC process, UV light (254 nm) was used in the presence of the Ti/TiO_2 catalyst (rutile). The EO process was applied to the RNO solution using the Ti/TiO_2 catalyst at the anode, while in the PECO process the Ti/TiO_2 photoanode (rutile) was exposed to UV irradiation (254 nm) and an external potential. The results of RNO degradation using different experimental conditions are shown in Figure 5-5. As is observed from this data, the bleaching rate of RNO increased with treatment time. The ROS were produced continuously over time and rapidly oxidised the nitroso groups. The RNO removal rate recorded in the solution over 120 min using the DP process was 6.52 10^{-3} mM h^{-1}. By comparison, exposure to the Ti/TiO_2 electrode (rutile) under UV irradiation (PC process) increases the degradation rate of RNO (6.69 10^{-3} mM h^{-1}). In the PC process, the photogeneration of oxidising species, such as hydroxyl radicals or holes, leads to their reaction with the conjugated double bonds in the π system of RNO and promotes thus the bleaching of RNO (Simonsen et al., 2010). According to Zang et al. (1997), the oxidation process is thermodynamically favoured because the VB of TiO_2 (+ 2.5 V/NHE at pH 7) is much higher than the oxidation potential of RNO (+ 0.3 V/NHE at pH 7). Furthermore, the degradation rate of RNO by the EO process was tested using rutile Ti/TiO_2 as an anode at 0.1 A. The removal rate of RNO recorded over 120 min of treatment was 7.12 10^{-3} mM h^{-1}. However, a more rapid RNO removal rate (15.9 10^{-3} mM h^{-1}) was recorded over 120 min using the PECO process with the Ti/TiO_2 photo-anode (rutile) at 0.1 A. In the PECO process, UV radiation activates the Ti/TiO_2 semi-conductor by ejecting an electron from the VB to the CB, while the applied external potential prevents recombination of the electron-

hole pairs. These charge carriers (e^-/h^+) can migrate to the surface of the catalyst, where they are then available to undergo redox reactions with substrates (Yang et al., 2009).

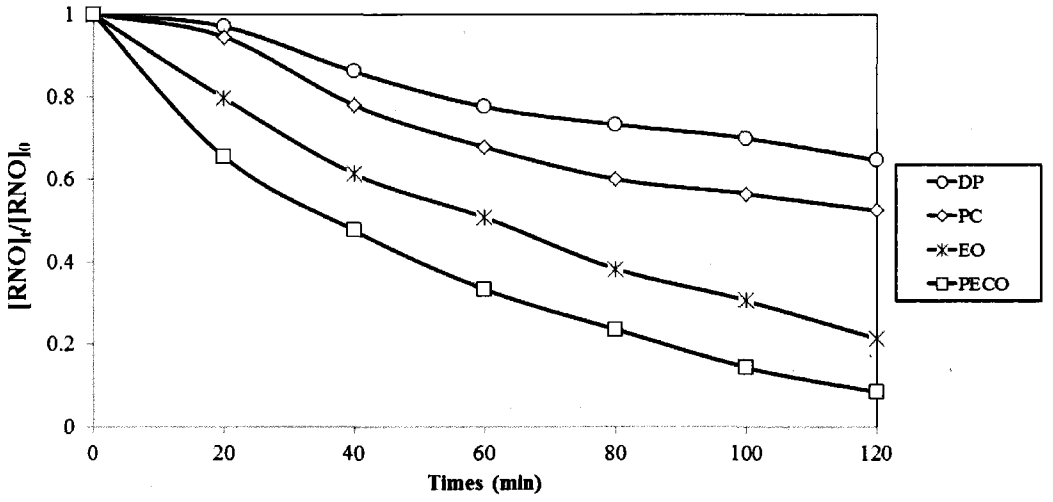


Figure 5-5 Bleaching of RNO using different processes.

The RNO bleaching rate was determined under DP, PC, EO and PECO conditions. The oxidizing species (i.e., OH°, O_3, h^+) production rate is equal to the RNO disappearance rate according to Equation 5-5.

Équation 5-5
$$r = \frac{d[RNO]}{dt} = -k.[RNO]$$

Where "[RNO]" is the concentration of RNO, "k" is the first order reaction rate constant (t^{-1}) and "r" is the production rate of oxidizing species (such as OH°, h^+, O_3).

Integration of Equation 5-5 gives:

Équation 5-6 $$Ln\left(\frac{C_0}{C}\right) = k.t$$

Where "C_0" is the initial concentration of RNO, "C" is the concentration of RNO at time t and "t" is the reaction time. The reaction rate constant "k" could be calculated from the slope of a plot of (t) versus Ln (C_0/C) from Equation 5- 6.

Figure 5-6 shows that the RNO disappearance rate follows a first-order kinetic model. The first-order kinetic reaction rate constant in the PECO process was 0.02 min^{-1}. By comparison, the values of the apparent reaction rate constants for the DP, PC and EO processes were 0.0038 min^{-1}, 0.0058 min^{-1} and 0.012 min^{-1}, respectively. The apparent reaction rate constant found for the PECO process was 3.4 times higher than that recorded under the PC conditions and 1.67 times higher than that measured using EO conditions. The contribution of external potential applied in photoelectrocatalytic process influences the production rate of oxidizing species (OH°, h^+, O_3) and consequently the kinetic rate of pollutant degradation (Daghrir et al., 2012). In the PECO process, the applied potential reduces the recombination rate of the photogenerated electron-hole pairs, enhances the production rate of oxidizing species and consequently increases the bleaching rate of RNO. Therefore, the electrons and holes have more opportunities to participate in the degradation of RNO directly on the surface of nanostructured Ti/TiO_2 photo-anode (adsorption) or indirectly by reacting with oxidant species such as hydroxyl radicals (Adams et al., 2002). RNO molecules were firstly adsorbed on Ti/TiO_2 and subsequently, the reactive oxygen species such as OH°, h^+, etc predominantly attack the ring structure and induce the cleavage of the RNO. The mechanism of the adsorption of organic pollutant (such as rhodamine) on the photocatalyst surface (TiO_2 or TiO_2/SnO_2) using photocatalytic process has been widely highlighted by Chen et al. (2003). This work provide that the photocatalytic degradation of dye proceeds on the surface of the

photo-catalyst rather than on the bulk solution and the reactive oxygen species preferentially attack the molecular portion directly connected to the catalyst surface. However, the pollutant adsorbed on the surface of the catalyst can inhibit the reaction between the photo-generated holes (or hydroxyl radicals) and pollutant, and consequently decrease the degradation rate of pollutant (Ding et al., 2010). A far as, the competition reaction between intermediate products for reacting with hydroxyl radicals could also inhibit the kinetic degradation of pollutant (Wang et al., 2009).

Several researchers (Wang et al., 2009; Ding et al., 2010; Leng et al., 2006) have shown that the efficiency of removing pollutants using the PECO process is influenced by various operating factors such as external potential, pH, UV light intensity and material phase structure. These parameters influence the oxidation potential, and consequently pollutant removal. Thus, the next step in our study was to investigate the effect of various operating parameters on the bleaching rate of RNO using the PECO process.

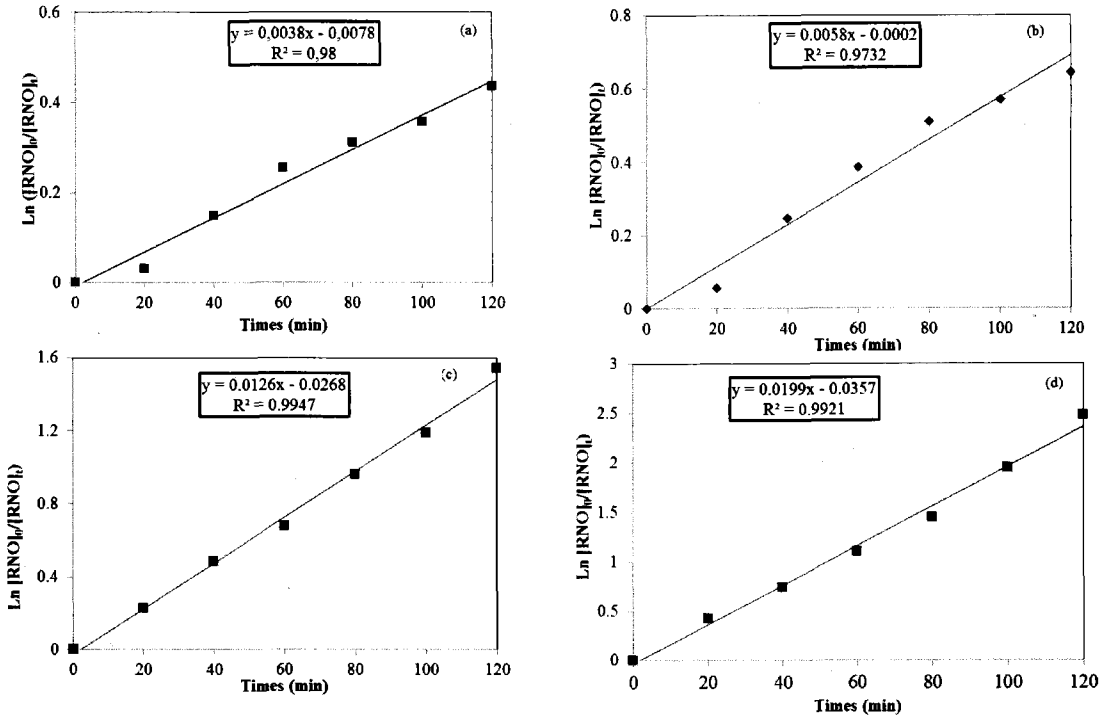


Figure 5-6 Kinetic studies of bleaching of RNO using (a) DP (b) PC (c) EO and (d) PECO processes.

5.5.3 Effect of the crystallographic structure

Three different structures of Ti/TiO_2 films (anatase, rutile, amorphous) were used for the PECO process to compare RNO removal efficiencies. The RNO removal rates using different experimental conditions (tests T1 to T6) are shown in Table 5-1. For amorphous Ti/TiO_2, the RNO removal rate was slower than that recorded using anatase and rutile Ti/TiO_2 structures. The amorphous structure of Ti/TiO_2 contains large amounts of defects that can lead to an increase in the number of recombination sites for photo-generated electron-hole pairs, and consequently leads to a relatively low concentration of oxidising species (Xiang et al., 2011; Yu et al., 2007a; Yu et al., 2007b). The RNO degradation rate using the rutile structure was lower than that recording when using the anatase structure. RNO removal rates were 0.013 ± 0.0008 mMh^{-1} and 0.010 ± 0.0008 mMh^{-1} over 120 min using rutile Ti/TiO_2 at 0.1 A

and 0.05 A, respectively. In comparison, for the same current intensities (0.1 A and 0.05 A), the average RNO removal rates using anatase Ti/TiO_2 were 0.018 ± 0.002 mM h^{-1} and 0.013 ± 0.001 mM h^{-1}, respectively. This result was not surprising because the band gap energy of the anatase phase (3.23 eV) is wider than that of the rutile phase (3.02 eV) (Yoon et al., 2006). This lower band gap energy of the rutile phase promotes the recombination of electrons and holes on the surface of the structure and reduces the production of oxidant species, such as hydroxyl radical. Thus, the anatase Ti/TiO_2 structure was selected for the next step of the experiments.

Tableau 5-1 Effect of crystallographic structure on the rate of RNO removal.

Parameters	PECO Process					
	Test 1	**Test 2**	**Test 3**	**Test 4**	**Test 5**	**Test 6**
Intensity (A)	0.1	0.1	0.1	0.05	0.05	0.05
Treatment times (min)	120	120	120	120	120	120
UV light intensity ($\mu W\ cm^{-2}$)	6900	6900	6900	6900	6900	6900
UV lamp position	Internal	Internal	Internal	Internal	Internal	Internal
Electrolyte (Na_2SO_4 M)	0.05	0.05	0.05	0.05	0.05	0.05
Type of cathode	Stainless steel	Stainless steel	Stainless steel	Stainless steel	Stainless steel	Stainless steel
Type of anode Structure (Ti/TiO_2)	rutile	anatase	amorphous	rutile	anatase	amorphous
Rate of RNO removal ($mM\ h^{-1}$)	0.12 ± 0.007	0.16 ± 0.02	0.10 ± 0.01	0.09 ± 0.007	0.12 ± 0.01	0.09 ± 0.015

PECO: Photoelecrtrocatalytic oxidation

5.5.4 Effect of external potential

According to the literature (Wang et al., 2009; Selcuk et al., 2003), external electrical potential is one of the key factors that improve photoelectrocatalytic efficiency. Applying an external potential at the TiO_2 photo-anode improves the separation of the photogenerated electrons and holes and prevents recombination. In our study, the effect of current intensity (from 0.02 A to 0.1 A) was explored in the PECO process with irradiation at 254 nm using anatase Ti/TiO_2. Figure 5-7 shows the RNO degradation rate as a function of current intensity applied over the treatment time of 120 min. It can be observed that the RNO bleaching efficiency increased when the applied current increased from 0.02 A to 0.1 A (from 7.2 V to 13.1 V). The maximum RNO bleaching rate ($17.3\ 10^{-3}$ mM h^{-1}) was obtained at 0.1 A over 120 min. In the PECO process, the electrical potential applied prevents the recombination of electron-hole pairs, increases the active hole lifetime, and consequently increases the concentration of oxidant species, such as hydroxyl radicals (Ding et al., 2010; An et al., 2004; Vinodgopal et al., 1993). The effect of electrical potential on hydroxyl radical production has been studied by Jiang et al. (2006). That study showed that the total concentration of hydroxyl radicals (higher than 20 μmol L^{-1}) generated under UV irradiation (20 W) was effectively enhanced with a small applied potential (0.6 V). Therefore, the current intensity selected for the next step of optimisation of the PECO process was 0.1 A.

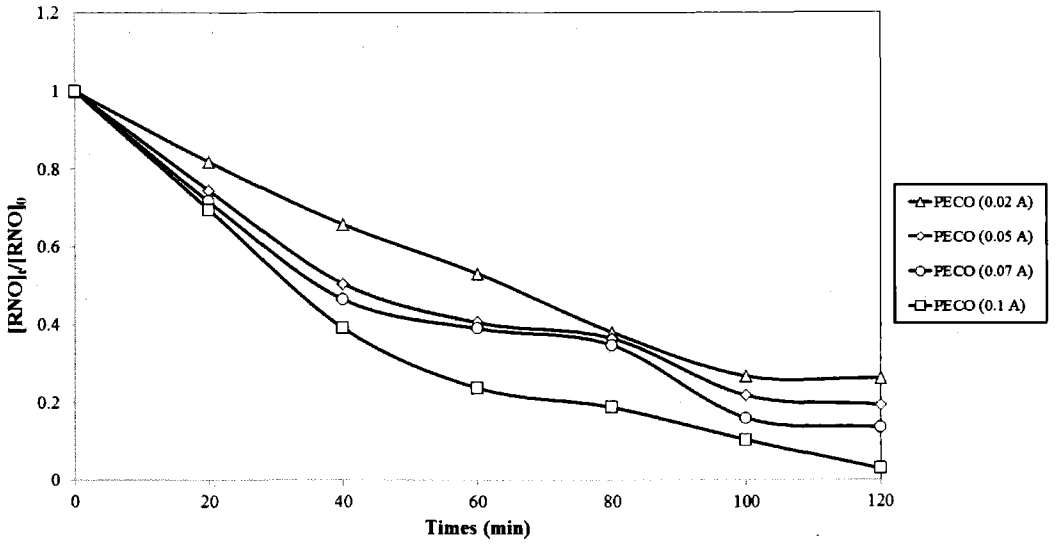


Figure 5-7 Bleaching of RNO using the PECO process under different current intensities (Effect of external potential) (at 254 nm and using Ti/TiO_2 anatase).

5.5.5 Effect of light intensity

In the PC and PECO processes, the recombination of electron-hole pairs is a limiting step (Venkatachalam et al., 2007). By increasing the intensity of the incident light, the probability of catalyst excitation and the re-excitation of recombined electrons are increased (Wang et al., 2009). To assess the effect of light intensity (6900 μW cm^{-2} versus 300 μW cm^{-2}) on the RNO bleaching rate, experiments using the DP, PC and PECO processes were carried out over 120 min of treatment time. The oxidative performance of the DP, PC and PECO processes (formation of active oxidant species) was evaluated by comparing the RNO bleaching rate under different light intensities. The results of RNO degradation using different experimental conditions are shown in Figure 5-8. These results revealed that the bleaching rate increased with increasing the light intensity from 300 μW cm^{-2} to 6900 μW cm^{-2}. In the DP, PC and

PECO processes, the removal rates of RNO recorded using a light intensity of 6900 $\mu W\ cm^{-2}$ (254 nm) were 6.52 10^{-3} mM h^{-1}, 8.55 10^{-3} mM h^{-1} and 17.3 10^{-3} mM h^{-1}, respectively. By comparison, the RNO removal rates detected using a light intensity of 300 $\mu W\ cm^{-2}$ (365 nm) were 1.26 10^{-3} mM h^{-1} (DP), 5.36 10^{-3} mM h^{-1} (PC) and 15.7 10^{-3} mM (PECO). Thus, the decrease in the wavelength from 365 nm (0.3 mW cm^{-2}) to 254 nm (6.9 mW cm^{-2}) corresponds to an increase in the energy of the incident photon by a factor of 1.43 (according to the Planck equation $E = h\ c/\lambda$), whereas in terms of light intensity a factor of 23 is introduced. Thus, this higher degradation rate of RNO recorded by PECO process is mainly attributed to the effect of light intensity. The increase in the light intensity promotes the formation of reactive oxygen species (such as hydroxyl radicals) and improves the RNO bleaching rate. The effect of light intensity on the degradation of 4-chlorophenol using the photoelectrocatalytic process was also studied by Wang et al. (2009). Increasing light intensity (from 700 $\mu W\ cm^{-2}$ to 2.5 mW cm^{-2}) enhances the formation of hydroxyl radicals and improves the degradation rate of 4-chlorophenol (95 % at 2.5 mW cm^{-2}). It has been proven by previous research (Li et al., 2002) that the degradation rate of organic pollutant is proportional to the light intensity ($k^{\circ} = k_2\ I^b$, where k° is the degradation reaction rate; I the light intensity; and k_2 and b are the kinetic constants). As the photoelectrocatalytic-bleaching rate of RNO was found to depend strongly of the applied light intensity applied to the surface of the catalysts, UV radiation with a light intensity of 6900 $\mu W\ cm^{-1}$ was selected for further study.

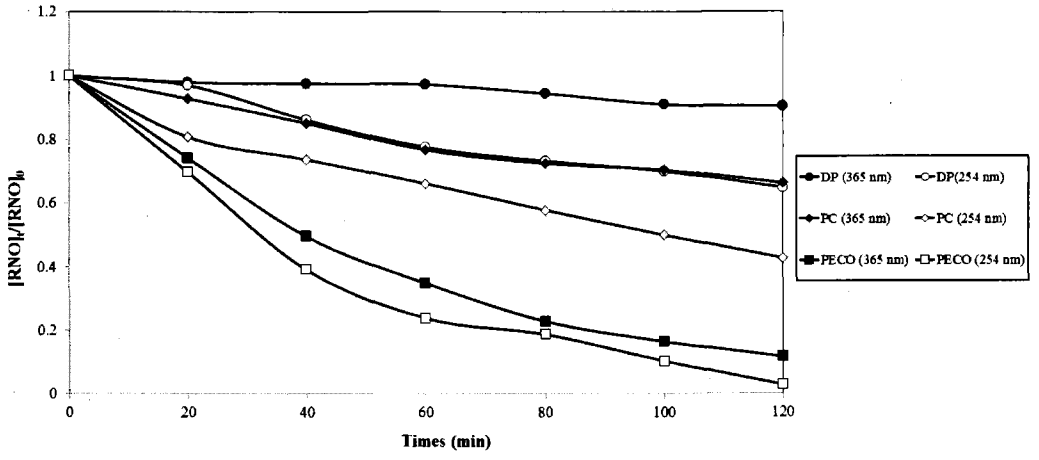


Figure 5-8 Bleaching of RNO using the PECO process (at 0.1 A and using Ti/TiO_2 anatase) under different light intensities.

5.5.6 Effect of pH

In photocatalytic reactions, pH is one of the most important parameters that influence the degradation of pollutants (Wang et al., 2009; Liang et al., 2008; Gaya and Abdullah, 2008; Quan et al., 2007). Solution pH affects the adsorption capacity and dissociation of the target compounds, the charge distribution of the photocatalyst surface, and the oxidation potential of the VB (Wang et al., 2009; Quan et al., 2007; Chong et al., 2010). To investigate the effect of pH on the bleaching rate using the PECO process, the pH of the RNO solution was adjusted using 5 M NaOH or 1.5 M HCl. In a pH range of 6.2-10, the maximum RNO absorption peak is 440 nm, whereas at a pH value below 6.2, the maximum RNO absorption peak shifts to 350 nm (Simonsen et al., 2010; Muff et al., 2011). According to Simonsen et al. (2010), the loss of the light absorption proprieties (from 440 nm to 350 nm) under acidic conditions is

due to interaction of protons with the nitrogen atoms (in the tertiary amine or in the nitroso group) present in RNO molecule.

Équation 5-7 $RNO_{(aq)} + H^{+} \leftrightarrow RNOH^{+}_{(aq)}$

The effect of pH on RNO degradation is shown in Figure 5-9. With an increase in solution pH (from 2.7 to 11), the RNO bleaching rate (R_0) increased. The use of neutral and alkaline pH conditions was more beneficial to RNO bleaching. From the Figure 5-9, we see that the highest bleaching rate (17.7 10^{-3} mM^{-1} h^{-1}) was recorded at a pH value of 7. For pH values above 7, the bleaching rate reaches a plateau. The changes in the RNO degradation rate with varying pH values can be attributed to variation of the acid/base properties of the TiO_2 surface (Simonsen et al., 2010). When the pH is below 3.7, the TiO_2 surface becomes positively charged ($TiOH_2^{+}$) and strongly repels the RNO molecule, which can also possess a positive charge ($RNOH^{+}$). For pH values between 3.7 and 6.5, the bleaching rate was enhanced. In this range, a slight repulsion between the positively charged RNO molecule ($RNOH^{+}$) and the surface of TiO_2 (slightly charged) (Zang et al., 1997). For pH values above 6.5, the electrostatic attraction between the negatively charged TiO_2 surface (TiO^{-}) and the RNO molecule was enhanced, and the bleaching rate increased. The results recorded in our study are consistent with the results obtained by Zang et al. (1997) who studied the effect of pH on RNO bleaching using the PC process. These results demonstrate clearly that a pH value of 7.0 is optimal for effective RNO bleaching. According to previous research work (Xu et Langford 2001; Zhao et al., 1998), the adsorption of organic molecules on the surface of photocatalysts had been proved to influence greatly the photocatalytic degradation of the organic compounds. For instance, TiO_2 and TiO_2/SnO_2 systems were investigated by Chen et al. (2003) to understand the influence of the adsorption mode and illumination radiation in the

degradation of Rhodamine B. The adsorption of rhodamine B on the TiO_2/SiO_2 surface has been recorded by the positively-charged diethylamino group while in the case of TiO_2, it adsorbs through the negatively-charged carboxyl group (Chen et al., 2003). Subsequently, the reactive oxygen species produced by photocatalytic process ensure the degradation of rhodhamine.

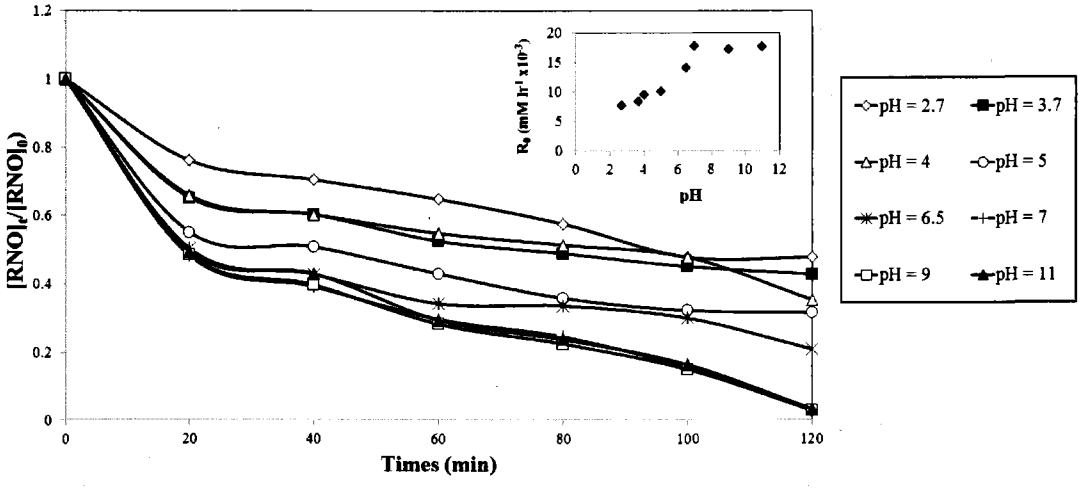


Figure 5-9 Bleaching of RNO using the PECO process (at 0.1 A under 254 nm using Ti/TiO_2 anatase) at different pH.

5.5.7 Effect of H_2O_2 produced at the cathode electrode

The main objective is to evaluate the effect of ROS produced *in situ* on the RNO bleaching efficiency. ROS, such as H_2O_2, can be generated at the cathode (Xie and Li, 2006). The addition of oxidising species, such as H_2O_2 is beneficial for photocatalytic reaction by trapping the electron in the CB and generating more hydroxyl radicals (Xie and Li, 2006; Sohrabi and Ghavami, 2010).

Three types of cathode electrodes (SS, Gr, and VC) were tested to evaluate their capacity for H_2O_2 production in the photoelectrocatalytic cell using a solution of distilled water and

Na_2SO_4 (0.05 M) without the addition of RNO. Experiments were performed using Ti/TiO_2 (anatase) as the photo-anode with (or without) UV irradiation (254 nm). Hydrogen peroxide concentrations generated under the different experimental conditions are shown in Figure 5-10. The maximum concentration of H_2O_2 (0.23 mM) was recorded after a treatment time of 120 min using VC as the cathode at a current intensity of 0.1 A without UV illumination. Under the same conditions, the concentration of H_2O_2 detected after 120 min using Gr as the cathode was 0.15 mM. Recent studies have demonstrated that VC and Gr used as a cathode material can lead to the electrochemical generation of H_2O_2 (Xie and Li, 2006). However, it was surprising to measure a residual H_2O_2 concentration in solution using SS as a cathode material.

In fact, the H_2O_2 (~ 0.09 mM) produced during 120 min of electrolysis was not produced at the SS cathode, but it was produced on the photo-anode material. The same trend has been also obtained by Daghrir et al. (2013) while studying the photoelectrocatalytic oxidation of CTC using different cathode materials. The residual H_2O_2 concentration recorded at 0.39 A of current intensity, after 120 min of treatment time and using Ti/TiO_2 (anatase) as anode and SS as cathode was 0.09 ± 0.002 mM. The observed peroxide was mainly formed during reactions (Equations 5.8-5.14) occurring at the surface of the Ti/TiO_2 catalyst (Daghrir et al., 2013; Macphee et al., 2011). H_2O_2 is one of the oxidising species that can be formed on the surface of Ti/TiO_2 in the presence or in the absence of UV irradiation. Indeed, in the absence of UV irradiation, only the applied current (or the potential difference) during electrolysis results in excitation of the Ti/TiO_2 catalyst. Under these conditions, adsorbed oxygen ($O_{2(ads)}$) can directly participate in the reaction by trapping the electron (e^-) present in the CB, generating superoxide anion ($O_2^{\circ-}$), and subsequently H_2O_2. The reduction mechanism of O_2 to generate $O_2^{\circ-}$ is thermodynamic favoured as the conduction band of TiO_2 (-0.52V) is much electronegative than reduction potential of $O_2/O_2^{\circ-}$ (-0.33 V) (Wood, 1998).

Équation 5-8 $e^- + O_{2\,(ads)} \rightarrow O_2^{\circ -}$

Équation 5-9 $O_2^{\circ -} + H^+ \rightarrow HO_2^{\circ}$

Équation 5-10 $2HO_2^{\circ} \rightarrow H_2O_2 + O_2$

Équation 5-11 $O_2^{\circ -} + HO_2^{\circ} \rightarrow O_2 + HO_2^-$

Équation 5-12 $HO_2^- + H^+ \rightarrow H_2O_2$

Équation 5-13 $O_2 + 2\acute{e}_{CB} + 2H^+ \rightarrow H_2O_2$

Équation 5-14 $2H_2O + 2h^+_{VB} \rightarrow H_2O_2 + 2H^+_{aq}$

Nevertheless, under UV irradiation (254 nm), H_2O_2 concentrations recorded after 120 min of treatment at a current intensity of 0.1 A using VC, Gr and SS as the cathode were 0.15 mM, 0.11 mM and 0.07 mM, respectively. The decrease in the concentration of H_2O_2 was attributed to hydroxyl radical formation, which is generated from the decomposition of H_2O_2 under UV irradiation (Equation 5-15) (Ollis et al., 1991; Hua et al., 1995; Tizaoui et al., 2011).

Équation 5-15 $H_2O_2 + h\nu \rightarrow 2OH^{\circ}$

To evaluate the effect of the cathode on the RNO bleaching rate, additional experiments were carried out using the following conditions: 0.1 A under, UV irradiation at 254 nm, 4.80 10^{-5} M RNO. The different cathode electrode materials (SS, Gr, and VC) were explored. The bleaching rate recorded using VC as a cathode material was 22.6 10^{-3} mM h^{-1}. By comparison, the RNO bleaching rates recorded using SS and Gr as cathode electrodes were 15.8 10^{-3} mM h^{-1} and 19.2 10^{-3} mM h^{-1}, respectively. The significantly higher rate (22.6 10^{-3} mM h^{-1}) of

RNO bleaching recorded using VC as cathode and TiO_2 (anatase form) as photoanode is mainly due the oxidizing species (OH°, h^+, O_3) generated by PECO process. Besides, the bleaching rate of RNO may be due to the reductive mechanism. The reduction potential of RNO has been reported to be +0.04V versus NHE at pH 7.0, which is more electropositive than the conduction band of TiO_2 (-0.52 V) (Zang et al., 1997). Thus, the photo-generated electrons on the conduction band are able to reduce RNO. The reduction process is believed to bring an electron into the antibonding π electron system of RNO promoting the decrease of the total bonding energy of the π electron system and cleave the bond (Simonsen et al., 2010). It could be interesting to compare the bleaching rate of RNO recorded by PECO process with those obtained in others experimental conditions. Simonsen et al. (2010) indicated that the photocatalytic bleaching rate of RNO using TiO_2 coated liner under UV irradiation (14 W low pressure lamp, 254 nm, 20 mW cm^{-2}) is 8.9 10^{-9} M s^{-1}. This bleaching rate reported in the literature is higher than those recorded in the present study. The corresponding bleaching rate recorded by PECO process in our study (62 10^{-10} M s^{-1}) was lower than that recorded by Simonsen et al. (2010). The contribution of experimental conditions such as the light intensity influences the production rate of oxidizing species (h^+, OH°, etc) and consequently the bleaching rate of RNO. The UV light intensity imposed during the photoelectrocatalytic process (6.9 mW cm^{-2}) was lower than the UV light imposed by Simonsen et al. (2010).

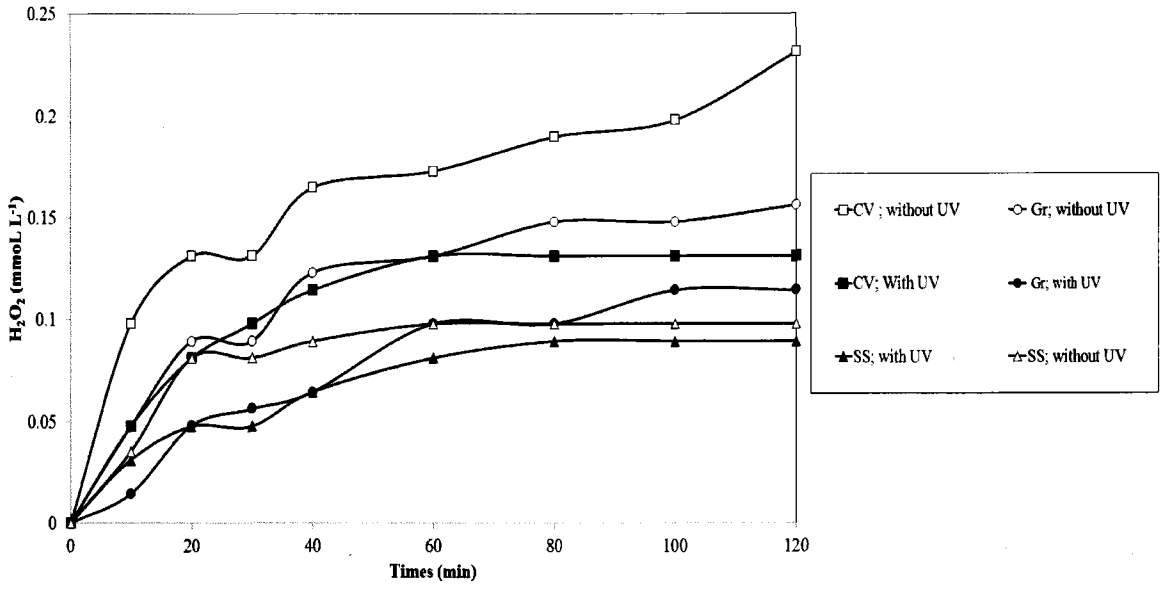


Figure 5-10 H_2O_2 production during electrolysis at 0.1 A and under 254 nm.

5.5.8 Effect of ozone production

Ozone is a very strong oxidant (E° = 1.51 V/ENH) that can be generated by electrolytic oxidation of a water molecule (Equation 5-16) (Kitsuka et al., 2009). The capacity for ozone production in the photoelectrocatalytic cell under the typical synthetic conditions (distilled water + Na_2SO_4 (0.05 M) without RNO addition) was evaluated. The final concentration of ozone recorded after 120 min of electrolysis at 0.1 A using Ti/TiO_2 (anatase) as the photo-anode and VC as the cathode with UV irradiation (254 nm) was approximately 0.313 μM. Ozone generated *in situ* can directly participate in the bleaching of RNO (Simonsen et al., 2010). However, when the photocatalytic reaction was initiated (under UV radiation), hydroxyl radicals were generated from the decomposition of ozone (Equations 5-17-5-19)) (Hong et al., 2007). The decomposition of ROS (such as H_2O_2 and O_3) increases the hydroxyl radical concentration and leads to an enhanced RNO bleaching rate.

Équation 5-16 $3\ H_2O \rightarrow O_3 + 6\ H^+ + 6e^-$

Équation 5-17 $O_3 + h\nu \rightarrow O_2 + O°$

Équation 5-18 $O° + H_2O \rightarrow 2OH°$

Équation 5-19 $O_3 + OH° \rightarrow HO_2^{\circ} + O_2$

5.6 Conclusion

In this study, a rectangular Ti/TiO_2 electrode was prepared by a PLD method. The TiO_2 coating formed at 600°C and 400°C is very uniform in thickness and forms a continuous interface with the substrate. In addition, X-ray diffraction analysis indicated that the TiO_2 coating formed on the Ti-grid is of the rutile phase and the coating formed on Si is of the anatase phase. The main (110) and (101) XRD peaks of the rutile and anatase structures are broader in the case of TiO_2 deposited onto the Ti grid than on the Si substrate. Using Ti/TiO_2 nanostructured electrodes, a photoelectrocatalytic cell was constructed and evaluated in terms of its capacity to degrade RNO. The current intensity, crystallographic structure of the Ti/TiO_2 anode, type of cathode material, UV irradiation and initial pH all had a significant influence on the RNO bleaching rate. The photoelectrocatalytic cell prepared using anatase Ti/TiO_2 as the photo-anode and VC as the cathode electrode, operated at a current of 0.1 A for 120 min with UV irradiation (254 nm), was found to be the best for removing large amounts of RNO at a rate of 22.63 10^{-3} mM h^{-1}. However, the identification of by-products needs to be rigorously verified and a mechanism of RNO degradation should be proposed. The photoelectrocatalytic technique could form the basis of a process capable of removing refractory organic compounds from many natural and wastewater sources (drinking water, industrial and municipal wastewater). The next step in this investigation should involve the study of the treatment of water contaminated by emerging and persistent organic pollutants

(POPs), such as antibiotics, pesticides, estrogenic compounds and alkylphenols, using a surface response methodology.

5.7 Acknowledgments

Sincere thanks are extended to the National Sciences, Engineering Research Council of Canada and Premier Tech Ltée for their financial support of this study.

5.8 References

Adams C, Wang MY, Loftin K & Meyer M (2002) Removal of antibiotics from surface and distilled water in conventional water treatment processes. *J. Environ. Eng.* 128: 253-260.

An T, Zhang W, Li G, Xiao X, Sheng G, Fu J & Zhu X, Photoelectrocatalytic degradation of quinolone with a novel three-dimentional electrode-packed bed photocatalytic reactor. *J. Photochem. Photobiol. A.* 161: 233-242.

Bader H & Hoigné J (1981) Determination of ozone in water by the indigo method. *Water Res.* 15 (4): 449-456.

Burda C, Lou Y, Chen X, Samia A C S, Stout J & Gole JL (2003) Enhanced Nitrogen doping in TiO_2 nanoparticles. *Nano Lett.* 3: 1049-1051.

Chen F, Zhao J & Hidaka H (2003) Highly selective deethylation of rhodamine B: Adsorption and photooxidation pathways of the dye on the TiO_2/SiO_2 composite photocatalyst. *Int. J. Photoenergy* 5(4) 209-217.

Chong MN, Jin B, Chow CWK & Saint C (2010) Recent developpements in photocatalytic water treatment technology: A review. *Water Res.* 44 (10): 2997-3027.

Cushing SK, Li J, Meng F, Senty TR, Suri S, Zhi M, Li M, Bristow AD & Wu N (2012) Photocatalytic Activity Enhanced by Plasmonic Resonant Energy Transfer from Metal to Semiconductor. *J. Am. Chem. Soc.* 134 (36): 15033–15041.

Daghrir R, Drogui P & El-Khakani MA (2013) Photoelectrocatalytic degradation of chlortetracycline using Ti/TiO_2 photo-anode with simultaneous H_2O_2 production. *Electrochem. Acta* 87: 18-31.

Daghrir R, Drogui, P & Didier, R (2012) Photoelectrocatalytic technologies for environmental applications. *J. photochem. Photobiol. A.* 238: 41-52.

Daghrir R, Drogui P, Ka I & El-Khakani MA (2012) Photoelectrocatalytic degradation of chlortetracycline using Ti/TiO_2 nanostructured electrodes deposited by means of a Pulsed Laser deposition process. *J. Hazard. Mater.* 199–200: 15–24.

Desbiens E & El Khakani MA (2003) Growth of high-K silicon oxynitride thin films by means of a pulsed laser deposition-atomic nitrogen plasma source hybrid system for gate dielectric applications. *J. Appl. Phys.* 94(9): 5969-5975.

Ding Y, Yang C, Zhu L & Zhang J (2010) Photoelectrochemical activity of liquid phase deposited TiO_2 film for degradation of benzotriazole. *J. Hazard. Mater.* 175: 96-103.

Fang D, Luo Z, Huang K & Lagoudas DC (2011) Effect of heat treatment on morphology, crystalline structure and photocatalysis properties of TiO_2 nanotubes on Ti substrate and freestanding membrane. *Appl. Surf. Sci.* 257 (15): 6451-6461.

Fukahori S, Ichiura H, Kitaoka T & Tanaka H (2003) Photocatalytic Decomposition of Bisphenol A in Water Using Composite TiO_2-Zeolite Sheets Prepared by a Papermaking Technique. *Environ. Sci. Technol.* 37: 1048–1051.

Fujishima A, Rao TN & Tryk AD (2000) Titanium dioxide photocatalysis. *J. Photochem. Photobiol.C.* 1: 1-21.

Gaya UI & Abdullah AH (2008) Heterogeneous photocatalytic degradation of organic contaminants over titanium dioxide: A review of fundamentals, progress and problems. *J.Photochem. Photobiol.C.* 9 (1): 1-12.

Guinier A (1962) *Théorie et Technique de la radiocristallographie.* 3rd ed. Dunod, Paris, 740p.

Halpern HJ, Yu C, Barth E, Peric M & Rosen GM (1995) In situ detection, by spin trapping, of hydroxyl radical markers produced from ionizing radiation in the tumor of a living mouse. *Proc. Nat. Acad.Sci.* USA 92 (3): 796-800.

Hidaka H, Nohara K, Zhao J, Serpone N & Pelizzetti, E (1992) Photo-oxidative degradation of the pesticide permethrin catalyzed by irradiated TiO_2 semiconductor slurries in aqueous media. *J. Photochem. Photobiol. A.* 64 (2): 247-254.

Hoffmann MR, Martin ST, Choi W & Bahnemann DW (1995) Evironmental applications of semiconductor photocatalysis. *Chem. Rev.* 95 (1): 69-96.

Hong Q, De-zhi S & Guo-qing C (2007) Formaldehyde degradation by UV/TiO_2/O_3 process using continuous flow mode. *J. Environ. Sci.* 19: 1136-1140.

Hua Z, Manping Z, Zongfeng X & Low GKC (1995) Titanium dioxide mediated photocatalytic degradation of monocrotophos. *Water Res.* 29 (12): 2681-2688.

Ishibashi Ki, Fujishima A, Watanabe T & Hashimoto K (2000) Quantum yields of active oxidative species formed on TiO_2 photocatalyst. *J Photochem Photobiol A* 134 (1-2): 139-142.

Ishibashi Ki, Fujishima A, Watanabe T & Hashimoto K (2000) Detection of active oxidative species in TiO_2 photocatalysis using the fluorescence technique. *Electrochem. Commun.* 2 (3): 207-210.

Jaroenworaluck A, Regonini D, Bowen CR & Stevens R(2010) A microscopy study of the effect of heat treatment on the structure and properties of anodized TiO_2 nanotubes. *Appl. Surf. Sci.* 256: 2672-2679.

Jen JF, Leu MF &Yang TC (1998) Determination of hydroxyl radicals in an advanced oxidation process with salicylic acid trapping and liquid chromatography. *J. Chromatogr. A.* 796 (2): 283-288.

Jiang YL, Liu HL, Wang QH & Jiang ZH (2006) Determination of hydroxyl radicals in TiO_2/Ti Photoelectrocatalytic oxidation system using $Fe(phen)_3^{2+}$ spectrophotometry. *J. Environ. Sci.* 18(1): 158-161.

Kaniou S, Pitarakis K, Barlagianni I & Poulios I (2005) Photocatalyticoxidation of Sulfamethazine. *Chemosphere* 60: 372-380.

Kim CS, Kwon IM, Moon BK, Jeong JH, Choi BC, Kim JH, Choi H, Yi SS, Yoo DH, Hong KS, Park JH & Lee HS (2007) Synthesis and particle size effect on the phase transformation of nanocrystalline TiO_2. *Mater. Sci. Eng.* C 27: 1343-1346.

Kitazawa Si, Choi Y, Yamamoto Sh & Yamaki T (2006) Rutile and anatase mixed crystal TiO_2 thin films prepared by pulsed laser deposition. *Thin Solid Films* 515(4): 1901-1904.

Kitsuka K, Kaneda K, Ikematsu M, Iseki M, Mushiake K & Ohsaka T (2009) Ex situ and in situ characterization studies of spin-coated TiO_2 film electrodes for the electrochemical ozone production process. *Electrochim. Acta* 55 (1): 31-36.

Kraljié I & Trumbore CN (1965) p-Nitrosodimethylaniline as an OH radical scavenger in radiation chemistry. *J. Am. Chem. Soc.* 87: 2547-2550.

Leng WH, Zhu WC, Ni J, Zhang Z, Zhang JQ & Cao CN (2006) Photoelectrocatalytic destruction of organics using TiO_2 as photoanode with simultaneous production of H_2O_2 at the cathode. *Appl. Catal. A.* 300 (1): 24-35.

Li J, Li LJ, Zheng L, Xian Y & Jin L (2006) photoelectrocatalytic degradation of rodhamine B using Ti/TiO_2 electrode prepared by laser calcination method. *Electrochim. Acta.* 51(23): 4942 -4949.

Li, XZ, Li FB, Fan CM & Sun YP (2002) Photoelectrocatalytic degradation of humic acid in aqueous solution using a Ti/TiO_2 mesh photoelectrode. *Water Res.* 36(9): 2215-2224.

Li XZ, Liu HL, Yue PT & Sun YP (2000) Photoelectrocatalytic oxidation of rose Bengal in aqueous solution using a Ti/TiO_2 mesh electrode. *Environ. Sci. Technol.* 34 (20): 4401-4406.

Liang HC, Li XZ, Yang YH & Sze KH (2008) Effects of dissolved oxygen, pH, and anions on the 2,3-dichlorophenol degradation by photocatalytic reaction with anodic TiO_2 nanotube films. *Chemosphere* 73 (5): 805-812.

Ma TY, Yuan ZY & Cao JL (2010) Hydrangea-Like Meso-/Macroporous $ZnO-CeO_2$ Binary Oxide Materials: Synthesis, Photocatalysis and CO Oxidation. *Eur. J. Inorg. Chem.* 2010 (5): 716-724.

Macphee DE, Rosenberg D, Skellern MG, Wells RP, Duffy JA & Killham KS (2011) A tungsten oxide-based photoelectrocatalyst for degradation of environmental comtaminants. *J. Solid State Electrochem.* 15 (1): 99-103.

Meng F, Hong Z, Arndt J, Li M, Zhi M, Yang F & Wu N (2012) Visible Light Photocatalytic Activity of Nitrogen-Doped $La_2Ti_2O_7$Nanosheets Originating from Band Gap Narrowing. *Nano. Res.* 5(3): 213–221.

Muff J, Bennedsen LR & Søgaard EG (2011) Study of electrochemical bleaching of p-nitrosodimethylaniline and its role hydroxyl radical probe compound. *J. Appl. Electrochem.* 41(5): 599-607.

Ollis DF, Pelizzetti E & Serpone N (1991) Photocatalysed destruction of water contaminants. *Environ. Sci. Technol.* 25 (9): 1522-1529.

Ozer RR & Ferry JL (2001) Investigation of the photocatalytic activity of TiO_2-polyoxometalate systems. *Environ. Sci. Technol.* 35(15): 3242-3246.

Quan X, Ruan X, Zhao H, Chen S & Zhao Y (2007) Photoelectrocatalytic degradation of pentachlorophenol in aqueous solution using a TiO_2 nanotube film electrode. *Environ. Pollut.* 147 (2): 409-414.

Regonini D, Jaroenworaluck A, Stevens R & Bowen CR (2010) Effect of heat treatment on the properties and structure of TiO_2 nanotubes: Phase composition and chemical composition. *Surf. Interface Anal.* 42: 139-144.

Reyes C, Fernandez J, Freer J, Mondaca MA, Zaror C, Malato S & Mansilla H (2006) Degradation and inactivation of tetracycline by TiO_2 photocatalysis. *J.Photochem. Photobiol. A.* 184:141–146.

Selcuk H, Sene JJ & Anderson MA (2003) Photoelectrocatalytic humic acid degradation kinetics and effect of pH, applied potential and inorganic ions. *J. Chem. Technol. Biotechnol.* 78 (9): 979-984.

Simonsen ME, Muff J, Bennedsen LR, Kowalski KP & Søgaard EG (2010) Photocatalytic bleaching of p-nitrosodimethylaniline and a comparison to the performance of other AOP technologies. *J. Photochem. Photobiol .A.* 216: 244-249.

Sohrabi MR & Ghavami M (2010) Comparison of Direct Yellow 12 dye degradation efficiency using UV/semiconductor and UV/H_2O_2/semiconductor systems. *Desalination* 252 (1-3): 157-162.

Teh CM, Mohamed AR (2011) Role of titanium dioxide and ion-doped titanium dioxide on phtotocatalytic degradation of organic pollutants (phenol compounds and dyes) in aqueous solutions: A review. *J. Alloys Compd.* 509: 1648-1660.

Tizaoui C, Mezughi K & Bickley R (2011) Heterogeneous photocatalytic removal of the herbicide clopyralid and its comparison with UV/H_2O_2 and ozone oxidation techniques. *Desalination* 273 (1): 197-204.

Venkatachalam N, Palanichamy M, Arabindoo B & Murugesan V (2007) Enhanced photocatalytic degradation of 4-chlorophenol by Zr^{4+} doped nano TiO_2. *J. Mol. Catal. A.* 266 (1-2): 158-165.

Vinodgopal K, Hotchandani S & Kamat PV (1993) Electrochemically assisted photocatalysis TiO_2 particulate film electrodes for photocatalytic degradation of 4-chlorophenol. *J. Phys. Chem.* 97: 9040-9044.

Wang N, Li X, Wang Y, Quan X & Chen G (2009) Evaluation of bias potential enhanced photocatalytic degradation of 4-chlorophenol with TiO_2 nanotube fabricated by anodic oxidation method. *Chem. Eng. J.* 146 (1): 30-35.

Waldner G, Pourmodjib M, Bauer R & Neumann-Spallart M (2003) Photoelectrocatalytic degradation of 4-chlorophenol oxalic acid on titanium dioxide electrodes. *Chemosphere* 50 (8): 989-998.

Wood PM (1998) The potential diagram for oxygen at pH 7. *Biochem.J.* 253: 287-289.

Xiang Q, Yu J & Wong PK (2011) Quantitative characterization of hydroxyl radicals produced by various photocatalysts. *J. Colloid Interface Sci.* 357 (1): 163-167.

Xie YB & Li XZ (2006) Degradation of bisphenol A in aqueous solution by H_2O_2 assisted photoelectrocatalytic oxidation. *J. Hazard. Mater. B.*138: 526-533.

Xu Y & Langford CH (2001) UV- or Visible-Light-Induced Degradation of X3B on TiO_2 Nanoparticles: The Influence of Adsorption. Langmuir 17: 897-902.

Yang J, Dai J, Chen C & Zhao J (2009) Effects of hydroxyl radicals and oxygen species on the 4-chlorophenol degradation by photoelectrocatalytic reactions with TiO_2-film electrodes. *J. Photochem. Photobiol. A.* 208: 66-77.

Yoon KH, Noha JS, Kwon CH & Muhammed M (2006) Photocatalytic behavior of TiO_2 thin films prepared by sol-gel process. *Mater. Chem.Phys.* 95 (1), 79-83.

Yu J, Zhang L, Cheng B & Su Y (2007a) Hydrothermal preparation and photocatalytic activity of hierarchically sponge-like macro-/mesoporous Titania. *J. Phys. Chem. C.* 111: 10582-10589.

Yu J, Wang G, Cheng B & Zhou M (2007b) Effects of hydrothermal temperature and time on the photocatalytic activity and microstructures of bimodal mesoporous TiO_2 powders. *Appl. Catal. B.* 69 (3-4): 171-180.

Zang L, Qu P, Zhao J, Shen T & Hidaka H (1997) Photocatalytic bleaching of p-nitrosodimethylaniline in TiO_2 aqueous suspensions: A kinetic treatment involving some primary events photoinduced on the particle surface. *J. Mol. Catal A.* 120 (1-3): 235-245.

Zhao J, Wu T, Wu K, Okikawa K, Hidaka H & Serpone N (1998) Photoassisted Degradation of Dye Pollutants.3. Degradation of the Cationic Dye Rhodamine B in Aqueous Anionic Surfactant/TiO_2Dispersions under Visible Light Irradiation: Evidence for the Need of Substrate Adsorption on TiO_2 Particles. *Environ. Sci. Technol.* 32: 2394-2400.

CHAPITRE 6

PHOTOELECTROCATALYTIC DEGRADATION OF CHLORTETRACYCLINE USING TI/TIO_2 NANOSTRUCTURED ELECTRODES DEPOSITED BY MEANS OF A PULSED LASER DEPOSITION PROCESS.

Le chapitre 6 est constitué de l'article suivant :

Rimeh Daghrir, Patrick Drogui, Ibrahima Ka, My Ali El Khakani, Photoelectrocatalytic degradation of chlortetracycline using Ti/TiO_2 nanostructured electrodes deposited by means of a Pulsed Laser Deposition process. *Journal of Hazardous Materials. 199-200 (2012) 15-24.*

6. PHOTOELECTROCATALYTIC DEGRADATION OF CHLORTETRACYCLINE USING TI/TIO_2 NANOSTRUCTURED ELECTRODES DEPOSITED BY MEANS OF A PULSED LASER DEPOSITION PROCESS

6.1 Abstract

Ti/TiO_2 electrode was prepared by means of the Pulsed Laser Deposition method and used in a photoelectrocatalytic oxidation (PECO) process in order to degrade chlortetracycline (CTC). The deposited TiO_2 coatings were found to be of rutile structure. High treatment efficiency of CTC was achieved by the PECO process compared to the conventional electrochemical oxidation, direct photolysis and photocatalysis processes. Several factors such as current intensity, treatment time, UV lamp position and initial concentration of CTC were investigated. Using a 2^4 factorial matrix, the best performance for CTC degradation (74.3% of removal) was obtained at a current intensity of 0.5 A during 120 min of treatment time and when the UV lamp was immersed in the solution in the presence of 25 mg L^{-1} of CTC. The current intensity and treatment time were the main parameters influencing the degradation rate of CTC. Subsequently, a central composite design methodology has been investigated to determine the optimal experimental parameters for CTC degradation. The PECO process applied under optimal conditions (at current intensity of 0.39 A during 120 min with internal position of the UV lamp) is able to oxidize around 74.2 ± 0.57%, of CTC.

6.2 Key words

Chlortetracycline hydrochloride, Photoelectrocatalytic oxidation, Titanium dioxide film, Pulsed Laser Deposition (PLD).

6.3 Introduction

In the past few years, there has been considerable interest to pharmaceuticals and personal care products (PPCPs) including antibiotics, hormones, anesthetics, etc. due to their discharges into the environment. These contaminants are soluble in surface water, groundwater, and even drinking water (Lòpez-Penalver et al., 2010; Tolls, 2001; Kolpin et al., 2002; Miao et al., 2004). Antibiotics belong to pharmaceutical compounds most often used as growth promoters of animals. The discharge of antibiotics into the environment is one of the major and global public health issues that need urgent action. Its annual usage has been globally estimated between 100,000 and 200,000 tones (Kuemmerer, 2003). Chlortetracycline (CTC); oxytetracycline (OTC); and tetracycline (TC) are the most often used throughout the world (Lòpez-Penalver et al., 2010; Heberer, 2002; Jeong et al., 2010; Halling-Sørensen, et al., 2002). Antibiotics or their metabolites have been detected in surface water, ground water, sewage water, and drinking water at concentrations ranging from ng L^{-1} to μg L^{-1} (Lòpez-Penalver et al., 2010; Kim et Tanaka, 2009; Bautitz et Nogueira, 2007). These findings have raised concern regarding potential human health effects caused by low levels of antibiotics in drinking water, as well as the transfer and spread of antibiotic resistant genes among microorganisms (Zhang et al., 2009). Globally, a very low proportion (<1%) of these antibiotic compounds participates to the total DOC from pollutants in contaminated water, but their presence in water has to be taken into account owing to their potential toxicity for human. Thus, it is of great importance to develop efficient and cost-effective treatment technologies for removal of such compounds.

Conventional wastewater treatments such as traditional biological treatment methods are not always able to remove completely antibiotic compounds (Lòpez-Penalver et al., 2010; Reyes et al., 2006). It has been found by Ingerslev and Halling-Sorensen (Ingerslev and Halling-Sorensen, 2000) that twelve sulfonamide antibiotics were not readily biodegradable in

activated sludge. Likewise, Kummerer and Hartmann (1997) investigated the effectiveness of the treatment of hospital and pharmaceutical wastewaters in several wastewater treatment plants in Germany. These works showed that many pharmaceutical products could not be oxidized during conventional biological treatments. However, other methods can be used to remove antibiotics such as adsorption, biosorption, ozonation, membrane techniques (reverse osmosis), advanced oxidation processes (AOPs), including O_3/H_2O_2, UV/O_3, UV/H_2O_2, H_2O_2/Fe^{2+}, etc. (Lòpez-Penalver et al., 2010; Rey et al., 1999; Adams et al., 2002; Ji et al., 2009). Among them, chemical oxidation processes have been successfully applied to degrade various pharmaceutical compounds present in contaminated water. UV and UV/H_2O_2 oxidation processes are used to degrade three antibiotics from tetracycline group (tetracycline; chlortetracycline; and oxytetracycline) (Lòpez-Penalver et al., 2010). In spite of the good oxidation of refractory organic pollutants, the complexity of these methods (advanced oxidation processes), high chemical consumption, and relatively high treatment costs constitute major barriers for large-scale applications (Martinez-Huitle and Ferro, 2006). In the same context, photocatalysis process combining UV and TiO_2 suspensions as catalyst was used by Reyes et al. (2006) to degrade tetracycline as a model of antibiotic compounds. Degradation around 50% was recorded after 10 min of treatment using 0.5 g L^{-1} of TiO_2 exposed to UV light. A renewed interest in photocatalysis has been spurred by the search for reliable, cost-effective water treatment processes. From this point of view, it can be interesting to develop photoelectrocatalytic oxidation (PECO) technique combining electrolytic and photocatalytic processes. This approach offers the possibility to delay the recombination of the electron–hole pairs (e^-_{CB}/h^+_{VB}) and the possibility to increase the lifetime of the latter. The applied external potential in PECO technique is the key factor because it accelerates the photocatalytic reaction. The aim of the present study is to evaluate the efficiency of a PECO process using UV light and nanocrystalline TiO_2 photo-anodes for

the efficient treatment of waters contaminated by CTC. To this end, an experimental design methodology (Myers and Montgomery, 2002) was put in place to investigate the influence of the principal experimental parameters (current intensity, treatment time, pollutant concentration, and UV lamp position) on the efficiency of the PECO process for CTC degradation. A second objective of this study was to use a statistical methodology for a rational analysis of the combination of operational factors that led to the best treatment process. Factorial design (FD) and central composite design (CCD) methodologies have been successively applied in order to point out the main and interaction effects of the factors and to optimize CTC degradation by the PECO process.

6.4 Materials and methods

6.4.1 Ti/TiO_2 electrode preparation

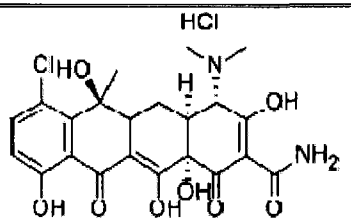
The titanium dioxide (TiO_2) coatings have been performed by means of a Pulsed Laser Deposition (PLD) method. A KrF excimer laser (wavelength = 248 nm, pulse duration = 15 ns) operating at a repetition rate of 30 Hz was focused, at an incidence angle of 45°, onto the TiO2 rotating target (99.95% purity). The on-target laser energy density was set to 4.5 J/cm^2. The TiO_2 films were deposited on both titanium grids (for photoelectrochemical studies) and on silicon substrates (for material characterizations purposes). The TiO_2 deposits were performed at a deposition temperature 600°C under an oxygen background pressure of 1 mTorr. The PLD deposition chamber was first turbo-pumped to about 10^{-6} Torr before filling it with oxygen. More details on the Pulsed Laser Deposition system and it schematics can be found elsewhere (Desbiens and El Khakani, 2003).

6.4.2 Preparation of the synthetic solution

Chlortetracycline hydrochloride ($C_{22}H_{24}Cl_2N_2O_8$) was an analytical grade reagent supplied by Sigma Aldrich (purity 78%). Its water solubility was 0.008 mol L^{-1} (Lòpez-Penalver et al.,

2010). Table 6-1 presents some chemicals properties of CTC (Qiang et Adams, 2004). CTC stock solution was prepared in a glass-tank containing 2 L of distilled water in which 100 mg of CTC was added. Solubilization of CTC was carried out at a high speed of 750 rpm for a 30 min. Mixing was achieved by a Teflon-covered stirring bar installed at the bottom of the beaker. Final concentration of CTC was 50 mg L^{-1}. In order to increase electrical conductivity in the solution, 0.05 mol L^{-1} of sodium sulfate was added.

Tableau 6-1 Chemical properties of Chlortetracycline hydrochloride.

Molecule	Molecular formula	Chemical structure	Molecular weight (g mol^{-1})	Solubility (mol L^{-1})	pK_{a1}*	pK_{a2}*	pK_{a3}*
CTC	$C_{22}H_{24}Cl_2N_2O_8$		515.3	0.008	3.3±0.3	7.55±0.02	9.3±0.3

*, *pk_a was determined by Qiang et al., (2004)*

6.4.3 Experimental devices

The reactor unit was made of acrylic material with a dimension of 12.7 cm (width), 16.51 cm (length), and 11.43 cm (depth). A quartz window (8.89 cm × 8.89 cm) was disposed on one face of the reactor for the photoelectrocatalysis experiments (Figure 6-1). All the assays were conducted in batch mode. The photoelectrocatalytic cell was comprised of one anode (Ti/TiO_2) and one cathode (inox), each one having a surface area of 110 cm^2 (10 cm width × 11 cm high), placed in parallel and were submerged in the solution. The electrodes were vertically installed on a perforated Plexiglas plate placed at 2 cm from the bottom of the cell. The inter-electrode gap was 1.0 cm. Both anode and cathode were connected respectively to the positive and negative outlets of a DC power supply Xantrex XFR 40-70 (Aca Tmetrix, Mississauga, ON, Canada) with a maximum current rating of 70 A at an open circuit potential of 40 V. The photoelectrocatalytic cell was operated with current intensities (from 0.16 A to 0.59 A) imposed during treatment period ranging from 40 to 120 min. The photo-anode was illuminated by a mercury lamp (light intensity = 6.9 mW cm^{-2}; λ_{max} = 254 nm) through the quartz window. The lamp was installed vertically outside or inside the reactor. The light intensity was measured with a photometer (Model PS-3, 99-0057-01, UVp Company; USA). The photoelectrocatalytic reactor was placed in a dark chamber in order to avoid interferences from the daylight. Mixing in the cell was achieved by a Teflon-covered stirring bar installed between the perforated plate and the bottom of the cell. All experiments were carried out at room temperature (25°C). For all tests a total volume of 1.0 L was used. An electrolyte concentration of 0.05 mol Na_2SO_4 L^{-1} was added in the synthetic solution. Sodium sulfate was analytical grade reagent and supplied by Mat Laboratory (Quebec, Qc, Canada).

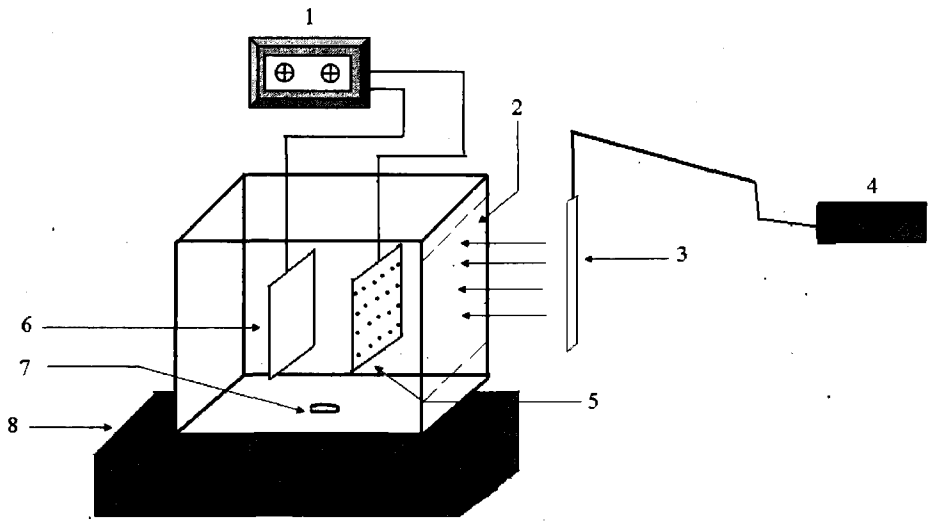


Figure 6-1 Schematic diagram of the photoelectrocatalytic reactor: (1) DC power supply (2) quartz window (3) UV lamp (4) photometer (5) photoanode (6) cathode (7) stirring bar (8) magnetic stirrer.

6.4.4 Experimental design

Response surface methodology (RSM) was applied to evaluate and determine the optimum operating conditions. RSM is a collection of mathematical and statistical methods for modeling, optimizing, and analyses a treatment process in which the response can be influenced by several variables (Zaroual et al., 2009). Both factorial design (FD) and central composite design (CCD) methodologies are widely used in RSM. FD was used in order to investigate the main and interaction effects of the factors on the degradation of CTC. Subsequently, CCD was employed to optimize PECO process in CTC degradation. A four-factorial and a two-level central composite design, with six replicate at the center point for each categorical factor, led to a total number of forty experiments employed for response surface modeling. The variables investigated in our study were: the applied current intensity

(X1), treatment time (X2), pollutant concentration (X3), and UV lamp position (X4). CTC degradation efficiency was considered as response (Y). The values of different variables were selected based on the preliminary assays.

6.4.5 Analytical details

The pH was determined using a pH-meter (Fisher Acumet model 915) equipped with a double-junction Cole-Palmer electrode with Ag/AgCl reference cell. The progress of photoelectrocatalysis degradation of CTC in the solution was firstly monitored by absorbance measurements using UV–vis absorption spectrophotometer (UV 0811 M136, Varian, Australia). The maximum absorption of the solution samples has been made at the wavelength of 368 nm in an optical quartz cell (1 cm). This absorption peak was chosen to evaluate the residual CTC concentration. A calibration curve of known CTC concentration versus absorbance (368 nm) was used to calculate the residual CTC concentrations. Likewise, the progress of photoelectrocatalytic degradation of CTC was monitored and quantified by LC/MS/MS (Thermo TSQ Quantum Access). The chromatographic column used was Hypersil Gold C18, particle size 3 μm and 2.1 ×100 mm inner diameter. The isocratic mobile phase was A: 50% H_2O + 0.1% formic acid and B: 50% CH_3CN + 0.1% formic acid at a flow rate of 200 μL min^{-1}. Mass spectral data shown in this study were acquired on a LCQ Duo ion trap tandem mass spectrometry equipped with an electrospray ionization (ESI) source operated in positive ion mode. Qualitative analysis of CTC was determined using standard addition method (SAM). SAM is based on the addition of small known quantities of analyte to the sample (Khandpur, 2006). The calibration curve of five points (from 0.1 mg L^{-1} to 20 mg L^{-1}) was prepared from a stock solution 20 mg L^{-1}. A certified control was prepared at concentration of 5 mg L^{-1} in the center of the curve. The percentage of recovery of the analyte at the end of the analysis was 83%.

6.4.6 Economic aspect

The economic study included chemical and energy consumption. The electric cost was estimated about of US$0.06 kW h^{-1}. A unit cost of US$0.30 kg^{-1} was used of electrolyte (Na_2SO_4 industrial grade). The total cost was evaluated in terms of U.S. dollars spent per cubic meter of treated solution (US$ m^{-3}).

6.5 Results and discussion

6.5.1 Characterization of the Ti/TiO_2 electrode

The surface morphology of the TiO_2 photocatalytic coating was examined by SEM observations. Figure 6-2a shows the top-view of the TiO_2 film deposited at 600°C onto silicon substrate. The coating is seen to be highly dense with fine-grained surface with more or less spherical features of few tens of nm of diameter (as shown in the higher magnification SEM image of Figure 6-2b). The cross-sectional SEM views reveal the columnar growth of the TiO_2 coating where The TiO_2 columns are seen to be densely packed (Figure 6-2d). Figure 6-2c also shows that the TiO_2 coating is very uniform in thickness and forms a very smooth and continuous interface with the underlying substrate.

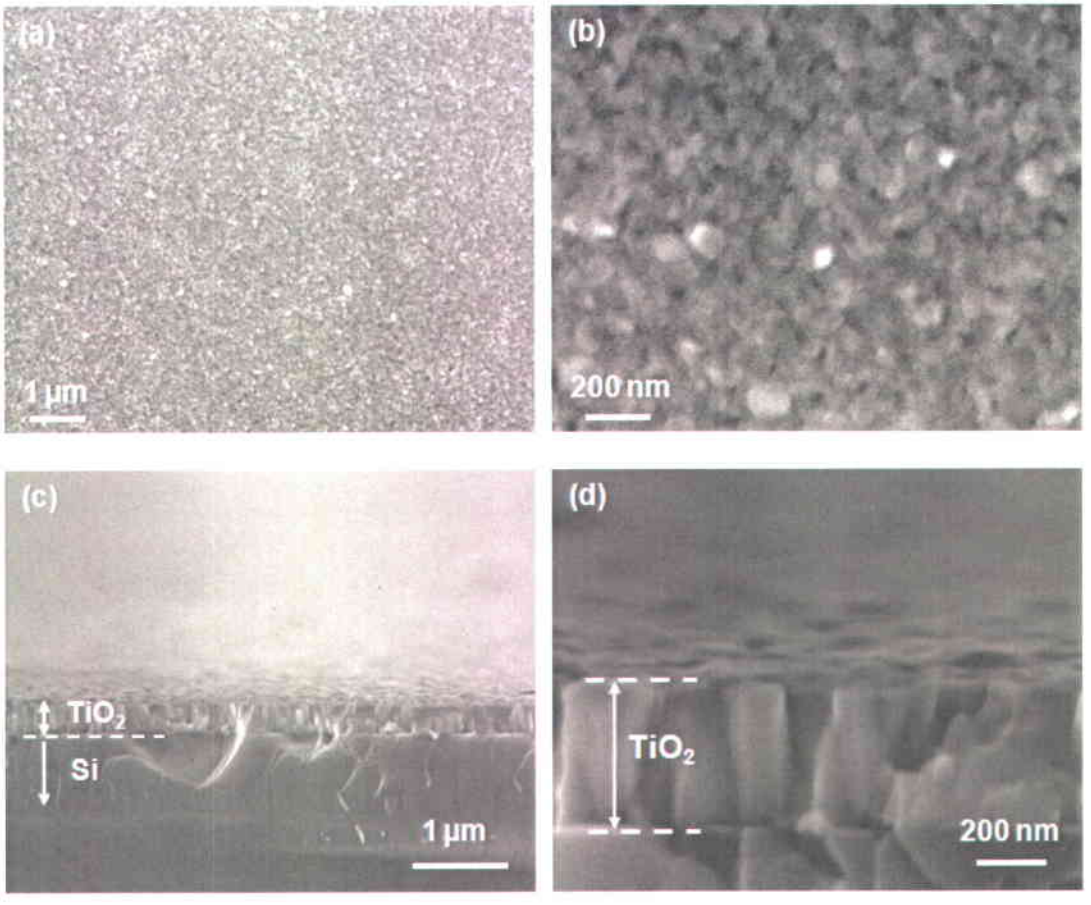


Figure 6-2 SEM images of the surface morphology of the TiO_2 film deposited at 600°C.

The XRD analysis (Figure 6-3) indicates that our TiO_2 coatings deposited at 600°C are polycrystalline and crystallize in the TiO_2 rutile phase, in accordance with literature data where the TiO_2 rutile phase is generally obtained for deposition temperatures above 550°C (Kitazawa et al., 2006; Jaroenworaluck et al., 2010; Regonini et al., 2010). The XRD spectrum of the TiO_2 coating onto the Ti-grid confirms the presence of the same TiO_2 rutile phase obtained on Si. The average size of the TiO_2 crystallites was estimated to about 29 nm on silicon while it is of ~10 nm on the Ti-grid substrates. Such a nanometric grain size is expected to have an important effect on the photocatalytic activity of the TiO_2 coating (Guinier, 1962; Kim et al., 2007). Indeed, with the decrease in particle size, the catalytic

activity is enhanced due to the huge increase in the surface area (or surface to volume ratio) of the material.

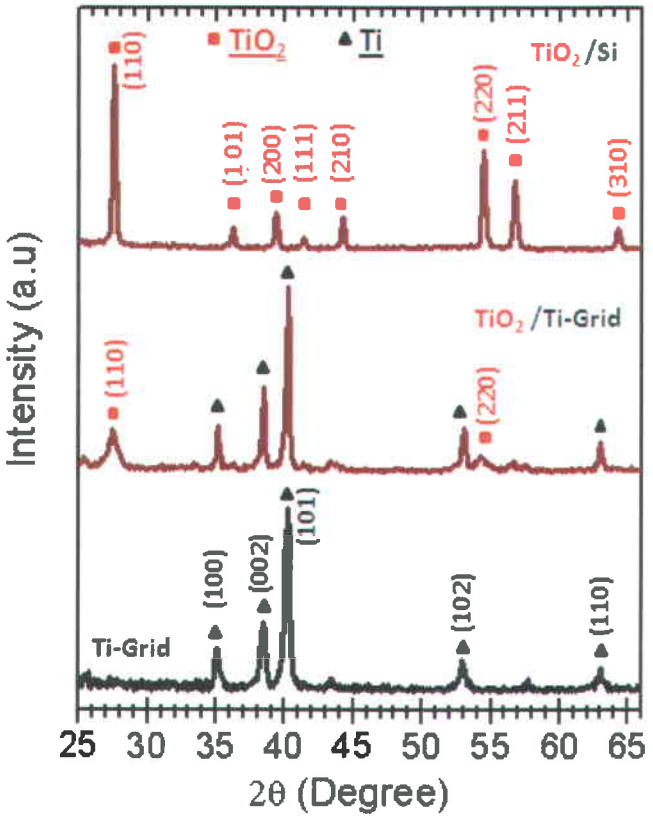


Figure 6-3 X-ray diffraction patterns of TiO_2 film coated on Ti grids and on Si substrates at 600°C.

6.5.2 Preliminary investigation of CTC degradation

Experiments using direct photolysis (DP), photo-catalysis (PC), electro-oxidation (EO) and PECO processes were carried out in order to compare the CTC degradation efficiencies (Table 6-2).

Tableau 6-2 Different processes used for degradation of CTC.

Parameters	Value	Process			
		PECO	PC	EO	DP
Intensity (A)	0.5	✓		✓	
Treatment time (min)	120	✓	✓	✓	✓
Light intensity ($\mu W\ cm^{-2}$)	6900	✓	✓		✓
UV lamp position	External	✓	✓		✓
	Internal	✓	✓		✓
Electrolyte (Na_2SO_4) (mol L^{-1})	0.05	✓		✓	
Type of Cathode	Inox	✓		✓	
Type of anode	Ti/Pt			✓	
	Ti/TiO_2	✓	✓	✓	
CTC (mmol L^{-1})	0.05	✓	✓	✓	✓

DP: Direct photolysis; PC: Photocatalysis; EO: Electro-oxidation; PECO: Photoelecrtrocatalytic- oxidation

The DP process consisted in treating the effluent using only UV irradiation light at 254 nm, whereas in the PC process UV light was used in the presence of Ti/TiO_2 catalyst. The EO process was applied to treat the effluent using Ti/TiO_2 catalyst and Ti/Pt anode electrodes, while in the PECO process; the Ti/TiO_2 photoanode was used under UV irradiation and an external potential. The results of CTC degradation using different experimental conditions (tests T1–T8) are shown in Table 6-3. As it can be been seen from these data, the CTC degradation rate is higher using internal UV illumination (see the tests T2, T4, and T8). Only 16% of CTC was oxidized using DP process with external UV configuration. By comparison, 37% of CTC was removed by DP with internal UV illumination. In the case of direct photolysis, UV radiations absorbed by H_2O molecules allow the generation of powerful oxidizing species such as the hydroxyl radicals ($OH^{\bullet}$) and hydrogen peroxide (H_2O_2) (Kim et Tanaka, 2009; Heit et al., 1998). The direct contact of UV light (internal UV illumination) with contaminated water induced high oxidative degradation. The high CTC degradation

using internal UV illumination can be due to the rapid increase of $HO^{\bullet}$ species concentration in the solution. The exposure of Ti/TiO_2 electrode under UV light (PC process) decreased the final CTC concentrations. The residual CTC concentrations recorded after 120 min of treatment were 25% and 47% under external and internal UV illumination, respectively. These results indicate that the system (UV and Ti/TiO_2 catalyst) is working in a photocatalytic regime. Furthermore, the degradation rate of CTC by EO process at a current intensity of 0.5 A was tested using Ti/Pt and Ti/TiO_2 as anodes. The final CTC concentration recorded using Ti/Pt anode was 60.1% (after 120 min) and 37.5% using Ti/TiO_2 anode (after 60 min) in the absence of UV light. The nature of the anode material used affected the ions conductivity in the solutions and influenced the performance of the system. In EO process, the conductivity of the solution affects the current efficiency, the cell voltage and the electrical energy consumed (Daneshvar et al., 2006). For the same current intensity imposed (0.5 A), Ti/Pt electrode used at the anode provided a relatively low electrical resistance of 14 Ω during 120 min of electrolysis, whereas a value of 60 Ω was recorded using Ti/TiO_2 anode electrodes during 60 min of electrolysis. The potential difference existing between the electrodes connected to the power supply increased from 9.4 V to 30 V using Ti/TiO_2 anode, whereas it varied from 5.8 V to 7 V using Ti/Pt anode. This situation may affect the treatment performance in a long-term experiment. It was the reason for which Ti/Pt was more effective than Ti/TiO_2 for CTC oxidation using EO process. However, a higher degradation efficiency was recorded (above 80%) by PECO process using Ti/TiO_2 photoanode at 0.5 A. In PECO process, UV radiation activates Ti/TiO_2 photoanode by transferring electrons from the valance band (VB) to the conduction band (CB), while at the same time the applied external potential prevents the recombination of photo-generated electron–hole pairs. Thus, the efficiency of CTC degradation was enhanced. Finally, PECO process was selected for the next step of this study using the experimental factorial design methodology.

Tableau 6-3 Chlortetracycline hydrochloride removal under various experimental conditions.

		Parameters							
Processes	**Tests**	**Intensity (A)**	**Times (min)**	**Anode**	**Cathode**	**Light intensity ($mW\ cm^{-2}$)**	**UV lamp position**	**Electrolyte (Na_2SO_4 $mol\ L^{-1}$)**	**CTC removal (%)**
DP	T1	-	120	-	-	6.9	External	-	16
	T2	-	120	-	-	6.9	Internal	-	37
PC	T3	-	120	Ti/TiO_2	-	6.9	External	-	25
	T4	-	120	Ti/TiO_2	-	6.9	Internal	-	47
EO	T5	0.5	120	Ti/Pt	Inox	-	-	0.05	60.1
	T6	0.5	60	Ti/TiO_2	Inox	-	-	0.05	37.5
PECO	T7	0.5	120	Ti/TiO_2	Inox	6.9	External	0.05	80.9
	T8	0.5	120	Ti/TiO_2	Inox	6.9	Internal	0.05	81.2

DP: Direct photolysis; PC: Photocatalysis; EO: Electro-oxidation; PECO: Photoelecrtrocatalytic- oxidation

6.5.3 Effect of the experiment parameters on the CTC degradation using the experimental factorial design methodology

The results presented above allowed us to clearly define the experimental region for RSM to study CTC degradation using the PECO process. The influence of different variables: current intensity (U1), treatment time (U2) pollutant concentration (U3), and UV lamp position (U4) on the CTC removal was investigated using factorial matrix (2^k, k being the number of factors; k = 4). The experiment region investigated for CTC degradation and the code values are shown in Table 6-4. The experimental results are presented in Table 6-5.

Tableau 6-4 Data for optimization operation: experimental range and levels of independent process variables.

Coded variables (X_i)	Factor (U_i)	Experimental field		$U_{i,0}$	ΔU_i
		Min value (-1)	Max value (+1)		
X_1	U_1 : Current intensity (A)	0.25	0.50	0.375	0.125
X_2	U_2 : Electrolysis time (min)	60	120	90	30
X_3	U_3 : CTC concentration (mg $L^{-1)}$	25	50	37.5	12.5
X_4	U_4 : UV Lamp position	External	Internal	-	-

With this design it was possible to calculate the principle effect of each factor and the interaction between them. The experimental response associated to a 2^4 factorial design (four variables) is represented by a linear polynomial model with interaction, as follows:

Équation 6-1

$$Y = b_0 + b_1 X_1 + b_2 X_2 + b_3 X_3 + b_4 X_4 + b_{12} X_1 X_2 + b_{13} X_1 X_3 + b_{14} X_1 X_4 + b_{23} X_2 X_3 + b_{24} X_2 X_4 + b_{34} X_3 X_4$$

Where, Y represents the experimental response (CTC degradation); b_0 represents the average value of the responses of the 16 assays; X_i the coded variable (−1 or +1); bi represents the principal effect of each factor i on the response and bij represents the interaction effect between factor i and factor j on the response. The coefficients of the model were calculated using the half-difference between the arithmetic average of the response values when the associated coded variable is at a level (+1) and the arithmetic average of the response values when the associated coded variable is at level (−1). Design-Expert® Program Software (Design Expert 7, Stat-Ease Inc., Minneapolis) was used to calculate the coefficient of the polynomial model.

Équation 6-2

$$Y = 50.85 + 12.06 X_1 + 5.65 X_2 - 2.73 X_3 - 2.18 X_4 - 0.36 X_1 X_2 + 1.11 X_1 X_3 + 0.81 X_1 X_4 + 0.35 X_2 X_3 - 0.55 X_2 X_4 + 0.60 X_3 X_4$$

The value of the regression coefficient R^2 was 0.996. The coefficient $b_0 = 50.85$ represents the average value of the response of 16 assays. According to Equation 6-2, it can also been seen that current intensity and treatment times have a positive effect on CTC degradation, whereas pollutant concentration and UV lamp position have a negative effect on CTC degradation. The interaction effects were globally weaker than the main effects.

Tableau 6-5 Experimental factorial matrix in the 2^4 design.

Assays	Experiment design				Experiment plan				Result, Y Degradation efficacy (%)
	X_1	X_2	X_3	X_4	U_1	U_2	U_3	U_4	
1	-1	-1	-1	-1	0.25 A	60 min	25	External	33.3
2	-1	+1	-1	-1	0.25 A	120 min	25	External	43.1
3	-1	-1	+1	-1	0.25 A	60 min	50	External	27.8
4	-1	+1	+1	-1	0.25 A	120 min	50	External	39
5	+1	-1	-1	-1	0.5 A	60 min	25	External	58.8
6	+1	+1	-1	-1	0.5 A	120 min	25	External	68
7	+1	-1	+1	-1	0.5 A	60 min	50	External	54.4
8	+1	+1	+1	-1	0.5 A	120 min	50	External	65
9	-1	-1	-1	+1	0.25 A	60 min	25	Internal	41.0
10	-1	+1	-1	+1	0.25 A	120 min	25	Internal	53.1
11	-1	-1	+1	+1	0.25 A	60 min	50	Internal	29.0
12	-1	+1	+1	+1	0.25 A	120 min	50	Internal	44
13	+1	-1	-1	+1	0.5 A	60 min	25	Internal	60
14	+1	+1	-1	+1	0.5 A	120 min	25	Internal	74.3
15	+1	-1	+1	+1	0.5A	60 min	50	Internal	57.3
16	+1	+1	+1	+1	0.5 A	120 min	50	Internal	68.5

The importance of the factors and interactions on CTC degradation has been put into evidence using Equation 6-3. Indeed, it is possible to give more significant information by calculating the contribution of each factor on the response.

Équation 6-3

$$P_i = \left(\frac{b_i^2}{\sum b_i^2} \right) * 100 \qquad (i \neq 0)$$

Where, b_i represents the estimation of the principal effect of the factor i. Thus, it is found that the contribution of current intensity and treatment time on CTC removal is around 76.2% and 16.7%, respectively, whereas that of pollutant concentration and UV lamp position account only for 4.0% and 2.5%, respectively (Figure 6-4).

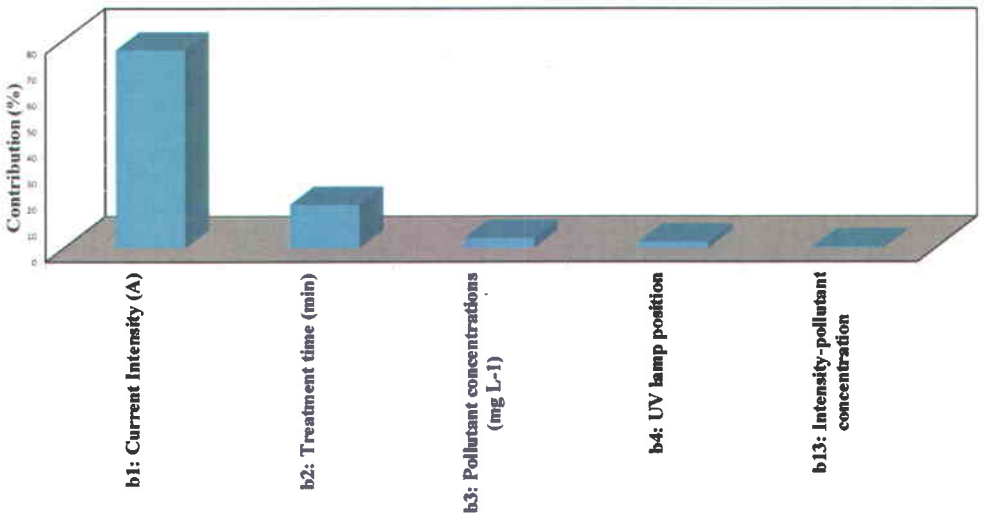


Figure 6-4 Graphical Pareto analysis of the effect of current intensity, treatment time, Pollutant concentration and UV lamp position on CTC degradation

With the exception of the interactions X_1X_3 (current intensity and pollutant concentration), the other interactions have a negligible effect. The interaction effect of X_1X_3 on CTC degradation is presented in Figure 6-5. Each point represents the combination between two factors: current intensity and pollutant concentration. At current intensity of 0.5 A and 50 mg L^{-1} of CTC concentration, an average reduction of 61.3% was recorded (assays 7, 8, 15, and 16). When pollutant concentration (X3) is fixed at the highest level (50 mg L^{-1}), current intensity has a significant influence on the removal of CTC. The degradation rate passed from 34.9% to 61.3% (a reduction gain of 27 units). When the pollutant concentration is fixed at the lowest level (25 mg L^{-1}), the degradation rate passed from 42.6% to 64.5% (a reduction gain of 22 units). Consequently, current intensity is a major factor that influences degradation rate of CTC, but it directly depends of pollutant concentration. In the PECO process, current intensity is a key factor that influences pollutant degradation efficiency. Current intensity supplied to the catalyzed Ti/TiO_2 electrode prevents the recombination of photo-generated electron–hole pairs (h^+/e^-) (Waldner et al., 2003; Li et al., 2002). Therefore, the electrons and holes have more opportunities to participate in degradation of CTC pollutant directly on the surface of nanostructured Ti/TiO_2 photoanode (adsorption) or indirectly by reacting with active species (such as hydroxyl radicals) (Adams et al., 2002). Furthermore, the PECO process was more effective at low CTC concentrations (25 mg L^{-1}). This result indicates that CTC degradation reaction is limited by the amount of reactive species (OH• radicals) produced by UV illumination. At higher pollutant concentration, the reactive species are insufficient for enhance degradation efficiency (Wang et al., 2009). According to Wang et al., (2009), the decrease in pollutant degradation efficiency can be attributed to the competition reaction between intermediate products for reacting with hydroxyl radicals. The influence of initial concentration of pollutant was also put into evidence by Ding et al., (2010) while studying photoelectrocalytic degradation of benzotriazole. The degradation experiments were

carried out at different initial concentrations (from 0.05 mM to 0.5 mM) in 0.5 M of Na_2SO_4 using a voltage of 0.8 V. The degradation efficiency was around 40% at initial concentration of 0.5 mM, whereas more than 99% of benzotriazole was removed at initial concentration of 0.05 mM. The decrease in degradation rate of pollutant while increasing the initial concentration increase can be explained in two ways. Firstly, the reaction between photogenerated holes (or hydroxyl radicals) and pollutant can be inhibited owing to adsorbed pollutant on the surface of the catalyst. Secondly, the UV radiations may be more adsorbed by pollutants rather than photocatalysts Ti/TiO_2 and consequently limits the catalytic reaction efficiency (Ding et al., 2010).

Finally, the factorial plan design was used to determine the interactions affecting the response and indicates that if the lowest or the highest levels of the factors are favourable or not. The results show that the response is greatly influenced by the factors having a significant effect. However, the factorial plan design cannot be used to determine the optimal conditions of CTC degradation. For this reason, a RSM should be used in a second step to determine the optimal conditions for CTC degradation.

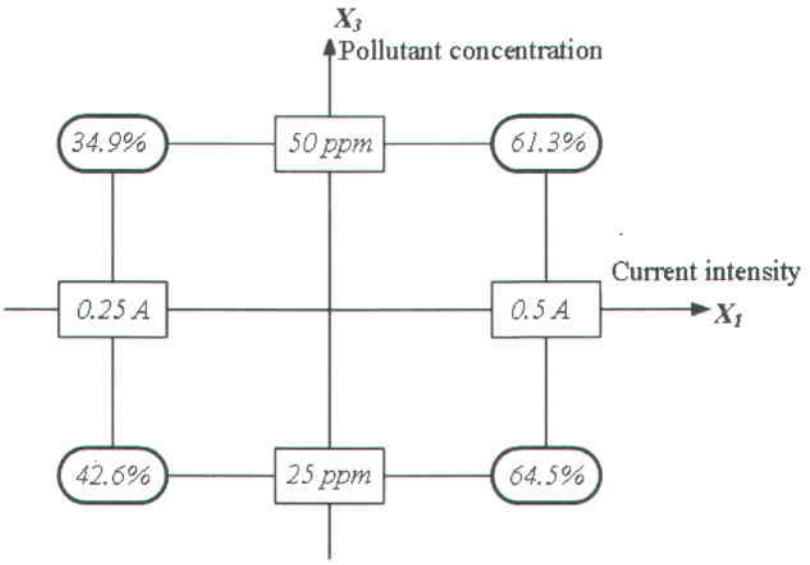


Figure 6-5 Interaction X_{13} between current intensity and pollutant concentration.

6.5.4 Optimization conditions for CTC degradation using central composite design (CCD) methodology

A two-level central composite experimental design, with six replicates at the center point leading to a total number of forty experiments was used for response surface modeling (Table 6-6). For the evaluation of experimental data, the response was described by a second-order model in the form of quadratic polynomial equation given below:

Équation 6-4

$$Y = b_0 + \sum_{i=1}^{k} b_i X_i + \sum_{i=1}^{*} b_{ii} X^2{}_i + \sum_{j} \sum_{i=2}^{*} b_{ij} X_i X_j + e_i$$

where Y is the experimental response; X_i and X_j are the independent variables; b_0 is the average of the experimental response; bi is the estimation of the principal effect of the factor j

on the response Y; b_{ii} is the estimation of the second effect of the factor i on the response Y; b_{ij} is the estimation of the interaction effect between i and j on the response Y and e_i represents the error on the response Y. All coefficients are calculated using the least square method (Myers et Montgomery, 2002):

Équation 6-5 $B = (X^T X)^{-1} X^T Y$

Where, B represents the vector of estimates of the coefficients; X is the model matrix, and Y is the vector of the experiment results. The variables (X_i) are coded according to the following equation (Tir et Moulai-Mostefa, 2008):

Équation 6-6 $\frac{U_i - U_{i0}}{\Delta U_i}$

Where $U_{i,0} = (U_{i,max} + U_{i,min}) / 2$ represents the value of U_i at the center; $\Delta U_i = (U_{i,max} - U_{i,min}) / 2$ is the value of variable change step and $U_{i\ max}$ and $U_{i\ min}$ are the maximum and the minimum values of the effective variable U_i, respectively. The coefficients of the polynomial model (quadratic model) were calculated using the Design-Expert ® Program Software:

For Internal UV lamp:

Équation 6-7
$$Y_1 = -23.0807 + 193.235\ X_1 + 0{,}7462\ X_2 - 0.3788\ X_3 - 0.0966\ X_1X_2$$
$$0.712\ X_1X_3 + 0.000933\ X_2X_3 - 174.967X_1^2 - 0.003095\ X_2^2 - 0.00216\ X_3^2$$

For External UV lamp:

Équation 6-8

$$Y_1 = -34.93077 + 204.20030\ X_1 + 0.76658X_2 - 0.34325\ X_3 - 0.0966\ X_1X_2$$
$$0.712\ X_1X_3 + 0.000933\ X_2X_3 - 174.967X_1^2 - 0.003095\ X_2^2 - 0.00216\ X_3^2$$

From these Equations 6.7 and 6.8, it can be seen that current intensity is very meaningful for CTC degradation using both internal and external UV position. Current intensity and treatment time are positive effect on the response compared to pollutant concentration, which has a negative effect on the removal of CTC. The predicted contour plots (curves of constant response) and the three-dimensional representation of the same plots are given in Figure 6-6. This figure clearly shows that CTC removal efficiency increased with increasing current intensity at all pollutant concentrations studied varying from 25 to 50 mg L^{-1} (for internal UV position). 63% CTC removal efficiency could be achieved at constant treatment time of 90 min (treatment time at the center of the experimental region investigated) while the current intensity was above 0.40 A for all concentrations of pollutant investigated varying from 25 to 50 mg L^{-1}. From the correlation between the current intensity and pollutant concentration, it can be concluded that the current intensity has more significant impact on CTC removal efficiency.

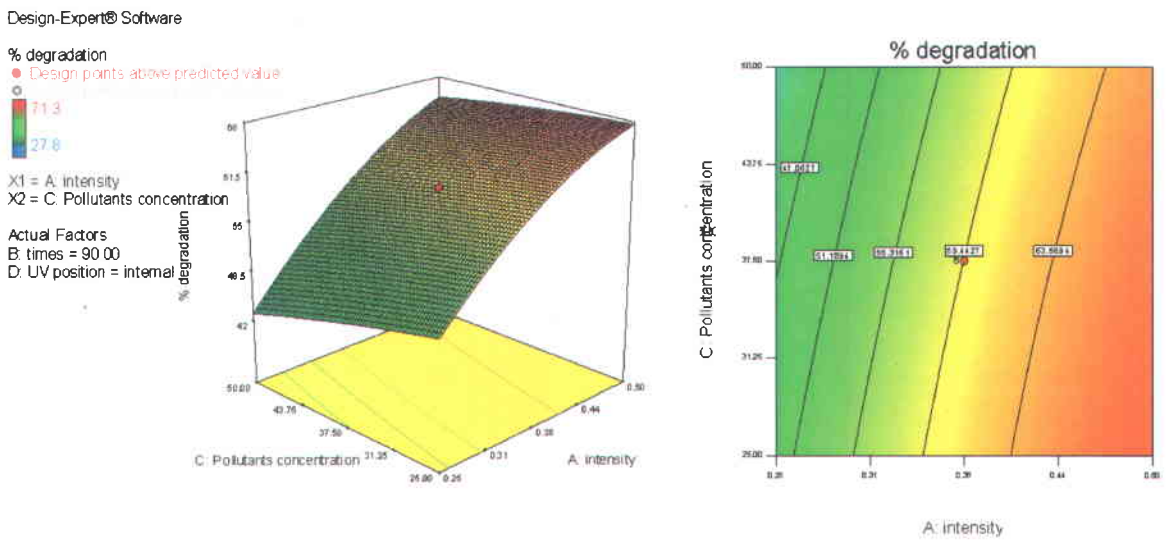


Figure 6-6 The effect of current intensity (A) and pollutant concentration (mg L^{-1}) on CTC removal (application time: 90 min) three-dimensional plot; results obtained from central composite matrix; Internal UV lamp position.

The comparison between actual (experimental) and predicted values of CTC degradation are presented in Figure 6-7. An agreement between actual and predicted values of CTC degradation is satisfactory and in accordance with the statistical significance of the quadratic model. Table 6-6 shows the analysis of variance (ANOVA) of regression parameters of the predicted response surface quadratic model for CTC removal using PECO process. As it can be seen from this table, the model F-value of 60.04 and a low probability value ($Pr > F = 0.0001$) indicate that the model is significant for CTC removal. The value of the correlation coefficient ($R^2 = 0.9678$) indicates that only 3.22% of the total variation could not be explained by the empirical model. According to Joglekar and May (1987), R^2 should be at least 0.80 for a good fit of a model. The R^2 value (0.9678) recorded in the present study for

CTC removal was higher than 0.80, indicating that the regression model explained the reaction well.

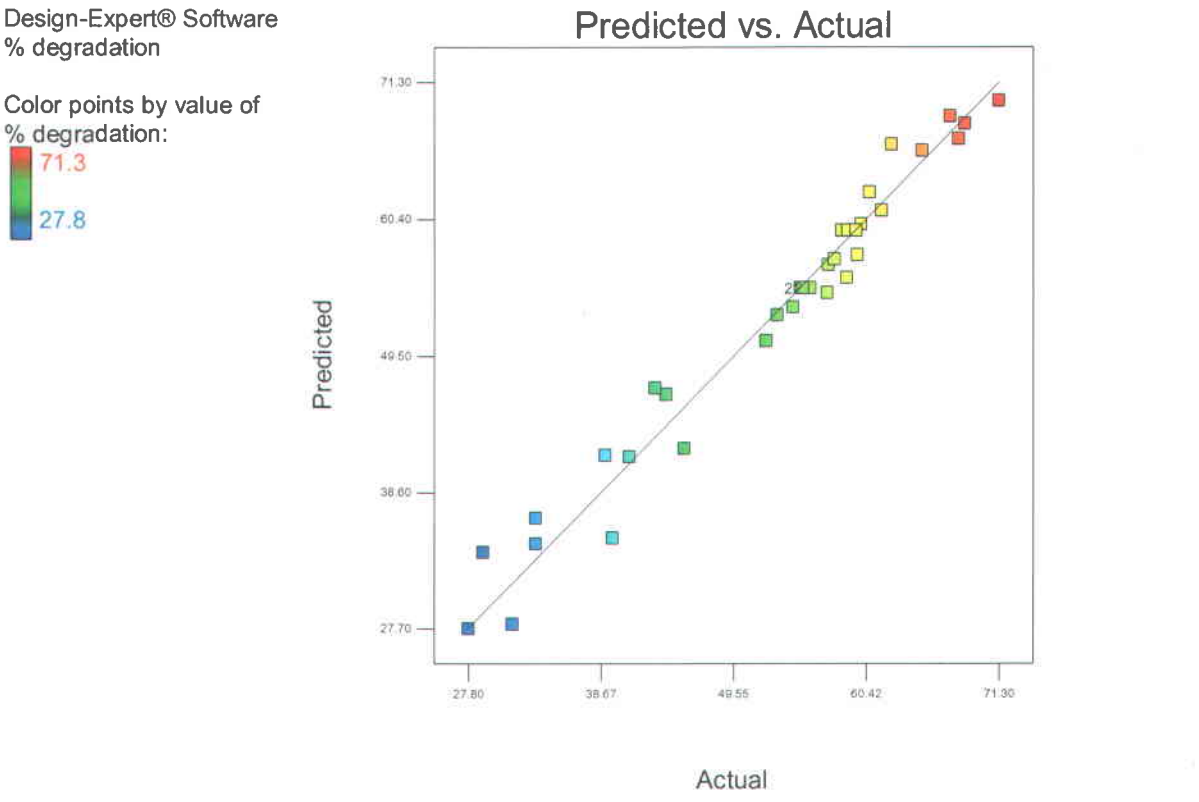


Figure 6-7 Comparison between actual and predicted values for CTC degradation.

Tableau 6-6 ANOVA results for the response surface quadratic for CTC degradation.

Source	Analysis of variance				
	d.f.[a]	Sum of square	Mean of square	F-value	Pr > F
Model	13	4857.49	373.65	60.04	< 0.0001
Residual	26	161.82	6.22	-	-
Lack of fit	16	160.12	10.01	58.81	< 0.0001
Pure error	10	1.70	0.17	-	-

[a] *Degree of freedom; F: Fisher coefficient;* R^2*=0.9678*

The main objective of the optimization is to determine the optimum values for CTC removal using the PECO process. The criteria selected for the optimization condition for CTC degradation are the following: (i) current intensity and pollutant concentration have to be minimized; (ii) treatment time has to be maximized, and (iii) UV lamp position was investigated in the experimental range. The optimization results of the process variables for CTC removal are shown in Table 6-7. The desirability function value was found as 0.905 for these optimum conditions. The theoretical response proposed by Design-Expert® Program Software for CTC degradation was 72.7%. To confirm the model adequacy and the validity of the optimization procedure, additional experiments were performed under optimal operating conditions. The average value of the experimental response measured using UV–vis absorption spectrophotometer is 74.2% ± 0.57%. This CTC degradation rate of ~74% was recorded at the end of this experiment, and is found to be very close to the value proposed by the model (72% of CTC degradation).

Tableau 6-7 Determination of optimum operating conditions proposed by Design-Expert ® Program Software.

Parameter	Optimum value
Applied electric current (A)	0.39
Treatment time (min)	120
Pollutant concentration (mg L^{-1})	25
UV lamp position	internal
Experimental response (%)	74.2 ± 0.57
Theoretical response (%)	72.73

However, experimental results determined using liquid chromatography mass spectrometer (LC/MS/MS) shows that the removal of CTC is around 97% ±1.12%. UV–vis absorption spectrophotometer is an indirect analytical method. According to Beer–Lambert law, the measure of the concentration of species can be determined from the measured absorbance. The presence of interfering substance can influence the absorption spectrum and consequently can modify the results. By comparison, LC/MS/MS technique, which combines simultaneously a powerful physical separation technique and a powerful technique of analysis and mass detection, has a very high sensitivity and selectivity towards several antibiotics (Hernàndez et al., 2007). It is worth noting that during the treatment, the pH varied from 4.82 ± 0.14 (initial value) to 7.67 ± 0.42. This variation could be probably attributed to by-products formation during the application of the PECO process. It is worth noting that hydroxyl radical produced at the surface of photo-anode could react with the CTC and lead to the formation of by-products. Subsequently, by-products can be oxidized by hydroxyl radical into further intermediates including ring-opened structures. The above mentioned hypothesis of intermediates and CO_2 formation was based on the results described elsewhere using hydroxyl radical as oxidant agent (Tran et al., 2010). According to Halling-Sørensen et al., (2002), the possible formation of by-products derived from CTC oxidation are: 5a,6-

anhydrochlorotetracycline hydrochloride (ACTC); 4-epi-chlorotetracycline hydrochloride (ECTC); 4-epi-anhydrochlorotetracycline hydrochloride (EACTC); iso-chlorotetracycline (iso-CTC); keto-chlorotetracycline (keto-CTC). At pH value between 3 and 6.5, ECTC, EACTC, ACTC, and keto-CTC are the predominant forms, while at pH value between 6.5 and 9, iso-CTC, keto-CTC (more predominate at this pH interval), demethylation of the isochlorotetracycline (DM-iso CTC) are the predominant ones. The pH, ions, and solvents clearly influence the predominant forms of CTC by-products present in the solution (Halling-Sørensen et al., 2002). In our study, the initial pH value of the CTC solution was 4.82 ± 0.14. This result demonstrates clearly that the by-products were formed after photoelectrocatalytic treatment of CTC solution. The by-products of CTC can interfere on the absorption spectrum of CTC and modify the removal rate of CTC during electrolysis. Photoelectrocatalytic treatment costs of CTC (including only chemical consumption and energy consumption) recorded in the best experimental condition was estimated to \$4.55 $\pm$0.01 m^{-3}. It is to be underlined that, sometimes by-products can be as toxic as the initial pollutant or more toxic than that the initial pollutant. To circumvent these drawbacks, by-products have to be further oxidized into water and carbon dioxide. In view of enhancing CTC removal and to avoid possible toxicity of treated-effluent, an additional parameter (X5) such as the type of supporting electrolyte (NaCl and Na_2SO_4) should be tested. Indeed, on Ti/TiO_2 photo-anode, chloride ions can be oxidized and form hypochlorous acid (HClO) in solution. HClO is powerful oxidant capable of oxidizing and modifying the structure of organic molecules (Drogui et al., 2007; Canizares et al., 2005) and leading to more oxidized and less toxic compounds. However, this alternative has to be carefully studied because of the possible formation of organochlorinated compounds, which can be more toxic than the initial pollutant. Another interesting alternative could be the use of another type of cathode material, such as vitreous carbon (VC) versus stainless steel (SS). It has been demonstrated that, on

vitreous carbon electrode, hydrogen peroxide (H_2O_2) can be electrochemically generated by cathodic reduction of dissolved oxygen (Xie and Li, 2002). This peroxide induces non offensive by-products contrarily to chlorine. Under UV irradiation, hydrogen peroxide can be decomposed into hydroxyl radical (in addition to hydroxyl radical produced on the surface of photocatalyst). This should contribute to enhance CTC degradation. Likewise, the addition of an electron acceptor (e.g. H_2O_2) should prevent the electron-hole recombination and increase the photocatalyst efficiency (Ozer and Ferry, 2001). According to previous studies (Xie and Li, 2002; Sohrabi and Ghavami, 2010; Ding et al., 2010), such an oxidant agent (H_2O_2) is beneficial for photocatalytic reaction by trapping the conduction band electron in order to generate more hydroxyl radical.

6.6 Conclusion

In this study, the Ti/TiO_2 rectangular electrode was prepared by a PLD method. It showed that the TiO2 coating at 600°C is very uniform in thickness and was found to be of rutile structure. By investigating the photoelectrocatalytic degradation process of CTC in aqueous medium using this electrode, current intensity and treatment time were found to be the most influent parameters. The contribution of current intensity and treatment time were 76.2% and 16.7%, respectively, while the contribution of pollutant concentration and UV lamp position represented only 4% and 2.5%, respectively. A central composite design was employed to define the optimal operating condition for CTC removal. Current intensity is very meaningful for CTC degradation using both internal and external UV lamp configuration. Current intensity and treatment time have positive effects on the response compared to the pollutant concentration which has a rather negative one on the removal of CTC. The PECO process applied under optimal conditions (at current intensity of 0.39 A during 120 min with internal position of the UV lamp) is able to oxidize around $74.2 \pm 0.57\%$, of CTC.

However, in view of enhancing CTC removal and to avoid possible toxicity of treated-effluent, another type of cathode material such as vitreous carbon (VC) should be tested. On such a cathode electrode, hydrogen peroxide (H_2O_2) can be electrochemically generated and decomposed into hydroxyl radical under UV irradiation. Likewise, the identification of by-products needs to be rigorously verified and a mechanism of CTC degradation should be proposed. The total organic carbon (TOC) should be measured to evaluate the level of the degradation and see if CTC is completely or partially transformed into water and carbon dioxide.

6.7 Acknowledgements

The authors acknowledge the financial support of the National Sciences, Engineering Research Council (NSERC) of Canada and Premier Tech Ltée.

6.8 References

Adams C, Wang MYLoftin K & Meyer M (2002) Removal of antibiotics from surface and distilled water in conventional water treatment processes. *J. Environ. Eng. Div. ASCE* 128: 253–260.

Bautitz IR & Nogueira RFP (2007) Degradation of tetracycline by photo-Fenton process-Solar irradiation and matrix effects. *J. Photochem. Photobiol. A* 184: 141–146.

Canizares P, Lobato J, Paz R, Saez CJet, M.A. Rodrigo MA, Electrochemical oxidation of phenolic wastes with boron-doped diamond anodes. *Water Res.* 39(2005) 2687–2703.

Daneshvar N, Oladegaragoze A, Djafarzadeh N (2006) Decolorization of basic dye solutions by electrocoagulation: an investigation of the effect of operational parameters. *J. Hazard. Mater. B.* 129: 116–122.

Desbiens E & El Khakani MA (2003) Growth of high-K silicon oxynitride thin films by means of a pulsed laser deposition-atomic nitrogen plasma source hybrid system for gate dielectric applications. *J. Appl. Phys.* 94 (9): 5969–5975.

Ding Y, Yang C, Zhu L & Zhang J (2010) Photoelectrochemical activity of liquid phase deposited TiO_2 film for degradation of benzotriazole. *J. Hazard. Mater.* 175: 96–103.

Drogui P, Blais JF & Mercier G (2007) Review of electrochemical technologies for environmental applications. *Recent Patent Eng.* 1: 257–272.

Guinier A (1962) *Théorie et Technique de la radiocristallographie.* 3rd ed., Dunod, Paris, 740p

Halling-Sørensen B, Sengeløv G & Tjørnelund J (2002) Toxicity of tetracyclines and tetracycline degradation products to environmentally relevant bacteria including

selected tetracycline-resistant bacteria, Arch. Environ. *Contam. Toxicol.* 42 (3): 263–271.

Heberer T (2002) Occurrence, fate, and removal of pharmaceutrical residues in the aquatic environment: a review of recent research data. *Toxicol. Lett.* 131 (1–2): 5–17.

Heit G, Neuner A, Saugy PY & Braun AM (1998) Vacuum-UV (172 nm) actinometry– the quantum yield of the photolysis of water. *J. Phys. Chem. A* 102: 5551–5561.

Hernàndez F, Sancho VJ, Ibànez M & Guerrero C (2007) Antibiotic residue determination in environmental waters by LC–MS, TrAC, Trends Anal. Chem. 26 (6): 466–485.

Ingerslev F & Halling-Sorensen B (2000) Importance of the test volume on the lag phase in biodegradation studies. *Environ. Toxicol. Chem.* 19 (10): 2443–2447.

Jaroenworaluck A, Regonini D, Bowen CR, Stevens R (2010) A microscopy study of the effect of heat treatment on the structure and properties of anodized TiO2 nanotubes. *Appl. Surf. Sci.* 256: 2672–2679.

Jeong J, Song W, Cooper WJ, Jung J & Greaves J (2010) Degradation of tetracycline antibiotics: mechanisms and kinetic studies for advanced oxidation/reduction processes. (2010) *Chemosphere* 78: 533–540.

Ji L, Chen W, Duan L & Zhu D (2009) Mechanisms for strong adsorption of tetracycline to carbon nanotubes: a comparative study using activated carbon and graphite as adsorbents. *Environ. Sci. Technol.* 43: 2322–2327.

Joglekar AM May AT (1987) *Product excellence through design of experiments.* Cereal Foods World 32: 857–868.

Kim I & Tanaka H (2009) Photodegradation characteristics of PPCPs in water with UV treatment. *Environ. Int.* 35: 793–802.

Kim CS, Kwon IM, Moon BK, Jeong JH, Choi BC, Kim JH, Choi H, Yi SS, Yoo DH, Hong KS, Park JH & Lee HS (2007) Synthesis and particle size effect on the phase transformation of nanocrystalline TiO_2. *Mater. Sci. Eng.* C 27: 1343–1346.

Kitazawa Si, Choi Y, Yamamoto Sh, Yamaki T (2006) Rutile and anatase mixed crystal TiO_2 thin film prepared by pulsed laser deposition. *Thin Solid Films* 515 (4):1901–1904.

Kolpin DW, Furlong ET, Meyer MT, Thurman EM, Zaugg SD, Barber LB & Buxton HT (2002) Pharmaceuticals, hormones, and other organic wastewater contaminants in U.S. streams, 1999–2000: a national reconnaissance. *Environ. Sci.Technol.* 36: 1202–1211.

Khandpur RS (2006) *Handbook of Analytical Instruments*, 2nd ed., Tata Mc Graw-Hill, p770.

Kummerer K (2003) Significance of antibiotics in the environment. *J. Antimicrob.Chemother.* 52 (1): 5–7.

Kummerer K, Hartmann TS & Meyer M (1997) Biodegradability of the anti-tumor agent ifosfamide and its occurrence in hospital effluents and communal sewage. *Water Res.* 31 (11): 2705–2710.

Li XZ, Li FB, Fan CM & Sun YP (2002) Photoelectrocatalytic degradation of humic acid in aqueous solution using a Ti/TiO_2 mesh photoelectrode. *Water Res.* 36: 2215–2224.

Lòpez-Penalver JJ, Sànchez-Polo M, Gòmez-Pacheco CV & Rivera-Utrilla J (2010) Photodegradation of tetracyclines in aqueous solution by using UV and UV/H_2O_2 oxidation processes. *J. Chem. Technol. Biotechnol.* 85 (10): 1325–1333.

Martinez-Huitle CA & Ferro S (2006) Electrochemical oxidation of organic pollutants for the wastewater treatment: direct and indirect processes. *Chem. Soc. Rev.* 35: 1324–1340.

Miao X, Bishay F, Chen M & Metcalfe CD (2004) Occurrence of antimicrobials in the final effluents of wastewater treatment plants in Canada. *Environ. Sci. Technol.* 38: 3533–3541.

Myers RH & Montgomery DC (2002) *Response Surface Methodology: Process and Product Optimization using Designed Experiments*. 2nd ed., John Wiley and Sons, New York, NY, 704p.

Ozer RR & Ferry JL (2001) Investigation of the photocatalytic activity of TiO_2–polyoxometalate systems. *Environ. Sci. Technol.* 35: 3242–3246.

Qiang Z & Adams C (2004) Potentiometric determination of acid dissociation constants (pKa) for human and veterinary antibiotics. *Water Res.* 38: 2874–2890.

Regonini D, Jaroenworaluck A, Stevens R & Bowen CR (2010) Effect of heat treatment on the properties and structure of TiO_2 nanotubes: phase composition and chemical composition. *Surf. Interface Anal.* 42: 139–144.

Reyes C, Fernandez J, Freer J, Mondaca MA, Zaror C, Malato S, H. Mansilla H (2006) Degradation and inactivation of tetracycline by TiO2 photocatalysis, *J.Photochem. Photobiol. A* 184: 141–146.

Rey RP, A.S. Padron AS, Leon PL, Pozo MM, Baluja C (1999) Ozonation of cytostatics in water medium. Nitrogen bases. *Ozone Sci. Eng.* 21: 69–77.

Sohrabi MR & Ghavami M (2010) Comparison of direct yellow 12 dye degradation efficiency using UV/semiconductor and UV/H_2O_2/semiconductor systems. *Desalination* 252: 157–162.

Tir M & Moulai-Mostefa N (2008) Optimization of oil removal from oily wastewater by electrocoagulation using response surface method. *J. Hazard. Mater.* 158: 107–115.

Tolls J (2001) Sorption of veterinary pharmaceuticals in soils: a review. *Environ. Sci. Technol.* 35: 3397–3406.

Tran L, Drogui P, Mercier G & Blais JF (2010) Comparison between Fenton oxidation process and electrochemical oxidation for PAH removal from an amophoteric surfactant solution. *J. Hazard. Mater.* 40: 1493–1510.

Waldner G, Pourmodjib M, Bauer R & Neumann-Spallart M (2003) Photoelectrocatalytic degradation of 4-chlorophenol and oxalic acid on titanium dioxide electrodes. *Chemosphere* 50: 989–998.

Xie YB & Li XZ (2006) Degradation of bisphenol A in aqueous solution by H_2O_2-assisted photoelectrocatalytic oxidation. *J. Hazard. Mater.* B138: 526–533.

Wang N, Li X, Wang Y, Quan X & Chen G (2009) Evaluation of bias potential enhanced photocatalytic degradation of 4-chlorophenol with TiO_2 nanotube fabricated by anodic oxidation method. *Chem. Eng. J.* 146: 30–35.

Zaroual Z, Chaair H, Essadki AH, El Ass K & Azzi M (2009) Optimizing the removal of trivalent chromium by electrocogulation using experimental design. *Chem. Eng. J.* 148: 488–495.

Zhang T, M. Zhang M, Zhang X & Fang HH (2009) Tetracycline resistance genes and tetracycline resistant lactose-fermenting enterobacteriaceae in activated sludge of sewage treatment plants. *Environ. Sci. Technol.* 438: 3455–3460.

CHAPITRE 7

PHOTOELECTROCATALYTIC OXIDATION OF CHLORTETRACYCLINE USING TI/TIO_2 PHOTO-ANODE WITH SIMULTANEOUS H_2O_2 PRODUCTION

Le chapitre 7 est constitué de l'article suivant :

Rimeh Daghrir, Patrick Drogui, My Ali El Khakani, Photoelectrocatalytic oxidation of chlortetracycline using Ti/TiO_2 photo-anode with simultaneous H_2O_2 production. *Electrochimica Acta. 87 (2013) 18-31.*

7. PHOTOELECTROCATALYTIC OXIDATION OF CHLORTETRACYCLINE USING TI/TIO_2 PHOTO ANODE WITH SIMULTANEOUS H_2O_2 PRODUCTION

7.1 Abstarct

This study investigated the photoelectrocatalytic oxidation (PECO) of chlortetracycline (CTC) in aqueous solution using a Ti/TiO_2 photocatalyst. The Ti/TiO_2 used as photo-anode was prepared by a pulsed laser deposition method (PLD). The PLD TiO_2 coatings were found to have rutile and anatase structures consisting of nano-cristallites of approximately 10 nm and 15 nm in diameter, respectively. The influence of various parameters such as crystallographic structure of Ti/TiO_2, cathode material and pH were evaluated. Experimental results revealed that a curret intensity of 0.39 A under UV irradiation (254 nm) for a period of treatment of 1230 min was beneficial for CTC oxidation. The initial CTC concentration (25 μg L^{-1}) could be optimmaly diminished up to 98.0 ± 0.2% while using a Ti/TiO_2 photo-anode having a crystallographic structure of anatase and using vitreous carbon as cathode. Under these conditions, a relatively high mineralization of (67.3 ± 2.15% of TOC removal and 69.3 ± 3.10% of TN removal) was recorded. The initial rate of photoelectrocatalytic degradation of CTC can be well described by the Langmuir-Hinshelwood (L-H) kinetic model (R^2 = 0.9996) with a reaction rate constant of 17.3 μg L^{-1} min^{-1}. Likewise, microtox (*Vibrio fisheri*), microalga (*Pseudokirchneriella Subcapitata*) and Daphnia (*Daphnia magna)* biotests revealed that the treated – effluent was not toxic compared to the untreated effluent.

7.2 Key words

Photoelectrocatalysis; Photo-anode; Chlortetracycline; Kinetics; Toxicity

7.3 Introduction

Pharmaceutical products (PPs) used in the medical field for preserving human and animal health have received recently a special attention and an increasing of concern. Among PPs, antibiotics are largely consumed in human medicine for therapeutic purposes and widely used in the livestock and poultry industries for preventing diseases or improving growth (Chen et al., 2011; Lee et al., 2011). According to previous studies (Martinez et al., 2011; Halling-Sorensen et al., 2011), the annual production volume of drugs has been estimated in several hundreds of tons. These substances are excreted by the organism, disposed from the households and released into the aquatic environment. They were detected in influents of wastewater treatment plants, in surface water, in ground water and even in drinking water (Martinez et al., 2011; Ternes, 1998; Kolpin et al., 2002; Petrovic et Barcelo, 2006). Due to their anti-bacterial properties, some of antibiotic compounds are not completely removed and inhibit the performance of biological processes (Lee et al., 2011; Carballa et al., 2004). Thus, their occurrence and persistence in the aquatic ecosystems lead to a negative effect on human life and cause troubles on aquatic systems (Lee et al., 2011; Yang and Carlson, 2004).

Chlortetracycline hydrochloride (CTC) belongs to the tetracycline (TCs) antibiotic groups. TCs are widely used throughout the world for veterinary purposes, for human therapy and in agriculture sector (Lopez-Penalver et al., 2010; Li et al., 2011; Daghrir et al., 2012). It has been reported by Halling-Sorensen et al. (2002), that the annual use of TCs (including CTC) in Europe in veterinary therapy field was about 2500 tons. Due to the high consumption of TCs through the world, recent researches have demonstrated that the residual TCs are detected in different environmental compartments: surface water (Li et al., 2011), ground water (Hernandez et al., 2007), agriculture wastewater (Shelver and Varel, 2012), municipal sewage (Chang et al., 2010), soil and sediments (Liu et al., 2009; Andreu et al., 2009). Thus, the presence of these residual concentrations in the environment has to be taken into account

due to their potential to disrupt the ecosystem equilibrium. Few previous studies have examined CTC in terms of toxicity to a variety of species. Wang et al. (2009) showed the inhibiting effects of CTC on the growth of freshwater algae, whereas Guo and Chen (2012) have reported that CTC had significantly toxic effect on freshwater phytoplankton species. Generally, biological treatment processes have been shown to be ineffective in the removal of antibiotics (Lee et al., 2011; Lopez-Penalver et al., 2010; Daghrir et al., 2012; Reyes et al., 2006). However, other methods can be used to remove antibiotics such as adsorption, biosorption, ozonation, membrane techniques (reverse osmosis), advanced oxidation processes (AOPs) including O_3/H_2O_2, UV/O_3, UV/H_2O_2, H_2O_2/Fe^{2+}, e.g. (Ji et al., 2009; Adams et al., 2002; Rey et al., 1999). Among them, oxidative treatments using AOPs have been successfully applied to degrade various pharmaceutical compounds present in polluted water. In spite of the good oxidation of refractory organic compounds, the complexity of these methods (AOPs), high chemical consumption and relatively higher treatment cost constitute major barriers for field application purposes (Martinez-Huitle and Ferro, 2006). A renewed interest in photoelectrocatalytic oxidation (PECO) technique combining both electrolytic and photocatalytic processes has been spurred by the search for reliable, cost-effective water treatment processes (Daghrir et al., 2012). The PECO process represents an example of electrochemical advanced oxidation processes (EAOPs) able to retard the recombination of the electron-hole pairs (e^-_{CB}/h^+_{VB}) photo-generated on the surface of the catalyst. Consequently, higher efficiency in the degradation of pollutants can be recorded (Daghrir et al., 2012; Frontistis et al., 2011; Liu et al., 2009). The PECO process has been studied for CTC degradation using a response surface methodology (Daghrir et al., 2012). The degradation experiments were carried out at different initial concentrations of CTC (from 25 mg L^{-1} to 50 mg L^{-1}) in 0.5 M of Na_2SO_4 using a current intensity varying from 0.25 to 0.50 A. High treatment efficiency of CTC was achieved by the PECO process compared to

the conventional electrochemical oxidation, direct photolysis and photocatalysis processes. The PECO process applied under optimal conditions (at current intensity of 0.39 A during 120 min with internal position of the UV lamp) is able to oxidize around 74.2 ± 0.57 %, of CTC. However, additional experiments are required to evaluate the effectiveness of the PECO process in the presence of a relatively low concentration of CTC (25 μg L^{-1}) while applying the optimal conditions determined elsewhere (Daghrir et al., 2012). Thus, the specific objectives of the present works are the followings: 1) evaluate the degradation efficiency and the mineralization rate of CTC (initial concentration of 25 μg L^{-1}) using different nanostructure of TiO_2 (anatase, rutile, amorphous); 2) evaluate the effect of other parameters (such as cathode material and initial pH) on CTC degradation; 3) study the kinetic of CTC degradation; 4) identify the CTC by-products and propose a mechanism (reaction pathways) for CTC degradation based on identified by-products and ; 5) Verify the quality of treated-effluents (versus untreated effluents) in terms of toxicological effects using some biotests.

7.4 Materials and methods

7.4.1 Preparation of the Ti/TiO_2 electrode

TiO_2 coatings were prepared using a pulsed laser deposition (PLD) method. A KrF excimer laser (wavelength = 248 nm, pulse durations 15 nanoseconds) operating at a repetition rate of 30 Hz was focused, at an incidence angle of 45°, onto the TiO_2 rotating target (99.95% purity). The on-target laser energy density was set to 4.5 J cm^{-2}. The TiO_2 films were deposited on both titanium grids (for photoelectrochemical studies) and on silicon substrates (for material characterisations). The TiO_2 films were deposited at a temperature of 600°C and 400°C, respectively, under an oxygen background pressure of 1 mTorr. The PLD deposition chamber was first turbo-pumped to approximately 10^{-6} Torr before filling it with oxygen. More details on the pulsed laser deposition system and it schematics can be found elsewhere (Desbiens and El Khakani, 2003). Prior to coating the substrates, the TiO_2 target was

systematically cleaned by laser-ablating its surface for 5 min. The nominal thickness of the coating was estimated to 400 nm for rutile TiO_2 forms and 1 μm for anatase TiO_2 forms. The film thickness was determined directly from cross-sectional scanning electron microscopy (SEM) observations. The crystallographic structure of the PLD-deposited TiO_2 films was examined by means of X-ray diffraction (XRD) using a Philips X'pert-MPD X-ray diffractometer (Cu K_α radiation) at a glancing incident angle of 1°.

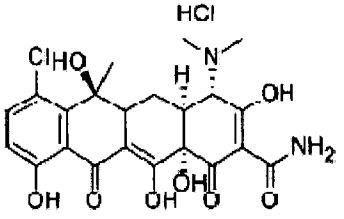
7.4.2 Preparation of the amorphous carbon electrode

The amorphous carbon (a-C) films were deposited by using the pulsed laser deposition (PLD) method. Thus, a KrF excimer laser (wavelength = 248 nm, pulse durations 15 ns, repetition rate = 30 Hz) was focused, at an incidence angle of 45°, onto a 2"-diameter graphite pellet. During the laser ablation, the graphite target is kept rotating while the Incident KrF-laser beam is swept laterally on the target surface, in order to perform a uniform erosion of the graphite pellet. The on-target laser energy density was set to ~4 J cm^{-2}. Prior to performing the coating, the PLD deposition chamber was first turbo-pumped to about 10^{-6} Torr, and the graphite target was in-situ cleaned by ablating its surface for 5 min while isolating the substrate from the ablation plume by a shutter. The a-C coatings were deposited on 1 cm-diameter polished-discs of titanium (for analyses purposes), and onto both sides of titanium grids specially designed for the photoelectrochemical studies. The PLD deposition of a-C films was achieved at two different deposition temperatures, namely 20°C (RT) and 600°C (HT). The typical thickness of the a-C coating, as deduced from cross-section scanning electron microscopy (SEM) observations is of ~500 nm.

7.4.3 Preparation of the synthetic solution

Chlortetracycline hydrochloride ($C_{22}H_{24}Cl_2N_2O_8$) was an analytical grade reagent supplied by Sigma Aldrich (purity 78 %). Its water solubility was 4.12 g L^{-1} (Lopez-Penalver et al., 2010). Table 7-1 presents some chemicals properties of CTC (Qiang and Adams, 2004; Kim et al., 2009). A stock solution (25 mg L^{-1} of CTC) was prepared in a glass-tank containing 1 L of distilled water in which 25 mg of CTC was added. Solubilisation of CTC was carried out at a high speed of 750 rpm for a 30 min. Mixing was achieved by a Teflon-covered stirring bar installed at the bottom of the beaker. At the end of this conditioning stage, a fraction of the mixture (1 mL) was transferred into a 2 L tank containing 1 L of distilled water. The resulting mixture constituted the synthetic CTC solution (final concentration of 25 μg L^{-1}) in which an electrolyte such as sulphate sodium was added to increase electrical conductivity.

Tableau 7-1 Chemical properties of Chlortetracycline hydrochloride.

Molecule	Molecular formula	Chemical structure	Molecular weight (g mol^{-1})	Solubility (mol L^{-1})	Log K_{OW}	pK_{a1}	pK_{a2}	pK_{a3}
CTC	$C_{22}H_{24}Cl_2N_2O_8$		515.3	0.008	-0.62	3.3±0.3	7.55±0.02	9.3±0.3

7.4.4 Experimental unit

The reactor unit was made of acrylic material with a dimension of 12.7 cm (width), 16.51 cm (length) and 11.43 cm (depth). A quartz window (8.89 cm x 8.89 cm) was disposed on one face of the reactor for the photo-electrocatalysis experiments (Figure 7-1). All the assays were conducted in batch mode. The photoelectrocatalytic cell was comprised of one anode (Ti/TiO_2) and one cathode, each one having a surface area of 110 cm^2 (10 cm width x 11 cm high), placed in parallel and were submerged in the solution. Different cathode materials were investigated: stainless steel (SS), vitreous carbon (VC), graphite (Gr) and amorphous carbon prepared at 20°C (a-C1) and at 600°C (a-C2). The electrodes were vertically installed on a perforated Plexiglas plate placed at 2 cm from the bottom of the cell. The inter-electrode gap was 1.0 cm. Both anode and cathode were connected respectively to the positive and negative outlet of a regulated DC power supply (PS 3030 D, Circuit-Test Electronics, Burnaby, BC, Canada) with a maximum current rating of 3.0 A at an open circuit potential of 30 V. The photoelectrocatalytic cell was operated with 0.39 A of current intensity imposed during a treatment period of 120 min (Daghrir et al., 2012). The photo-anode was illuminated by a mercury lamp (light intensity = 6.9 mW cm^{-2}; λ_{max} = 254 nm). The lamp was installed vertically inside the reactor. The light intensity was measured with a photometer (Model PS-3, 99-0057-01, UVp Company; USA). The photoelectrocatalytic reactor was placed in a dark chamber in order to avoid interferences from the daylight. Mixing in the cell was achieved by a Teflon-covered stirring bar installed between the perforated plate and the bottom of the cell. All experiments were carried out at room temperature (25°C). For all tests a total volume of 1.0 L was used.

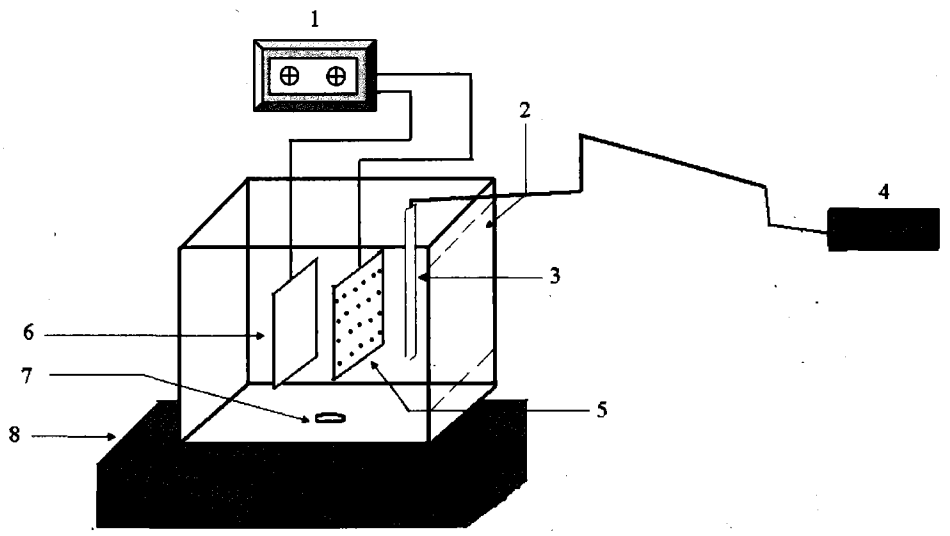


Figure 7-1 Schematic diagram of the photoelectrocatalytic reactor: (1) DC power supply (2) quartz window (3) UV lamp (4) photometer (5) photoanode (6) cathode (7) stirring bar (8) magnetic stirrer.

7.4.5 Experimental procedure

The first set of photoelectrocatalytic experiments consists to test successively different operating parameters such as the crystallographic structure of Ti/TiO_2 (anatase, rutile and amorphous), the type of cathode material (Gr, VC, a-C1, a-C2, SS), the concentrations of CTC (25-230 $\mu g\ L^{-1}$) and the initial pH (3.0 - 9.0), in view of determining the best operating conditions for treating CTC. The initial pH was adjusted using sulfuric acid (HCl, 1.5 mol L^{-1}) or sodium hydroxide (NaOH, 1.5 mol L^{-1}). Sodium sulphate, sodium hydroxide and chlorhydric acid were analytical grade reagents and supplied by Fisher scientific (Quebec, Qc, Canada). During these assays, the performance of the photoelectrocatalytic unit to oxidize CTC was evaluated by measuring simultaneously the residual concentration of CTC, total nitrogen (TN) and total organic carbon (TOC). The pH was also measured. Likewise, biotests

(Microtox, algae and Daphnia tests) were carried out to have information about the toxicity of the treated solution of CTC (versus untreated solution of CTC). To verify the effectiveness and the reproducibility of the photoelectrocatalytic process, the measure of all parameters were repeated in triplicate.

7.4.6 Analytical techniques

7.4.6.1 Operating parameters and organic measurements

The pH was determined using a pH-meter (Fisher Acumet model 915) equipped with a double-junction Cole-Palmer electrode with Ag/AgCl reference cell. NT and TOC measurements were performed using a Shimadzu TOC 5000A analyzer (Shimadzu Scientific Instruments Inc) equipped with an autosampler.

7.4.6.2 Measure of CTC concentration

The progress of the photoelectrocatalytic degradation of CTC and by-products was monitored and quantified by LC/MS/MS (Thermo TSQ Quantum Access). The chromatographic column used was Beta Basic C18, particle size 3 μm and 2.1 x 100 mm inner diameter. The isocratic mobile phase was A: 50% H_2O + 0.1% formic acid and B: 50% CH_3CN + 0.1% formic acid at a flow rate of 200 μL min^{-1}. Mass spectral data shown in this study were acquired on a LCQ Duo ion trap tandem mass spectrometry equipped with an electrospray ionisation (ESI) source operated in positive ion mode. Nitrogen was used as a sheath and auxiliary gas. Working conditions were as followed: spray voltage was 5000 V and capillary temperature was 345°C. Quantitative analysis of CTC was determined using sulfamethazine C_{13} as internal standard.

7.4.6.3 Toxicity tests

The quality of treated-solution (versus untreated solution) has been evaluated using a biotest battery to have information about its toxic effect. Microtox, microalga and *Daphnia* bioassay tests were applied. Microtox analysis is a standardized toxicity method using the luminescent

marine, Vibrio fisheri (Software MTX6, version 6.0, Microbics Corporation) (Environnement Canada, 1992; USEPA, 1993). This test consisted of one control and six serial dilutions of each sample (1.56, 3.13, 6.25, 12.5, 25.0, and 50%, v/v). The endpoint of Microtox test is the measurement of bioluminescence reduction. The bioluminescence emitted by V. fisheri was first measured after 10 min of incubation (without adding any sample, control assay), after which the CTC-solution (treated or untreated-solution) was added to the bacterial suspension. The bioluminescence reduction was determined after a 5, 15 and 30 min exposure to the contaminant. The effects of toxicity were expressed as percentage of luminescence inhibition at 15 min of exposure.

By comparison, Daphnia bioassay tests consist to determine the lethal concentration for which at least 50% of mortality of *Daphnia magna* is observed after 48 h exposure to the contaminant. This test consisted of one control and five serial dilutions of each sample (6.25, 12.5, 25.0, 50.0, and 100%, v/v). After 48 h exposure, the survival and death organisms was counted and the toxicity effect was evaluated using a statistic calculation software (Computer Basic, Spearman Karber tests, version 2.01, Microsoft) (Environnement Canada, 2000; Ministére de l'environnement du Québec, 2000).

The chronic toxicity of the CTC solution has been also evaluated using microalga *Pseudokirchneriella Subcapitata*. The endpoint of microalga test is the measure of the inhibition rate of the growth of *P. Subcapitata* after 72 h exposure to the contaminant. This test consisted of one control and seven serial dilutions of each sample (1.42; 2.85; 5.68; 11.36; 22.73; 45.45; and 90.91%, v/v). After 72 h exposure, the inhibition of growth rate of *P. Subcapitata* was measured and the toxicity effect was evaluated.

7.4.6.4 Measure of hydrogen peroxide concentrations

The hydrogen peroxide concentration was measured using volumetric dosage. The cerium ion solution (Ce $(SO_4)_2$, $2(NH_4)_2$ SO_4, 2 H_2O) (5.88 10^{-3} M) was used under acidic conditions (H_2SO_4, 9N) in the presence of three drops of $Fe(o\text{-}phen)_3^{2+}$ as an indicator. To quantitatively determine the concentration of hydrogen peroxide, a H_2O_2 calibration curve was obtained by plotting the cerium volume (mL) as a function of H_2O_2 concentration (from 0 moL L^{-1} to 2.94 10^{-3} moL L^{-1}). The gradual change of the solution colour from red to the blue indicates a total oxidation of hydrogen peroxide using a cerium solution

7.4.7 Economic aspect

The economic study included chemical and energy consumption. The electric cost was estimated about of 0.06 US$ kWh^{-1}. A unit cost of 0.30 US$ kg^{-1} was used for electrolyte consumption (Na_2SO_4 industrial grade). The total cost was evaluated in terms of U.S. dollars spent per cubic meter of treated solution (US$ m^{-3}).

7.5 Results and discussion

7.5.1 Characterization of the Ti/TiO_2 electrode

The surface morphology of the TiO_2 photocatalytic coating was examined by scanning electron microscopy. Figure 7-2 shows a top view of a TiO_2 film deposited at 600°C and 400°C onto silicon substrates. The coating is densely featured with fine spherical grains of a few tens of nanometers of diameters. By increasing the temperature from 400°C to 600°C, the deposited TiO_2 showed an increase in crystallite size.

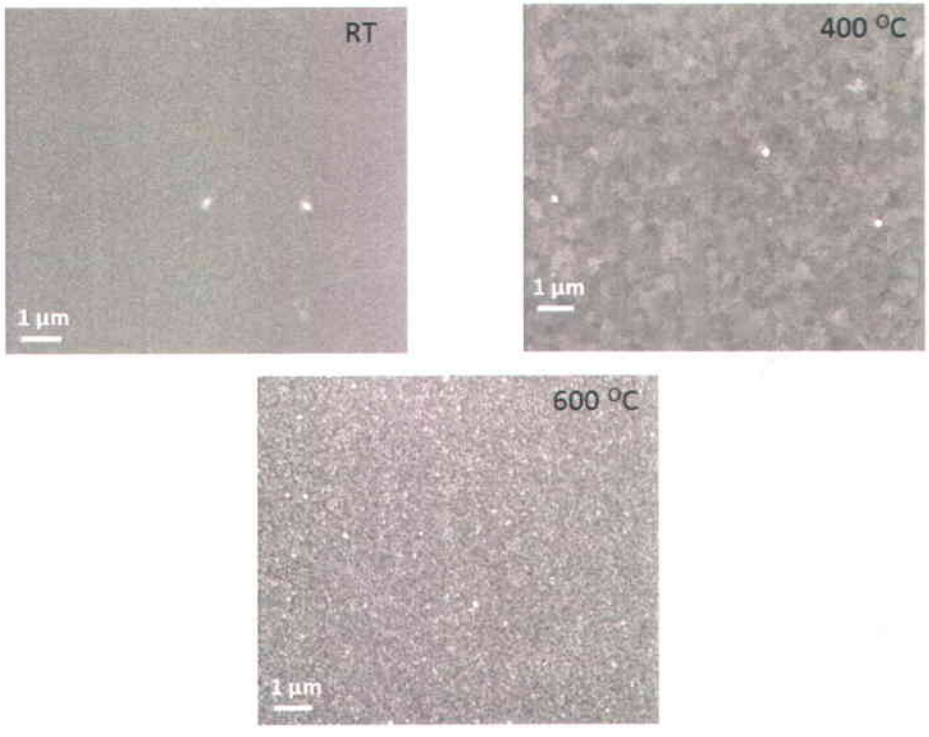


Figure 7-2 SEM views of PLD TiO_2 films deposited on Si at different deposition temperatures.

Figure 7-3a and b show that the TiO_2 columns are densely packed with a uniform thickness across the film, forming a smooth and continuous interface with the underlying substrate.

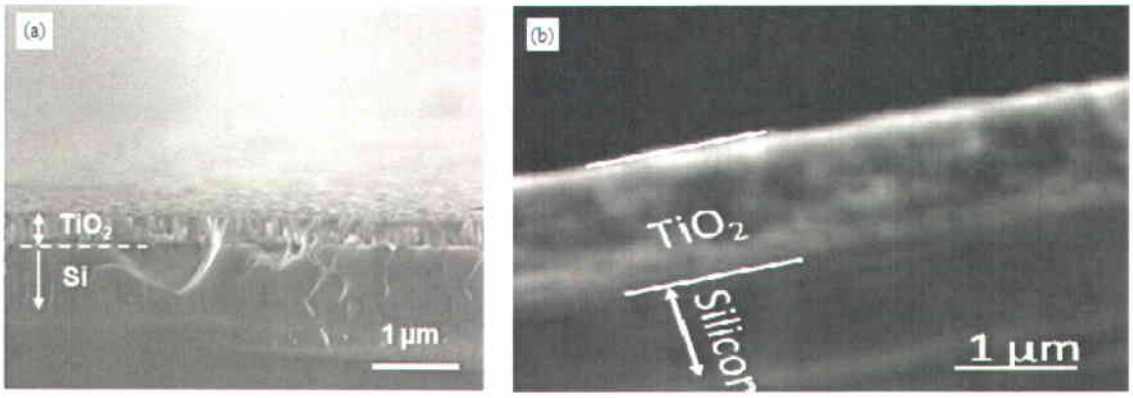


Figure 7-3 SEM views of PLD TiO_2 films deposited.

The crystallographic structure of the TiO_2 coating prepared by PLD was characterised by XRD. The XRD analysis indicates that our TiO_2 coatings deposited at 600°C and 400°C are polycrystalline and crystallize in the TiO_2 rutile phase and in the TiO_2 anatase phase, respectively (Figure 7-4a). The TiO_2 rutile phase is generally obtained for deposition at temperatures above 550°C (Kitazawa et al., 2006; Jaroenworaluck et al., 2010; Regonini et al., 2010), while at temperature below 500°C only the TiO_2 anatase phase is found (Regonini et al., 2010). The XRD spectrum of the TiO_2 coating on the Ti-grid confirms the presence of the same TiO_2 rutile phase and the same TiO_2 anatase phase obtained on Si (the peak intensities are less prominent than the peaks of the underlying metallic Ti grid because of the thinness of the TiO_2 coating compared to the Ti grid substrate) (Figure 7-4b and 7-4c). Interestingly, one can note that the main (110) and (101) XRD peak of the TiO_2 phase is broader in the case of the films deposited onto the Ti grid than on Si substrates. The average size of TiO_2 crystallites is smaller on the Ti grid than on Si. To quantify this substrate-dependent grain size effect, the average size (D) of the TiO_2 crystallites was estimated using the Debye–Scherer equation (Guinier, 1962):

Équation 7-1 $$D = \frac{0.9\ \lambda}{\Delta(2\theta)\cos\theta}$$

Where D is the grain size in a particular orientation (i.e.; (110) and (101) here), λ is the X-ray wavelength, θ is the diffraction angle corresponding to the particular orientation and (2θ) is the width at half maximum of the peak.

Thus, the average size of the TiO_2 rutile crystallites was estimated to approximately 29 nm on silicon and only approximately 10 nm on the Ti-grid substrates. By comparison, the average size of the TiO_2 anatase crystallites was estimated to approximately 26 nm on silicon and only approximately 15 nm on the Ti-grid substrates. The smoothness of the silicon substrate promotes the growth of TiO_2 crystallites with increasing temperature. The average size of the TiO_2 particles (anatase) deposited on the Ti-grid is greater than the average size of TiO_2 rutile structure deposited on the Ti-gird. This result agrees with the data obtained from the SEM images and is likely due to the rougher surface of the Ti grids compared to silicon grids. This nanometre scale grain size is expected to have an important effect on the photocatalytic activity of the TiO_2 coating (Kim et al., 2007). Indeed, with a decrease in particle size, the catalytic activity is enhanced due to the huge increase in the surface area (or surface to volume ratio) of the material.

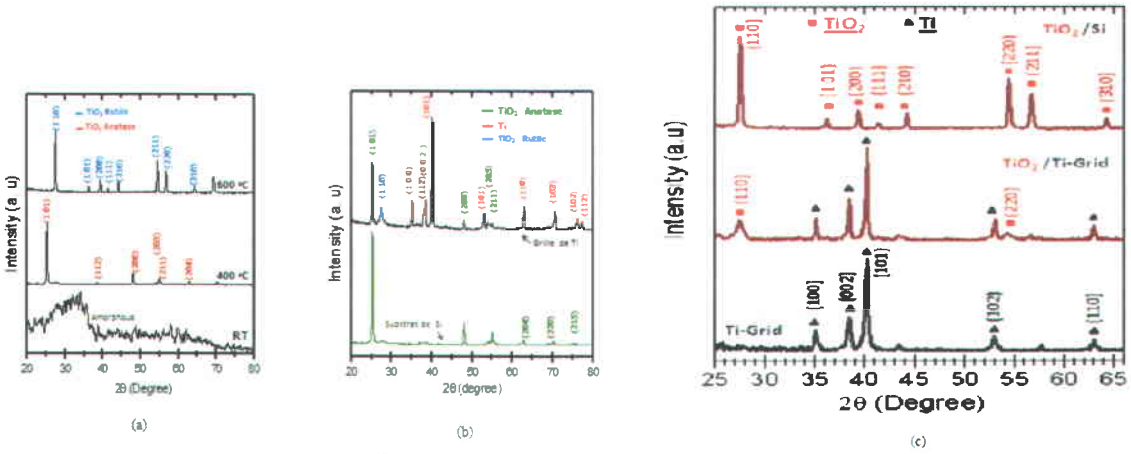


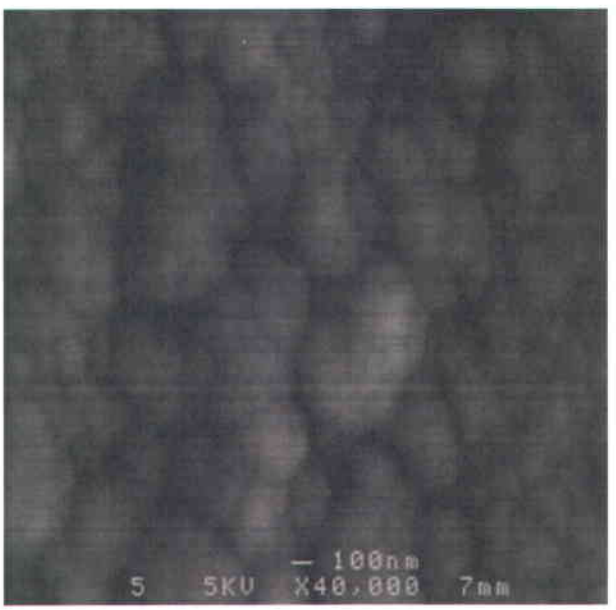
Figure 7-4 **X-ray diffraction patterns of TiO_2 film coated on titanium grids and on silicon substrates at 600°C and 400°C.**

7.5.2 Characterization of the carbon electrode

The surface morphology of the amorphous carbon (a-C) coatings was examined by scanning electron microscopy (SEM). Figure 7-5a shows a typical SEM-top-view of a carbon film deposited at 20°C onto a titanium disc. The coating is seen to be highly dense with fine grained pebbly surface with more or less spherical features. The size of these features is in the 100-300 nm range and are found to present finer substructures of few tens of nm-diameter (as shown in the higher magnification SEM image of Figure 7-5b.



(a)



(b)

Figure 7-5 SEM views of PLD amorphous carbon deposited on titanium at 20°C.

7.5.3 Effect of the Ti/TiO_2 crystallographic structure

According to several research studies (Ohtani et al., 1997; Sun and Xu, 2010; Yu et al., 2007), the physical properties of titanium dioxide such as crystallization, grain size, specific surface area, morphology and porosity influence the photocatalyic activity of titania. Experiments using different structures of Ti/TiO_2 film (anatase, rutile and amorphous) were carried out to evaluate the performance of the PECO process in treating CTC. In our study, the PECO process was applied during 120 min of treatment time at 0.39 A of current intensity with UV light irradiation at 254 nm (Daghrir et al., 2012). The initial concentration of CTC solution was 25 $\mu g\ L^{-1}$. The effectiveness of the PECO process was evaluated by measuring simultaneously the residual TN, TOC and CTC concentrations. The results are summarized in Table 7-2. The pH varied from 5.76 ± 0.26 (initial value) to 7.57 ± 0.23 using anatase and rutile as photoanodes, whereas a slight variation of pH was recorded after 120 min of treatment time using amorphous structure (from 5.75 ± 0.38 to 6.3 ± 0.31). The average initial value of TOC and NT recorded was 0.97 ± 0.27 mg L^{-1} and 0.17 ± 0.01 mg L^{-1}, respectively. After 120 min of PECO treatment, the removal rate of TOC was around 55.6 %, 41.0 % and 25.7 % using anatase, rutile and amorphous structure of Ti/TiO_2 as photoanode, respectively. The maximum removal of NT was recorded with anatase structure (63.1 %), whereas 58.8 % and 41.1 % of NT removal were recorded with rutile and amorphous structure, respectively. The CTC removal was 97.5 ± 0.6 %; 95 ± 1.6% and 84.5 ± 4.4% for anatase, rutile and amorphous structures, respectively. According to the above results, the photocatalytic activity recorded using amorphous structure of Ti/TiO_2 was weaker compared to the anatase and rutile forms of Ti/TiO_2. The large amounts of defects presents in amorphous structure of Ti/TiO_2 could lead to an increase in the number of recombination sites for electron-hole pairs (e^-/h^+) photo-generated by PECO process and consequently reduce the oxidation and the mineralization of CTC molecule (Xiang et al., 2011). Few studies have revealed the negligible

photocatalytic activity of amorphous TiO_2 compared to the anatase form (Ohtani et al., 1997; Yu et al., 2007). According to Ohtani et al. (1997), the lower photocatalytic activity recorded using amorphous TiO_2 is due to the impurities and micro-voids present in the structure, which lead to the recombination of e^-/h^+ photo-generated and decrease the photocatalytic efficiency. On the other hand, highest photocatalytic efficiency was recorded using anatase form compared to rutile form. This result was not surprising because the band gap of the anatase form (3.23 eV) is wider than that of the rutile form (3.02 eV) (Yoon et al., 2006). The lower band gap of TiO_2 rutile promotes the recombination of electrons-holes pairs (e^-/h^+) and reduces the photocatalytic efficiency (Yu et al., 2007). Furthemore, the physical properties (grain size, porosity, etc) and the crystal structure of TiO_2 often affect the photocatalytic activity (Sun and Xu, 2010). The octahedra of rutile are slightly ortho-rhombic and each octahedron is connected to 8 surrounding octahedrons (Fujishima et al., 2000). By comparison, the octahedra of anatase are distorted ortho-rhombic and each octahedron is connected to 10 surrounding octahedrons (Fujishima et al., 2000). According to Ma and Tu (2011), this difference in crystal structure between anatase and rutile could influence the activity of the photocatalytic reaction and could contribute to higher photocatalytic efficiency for anatase form.

Tableau 7-2 Effect of TiO_2 phase structure on the removal rate of CTC.

Parameters	PECO Process		
	Test 1	Test 2	Test 3
Intensity (A)	0.39	0.39	0.39
Treatment times (min)	120	120	120
Light intensity ($\mu W\ cm^{-2}$)	6900	6900	6900
UV lamp position	Internal	Internal	Internal
Electrolyte (Na_2SO_4 mol L^{-1})	0.05	0.05	0.05
$[CTC]^0$ concentrations ($\mu g\ L^{-1}$)	25	25	25
Type of cathode	SS	SS	SS
Type of anode	Ti/TiO_2 (anatase)	Ti/TiO_2 (rutile)	Ti/TiO_2 (amorphous)
Initial pH	5.75±0.38	5.77±0.17	5.75±0.38
Final pH	7.49±0.32	7.65±0.10	6.3±0.31
CTC removal (%)	97.5±0.6	95±1.6	84.5±4.4
TN initial (mg L^{-1})	0.19±0.12	0.17±0.03	0.17±0.02
TN final (mg L^{-1})	0.07±0.01	0.07±0.02	0.10±0.03
TOC initial (mg L^{-1})	1.06±0.21	1.17±0.42	0.66±0.42
TOC final (mg L^{-1})	0.47±0.03	0.69±0.41	0.49±0.41

PECO: Photoelecrtrocatalytic oxidation

7.5.4 Effect of the cathode material

The fast recombination of the photo-generated e^-/h^+ represents the major drawback of photocatalytic process (Martinez et al., 2011). Every recombination means a loss of hole that might otherwise have promoted the degradation reaction. This recombination between e^- and h^+ can be avoided by adding a proper electron acceptor to the system such as H_2O_2. H_2O_2 is

beneficial for photocatalytic reaction by trapping the electron in the conduction band and enhancing the oxidation rate of pollutant (Leng et al., 2006). According to previous studies (Leng et al., 2006; Xie and Li, 2006), several cathode materials including graphite, carbon felt, activated carbon fiber and vitreous carbon can be used for electrochemically production of H_2O_2.

Five type of cathode materials SS, Gr, VC, a-C1 and a-C2 were tested to evaluate their capacity for H_2O_2 production using distilled water in which Na_2SO_4 (0.05 M) was added. Experiments using Ti/TiO_2 (anatase) at the anode were carried out over 120 min of treatment time at 0.39 A of current intensity and 254 nm of UV light. Hydrogen peroxide concentrations generated under the different experimental conditions are shown in Figure 7-6. The maximum concentration of H_2O_2 (0.2 ± 0.01mM) was recorded after a treatment time of 120 min using VC. Under the same condition, only 0.16 ± 0.005 mM, 0.11 ± 0.0mM and 0.12 ± 0.005 mM of H_2O_2 were generated using Gr, a-C1 and a-C2, respectively. However, it was surprising to measure the residual concentration of H_2O_2 in the solution using SS as a cathode material (0.09 ± 0.002 mM). The H_2O_2 concentrations recorded was not produced at the SS. Additional experiment was carried out using Ti/IrO_2 at the anode and SS at the cathode. Under these conditions, H_2O_2 was not generated. According to Daghrir et al. (2012), the generation of H_2O_2 during the application of the PECO process takes place at the surface of the Ti/TiO_2 photo-catalyst. Under UV irradiation, H_2O_2 is decomposed and form hydroxyl radicals (Daghrir et al., 2012; Wang and Hong, 1999; Sontakke et al., 2011).

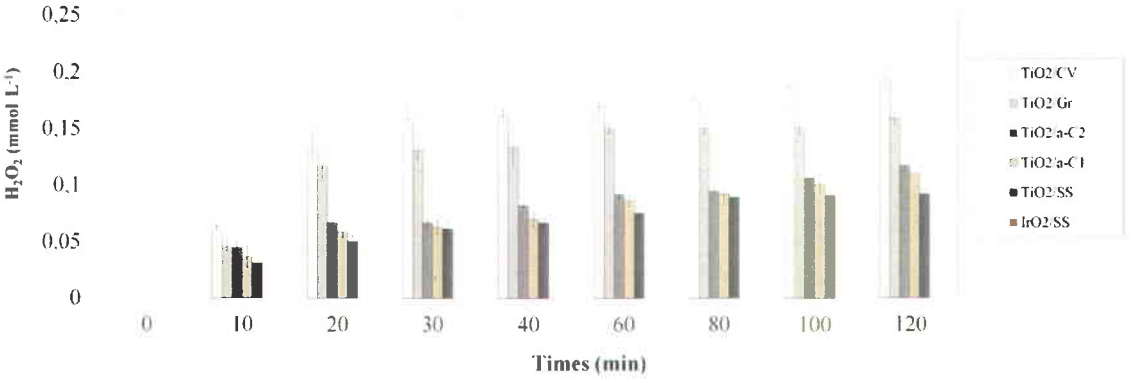


Figure 7-6 Hydrogen peroxide production using different cathode materials (at 0.39 A of current intensity and under 254 nm of UV irradiation).

To evaluate the effect of the cathode material on the photoelectrocatalytic degradation of CTC, additional experiments were carried out using the following conditions: 0.39 A of current intensity under UV irradiations (254 nm) and in the presence of 25 μg L^{-1} of initial CTC concentration. The different cathode electrode materials (SS, Gr, VC, a-C1 and a-C2) were respectively used. The results are shown in Table 7-3. Residual TN, TOC and CTC concentrations were measured. The initial pH value was 6.29 ± 0.30. After treatment, the final pH was 7.63 ± 0.21. The initial value of TOC and TN was 1.56 ± 0.37 mg L^{-1} and 0.27 ± 0.11 mg L^{-1}, respectively. Higher mineralization yield (67.3 ± 2.15 % of TOC removal and 69.3 ± 3.10 % of TN removal) was recorded using VC at the cathode. By comparison, only 55.6 ± 4.5% of TOC removal and 63.15 ± 2.35% of TN removal were obtained using SS as cathode electrode. The enhanced degradation recorded using VC at the cathode was mainly attributed to the effect of H_2O_2 electrochemically generated at the cathode (0.2 ± 0.01 mM). In photocatalytic process, H_2O_2 is considered as an efficient oxidant for organic compound oxidation (Carbajo et al., 2011). The CTC removal obtained at the end of the PECO treatment

using VC as cathode was around 98.0 ± 0.2%. By comparison, the degradation rate of CTC recorded after 120 min of treatment time using SS, Gr, a-C1 and a-C2 were 97.5 ± 0.6%, 97.2 ± 0.4%, 95.6 ± 0.4% and 96.3 ± 0.11 %, respectively. The influence of cathode materials was also put into evidence by Xie and Li (2006) while studying photoelectrocatalytic degradation of bisphenol A. The high efficiency of pollutant degradation (up to 99% of bisphenol A removal) recorded can be explained by the presence of H_2O_2 electrochemically generated. According to Xie and Li (2006), such an oxidant (H_2O_2) is beneficial for photoelectrocatalytic reactions by trapping the conduction band electrons in order to generate more hydroxyl radical (Eq. 2) and consequently to enhance the degradation of pollutant.

Équation 7-2 $H_2O_2 + e_{CB}^- \rightarrow OH^- + OH^{\bullet}$

Tableau 7-3 Effect of cathode materials on CTC degradation and mineralization.

Parameters	PECO Process				
	Test 1	**Test 2**	**Test 3**	**Test 4**	**Test 5**
Intensity (A)	0.39	0.39	0.39	0.39	0.39
Treatment times (min)	120	120	120	120	120
Light intensity ($\mu W\ cm^{-2}$)	6900	6900	6900	6900	6900
UV lamp position	Internal	Internal	Internal	Internal	Internal
Electrolyte (Na_2SO_4 mol L^{-1})	0.05	0.05	0.05	0.05	0.05
$[CTC]^0$ concentrations ($\mu g\ L^{-1}$)	25	25	25	25	25
Type of cathode	SS	Gr	VC	a-C1	a-C2
Type of anode	Ti/TiO_2 (anatase)	Ti/TiO_2 (anatase)	Ti/TiO_2 (anatase)	Ti/TiO_2 (anatase)	Ti/TiO_2 (anatase)
Initial pH	5.75±0.38	6.38±0.06	6.41±0.01	6.55±0.17	6.35±0.06
Final pH	7.49±0.32	7.5±0.14	7.8 ± 0.14	7.44±0.13	7.92±0.29
CTC removal (%)	97.5±0.6	97.2±0.4	98±0.2	95.6±0.4	96.3±0.11
TN initial ($mg\ L^{-1}$)	0.19±0.12	0.24±0.07	0.27±0.11	0.26±0.1	0.23±0.09
TN final ($mg\ L^{-1}$)	0.07±0.01	0.08±0.01	0.08±0.04	0.09±0.04	0.09±0.01
TOC initial ($mg\ L^{-1}$)	1.06+±0.21	1.4±0.32	1.56±0.37	1.5±0.1	1.43±0.40
TOC final ($mg\ L^{-1}$)	0.47± 0.03	0.60±0.20	0.51±0.16	0.7±0.17	0.6±0.1

PECO: Photoelecrtrocatalytic oxidation; SS: Stainless steel; Gr: graphite; VC: vitreous carbon; a-C1: amorphous carbon (20°C); a-C2: amorphous carbon (600°C)

7.5.5 Effect of the initial concentration of CTC

According to several authors (Daghrir et al., 2012; Wang et al., 2009; Ding et al., 2010), initial concentration of pollutant is a parameter that influences the efficiency of photoelectrocatalytic process. To evaluate the impact of the pollutant concentration on the efficiency of PECO process, various concentrations of CTC (from 32 μg L^{-1} to 230 μg L^{-1}) were tested. Experiments were carried out using anatase Ti/TiO_2 structure as photo-anode and VC at the cathode during 120 min of treatment time at 0.39 A of current intensity and 254 nm of UV light. The influence of the initial concentration of CTC on the photoelectrocatlytic oxidation and mineralization of CTC is shown in Table 7-4. When the pollutant concentration is fixed at the lowest level (32 μg L^{-1}), the degradation rate of CTC was 97.10 ± 0.47%. By comparison, only 92.34 ± 0.23% of CTC removal has been recorded when the pollutant concentration is fixed at the highest level (230 μg L^{-1}). Besides, 67.9% ± 1.11% and 51.66% ± 2.60% of TOC removal rate were recorded when the pollutant concentration is fixed at 32 μg L^{-1} and 230 μg L^{-1}, respectively. The same trend has been recorded by Frontistis et al., (2011), Wang et al., (2009) and Ding et al., (2010), while studying photoelectrocatalytic degradation of bisphenol-A, 4-chlorophenol and benzotriazole, respectively. During the photoelectrocatalytic process, the surface of the photo-catalyst may be covered by organic pollutants that inhibit its activity and consequently affect the purification performances (Daghrir et al., 2012). Besides, the decrease of the degradation rate while increasing the initial concentration of pollutant could be attributed to the insufficient concentration of ROS (H_2O_2, OH°, etc) by PECO process (Wang et al., 2009). Likewise, intermediates products of CTC produced during PECO treatment compete with CTC by reacting with ROS. Thus, lower rates of oxidation and mineralization of CTC are recorded at higher initial concentration of pollutant.

Tableau 7-4 Influence of the initial concentrations of pollutant on the photoelectrocatalytic oxidation of CTC (Ti/TiO_2 (anatase): anode and VC: cathode).

Parameters	PECO Process					
	Test 1	**Test 2**	**Test 3**	**Test 4**	**Test 5**	**Test 6**
Intensity (A)	0.39	0.39	0.39	0.39	0.39	0.39
Treatment times (min)	120	120	120	120	120	120
Light intensity ($\mu W\ cm^{-2}$)	6900	6900	6900	6900	6900	6900
UV lamp position	Internal	Internal	Internal	Internal	Internal	Internal
Electrolyte (Na_2SO_4 mol L^{-1})	0.05	0.05	0.05	0.05	0.05	0.05
$[CTC]^0$ concentrations ($\mu g\ L^{-1}$)	32	40	63	120	193	230
CTC removal (%)	97.30±0.47	97.21±0.06	96.4±0.32	94.0±0.79	92.9±0.30	92.34±0.23
TOC removal (%)	67.9± 1.11	67.25±1.01	66.7±1.71	65.82±2.55	59.64±3.05	51.66±2.60

PECO: photoelectrocatalytic oxidation

7.5.6 Effect of the initial pH on CTC degradation

In the field of wastewater treatment, pH is one of the most important parameters that influence the removal efficiency of pollutants (Daghrir et al., 2012; Wang et al., 2009; Quan et al., 2007). It affects the capacity of adsorption and dissociation of the target compounds, the distribution of charge on the surface of the photocatalyst and the oxidation potential of the valence band (Wang et al., 2009; Quan et al., 2007; Chong et al., 2010; Ahmed et al., 2011). Previous studies show that pH plays an important role in the adsorption (Gao and Pedersen, 2005; Parolo et al., 2008) and in the degradation processes of antibiotics (Rubert and Pedersen, 2006; Zhang and Huang, 2003). To study the impact of pH on the oxidation of pollutant, the point of zero charge (PZC) of the photo-catalyst TiO_2 has been used (Ding et al., 2010; Selcuk et al., 2003). For TiO_2, the PZC has a pH value of approximately 6 (pH_{PZC}) (Selcuk et al., 2003). The effect of pH value on the photoelectrocatalytic degradation of CTC (32 µg CTC L^{-1}) was carried out at 0.39 A of current intensity, under UV irradiation (254 nm) during 120 min of treatment time and at different initial pH values of 3.12, 5.51, 7.06 and 9.02. The effect of pH is shown in Figure 7-7a and b. The maximum photoelectrocatalytic degradation of CTC (97.3% ± 0.41%) was recorded without pH adjustment (Figure 7-7a). Beside, high mineralization of CTC was recorded without pH adjustment. The removal yield of TOC and TN recorded after 120 min of photoelectrocatalytic treatment was 67.9 ± 1.11% and 62.8 ± 0.32%, respectively (Figure 7-7b). The final value of pH recorded (after treatment) was 7.05 ± 0.33 compared to the initial value of 5.51 ± 0.16. The changes in the CTC degradation rate in function of pH variation can be attributed to the acid/base properties of the TiO_2 surface. For pH values lower than the PZC of TiO_2, the surface becomes positively charged ($TiOH_2^+$) and an electrostatic repulsion toward cationic compounds dominates, whereas when the pH values are higher than the PZC of TiO_2, the surface becomes negatively charged (TiO^-) and an electrostatic repulsion toward anionic compounds dominates (Daghrir

et al., 2012; Ahmed et al., 2011). According to the pK_a values (pk_{a1} = 3.30; pK_{a2} = 7.55 and pK_{a3} = 9.30), four different forms of CTC (fully protonated form ($CTCH_3^+$), zwitterionic form ($CTCH_2^{\pm}$), monoanion ($CTCH^-$) and dianion (CTC^{2-})) could be presented at different range of pH (Chen et al., 2012).

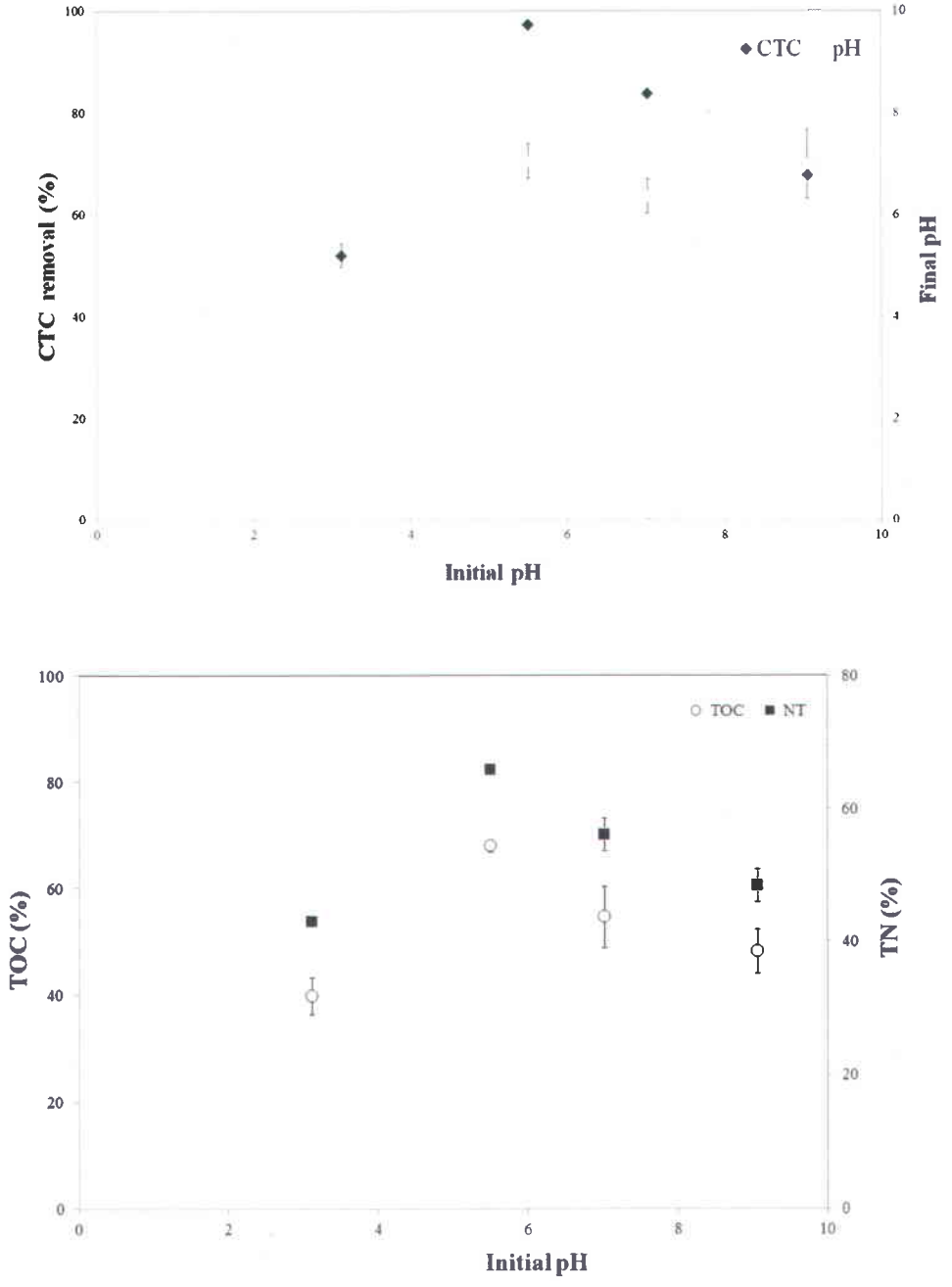
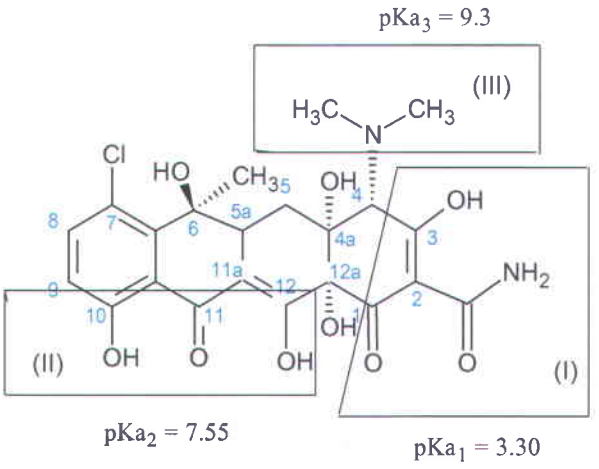


Figure 7-7 **Effect of the initial pH value on the oxidation and the mineralization of CTC (Ti/TiO_2; VC; 0.39 A of current intensity; 254 nm; $[CTC]^0 = 32\ \mu g\ L^{-1}$).**

Figure 7-8 presents the three distinct moieties of CTC, which correspond to tricarbonylamide (I), phenolic diketone (II) and dimethylamine (III). When the pH value is lower than 3.30, the dimethylamine moiety of CTC (C4) carried a positive charge at the position of the nitrogen atom and the other moieties were neutral. Thus, the cation $CTCH_3^+$ was the predominant form. In the pH range 3.30-7.55, the enolic group of the tricarbonylamide moiety (C1-C3) dissociates into an anion and the zwitterionic form ($CTCH_2^{\pm}$) of CTC became the dominant species. The amount of cationic form of CTC ($CTCH_3^+$) decrease and the zwitterionic form ($CTCH_2^{\pm}$) became predominant. When the pH value is higher than 7.55, the enolic groups of the phenolic diketone (C10-C12) begins to dissociate in the anionic form. When the pH value exceed pK_{a3} (9.30), the dimethylamine moiety of CTC become neutral, whereas the phenolic diketone and the tricarbonylamide moieties of CTC are in the anionic form (Chen et al., 2011). In our study, higher electrostatic attraction between the zwitterionic form of CTC ($CTCH_2^{\pm}$) and the positively charged surface of Ti/TiO_2 ($TiOH_2^+$) has been recorded at pH value around 6 and consequently higher oxidation and mineralization rate of CTC (97.3 ± 0.41% of CTC degradation and 67.9 ± 1.11% of TOC removal) was obtained.

Besides, higher oxidation and mineralization of CTC was recorded in basic medium (67.7 ± 2.29 % of CTC degradation and 48.2 ± 4.16% of TOC removal) compared to the acidic medium (51.9 ± 3.9% of CTC degradation and 39.8 ± 3.45% of TOC removal). In basic conditions, the hydroxyl ions present in relatively higher concentration react with the reactive holes on the surface of the Ti/TiO_2 to form strong oxidizing hydroxyl radicals ($E° = 2.81$ V at 25°C) (Equation 7-3).

Équation 7-3 $$OH^- + h^+ \rightarrow OH^{\circ -}$$



$$CTCH_3^+ \rightleftharpoons CTCH_2^{+-} \rightleftharpoons CTCH^- \rightleftharpoons CTC^{2-}$$

Figure 7-8 Chemical structure of CTC and the three distinct moieties (I) tricarbonylamide, (II) phenolic diketone and (III) dimethylamine.

7.5.7 Kinetic study of CTC degradation by PECO process

The kinetic study could be helpful to evaluate and to understand the mechanism of pollutant degradation. For practical applications, the kinetic degradation of CTC using the PECO process was investigated under the following conditions: Ti/TiO_2 photo-catalyst (anatase structure), VC at the cathode, 0.39 A of current intensity under UV irradiations (254 nm) during 120 min of treatment times and at initial concentration of CTC varying from 32 $\mu g\ L^{-1}$ to 230 $\mu g\ L^{-1}$. The progress of the photoelectrocatalytic degradation of CTC was monitored using LC/MS/MS technique. According to a great number of investigations (Frontistis et al., 2011; Liu et al., 2009; Selcuk et al., 2003), the Langmuir-Hinshelwood (L-H) kinetic model has been usually used to characterize the photoelectrocatalytic degradation of various organic compounds. The kinetic model data were estimated by regression analysis method using excel software. The L-H kinetic model is described by the following equation:

Équation 7-4 $$r = -\frac{dC}{dt} = k_r\theta = \frac{k_r KC}{1 + KC}$$

Where k_r is the reaction rate constant; K is the reactant adsorption constant; θ is the fraction of the surface of Ti/TiO_2 covered by CTC and C is the concentration of CTC at any time t.

At low CTC concentrations, there is no catalyst saturation and the photoelectrocatalytic disappearance of CTC can follow apparent first order kinetics model. In this case, Equation 7-4 can be simplified to an apparent first order kinetic model:

Équation 7-5 $$r = -\frac{d[C]}{dt} = k_r KC = k_{app} C$$

Where $k_{app} = k_r K$

The integration of Equation 7-5 gives:

Équation 7-6 $$\ln \frac{C_0}{C} = k_{app} t$$

Where C_0 is the initial concentration of CTC, C is the concentration of CTC at time t, k_{app} is the first order reaction rate constant (min^{-1}) and t is the reaction time. The reaction rate constant k_{app} could be calculated from the slope of a plot of Ln (C_0/C) versus (t).

The values of kinetic rate constants (k_{app}) corresponding to the different initial concentrations of CTC, along with their regression coefficients R^2 are provided in Table 7-5. Higher correlation coefficients R^2 were obtained from the pseudo-first order kinetic model at lower CTC concentrations. The corresponding kinetic constants k_{app} for CTC degradation passed from 18.7 10^{-3} min^{-1} (at 230 µg CTC L^{-1}) to 23.0 10^{-3} min^{-1} (at 32 µg CTC L^{-1}). Therefore, the pseudo-first-order kinetic model can describe the degradation of CTC using the PECO process. It could be interesting to compare the kinetic constant with values obtained in others experimental conditions. Liu et al. (2009) indicated that the photoelectrocatalytic degradation

of tetracycline (TC) on TiO_2 nanopore ($[TC]^0$ = 10 mg L^{-1}; 0.5 V of the applied potential; 2.5 mW cm^{-2} of UV light intensity and 3 h of treatment times) is well described by the pseudo-first order kinetic model. The apparent reaction constant value recorded under these conditions was 9.33 10^{-3} min^{-1}. The same trend has been also obtained by Wang et al. (2009) while studying the photoelectrocatalytic degradation of 4-chlorophenol (0.6 V of bias potential; 2.5 mW cm^{-2} of UV light intensity and $[4\text{-chlorophenol}]^0$ = 20 mg L^{-1}). The corresponding kinetic rate constant was 16.7 10^{-3} min^{-1}. These apparent reaction constant values reported in the literature are lower than those recorded in the present study. The corresponding kinetic rate recorded in our study (23.0 10^{-3} min^{-1} for 32 µg CTC L^{-1}) was 1.37 times and 2.46 times higher than that recorded by Wang et al. (2009) and Liu et al. (2009), respectively. The contribution of the light intensity in photoelectrocatalytic process influences the production rate of reactive oxygen species (OH°, O_2°, H_2O_2, etc) and consequently the kinetic rate of pollutant degradation (Daghrir et al., 2012; Wang et al., 2009). The UV light intensity imposed during the photoelectrocatalytic oxidation of CTC (6.9 mW cm^{-2}) was higher than the UV light intensity imposed by Wang et al. (2009) and Liu et al. (2009).

Tableau 7-5 Kinetic parameters for CTC degradation

Initial CTC concentrations (µg L^{-1})	Pseudo-first order kinetic		
	k_{app} 10^{-3} (min^{-1})	R^2	$t_{(1/2)}$ min
32	23.0	0.957	30.13
63	22.1	0.955	31.36
120	21.5	0.957	32.23
193	20.1	0.955	34.48
230	18.7	0.956	37.06

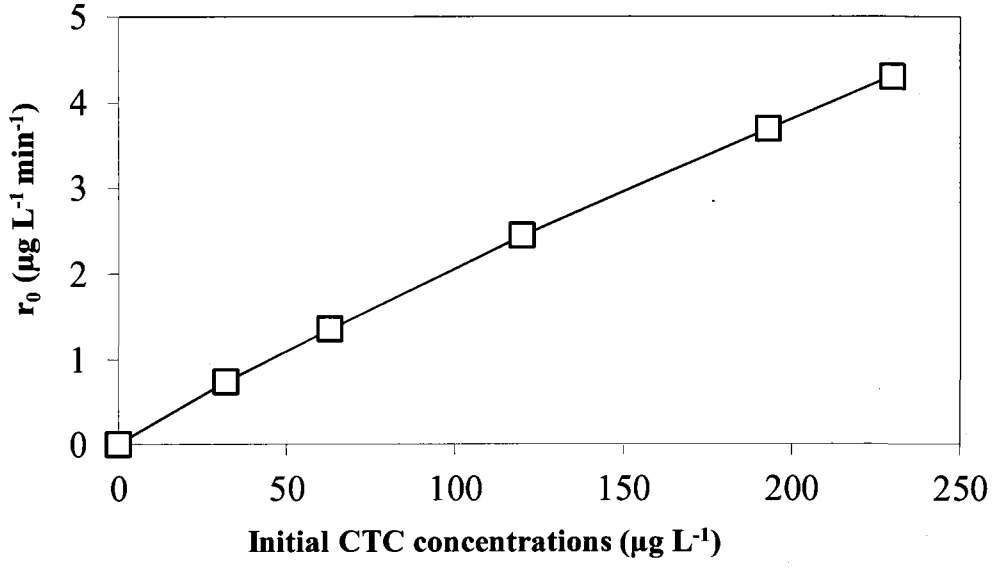
Furthermore, the higher concentrations of pollutant influence the kinetic degradation (Wang et al., (2009). The photoelectrocatalytic degradation rate of CTC could be expressed as a function of concentration according to the following equation:

Équation 7-7 $$r_0 = \frac{k_r K C_0}{1 + K C_0}$$

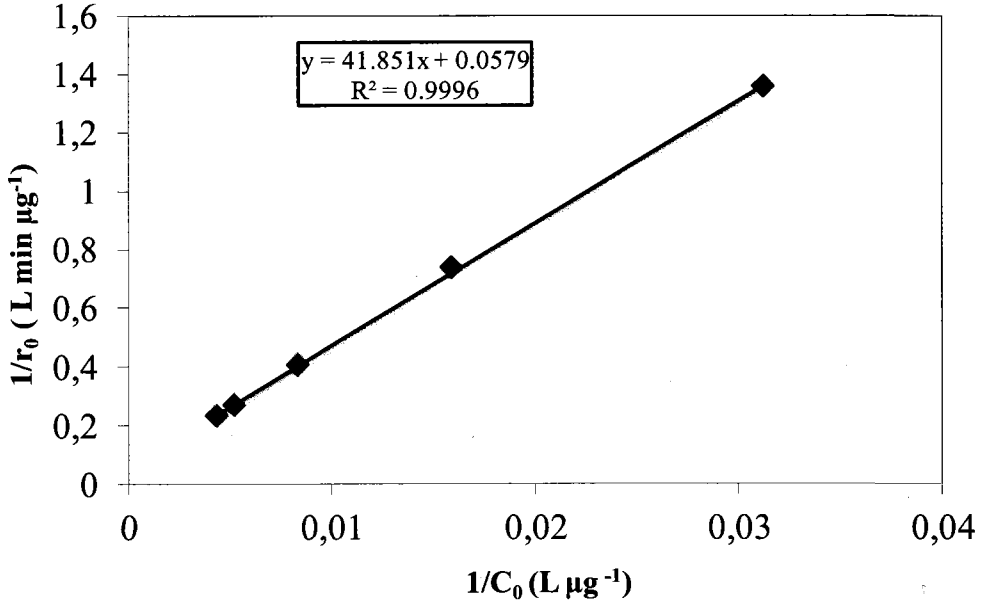
Where, r_0 is the initial rate of photoelectrocatalytic degrdation of CTC and C_0 is the initial concentration of CTC. The influence of the initial concentrations of pollutant on the initial rate of photoelectrocatalytic degradation of CTC is shown in Figure 7-9a. The degradation rate of pollutant increases with the initial concentrations of CTC. The inverse of Equation 7-7 gives the dependence of $1/r_0$ values on the corresponding $1/C_0$ values of CTC concentrations:

Équation 7-8 $$\frac{1}{r_0} = \frac{1}{k_r} + \frac{1}{K k_r}\frac{1}{C_0}$$

The linear variation of the plot $1/r_0$ versus $1/C_0$ represented in Figure 7-9b confirms the Langmuir-Hinshelwood (L-H) relationship for the initial rate of CTC degradation. The value of k_r and K calculated from the slop and the intercept of the straight line ($R^2 = 0.9996$) were 17.271 $\mu g\ L^{-1}\ min^{-1}$ and 1.38 10^{-3} L μg^{-1}, respectively.



(a)



(b)

Figure 7-9 **(a) Variation of the initial rate of CTC degradation versus different initial concentration and (b) the linear variation of the plot $1/r_0$ versus $1/C_0$ in the Langmuir-Hinshelwood kinetic model (Ti/TiO_2; VC; 0.39 A of current intensity; 254 nm of UV light).**

7.5.8 By-products identification and proposed mechanism of CTC degradation

Our intention is to follow the formation of some by products while treating the synthetic CTC solution using the PECO process. With LC/MS/MS analysis, two CTC by-products were confirmed via comparison with authentic standards and four CTC by-products were idententified on the basis of their mass spectra. The LC/MS/MS chromatogram and the individual MS spectra of possible transformation of CTC are shown in Figure 7-10, and the proposed mechanism of CTC degradation by PECO process is depicted in Figure 7-11. The product ions at m/z 462 were obtained from the precursor ions m/z 479 (CTC) corresponding to I-CTC (t_R= 6.93 min). This product has been identified and confirmed with the standard value under the same analysis conditions using LC/MS/MS. Under alkaline conditions, CTC could be converted to Iso-CTC. The bond between C_6 and C_{11a} atoms (Figure 7-8) could be catalyzed at the TiO_2 surface to yield Iso-CTC. An additional product ion at 511.18 was also obtained (t_R= 10.25 min). This product was assigned to comprise an iso-CTC with two additional hydroxyl groups. The product ion m/z 495.19 (t_R = 12.28 min) was the intermediate product of m/z 511.18. Besides, N- dedismethyl-CTC (N-DDM-CTC, m/z = 467.15) and N-demethyl-CTC (N-DM-CTC, m/z = 481.20) are two by-products of CTC formed by the loss of methyl groups from the dimethylamine moiety at the C_4 position of CTC. N-DDM-CTC (t_R = 5.47 min) is formed by a loss of two methyl groups, whereas N-DM-CTC (t_R = 13.52 min) is formed by loss of one methyl group. Moreover, two products contained the molecular ions of m/z 451 (t_R = 9.15 min) and m/z 465 (t_R = 14.61 min) have been also identified in the sample. The difference between the molecular weight of these two compounds and CTC (m/z 479) was equal to 28 and 14, respectively. This result indicates the possibility of losing two methyl groups and one methyl group from the dimethylamine moiety of CTC. We suggest that these two CTC-by-products are 4-epi-N- dedismethyl-CTC (EN- DDM-CTC; t_R = 9.15 min) and 4-epi-N-demethyl-CTC (EN-DM-CTC; t_R = 14.61 min), respectively. It could be

also possible to form epidemoclocycline (m/z = 465.21) by loss of methyl group from the C6 position of CTC. This product was identified and confirmed with the standard value under the same analysis conditions by LC/MS/MS. Tetracycline (m/z = 445.19) is another by-product of CTC resulting from the dechlorination of CTC.

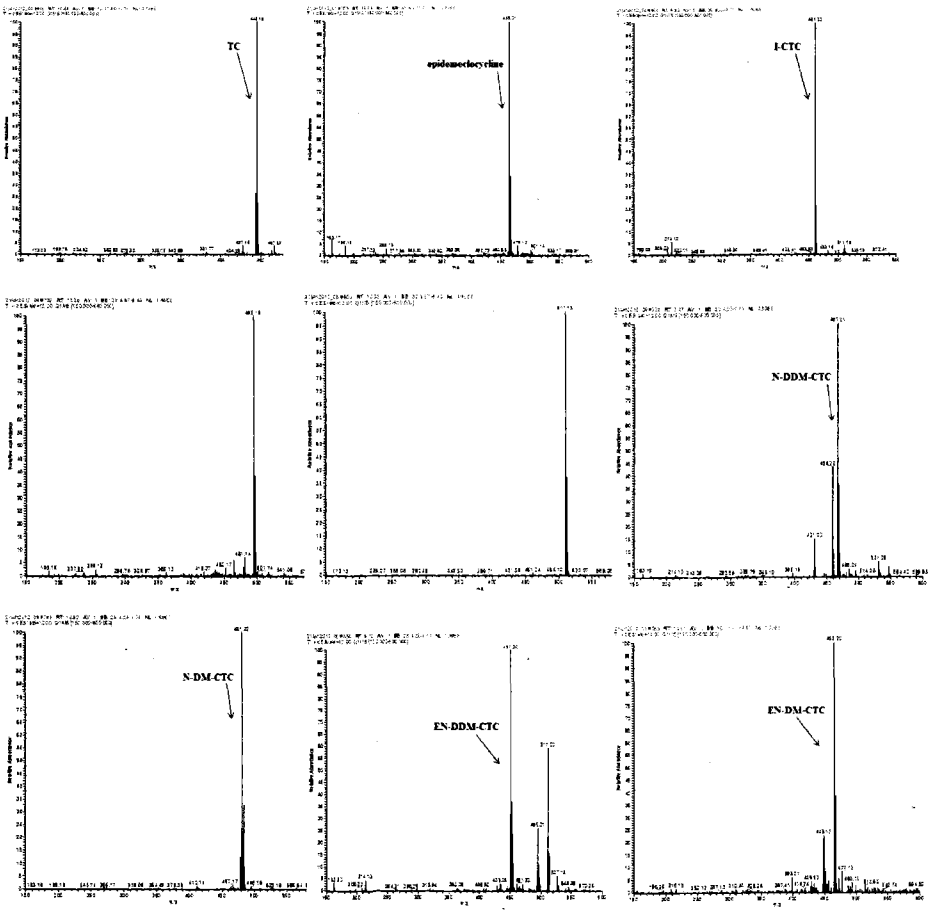


Figure 7-10 (a) LC/MS/MS chromatogram presented with (b) individual MS spectra of possible by-products of CTC by PECO process.

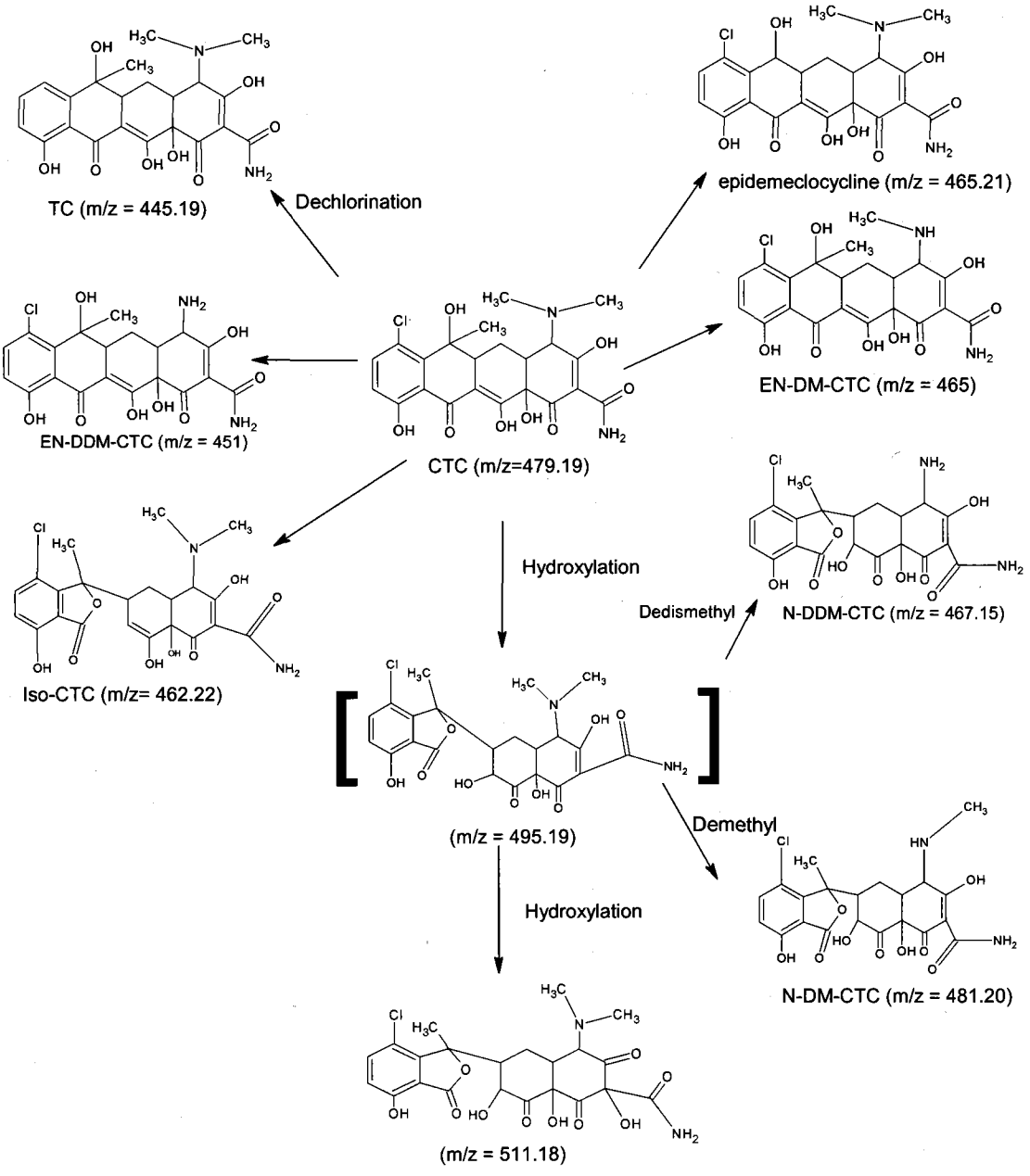


Figure 7-11 The chemical structure and the proposed photoelectrocatalytic degradation pathways of CTC.

7.5.9 Aquatic toxicity studies

Microtox, Microalga and Daphnia bioassay tests were carried out to estimate the toxic effect of the initial and treated CTC solution under optimum experimental conditions. The partial mineralization of CTC and the formation of by-products after treatment could influence the

toxicity effect. Toxicity measurements recorded before and after treatment in optimal conditions are summarized in Table 7-6. Microtox and microalga tests carried under optimal conditions show a reduction of the toxicity while applying PECO process during 120 min. At exposure time of 15 min, the inhibition percentage of V. fisheri measured in the initial solution (for 32 μg L^{-1} of CTC) was 9.1 %, whereas at the end of PECO treatment lower inhibition of bioluminescence (2.0 %) has been recorded. Besides, results show a reduction of the inhibition of the growth rate of *P. Subcapitata* while applying photoelectrocatalytic treatment. After 72 h exposure to the contaminant, the inhibition rate passed from 3.3 ± 0.28 TU to 1.25± 0.21 TU. Results indicate also that the residual concentrations of CTC and the by-products recorded under optimal conditions have no influence on the Daphnia magna (toxicity lower than 1 TU). Finally, the photoelectrocatalytic treatment costs of CTC (including chemical consumption and energy consumption) recorded was estimated to \$4.52±0.01 m^{-3}.

Tableau 7-6 Toxicity measurements before and after PECO treatment in optimal conditions.

Parameters	Solution treatment	
	Before	After
Daphnia magna test (TU)	< 1	< 1
Vibrio fisheri test (Microtox) (%)	9.1	2.0
Pseudokirchneriella Subcapitata test (TU)	3.3±0.28	1.25±0.21

TU : toxicity unit

7.6 Conclusion

In this study, the Ti/TiO_2 rectangular electrode was prepared by a PLD method. It showed that the TiO_2 coating at 400°C and 600°C is very uniform in thickness and was found to be of anatase structure and rutile structure, respectively. The investigation of the photoelectrocatalytic oxidation process on the CTC degradation shows that crystallographic structure of Ti/TiO_2, pollutant concentration, cathode material, initial pH value influence the treatment efficiency of CTC. The photoelectrocatalytic treatment of CTC during 120 min using anatase forms of Ti/TiO_2 as photo anode, vitreous carbon as cathode at 0.39 A of current intensity under UV irradiations (245 nm) and without adjustment of pH (6.29 ± 0.30) ensures a higher oxidation (98.0 ± 0.2 %) and higher mineralization rates of CTC (67.3 ± 2.15% of TOC removal and 69.3 ± 3.10% of TN removal). The analysis using LC/MS/MS technique shows that tetracycline, Iso-CTC, epidemeclocycline, N- dedismethyl-CTC, N-demethyl-CTC, 4-epi-N dedismethyl-CTC and 4-epi-N demethyl-CTC are the main by-products of CTC. Toxicity studies with results obtained by microtox, microalga and daphnia bioassay evaluation confirmed the effectiveness of the photoelectrocatalytic process for CTC degradation. The Langmuir-Hinshelwood (L-H) kinetic model ($R^2 = 0.9996$) showed a good agreement for the initial rates of photoelectrocatalytic degradation of CTC with the appropriate reaction rate constant and the reactant adsorption constant values of 17.271 $\mu g\ L^{-1}$ min and 1.38 10^{-3} L μg^{-1}, respectively.

7.7 Acknowledgments

Sincere thanks are extended to the National Sciences, Engineering Research Council of Canada and Premier Tech Ltée for their financial to this study.

7.8 References

Adams C, Wang MY, Loftin K & Meyer M (2002) Removal of antibiotics from surface and distilled water in conventional water treatment processes. *J.Environ.Eng.Div.ASCE.* 128:253-260.

Ahmed S, Rasul MG, Brown R & Hashib MA (2011) Inluence of parameters on the heterogeneous photocatalytic degradation of pesticides and phenolic contaminants in wastewater: A short review. *J. Environ. Manag.* 92:311-330.

Andreu V, Vazguez-Roig P, Blasco C & Pico Y (2009) Determination of tetracycline residues in soil by pressurized liquid extraction and liquid chromatography tandem mass spectrometry. *Anal. Bioanal. Chem.* 394(5):1329-1339.

Carbajo J, Adàn C, Rey A, Martinez-Arias A & Bahamonde A (2011) Optimization of H_2O_2 use during the photocatalytic degradation of ethidium bromide with TiO_2 and iron-doped TiO_2 catalysts. *Appl.Catal. B: Environ.*102:85-93.

Carballa M, Omil F, Lema JM, Llompart M, Garcia-Jares C, Rodriguez I, Gomez M & Ternes T (2004) Behavior of pharmaceuticals, cosmetics and hormones in a sewage treatment plant. *Water Res.* 38(12): 2918-2926.

Chang X, Meyer MT, Liu X, Zhao Q, Chen H, Chen JA, Qui, Z, Yang L, Cao J & Shu W (2010) Determination of antibiotics in sewage from hospitals, nursery and slaughter house, wastewater treatment plant and source water in Chongqing region of three Gorge Reservoir in China. *Environ. Pollut.* 158(5): 1444-1450.

Chen G, Zhao L & Dong Y-h (2011) Oxidative degradation kinetics and products of chlortetracycline by manganese dioxide. *J. Hazard. Mater.* 193: 128-138.

Chen Y, Li H, Wang Z, Tao T, Wei D & Hu C (2012) Photolysis of chlortetracycline

in aqueous solution: Kinetics, toxicity and products. *J.Environ.Sci.* 24(2): 254-260.

Chong MN, Jin B, Chow CWK & Saint C (2010) Recent developments in photocatalytic water treatment technology: A review. *Water Res.* 44(10): 2997-3027.

Daghrir R, Drogui P, Ka I & El Khakani MA (2012) Photoelectrocatalytic degradation of chlortetracycline using Ti/TiO_2 nanostructured electrodes deposited by means of pulsed Laser deposition process. *J. Hazard. Mater.* 199-200: 15-24.

Daghrir R, Drogui P & Didier R (2012) Photoelectrocatalytic technologies for environmental applications. *J. Photochem. Photobiol.A.* 238: 41-52.

Desbiens E & El Khakani MA (2003) Growth of high-K silicon oxynitride thin films by means of a pulsed laser deposition-atomic nitrogen plasma source hybrid system for gate dielectric applications. *J Appl.Phys.* 94 (9): 5969-5976.

Ding Y, Yang C, Zhu L & Zhang J (2010) Photoelectrochemical activity of liquid phase deposited TiO_2 film for degradation of benzotriazole. *J Hazard.Mater.* 175: 96-103.

Fujishima A, Rao TN & Tryk AD (2000) Titanium dioxide photocatalysis. *J.Photochem. Photobiol. C.* 1(1):1-21.

Frontistis Z, Daskalaki VM, Katsaounis A, Poulios I & Mantzavinos D (2011) Electrochemical enhancement of solar photocatalysis: Degradation of endocrine distruptor bisphenol A on Ti/TiO_2 films. *Water Res.* 45: 2996-3004.

Gao J & Pedersen JA (2005) Adsorption of sulfonamide antimicrobial agents to clay minerals. *Environ. Sci.Technol.*39(24): 9509-9516.

Guinier A (1962) *Théorie et Technique de la radiocristallographie*. 3rd ed., Dunod, Paris, 740p.

Guo RX &Chen JQ (2012) Phytoplankton toxicity of the antibiotic chlortetracycline and its UV light degradation products. *Chemosphere* 87: 1254.

Kim I, Yamashita N & Tanaka H (2009) Photodegradation of pharmaceuticals and personal care products during UV and UV/H2O2 treatments. Chemosphere 77: 518-525.

Halling-Sorensen B, Nors Nielsen S, Lansky PF, Ingerslev F, Holten Lutzhoft HC & Jorgensen SE (1998) Occurrence, fate and effects of pharmaceuticals in the environment-a review. *Chemosphere* 36: 357-393.

Halling-Sorensen B, Sengelov G, Tjornelund J (2002) Toxicity of tetracyclines and tetracycline degradation products to environmentally relevant bacteria including selected tetracycline-resistant bacteria. *Arch. Environ. Cont. Tox.* 42(3): 263-271.

Hernandez F, Sancho JV, Ibanez M, Guerrero C (2007) Antibiotic residue determination in environment waters by LC-MS. *TrAC-Trends Anal. Chem.* 26(6): 466-485.

Jaroenworaluck A, Regonini D, Bowen CR & Stevens R (2010) A microscopy study of the effect of heat treatment on the structure and properties of anodized TiO_2 nanotubes. *Appl. Surf. Sci.* 256: 2672-2679.

Ji L, Chen W, Duan L & Zhu D (2009) Mechanisms for strong adsorption of tetracycline to carbon nanotubes: A comparative study using activated carbon and graphite as adsorbents. *Environ. Sci. Technol.* 43: 2322-2327.

Kim CS, Kwon IM, Moon BK, Jeong JH, Choi BC, Kim JH, Choi H, Yi SS, Yoo DH, Hong KS, Park JH & Lee HS (2007) Synthesis and particle size effect on the phase transformation of nanocristalline TiO_2. *Mater.Sci. & Eng. C* 27:1343-1346.

Kitazawa Si, Choi Y, Yamamoto Sh, Yamaki T (2006) Rutile and anatase mixed crystal TiO_2 thin films prepared by pulsed laser deposition. *Thin. Solid. Films.* 515(4): 1901-1904.

Kolpin DW, Furlong ET, Meyers MT, Thurman EM, Zaugg SD, Barber LB & Buxton HT (2002) Pharmaceuticals, hormones and other organic wastewater contaminants in U.S. streams, 1999–2000: A national reconnaissance. *Environ.Sci.Technol.* 36(6): 1202-1211.

Lee S, Kang Su-Il, Lim JL, Huh YJ, Kim KS & Cho J (2011) Evaluating controllability of pharmaceuticals and metabolites in biologically engineered processes using corresponding octanol-water distribution coefficient. *Ecol. Eng.* 37:1595-1600.

Leng WH, Zhu WC, Ni J, Zhang Z, Zhang JQ & Cao CN (2006) Photoelectrocatalytic destruction of organics using TiO_2 as photoanode with simultaneous production of H_2O_2 at the cathode. *Appl. Catal.A.* 300 (1): 24-35.

Liu F, Ying GG, Tao R, Zhao JL, Yang JF & Zhao LF (2009) Effects of six selected antibiotics on plant growth and soil microbial and enzymatic activities. *Environ.Pollut.* 157(5): 1636-1642.

Liu Y, Gan X, Zhou B, Xiong B, Li J, Dong C, Bai J & Cai W (2009) Photoelectrocatalytic degradation of tetracycline by highly effective TiO_2 nanopore arrays electrode. *J. Hazard. Mater.*171: 678-683.

Lopez-Penalver JJ, Sànchez-Polo M, Gòmez-Pacheco CV & Rivera-Utrilla J (2010) Photodegradation of tetracyclines in aqueous solution by using UV and UV/H_2O_2 oxidation processes. *J.Chem.Technol. Biot.* 85(10): 1325-1333.

Li R, Zhang Y, Lee CC, Liu L & Huang Y (2011) Hydropholic interaction chromatography separation mechanisms of tetracyclines on amino-bonded silica column. *J.Sep. Sci.* 34 (13): 1508-1516.

Ma L & Tu SX (2011) Removal of Arsenic from aqueous solution by two types of nano TiO_2 crystals. *Environ. Chem.Lett.* 9: 465-472.

Martinez C, Canle ML, Fernàndez MI, Santaballa JA & Faria J (2011) Kinetics and mechanism of aqueous degrdation of carbamazepine by heterogenous photocatalysis using nanocristalline TiO_2, ZnO_2 and multi-walled carbon nanotube-anatase composites. *Appl. Catal.B: Environ.* 102: 563-571.

Martinez-Huitle CA & Ferro S (2006) Electrochemical oxidation of organic pollutants for the wastewater treatment: direct and indirect processes. *Chem.Soc. Rev.*35: 1324-1340.

Ohtani B, Ogawa Y & Nishimoto S-I (1997) Photocatalytic activity of amorphousanatase mixture of titanium (IV) oxide particles suspended in aqueous solutions. *J.phys.Chem. B.* 101(19): 3746-3752.

Parolo ME, Savini MC, Vallés JM, Baschini MT & Avena MJ (2008) Tetracycline adsorption on montmorillonite: pH and ionic strength effects. Appl.Clay Sci. 40(1-4): 179-186.

Petrovic M & Barcelo D (2006) Liquid chromatography-mass spectrometry in the analysis of emerging environmental contaminant. *Anal. Bioanal. Chem.*385 (3): 422-424.

Qiang Z & Adams C (2004) Potentiometric determination of acid dissociation constants (pKa) for human and veterinary antibiotics. *Water Res.* 38: 2874-2890.

Quan X, Ruan X, Zhao H, Chen S & Zhao Y (2007) Photoelectrocatalytic degradation of pentachlorophenol in aqueous solution using a TiO_2 nanotube film electrode. *Environ. Pollut.*147(2): 409-414.

Regonini D, Jaroenworaluck A, Stevens R & Bowen CR. Effect of heat treatment on the properties and structure of TiO_2 nanotubes: phase composition and chemical composition. *Surf. Inter.Anal.* 42:139-144.

Reyes C, Fernandez J, Freer J, Mondaca MA, Zaror C, Malato S & Mansilla H (2006) Degradation and inactivation of tetracycline by TiO_2 photocatalysis. *J.Photochem. Photobiol.A.* 184:141-146.

Rey RP, Padron AS, Leon PL, Pozo MM & Baluja C (1999) Ozone of cytostatics in water medium. Nitrogen bases. *Ozone Sci. Eng.* 2: 69-77.

Rubert IV KF & Pedersen JA (2006) Kinetics of oxytetracycline reaction with a hydrous manganese oxide. *Environ. Sci. Technol.* 40(23): 7216-7221.

Selcuk H, Sene JJ & Anderson MA (2003) Photoelectrocatalytic humic acid degradation kinetics and effect of pH, applied potential and inorganic ions. *J Chem.Technol. Biotechnol.* 78: 979-984.

Sontakke S, Modak J & Madras G (2011) Effect of inorganic ions, H_2O_2 and pH on the photocatalytic inactivation of Escherichia coli with silver impregnated combustion synthesized TiO_2 catalyst. *Appl. Catal. B: Environ.*106: 453-459.

Shelver WL & Varel VH (2012) Development of a UHPLC-MS-MS method for the measurement of chlortetracycline degradation in swine manure. *Anal. Bioanal.Chem.* 402: 1931-1939.

Sun Q & Xu Y (2010) Evaluating intrinsic photocatalytic activities of anatase and rutile TiO_2 for organic degradation in water. J phys. Chem.C 114 (44): 18911-18918.

Ternes TA (1998) Occurrence of drugs in German sewage treatment plants and rivers. Water Res. 32 (11): 3245-3260.

Wang MC, Zhong WY & Chen JQ (2011) Effects of Chlortetracycline hydrochloride and its UV degradation products on growth of freshwater algae. J. *Anhui Agricul.Sci.*39: 4155.

Wang N, Li X, Wang Y, Quan X & Chen G (2009) Evaluation of bias potential enhanced photocatalytic degradation of 4-chlorophenol with TiO_2 nanotube fabricated by anodic oxidation method. *Chem. Eng. J.* 146: 30-35.

Wang Y & Hong CS (1999) Effect of hydrogen peroxide, periodate and persulfate on photocalysis of 2-chlorobiphenyl in aqueous TiO_2 suspensions. *Water Res.* 33: 2031-2036.

Xiang Q, Yu J & Wong PK (2011) Quantitative characterization of hydroxyl radicals produced by various photocatalysts. *J Colloid.Interf. Sci.* 357 (1):163-167.

Xie YB & Li XZ (2006) Degradation of Bisphenol A in aqueous solution by H_2O_2- assisted photoelectrocatalytic oxidation. *J Hazard. Mater.* B138: 526-533.

Yang S & Carlson K (2004) Routine monitoring of antibiotics in water and wastewater with a radioimmunoassay technique. *Water Res.* 38(14-15): 3155-3166.

Yoon H, Noha JS, Kwon CH & Muhammed M (2006) Photocatalytic behavior of TiO_2 thin films prepared by sol–gel process. *Mater. Chem. Phys* 95 (1): 79-83.

Yu J, Wang G, Cheng B & Zhou M (2007) Effects of hydrothermal temperature and time on the photocatalytic activity and microstructures of bimodal mesoporous TiO_2 powders. *Appl.Catal. B. Environ.* 69: 171-180.

Zhang H & Huang CH (2003) Oxidative transformation of ticlosan and chlorophene by manganese oxides. *Environ. Sci. Technol.* 37(11): 2421-2430.

CHAPITRE 8

ELECTROCHEMICAL DEGRADATION OF CHLORTETRACYCLINE USING N-DOPED TI/TiO_2 PHOTOANODE UNDER SUNLIGHT IRRADIATIONS

Le chapitre 8 est constitué de l'article suivant :

Rimeh Daghrir, Patrick Drogui, Nazar Delegan, My Ali El Khakani, Electrochemical degradation of chlortetracycline using N-doped Ti/TiO_2 photoanode under sunlight irradiations, *Water Research (Accepted)*.

8. ELECTROCHEMICAL DEGRADATION OF CHLORTETRACYCLINE USING N-DOPED TI/TiO_2 PHOTOANODE UNDER SUNLIGHT IRRADIATIONS

8.1 Abstract

The appearance and the persistence of pharmaceutical products in the aquatic environment urgently call for the development of an innovative and practical water treatment technology. This study deals with the development of nanostructured nitrogen-doped TiO_2 photoanodes and their subsequent use for chlortetracycline (CTC) photoelectrocatalytic oxidation under visible light. The N-doped TiO_2 photoanodes with different nitrogen contents were prepared by means of a radiofrequency magnetron sputtering (RF-MS) process, with the objective to tune shift their optical absorption from the UV towards the visible. The N-doped TiO_2 consist of nanostructured anatase phase with average TiO_2 nanocrystallite size of 29 nm. The nitrogen doping is clearly shown to produce the desired red shift of the absorption onset of the TiO_2 coatings (from ~380 nm to ~550 nm). Likewise, the N-doped TiO_2 are found to be highly photo-electroactive not only under the UV light but most interestingly under the visible light as well. Using the optimal N-doped photoanodes, 99.6% of CTC (100 $\mu g\ L^{-1}$) was successfully degraded after 180 min of treatment time with a current intensity of 0.6 A. Under these conditions, a relatively high mineralization of CTC (92.5% ±0.26 % of TOC removal and 90.3%±1.1% of TN removal) was achieved.

8.2 Key words

Photoelectrocatalytic oxidation; magnetron sputtering process; N-doped TiO_2; Chlortetracycline.

8.3 Introduction

The occurrence and the fate of endocrine disrupting compounds (EDC) in aqueous environment have received considerable interest over the past several years due to their adverse effects on aquatic organisms (Daskalaki et al., 2012). Antibiotics are extensively used in human and veterinary medicine for preventing or treating diseases, increasing feed efficiency and improving growth rate for livestock (Sarmah et al., 2006; Kummerer, 2009; Homem and Santos, 2011; Gao et al., 2012). After consumption by humans and animals, antibiotics are thrown out via urine or feces in both unchanged and/or metabolized forms. These contaminants are soluble in water and are detected in soils, sediments, surface water, drinking water, and wastewater at concentrations ranging from ng/L to μg/L (Gao et al., 2012; Chenxi et al., 2006).

Chlortetracycline hydrochloride (CTC) belongs to the tetracycline (TCs) antibiotic groups. TCs are bacteriostatic agents used in both human and animal medicine for treating infections caused by strains of Gram negative and Gram positive bacilli streptococci, Rickettsia bacteria and spiroquetes, among others. Besides, TCs are extensively administered as an additive in avian, cattle and pig feed to promote growth. Due to its widespread usage, the introduction of these residual compounds into environment through different sources will lead to serious environmental problems including ecological risk and human health damage. Few previous studies have examined the CTC toxicity to a variety of species. Wang and his co-workers (2011) showed that CTC has negative effect on the growth of freshwater algae, whereas Guo and Chen (2012) have reported that CTC had significantly toxic effects on freshwater phytoplankton species. Accordingly, the removal of CTC from aquatic matrix is become as important for environmental protection.

Generally, the wastewater treatment plants (WWTPs) using conventional activated sludge treatment process are not designed to effectively remove this micropollutant. For instance, the

removal efficiency of TCs varied significantly from 12% (Spongberg and Witter, 2008) to 80% (Karthikeyan and Meyer, 2006). Physicochemical methods such as adsorption using activated carbon have been applied by Choi et al. (2008) to remove more than 68 % of TCs (tetracycline, doxycycline-hyclate, and chlortetracycline-HCl). The main disadvantage of such methods is that they do not destroy the pollutants but transfer the pollutant from one phase to another (Tahir and Rauf, 2006; Ozcan et al., 2004). Likewise, chemical oxidation processes using UV/H_2O_2 and O_3 have been successfully applied to degrade CTC (Lopez-Penalver et al., 2010; Kim et al., 2012). However, the high chemical consumption, the complexity of these methods and the relatively high treatment cost represent the major drawbacks that limit their implementation at large scale (Daghrir et al., 2012; Martinez-Huitle and Ferro, 2006).

Photoelectrocatalytic oxidation (PECO) processes combining both photocatalytic and electrolytic processes have been evolved as an efficient technique for the removal of organic contaminants and pathogens in aqueous matrices (Daghrir et al., 2012; Wang et al., 2010; Frontistis et al., 2011; Hou et al., 2012; Daghrir et al., 2013). Owing to the external potential applied, the PECO process is able to retard the recombination of the electron/hole pairs (e^-_{CB}/h^+_{VB}) photo-generated on the surface of the catalyst and consequently to ensure higher efficiency in the degradation of pollutants (Frontistis et al., 2011; Daghrir et al., 2012; Liu et al., 2009).

Among the various semiconductors, titanium dioxide (TiO_2) is the prime photocatalytic candidate owing to its promising physical and chemical properties such as: high oxidation efficiency, non-toxicity, low cost, high photostability, chemical inertness and environmentally friendly nature (Ouyang et al., 2012; Valentin et al., 2007; Peng et al., 2012; Kuo et al., 2010). However, TiO_2 can only be activated under UV irradiation using a wavelength lower than 387 nm, this is due to its large optical band gap (~ 3.2 eV). Thus, only a small fraction of solar light (less than 5% of solar energy is emitted as UV irradiation) is actually photoconverted by

pure TiO_2 (Ren et al., 2007). This drawback limits the use of TiO_2 at large scale application. For the sake of efficient utilization of sunlight, great deals of efforts have been made to extend the absorption of TiO_2 into the visible light region (Wu et al., 2010; Yap et al., 2010; Cheng et al., 2013). Impurity doping of TiO_2 (either cations or anions) is one of the typical approaches that has been applied by several research works to extend the spectral response to visible light region (Valentin et al., 2007; Wang and Lewis, 2005; Chen et al., 2007; Park et al., 2006). Doping pure TiO_2 with anions such as nitrogen has been shown to create an effective red shift in the absorption spectra of the TiO_2 well into the visible spectrum (Asahi et al., 2001; Ananapattarachai et al., 2009; Kang et al., 2008; Choi et al., 2007). The usage of a higher portion of the solar energy spectrum will promote exciton generation to be used in photo-electro-catalytic reactions (Daghrir et al., 2013).

The aim of the present work is to evaluate the potential of a PECO process using N-doped TiO_2 photoanodes deposited by means of a magnetron sputtering process for the treatment of waters contaminated by CTC under solar irradiation (1.5 AM). Thus, after optimizing the nanostructure and the optoelectronic properties (namely bandgap narrowing) of N-doped TiO_2 photoanodes, the latter were successfully used to investigate their degradation efficiency and mineralization rate for CTC under sun irradiation conditions. By carrying out systematic studies of the effect of different operating parameters (such as current intensity, treatment time and type of photoanode), we were able to identify the optimal processing conditions that lead not only to a full degradation of CTC (of up to 99,6%), but also to its mineralization (of up to 92.5%) into CO_2 and H_2O. Possible CTC degradation pathways under visible light irradiation are discussed.

8.4 Material and methods

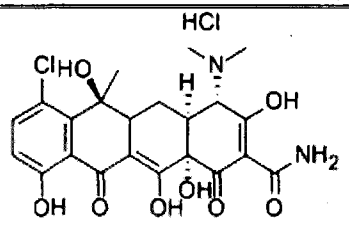
8.4.1 N-doped TiO_2 Photoanodes preparation

The photoanodes were prepared by depositing N-doped TiO_2 coatings onto Ti metallic grids by means of a radiofrequency magnetron sputtering (MS) process, which permits their *in-situ* doping through the incorporation of nitrogen (N) gas with the argon (Ar) during the sputtering process. The nitrogen content of the N-doped TiO_2 coatings was controlled by adjusting the $[N_2]/([Ar]+[N_2])$ gas flow ratio during the sputter-deposition process, while keeping the total pressure at 1.4 mTorr in the deposition chamber. The background chamber pressure prior to deposition between each deposit was kept at an ultra-high vacuum value as low as ~2 x 10^{-8} Torr. The deposition temperature of the N-doped coatings was maintained at 650°C, while the RF power for the magnetron sputtering was set at 350 W. More experimental details on our MS system can be found elsewhere (Brassard et al., 2006; Hajjaji et al., 2011). Thus, N-doped TiO_2 photoanodes with N contents ranging from 0 to ~6 at.% have been successfully achieved.

8.4.2 Synthetic solution preparation

Chlortetracycline hydrochloride ($C_{22}H_{24}Cl_2N_2O_8$) was an analytical grade reagent supplied by Sigma Aldrich (purity 78 %). Its water solubility was 4.12 g L^{-1} (Lopez-Penalver et al., 2010). Table 8-1 presents some physico-chemicals properties of CTC (Kim et al., 2012; Qiang and Adams, 2004; Kim et al., 2009). CTC stock solution was prepared in deionized water at 1 mg L^{-1} and kept at 4°C. Synthetic solution of CTC was made by diluting the CTC stock solution in deionized water. Final concentration of CTC was 100 µg L^{-1}. In order to increase the electrical conductivity in the solution, 0.07 mol L^{-1} of sodium sulfate was added.

Tableau 8-1 Physico-chemical properties of Chlortetracycline hydrochloride.

Molecule	Molecular formula	Chemical structure	Molecular weight (g mol^{-1})	Solubility (mol/L^{-1})	Log K_{OW}	Henry's law constant (atm m^3 mol^{-1})	Isoelectric point	pK_{a1}	pK_{a2}	pK_{a3}
CTC	$C_{22}H_{24}Cl_2N_2O_8$		515.3	0.008	-0.62	3.45 E-24	2.27	3.3±0.3	7.55±0.02	9.3±0.3

8.4.3 Photoelectrocatalytic cell

The photoelectrocatalytic cell used was 1 L of capacity and was made of PVC material with a dimension of 13 cm (depth) x 10 cm (width) x 10 cm (length). The photoelectrocatalytic reactor was comprised of two parallel pieces of vitreous carbon plates (6 cm height x 4 cm width) each, having a surface area of 24 cm^2 and situated 6 cm apart. The vitreous carbon plates were used as cathode electrodes. The anode consists of Ti expanded grid coated with the TiO_2 coating (either undoped or N-doped at different N contents) was horizontally installed between the two vertically installed cathodes. The dimensions of the anode are 6 cm height x 4 cm width. The electrodes were installed on a perforated Plexiglas plate placed at 2 cm from the bottom of the cell (see Figure 8-1).

8.4.4 Experimental setup

The assays were carried out in a closed loop as depicted schematically in Figure 8-1. A 0.6 L of PVC tank (1), a peristaltic recycling pump (2) and the photoelectrocatalytic cell (3) constitute the loop. All the essays were conducted in batch recirculation mode with a flow of CTC synthetic solution entering the bottom of the cell. A recycle flow rate of 0.25 L min^{-1} was maintained using a peristaltic recycling pump (Master flex, Model 77200-50, USA). The photoelectrocatalytic cell was operated under galvanostatic conditions, with current intensity in the range 0.1-0.8 A imposed during a treatment period varying from 20 min to 240 min. Current intensity was imposed by means of DC power source, PS 3030 D, Circuit-Test Electronics (Burnaby, BC, Canada) with a maximum current rating of 3.0 A at an open circuit potential of 30 V. The photo-anode (undoped Ti/TiO_2 or N-doped Ti/TiO_2) was illuminated under visible irradiation using a solar simulator model SS50AAA (Photo emission Tech., INC, Camarillo, USA) equipped with a 150 W xenon lamp. All experiments were carried out under AM 1.5 solar illumination conditions. For all tests, a total volume of 0.6 L was used. A concentration of 0.07 mol Na_2SO_4 L^{-1} was added in the synthetic solution to increase its

electrical conductivity. Sodium sulfate was analytical grade reagent supplied by Mat laboratory (Quebec, Qc, Canada).

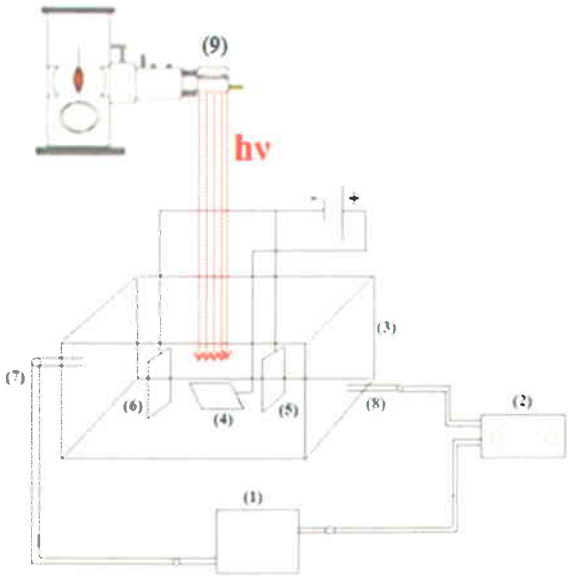


Figure 8-1 **Schematic diagram of the experimental setup: (1) PVC tank, (2) peristaltic recycling pump, (3) photoelectrocatalytic reactor, (4) N-doped TiO_2 photocatalyst, (5) and (6) vitreous carbon, (7) in let, (8) out let, (9) Solar simulator.**

8.4.5 Experimental procedure

The first-set of experiments were carried out to evaluate the efficiency of PECO process for the treatment of CTC synthetic solution using Ti/TiO_2 photo-anode respectively doped with different contents of nitrogen (from 0 at.% to 5.8 at.% of nitrogen contents). The PECO process was applied during 120 min of treatment time at 0.39 A of current intensity and under visible illumination (solar simulator). In view of determining the optimal conditions (reduce

cost and increase effectiveness) for treating CTC by PECO process, different operating parameters such as current intensity (from 0.1 to 0.8 A) and treatment time (ranging from 20 min to 240 min) were successively tested. During these essays, the effectiveness of the photoelectrocatalytic process was evaluated by simultaneously measuring the residual concentration of CTC, total nitrogen (TN) and total organic carbon (TOC). The pH was also measured. To check the effectiveness and the reproducibility of the photoelectrocatalytic process, the measure of all parameters were repeated in triplicate.

8.4.6 Analytical technique

The pH was determined using a pH-meter (Fisher Acumet model 915) equipped with a double-junction Cole-Palmer electrode with Ag/AgCl reference cell. NT and TOC measurements were performed using a Shimadzu TOC 5000A analyzer (Shimadzu Scientific Instruments Inc) equipped with an autosampler.

The progress of the photoelectrocatalytic degradation of CTC and by-products was monitored and quantified by LC/MS/MS (Thermo TSQ Quantum Access). The chromatographic column used was Beta Basic C18, particle size 3 μm and 2.1 x 100 mm inner diameter. The mobile phase consisted of a mixture of 0.1% formic acid in water (v/v) (component A) and 0.1% formic acid in acetonitrile (component B). A gradient elution program at a 0.2 mL min^{-1} flow rate was used to achieve the separation. The program begins with an isocratic step at 90% A and 10% B for 2 min followed by a linear elution gradient from 90% to 30% A and from 10% to 70% B in 10 min more, and returned to initial condition. 18.5 min were waited between injections. Mass spectral data shown in this study were acquired on a LCQ Duo ion trap tandem mass spectrometry equipped with an electrospray ionization (ESI) source operated in positive ion mode. Nitrogen was used as a sheath and auxiliary gas. Working conditions were as followed: spray voltage was 5000 V and capillary temperature was 345°C. Quantitative analysis of CTC was determined using sulfamethazine C13 as internal standard.

8.4.7 Economic aspect

Evaluation of operation costs related to the photoelectrocatalytic treatment process included chemical and energy consumption. The electrolyte (Na_2SO_4 industrial grade) provided by Mat laboratory (Quebec, Canada) was estimated at a unit cost of 0.30 US$ kg^{-1}. The energy consumed was estimated at a cost of 0.06 US$ kWh^{-1}, which corresponded to the cost in the province of Quebec (Canada). The total cost was evaluated in terms of U.S. dollars spent per cubic meter of treated solution (US$ m^{-3}).

8.5 Results and Discussion

8.5.1 Photoanode characterization

The chemical composition of the N-doped TiO_2 coatings was determined by means of X-ray Photoelectron Spectroscopy (XPS). The XPS spectra were collected by using the VG Escalab 220i XL spectrophotometer equipped with an Al-K_α (1486.6 eV) monochromatic source, after a systematic *in-situ* surface cleaning by means of Ar^+ ion sputtering. Thus, the variation of the $[N_2]/([Ar]+[N_2])$ gas flow ratio between 0 and 20% during the sputtering process has led to an incorporated N content in the films varying from 0 to 5.8 at.%, respectively.

The crystalline structure of the TiO_2 films was characterized by the X-ray diffraction (XRD) technique using the Panalytical X-Pert Pro diffractomter with the Cu-K_α radiation (1.5418 Å). Figure 8-2 shows the XRD spectra of the sputter-deposited N-doped TiO_2 films for different N contents. All the N-doped TiO_2 films were found to crystallise in the anatase phase irrespective to their N content. Nevertheless, the (101) anatase peak (located at $2\theta \approx 25.3°$) is seen to broaden slightly as the N content is increased from 0 to 3.4 at.%, suggesting a decrease in the TiO_2 crystallite size with increasing N contents.

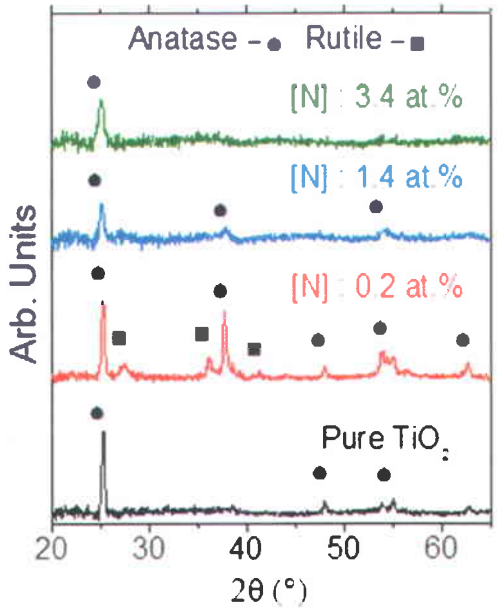


Figure 8-2 X-ray diffraction patterns of pure TiO_2 and N-doped TiO_2 coatings prepared at 650°C, by means of a magnetron sputtering process.

In order to estimate the anatase crystallite size effect, the average particle size (D) of the TiO_2 crystallites on the anatase (101) diffraction, we have used the Debye–Scherer formula (Guinier, 1962): $D = \frac{0.9\ \lambda}{\Delta(2\theta)\cos\theta}$, where D is the crystallite size in a particular orientation (i.e.; (110) here), λ is the x-ray wavelength, θ is the diffraction angle corresponding to the particular orientation and Δ(2θ) is the width at half maximum of the peak. Thus, the TiO_2 crystallite size was found to decrease from ~51 nm for pure TiO_2 ([N] = 0 at.%) down to ~29 nm for N-doped TiO_2 films with [N] = 3.4 at.% (Figure 8-3). This nanometer scale of the TiO_2 nanocrystallites is expected to enhance the photocatalytic activity of these N-doped TiO_2 coating, because of the nanostructuring induced increase of the surface area of the material (Kim et al., 2007). One can note that for the [N] = 0.2 at.% content, in addition to the (101),

(103), (200), (105) and (213) anatase diffraction peaks (appearing at the respective positions of 2θ of 25.3°, 37.9°, 48.4°, 55.3°, and 62.7°), the XRD spectra of the N-doped TiO_2 films exhibit also some less intense peaks of the rutile phase (i.e. the (110), (101), and (200) rutile diffraction peaks appearing at 27.5°, 36.0°, and 39.3°, respectively).

The rutile phase of the TiO_2 is more densely packed than the anatase one, whereas the latter is well known to be the most photoactive form of TiO_2 (Tsai and Cheng, 1997; Ohno et al., 2001; Sakatani et al., 2006). Our N-doped TiO_2 films with the 0.2 at.% N content seem to consist of a mixture of anatase (as a prominent component) and rutile. Actually, the TiO_2 powder (Degussa, P-25), which is considered as a standard material in the field of photocatalysis, contains anatase and rutile phases in a ratio of about 4:1 (Carp et al., 2004).

The film thickness and morphology of the N-doped TiO_2 films were systematically examined by scanning electron microscopy, using a Jeol JSM-6300F microscope. Figure 8-3 shows a typical cross-section view SEM micrograph of the N-doped TiO_2 films deposited onto silicon substrate (for SEM observation purposes). Regardless of the N content of the films, they were found to exhibit a relatively dense columnar morphology with a certain inter-columnar porosity. The thickness of N-doped TiO_2 coatings is uniform and is of ~560 nm.

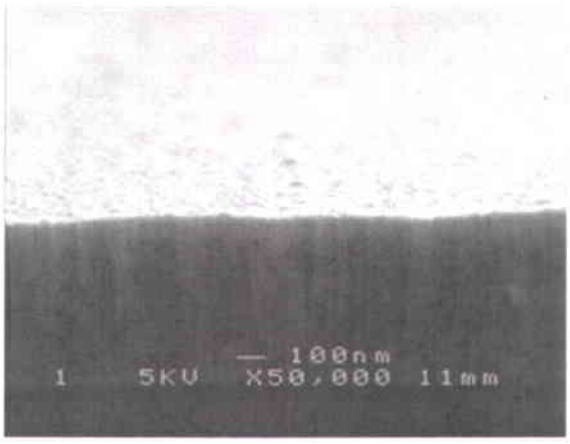


Figure 8-3 Typical SEM micrograph of the sputter-deposited N-doped TiO_2 films.

To study the effectiveness of the N doping on the optoelectronic properties of the N-doped TiO_2 films, we have used the UV-Vis absorption spectroscopy. The UV-Vis spectra of the N-doped TiO_2 films deposited onto quartz subsrates were acquired using a Varian-Cary 5000 spectrophotometer. Figure 8-4 clearly shows that as the N content of the films is increased from 0 up to 5.8 at.%, their onset of absorption is red-shifted from the UV towards the visible (from ~380 nm for the undoped-TiO_2 films to ~550 nm for the N-doped TiO_2 ones with a N content of 3.4 at.%). These results are in accordance with those reported by Asahi et al. (2001) and Zhao et al. (2008), where the nitrogen doping of the TiO_2 films increases their absorption component in the visible. By analyzing the UV-Vis spectra of the N-doped TiO_2 films, we were able to extract their corresponding absorption coefficient as a function of the wavelength (Wu et al., 2004). Then, the absorption coefficients of the N-doped films were plotted across the wavelength to generate their corresponding Tauc plots, and deduce their corresponding optical band-gap (Wu et al., 2004). The inset of Figure 8-4 shows the variation of the band-gap of the N-doped TiO_2 films as a function of their N content. It is clearly seen that the band-gap decreases from 3.2 eV (for the undoped anatase TiO_2 films) to a value as low as 2.3 eV (for N-doped TiO_2 films at a N content of 3.4 at.%). It important to note that increasing further the N doping of the films up to 5.8 at.% does not lead to additional band-gap narrowing. The N content of 3.4 at.% arises as the optimal value that leads to the most effective narrowing of the bandgap to 2.3 eV. Interestingly, this band-gap value of 2.3 eV corresponds to a wavelength of 539 nm, which is very close to the sun peak power. This results is extremely important as the photo-anode developed here are expected to not only operate under the sun light (in stead of the classical UV exposure), but also their absorption characteristics match well with the wavelength at which the sun emits a maximum of photons in the visible. This promises a strong photoresponse of the N-doped TiO_2 photoanodes (with the optimal N content of 3.4 at.%), with an enhanced creation of excitons under the visible

light of the sun. Such an enhanced absorption in the visible would result in higher photocatalytic performance (Peng et al., 2012; Cheng et al., 2013; Ananapattarachai et al., 2009; Senthilnathan and Philip, 2010). The photocatalytic behavior of the N-doped TiO_2 photoanodes will be investigated hereafter as a function of their N content.

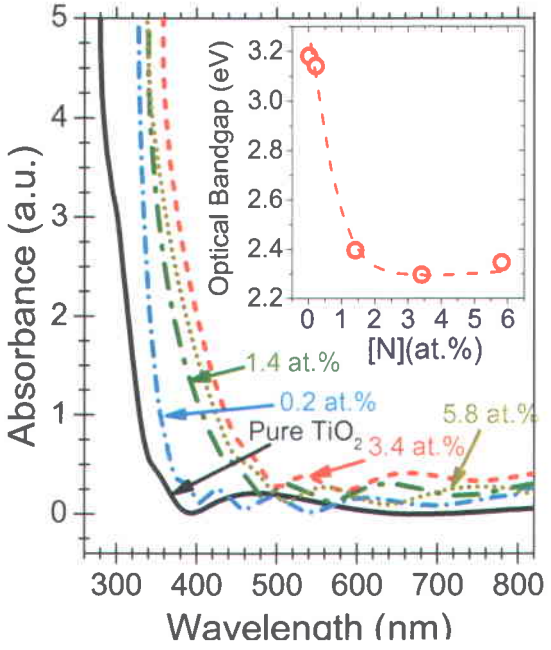


Figure 8-4 **UV-Vis absorbance spectra of the N-doped TiO_2 films with various nitrogen contents (indicated by the arrows). The inset shows the variation of the optical bandgap of the N-doped TiO_2 films as a function of their N content.**

8.5.2 Effect of nitrogen content on the photoelectrocatalytic properties of N-doped TiO2 photoanodes

The photoelectrocatalytic degradation of CTC (100 μg L^{-1}) was investigated by using N-doped TiO_2 photoanodes containing different contents of nitrogen (namely undoped (0 at.%); 0.2 at.%; 0.32 at.%; 1.4 at.%; 3.4 at.% and 5.8 at.%). The PECO treatment was carried out

under simulated sunlight irradiation for a period of 120min at a 0.39 A of current intensity. The performances of these photoanodes for CTC degradation were evaluated by simultaneously measuring the residual concentrations of TN, TOC and CTC (Figure 8-5). The initial values of TOC and TN were 2.8 ± 0.1 mg L^{-1} and 0.54 ± 0.01 mg L^{-1}, respectively.

The increase in the nitrogen content doping TiO_2 enhances the oxidation efficiency of CTC by PECO process. A removal rate of 82.4 ± 0.3% of CTC was recorded after 120 min of treatment time using 0.2 at.% N-doped TiO_2 photoanode, whereas 87.4±0.1% and 91.6±0.2% of CTC removal have been recorded within the same irradiation time using 0.32 at.% and 1.4 at.% of nitrogen contents, respectively. The mineralization rate of CTC was also greatly improved by increasing the nitrogen content in TiO_2 photo-anode. The residual concentrations of TOC and TN recorded using 0.2 at.% N-doped TiO_2 were 1.1±0.06 mg L^{-1} and 0.21±0.0 mg L^{-1}. By comparison, 0.72 ± 0.01 mg L^{-1} and 0.15 ± 0.01 mg L^{-1} have been respectively recorded using 1.4 at.% of nitrogen content in TiO_2 photoanode. The shift in the band gap transition of the doped TiO_2 (from 3.2 eV to 2.3 eV) promotes the absorption in the visible irradiation and consequently increases the photo-electro-catalytic degradation of CTC (Asahi et al., 2001; Burda et al., 2003).

Nevertheless, the increase of nitrogen content from 3.4 at.% to 5.8 at.% reduces the oxidation efficiency of CTC by PECO process. The photocatalytic activity of N-doped TiO_2 having 5.8 at.% of nitrogen content was lower compared to that containing 3.4 at.%. The photoelectrocatalytic degradation of CTC using 5.8 at.% of nitrogen content in TiO_2 photoanode was 84.8±0.0%. Under these conditions, the residual concentrations of TOC and TN recoded after 120 min of treatment time were 0.88±0.06 mg L^{-1} and 0.19±0.01 mg L^{-1}, respectively. This lower photocatalytic activity of photo-catalyst recorded was mainly attributed to the occupation of the surface active sites by excess nitrogen. According to Lin et

al. (2011), the excess of nitrogen could decrease the number of active sites of the catalyst and consequently reduce the photocatalytic efficiency.

Among all the photo-anodes, N-doped TiO_2 having 3.4 at.% of nitrogen content exhibited the highest PECO activity. After 120 min of treatment, higher mineralization rate has been also recorded. The residual concentration of TOC and TN recorded were 0.56±0.02 mg L^{-1} and 0.12±0.01 mg L^{-1}, respectively. Besides, the maximum photoelectrocatalytic degradation of CTC (98.2 ± 0.1%) was recorded using the N-doped TiO_2 photoanode with the optimal N content of 3.4 at.%. By comparison, for the undoped TiO_2 photoanode, only 75.2 ± 0.5% of CTC removal rate has been achieved after 120 min of treatment. This shows that N-doping of the TiO_2 photoanodes at the optimal content of 3.4 at.% enhances their PECO degradation efficiency towards CTC by 30% in comparison to undoped TiO_2. Moreover, the residual concentrations of TOC and TN recorded using undoped TiO_2 photoanodes were 1.3±0.0 mg L^{-1} and 0.21 ± 0.01 mg L^{-1}, respectively. The enhanced PECO activity of the N-doped TiO_2 photoanodes is a consequence of their narrower bandgap (as evidenced by the above-discussed results of Figure 5). The narrower is the bandgap, the higher is number of harvested visible photons that lead to a higher number of photogenerated excitonst (Peng et al., 2012; Wu et al., 2010; Ao et al., 2009; Trenczek-Zajac et al., 2009).

The influence of nitrogen content was also put into evidence by Ananpattarachai et al. (2009) and Cheng et al. (2013) while studying the photocatalytic degradation of 2-chlorophenol and rhodamine B, respectively. The degradation experiments of 2-chlorophenol were carried out at different nitrogen contents (from 0 to 5.01% of N content) during 50 min of treatment time. The degradation efficiency was around 49% using 0.64% of N content, while 66% of 2-Chlorophenol was removed using 4.11% of N content. The limited degradation rate of pollutant using lower nitrogen content was mainly due to the fact that the band gap of TiO_2

photoanode was not sufficiently reduced causing lower photocatalytic efficiency (Ananpattarachai et al., 2009).

Finally, 3.4 at.% N-doped TiO_2 photo-catalyst used in PECO process has the capacity to produce the highest level of photo-generated electrons and holes to oxidize CTC. Thereby, N-doped Ti/TiO_2 photoanode with 3.4 at.% of nitrogen content arises as the optimal N doping concentration, and was consequently selected to further optimize the PECO process, as it will be shown hereafter.

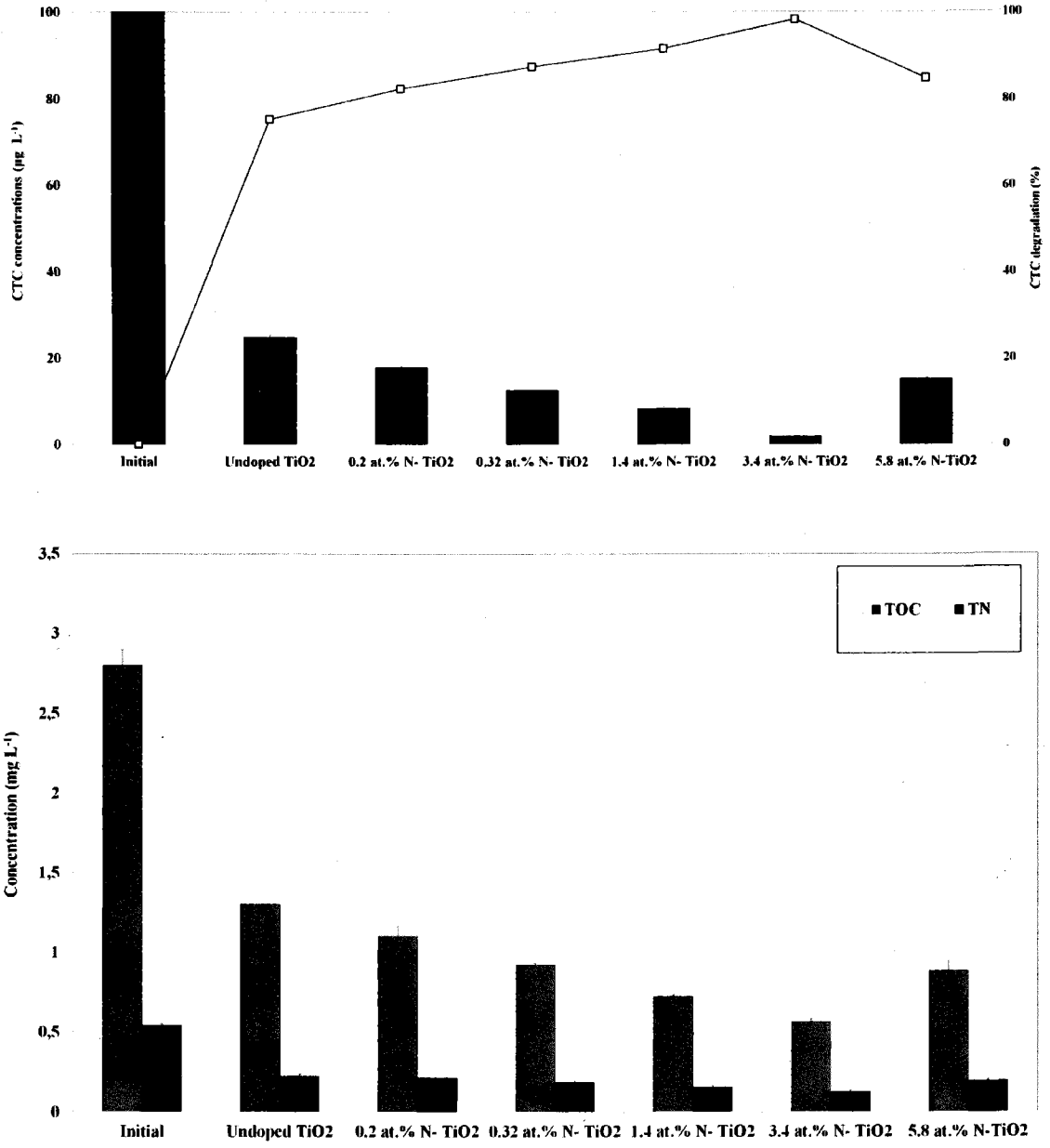


Figure 8-5 **Effect of nitrogen content doped TiO_2 photoanode on the oxidation and the mineralization of CTC (VC as cathode; 0.39 A of current intensity; visible irradiation; [CTC]°= 100 µg L^{-1}).**

8.5.3 Effect of current intensity

Applying an external potential is one of the key factor that improve the photoelectrocatalytic efficiency (Daghrir et al., 2012; Han et al., 2010; Chai et al., 2012). The effect of current intensity (0.1 A to 0.8 A) on CTC degradation was explored at 100 μg L^{-1} initial concentration, using 3.4 at.% N-doped TiO_2 photoanode. As shown in Figure 8-6, the degradation rate of CTC increased with the current intensity. The best performance of CTC degradation (99.1% ± 0.05%) was recorded for 0.6A. Likewise, TOC and TN could be removed up to 86.2% ±2.9% and 83.5% ± 2.1%, respectively when a current intensity of 0.6A was imposed.

During the PECO treatment, the electrical potential applied prevents the recombination of electron-hole pairs, increases the active holes lifetime, and consequently increases the concentration of reactive oxygen species such as hydroxyl radicals (Daghrir et al., 2013; Ding et al., 2010). However, applying higher current intensity (0.8 A) did not practically improve the oxidation and the mineralization of CTC. A removal rate of 99.1±0.1% of CTC was recorded at 0.8 A of current intensity imposed, while the removal of TOC and TN obtained were 87.9%±2.3% and 84.7±1.25%, respectively. As reported by Daghrir et al. (2012), the increase of current intensity above the optimal value decrease the degradation efficiency of pollutant and it may also have no effect on the degradation. In the full depletion conditions, the electrons are drawn inside the semiconductor and are extracted at the back contact. Under these conditions, the kinetic of the reaction is only limited by the photon flux (Neuman-Spallart, 2007).

On the other hand, the choice of intensity is not only dictated by the removal efficiency of CTC, but also by the cost of energy consumed. An increase in current intensity from 0.1 A to 0.8 A causes an increase in energy consumption from 2.4 kWh m^{-3} to 49.6 kWh m^{-}

[3].Therefore, the optimal current intensity of 0.6 A was selected as the best trade-off for not only CTC degradation but also for its effective mineralization.

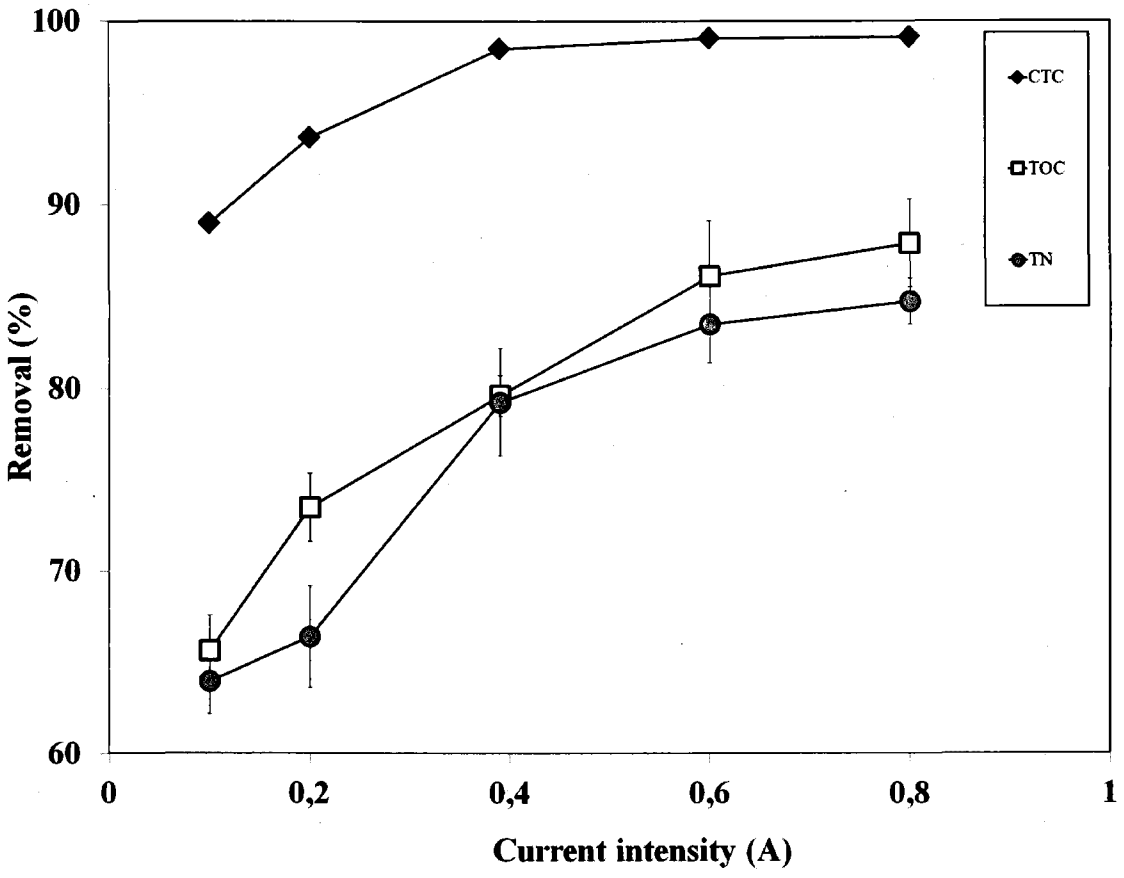


Figure 8-6 Effect of current intensity on CTC degradation and mineralization using PECO process (3.4 at.% N-doped TiO_2 photoanode; treatment time =120 min; [CTC]° = 100 μg L^{-1}).

8.5.4 Effect of treatment time

The effect of treatment time ranging between 20 min and 240 min on the CTC oxidation was investigated using the optimal 3.4 at.% N-doped TiO_2 photoanode, at the selected current intensity of 0.6 A for the degradation of an initial CTC concentration of 100 μg L^{-1}. The CTC degradation rate increased with the treatment time (Figure 8-7). The increase of treatment

time from 20 min to 240 min promotes the degradation of CTC from 48.7%±1.5% to 99.6%±0.0%, respectively. Moreover, the removal of TOC and TN reached 92.5% ±0.26% and 90.3%±1.1%, respectively, after 180 min of treatment time and remains constant up to 240 min. Thus, it is clear that 180 min of photoelectrocatalytic treatment is required to produce sufficient amount of reactive oxygen species and consequently to promote higher CTC degradation. Under these conditions, the consumed energy recorded was 45.6 kWh m^{-3}.

To further understand and evaluate the mechanism of pollutant degradation, the kinetic study for CTC decay is analyzed in details. CTC degradation by PECO process could be described by pseudo-first order kinetics (Daghrir et al., 2013), as follow:

Équation 8-1 $$-\frac{d[C]}{dt} = k_{PECO}\, C$$

The integration of equation 8.1 gives:

Équation 8-2 $$\ln\frac{C_0}{C} = k_{PECO}\, t$$

Where C_0 is the initial CTC concentration, C is the concentration of CTC at time t, k_{PECO} is the apparent kinetic constant (min^{-1}) and t is the reaction time. The reaction rate constant "k_{PECO}" could be calculated from the slope value of the plot (t) versus $Ln(C_0/C)$ of Equation 8.2.

Higher correlation coefficient (R^2 = 0.97) was obtained from the pseudo-first order kinetic model. The reaction rate constant k_{PECO} for CTC degradation was 32.1 10^{-3} min^{-1}. It is interesting to compare the constant rate of CTC degradation under visible irradiation with those obtained under different experimental conditions. Daghrir et al. (2013) indicated that the

photoelectrocatalytic degradation of CTC on TiO_2 nanostructured electrodes ($[CTC]_0$ = 32.1μg L^{-1}; 0.39 A of current intensity; 6.9mW cm^{-2} of UV light intensity and 120 min of treatment times) is well described by the pseudo-first order kinetic model. The corresponding kinetic rate constant recorded under these conditions was 23.0 10^{-3} min^{-1}. This apparent reaction constant value is 1.4 times lower than this recorded in the present study (32.1 10^{-3} min^{-1}). The same trend has been also obtained by Peng et al. (2012) while studying the photoelectrocatalytic degradation of methyl orange using N-doped TiO_2 thin film as photoanode. The corresponding kinetic rate constant was 137.4 10^{-3} min^{-1}. The reaction rate of methyl orange was 4.2 times greater than that CTC. The difference may be due to the higher external potential applied while treating the methyl orange (2.0 V). Greater external potential applied during the photoelectrocatalytic treatment could enhance the separation of photo-generated electrons and holes which promote higher oxidation reactions of pollutant (Peng et al., 2012).

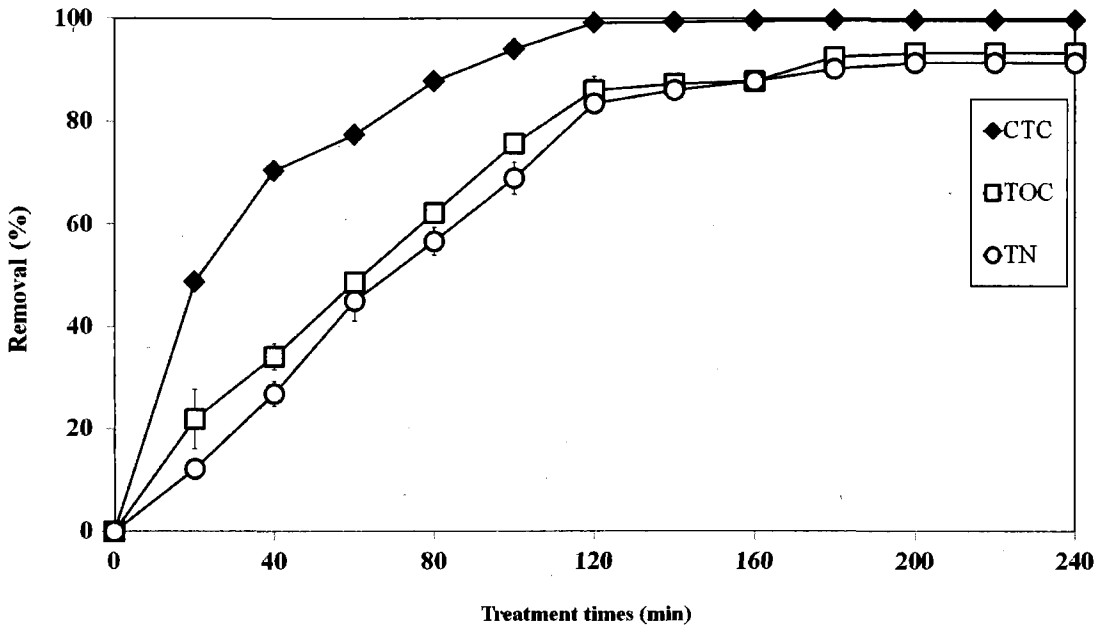


Figure 8-7 Effect of treatment time on CTC degradation and mineralization using PECO process (N-doped TiO_2 photoanode with a N content of 3.4 at.%; Current intensity = 0.6 A; $[CTC]^\circ = 100\ \mu g\ L^{-1}$).

8.5.5 By-products identification and proposed mechanism of CTC degradation

Our intention is to follow the formation of some by-products and possibly identify chemical structures while treating synthetic solution of CTC under visible irradiation. The photoelectrocatalytic cell was operated under the following conditions: 3.4 at.% N-doped TiO_2 photoanode at 0.6 A of current intensity under visible light during 180 min of treatment time. Based on the found primary intermediates, reaction pathways of the CTC degradation can be proposed (Figure 8-8).

The CTC by-products were identified on the basis of their mass spectra using LC/MS/MS analysis. The product ion at m/z 462 were obtained from the precursor ions m/z 479 (CTC) corresponding to Iso-CTC. Under alkaline conditions, the bond between C_6 and C_{11a} atoms could be catalyzed at the surface of TiO_2 to yield Iso-CTC (Daghrir et al., 2013). Besides, N-

dedismethyl-CTC (N-DDM-CTC, m/z = 467.15) is a by-product of CTC formed by a loss of two methyl groups from the dimethylamine moiety at the C4 position of CTC. The product ion m/z 495.19 was the intermediate product of m/z 467.15. The dechlorination of N-DDM-CTC results in the formation of N-dedismethyl TC (N-DDM-TC). During the photoelectrocatalytic reactions, hydroxyl radicals (OH°) are the most important oxidizing species which can eventually attack and transform the organic molecules to inorganic micro molecule (Kaneco et al., 2004; Bu and Zhuang, 2013). The scission of the amino group from alkyl amine at the C2 and C4 position of N-DDM-TC via hydroxyl radical promotes the formation of ammonia (NH_3). The cleavage of the amino group at the C2 and C4 position of N-DDM-TC forms carboxylic acid and ketone group, respectively.

Furthermore, the attack of OH° radicals may produce bicyclic and tricyclic aromatics intermediates. These intermediates are further oxidized through ring rupturing reaction into aliphatic compounds containing formic acid, acetic acid, methyl acetate and acetaldehyde, which subsequently oxidized into water and carbon dioxide (Bu and Zhuang, 2013).

Moreover, the photocatalytic oxidation of ammonia on the surface of the N-doped TiO_2 photoanode takes places through parallel and consecutive reaction steps leading to the formation of different products. The photoelectrocatalytic oxidation of ammonia into nitrate occurs through a series of consecutive reactions. The interaction of ammonia with a higher number of holes (h^+) created at the valence band of TiO_2 promotes the formation of nitrate (Murgia et al., 2005). Nitrite anions are the intermediates species detected during the oxidation reactions (Altomare and Selli, 2013). Another possible pathway for the oxidation of ammonia would be the reaction with hydroxyl radical (or photo-generated holes) to form $(NH_2)_x$ radical species (hydroxylamine and/or hydrazine), which are subsequently transformed into N_2 through their diffusion and recombination with other nitrogen-containing species (Altomare and Selli, 2013; Kolinko and Kozlov, 2009).

Finally, the photoelectrocatalytic treatment costs of CTC (including chemical consumption and energy consumption) recorded was estimated to \$5.71 ±0.01 m^{-3}.

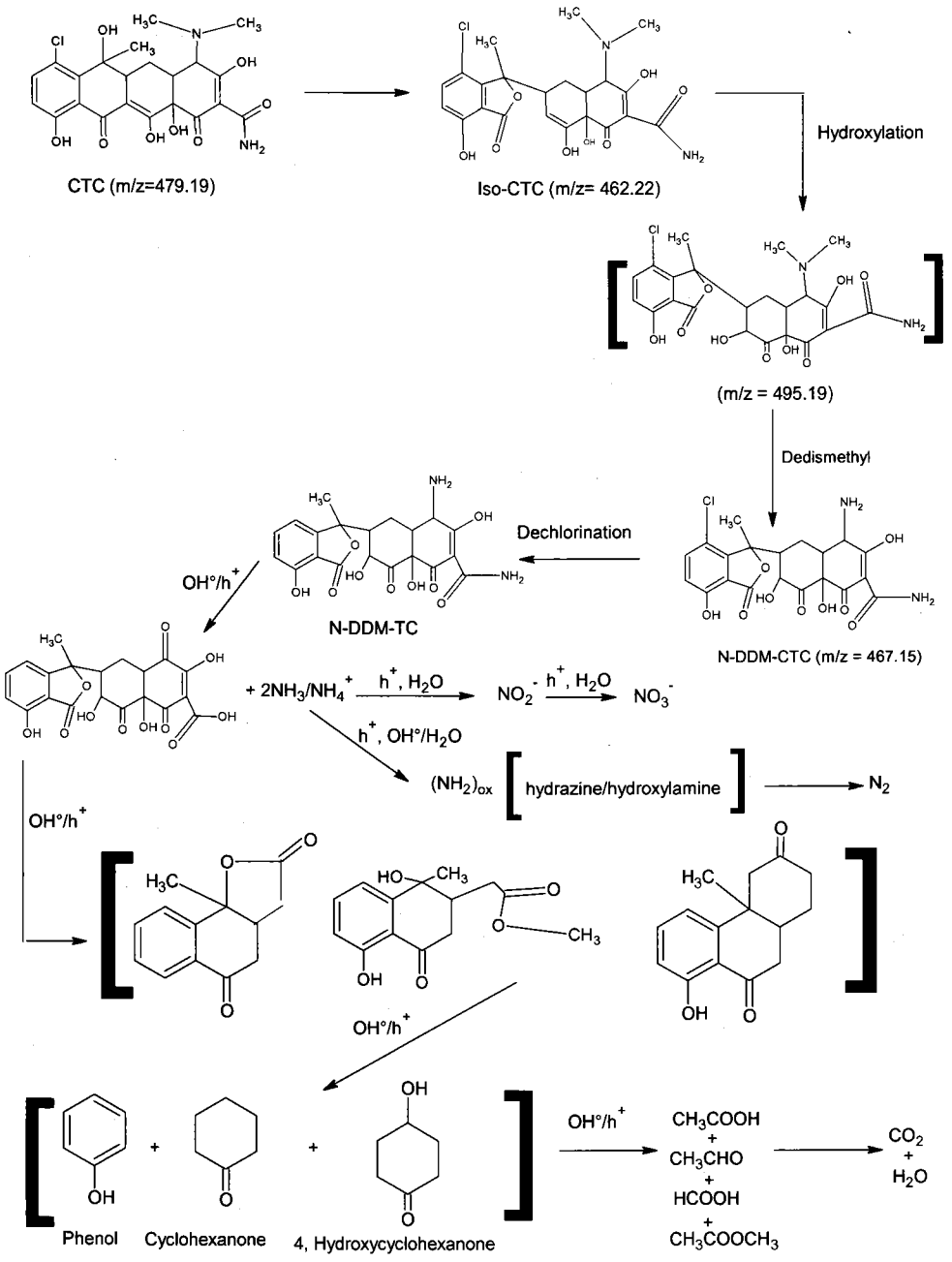


Figure 8-8 Proposed photoelectrocatalytic degradation pathways of CTC under visible irradiation using 3.4 at.% N-doped TiO_2 photoanode.

8.6 Conclusion

In this study, the N-doped TiO_2 film was prepared by means of a radiofrequency magnetron sputtering process. The N-doped TiO_2 consist of nanostructured anatase phase with average TiO_2 nanocrystallite size of 29 nm. The nitrogen doping of the TiO_2 films increases their absorption component in the visible (from ~380 nm to ~550 nm). The investigation of the photoelectrocatalytic oxidation process on the CTC degradation shows that N content doped TiO_2 photoanode, current intensity and treatment time influence the degradation efficiency of CTC. Using the optimal N-doped photoanode at a current intensity of 0.6 A and during 180 min of treatment time ensures a higher oxidation (99.6%) and a higher mineralization of CTC (92.5% ±0.26 % of TOC removal and 90.3%±1.1% of TN removal). During the treatment, CTC was mainly transformed into CO_2 and H_2O.

8.7 Acknowledgments

The authors would like to acknowledge the financial support of the National Sciences and Engineering Research Council (NSERC) of Canada, Premier Tech Ltee, and the PSR-SIIRI Program of the MDEIE Ministry of Quebec.

8.8 References

Altomare M & Selli E (2013) Effects of metal nanoparticles deposition on the photocatalytic oxidation of ammonia in TiO_2 aqueous suspensions. *Catal.Today* 209:127-133.

Ananapattarachai J, Kajitvichyanukul P & Seraphin S (2009) Visible light absorption ability and photocatalytic oxidation activity of various interstitial N-doped TiO_2 prepared from different nitrogen dopants. *J Hazard. Mater.*168: 253-261.

Ao Y, Xu J, Fu D & Yuan C (2009) A simple method to prepare N-doped titania hollow spheres with high photocatalytic activity under visible light. *J. Hazard.Mater.*167: 413-417.

Asahi R, Morikawa T, Ohwaki T, Aoki K & Taga Y (2001) Visible light photocatalysis in nitrogen-doped titanium oxides. *Science* 293 (5528): 269-271.

Bu D & Zhuang H (2013) Biotemplated synthesis of high specific surface area copper-doped hollow spherical titania and its photocatalytic research for degradating chlorotetracycline. *App. Surf. Sci.* 265: 677-685.

Burda C, Lou Y, Chen X, Samia ACS, Stout J & Gole JL (2003) Enhanced nitrogen doping in TiO_2 nanoparticles. *Nano Lett.* 3: 1049-1051.

Brassard D, Sarkar DK, El Khakani MA & Ouellet L (2006) Compositional effect on the dielectric properties of high-k titanium silicate thin films deposited by means of a co-sputtering process. *J. Vac. Sci & Technol.A* 24: 600-605.

Carp O, Huisman C & Reller A (2004) Photoinduced reactivity of titanium dioxide. *Prog. Solid State Ch.* 32: 33–177.

Chai S, Zhao G, Zhang Yn, Wang Y, Nong F, Li M & Li D (2012) Selective photoelectrocatalytic degradation of recalcitrant contaminant driven by an n-P

Heterojunction Nanoelectrode with Molecular Recognition Ability. *Environ. Sci. & Technol.* 46: 10182-10190.

Chen D, Jiang Z, Geng J, Wang Q & Yang D (2007) Carbon and nitrogen Co-doped TiO_2 with enhanced visible light photocatalytic activity. *Ind. Eng. Chem. Res.* 46: 2741-2746.

Cheng X, Yu X, Xing Z (2013) Enhanced photoelectric property and visible activity of nitrogen doped TiO_2 synthesized from different nitrogen dopants. *App. Surf. Sci.* 268: 204-208.

Chenxi W, Spongberg AL & Witter JD (2008) Determination of the persistence of pharmaceuticals in biosolids using liquid-chromatography tandem mass spectrometry. *Chemosphere* 73: 511-518.

Choi KJ, Kim SG & Kim SH (2008) Removal of antibiotics by coagulation and granular activated carbon filtration. *J Hazard. Mater.* 151, 38–43.

Choi H, Antoniou MG, Pelaez M, De La Cruz, AA, Shoemaker JA & Dionysiou DD (2007) Mesoporous Nitrogen-Doped TiO_2 for the photocatalytic destruction of the Cyanobacterial toxin Microcystin-LR under visible light irradiation. *Environ.Sci. Technol.* 41:7530-7535.

Daghrir R, Drogui P, El Khakani MA (2013) Photoelectrocatalytic oxidation of chlortetracycline using Ti/TiO_2 photo-anode with simultaneous H_2O_2 production. Electrochim. Acta 87: 18-31.

Daghrir R, Drogui P, Ka I & El Khakani MA (2012) Photoelectrocatalytic degradation of chlortetracycline using Ti/TiO_2 nanostructured electrodes deposited by means of a pulsed Laser deposition process. *J. Hazard.Mater.* 199–200: 15-24.

Daghrir R, Drogui P & Didier R (2012) Photoelectrocatalytic technologies for environmental applications. *J.photochem.photobiol. A.* 238: 41-52.

Daskalaki VM, Fulgione I, Frontistis Z, Rizzo L & Mantzavinos D (2012) Solar light-induced photoelectrocatalytic degradation of bisphenol-A on TiO_2/ITO film anode and BDD cathode. *Catal.Today* 209:74-78.

Ding Y, Yang C, Zhu L & Zhang J (2010) Photoelectrochemical activity of liquid phase deposited TiO_2 film for degradation of benzotriazole. *J Hazard.Mater.*175: 96–103.

Frontistis Z, Daskalaki VM, Katsaounis A, Poulios I & Mantzavinos D (2011) Electrochemical enhancement of solar photocatalysis: Degradation of endocrine distruptor bisphenol A on Ti/TiO_2 films. *Water Res.* 45: 2996-3004.

Gao P, Ding Y, Li H & Xagoraraki I (2012) Occurrence of pharmaceuticals in a municipal wastewater treatment plant: mass balance and removal processes. *Chemosphere* 88: 17-24.

Guinier A (1962) Théorie et Technique de la radiocristallographie, 3rd ed., Dunod, Paris, 740p.

Guo RX & Chen JQ (2012) Phytoplankton toxicity of the antibiotic chlortetracycline and its UV light degradation products. *Chemosphere* 87: 1254-1259.

Hajjaji A, Gaidi M, Bessais B & El Khakani MA (2011) Effect of Cr incorporation on the structural and optoelectronic properties of TiO_2: Cr deposited by means of a magnetron co-sputtering process. *App.Surf. Sci.* 257: 10351-10357.

Han L, Xin Y, Liu H, Ma X & Tang G (2010) Photoelectrocatalytic properties of nitrogen doped TiO_2/Ti photoelectrode prepared by plasma based ion implantation under visible light. *J. Hazard. Mater.* 175: 524-531.

Homem V & Santos L (2011) Degradation and removal methods of antibiotics from aqueous matrices-A review. *J. Environ. Manage.* 92: 2304-2347.

Hou Y, Li X, Zhao Q, Chen G, Raston CL (2012) Role of Hydroxyl Radicals and Mechanism of *Escherichia coli* Inactivation on Ag/AgBr/TiO_2 Nanotube Array Electrode under Visible Light Irradiation. *Environ. Sci. Technol.* 46: 4042-4050.

Karthikeyan KG & Meyer MT (2006) Occurrence of antibiotics in wastewater treatment facilities in Wisconsin, USA. *Sci. Total Enviro.*361: 196–207.

Kaneco S, Rahman MA, Suzuki T, Katsumata H & Ohta K (2004) Optimization of solar photocatalytic degradation conditions of bisphenol A in water using titanium dioxide. *J. Photochem.Photobiol.A* 163, 419-424.

Kang IC, Zhang Q, Yin S, Sato T & Saito F (2008) Improvement in photocatalytic activity of TiO_2 under visible irradiation through addition of N-TiO_2. Environ. Sci. Technol.42: 3622-3626.

Kolinko PA & Kozlov DV (2009) Products distribution during the gas phase photocatalytic oxidation of ammonia over the various titania based photocatalysts. *App.Catal. B* 90: 126-131.

Kim TH, Kim SD, Kim HY, Lim SJ, Lee M & Yu S (2012) Degradation and toxicity assessment of sulfamethoxazole and chlortetracycline using electron beam, ozone and UV. *J.Hazard.Mater.*227-228: 237-242.

Kim CS, Kwon IM, Moon BK, Jeong JH, Choi BC, Kim JH, Choi H, Yi SS, Yoo DH, Hong, KS, Park JH & Lee HS (2007) Synthesis and particle size effect on the phase transformation of nanocrystalline TiO_2. *Mater. Sci. En. C* 27: 1343–1346.

Kim I, Yamashita N, Tanaka H (2009) Photodegradation of pharmaceuticals and personal care products during UV and UV/H_2O_2 treatments. *Chemosphere* 77: 518-525.

Kummerer K (2009) Antibiotics in the aquatic environment—a review-part I. *Chemosphere* 75: 417–434.

Kuo CY, Wu CH, Lin HY (2010) Photocatalytic degradation of bisphenol A in a visible light/TiO_2 system. *Desalination* 256: 37-42.

Lopez-Penalver JJ, Sanchez-Polo M, Gomez-Pacheco CV & Rivera-Utrilla J (2010) Photodegradation of tetracyclines in aqueous solution by using UV and UV/H_2O_2 oxidation processes. *J Chem. Technol. Biotechnol.* 85: 1325–1333.

Lin YH, Chiu TC, Hsueh HT & Chu H (2011) N-doped TiO_2 photo-catalyst for the degradation of 1, 2 dichloroethane under fluorescent light. *App. Surf. Sci.* 258: 1581-1586.

Liu Y, Gan X, Zhou B, Xiong B, Li J, Dong C, Bai J & Cai W (2009) Photoelectrocatalytic degradation of tetracycline by highly effective TiO_2 nanopore arrays electrode. *J. Hazard. Mater.* 171: 678-683.

Martinez-Huitle CA & Ferro S (2006) Electrochemical oxidation of organic pollutants for the wastewater treatment: direct and indirect processes. *Chem. Soc. Rev.* 35: 1324-1340.

Murgia SM, Poletti A, Selvaggi R (2005) Photocatalytic degradation of high ammonia concentration water solutions by TiO_2. *Annali di Chimica* 95: 1-9.

Neuman-Spallart M (2007) Aspects of Photocatalysis on Semiconductors: Photoelectrocatalysis. *Chimica Inter. J. Chem.* 61: 806–809.

Ohno T, Sarukawa K & Matsumura M (2001) Photocatalytic Activities of Pure Rutile Particles Isolated from TiO_2Powder by Dissolving the Anatase Component in HF Solution. *J. Phys.Chem. B.* 105: 2417–2420.

Ouyang J, Chang M & Li X (2012) CdS-sensitized ZnO nanorod arrays coated with TiO_2 layer for visible light photoelectrocatalysis. *J. Mater. Sci.* 47: 4187-4193.

Ozcan AS, Erdem B & Ozcan A (2004) Adsorption of Acid Blue 193 from aqueous solutions onto Na-bentonite and DTMA-bentonite. *J Colloid Inter. Sci.* 280, 44-54.

Park JH, Kim S, Bard AJ (2006) Novel Carbon-doped TiO_2 nanotube arrays with high aspect Ratios for efficient solar water splitting. *Nano Lett.* 6: 24-28.

Peng YP, Yassitepe E, Yeh YT, Ruzybayev I, Shah SI, Huang CP (2012) Photoelectrochemical degradation of azo dye over pulsed laser deposited nitrogen-doped TiO_2 thin film. *App.Catal. B.* 125: 465-472.

Qiang Z & Adams C (2004) Potentiometric determination of acid dissociation constants (pKa) for human and veterinary antibiotics. *Water Res.* 38: 2874-2890.

Ren W, Ai Z, Jia F, Zhang L, Fan X, Zou Z (2007) Low temperature preparation and visible light photocatalytic activity of mesoporous carbon-doped crystalline TiO_2. *App.Catal.B* 69: 138-144.

Sakatani Y, Grosso D, Nicole L, Boissière C, Soler-Illia G, Sanchez C (2006) Optimized photocatalytic activity of grid-like mesoporous TiO_2 films: effect of crystallinity, pore size distribution, and pore accessibility. *J. Mater. Chem.*16: 77-82.

Sarmah AK, Meyer MT, Boxall ABA (2006) A global perspective on the use, sales, exposure pathways, occurrence, fate and effects of veterinary antibiotics (VAs) in the environment. *Chemosphere* 65: 725–759.

Senthilnathan J, Philip L (2010) Photocatalytic degradation of lindane under UV and visible light using N-doped TiO_2. *Chem. Eng.J.*161: 83-92.

Spongberg AL, Witter JD (2008) Pharmaceutical compounds in the wastewater process stream in Northwest Ohio. *Sci. Total Environ.* 397, 148–157.

Tahir SS, Rauf N (2006) Removal of a cationic dye from aqueous solutions by adsorption onto bentonite clay. *Chemosphere* 63: 1842-1848.

Trenczek-Zajac A, Kowalski K, Zakrzewska K, Radecka M (2009) Nitrogen-doped titanium dioxide-Characterization of structural and optical properties. *Mater. Res. Bull.* 44: 1547-1552.

Tsai SJ, Cheng S (1997) Effect of TiO_2 crystalline structure in photocatalytic degradation of phenolic contaminants. *Catal. Today* 33: 227-237.

Valentin CD, Finazzi E, Pacchioni G, Selloni A, Livraghi S, Paganini, MC, Giamello E (2007) N-doped TiO_2: Theory and experiment. *Chem. Phys.* 339: 44-56.

Wang MC, Zhong WY, Chen JQ (2011) Effects of Chlortetracycline hydrochloride and its UV degradation products on growth of freshwater algae. *J Anhui Agricul. Sci.* 39: 4155-4157.

Wang H & Lewis JP (2005) Effects of dopant states on photoactivity in carbon-doped TiO_2. *J. Phys. Conden. Matt.* 17: L209-L213.

Wang WY, Yang ML & Ku Y(2010) Photoelectrocatalytic decomposition of dye in aqueous solution using Nafion as an electrolyte. *Chem. Eng.J.*165: 273-280.

Wu PG, Ma CH, Shang JK (2004) Effects of nitrogen doping on optical properties of TiO_2 thin films. *Appl. Phys. A.* 81: 1411-1417.

Wu D, Long M, Cai W, Chen C & Wu, Y (2010) Low temperature hydrothermal synthesis of N-doped TiO_2 photocatalyst with high visible light activity. J. Alloys Compd. 502: 289-294.

Yap PS, Lim T.T, Lim M & Srinivasan M (2010) Synthesis and characterization of nitrogen-doped TiO_2/AC composite for the adsorption-photocatalytic degradation of aqueous bisphenol-A using solar light. *Catal.Today* 151: 8-13.

Zhao L, Jiang Q & Lian J (2008) Visible-light photocatalytic activity of nitrogen-doped TiO_2 thin film prepared by pulsed laser deposition. *App. Surf. Sci.* 245: 4620-4625.

CHAPITRE 9

REMOVAL OF CHLORTETRACYCLINE FROM SPIKED MUNICIPAL WASTEWATER USING A PHOTOELECTROCATALYTIC PROCESS OPERATED UNDER SUNLIGHT IRRADIATIONS

Le chapitre 9 est constitué de l'article suivant :

Rimeh Daghrir, Patrick Drogui, Nazar Delegan, My Ali El Khakani, Removal of chlortetracycline from spiked municipal wastewater using a photoelectrocatalytic process operated under sunlight irradiations, accepted for publication in *Science of the Total Environment (STOTEN-D-13-01649R1).*

9. REMOVAL OF CHLORTETRACYCLINE FROM SPIKED MUNICIPAL WASTEWATER USING A PHOTOELECTROCATALYTIC PROCESS OPERATED UNDER SUNLIGHT IRRADIATIONS

9.1 Abstract

The degradation of chlortetracycline in synthetic solution and in municipal effluent was investigated using a photoelectrocatalytic oxidation process under visible irradiation. The N-doped TiO_2 used as photoanode with 3.4%at of nitrogen content was prepared by means of a radiofrequency magnetron sputtering (RF-MS) process. Under visible irradiation, higher photoelectrocatalytic removal efficiency of CTC was recorded using N-doped TiO_2 compared to the conventional electrochemical oxidation, direct photolysis and photocatalysis processes. The photoelectrocatalytic process operated at 0.6 A of current intensity during 180 min of treatment time promotes the degradation of 99.1 ± 0.1 % of CTC. Under these conditions, a removal rate of 85.4 ± 3.6%, 87.4 ± 3.1% and 55.7 ± 2.9 % of TOC, TN and NH_4^+ have been recorded. During the treatment, CTC was mainly transformed into CO_2 and H_2O. The process was also found to be effective in removing indicator of pathogens such as fecal coliform (log-inactivation was higher than 1.2 units).

9.2 Key words

Photoelectrocatalytic oxidation; Sunlight irradiation; Chlortetracycline, Municipal wastewater

9.3 Introduction

The discharge of antibiotics into the environment is one of the major and global public health issues that need urgent action. During their use, antibiotics cannot be absorbed or metabolized entirely in vivo and a significant fraction (from 30 to 90 %) is excreted in metabolite forms into the environment via urine and feces (Zhou et al., 2012; Hu et al., 2010; Bound and Voulvoulis, 2004). Residues of antibiotics, including chlortetracycline discharged from municipal wastewater treatment plants and agricultural runoff, are frequently detected in surface water, ground water et even drinking water (Li et al., 2011; Hernandez et al., 2007; Miao et al., 2004; Kolpin et al., 2002). By considering the risks of antibiotics in the ecosystem caused by their lower concentrations in aquatic environment, as well as the transfer and spread of antibiotics resistant genes among microorganisms, it is of great importance to develop efficient and cost effective treatment technologies for removal of such compounds (Zhang *et al.* 2009).

In order to treat effectively Chlortetracycline in wastewater or natural water (surface and ground water), a new category of treatment has been investigated corresponding to advanced oxidation processes (AOPs). Among AOPs, photoelectrocatalytic oxidation (PECO) technique combining photocatalytic and electrochemical process is very interesting due to its "green" aspect, its flexibility and its higher efficiency to completely eradicate these micro-pollutants including chlortetracycline (Daghrir et al., 2013). Owing to the external potential applied, the PECO process is able to retard the recombination of the electron/hole pairs (e^-_{CB}/h^+_{VB}) photo-generated on the surface of the catalyst and consequently to ensure higher efficiency in the degradation of pollutants (Frontistis et al., 2011; Daghrir et al., 2012; Liu et al., 2009).

Among the various semiconductors, titanium dioxide (TiO_2) is the prime photocatalytic candidate owing to its promising physical and chemical properties (Ouyang et al., 2012; Peng

et al., 2012). Due to its large band gap (3.0-3.2 eV), TiO_2 can only be activated under UV irradiation having a wavelength lower than 387 nm. Thus, only a small fraction of solar light (less than 5% of solar energy is emitted as UV irradiation) is actually photoconverted by pure TiO_2 (Ren et al., 2007). This major drawback limits the environmental application of TiO_2 at large scale. In order to avoid this inconvenient, research is now focused on to achieve high photocatalytic efficiency with TiO_2 under visible light (Rehman et al., 2009). Doping TiO_2 with anion such as nitrogen is one of the typical approaches that has been applied by several research works to extend the absorption spectra of the TiO_2 well into the visible spectrum (Ananapattarachai et al., 2009; Kang et al., 2008; Choi et al., 2007).

In this context, it could be interesting to use the N-doped TiO_2 photoanode in the photoelectrocatalytic oxidation process in order to remove CTC from MWW under visible irradiation. The main objective of this study is to develop at the laboratory scale a photoelectrocatalytic oxidation process using N-doped TiO_2 photoanode deposited by means of a magnetron sputtering process and to evaluate its performance in treating MWW contaminated by CTC in batch recirculation mode under solar irradiation (1.5 AM).

9.4 Materials and methods

9.4.1 Preparation of the synthetic solution

Analytical grade chlortetracycline hydrochloride (CTC, $C_{22}H_{24}Cl_2N_2O_8$) (purity 78%) was acquired from Sigma-Aldrich. CTC stock solution was prepared in deionized water at 1 mg L^{-1} and kept at 4°C. Synthetic solution of CTC was made by diluting the CTC stock solution in deionized water. Final concentration of CTC was 100 µg L^{-1}. In order to increase the electrical conductivity in the solution, 0.07 mol L^{-1} of sodium sulfate was added.

9.4.2 Wastewater CTC-spiking

The municipal wastewaters (MWW) used throughout this study was an effluent provided from Quebec Urban Community (CUQ) wastewater treatment plant (WTP, Beauport, Quebec city, Quebec, Canada). It is a conventional WTP having a physicochemical pre-treatment followed by a bio-filtration process. The effluents were sampled at the outlet of the bio-filtration unit. Samples were collected and stored in polypropylene bottles and kept at 4°C until use. The treated-effluent had an initial content of COD of 56.7 ± 9 mg L^{-1}, TOC of 16.5 ± 1.2 mg L^{-1}, TN of 17.9 ± 2.2 mg L^{-1}, fecal coliform of 1900 ± 565 UFC/100 mL, ammonia of 10.5 ± 0.3 mg L^{-1}, pH of 6.9 ± 0.18 and conductivity of 1018 ± 12 µs cm^{-1}. In view of testing the photoelectrocatalytic oxidation process on real effluent containing refractory organic pollutants (refractory COD) and to simulate CTC contamination, wastewater samples were enriched with CTC (100 µg L^{-1}). Mixing and stirring time of 10 min was required to completely dissolve CTC prior to the photoelectrochemical treatment.

9.4.3 Photoelectrocatalytic cell

The photoelectrocatalytic cell used was 1 L of capacity and was made of PVC material with a dimension of 13 cm (depth) x 10 cm (width) x 10 cm (length). The photoelectrocatalytic reactor was comprised of two parallel pieces of vitreous carbon plates (6 cm height x 4 cm width) each, having a surface area of 24 cm^2 and situated 6 cm apart. The vitreous carbon plates were used as cathode electrodes. The photoanode consists of Ti expanded grid coated with the TiO_2 coating (either undoped or N-doped) was horizontally installed between the two vertically installed cathodes. The photoanode was prepared by depositing N-doped TiO_2 coatings onto Ti metallic grids by means of a radiofrequency magnetron sputtering (MS) process, which permits their *in-situ* doping through the incorporation of nitrogen (N) gas with the argon (Ar) during the sputtering process. The nitrogen content of the N-doped TiO_2 coatings was controlled by adjusting the $[N_2]/([Ar]+[N_2])$ gas flow ratio during the sputter-

deposition process, while keeping the total pressure at 1.4 mTorr in the deposition chamber. Thus, N-doped TiO_2 photoanode with N contents of 3.4 at.% has been successfully achieved. More experimental details on our MS system can be found elsewhere (Brassard et al., 2006; Hajjaji et al., 2011). The dimensions of the anode are 6 cm height x 4 cm width. The electrodes were installed on a perforated Plexiglas plate placed at 2 cm from the bottom of the cell.

9.4.4 Experimental setup

The essays were carried out in a closed loop as depicted schematically in Figure 9-1. A 0.6 L of PVC tank (1), a peristaltic recycling pump (2) and the photoelectrocatalytic cell (3) constitute the loop. All the essays were conducted in batch recirculation mode with a flow of effluent entering the bottom of the cell. A recycle flow rate of 0.25 L min^{-1} was maintained using a peristaltic recycling pump (Master flex, Model 77200-50, USA). The photoelectrocatalytic cell was operated under galvanostatic conditions, with 0.6 A of current intensity imposed during 180 min of treatment period. Current intensity was imposed by means of DC power source, PS 3030 D, Circuit-Test Electronics (Burnaby, BC, Canada) with a maximum current rating of 3.0 A at an open circuit potential of 30 V. The photo-anode (undoped Ti/TiO_2 or N-doped Ti/TiO_2) was illuminated under visible irradiation using a solar simulator model SS50AAA (Photo emission Tech., INC, Camarillo, USA) equipped with a 150 W xenon lamp. All experiments were carried out under AM 1.5 solar illumination conditions. For all tests, a total volume of 0.6 L was used.

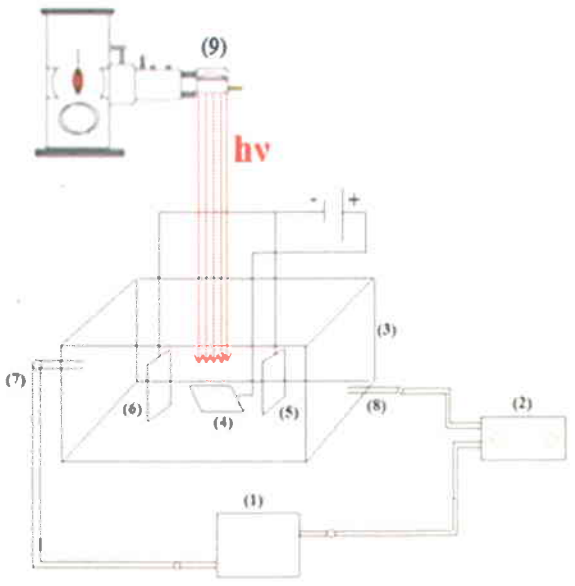


Figure 9-1 **Schematic diagram of the experimental setup: (1) PVC tank, (2) peristaltic recycling pump, (3) photoelectrocatalytic reactor, (4) N-doped TiO_2 photocatalyst, (5) and (6) vitreous carbon, (7) in let, (8) out let, (9) Solar simulator.**

9.4.5 Experimental procedure

A preliminary investigation was conducted to compare the removal efficiencies of CTC using direct photolysis (DP), electrooxidation (EO), photocatalysis (PC) and photoelectrocatalytic oxidation (PECO) processes. DP process consists in exposing CTC solution to visible irradiation in the absence of catalyst. PC process combined visible irradiations and N-doped TiO_2 photocatalyst (or undoped TiO_2). EO process was carried using N-doped TiO_2 as anode electrode without visible irradiations. PECO process consists in treating the effluent using N-doped TiO_2 (or undoped TiO_2) photoanode and connected to a DC power source (to apply an external potential) under visible irradiation. The effectiveness of each process was evaluated

using the synthetic CTC solution (100 μg L^{-1}). In order to increase the electrical conductivity in the solution, 0.07 mol L^{-1} of sodium sulfate was added. Experiments were carried out over 180 min. During these assays, only the residual CTC, TOC and TN concentrations were measured.

Subsequently, MWW was artificially contaminated by CTC (100 μg L^{-1}) and subjected to treatment using PECO process operated at 0.6 A of current intensity during 180 min of electrolysis times. During these assays, the effectiveness of the process was evaluated by measuring the residual CTC, TOC, COD, TN, NH_4^+, nitrite, nitrate and fecal coliform concentrations.

9.4.6 Analytical technique

The pH was determined using a pH-meter (Fisher Acumet model 915) equipped with a double junction Cole-Palmer electrode with Ag/AgCl reference cell. A conductivity meter (Oakton Model 510) was used to determine the ionic conductivity of the effluent. COD determination was measured based on APHA (1999) and a reading spectrophotometer UV 0811 M136 (Varian, Australia). TN and TOC measurements were performed using a Shimadzu TOC 5000A analyzer (Shimadzu Scientific Instruments Inc) equipped with an autosampler. Ammonium nitrogen, phosphate ions, nitrites and nitrates were measured using Lachat analyzer (Model FIA, Zellweger Analytics, Lachat Instrument Division, WI., USA). Analysis of fecal coliform was carried out in duplicate by Bodycote Laboratory (Quebec, Qc, Canada). The progress of the photoelectrocatalytic degradation of CTC was monitored and quantified by LC/MS/MS (Thermo TSQ Quantum Access). The chromatographic column used was Beta Basic C18, particle size 3 μm and 2.1 x 100 mm inner diameter. The mobile phase consisted of a mixture of 0.1% formic acid in water (v/v) (component A) and 0.1% formic acid in acetonitrile (component B). A gradient elution program at a 0.2 mL min^{-1} flow rate was used to achieve the separation. The program begins with an isocratic step at 90% A and 10% B for

2 min followed by a linear elution gradient from 90% to 30% A and from 10% to 70% B in 10 min more, and returned to initial condition. 18.5 min were waited between injections. Mass spectral data shown in this study were acquired on a LCQ Duo ion trap tandem mass spectrometry equipped with an electrospray ionization (ESI) source operated in positive ion mode. Nitrogen was used as a sheath and auxiliary gas. Working conditions were as followed: spray voltage was 5000 V and capillary temperature was 345°C. Quantitative analysis of CTC was determined using sulfamethazine C13 as internal standard.

9.4.7 Economics

Evaluation of operation costs related to the photoelectrocatalytic treatment process included energy consumption. The energy consumed was estimated at a cost of 0.06 US$ kWh^{-1}, which corresponded to the cost in the province of Quebec (Canada). The total cost was evaluated in terms of U.S. dollars spent per cubic meter of treated solution (US$ m^{-3}).

9.5 Results and discussions

9.5.1 Preliminary investigations of CTC degradation

The effectiveness of the different processes was evaluated by measuring simultaneously the residual concentrations of TN, TOC and CTC (Table 9-1). As it is observed from these data, higher degradation rate of CTC has been recorded after 180 min of treatment time. The CTC removal rate recorded in the solution using the DP process was 40.7 %±1.6%, whereas the TOC and TN removal rates were 21.4 ± 2.1% and 29.6 ±1.8%, respectively. In this case, the decomposition of CTC is caused by the artificial sunlight from solar simulator. Under sunlight irradiation, powerful oxygen species such as H_2O_2 and OH° could be generated in water (Vialaton and Richard, 2002; Vaughan and Blough, 1998). Furthermore, the degradation rate of CTC increased when the PC process was applied in the presence of N-doped TiO_2 photocatalyst. For instance, after 180 min of treatment time, a CTC removal rate of

81.3±1.0 % was recorded. Likewise, 60.7 % ± 1.9 % of TOC and 59.3 % ± 2.8% of TN were simultaneously removed. However, the CTC degradation rate decreased to 59.4 ± 2.2% when the undoped TiO_2 photocatalyst was used in the PC process. Indeed, nitrogen doping TiO_2 narrows the band gap of the photo-catalyst from 3.2 eV to 2.3 eV and shifts its optical response to the visible light region. The localized mid-gap state above the top of the valence band is responsible to increase the photoactivity of TiO_2 in visible region (Zhang et al. 2010; Cheng et al. 2013). Under visible illumination, the nitrogen ions doping TiO_2 can act as electron traps facilitating the separation of photo-generated carriers (e^-/h^+), which can undergo redox reactions with substrate (Ilieva et al., 2012).

The degradation rate of CTC using the EO process operated at a current intensity of 0.6 A was also tested. After 180 min of treatment time, the degradation rate of CTC was 62.7 ± 2.3%. Likewise, 41.0 ± 1.0 % of TOC and 44.5 ± 1.8% of TN were simultaneously recorded using EO process. By comparison, higher degradation efficiency of CTC (99.6%) was recorded using the PECO process in the presence of N-doped TiO_2 photoanode and operated at 0.6 A of current intensity. In addition, higher mineralization rate was recorded. Within the same irradiation time, the degradation rate of TOC reached 92.5 ± 0.26 %, whereas the degradation rate of TN was 90.3 ± 1.1%. However, using the undoped TiO_2 photoanode in the PECO process, only 78.5 ± 0.2% of CTC removal rate was recorded (in comparison to 99.6% measured for the doped TiO_2 photoanode). The enhanced PECO activity using N-doped TiO_2 photoanode is a consequence of the narrower band-gap. The narrower is the band-gap, the higher is number of harvested visible photons that lead to a higher number of photogenerated excitonst (Peng et al., 2012; Wu et al., 2010; Ao et al., 2009; Trenczek-Zajac et al., 2009). The external potential applied in the PECO process is also a key factor that improves the degradation efficiency of pollutants (Daghrir et al., 2012). The PECO technique combining electrochemical oxidation and photocatalysis processes promotes the separation between the

electrons and holes photo-generated which participate in the redox reactions and lead to enhance the photocatalytic activity (Daghrir et al., 2013). This trend has been also recorded by Peng and his co-workers (2012) while treating the methyl orange as an azo dye using N-doped TiO_2 photocatalyst. The complete removal of 1.0 mg L^{-1} of methyl orange was observed after 40 min using photoelectrocatalytic process, while only 5.1%, 14.9 % and 36.3 % of the methyl orange removal was achieved by the DP, EO and PC processes, respectively. The application of PECO process provided the most powerful way to degrade pollutants owing to the synergetic effect by combining EO and PC processes (Zhao et al. 2006; Peng et al. 2012).

Tableau 9-1 Different processes used for CTC degradation

Parameters	Values	Processes					
		DP	EO	PC		PECO	
		Test 1	Test 2	Test 3	Test 4	Test 5	Test 6
Photo-catalyst	Undoped-TiO_2			✓		✓	
	3.4 at% N-Doped TiO_2		✓		✓		✓
Cathode	VC					✓	✓
Current intensity (A)	0.6					✓	✓
Visible irradiation	Solar simulator	✓		✓	✓	✓	✓
Treatment time (min)	180	✓	✓	✓	✓	✓	✓
Initial CTC concentrations ($\mu g\ L^{-1}$)	100	✓	✓	✓	✓	✓	✓
Electrolyte (Na_2SO_4) ($mol\ L^{-1}$)	0.07		✓			✓	✓
Initial pH		6.86±0.10	6.86±0.10	6.86±0.10	6.86±0.10	6.86±0.10	6.86±0.10
Final pH		5.89±0.30	7.39±0.20	7.32±0.10	7.86±0.32	7.41±0.10	7.56±0.30
TN initial ($mg\ L^{-1}$)		0.54±0.01	0.54±0.01	0.54±0.10	0.54±0.01	0.54±0.01	0.54±0.01
TN final ($mg\ L^{-1}$)		0.38±0.01	0.30±0.01	0.36±0.01	0.22±0.01	0.19±0.01	0.05±0.01
TOC initial ($mg\ L^{-1}$)		2.8±0.10	2.8±0.10	2.8±0.10	2.8±0.10	2.8±0.10	2.8±0.10
TOC final ($mg\ L^{-1}$)		2.2±0.05	1.65±0.03	1.9±0.02	1.1±0.01	1.2±0.0	0.20 ±0.01
CTC removal (%)		42.8±1.6	62.7±2.3	59.4±2.2	81.3±1.0	78.5±0.2	99.6±0.0

DP Direct photolysis; EO: electrooxidation; PC: photocatalysis; PECO: photoelectrocatalytic oxidation

9.5.2 Photoelectrocatalytic treatment of MWW contaminated by CTC

The effectiveness of the photoelectrocatalytic cell in treating wastewater effluent contaminated by CTC (around 100 $\mu g\ L^{-1}$) was evaluated at a current intensity of 0.6 A during 180 min of treatment time using N-doped TiO_2 as photoanode and vitreous carbon as cathode. The objective was to test the effectiveness of the photoelectrocatalytic cell as tertiary treatment to remove CTC in the presence of other types of organic, inorganic and microbial pollutants. It was important to determine whether the results of these tests are reproducible or not. For that, the experiments were repeated in triplicate to verify the effectiveness and reproducibility of PECO performance in treating municipal wastewater effluent contaminated by CTC. The variation of CTC, TN, TOC, NO_2^-/NO_3^- and NH_4^+ as a function of treatment time is shown in Figure 9-2. The increase of treatment time from 30 min to 180 min promotes the degradation of CTC from $61.1 \pm 2.0\%$ to $99.1 \pm 0.1\%$, respectively. Moreover, the removal of TOC and TN reached $85.4 \pm 3.6\%$ and $87.4 \pm 3.1\%$, respectively, after 180 min of treatment time. The relatively higher yield of TOC removal indicated that the major fraction of organic compounds was completely oxidized into water and carbon dioxide. Thus, it is clear that 180 min of photoelectrocatalytic treatment is required to produce sufficient amount of reactive oxygen species for CTC oxidation. Furthermore, the removal rate of NH_4^+ and NO_2^-/NO_3^- reached $55.7 \pm 2.9\ \%$ and $71.1\% \pm 3.1\%$, respectively. The oxidation of NH_4^+ on the surface of N-doped TiO_2 photoanode into nitrate occurs through a series of consecutive reactions. A higher number of holes (h^+) created at the valence band of TiO_2 promote the oxidation of NH_4^+ into NO_3^- (Murgia et al., 2005). Nitrite anions are the intermediates species detected during ammonia oxidation (Altomare and Selli, 2013). Another possible pathway for the oxidation of NH_4^+ would be the reaction with OH° (or with photo-generated holes) to form $(NH_2)_x$ radical species (hydroxylamine and/or hydrazine), which are subsequently transformed into N_2 through their diffusion and recombination with other nitrogen-containing

species (Altomare and Selli, 2013; Kolinko and Kozlov, 2009). On the other hand, higher removal efficiency of COD (97.5 ± 1.2%) and fecal coliforms (94.8%; log-inactivation >1.2-log units) has been recorded after 180 min of treatment. Thereby, PECO technique could be the basis of a tertiary treatment process of wastewater able to upgrade water quality by providing both high disinfection and removal of persistent organic compounds. Finally, the photoelectrocatalytic treatment cost (including only energy consumption) was estimated to $\$4.17 \pm 0.01\ m^{-3}$.

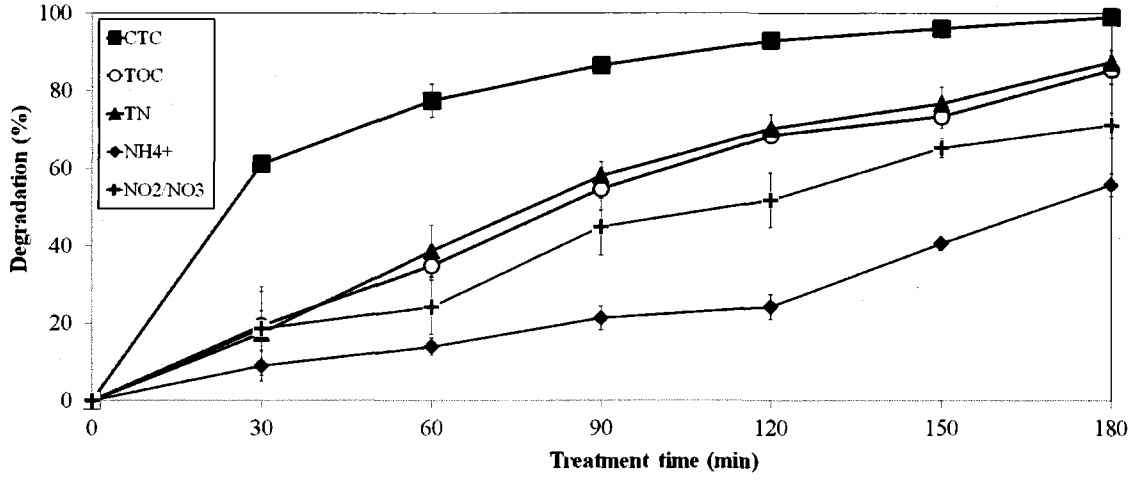


Figure 9-2 Photoelectrocatalytic treatment of municipal wastewater contaminated by CTC under visible irradiation ([CTC]° = 100 µg L^{-1}; [TOC]° = 18.7±1.2 mg L^{-1}; [TN]° = 19.8±2.1 mg L^{-1}; [NH_4^+]° = 12.7±0.5 mg L^{-1}; [NO_2^-+NO_3^-]° = 1.68 ± 0.05 mg L^{-1}).

9.6 Conclusion

This study investigated the treatment of MWW contaminated by CTC in batch recirculation mode using a photoelectrocatalytic cell. High treatment efficiency of CTC was achieved by the PECO process (99.6%) compared to the conventional electrochemical oxidation, direct photolysis and photocatalysis processes. The PECO process using N-doped TiO_2 photoanode

is a feasible technology for the treatment of MWW contaminated by CTC. After 180 min of photoelectrocatalytic treatment, the removal efficiency of CTC, TOC, TN and NH_4^+ recorded at 0.6 A of current intensity and using N-doped TiO_2 as photoanode were $99.1 \pm 0.1\%$, $85.4 \pm 3.6\%$ and $87.4 \pm 3.1\%$ and $55.7 \pm 2.9\%$, respectively. The PECO process was also found to be effective in removing fecal coliform (log-inactivation was higher than 1.2 units). The PECO process is a promising technology that can be used as tertiary treatment for disinfection and to remove emerging pollutants from MWW.

9.7 Acknowledgments

The authors would like to acknowledge the financial support of the National Sciences and Engineering Research Council (NSERC) of Canada, Premier Tech Ltee, and the PSR-SIIRI Program of the MDEIE Ministry of Quebec.

9.8 References

Altomare M & Selli E (2013) Effects of metal nanoparticles deposition on the photocatalytic oxidation of ammonia in TiO_2 aqueous suspensions. *Catal. Today* 209: 127-133.

Ananapattarachai J, Kajitvichyanukul P, Seraphin S (2009) Visible light absorption ability and photocatalytic oxidation activity of various interstitial N-doped TiO_2 prepared from different nitrogen dopants. *J Hazard. Mater.* 168: 253-261.

Ao Y, Xu J, Fu D, Yuan C (2009) A simple method to prepare N-doped titania hollow spheres with high photocatalytic activity under visible light. *J. Hazard.Mater.* 167: 413-417.

Bound JP & Voulvoulis N (2004) Pharmaceuticals in the aquatic environment-a comparison of risk assessment strategies. *Chemosphere* 56: 1143–1155.

Brassard D, Sarkar DK, El Khakani MA & Ouellet L (2006) Compositional effect on the dielectric properties of high-k titanium silicate thin films deposited by means of a co-sputtering process. *J. Vacu. Sci. Technol. A* 24: 600-605.

Cheng X, Yu X & Xing Z (2013) Enhanced photoelectric property and visible activity of nitrogen doped TiO_2 synthesized from different nitrogen dopants. *Appl. Surf. Sci.* 268: 204-208.

Choi H, Antoniou MG, Pelaez M, De La Cruz AA, Shoemaker JA, Dionysiou DD (2007) Mesoporous Nitrogen-Doped TiO_2 for the photocatalytic destruction of the Cyanobacterial toxin Microcystin-LR under visible light irradiation. *Environ. Sci. Technol.* 41: 7530-7535.

Daghrir R, Drogui P, El Khakani MA (2013) Photoelectrocatalytic oxidation of chlortetracycline using Ti/TiO_2 photo-anode with simultaneous H_2O_2 production. *Electrochim. Acta* 87: 18-31.

Daghrir R, Drogui P, Ka I & El Khakani MA (2012) Photoelectrocatalytic degradation of chlortetracycline using Ti/TiO_2 nanostructured electrodes deposited by means of a pulsed Laser deposition process. *J. Hazard.Mater.* 199–200: 15-24.

Frontistis Z, Daskalaki VM, Katsaounis A, Poulios I & Mantzavinos D (2011) Electrochemical enhancement of solar photocatalysis: Degradation of endocrine distruptor bisphenol A on Ti/TiO_2 films. *Water Res.* 45: 2996-3004.

Hajjaji A, Gaidi M, Bessais B, El Khakani MA (2011) Effect of Cr incorporation on the structural and optoelectronic propert ies of TiO_2: Cr deposited by means of a magnetron co-sputtering process. *Appl. Surf. Sci.* 25: 10351-10357.

Hernandez F, Sancho JV, Ibanez M, Guerrero C (2007) Antibiotic residue determination in environment waters by LC-MS. *TrACTrend Anal. Chem.* 26: 466–485.

Hu X, Zhou Q & Luo Y (2010) Occurrence and source analysis of typical veterinary antibiotics in manure, soil, vegetables and groundwater from organic vegetable bases, northern China. *Environ. Pollut.* 158: 2992–2998.

Ilieva M, Nakova A, Tsakova V (2012) TiO_2/WO_3 hybrid structures produced through a sacrificial polymer layer technique for pollutant photo-and photoelectrooxidation under ultraviolet and visible light illumination. *J. Appl. Electrochem.* 42: 121-129.

Kang IC, Zhang Q, Yin S, Sato T, Saito F (2008) Improvement in photocatalytic activity of TiO_2 under visible irradiation through addition of $N\text{-}TiO_2$. *Environ. Sci. Technol.* 42: 3622-3626.

Kolpin DW, Furlong ET, Meyer MT, Thurman EM, Zaugg SD, Barber LB & Buxton HT (2002) Pharmaceuticals, hormones, and other organic wastewater contaminants in U.S. streams, 1999-2000: A national reconnaissance. *Environ. Sci. Technol.* 36: 1202-1211.

Kolinko PA & Kozlov DV (2009) Products distribution during the gas phase photocatalytic oxidation of ammonia over the various titania based photocatalysts. *Appl. Catal. B.* 90: 126-131.

Li R, Zhang Y, Lee CC, Liu L & Huang Y (2011) Hydrauphilic interaction chromatography separation mechanisms of tetracyclines on amino-bonded silica column. *J. Sep. Sci.* 34: 1508–1516.

Liu Y, Gan X, Zhou B, Xiong B, Li J, Dong C, Bai J & Cai W (2009) Photoelectrocatalytic degradation of tetracycline by highly effective TiO_2 nanopore arrays electrode. *J Hazard.Mater.* 17: 678-683.

Miao X, Bishay F, Chen M & Metcalfe CD (2004) Occurrence of antimicrobials in the final effluents of wastewater treatment plants in Canada. *Environ. Sci. Technol.* 38: 3533-3541.

Murgia SM, Poletti A, Selvaggi R (2005) Photocatalytic degradation of high ammonia concentration water solutions by TiO_2. *Annali di Chimica* 95: 1-9.

Ouyang J, Chang M, Li X (2012) CdS-sensitized ZnO nanorod arrays coated with TiO_2 layer for visible light photoelectrocatalysis. *J. Mater. Sci.* 47: 4187-4193.

Peng YP, Yassitepe E, Yeh YT, Ruzybayev I, Shah SI, Huang CP (2012) Photoelectrochemical degradation of azo dye over pulsed laser deposited nitrogen-doped TiO_2 thin film. *Appl. Catal.B.* 125: 465-472.

Ren W, Ai Z, Jia F, Zhang L, Fan X & Zou Z (2007) Low temperature preparation and visible light photocatalytic activity of mesoporous carbon-doped crystalline TiO_2. *Appl.Catal. B.* 69: 138-144.

Rehman S, Ullah R, Butt AM & Gohar ND (2009) Strategies of making TiO2 and ZnO visible light active. *J. Hazard. Mater.* 170: 560-569.

Trenczek-Zajac A, Kowalski K, Zakrzewska K, Radecka M (2009) Nitrogen-doped titanium dioxide-Characterization of structural and optical properties. *Mater. Res. Bull.* 44: 1547-1552.

Vaughan P & Blough NV (1998) Photochemical formation of hydroxyl radical by constituents of natural waters. *Environ. Sci. Technol.* 32: 2947-2953.

Vialaton D & Richard C (2002) Phototransformation of aromatic pollutants in solar light: photolysis versus photosensitized reaction under natural water conditions. *Aquatic Sci.* 64: 207-215.

Wu D, Long M, Cai W, Chen C, Wu Y (2010) Low temperature hydrothermal synthesis of N-doped TiO_2 photocatalyst with high visible light activity. *J. Alloy. Compd.* 502: 289-294.

Zhang T, Zhang M, Zhang X & Fang HH (2009) Tetracycline resistance genes and tetracycline resistant lactose-fermenting enterobacteriaceae in activated sludge of sewage treatment plants. *Environ. Sci. Technol.* 438: 3455-3460.

Zhang J, Wu Y, Xing M, Khan Leghari SA, Sajjad S (2010) Development of modified N doped TiO_2 photocatalyst with metals, nonmetals and metal oxides. *Energy Environ. Sci.* 3: 715-726.

Zhao L, Jiang Q, Lian J (2008) Visible-light photocatalytic activity of nitrogen-doped TiO_2 thin film prepared by pulsed laser deposition. *Appl. Surf. Sci.* 245: 4620-4625.

Zhou Q, Zhang MC, Shuang CD, Li ZQ & Li AM (2012) Preparation of a novel magnetic powder resin for the rapid removal of tetracycline in the aquatic environment. *Chin. Chem. Lett.* 23: 745–748.

CHAPITRE 10

PHOTOELECTROCATALYTIC DEGRADATION OF CARBAMAZEPINE USING TI/TIO_2 NANOSTRUCTURED ELECTRODES DEPOSITED BY MEANS OF A PULSED LASER DEPOSITION PROCESS

Le chapitre 10 est constitué de l'article suivant :

Rimeh Daghrir, Patrick Drogui, Aicha Dimboukou-Mpira, My Ali El Khakani, Photoelectrocatalytic degradation of carbamazepine using Ti/TiO_2 nanostructured electrodes deposited by means of a pulsed Laser deposition process, *Chemosphere (Accepted)*.

10. PHOTOELECTROCATALYTIC DEGRADATION OF CARBAMAZEPINE USING TI/TiO_2 NANOSTRUCTURED ELECTRODES DEPOSITED BY MEANS OF A PULSED LASER DEPOSITION PROCESS

10.1 Abstract

The objective of the present work is to evaluate the potential of photoelectrocatalytic oxidation (PECO) process using Ti/TiO_2 for the degradation of carbamazepine (CBZ). Ti/TiO_2 prepared by Pulsed Laser Deposition (PLD) has been used as a photo-catalyst in a photoelectrocatalytic cell. The PLD TiO_2 coatings were found to be of anatase structure consisting of nanocrystallites of approximately 15 nm in diameter. Factorial and central composite design methodologies were successively employed to define the optimal operating conditions for CBZ degradation. Several factors such as current intensity, treatment time, pollutant concentration and cathode material were investigated. Using a 2^4 factorial matrix, the best performance for CBZ degradation (53.5 %) was obtained at a current intensity of 0.1 A during 120 min of treatment time and when the vitreous carbon (VC) was used at the cathode in the presence of 10 mg L^{-1} of CBZ. Treatment time and pollutant concentration were found to be very meaningful for CBZ removal. The PECO process applied under optimal conditions (at current intensity of 0.3 A during 120 min in the presence of 10 mg L^{-1} of CBZ with VC at the cathode) is able to oxidize around 73.5 % ± 2.8 % of CBZ and to ensure 21.2 % ± 7.7 % of mineralization. During PECO process, CBZ was mainly transformed to acridine and anthranilic acid. Microtox biotests (*Vibrio fisheri*) showed that the treated – effluent was not toxic. The pseudo-second order kinetic model (k_2 = 6 10^{-4} L mg^{-1} min^{-1}) described very well the oxidation of CBZ.

10.2 Keywords

Photoelectrocatalytic oxidation; Carbamazepine; Titanium dioxide; Vitreous carbon; Pulsed laser deposition.

10.3 Introduction

In recent years, the impact of toxic organic compounds called endocrine-disrupting compounds (EDC) in wastewater and their fate during wastewater treatment plants (WWTPs) is becoming an important environmental and health issues. Pharmaceutical products (PPs) found in the environment belong to this type of pollutants. The high consumption of these products leads to their accumulation in the aquatic environment (Marin-Diaz et al., 2009; Ching and Jin, 2012). Among the large number of registered PPs, carbamazepine (CBZ), *5H*-dibenzo[b, f] azepine-5-carboxamide, is an antiepileptic drug used as sedative (Chong et al., 2011; Scheytt et al., 2005). According to previous studies (Martinez et al., 2011; Prajapati et al., 2007; Vogna et al., 2004), CBZ is used to control seizures, to relieve chronic pain and to treat different psychiatric disorders. Due to the high consumption of CBZ throughout the world (1014 ton per year) (Zhang et al., 2008; Calisto et al., 2011), recent researches have demonstrated that the residual concentrations of CBZ are detected in different environmental matrices: surface water (Metcalfe et al., 2003; Ternes, 1998), ground water (Focazio et al., 2008; Lapworth et al., 2012), in WWTPs (Hummel et al., 2006; Bahlmann et al., 2009) and even in drinking water (Heberer et al., 2002). These occurrences of CBZ in aquatic environment are mainly due to the inappropriate treatment methods applied in WWTPs (Calisto et al., 2011). The removal efficiency of CBZ in WWTP is typically below 10 % (Zhang et al., 2008). The effect of CBZ on aquatic life including bacteria, algae, fish and invertebrates has been evaluated as dangerous (Ferrari et al., 2003). Due to their adverse effects, efficient treatment technology is highly desired in order to remove this pollution from aquatic environment.

Advanced oxidation processes (AOPs) have been proposed as alternative methods to remove many toxic and bio-recalcitrant compounds in wastewater (Chong et al., 2011; Laera et al., 2011; Saien and Khezrianjoo, 2008). Chemical oxidation process using UV/H_2O_2 has been

investigated by Vogna et al. (2004) to degrade CBZ. Other advanced treatment technologies such as ozonation, UV irradiation and adsorption using granular activated carbon (GAC) are found to be effective in removing CBZ (Ternes et al., 2002; Esplugas et al., 2007). In spite of the good oxidation of CBZ, the high chemical consumption of H_2O_2 or O_3 and the relatively high treatment costs constitute the major barriers for large scale applications (Martinez-Huitle and Ferro, 2006). Besides, adsorption using granular activated carbon (GAC) creates secondary pollution by transferring the pollutant from one phase (liquid phase) to another (solid phase) rather than being completely eliminated (Chong et al., 2004).

Over the last few years, photocatalytic (PC) process using TiO_2 photocatalyst under UV irradiations was found to be one of the most powerful techniques to remove recalcitrant organic pollutants (Chong and Jin, 2012). The conventional PC process consists of ejecting an electron from the valence band (VB) to the conduction band (CB) of the TiO_2 semi-conductor, thereby creating an "h^+" hole in the valence band. These charge carriers (e^-/h^+) can migrate to the surface of the catalyst, where they are then available to undergo redox reactions with substrates (Yang et al., 2009). However, the fast recombination of the photo-generated electron/hole (e^-/h^+) represents the major drawback of PC applications (Waldner et al., 2003). Recently, photoelectrocatalytic oxidation (PECO) technique combining both electrochemical and PC technologies has been finding increased use (Daghrir et al., 2012). In the photoelectrocatalytic process, applying an external potential prevents charge recombination, increases the lifetimes of the active holes and consequently increase the degradation efficiency of the organic compounds (Daghrir et al., 2012; Frontistis et al., 2011; Liu et al., 2009). Another interesting advantage of the PECO process could be the use of a cathode material, such as VC on which hydrogen peroxide (H_2O_2) can be electrochemically generated by cathodic reduction of dissolved oxygen (Xie and Li., 2006). Such an oxidant agent (H_2O_2)

is beneficial for PC reaction by trapping the conduction band electron in order to generate more hydroxyl radicals (Sohrabi and Ghavami, 2010).

The aim of the present study is to evaluate the potential of a PECO process using nanocrystalline TiO_2 photo-anodes prepared by means of a pulsed laser deposition (PLD) method for the treatment of waters contaminated by CBZ. The specific objectives of the present works are the followings: (1) identify the CBZ by-products and propose a mechanism (reaction pathways) for CBZ degradation based on identified by-products; (2) study the kinetic of CBZ degradation and; (3) Verify the quality of treated-effluents (versus untreated effluents) in terms of toxicological effect.

10.4 Materials and methods

10.4.1 Preparation of the Ti/TiO_2 electrode

The titanium dioxide (TiO_2) coatings have been performed by means of a PLD method (Desbiens and El Khakani, 2003). A KrF excimer laser (wavelength = 248 nm, pulse duration = 15 nanoseconds) operating at a repetition rate of 30 Hz was focused, at an incidence angle of 45°, onto the TiO_2 rotating target (99.95% purity). The on-target laser energy density was set to 4.5 J cm^{-2}. The TiO_2 films were deposited on both titanium grids (for photoelectrochemical studies) and on silicon substrates (for material characterizations purposes). The TiO_2 deposits were performed at a deposition temperature 400°C under an oxygen background pressure of 1 mTorr. The PLD deposition chamber was first turbo-pumped to about 10^{-6} Torr before filling it with oxygen. Prior to coating the substrates, the TiO_2 target was systematically cleaned by laser-ablating its surface for 5 min. The nominal thickness of the coating was estimated to 1 μm, as determined directly from cross-sectional scanning electron microscopy (SEM) observations. The crystallographic structure of the PLD-

deposited TiO_2 films was examined by means of X-ray diffraction (XRD) technique using a Philips X'pert-MPD X-ray diffractometer (Cu K_α radiation) at a glancing incident angle of 1°.

10.4.2 Preparation of the amorphous carbon electrode

The amorphous carbon (a-C) films were deposited by using the PLD method. Thus, a KrF excimer laser (wavelength = 248 nm, pulse durations 15 ns, repetition rate = 30 Hz) was focused, at an incidence angle of 45°, onto a 2"-diameter graphite pellet. During the laser ablation, the graphite target is kept rotating while the Incident KrF-laser beam is swept laterally on the target surface, in order to perform a uniform erosion of the graphite pellet. The on-target laser energy density was set to ~4 J cm^{-2}. Prior to performing the coating, the PLD deposition chamber was first turbo-pumped to about 10^{-6} Torr, and the graphite target was in-situ cleaned by ablating its surface for 5 min while isolating the substrate from the ablation plume by a shutter. The a-C coatings were deposited on 1 cm diameter polished-discs of titanium (for analyses purposes), and onto both sides of titanium grids specially designed for the photoelectrochemical studies. The PLD deposition of a-C films was achieved at two different deposition temperatures, namely 20°C (RT) (a-C1) and 600°C (HT) (a-C2). The typical thickness of the a-C coating, as deduced from cross-section scanning electron microscopy (SEM) observations is of ~500 nm.

10.4.3 Preparation of the synthetic solutions

The synthetic solution was prepared from distilled water with the addition of 0.05 mol/L of Na_2SO_4 to improve the electrical conductivity. This type of solution was used to evaluate the capacity of the electrolytic cell to produce reactive oxygen species (ROS). Another type of synthetic solution containing Na_2SO_4 was artificially contaminated by CBZ. CBZ ($C_{15}H_{12}N_2O$; CAS 298-48-4) was an analytical grade reagent supplied by sigma Aldrich (purity 99%). Its water solubility is 112 mg L^{-1} (Ferrari et al., 2004) and its vapor pressure

(1.4. 10^{-7} mmHg at 25°C) is relatively low indicating that this molecule is weakly lost by volatilization. Its octanol–water partition coefficient (log K_{ow} = 2.45) indicates the hydrophilic character of this molecule (Scheytti et al., 2005; Lee et al., 2011). CBZ stock solution was prepared in deionized water at 28.6 mg L^{-1}. Synthetic solution of CBZ was made by diluting the CBZ stock solution in deionized water (final concentration of 20 mg L^{-1}). Sodium sulphate was analytical grade reagent and supplied by Mat laboratory (Quebec, Qc, Canada).

10.4.4 Experimental devices

The reactor unit was made of acrylic material with a dimension of 12.7 cm (width), 16.51 cm (length) and 11.43 cm (depth) (Figure 10-1). All the assays were conducted in batch mode. The photoelectrocatalytic cell was comprised of one anode (Ti/TiO_2) and one cathode (SS, VC, Gr, a-C1 and a-C2), each one having a surface area of 110 cm^2 (10 cm width x 11 cm high), placed in parallel and were submerged in the solution. The electrodes were vertically installed on a perforated plexiglas plate placed at 2 cm from the bottom of the cell. The inter-electrode gap was 1.0 cm. Both anode and cathode were connected respectively to the positive and negative outlets of a DC power supply PS 3030 D (Circuit-Test Electronics, Burnaby, BC, Canada) with a maximum current rating of 3 A at an open circuit potential of 30 V. The photoelectrocatalytic cell was operated with current intensities (from 0.03 A to 0.37 A) imposed during treatment period ranging from 39.5 to 140.5 min. The photo-anode was illuminated by a mercury lamp (light intensity = 6.9 mW cm^{-2}; λ_{max} = 254 nm). The lamp was installed vertically inside the reactor. The light intensity was measured with a photometer (Model PS-3, 99-0057-01, UVp Company; USA). The photoelectrocatalytic reactor was placed in a dark chamber in order to avoid interferences from the daylight. Mixing in the cell was achieved by a Teflon-covered stirring bar installed between the perforated plate and the bottom of the cell. All experiments were carried out at room temperature (25°C). For all tests a total volume of 1.0 L was used.

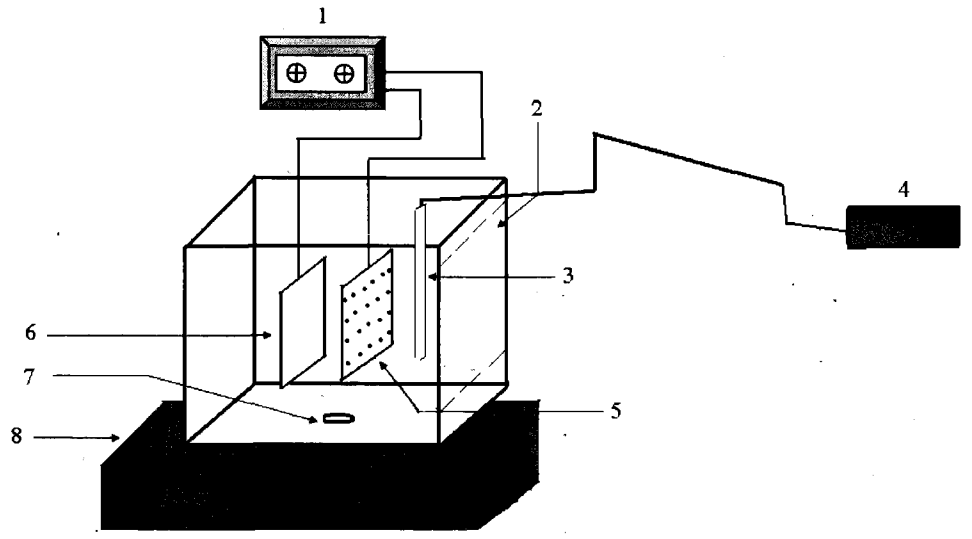


Figure 10-1 Schematic diagram of the photoelectrocatalytic reactor: (1) DC power supply (2) quartz window (3) UV lamp (4) photometer (5) photoanode (6) cathode (7) stirring bar (8) magnetic stirrer.

10.4.5 Experimental design

Response surface methodology (RSM) was applied to evaluate and determine the optimum operating conditions. RSM is a collection of mathematical and statistical methods for modeling, optimizing and analyzing a treatment process in which the response can be influenced by several variables (Zaroual., 2009). Both Factorial Design (FD) and Central Composite Design (CCD) methodologies are widely used in RSM. FD was used in order to investigate the main and interaction effects of the factors on the degradation of CBZ. Subsequently, CCD was employed to optimize PECO process in CBZ degradation. The variables investigated in our study were: the applied current intensity (X1), treatment time (X2), pollutant concentration (X3) and cathode material (X4). CBZ degradation efficiency

was considered as response (Y). The values of different variables were selected based on the preliminary assays.

10.4.6 Analytical details

The progress of photoelectrocatalytic degradation of CBZ in the solution was firstly monitored by measurements of relative absorbance using UV-visible absorption spectrophotometer (UV 0811 M136, Varian, Australia). The maximum absorption of the CBZ solution samples has been made at the wavelength of 286 nm in an optical quartz cell (1 cm). A calibration curve of known CBZ concentration versus relative absorbance was used to calculate the residual CBZ concentrations.

Likewise, the progress of photoelectrocatalytic degradation of CBZ and by-products (acridine and anthranilic acid) was monitored and quantified by LC/MS/MS (Thermo TSQ Quantum Access). The chromatographic column used was Hypersil Gold C18, particle size 3 μm and 2.1 x 100 mm inner diameter. The isocratic mobile phase was A: 50% H_2O + 0.1% formic acid and B: 50% CH_3CN + 0.1% formic acid at a flow rate of 200 μL/min. Mass spectral data shown in this study were acquired on a LCQ Duo ion trap tandem mass spectrometry equipped with an electrospray ionization (ESI) source operated in positive ion mode. Nitrogen was used as a sheath and auxiliary gas. Working conditions were as followed: spray voltage was 4500 V and capillary temperature was 300°C. Quantitative analysis of CBZ, acridine and anthranilic acid was determined using sulfamethazine C_{13} as internal standard.

The hydrogen peroxide concentration was measured using a volumetric dosage (Sigler and Masters., 1957). To quantitatively determine the concentration of hydrogen peroxide, the H_2O_2 calibration curve was obtained by plotting the cerium volume (mL) as a function of H_2O_2 concentration (from 0 mg L^{-1} to 100 mg L^{-1}) (Mespléde and Randon, 2004).

The rate of ROS production (OH°, O_3) was monitored by absorbance measurements of RNO at 440 nm using an UV-visible absorption spectrophotometer (UV 0811 M136, Varian, Australia). The RNO calibration curve was obtained by plotting the RNO absorbance at 440 nm as a function of RNO concentration (from 0.0 mg L^{-1} to 8 mg L^{-1}) (Simonsen et al., 2010).

The quality of treated CBZ solution (versus untreated CBZ solution) has been evaluated using a Microtox tests in order to determine its toxic effects. Toxicity tests were carried out in duplicate by Exova Laboratory (Quebec, Qu, Canada). Microtox analysis is a standardized toxicity method using the luminescent marine, Vibrio fisheri. The endpoint of Microtox test is the measurement of bioluminescence reduction. The bioluminescence reduction was determined after a 5, 15 and 30 min exposure to the contaminant. The effects of toxicity were expressed as percentage of luminescence inhibition at 15 min of exposure.

10.4.7 Economic aspect

The economic study included chemical and energy consumption. The electric cost was estimated about of 0.06 US$ kWh^{-1}. A unit cost of 0.30 US$ kg^{-1} was used of electrolyte (Na_2SO_4 industrial grade). The total cost was evaluated in terms of U.S. dollars spent per cubic meter of treated solution (US$ m^{-3}).

10.5 Results and discussions

10.5.1 Characterization of the Ti/TiO_2 electrode

The surface morphology of the TiO_2 photocatalytic coating was examined by SEM. Figure 10-2 shows a top view of a TiO_2 film deposited at 400°C onto silicon substrates. The coating is densely packed with a very smooth surface, where no specific features can be distinguished from the SEM images.

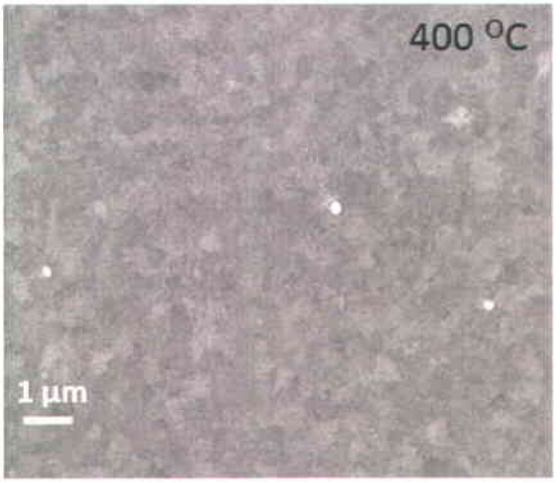


Figure 10-2 SEM image of the surface morphology of the TiO_2 film deposited at 400°C.

Besides, Figure 10-3 (a, b) shows the very uniform thickness of the TiO_2 films. The morphology of the TiO_2 films is seen be characterized by densely packed TiO_2 columns with a very smooth top surface and a continuous interface with the underlying substrate.

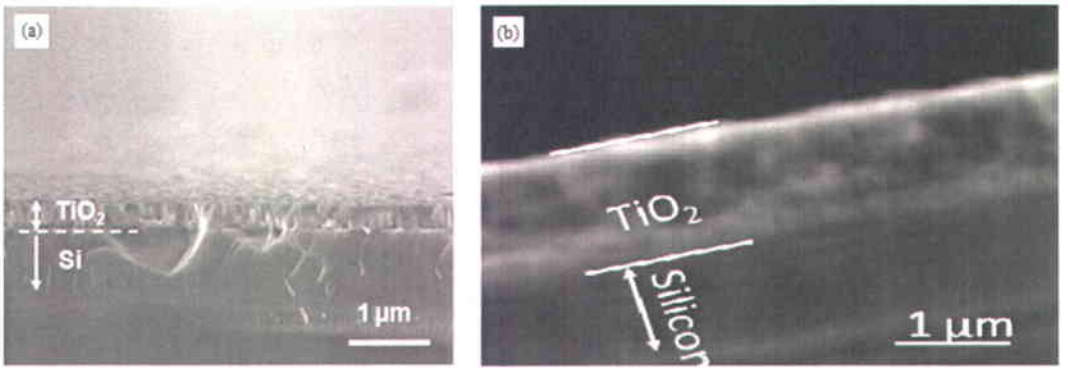


Figure 10-3 SEM views of PLD TiO_2 films deposited on silicon.

The crystallographic structure of the TiO_2 coating prepared by PLD was characterised by XRD (Figure 10-4). The XRD analysis indicates that our TiO_2 coatings deposited at 400°C

are polycrystalline and crystallize in the TiO_2 anatase phase. According to Regonini et al. (2010), the TiO_2 anatase phase is generally obtained for deposition at temperatures below 500°C. The XRD spectrum of the TiO_2 coating on the Ti-grid confirms the presence of the same TiO_2 anatase phase obtained on Si (the peak intensities are less prominent than the peaks of the underlying metallic Ti grid because of the thinness of the TiO_2 coating compared to the Ti grid substrate). Interestingly, one can note that the main (101) XRD peak of the TiO_2 phase is broader in the case of the films deposited onto the Ti grid than on Si substrates. The average size of TiO_2 crystallites is smaller on the Ti grid than on Si. To quantify this substrate-dependent grain size effect, the average size (D) of the TiO_2 crystallites was estimated using the Debye–Scherer equation (Guinier, 1962):

Équation 10-1 $$D = \frac{0.9\ \lambda}{\Delta(2\theta)\cos\theta}$$

Where D is the grain size in a particular orientation (i.e.; (101) here), λ is the X-ray wavelength, θ is the diffraction angle corresponding to the particular orientation and (2θ) is the width at half maximum of the peak.

The average size of the TiO_2 anatase crystallites was estimated to approximately 26 nm on silicon and only approximately 15 nm on the Ti-grid substrates. This results is likely due to the rougher surface of the Ti grids compared to the silicon substrate. The smoothness of the silicon substrate promotes the growth of relatively larger TiO_2 crystallites with increasing temperatures. The same trends have been also recorded by Alekhin et al. (2010). At numbers of reaction cycles constant (N = 3600), the crystallite size for TiO_2 film grown on a Ti-substrate (76 nm) is lower (35%) compared to the TiO_2 film grown on a Si-substrate. This difference is mainly attributed to the surface of the Ti-substrate which is rougher compared to

the surface of the Si-substrate (Alekhin et al., 2010). The roughness of the substrate affects directly the surface diffusivity of the ablated species, which in turn govern the TiO_2 crystallites growth. This nanometer scale grain size is expected to have an important effect on the photocatalytic activity of the TiO_2 coating (Kim et al., 2007). Indeed, with a decrease in particle size, the catalytic activity is enhanced due to the huge increase in the surface area (or surface to volume ratio) of the material. TiO_2 used as photocalyst is largely affected by the surface properties of its nanocrystals. Indeed, the catalytic activity of the photo-catalyst is enhanced with decrease in particle size of TiO_2 to the nanometer scale because the optical band gap is widened due to the quantum size effect combined with the increase in the surface area (Mills and Le Hunte., 1997; Colmenares et al., 2009; Anpo et al., 1987). This phenomenon has been observed by Anpo et al. (2006). Higher photocatalytic activity has been reported when the size of the TiO_2 particles is below 10 nm.

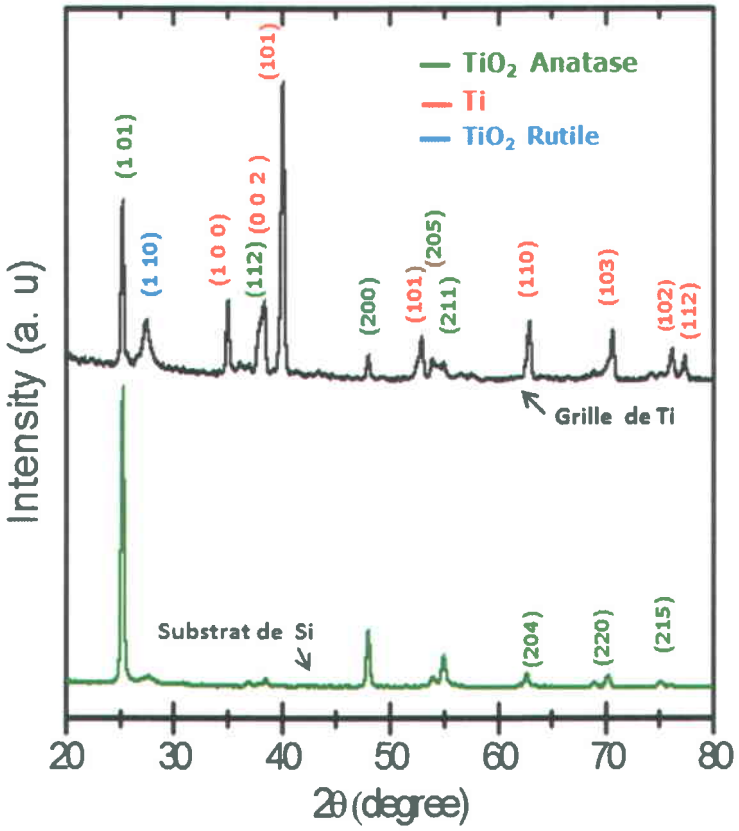


Figure 10-4 X-ray diffraction patterns of TiO_2 film coated on silicon substrates and on titanium grids at 400°C.

10.5.2 Characterization of the nanostructured carbon electrode

The surface morphology of the amorphous carbon (a-C) coatings was examined by SEM. Figure 10-5a shows a typical SEM-top-view of a carbon film deposited at 20°C onto a titanium disc. The coating is seen to be highly dense with fine grained pebbly surface with more or less spherical features. These features are seen to have a size in the 100-300 nm range, and present a "cauli-flower-like" morphology with a finer substructure that can be perceived in the SEM image of Figure 10-5b.

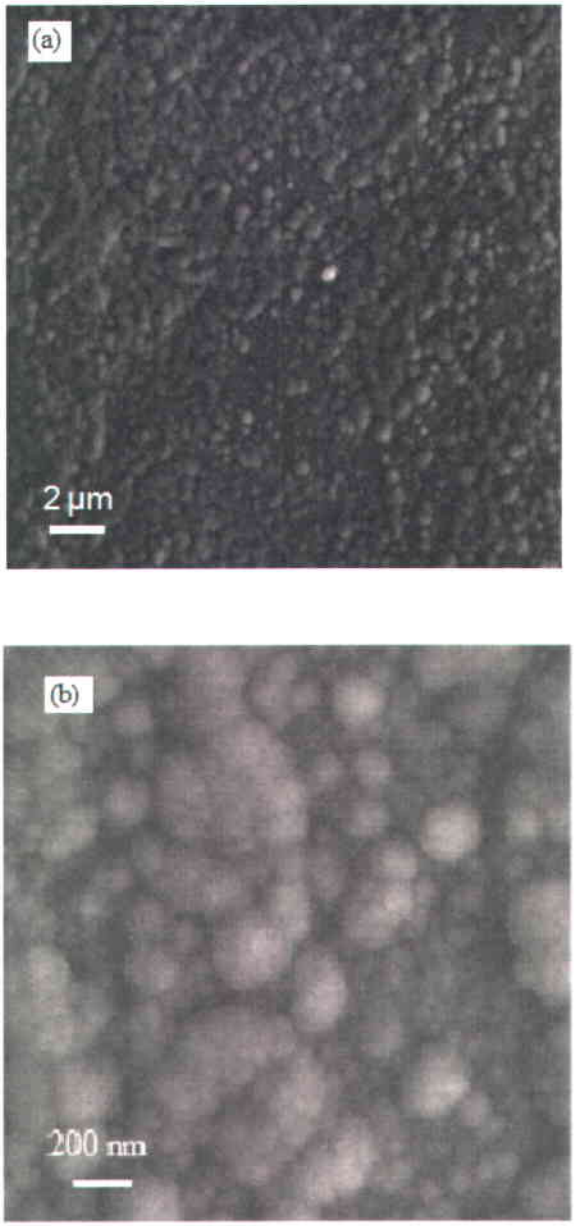


Figure 10-5 SEM views of PLD amorphous carbon deposited on Ti at 20 °C.

10.5.3 Efficacy of the PECO process in removing CBZ using different types of cathode electrodes

To clearly define the experimental region for the RSM study, a preliminary galvanostatic study was performed by applying a current intensity of 0.1 A for 120 min using different

types of cathode materials: SS, VC, Gr and nanostructured a-C_1 and a-C_2. During these tests, Ti/TiO_2 nanostructured was used as photo-anode under UV irradiation at 254 nm (Table 10-1). The maximum degradation of CBZ has been recorded using VC as cathode material (51 ± 2.6 %), whereas the lowest CBZ removal was recorded with SS (37.2 ± 2.01 %). The best performance of CBZ degradation using VC can be attributed to the capacity of the cell to produce more H_2O_2, which oxidant effect is beneficial for PC reaction by trapping the electron in the CB and enhancing the oxidation rate of pollutant (Leng et al., 2006). Such oxidant (H_2O_2) can be generated at the cathode (Xie and Li, 2006). The capacity of the photoelectrocatalytic cell to produce H_2O_2 was tested using distilled water containing Na_2SO_4 (0.05 M) without the addition of CBZ. The maximum H_2O_2 concentration (0.14 ± 0.01 mmol L^{-1}) has been recorded using VC as cathode. It is worth noting that, those values recorded were the residual H_2O_2 concentration, since UV irradiation was able to react with H_2O_2 to form OH° (Carbajo et al., 2011). However, it was surprising to measure a residual H_2O_2 concentration in solution using SS as a cathode material, whereas the literature reveals that H_2O_2 can be formed during electrolysis when graphite, carbon felt, activated carbon fiber or vitreous carbon are used as cathode electrodes. In fact, the residual H_2O_2 concentration (~ 0.09 mM) recorded using SS electrode was mainly attributed to oxidoreduction reactions occurring at the surface of the Ti/TiO_2 photocatalyst (Daghrir et al., 2013). Finally, VC and SS cathode electrodes were selected for the next step of this study dealing with FD methodology. Nevertheless, it is worth underlying that nanostructured a-C coated electrodes exhibited degradation capacity of CBZ that advantageously compares with that of VC if one considers the relatively high cost of VC and the relatively thin film of a-C required to use it as an effective cathode.

Tableau 10-1 Effect of cathode materials on CBZ degradation.

Parameters	PECO Process				
	Test 1	Test 2	Test 3	Test 4	Test 5
Intensity (A)	0.1	0.1	0.1	0.1	0.1
Treatment times (min)	120	120	120	120	120
Light intensity ($\mu W\ cm^{-2}$)	6900	6900	6900	6900	6900
UV lamp position	Internal	Internal	Internal	Internal	Internal
Initial CBZ concentrations ($mg\ L^{-1}$)	13.4±1.3	13.4±1.3	13.4±1.3	13.4±1.3	13.4±1.3
Electrolyte (Na_2SO_4 $mol\ L^{-1}$)	0.05	0.05	0.05	0.05	0.05
Type of cathode	SS	Gr	VC	AC1	AC2
Type of anode	Ti/TiO_2 (anatase)	Ti/TiO_2 (anatase)	Ti/TiO_2 (anatase)	Ti/TiO_2 (anatase)	Ti/TiO_2 (anatase)
H_2O_2 concentration ($mmol\ L^{-1}$)	0.09±0.002	0.11±0.0	0.14±0.01	0.10±0.002	0.11±0.005
CBZ removal (%)	37.2±2.01	41.3±4.08	51±2.6	41.4±1.5	39.4±3.3

PECO: Photoelecrtrocatalytic oxidation; SS: Stainless steel; Gr: graphite; VC: vitreous carbon; AC1: amorphous carbon (20°C); AC2: amorphous carbon (600°C)

10.5.4 Effect of the experiment parameters on the CBZ degradation using the experimental factorial design methodology

The results presented above allowed us to clearly define the experimental region for RSM to study CBZ degradation using the PECO process. The experiment region investigated for CBZ degradation and the experimental results are presented in Table 10-2. The experimental response associated to a 2^4 FD (four variables) is represented by a linear polynomial model with interaction, as follows:

Équation 10-2

$$Y = b_0 + b_1 X_1 + b_2 X_2 + b_3 X_3 + b_4 X_4 + b_{12} X_1 X_2 + b_{13} X_1 X_3 + b_{14} X_1 X_4 + b_{23} X_2 X_3 + b_{24} X_2 X_4 + b_{34} X_3 X_4$$

Where Y represents the experimental response (CBZ degradation); b_0 represents the average value of the responses of the 16 assays; X_i the coded variable (-1 or +1); b_i represents the principal effect of each factor i on the response and b_{ij} represents the interaction effect between factor i and factor j on the response. The coefficients of the polynomial model were calculated using the Design-Expert ® Program Software (Design Expert 7, Stat-Ease Inc., Minneapolis).

Équation 10-3

$$Y = 36.15 + 0.79 X_1 + 7.65 X_2 - 4.40 X_3 - 1.41 X_4 - 0.088 X_1X_2 + 0.037 X_1X_3 - 1.53 X_1X_4 - 0.80 X_2X_3 - 0.54 X_2X_4 + 1.29 X_3X_4$$

The value of the regression coefficient R^2 was 0.992. From Equation 10.3, it can be seen that the electrolysis time (b_1 = + 7.65) greatly influenced the rate of CBZ oxidation. The rate of CBZ oxidation increases on average of 15.3 % (2 x 7.65) when the treatment time goes from 60 to 120 min. The second most important factor on CBZ oxidation is the pollutant concentration with a negative effect (b_3 = - 4.40). The rate of CBZ oxidation decreased on average of 8.80 % (2 x 4.40) when the pollutant concentration goes from 10 to 20 mg L^{-1}. However, the effects of current intensity (b_1= + 0.79) and cathode material (b_4 = - 1.41) are relatively weak. Among the interaction terms, (X_1X_4) and (X_3X_4) have the most important

coefficient (b_{14} = - 1.53 and b_{34} = + 1.29, respectively). Pareto analysis can be used to give more significant information to interpret these results (Myers and Montgomery, 2002; Haaland, 1989). Indeed, this analysis gives more significant information by calculating the contribution of each factor on the response (Equation10-4).

Équation 10-4 $$P_i = \left(\frac{b_i^2}{\sum b_i^2} \right) * 100 \qquad (i \neq 0)$$

Where b_i represents the estimation of the principal effect of the factor i. Thus, it is found that the contribution of treatment time and pollutant concentration on CBZ removal is around 70.6% and 23.3%, respectively, whereas that of cathode material and current intensity account only for 2.4% and 0.75%, respectively (Figure 10-6).

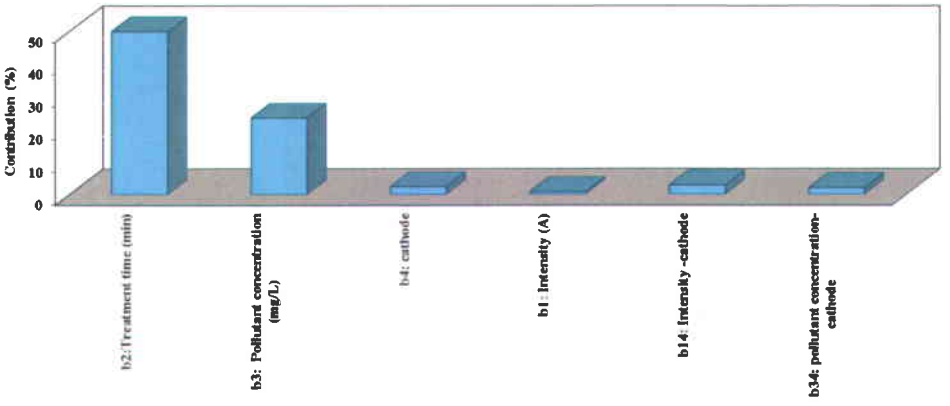


Figure 10-6 Graphical Pareto analysis of the effect of current intensity, treatment time, pollutant concentration and cathode material.

The interpretation of the interactions effect of X_1X_4 and X_3X_4 on CBZ degradation can be facilitated by seeing the Figure 10-7 and the Figure 10-8, respectively. Considering for

example the interaction X_3X_4 (Figure 10-8), it can be seen that when the cathode material (variable X_4) is fixed at the lowest level (i.e., VC is imposed), the pollutant concentration (X_3) has a significant influence on the response, the average rate of CBZ degradation increased from 31.8% to 43.9% (an abatement gain of 12.1 units was recorded). However, if the cathode material is fixed at the highest level (i.e., SS is imposed), the average rate of CBZ degradation passed from 31.4% to 37.8% (an abatement gain of 6.4%). Consequently, the cathode material influences the rate of CBZ oxidation, but it directly depends on the initial concentration of pollutant imposed.

Compared to conventional PC process, the use of cathode material such as VC represents an interesting advantage in PECO process, on which H_2O_2 can be electrochemically generated by cathodic reduction of dissolved oxygen (Xie and Li, 2006). Under UV radiation, H_2O_2 can be decomposed into OH°. Likewise, the addition of an electron acceptor (e.g. H_2O_2) should prevent the electron-hole recombination and increase the photocatalyst efficiency (Ozer and Ferry, 2001). Such an oxidant agent (H_2O_2) is beneficial for PC reaction by trapping the conduction band electron in order to generate more OH° (Daghrir et al., 2013). Furthermore, the PECO process was more effective at low CBZ concentrations (10 mg L^{-1}). This result indicates that CBZ removal is limited by the amount of ROS produced. The ROS are insufficient for enhance degradation efficiency at higher pollutant concentrations (Wang et al., 2009). The decrease of pollutant degradation efficiency (in the presence of high initial concentration of pollutant) can be attributed to the competitive reaction of the oxidation of the intermediates by OH° (Wang et al., 2009). The influence of initial concentration of pollutant was put into evidence by Daghrir et al. (2012) and Ding et al. (2010) while studying photoelectrocatalytic degradation of chlortetracycline and benzotrialzole, respectively. The degradation experiments of chlortetracycline were carried out at different initial concentrations (from 25 mg L^{-1} to 50 mg L^{-1}) in 0.5 M of Na_2SO_4 at 0.25 A and 0.5 A of

current intensity. The degradation efficiency was around 61.3 % at initial concentration of 50 mg L^{-1}, whereas 64.5 % of chlortetracycline has been removed at initial concentration of 25 mg L^{-1} of pollutant. The same trend has been also recorded by Ding et al. (2010), when more than 99 % of benzotriazole was removed at the lowest initial concentration (0.05 mM). The decrease in degradation rate of pollutant while increasing the initial concentration can be explained in two ways. Firstly, the reaction between photogenerated holes (or OH°) and pollutant can be inhibited owing to adsorbed pollutant on the surface of the catalyst. Secondly, the UV radiations may be more adsorbed by pollutants rather than photocatalyst Ti/TiO_2 and consequently limits the catalytic reaction efficiency (Ding et al., 2010).

Finally, the FD was useful to determine the interactions affecting the response and indicates if the lowest or the highest levels of the factors are favourable or not. However, this type of model cannot be used to predict or to determine the optimization conditions. For this reason, a RSM should be used in a second step to determine the optimal operating conditions for CBZ degradation.

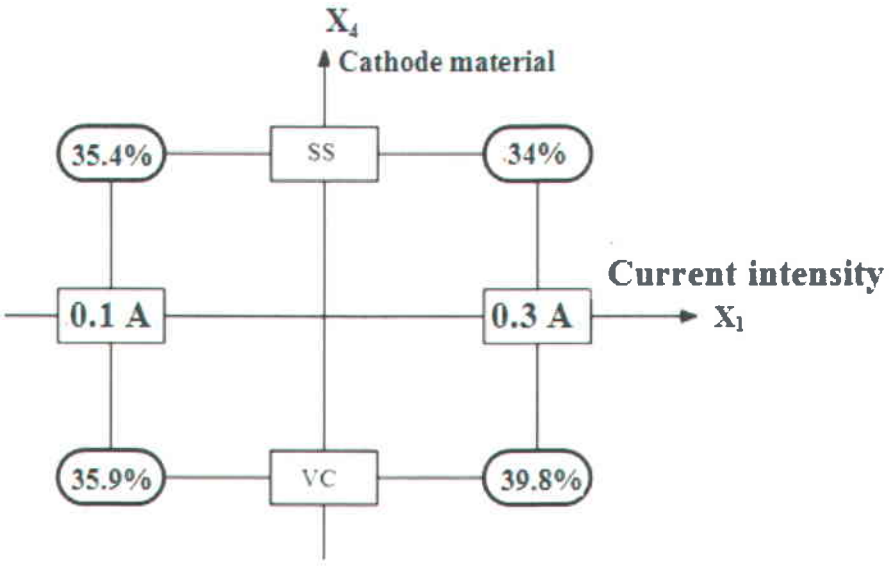


Figure 10-7 Interaction X_{14} between current intensity and cathode material.

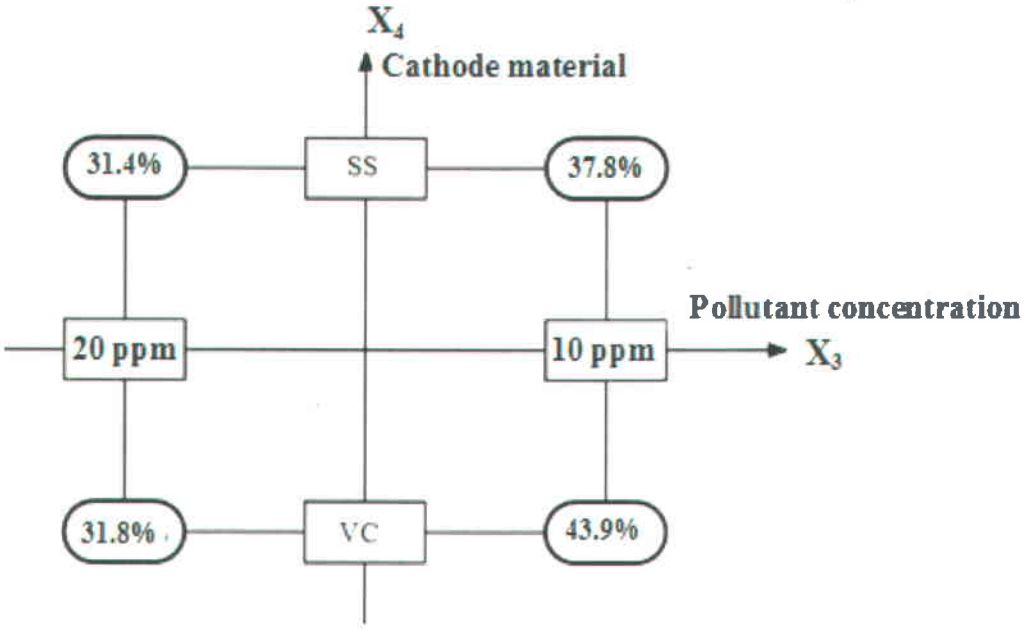


Figure 10-8 Interaction X_{34} between pollutant concentration and cathode material

.

Tableau 10-2 Experimental region and experimental results from Factorial Design matrix (2^4).

Coded variables (X_i)	Factor (U_i)	Experimental field		$U_{i,0}$	ΔU_i
		Min value (-1)	Max value (+1)		
X_1	U_1 : curent intensity (A)	0.10	0.30	0.2	0.1
X_2	U_2 : Treatment time (min)	60	120	90	30
X_3	U_3 : CBZ concentration (mg L^{-1})	10	20	15	5
X_4	U4: Cathode material	VC	SS	-	-

Test	Experimental design				Experimental plan				Experimental Responses
	X1	X3	X2	X4	U1	U2	U3	U_4	Result, Y Degradation efficacy (%)
1	-1	-1	-1	-1	0.10 A	60 min	10	VC	31.5
2	-1	+1	-1	-1	0.10 A	120 min	10	VC	53.6
3	-1	-1	+1	-1	0.10 A	60 min	20	VC	23
4	-1	+1	+1	-1	0.10 A	120 min	20	VC	35.5
5	+1	-1	-1	-1	0.30 A	60 min	10	VC	37
6	+1	+1	-1	-1	0.30 A	120 min	10	VC	53.5
7	+1	-1	+1	-1	0.30 A	60 min	20	VC	25.9
8	+1	+1	+1	-1	0.30 A	120 min	20	VC	43
9	-1	-1	-1	+1	0.10 A	60 min	10	SS	30.4
10	-1	+1	-1	+1	0.10 A	120 min	10	SS	46.3
11	-1	-1	+1	+1	0.10 A	60 min	20	SS	25.6
12	-1	+1	+1	+1	0.10 A	120 min	20	SS	39.6
13	+1	-1	-1	+1	0.30 A	60 min	10	SS	29.5
14	+1	+1	-1	+1	0.30 A	120 min	10	SS	45.2
15	+1	-1	+1	+1	0.30A	60 min	20	SS	25
16	+1	+1	+1	+1	0.30 A	120 min	20	SS	36.3

10.5.5 Optimization conditions for CBZ degradation using central composite design (CCD) methodology

One of the advantages of CCD is the possibility to explore the whole of the experimental region and the usefulness of interpolating the response. For the evaluation of data, the experimental response associated to a CCD matrix (Table 10-3) was described by a second-order model in the form of quadratic polynomial equation given below:

Équation 10-5

$$Y = b_0 + \sum_{i=1}^{k} b_i X_i + \sum_{i=1}^{k} b_{ii} X_i^{\,2} + \sum_{j} \sum_{i=2}^{k} b_{ij} X_i X_j + e_i$$

Where Y is the experimental response; X_i and X_j are the independent variables; b_0 is the average of the experimental response; b_i is the estimation of the principal effect of the factor i on the response Y; b_{ii} is the estimation of the second effect of the factor i on the response Y; b_{ij} is the estimation of the interaction effect between i and j on the response Y and e_i represents the error on the response Y. The coefficients of the polynomial model were calculated using the Design-Expert® Program Software:

For SS electrode:

Équation 10-6

$$Y_1 = 2.28525 - 54.02954\,X_1 + 0.57154\,X_2 + 1.01299\,X_3 - 0.08125\,X_1X_2 + 0.38750\,X_1X_3 - 6.37510^{-3}\,X_2X_3 + 121.86609\,X_1^2 - 1.1208110^{-3}\,X_2^2 - 0.039642\,X_3^2$$

For VC electrode:

Équation 10-7

$$Y_2 = 5.26173 - 32.59849\,X_1 + 0.58311\,X_2 + 0.70871\,X_3 - 0.08125\,X_1X_2 + 0.38750\,X_1X_3 - 6.37510^{-3}\,X_2X_3 + 121.86609\,X_1^2 - 1.1208110^{-3}\,X_2^2 - 0.039642\,X_3^2$$

From these Equations (10.6) and (10.7)), it can be seen that the current intensity is very meaningful for CBZ degradation using both SS and VC as cathode material. The predicted contour plot (curve of constant response) is given in Figure 10-9. When the treatment time was kept constant at 90 min (electrolysis time at the center of the experimental region

investigated), CBZ removal efficiency decreased with increasing pollutant concentration for all current intensities studied. As seen from the contour plot, more than 44% of CBZ removal could be recorded at 90 min while the current intensities were higher than 0.22 A and the pollutant concentration lower than 12.5 mg L^{-1}. In terms of optimization, the pollutant concentration has a more significant impact on CBZ removal efficiency.

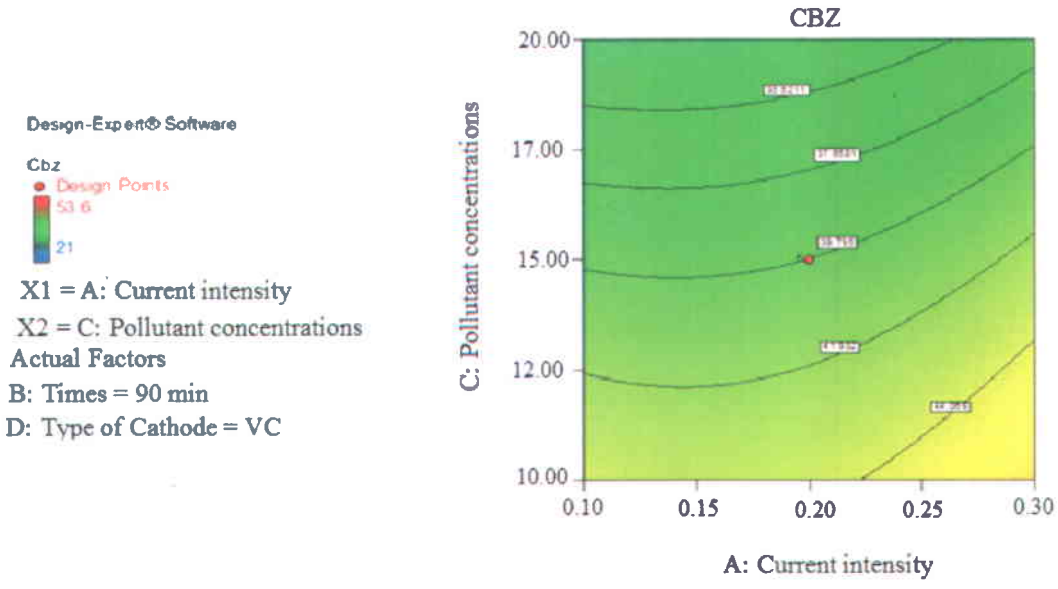


Figure 10-9 The effect of current intensity (A) and pollutant concentration (mg L^{-1}) on CBZ removal (application time: 90 min); VC as cathode.

Tableau 10-3 Central composite matrix and experimental results

Experiment number	Experimental design			Experimental plan			Result, Y Degradation efficacy (%)
	X_1	X_2	X_3	U_1	U_2	U_3	
For VC (U_4)							
17	-1.68	0	0	0.03	90	15	44
18	1.68	0	0	0.37	90	15	46.5
19	0	-1.68	0	0.2	39.5	15	21.6
20	0	1.68	0	0.2	140.5	15	49.7
21	0	0	-1.68	0.2	90	6.59	43
22	0	0	1.68	0.2	90	23.5	32
23	0	0	0	0.2	90	15	37
24	0	0	0	0.2	90	15	43
25	0	0	0	0.2	90	15	42
26	0	0	0	0.2	90	15	41
27	0	0	0	0.2	90	15	37
28	0	0	0	0.2	90	15	43
For SS (U_4)							
29	-1.68	0	0	0.03	90	15	41
30	1.68	0	0	0.37	90	15	39
31	0	-1.68	0	0.2	39.5	15	18.4
32	0	1.68	0	0.2	140.5	15	44.5
33	0	0	-1.68	0.2	90	6.59	41.5
34	0	0	1.68	0.2	90	23.5	29
35	0	0	0	0.2	90	15	37
36	0	0	0	0.2	90	15	39
37	0	0	0	0.2	90	15	34
38	0	0	0	0.2	90	15	33
39	0	0	0	0.2	90	15	34
40	0	0	0	0.2	90	15	32.6

Table 10-4 shows the analysis of variance (ANOVA) of regression parameters of the predicted response surface quadratic model for CBZ removal using PECO process. The model F-value of 60.02 and a low probability value (Pr > F = 0.0001) indicate that the model is significant for CBZ removal. The value of the correlation coefficient (R^2 = 0.9347) indicates that only 6.53% of the total variation could not be explained by the empirical model.

Tableau 10-4 ANOVA results for CBZ degradation.

Source	Analysis of variance				
	d.f.[a]	Sum of square	Mean of square	F-value	Pr > F
Model	13	2492.04	191.70	60.02	< 0.0001
Residual	26	174.08	6.70	-	-
Lack of fit	16	107.25	6.70	55.85	< 0.0001
Pure error	10	66.83	6.68	-	-

[a] *Degree of freedom; F: Fisher coefficient;* R^2*=0.9347.*

An agreement between actual and predicted values of CBZ degradation is satisfactory and consistent with the quadratic model (Figure 10-10). According to Joglekar and May (1987), R^2 should be at least 0.80 for a good fit of model. The R^2 value (0.9347) recorded in the present study for CBZ removal was higher than 0.80, indicating that the regression model explained the reaction well.

The main objective of the optimization is to determine the optimum values for CBZ removal using the PECO process. The criteria selected for the optimization condition for CBZ degradation are the following: (i) pollutant concentration has to be minimized (ii) treatment time has to be maximized and (iii) current intensity and cathode material were investigated in

the experimental range. The optimum operating conditions proposed by the Design Expert Program software are the following: 0.3 A of current intensity imposed during 120 min of treatment times using VC as cathode and at 10 mg L^{-1} of initial concentration of CBZ. The desirability function value was found as 1.00 for these optimum conditions. The average value of the CBZ removal measured using UV-vis absorption spectrophotometer is 49.1% ± 2.1%. This result was recorded at the end of this experiment, and is found to be very close to the value proposed by the model (54% of CBZ degradation).

However, experimental results determined using LC/MS/MS show that the removal of CBZ is around 73.5% ± 2.8%. UV–vis absorption spectrophotometer is an indirect analytical method. According to Beer-Lambert law, the measure of the concentration of species can be determined from the measured absorbance. The presence of interfering substances can influence the absorption spectrum and consequently can modify the results. By comparison, LC/MS/MS analysis is a technique combining simultaneously a powerful physical separation technique and powerful technique of analysis and mass detection. LC/MS/MS technique has a very high sensitivity and selectivity towards several compounds (Hernàndez et al., 2007). It is worth noting that during the treatment, the pH varied from 5.54 to 7.3. This variation could probably attributed to CBZ by-product formation during the application of the PECO process.

Besides, to confirm the superiority of PECO process on CBZ degradation, complementary tests were carried out using conventional PC process in optimal conditions (254 nm of UV irradiations was imposed during 120 min of treatment times, in the presence of the Ti/TiO_2 catalyst and at initial CBZ concentrations of 10 mg L^{-1}). The degradation rate of CBZ recorded using LC/MS/MS technique was 57.81±1.38%. Thus, it is clear that current intensity (0.3 A) applied during the treatment confirm the superiority of the PECO process.

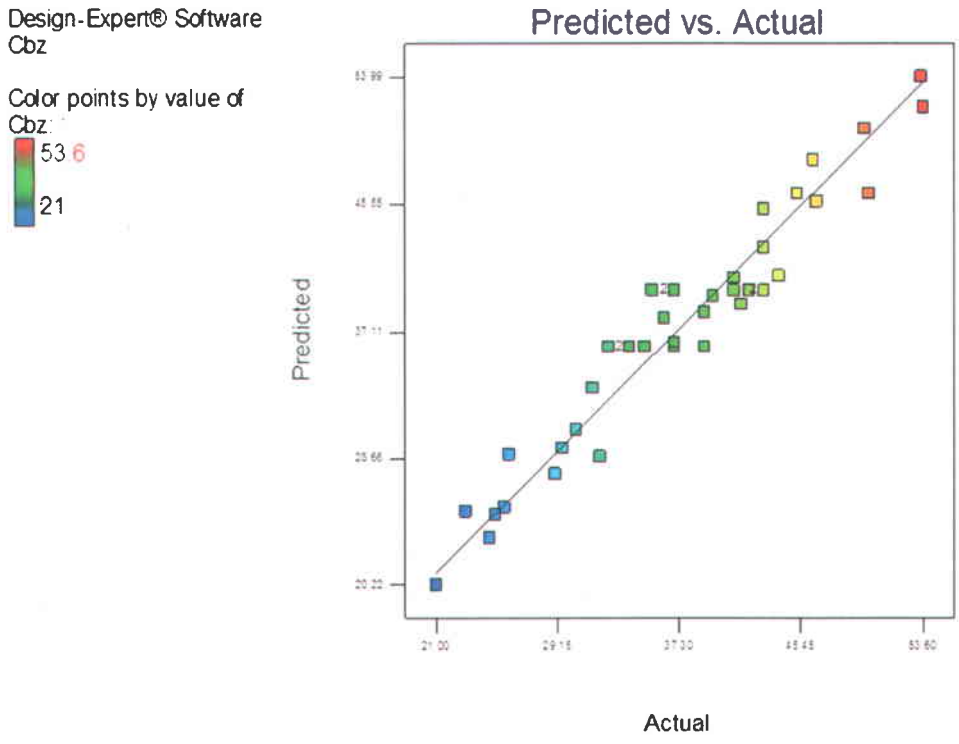


Figure 10-10 **Comparison between actual and predicted values for CBZ degradation**

10.5.6 By-products formation and proposed mechanism of CBZ degradation

Our intention is to follow the formation of some by products while treating the synthetic CBZ solution using the PECO process. LC/MS/MS analysis showed the detection of acridine and anthranilic acid as by-products of CBZ. The average concentrations of acridine and anthranilic acid recorded at the end of PECO process was 0.77 µM and 0.06 µM, respectively. By comparison, the residual concentration of acridine and anthranilic acid recorded after PC process was 1.13 µM and 0.12 µM, respectively. This difference is mainly due to the current intensity applied which increases the degradation efficiency of the organic compounds.

Considering the two by-products described above, the proposed mechanism of CBZ degradation by PECO process is shown in Figure 10-11. Firstly, OH° produced by PECO process react with CBZ at the 10 position and lead to the formation of radical intermediates that can evolve to form 10, 11-epoxycarbamazepine. Subsequently, ring contraction in 10, 11-epoxycarbamazepine by loss of the $-CONH_2$ group leads to 9-acridine- 9-carboxaldehyde as intermediate. This latter will decompose to give acridine. An alternatively pathway would lead by the reaction of CBZ with OH° to the formation of hydroxylated derivatives which breakdown yields anthranilic acid and salicylic acid.

On the other hand, the residual concentration of total organic carbon (TOC) recorded at the end of treatment was 5.78±0.60 mg L^{-1} compared to 7.33±0.11 mg L^{-1} measured in the initial CBZ solution (21.2% ± 7.7% of TOC removal). Only a small fraction of CBZ was completely oxidized into water and carbon dioxide. The majority of the pollutant was transformed into by-products. Besides, Microtox tests carried out under optimal conditions show a decrease in the percentage of luminescence inhibition while applying PECO process. The percentage of the inhibition initially measured was 32.25% ± 4.73%, whereas the percentage of the inhibition recorded at the end of the treatment was 20.45% ± 11.24%. Under these conditions, the residual concentration of CBZ and by-products (acridine and salicylic acid) are not toxic on V. fisheri.

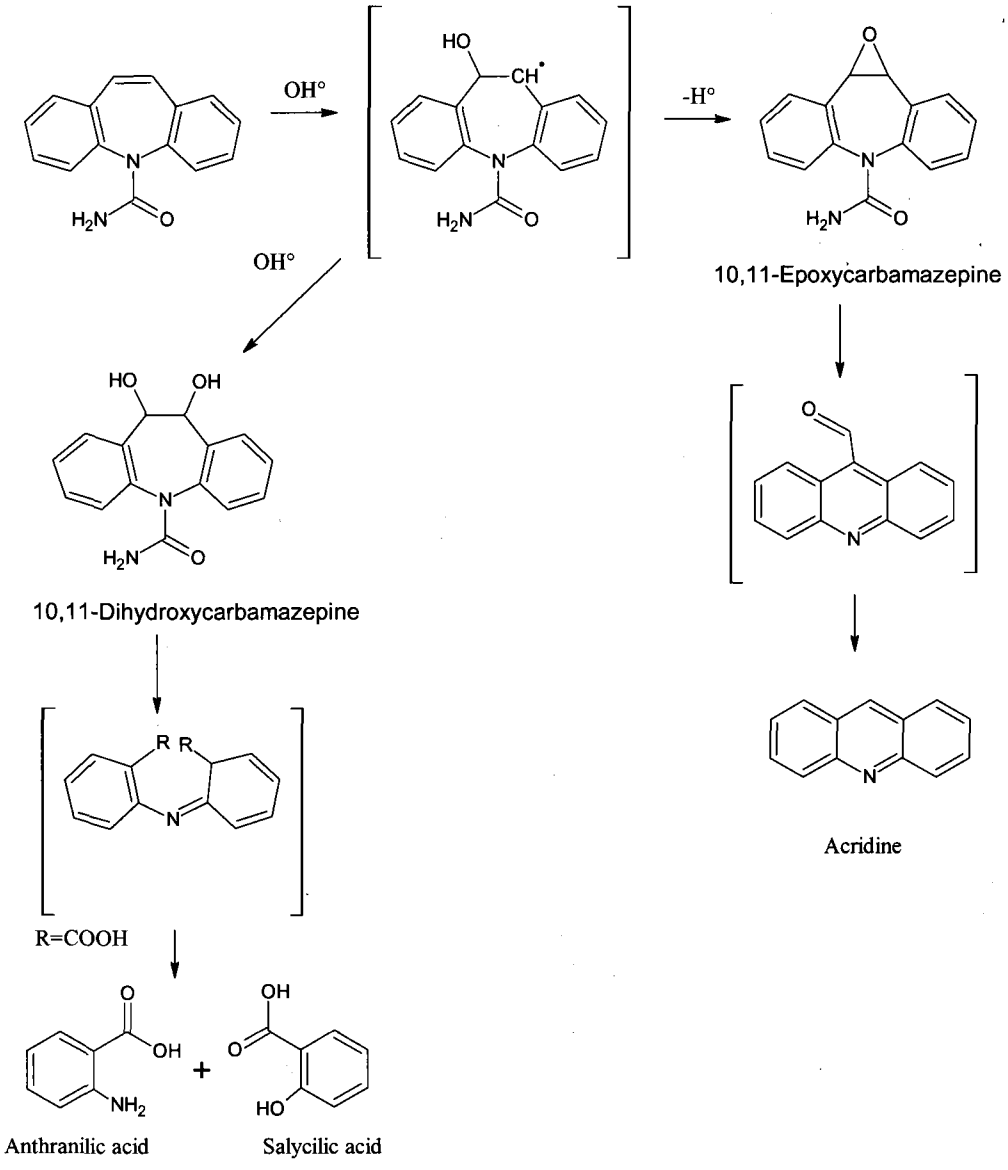


Figure 10-11 Reaction mechanism proposed for the photoelectrocatalytic degradation of CBZ.

10.5.7 Kinetics study of CBZ degradation by PECO process

Kinetic study could be helpful to evaluate and to understand the mechanism of pollutant degradation (Thabet and El-Zomrawy, 2011). To evaluate the degradation rate of CBZ, the

kinetic data were analyzed using different kinetic models: pseudo-first order kinetic model and pseudo-second order kinetic model.

The pseudo-first order kinetic model is described by the following equation:

Équation 10-8 $$Ln\frac{C_0}{C} = k_1 t$$

For the pseudo-second order kinetic model, the equation described below has been applied:

Équation 10-9 $$\frac{1}{C} - \frac{1}{C_0} = k_2 t$$

Where C_0 is the initial concentration of CBZ, C is the concentration of CBZ at time t, k_1 is the first order reaction rate constant (min^{-1}), k_2 is the second order reaction rate constant (L mg^{-1} mn^{-1}) and t is the reaction time.

For practical applications, the degradation kinetics of CBZ using the PECO process was investigated under optimum conditions. The kinetic rate constants k_1 and k_2 were 4 10^{-3} min^{-1} and 6 10^{-4} L mg^{-1} mn^{-1}, respectively. The best fitting model was selected according to regression coefficient (R^2) value. The calculated value of R^2 from the pseudo-first order kinetic model (R^2 = 0.910) was lower than the value obtained from the pseudo-second order kinetic model (R^2 = 0.994). These results showed that the pseudo-second order kinetic model describes very well the degradation of CBZ by PECO process. It is interesting to compare the kinetic constant with values obtained in others experimental conditions. Martinez et al (2011) indicated that the degradation kinetic of CBZ using PC process (0.5 g L^{-1} of P25 and 5 mM H_2O_2) is well described by the pseudo-first order kinetic model. The kinetic rate constant recorded was 0.3144 min^{-1}. However, pseudo-second order kinetic model for the CBZ degradation (1.92 10^9 L mol^{-1} s^{-1}) have been recorded by Matta et al. (2011) using sulfate radical oxidation. The same trend has been also recorded by Rosal et al. (2008) using ozonation process with 38–40 g N^{-1} m^{-3} of ozone concentration in gas and 1 g L^{-1} of TiO_2 as

catalyst. The corresponding kinetic constant ($4.25\ 10^{-3} \pm 9.7\ 10^{-4}$ L $mmol^{-1}s^{-1}$) was 1.8 times higher than that recorded in our study ($k_2 = 2.36\ 10^{-3}$ L $mmoL^{-1}\ s^{-1}$). In the study of Rosal et al. (2008), the CBZ degradation is obtained owing to the high ozone concentration (38–40 g $N^{-1}\ m^{-3}$) introduced in the reactor and the amount of OH° produced by decomposition of ozone. By comparison, the rate of ROS (OH° and O_3) generated by PECO process was 6.07 ± 0.06 mg L^{-1}. The rate of oxidant species produced influences the kinetic rate of pollutant degradation.

Finally, the photoelectrocatalytic treatment cost of CBZ (including only chemical consumption and energy consumption) recorded in the optimal conditions was estimated to 2.98 ± 0.1 \$ m^{-3}.

10.6 Conclusion

In this study, the Ti/TiO_2 rectangular electrode was prepared by a PLD method. It showed that the TiO_2 coating at 400°C is very uniform in thickness and was found to be of anatase structure. By investigating the PECO process for CBZ degradation in aqueous medium using Ti/TiO_2 electrode, treatment time and pollutant concentration were found to be the most influent parameters. The contribution of treatment time and pollutant concentration on CBZ degradation were 70.6% and 23.3%, respectively, whereas the contributions of cathode material and current intensity were 2.4% and 0.75%, respectively. A central composite design was employed to define the optimal operating conditions for CBZ oxidation. The PECO process applied under optimal conditions is able to oxidize 73.5% ± 2.8% of CBZ and to ensure partial mineralization (21.2% ± 7.7%). The analysis using LC/MS/MS technique shows that acridine and anthranilic acid are the two by-products of CBZ. The kinetic study shows that the pseudo-second-order kinetic model ($k_2 = 6\ 10^{-4}$ L $mg^{-1}min^{-1}$) describes well the oxidation of CBZ by PECO process.

10.7 Acknowledgments

Sincere thanks are extended to the National Sciences, Engineering Research Council of Canada and Premier Tech Ltée for their financial to this study.

10.8 References

Alekhin AP, Gudkova SA, Markeev AM, Mitiaev AS, Sigarev AA & Toknova VF (2010). Structural properties of the titanium dioxide thin films grown by atomic layer deposition at various numbers of reaction cycles. *Appl. Surf. Sci.* 257: 186-191.

Anpo M, Shima T, Kodama S & Kubokawa Y (1987) Photocatalytic hydrogenation of CH_3CCH with H_2O on small-particle TiO_2: Size quantization effects and reaction intermediates. *J. Phys. Chem.* 91: 4305-4310.

Bahlmann A, Weller MG, Panne U & Schneider RJ (2009) Monitoring carbamazepine in surface and wastewaters by an immunoassay based on a monoclonal antibody. *Anal. Bioanal. Chem.* 395(6): 1809-1820.

Calisto V, Domingues MRM, Erny GL & Esteves VI (2011) Direct photodegradation of carbamazepine followed by micellar electrokinetic chromatography and mass spectrometry. *Water Res.* 45: 1095-1104.

Carbajo J, Adàn C, Rey A, Martinez-Arias A & Bahamonde A (2011) Optimization of H_2O_2 use during the photocatalytic degradation of ethidium bromide with TiO_2 and iron-doped TiO_2 catalysts. *App.Catal. B.* 102: 85-93.

Chong MN & Jin B (2012) Photocatalytic treatment of high concentration carbamazepine in synthetic hospital wastewater. *J. Hazard. Mater.* 199-200: 135-142.

Chong MN, Jin B, Laera G & Saint CP (2011) Evaluating the photodegradation of Carbamazepine in a sequential batch photoreactor system: Impacts of effluent organic matter and inorganic ions. *Chem. Eng. J.* 174: 595-602.

Colmenares JC, Luque R, Campelo JM, Colmenares F, Karpinski Z & Romero AA (2009) Nanostructured Photocatalysts and Their Applications in the Photocatalytic Transformation of Lignocellulosic Biomass: An Overview. *Materials* 2: 2228-2258.

Daghrir R, Drogui P & El Khakani MA (2013) Photoelectrocatalytic oxidation of chlortetracycline using Ti/TiO_2 photoanode with simultaneous H_2O_2 production. *Electrochim. Acta.* 87: 18-52.

Daghrir R, Drogui P & Robert D (2012) Photoelectrocatalytic technologies for environmental applications. *J. Photochem. Photobiol. A* 238: 41-52.

Daghrir R, Drogui P, Ka I & El-Khakani MA (2012) Photoelectrocatalytic degradation of chlortetracycline using Ti/TiO_2 nanostructured electrode deposited by means of pulsed Laser deposition process. *J. Hazard. Mater.* 199-200: 15-24.

Desbiens E & El Khakani MA (2003) Growth of high-K silicon oxynitride thin films by means of a pulsed laser deposition-atomic nitrogen plasma source hybrid system for gate dielectric applications. *J. Appl.Phys.* 94 (9): 5969–5975.

Ding Y, Yang C, Zhu L & Zhang J (2010) Photoelectrochemical activity of liquid phase deposited TiO_2 film for degradation of benzotriazole. *J.Hazard.Mater.* 175:96-103.

Esplugas S, Bila DM, Krause LGT & Dezotti M (2007) Ozonation and advanced oxidation technologies to remove endocrine disrupting chemicals (EDCs) and pharmaceuticals and personal care products (PPCPs) in water effluents. *J. Hazard. Mater.* 149: 631-642.

Ferrari B, Paxéus N, Giudice RL, Pollio A & Garric J (2003). Ecotoxicological impact of pharmaceuticals found in treated wastewaters: Study of carbamazepine, clofibric acid, and diclofenac. *Ecotox. Environ. Safe.* 55 (3): 359-370.

Ferrari B, Mons R, Vollat B, Fraysse B, Paxéus N, Lo Giudice R, Pollio A & Garric J (2004) Environmental risk assessment of six human pharmaceuticals: Are the current environmental risk assessment procedures sufficient for the protection of the aquatic environment? *Environ. Toxicol. Chem.* 23(5): 1344-1354.

Focazio MJ, Kolpin DW, Barnes KK, Furlong ET, Meyer, MT, Zaugg SD, Barber LB & Thurman ME (2008) A national reconnaissance for pharmaceuticals and other organic wastewater contaminants in the United States - II) Untreated drinking water sources. *Sci. Total. Environ.* 402 (2-3): 201-216.

Frontistis Z, Daskalaki VM, Katsaounis A, Poulios I & Mantzavinos D (2011) Electrochemical enhancement of solar photocatalysis: Degradation of endocrine disruptor bisphenol-A on Ti/TiO_2 films. *Water Res.* 45: 2996-3004.

Guinier, A (1962) *Théorie et Technique de la radiocristallographie.* 3rd ed. Dunod, Paris. P740.

Haaland DP (1989) *Experimental design in biotechnology. Statistics: textbooks and monographs.* Vol 105, Dekker, New York, p 201.

Heberer T (2002) Occurrence, fate, and removal of pharmaceutical residues in the aquatic environment: A review of recent research data. *Toxicol Lett.*131: 5–17.

Heberer Th, Reddersen K & Mechlinski A (2002) From municipal sewage to drinking water: Fate and removal of pharmaceutical residues in the aquatic environment in urban areas. *Water Sci. Technol,* 46 (3): 81-88.

Hernàndez F, Sancho VJ, Ibànez M & Guerrero C (2007) Antibiotic residue determination in environmental waters by LC-MS. *Trends Anal. Chem.* 26 (6): 466–485.

Hummel D, Loffler D, Fink G & Ternes TA (2006) Simultaneous determination of psychoactive drugs and their metabolites in aqueous matrices by liquid chromatography mass spectrometry. *Environ. Sci. Technol.* 40 (23): 7321-7328.

Joglekar AM & May AT (1987) Product excellence through design of experiments. *Cereal Food World* 32: 857–868.

Kim CS, Kwon IM, Moon BK, Jeong JH, Choi BC, Kim JH, Choi H, Yi SS, Yoo DH, Hong KS, Park JH & Lee HS (2007) Synthesis and particle size effect on the phase transformation of nanocrystalline TiO_2. *Mat Sci Eng C* 27: 1343–1346.

Laera G, Chong MN, Jin B & Lopez A (2011) An integrated MBR-TiO_2 photocatalysis process for the removal of Carbamazepine from simulated pharmaceutical industrial effluent. *Bioresource Technol.* 102: 7012-7015.

Lapworth DJ, Baran N, Stuart ME & Ward RS (2012) Emerging organic contaminants in groundwater: A review of sources, fate and occurrence. *Environ. Pollut.* 163: 287-303.

Lee S, Kang Su-Il, Lim JL, Huh YJ, Kim KS & Cho J (2011) Evaluating controllability of pharmaceuticals and metabolites in biologically engineered processes, using corresponding octanol–water distribution coefficient. *Ecol. Eng.* 37: 1595-1600.

Leng WH, Zhu WC, Ni J, Zhang Z, Zhang JQ & Cao CN (2006) Photoelectrocatalytic destruction of organics using TiO_2 as photoanode with simultenous production of H_2O_2 at the cathode. *App. Catal. A* 300: 24-35.

Liu Y, Gan X, Zhou B, Xiong B, Li J, Dong C, Bai J & Cai W (2009) Photoelectrocatalytic degradation of tetracycline by highly effective TiO_2 nanopore arrays electrode. *J. Hazard. Mater.* 171: 678-683.

Martinez C, Canle ML, Fernàndez MI, Santaballa JA & Faria J (2011) Aqueous degradation of diclofenac by heterogeneous photocatalysis using nanostructured materials. *Appl. Catal. B-Environ.* 102: 563-571.

Martin-Diaz L, Franzellitti S, Buratti S, Valbonesi P, Capuzzo A & Fabbri E (2009) Effects of environmental concentrations of the antiepilectic drug carbamazepine on biomarkers and cAMP-mediated cell signaling in the mussel *Mytilus galloprovincialis. Aquat. Toxicol.* 94: 177-185.

Martinez-Huitle CA & Ferro, S (2006) Electrochemical oxidation of organic pollutants for the wastewater treatment: Direct and indirect processes. *Chem. Soc. Rev.* 35 (12): 1324-1340.

Matta R, Tlili S, Chiron S & Barbati S (2011) Removal of carbamazepine from urban wastewater by sulfate radical oxidation. *Environ. Chem. Lett.* 9: 347-353.

Metcalfe CD, Koenig BG, Bennie DT, Servos M, Ternes TA & Hirsch R (2003) Occurrence of neutral and acidic drugs in the effluents of canadian sewage treatment plants. *Environ. Toxicol. Chem.* 22 (12): 2872-2880.

Mesplède J & Randon J (2004) *100 manipulations de chimie générale et analytique*. Ed. Bréal, p289.

Mills A & Le Hunte S (1997) An overview of semiconductor photocatalysis. *J. Photoch. Photobio. A* 108 (1):1-35.

Myers RH & Montgomery DC (2002) *Response surface Methodology: Process and product optimization using Designed Experiments*. 2nd ed. John Wiley and Sons, New York, p704.

Ozer RR & Ferry JL (2001) Investigation of the photocatalytic activity of TiO_2-polyoxometalate systems. *Environ. Sci. Technol.* 35 (15): 3242-3246.

Prajapati S, Gohel M, Patel L (2007) Studies to enhance dissolution properties of carbamazepine. *Indian. J. pharm. Sci.* 69 (3): 427-430.

Regonini D, Jaroenworaluck A, Stevens R & Bowen CR (2010) Effect of heat treatment on the properties and structure of TiO_2 nanotubes: Phase composition and chemical composition. *Surf. Interface Anal.* 42: 139–144.

Rosal R, Rodriguez A, Gonzalo MS & Garcia-Calvo E (2008) Catalytic ozonation of naproxen and carbamazepine on titanium dioxide. *App. Catal. B* 84(1-2): 48-57.

Saien J & Khezrianjoo S (2008) Degradation of the fungicide carbendazim in aqueous solutions with UV/TiO_2 process: Optimization, kinetics and toxicity studies. *J. Hazard. Mater.* 157: 269-276.

Scheytt T, Mersmann P, Lindstadt R & Heberer T (2005) 1-Octanol/water partition coefficients of 5 pharmaceuticals from human medical care: Carbamazepine, clofibric acid, diclofenac, ibuprofen, and propyphenazone. *Water Air Soil Poll.* 165: 3-11.

Sigler PB & Masters BJ (1957) The hydrogen peroxide-induced Ce*(III)-Ce(IV) exchange system. *J. Am. Chem. Soc.* 79:6353– 6357.

Simonsen ME Muff J, Bennedsen LR, Kowalski KP & SOgaard EG (2010) Photocatalytic bleaching of p-nitrosodimethylaniline and a comparison to the performance of other AOP technologies. *J. Photochem. Photobiol. A* 216: 244-249.

Sohrabi MR & Ghavami M (2010) Comparison of Direct Yellow 12 dye degradation efficiency using UV/semiconductor and UV/H_2O_2/semiconductor systems. *Desalination* 252: 157–162.

Ternes TA (1998) Occurrence of drugs in German sewage treatment plants and rivers. *Water Res.* 32 (11): 3245-3260.

Ternes A, Meisenheimer M, McDowell D, Sacher F, Brauch HJ, Haist-Gulde B, Preuss G, Wilme U & Zulei-Seibert N (2002) Removal of pharmaceuticals during drinking water treatment. *Environ. Sci. Technol.* 36: 3855-3863.

Thabet M & El-Zomrawy AA (2011) Degradation of acid red 17 dye with ammonium persulphate in acidic solution using photoelectrocatalytic methods. *Arab. J. Chem.* http://dx.doi.org/10.1016/j.arabjc.2011.03.001.

Vogna D, Marotta R, Andreozzi R, Napolitano A & d'Ischia M, (2004) Kinetic and chemical assessment of the UV/H_2O_2 treatment of antiepileptic drug carbamazepine. *Chemosphere* 54: 497-505.

Waldner G, Pourmodjib M, Bauer R & Neumann-Spallart M (2003) Photoelectrocatalytic degradation of 4-chlorophenol and oxalic acid on titanium dioxide electrodes. *Chemosphere* 50: 989-998.

Wang N, Li X, Wang Y, Quan X & Chen G (2009) Evaluation of bias potential enhanced photocatalytic degradation of 4-chlorophenol with TiO_2 nanotube fabricated by anodic oxidation method. *Chem. Eng. J.* 146: 30–35.

Xie YB & Li XZ (2006) Degradation of bisphenol A in aqueous solution by H_2O_2-assisted photoelectrocatalytic oxidation. *J. Hazard. Mater.* B138: 526-533.

Yang J, Dai J, Chen C & Zhao J (2009) Effects of hydroxyl radicals and oxygen species on the 4-chlorophenol degradation by photoelectrocatalytic reactions with TiO_2-film electrodes. *J. Photochem. Photobiol. A* 208: 66-77.

Zaroual Z, Chaair H, Essadki AH, El Ass K & Azzi M (2009) Optimizing the removal of trivalent chromium by electrocoagulation using experimental design. *Chem. Eng. J.* 148: 488-495

Zhang Y, Geißen SU & Gal C (2008) Carbamazepine and diclofenac: Removal in wastewater treatment plants and occurrence in water bodies. *Chemosphere* 73 (8): 1151-1161.

ANNEXES

Annexe 1 : Données complémentaires au chapitre 1.

Estimation des coûts de traitement des eaux usées par les POAs

Tableau A Estimation des coûts de traitement des eaux usées Par les POAs

Technologie	Type d'effluent	Coûts ($\$ m^{-3}$)	Données pour estimer les coûts de traitement		Références
			Débit ($m^3 J^{-1}$)	Autres	
Oxydation photoélectrocatalytique utilisant des cellules solaires	Effluents synthétiques (acid dye provenant des industries de textiles)	9.42	-	• C'est le coût opérationnel (coût de l'énergie, coût du photocatalyseur et coût de la consommation de l'électrolyte) pour une élimination de 50 mg L^{-1} de l'acide dye. • Volume de pollunat traité = 1 m^3	Olya et al., (2013)
PhotoélectroFenton-photocatalytique (utilisant une lampe UV)	Acide Yellow 36 (AY 36)	0.63	-	• Coût opérationnel pour une élimination de 84.23% de AY 36 (25 mg L^{-1}). • Volume du polluant traité = 1 L.	Khataee et al., (2012)
Photocatalytique (utilisant des radiations solaires)	Acide dichloroacetique	-	-	• Coût opérationnel total de 26.18 $\$ Kg^{-1}$ d'acide dichloroacetique (coût du catalyseur et coût de la consommation chimique de Fe^{2+} et de H_2O_2. • Volume de pollunat traité = 22 L	Marugan et al., (2007)
Photo-Fenton: lumière UV artificielle + addition initiale de H_2O_2	Effluents industriels	48.83	-	• Coût opérationnel incluant le coût de l'électricité et la consommation de produits chimiques. • Usine Pilote UV: coût = 21.704$; valeur de récupération = 2170$; durée de vie utile estimée = 10 année; coût de maintenance = 434$/année; Charge d'utilisation = 1953$. • Collecteur parabolique solaire : coût = 28.486$; valeur de récupération = 2848$; durée de vie utile estimée = 10 année; coût de maintenance = 596$/année; Charge d'utilisation = 2563$. • Plusque 10 mg L^{-1} de cyanide et 1700 mg L^{-1} de formates	Duran et al., (2012)
Photo-Fenton modifié: lumière UV artificielle + addition continue de H_2O_2		16.3	33.6		
Photo-Fenton : lumière solaire (collecteur parabolique)		8.14	-		

Tableau A Estimation des coûts de traitement des eaux usées Par les POAs (*suite*)

Technologie	Type d'effluent	Coûts ($\$ m^{-3}$)	Données pour estimer les coûts de traitement		Références
			Débit ($m^3 J^{-1}$)	Autres	
Oxydation photocatalytique (UV) Photo-Fenton	Effluents industriels	24.41 12.88	- -	• Coût opérationnel calculé pour une réduction de la DCO de plus de 90%; concentration initiale de la [DCO]° = 300 mg L^{-1}.	Martinetti, (2007)
O_3 O_3/UV O_3/UV/H_2O_2	Effluents industriels	11.27 16.12 17.39	1	• Coût opérationnel incluant : coût de l'électricité, génération *in-situ* de l'oxygène; Lampe UV, produits chimiques ajoutés. • [DCO]° = 4650 mg O_2 L^{-1}	Lucas et al., (2010)
Oxydation électrochimique	Effluents industriels	5.47-8.44	-	• Coût opérationnel pour une élimination de la DCO de 74-93% ([DCO]° = 1084-8877 mg L^{-1}).	Rajkumar et Palanivelu, (2004)
Ozonation Fenton Oxydation électrochimique	Mélange de composés organiques (Acide Butyrique, 2-propanol, 4-chlorophenol, 2-Naphthol, huile d'olive, etc)	97-278 2.71-96 12.2-47.5	1	C'est le coût opérationnel calculé pour une élimination de 85% de DCO coût d'investissement: • 13871-24666 (Fenton) • 82849-167434 (Ozonation) • 27895-142310 (oxydation électrochimique)	Canizares et al., (2009)